

Coal Science II

Coal Science II

Harold H. Schobert, EDITOR
The Pennsylvania State University

Keith D. Bartle, EDITOR
University of Leeds

Leo J. Lynch, EDITOR
Commonwealth Scientific and Industrial Research Organisation

Developed from a symposium sponsored
by the Division of Fuel Chemistry
of the American Chemical Society
at the 198th National Meeting
Miami Beach, Florida, September 10–15, 1989





Library of Congress Cataloging-in-Publication Data

Coal science II / Harold H. Schobert, editor, Keith D. Bartle, editor, Leo J. Lynch, editor ; developed from a symposium sponsored by the Division of Fuel Chemistry of the American Chemical Society at the 198th National Meeting, Miami Beach, Florida, September 10–15, 1989.

p. cm.—(ACS symposium series; 461)

Symposium in honor of Peter Given.

Includes bibliographical references and index.


ISBN 0–8412–2005–0 : \$77.95

1. Coal—Congresses. 2. Given, P. H. (Peter Hervey), 1918–1988.

I. Schobert, Harold H., 1943– . II. Bartle, Keith D. III. Lynch, Leo J., 1940– . IV. Given, P. H. (Peter Hervey), 1918–1988. V. American Chemical Society. Division of Fuel Chemistry. VI. American Chemical Society. Meeting (198th: 1989: Miami Beach, Fla.) VII. Series.

TP325.C533 1991
662.6'2—dc20

91–11387
CIP

The paper used in this publication meets the minimum requirements of American National Standard for Information Sciences—Permanence of Paper for Printed Library Materials, ANSI Z39.48–1984. 

Copyright © 1991

American Chemical Society

All Rights Reserved. The appearance of the code at the bottom of the first page of each chapter in this volume indicates the copyright owner's consent that reprographic copies of the chapter may be made for personal or internal use or for the personal or internal use of specific clients. This consent is given on the condition, however, that the copier pay the stated per-copy fee through the Copyright Clearance Center, Inc., 27 Congress Street, Salem, MA 01970, for copying beyond that permitted by Sections 107 or 108 of the U.S. Copyright Law. This consent does not extend to copying or transmission by any means—graphic or electronic—for any other purpose, such as for general distribution, for advertising or promotional purposes, for creating a new collective work, for resale, or for information storage and retrieval systems. The copying fee for each chapter is indicated in the code at the bottom of the first page of the chapter.

The citation of trade names and/or names of manufacturers in this publication is not to be construed as an endorsement or as approval by ACS of the commercial products or services referred herein; nor should the mere reference herein to any drawing, specification, chemical process, or other data be regarded as a license or as a conveyance of any right or permission to the holder, reader, or any other person or corporation, to manufacture, reproduce, use, or sell any patented invention or copyrighted work that may in any way be related thereto. Registered names, trademarks, etc., used in this publication, even without specific indication thereof, are not to be considered unprotected by law.

PRINTED IN THE UNITED STATES OF AMERICA

American Chemical Society
Library
1155 16th St., N.W.
Washington, D.C. 20036

ACS Symposium Series

M. Joan Comstock, *Series Editor*

1991 ACS Books Advisory Board

V. Dean Adams
Tennessee Technological
University

Paul S. Anderson
Merck Sharp & Dohme
Research Laboratories

Alexis T. Bell
University of California—Berkeley

Malcolm H. Chisholm
Indiana University

Natalie Foster
Lehigh University

Dennis W. Hess
University of California—Berkeley

Mary A. Kaiser
E. I. du Pont de Nemours and
Company

Gretchen S. Kohl
Dow-Corning Corporation

Michael R. Ladisch
Purdue University

Bonnie Lawlor
Institute for Scientific Information

John L. Massingill
Dow Chemical Company

Robert McGorin
Kraft General Foods

Julius J. Menn
Plant Sciences Institute,
U.S. Department of Agriculture

Marshall Phillips
Office of Agricultural Biotechnology,
U.S. Department of Agriculture

Daniel M. Quinn
University of Iowa

A. Truman Schwartz
Macalaster College

Stephen A. Szabo
Conoco Inc.

Robert A. Weiss
University of Connecticut

Foreword

THE ACS SYMPOSIUM SERIES was founded in 1974 to provide a medium for publishing symposia quickly in book form. The format of the Series parallels that of the continuing ADVANCES IN CHEMISTRY SERIES except that, in order to save time, the papers are not typeset, but are reproduced as they are submitted by the authors in camera-ready form. Papers are reviewed under the supervision of the editors with the assistance of the Advisory Board and are selected to maintain the integrity of the symposia. Both reviews and reports of research are acceptable, because symposia may embrace both types of presentation. However, verbatim reproductions of previously published papers are not accepted.



Dedicated to the memory of Peter H. Given

Preface

COAL SCIENCE IS THE DISCIPLINE that investigates the geochemical origins of coal in the environment, the chemical constitution and physical properties of coal, and the fundamental basis of the reactions of coal. Coal science is distinct from coal technology in that coal science is not concerned with the development of specific processes for coal use. Ideally, the two disciplines should be closely allied because research in coal science provides new knowledge and ideas that could be adopted for the development and improvement of coal technology. In return, technological problems raise questions that require new research initiatives in the coal science laboratory. To be sure, a rough-and-ready body of coal technology can be erected, and—it might be argued—*has* been erected on a foundation of empirical results of poorly characterized materials of uncertain origin. However, as Leonardo da Vinci said, “Those who are in love with practice without science are like sailors who get into a ship without rudder or compass and can never be certain where they are going.” The discipline of coal science is a fascinating intellectual endeavor and the essential foundation of new processes for using this important natural resource as we move into the 21st century.

About 25 years ago, a major conference on coal science was held at The Pennsylvania State University. The papers presented at that conference were subsequently published as *Coal Science*, an out-of-print volume in the *Advances in Chemistry Series* of the American Chemical Society. Some of the chapters in that volume are still cited in current literature, a testament to the quality and continuing relevance of that work to the field of coal science. The conference organizer, Peter Given, had come to Penn State a few years earlier after a 10-year career with the British Coal Utilization Research Association. Even then, Given had established a reputation as a significant contributor to coal science. In the following years, he came to be recognized as one of the dominant coal scientists of the post-World War II era.

Peter Given retired from Penn State in 1985 and returned to his native England with ambitious plans to continue writing books and papers. Sadly, health problems intruded on these plans. Given died unexpectedly in April 1988. His death occurred almost a quarter century after the outstanding conference that he was instrumental in organizing; this occurrence suggested that a new symposium on coal science might serve two purposes. First, such a conference could be a tribute to this giant in

coal science. Second, the conference would provide an opportunity to take another look at the field after 25 years. The culmination of this idea was a symposium entitled “Advances in Coal Science: A Symposium in Remembrance of Peter Given.” After very kind and warm introductory remarks by Peter’s wife, Barbara Given, the symposium proceeded with 40 papers presented by authors from eight nations. Attendance was high, and the discussions were often quite spirited in a way that Peter Given would have richly enjoyed. This book represents the permanent record of the Given symposium.

Coal science is a vigorous, albeit small, field. Some research topics that were popular 25 years ago have withered while some new ones have become of vigorous interest; others seem to either come and go in cycles or serenely sail on forever. Unquestionably, the largest changes in the field have been the application of sophisticated instrumental analytical techniques to problems in coal science and the wealth of new insights and data these results have provided us. The chapters have been arranged to fit the major cornerstones of coal science: geochemistry, structure and properties, and reactivity. We have no doubt that a quarter century hence the contributions of Peter Given will continue to be cited and referenced. We hope the chapters in this book will prove to be durable and will serve as a fitting tribute to this great scientist.

Acknowledgments

This book would not have been possible without the efforts of all the authors who participated in the symposium on which this book is based and without the efforts of the many anonymous reviewers who provided useful comments. We are also very pleased to thank the Petroleum Research Fund, the Amoco Corporation, and The Pennsylvania State University for generous financial support that made it possible for some of our participants from overseas to attend the symposium.

HAROLD H. SCHOBERT
The Pennsylvania State University
University Park, PA 16802

KEITH D. BARTLE
University of Leeds
Leeds LS2 9JT, England

LEO J. LYNCH
Commonwealth Scientific and Industrial Research Organisation
North Ryde, New South Wales, Australia 2032

January 1991

Chapter 1

Peter Given: An Appreciation

Harold H. Schobert

Fuel Science Program, Department of Materials Science
and Engineering, The Pennsylvania State University,
University Park, PA 16802

This chapter provides some brief biographical information about Peter Given and his impact on the field of coal science. His contributions to the profession are measured and explained by comparing some of the papers presented at the 1964 American Conference on Coal Science, which he organized, and the 1989 symposium held in his memory and organized by the Division of Fuel Chemistry as part of the 198th national meeting of the American Chemical Society.

Peter Given

Peter Hervey Given was born in 1918. He was educated at Oxford University, receiving a B.A. in Chemistry in St. Peter's Hall, Oxford, and the M.A. and D.Phil. in the Dyson Perris Laboratory under the direction of Professors D. Ll. Hammick and Sir Robert Robinson (who was the Nobel laureate in chemistry for 1947). Given's thesis research dealt with carbonium ion reactions of aromatic hydrocarbons on cracking catalysts (1-3).

Peter Given joined the staff of the British Coal Utilization Research Association in 1945. From 1950 to 1960 he served as the head of the organic chemistry section. Many of his research activities at BCURA were quite different from those of his later, and perhaps better known, career at Penn State. In particular, he was involved in studies of the chemistry of phenols and their reactions on catalysts (e.g., 4-6), and was awarded a patent for improvements in processing of phenols (7). A second research area, which resulted in eighteen contributions to the literature from the mid-1950's through 1960, was a study of the electrochemical reactions of organic compounds, particularly with an emphasis on polarography (8-15). The electrochemical work also extended to coal extracts (16,17) and to coal (18). This phase of Peter Given's career culminated with the publication of the classic article on the distribution of hydrogen in coal and its relationship to the structure of coal, and the model structure which has now become almost universally known as "the Given structure" (19).

In 1961 Peter Given joined the faculty of The Pennsylvania State University as Associate Professor of Fuel Technology. He stayed at Penn State until his retirement in 1986. Promotion to professor came in 1962. In 1965 he became chairman of what was then the Department of Fuel Technology. Internal reorganization at Penn State in the late 60's led to Fuel Technology becoming the Fuel Science program of the

Department of Materials Science and Engineering; Given became the first program chairman and served until 1969. These details of academia aside, it was at Penn State that Given's career as coal scientist flourished.

Collaboration with colleagues in the College of Mineral Industries (now the College of Earth and Mineral Sciences) sparked a strong interest in the earth sciences, especially organic geochemistry, and led to a long and fruitful collaboration with geoscientists, most notably William Spackman. Writing in 1979, Peter Given said that, "Not long after I was appointed to Fuel Tech at Penn State in 1961, I concluded that an effective Fuel Tech of the type I was appointed to provide needed an organic geochemical component. ... In my current research on the applied chemistry of coal utilization, [this, I believe, was in reference to his extensive study of the relationship of coal characteristics to liquefaction behavior] I am constantly forced to regard the geochemistry and geology of coals in relation to what we find" (20). Within two years of joining the Penn State faculty, Given had already begun research on coal structure that was intended to draw on findings from geology, paleobotany, and petrography. In an overview article on coal research written in 1965, he discussed the interactions of coal research with the geological sciences, including the importance of coalified tree stumps in the development of Wegener's hypothesis of continental drift and the identification of coal-like material of high carbon content in the Gunflint chert as part of Barghoorn's pioneering studies of life in the Precambrian (21). By the early 70's Given was involved in studies of the Everglades peat with Spackman, exploring what he referred to as the "fascinating interface of biochemistry with organic and inorganic geochemistry" (22). In a brief biographical note, probably prepared about the time of his retirement, Peter Given referred to his career interest in the "bio-geochemistry of coal."

In the mid-70's Peter Given began a decade-long study of coal liquefaction, with particular emphasis on the geochemical and structural characteristics of coal that lead to high yields of distillable products. Ten years later, in the mid-80's, he was publishing vigorously in the areas of geochemistry, coal structure, and liquefaction chemistry, with 26 papers in the years 1983-86. Undoubtedly 1984 marked the zenith of his career, when he became the first non-American to receive the Henry H. Storch Award for outstanding research in fuel chemistry, and published the classic "An Essay on the Organic Geochemistry of Coal" (23).

During his career Peter Given published about 150 papers, was a vigorous participant in scientific meetings, taught Fuel Science courses on the chemistry of fuels and on coal structure, maintained an active group of graduate students and extensive informal collaboration with coal scientists around the world. His encyclopediac knowledge of the coal literature and of the composition and properties of coals was probably unparalleled. He was a tireless worker; there are legends of his appearing in the laboratory at 2 a.m., attired in robe and pajamas, because he had suddenly had an idea at home and wanted to be sure that the appropriate coal samples were on hand to test it. And yet this was not all. Peter Given had a remarkably rich intellectual and personal life. His interests outside the laboratory included antique furniture, photography, the layout of gardens and landscapes, and archaeology and the studies of early cultures. This last led to his development and teaching of a popular course "Materials in Ancient and Modern Cultures," which synthesized his interests in materials science, industrial archaeology, and history. He was interested in athletics, being an excellent swimmer and an enthusiastic attendant (and photographer) of athletic events. He was a long-standing member of the State College Choral Society, with a particular interest in medieval music.

Peter Given died suddenly on April 2, 1988 in Stroud, Gloucestershire, England. He left us the 150 or so papers, and some ways of attacking the fascinating, maddening problems of coal chemistry: the appreciation for the interplay of geochemistry and the chemistry of coal utilization, and the statistical manipulation of

bodies of data on coal characteristics and reactions. "The measure of any man lies not in his own lifetime, but in what he enables his successors to achieve (24)." For those of us who were privileged to know and work with Peter Given, he will always be with us.

"I shall have lived a little while
Before I die for ever." (25).

The Given Symposium

In 1964 The Pennsylvania State University, along with other organizations, sponsored The American Conference on Coal Science, held at Penn State in June of that year. The other sponsoring organizations were the American Chemical Society Division of Fuel Chemistry, the Geological Society of America, and the Organic Geochemistry Group of the Geochemical Society. Peter Given was the conference chairman. The papers contributed to that conference were subsequently published as a volume in the *Advances in Chemistry Series, Coal Science* (26). The 1964 conference included 47 papers on the topics of coal origins and metamorphosis, coal as an organic rock, the physical and chemical structure of coals, and the reactivity and reactions of coal.

In 1989 the American Chemical Society Division of Fuel Chemistry sponsored a symposium "Advances in Coal Science: A Symposium in Remembrance of Peter Given" as part of the program for the 198th national American Chemical Society meeting, held in Miami Beach in September. That symposium featured 35 papers, in the categories of coal geochemistry, coal structure, liquefaction and co-processing, and other aspects of thermoplasticity and coal reactivity. Because the *Advances in Coal Science* symposium to commemorate the career of Peter Given was held exactly a quarter-century after the American Conference on Coal Science, which he organized, a comparison of the two events makes it possible to provide some assessment of the changes in the field of coal science in the past 25 years and of Peter Given's impact on the field. In making such comparison, one must of course recognize that the content of any symposium or conference ultimately derives from the efforts of those who have contributed papers to it, and therefore the extent to which the selection of topics and papers represents a valid sample of the current major research problems in the field and of the leading practitioners is problematical. This is especially the case with the comparison being made here, because of the much more significant role of the geological organizations in the 1964 conference. Those caveats notwithstanding, however, a comparison of the papers presented and of the references to Peter Given's work do serve to illuminate somewhat the changes in coal science and of Given's contributions to it in the course of 25 years.

Several research topics were represented by papers at both meetings, and these topics must be counted among the "hardy perennials" in the field of coal science. Coalification, particularly the behavior of humic acids and the conversion of woody tissue to coal, is one such topic. The 1964 conference had three papers in this area (27-29). Phenolic compounds were recognized as being important in the formation of humic substances, and humification was known to be accompanied by a decrease in the methoxyl content (27). Single pieces of wood change heterogeneously to coal (29). Undoubtedly the greatest single change to occur in coal science in the past quarter-century is the increasing availability of highly sophisticated analytical instrumentation to be brought to bear on problems of the characterization of coals, of coalification, and of coal reactivity. The work reported in 1964 relied heavily on wet chemical methods (27), optical microscopy (29), and electron paramagnetic resonance spectrometry (28). The controlled electrolytic reduction of humic acids and hydroquinones reported by Given and co-workers in 1959 (30) was related to the information obtained by EPR examination of humic substances, with particular

relevance for a proposed humic acid model structure based on hydroquinone moieties (28). In 1989 Hatcher and Lerch reported on the survival of lignin units in coalified wood (31). That work relied heavily on pyrolysis-gas chromatography-mass spectrometry examination of fossil wood samples. The importance of phenol and methoxyphenol compounds was again emphasized, and the work showed that lignin structural units can be preserved in samples even as old as the Carboniferous. Reference was made to a prior study by Given and colleagues on the Curie point pyrolysis-gas chromatography-mass spectrometry of Paleocene and Eocene lignites (32), which curiously showed only traces of methoxyphenols. The work reported by Hatcher and Lerch is a continuation of a very fruitful research program which has relied not only on Py/GC/MS but also on ^{13}C nuclear magnetic resonance spectroscopy (e.g., 33).

The occurrence and incorporation of minor elements in coals was discussed in two papers at the 1964 conference (34,35). The distribution of elements and their modes of occurrence in coals was, and remains today, a concern. Much of the early work relied on detailed analyses of float-sink samples (34). It was in later years that Peter Given became active in detailed research on the inorganic components of coals (e.g., 36). Miller and Given's work on the association of inorganic components and minerals with coals (36) was noted in the present study of inorganic associations with South Australian lignites presented in 1989 by Quast and Readett (37). As in other areas of coal science, researchers studying the inorganic/organic relationships in coals now have available a variety of powerful analytical instrumentation, the uses and misuses of which have been discussed in the useful review by Robbins (38). An earlier review by Given and Yarzab called attention to some of the problems in coal analysis posed by the presence of mineral matter (39). Even the isolation of the inorganic components for subsequent characterization can be fraught with subtle complexities, such as the fixation of organic nitrogen as nitrate during the low temperature ashing of coals (40).

The macromolecular structures of coals and the variation of structure with rank has of course been a topic of great interest and controversy in coal science for decades. In the 1964 conference Peter Given was a co-author of a contribution on the EPR of macerals (41), which drew on some of his previous work in this area (30, 42). Given's work on the organic structural relationships in coal macerals (42) was also of relevance in a detailed study of maceral structures by Tschamler and deRuiter (43). Of particular interest was the determination of the amount of oxygen incorporated in phenolic groups (42) and the use of infrared measurements to assess the phenolic hydrogen (43); the results showing reasonable agreement. Given had also shown that the carbonyl groups in coals were not identified unambiguously, in that they could be quinonoid or ketonic (44); this work was of importance to developing an understanding of the total distribution of the carbon in coal, that distribution influencing in turn the measurement of aliphatic structures in coal from pyrolysis studies (45). The problem of making a total assignment of carbon still remains. In 1964 NMR studies, especially ^{13}C NMR, of coals were in their infancy (e.g., 46); since then, NMR has become a standard technique for coal structural studies. Sethi, for example, demonstrated the applicability of NMR to the assignment of methyl, methylene, methine, and quaternary structures (47).

One of the dominant issues in coal structure to re-emerge in the past decade is the two-phase concept of coal structure. A very spirited discussion of this topic was a feature of the 1989 symposium (48-52). Peter Given played a central role in the recent work on the two-phase concept, particularly in fostering the usage of the terms "mobile phase" and "macromolecular network" (23,53-55) and in organizing the "debate in print" (54), which has become a landmark papers in coal structure. In particular, the debate in print (54) was cited by all of the contributors to the 1989 discussion of the mobile phase (48-52). Given's work on the mobile phase was a

foundation for much of the research reported in the 1989 symposium. Particularly noteworthy were the observations of the early release of paraffins during mild pyrolysis, and the formation of n-alkyl aromatics and n-alkanes in quantities much higher than obtainable from mild Soxhlet extraction (56-58), which helped develop the idea that the mobile phase is clathrated in the macromolecular network (59). In recent years the study of the two-phase concept of coal structure has benefitted greatly as a result of the availability of powerful instrumental techniques, such as pyrolysis/field ionization mass spectrometry (48,51) and NMR spectroscopy (47,52).

Incorporation of heteroatoms in coal and their distribution among various functional groups is another of the topics of interest in both the 1964 and 1989 meetings. The application of instrumental methods to determination of functional groups, such as the infrared determination of carboxyl groups in coal macerals (60), was still in early stages in 1964. A report at the 1989 symposium discussed the use of high resolution mass spectrometry for speciation of oxygen compounds in benzene/methanol extracts of coals (61). This study drew in part from the work of Peter Given and his students on phenolic (62), carbonyl (44,63), and carboxyl groups (64). Gorbaty and colleagues reported in 1989 in powerful new techniques, x-ray photoelectron spectroscopy (65) and x-ray absorption near-edge spectroscopy (66), for speciation of organic sulfur forms in coals. Peter Given had published some discussion of the structural implications of very high organic sulfur contents, particularly in the interesting Rasa lignite from Yugoslavia (53), but his principal interest in organic sulfur seemed to be in its implications for liquefaction chemistry.

Although studies of the structure of coal have always been of interest to coal scientists, and have been studied extensively by both reaction chemistry and by the newer, powerful analytical methods, Carlson's 1989 paper on the computer-assisted modelling of coal structures (67) represents the application of an even newer, and potentially more powerful technique. Carlson's modelling included the famous "Given structure" which was proposed in 1960 (19), although this is a structure in which Given himself later seemed to put little credence. It is interesting that the Given structure, which had been published several years before the 1964 conference, was not cited in any of the papers published from that conference, but remains of interest today, even appearing in a textbook published in 1986 (68).

One of Peter Given's major undertakings in the last decade of his career was the effort to correlate liquefaction reactivity with chemical properties and structure of coals. Some of the contributions have been well summarized by Baldwin (69). Particularly noteworthy was the classic study of the liquefaction behavior of 104 coals, which was also a pioneering effort on the introduction of cluster analysis to classifying the behavior of coals (62). This major study was also cited by other investigators reporting liquefaction studies in the 1989 symposium (70,71). Among the important contributions by Given and his students on relating liquefaction behavior to structure (e.g., 72,73), was the study of reactivity correlations for 26 high volatile bituminous coals of high sulfur content (74), and the conclusion that the role of sulfur in liquefaction reactivity "needs more study" (73). Indeed, the study of liquefaction reactivity of high-sulfur coals is now continuing at Penn State (71).

Acknowledgments

I am grateful for the kind assistance provided by Judy Kiusalaas, College of Earth and Mineral Sciences, The Pennsylvania State University, who provided some materials and information on Peter Given's early years at Penn State.

LITERATURE CITED

1. Given, P.H.; Hammick, D.Ll. J. Chem. Soc. 1947, 928.
2. Given, P.H.; Hammick, D. Ll. J. Chem. Soc. 1948, 2154.
3. Given, P.H.; Hammick, D. Ll. J. Chem. Soc. 1949, 1779.
4. Given, P.H. Chem. and Ind. 1956, 525.
5. Given, P.H. J. Appl. Chem. 1957, 7, 172.
6. Given, P.H. J. Appl. Chem. 1957, 7, 182.
7. Given, P.H. British Patent 695 464, 1953.
8. Given, P.H. Nature 1958, 181, 1001.
9. Given, P.H.; Schoen, J.M.; Peover, M.E. J. Chem. Soc. 1958, 2674.
10. Given, P.H. J. Chem. Soc. 1958, 2684.
11. Given, P.H.; Peover, M.E. Nature 1958, 182, 1226.
12. Given, P.H.; Peover, M.E. J. Chem. Soc. 1959, 1602.
13. Given, P.H.; Peover, M.E. Nature, 1959, 184, 1064.
14. Given, P.H.; Peover, M.E. J. Chem. Soc. 1960, 385.
15. Given, P.H.; Peover, M.E. J. Chem. Soc. 1960, 465.
16. Given, P.H.; Schoen, J.M. J. Chem. Soc. 1958, 2680.
17. Given, P.H.; Peover, M.E. Fuel 1960, 39, 463.
18. Given, P.H. Nature 1958, 181, 1059.
19. Given, P.H. Fuel 1960, 39, 147.
20. Given, P.H. Unpublished memorandum, The Pennsylvania State University, 1979.
21. Given, P.H. Mineral Industries 1965, 34(2), 2.
22. Given, P.H. Earth and Mineral Sci. 1972, 41(7), 49.
23. Given, P. H. In Coal Science; Gorbaty, M.L.; Larsen, J. W.; Wender, I., Eds.; Academic Press: New York, 1984; Vol. 3, p.65.
24. Morris, J. The Age of Arthur; Charles Scribner's Sons: New York, 1973; p. 510.
25. Housman, A.E. A Shropshire Lad; The Folio Society: London, 1986; p. 92.
26. Gould, R. F. (ed.) Coal Science; American Chemical Society: Washington, 1966.
27. Flaig, W. In Coal Science; Gould, R. F., Ed.; American Chemical Society: Washington, 1966; Chapter 5.
28. Steelink, C. In Coal Science; Gould, R. F., Ed.; American Chemical Society, Washington, 1966; Chapter 7.
29. Spackman, W.; Barghoorn, E. S. In Coal Science; Gould, R. F., Ed.; American Chemical Society, Washington, 1966; Chapter 45.
30. Austen, D. E. G.; Given, P. H.; Ingram, D. J. E.; Peover, M. E. Fuel 1959, 38, 309.
31. Hatcher, P. G.; Lerch, H. E. III. Amer. Chem. Soc. Div. Fuel Chem. Preprints, 1989, 34(3), 617.
32. Nip, M.; deLeeuw, J. W.; Schenck, P. A.; Meuzelaar, H. L. C.; Stout, S. A.; Given, P. H.; Boon, J. J. J. Anal. Appl. Pyrol. 1985, 8, 221.
33. Hatcher, P. G.; Lerch, H. E. III; Kotra, R. K.; Verheyen, T. V. Fuel 1988, 67, 1069; and references cited therein.
34. Zubovic, P. In Coal Science; Gould, R. F., Ed.; American Chemical Society: Washington, 1966; Chapter 13.
35. Zubovic, P. In Coal Science; Gould, R. F., Ed.; American Chemical Society: Washington, 1966; Chapter 14.
36. Miller, R. N.; Given, P. H. Geochim. et Cosmochim. Acta 1986, 50, 2033.
37. Quast, K. B.; Readett, D. J. Amer. Chem. Soc. Div. Fuel Chem. Preprints 1989, 34(3), 640.

38. Robbins, G. A. Amer. Chem. Soc. Div. Fuel Chem. Preprints 1989, **34**(3), 656.
39. Given, P. H.; Yarzab, R. F. In Analytical Methods for Coal and Coal Products; Karr, C., Jr. Ed.; Academic Press: New York, 1978; Vol. II, Chapter 1.
40. Painter, P. C.; Youtcheff, J.; Given, P. H. Fuel, 1980, **59**, 523.
41. Austen, D. E. G.; Ingram, D. J. E.; Given, P. H.; Binder, C. R.; Hill, L. W. In Coal Science; Gould, R. F., Ed.; American Chemical Society: Washington, 1966; Chapter 21.
42. Given, P. H.; Peover, M. E.; Wyss, W. F. Fuel 1960, **39**, 323.
43. Tschamler, H.; deRuiter, E. In Coal Science; Gould, R. F., Ed.; American Chemical Society, Washington, 1966; Chapter 20.
44. Given, P. H.; Peover, M. E. J. Chem. Soc., 1960, 394.
45. Mazumdar, B. K.; Ganguly, S.; Sanyal, P. K.; Lahiri, A. In Coal Science; Gould, R.F., Ed.; American Chemical Society: Washington, 1966; Chapter 30.
46. Retcofsky, H. L.; Friedel, R. A. In Coal Science; Gould, R. F., Ed.; American Chemical Society: Washington, 1966; Chapter 32.
47. Sethi, N. K. Amer. Chem. Soc. Div. Fuel Chem. Preprints 1989, **34**(3), 714.
48. Marzec, A.; Schulten, H. R. Amer. Chem. Soc. Div. Fuel Chem. Preprints 1989, **34**(3), 668.
49. Derbyshire, F. J.; Davis, A.; Lin, R. Amer. Chem. Soc. Div. Fuel Chem. Preprints 1989, **34**(3), 676.
50. Nishioka, M. Amer. Chem. Soc. Div. Fuel Chem. Preprints 1989, **34**(3), 685.
51. Meuzelaar, H. L. C.; Yun, Y.; Simmleit, N.; Schulten, H. R. Amer. Chem. Soc. Div. Fuel Chem. Preprints 1989, **34**(3), 693.
52. Sakurovs, R.; Lynch, L. J.; Barton, W. A. Amer. Chem. Soc. Div. Fuel Chem. Preprints 1989, **34**(3), 702.
53. Given, P. H. Prog. Energy Combust. Sci. 1984, **10**, 149.
54. Given, P. H.; Marzec, A.; Barton, W. A.; Lynch, L. J.; Gerstein, B. C. Fuel 1988, **65**, 155.
55. Kamienski, B.; Pruski, M.; Gerstein, B. C.; Given, P. H. Energy Fuels 1987, **1**, 45.
56. Mudamburi, Z.; Given, P. H. Org. Geochem. 1985, **8**, 221.
57. Mudamburi, Z.; Given, P. H. Org. Geochem. 1985, **8**, 441.
58. Youtcheff, J. S.; Given, P. H.; Baset, Z.; Sundaram, M. S. Org. Geochem. 1983, **5**, 157.
59. Given, P. H.; Marzec, A. Fuel 1988, **67**, 242.
60. Murchison, D. G. In Coal Science; Gould, R. F., Ed.; American Chemical Society: Washington, 1966; Chapter 19.
61. Neill, P. H.; Xia, Y. J.; Winans, R. E. Amer. Chem. Soc. Div. Fuel Chem. Preprints 1989, **34**(3), 745.
62. Yarzab, R. F.; Given, P. H.; Davis, A.; Spackman, W. Fuel 1980, **59**, 81.
63. Given, P. H.; Peover, M. E. J. Inst. Fuel 1958, A-33.
64. Miller, R. N.; Yarzab, R. F.; Given, P. H. Fuel 1979, **58**, 4.
65. Kelemen, S. R.; George, G. N.; Gorbaty, M. L. Amer. Chem. Soc. Div. Fuel Chem. Preprints 1989, **34**(3), 729.
66. Gorbaty, M. L.; George, G. N.; Kelemen, S. R. Amer. Chem. Soc. Div. Fuel Chem. Preprints 1989, **34**(3), 738.
67. Carlson, G. A.; Granoff, B. Amer. Chem. Soc. Div. Fuel Chem. Preprints 1989, **34**(3), 780.
68. Hessley, R. K.; Reasoner, J. W.; Riley, J. T. Coal Science; John Wiley and Sons: New York, 1986; p. 121.
69. Baldwin, R. M. Amer. Chem. Soc. Div. Fuel Chem. Preprints 1989, **34**(3), 787.

70. Snape, C. E.; Derbyshire, F. J.; Stephens, H. P.; Kottenstette, R. J.; Smith, N. W. Amer. Chem. Soc. Div. Fuel Chem. Preprints 1989, 34(3), 793.
71. Garcia, A. B.; Schobert, H. H. Amer. Chem. Soc. Div. Fuel Chem. Preprints 1989, 34(3), 819.
72. Given, P. H.; Spackman, W.; Davis, A.; Jenkins, R. G. In Coal Liquefaction Fundamentals; Whitehurst, D. D., Ed.; American Chemical Society: Washington, 1980; Chapter 1.
73. Neill, P. H.; Shadle, L. J.; Given, P. H. Fuel 1988, 67, 1459.
74. Shadle, L. J.; Neill, P. H.; Given, P. H. Fuel 1988. 67, 1465.

RECEIVED December 26, 1990

Chapter 2

Survival of Lignin-Derived Structural Units in Ancient Coalified Wood Samples

Patrick G. Hatcher¹ and Harry E. Lerch, III

U.S. Geological Survey, Reston, VA 22092

Analysis of five Cretaceous and one Carboniferous fossil wood samples of lignite rank by pyrolysis-gas chromatography-mass spectrometry has revealed the presence of lignin-derived compounds such as phenols and methoxyphenols. The Cretaceous lignitic woods, produced a suite of methoxyphenols similar to those produced from pyrolysis of modern lignin and degraded wood. Distributions of these products indicate that the lignin structural units of the Cretaceous lignitic wood samples are preserved to varying degrees. The Carboniferous lignitic wood produced only traces of methoxyphenols, but phenols were abundant. This is an indication that lignin or lignin-like biomarkers such as methoxyphenols can survive in geological materials as old as the Carboniferous.

Lignin is a major biochemical component of woody tissue; however, it rarely survives early stages of coalification unchanged. Biochemical and chemical alteration during burial limit the extent to which lignin biomarkers can be preserved and recognized in the geologic record. The coalification of wood has been thought to involve primarily the removal of carbohydrates and the alteration of lignin to form aromatic structures containing few substituents other than alkyl groups [1]. Lignin from gymnosperms is composed of methoxylated phenolic ethers (guaiacyl units) having a three-carbon side chain linked to adjacent guaiacyl units through the ether bond; lignin from angiosperms also contains these guaiacyl units but additionally contains aromatic rings with two methoxyls and one aryl ether group (syringyl units). During peatification and coalification, the methoxyl group is lost from guaiacyl and syringyl units first via demethylation, and the resulting alkylated catechols are converted to alkylated phenols [1]. Thus, while the methoxyphenol structure provides a positive fingerprint for lignin, it can be altered at an early stage

¹Current address: Fuel Science Program, 209 Academic Projects Building, The Pennsylvania State University, University Park, PA 16802

of coalification [2]. Usually, methoxyphenols do not survive to the stage of subbituminous coal rank [1]. Thus, the best hope of finding the methoxyphenol biomarkers resides in finding coalified woods that have not been coalified beyond the lignite stage of coalification.

Lignin-derived compounds have been observed in pyrolysis products of low rank coals and associated woody tissue [1-6]. Mycke and Michaelis [7] isolated lignin-derived methoxyphenols from a Miocene coal by catalytic hydrogenolysis. Sigleo [8] reported the presence of phenolic compounds derived from alteration of lignin in pyrolysis products of silicified woody tissue as old as Triassic age. However, no methoxyphenols, that would clearly relate back to lignin structures, could be identified in Sigleo's samples. No doubt, the phenols were originally derived from lignin altered by geochemical processes. Hayatsu *et al.* [9] similarly reported the presence of lignin-derived phenolic products from copper-oxide oxidation of several coal samples. They, too, were unable to identify methoxylated phenols in their products. Recently, Nip *et al.* [4] subjected two lignite samples, one of Paleocene age and the other of Eocene age, to Curie-point pyrolysis-mass spectrometry. The data indicated only traces of methoxyphenols. They were puzzled by the low abundance of phenols in general, because the petrographic data indicated large amounts of huminite macerals derived from woody tissue. In a study of fossil woods ranging in age from Holocene to Carboniferous, Logan and Thomas [10] detected methoxyphenols by the cupric oxide oxidation method. They claim to have identified vanillin and acetovanillone in substantial quantities in Carboniferous wood; however, it is a bit disconcerting that the reported yields of these oxidation products are greater than in Holocene wood.

The most definitive identification of lignin-derived pyrolysis products in coalified wood samples as old as Paleocene age was reported in a study of coalified wood by Stout *et al.* [2]. They identified numerous lignin-derived methoxyphenols in angiospermous and gymnospermous wood samples from various lignites by Curie-point pyrolysis-gas chromatography-mass spectrometry. In a study of lignitic gymnospermous wood samples of Cretaceous and younger ages by analytical pyrolysis [6], we reported the presence of methoxyphenols in the pyrolyzates. Many of these methoxyphenols had associated propenyl side chains indicative of the presence of well-preserved lignin residues.

In an attempt to delineate the degree of preservation of lignin in pre-Tertiary coal, we examined numerous coalified wood samples ranging in age from Carboniferous to Cretaceous. The samples were initially screened by solid-state ^{13}C nuclear magnetic resonance to detect the possible presence of methoxyl carbon. Once such carbons were detected, the samples were subjected to analytical pyrolysis to determine the relative yields of methoxyphenols which would provide an indication of the state of preservation of the lignin-derived structural units. We report here on the identification of lignin-derived methoxyphenols in the coalified wood samples selected for analytical pyrolysis.

Samples and Methods

Samples of coalified wood (xylem) were obtained from Carboniferous and younger strata in various locales. Most samples were derived from coalified gymnospermous xylem (Table 1). A sample of coalified wood was collected by D. Gottfried (U.S. Geological survey) from the Magothy Formation (Upper Cretaceous) at the C&O canal near Bethel, Maryland. A Byrd Stadium lignitic wood was collected by the late I.A. Breger (U.S. Geological Survey) from an excavation for Byrd Stadium on the campus of the University of Maryland. The

coalified logs at this site were buried in an upright position in sediments of the Potomac Group (Lower Cretaceous). Wayne Newell (U.S. Geological Survey) graciously provided a sample (Stafford lignite) of coalified wood buried in sediments of the Potomac group (Lower Cretaceous) near Stafford, Virginia. Another sample was obtained by Roger Thomas (U.S. Geological Survey) from the Patapsco Formation of the Potomac Group (Lower Cretaceous) near the intersection of I-95 and I-695 in Landsdown, Maryland. Another sample (Long Island Lignite) was obtained by Byron Stone (U.S. Geological Survey) from Pleistocene clay in the Nassau Brick Co. clay pit on Long Island, New York; the sample probably was reworked from the Magothy Formation (Upper Cretaceous). Finally, a sample (from the Carboniferous lignite deposits of the Moscow Basin, USSR, Kurovskaya mine No. 1) was obtained from the collection of the late I.A. Breger. The coalified wood occurred as bright, shiny lenses within the coal groundmass. These were hand-picked to isolate sufficient material for analysis.

Table 1. Elemental compositions (dry mineral-matter free) for coalified wood samples

<u>Lignite Sample</u>	<u>Age</u>	<u>Wood type</u>	<u>%C</u>	<u>%H</u>	<u>%N</u>	<u>%O</u>
Stafford	K	G	74.9	4.98	0.58	18.9
Long Island	K	NA	61.1	4.57	0.33	34.0
Patapsco	K	G	65.7	5.00	0.27	29.3
Byrd Stadium	K	G	59.2	3.17	0.21	36.3
Magothy	K	G	72.2	4.43	0.21	22.0
Moscow Basin	C	NA	NA	NA	NA	NA

K - Cretaceous

C - Carboniferous

G - gymnospermous wood

NA - data not available

Pyrolysis-gas chromatography-mass spectrometry was performed on a Dupont 490B gas chromatograph-mass spectrometer system interfaced with a Technivent Vector 1 data system and a Chemical Data Systems Model 120 pyroprobe. Pyrolysis-gas chromatography was performed with a Perkin-Elmer Sigma 2B gas chromatograph interfaced to the pyroprobe. The fused silica column was a 50% phenylmethylsilicone phase available from Hewlett-Packard. Operating conditions and specific methodologies have been given in a previous report [6].

The presence of lignin structural units was confirmed by retention time data and by comparisons of mass spectra to library spectra, to spectra of authentic standards, and to published mass spectra of lignin phenols [11].

Results and Discussion

All the coalified wood samples examined in this report were of lignite rank, as determined by their elemental compositions (Table 1). The one sample from the Moscow Basin was not analyzed for its elemental composition but was collected from a well-known Carboniferous lignite deposit. Figure 1 shows the solid-state ^{13}C NMR data for some of the samples. Though the spectra show a large, broad

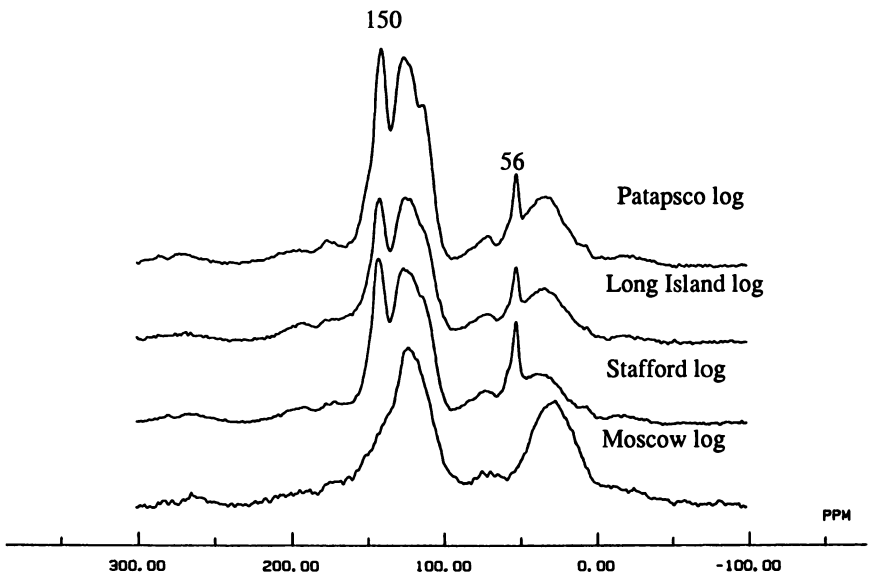


Figure 1. Solid state ¹³C NMR spectra of lignitic wood samples.

aromatic signal between 100 and 160 ppm, the peak at about 150 ppm is well resolved. This peak is most likely that of resonances from O-substituted aromatic carbons (Ar-O) in catechol-like structures. The peak at 56 ppm for methoxyl carbons indicated that some of these Ar-O resonances are from methoxyl groups attached to aromatic rings [12]. Clearly, the presence of methoxyphenols, as found in lignin, is suggested by the NMR data. The sample from the Moscow Basin shows only a trace of a peak at 56ppm, suggesting that if methoxyphenols were present, they would be so in only trace quantities.

Pyrolysis of Cretaceous lignitic xylem has been shown in a previous report [6] to yield abundant quantities of methoxyphenols derived from the lignin residues preserved in the lignitic woods. The state of preservation can be determined by the abundance of methoxyphenols relative to other altered lignin byproducts such as the phenols and catechols. Figure 2 shows the pyrograms for samples of the five Cretaceous lignitic woods in which the state of preservation of lignin varies widely. Peaks for guaiacol, 4-methylguaiacol, 4-vinylguaiacol, 4-ethylguaiacol, eugenol, *cis*- and *trans*-isoeugenol, vanillin, and acetoguaiacone are clearly the major products in the Long Island, Patapsco, and Stafford lignitic wood samples suggesting that the lignin-derived structures are relatively well preserved. These specific methoxyphenols are clearly derived from lignin precursors or partially altered lignin that has survived in the lignitic wood samples [2]. Extensively altered lignin products such as phenol, the cresol isomers, catechol isomers, and the alkylphenols [4] are also major components of the pyrogram, but they are subordinate to the methoxyphenols in these three lignitic woods. In the Magothy and Byrd Stadium lignitic woods, the phenols and cresols are dominant over the methoxyphenols, indicating that the lignin residues in this sample are significantly more altered than in the other Cretaceous lignitic wood samples. The degree of lignin preservation varies widely among the Cretaceous lignitic wood samples. Analytical pyrolysis of gymnospermous lignin that is minimally altered has been shown to yield the same products as those mentioned above for the three least coalified wood samples, although the relative peak intensities may vary [11,13-15]. Figure 3 shows a pyrogram for a Holocene gymnospermous log (Atlantic White Cedar, *Chamaecyparis thyoides*) buried in peat from the Great Dismal Swamp, Virginia. Previous studies have shown that most of the cellulosic components of this sample have been degraded microbiologically, leaving lignin relatively unaltered [1]. The pyrogram confirms this by showing a product distribution that is typical of relatively intact lignin [11,14]; the broad peak for levoglucosan indicates a small amount of cellulosic material is present [2]. The four largest peaks are for 4-methylguaiacol, 4-vinylguaiacol, guaiacol, and *trans*-isoeugenol in decreasing order of intensity. The relatively high abundance of methoxyphenols having the 3-carbon side chain intact (eugenol, the isoeugenols, coniferaldehyde, and guaiacylpropan-2-one) versus those with modified side chains (methylvanillate, vanilloyl methyl ketone, and vanillic acid) is further evidence that the lignin is not altered extensively [14]. Also, the presence of only trace levels of phenols, cresols, and catechols in the buried Holocene log is additional evidence for a relatively unaltered lignin. Saiz-Jimenez *et al* [15] have similarly observed that wood buried in anaerobic environments can contain lignin that is rather well preserved.

The relatively low yield of methoxyphenols having the 3-carbon side chain intact (relative to the other methoxyphenols) in the Cretaceous lignitic wood samples (Figure 2) can be expressed as the ratio of peak areas for guaiacol/*trans*-isoeugenol. This ratio is 1.3 for the modern buried cedar (Figure 3), whereas the Cretaceous lignitic samples have values that range from 4.8 to 11. This more than five-fold increase in the ratio is indicative of the fact that the lignin molecules in the Cretaceous lignitic woods are significantly altered at the side-chain sites.

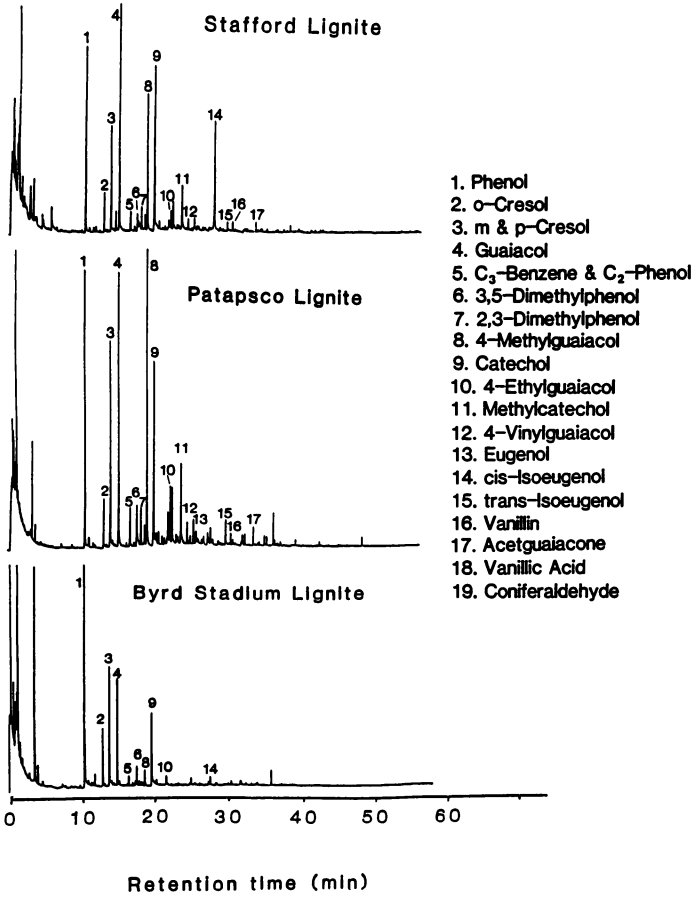


Figure 2a. Py/gc traces of Lower Cretaceous lignitic wood samples.

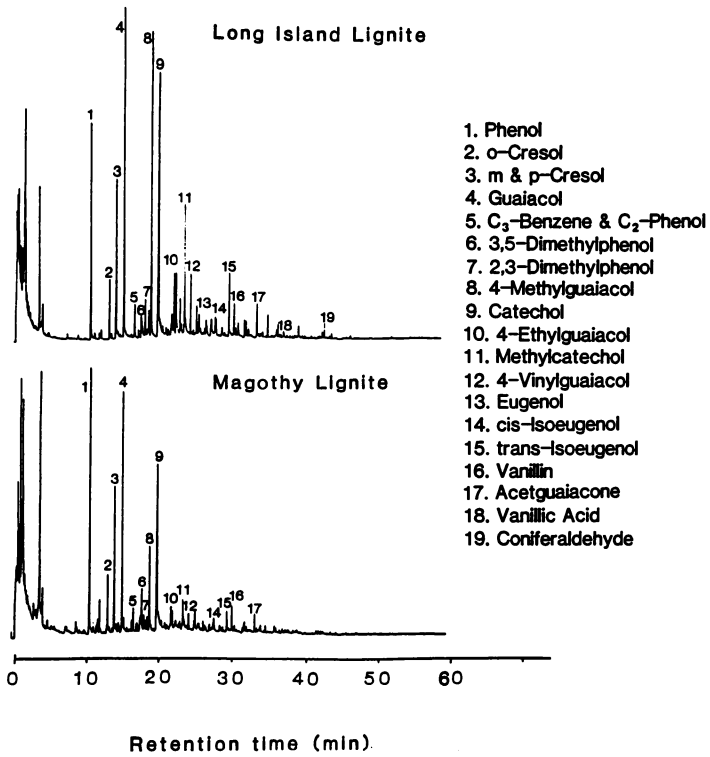
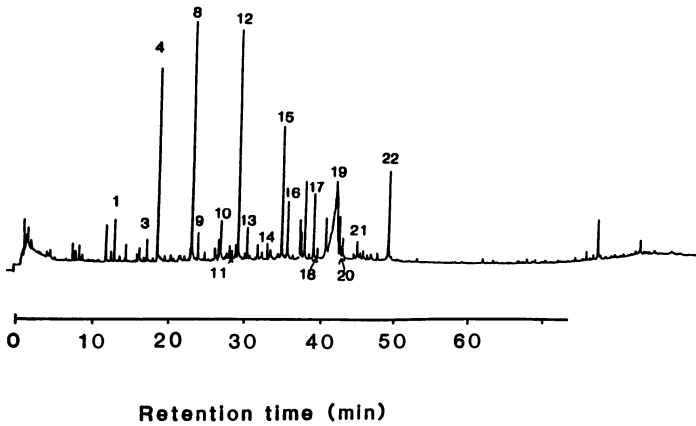


Figure 2b. Py/gc traces of Upper Cretaceous lignitic wood samples.



1. Phenol
2. o-Cresol
3. m&p-Cresol
4. Guaiacol
5. 2,4 & 2,5-Dimethylphenol
6. 3,5-Dimethylphenol
7. 2,3-Dimethylphenol
8. 4-Methylguaiacol
9. Catechol
10. 4-Ethylguaiacol
11. Methylcatechol
12. 4-Vinylguaiacol
13. Eugenol
14. cis-Isoeugenol
15. trans-Isoeugenol
16. Vanillin
17. Acetoguaiacone
18. Methylvanillate
19. Levoglucosan
20. Vanillic acid
21. Guaiacylacetic acid
22. Coniferaldehyde

Figure 3. Py/gc trace of buried cedar wood from the Dismal Swamp, VA.

Although the lignin-derived methoxyphenols are important components of the pyrolysis products of the Cretaceous lignitic woods, phenols, catechols, and methylated phenols are also abundant. The ratios of total phenols + catechols to total methoxyphenols range from 1.0 to 5.5 in the lignitic woods. In the buried cedar, this ratio is 0.10, indicative of the fact that lignin-derived methoxyphenols are the principal constituents and the phenols and catechols, the products of altered lignin, are subordinate. Sigleo [8] suggested that phenols, cresols, and catechols in pyrolysis products of 200-million-year-old petrified wood are derived from altered lignin. We support this conclusion, primarily because lignin is the most likely source of phenols in the lignitic woods and because of the abundance of lignin-derived methoxyphenols which are co-produced during pyrolysis. However, Sigleo [8] did not report *ortho*-methoxyphenols which would have provided unambiguous ties to lignin.

The pyrolysis data for the Carboniferous lignitic wood from the Moscow Basin are shown in Figure 4. The major pyrolysis products are alkylbenzenes, but phenol and alkylphenols comprise major peaks in the pyrogram (Figure 4a). Only a trace of methoxyphenol (Figure 4b) and methylmethoxyphenols (Figure 4c) could be detected in the sample. However, the trace presence of these two methoxyphenols is clear indication that lignin or a lignin-like material was present in the wood and that only a trace of it remains, albeit in a highly altered form. Thus, the presence of the methoxyphenols in pyrolysis products indicates that lignin-like components have survived for approximately 300 million years. That the specific peak was indeed methoxyphenol was determined by retention time and by examination of the fragment ions at m/z 109 and 81. Similarly, the verification of the presence of methylmethoxyphenol was made by retention time and by examination of fragment ions at m/z 123 and 95. Direct comparison of mass spectra to library spectra of authentic methoxyphenols was not possible due to the trace quantities and the complexity of the pyrolysis mixture in the retention-time windows for elution of the methoxyphenols.

The phenol, the cresol isomers, and the dimethylphenols, major pyrolysis products in the Moscow wood sample, are probably also derived from lignin precursors that have been altered through coalification reactions. Hatcher *et al.* [6] have shown that an increase is observed in the relative proportion of phenols and cresols as rank of coalified wood samples increases to subbituminous coal. Comparing the distribution of pyrolysis products from the Moscow wood to that of other coalified wood samples of Hatcher *et al.* [6] allows us to deduce that the Moscow wood is more similar to coalified wood of subbituminous rank than it is of coalified wood of lignite rank, assuming that its lignin was originally similar to lignin in Cretaceous or younger woods.

Conclusions

The analysis of lignitic woods by analytical pyrolysis has shown that lignin structural units can be preserved as biomarkers in samples as old as Carboniferous age, or approximately 300 million years. At least half or more of the pyrolysis products in lignitic wood of Cretaceous age are methoxyphenols characteristic of lignin. The product distributions in these Cretaceous samples indicate that the lignin is mainly altered in the 3-carbon side chains. Phenols, cresols, catechols, and other methylated phenols account for most of the remaining pyrolysis products. It is likely that these products are also derived from lignin, especially lignin that has been altered by coalification reactions.

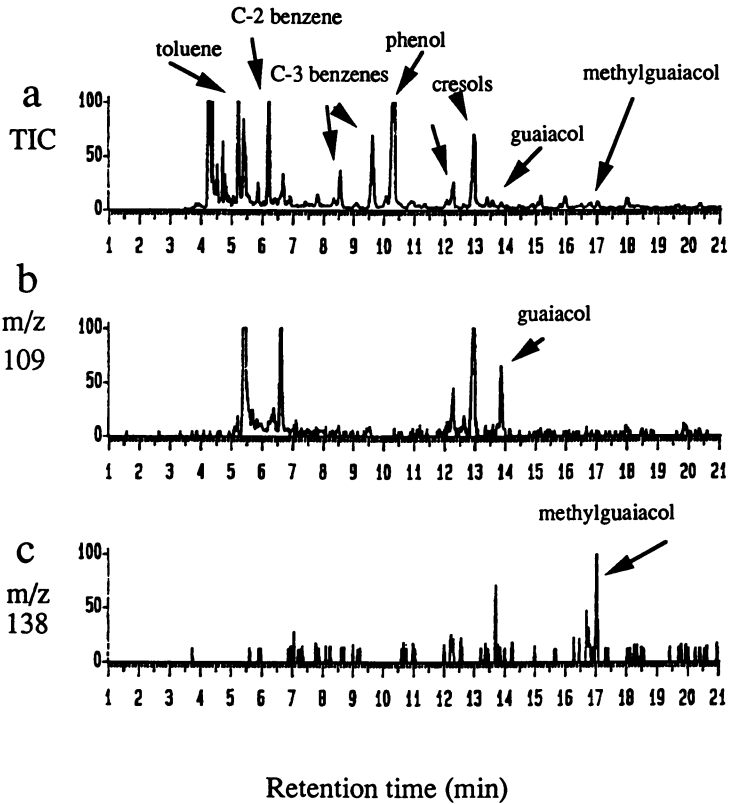


Figure 4. Py/gc/ms traces of coalified wood from the Moscow Basin. a) total ion chromatogram, b) mass chromatogram $m/z=109$, c) mass chromatogram $m/z=138$.

Acknowledgments

We thank our colleagues at the U.S. Geological Survey, Roger Thomas, David Gottfried, Byron Stone, and Wayne Newell, for providing samples for this study. We also thank Scott A. Stout for his valuable comments on the paper.

References

1. Hatcher, P.G.; Lerch, H. E., III; and Verheyen, T. V. Int. J. Coal Geol., 1989, **13**, 65-97.
2. Stout, S. A.; Boon, J.J.; and Spackman, W. Geochim. Cosmochim. Acta, 1988, **52**, 405-414.
3. Philp, R.P.; Russell, N.J.; Gilbert, T.D.; and Friedrich, J.M. J. Anal. Appl. Pyrol., 1982, **4**, 143-161.
4. Nip, M.; de Leeuw, J.W.; Schenck, P.A.; Meuzelaar, H.L.C.; Stout, S.A.; Given, P.H., Boon, J.J. J. Anal. Appl. Pyrol., 1985, **8**, 221-239.
5. Chaffee, A.L.; Johns, R.B.; Baerken, N.J.; de Leeuw, J.W.; Schenck, P.P.; Boon, J. J. Org. Geochem., 1984, **6**, 409-416.
6. Hatcher, P.G.; Lerch, H.E., III; Kotra, R.K.; Verheyen, T.V. Fuel, 1988, **67**, 1069-1075.
7. Mycke, B.; Michaelis, W. Naturwissenschaften, 1986, **73**, 731-734.
8. Sigleo, A.C. Geochim. Cosmochim. Acta, 1978, **42**, 1397-1405.
9. Hayatsu, R.; Winans, R.E.; McBeth, R.L.; Scott, R.G.; Moore, L.P.; Studier, N.H. Nature, 1979, **278**, 41-43.
10. Logan, K. J.; Thomas, B. A. New Phytol., 1987, **105**, 157-173.
11. Obst, J.R. J. Wood Chem. Technol., 1983, **3**, 337-397.
12. Hatcher, P. G.; Breger, I. A.; Szeverenyi, N.; Maciel, G. E. Org. Geochem., 1982, **4**, 9-18.
13. van de Meent, D.; Brown, S.C.; Philp, R.P.; Simoneit, B.R.T. Geochim. Cosmochim. Acta, 1980, **44**, 999-1013.
14. Saiz-Jimenez, C.; de Leeuw, J.W. Org. Geochem., 1984, **6**, 417-422.
15. Saiz-Jimenez, D.; Boon, J.J.; Hedges, J.I.; Hessels, J.K.C.; de Leeuw, J.W. J. Anal. Appl. Pyrol., 1987, **11**, 437-450.

RECEIVED February 26, 1991

Chapter 3

Minerals and Inorganic Components Associated with South Australian Lignites

Keith B. Quast and David J. Readett¹

Metallurgy Department, South Australia Institute of Technology,
The Levels, South Australia 5095, Australia

Minerals and other inorganic components from the South Australian lignite deposits have been studied using both standard and specifically developed analytical techniques. Techniques used included scanning electron microscopy with both back scattered electron imaging and energy dispersive spectrography, x-ray diffraction, leaching and mechanical dewatering. The inorganics within the lignite samples showed variations in amount and chemical composition between deposits and within the same deposit. Quartz and kaolinite were the predominant minerals and also exhibited major variations in size and distribution within and between deposits.

Introduction and Literature Review.

South Australia contains large reserves of low rank Permian to Jurassic sub-bituminous coal and Tertiary lignite (1). Samples from several of these deposits have been evaluated since the mid 1970's to assess their suitability for power generation (2). Of the lignites, the Bowmans (1600 million t) and Lochiel (600 million t) deposits from the Northern St. Vincent Basin (see Figure 1) have been the subject of extensive research. Both these lignites contain in excess of 55% moisture, and very high sodium, chlorine and sulphur contents, all of which create problems for subsequent utilization. Combustion trials on both Bowmans and Lochiel lignites have been conducted (2) as well as pilot scale gasification and circulating fluidized bed combustion tests (3). Results show that the non-carbonaceous components of the lignite may cause major technical and economic problems. Consequently, an extensive research program has been conducted at the S.A. Institute of Technology to determine both the minerals and inorganics present and their distribution in South Australian lignites. A major part of this project was the development of techniques to enable the analysis of minerals using scanning electron microscopy (SEM) with back

¹Current address: Mount Isa Mines Limited, Mount Isa, Queensland, Australia

scattered electron (BSE) imaging, energy dispersive x-ray spectrography (EDS), x-ray diffraction (XRD) and mechanical dewatering to extract water for subsequent analysis.

The occurrence of non-carbonaceous material in coals has been the subject of much research, especially in relation to its effect on utilization and ash formation (4-14). In contrast to high rank coals in which minerals constitute almost all of the non-carbonaceous fraction, the low rank coals have two categories of non-carbonaceous material: minerals which occur as discrete particles of quartz, marcasite, clays, etc. and inorganics which occur as water soluble salts and exchangeable ions such as NaCl, Na_2SO_4 , Al^{3+} , etc. (15-17).

Much of the literature published on minerals is based on high rank coals, but can be related to low rank coals (18). In general, the silicate minerals represent the major component of the minerals contained in coal. The most common analytical methods for mineral characterisation and analysis are listed in (19) and covered in detail in the "Analytical Methods for Coal and Coal Products" series (20).

The majority of the early studies on inorganics was based on the determination of the chloride content, its mode of occurrence, and why it was present (21-28). It is only in more recent years with the increase in low rank coal utilization where the inorganics have a considerable economic impact that detailed research on inorganics has been undertaken (17-18, 29-32). This work indicates that the inorganics in low rank coals exist in two forms: as free ions present in the water associated with the coal and as cations exchanged on to the surface functional groups of the coal. Analysis of the inorganics is most commonly done using leaching to extract the inorganics, followed by atomic absorption techniques for cations and standard chemical analysis for anions.

Experimental Procedures and Results.

Coal Samples Examined

Typical analyses of the four South Australian lignites are given in Table I (1, 33). They are all ranked as Lignite B on the ASTM system. Several different samples of Lochiel and Kingston lignites were examined and these are identified as "1", "2" etc.

Techniques Used in this Study.

SEM-BSE/SEM-EDS

A Cambridge Stereoscan 100 scanning electron microscope with a KEVEX energy dispersive spectrography unit was used in all the experimental work. In order to ensure optimum conditions for analysis, it was necessary to use polished sections of lignite samples. Lignite samples were crushed to pass 2 mm, screened at 0.21 mm, and allowed to air equilibrate at 20°C for 2 days. These partially dried samples were then impregnated with epoxy resin. After the resin had set, each sample was polished using diamond paste and kerosene as a lubricant. Prior to viewing under the SEM, each polished section was coated with a fine layer of amorphous carbon using a vacuum arc

Table I. Typical Analyses of South Australian Lignites

	Bowmans	Lochiel	Sedan	Kingston
Moisture (%)	56	63	59	53
Higher Heating Value (MJ/Kg)	10.6	9.1	9.1	10.6
% Ash (db)	14	16	20	15
% Sodium (db)	1.6	1.0	0.6	0.9
% Chlorine (db)	1.5	0.5	0.3	0.2
% Sulphur (db)	5.0	2.8	5.5	2.9
% Volatile Matter (db)	46.7	49.9	43.9	46.9
% Carbon (db)	59.7	57.8	54.7	59.2
% Hydrogen (db)	3.9	4.7	4.1	4.1
% Nitrogen (db)	0.4	0.6	0.5	0.6
% Oxygen (db)	17.0	18.2	15.0	18.3

coater to ensure adequate electrical conductivity to prevent charging.

To enable detection of fine mineral particles (<20 μ m), back-scattered electron imaging was used. Once the minerals were detected, EDS was used for analysis. Selected lignite particles were scanned to determine the distribution of minerals. Mineral types were then differentiated by variation in back scatter intensity and identified using EDS. The relative proportions (major, minor) and size and spatial distributions of the minerals were recorded. The overall surface of the polished section was viewed and "massive" minerals were analyzed and their distribution and size recorded.

Inorganic analysis was conducted in conjunction with the mineral analysis. Particles analyzed previously for mineral content were analyzed for their inorganic content, and an overall analysis conducted. The resultant EDS spectra output was fed into a spreadsheet software package which was adapted by the authors to allow the calculation of a quantitative elemental analysis.

X-Ray Diffraction.

Lignite samples were predried at 105 $^{\circ}$ C for 2 hours to remove the water which is a major component; hence its removal, in effect, concentrates the mineral species. After drying, the samples were crushed using a mortar and pestle to pass 75 μ m. The dried lignite powder was then mounted in a standard aluminium mounting plate and placed in a Philips x-ray diffractometer with a Rigaku power source. A Co x-ray tube was used to suppress fluorescence of any elemental species. The resultant diffraction pattern was resolved using the JCPDS -ICDD Powder diffraction index.

Leaching.

Standard procedures using leaching for determining inorganic species in low rank coals are well established. The procedures adopted for this study are given below. All lignite samples were crushed finer

than 1 mm and dried at 105°C for 2 hours. Samples weighing 2 g were mixed with 100 ml of distilled water and agitated for 1 hour. The resultant slurry was filtered and analyzed. The amounts of water soluble inorganics were calculated on a dry coal basis. For the acid extraction, 100 ml distilled water and 15 ml concentrated A.R. nitric acid were added, and the slurry boiled and simmered for 1 hour on a hot plate. The resultant slurry was filtered and analyzed to allow total inorganics present in the sample to be calculated.

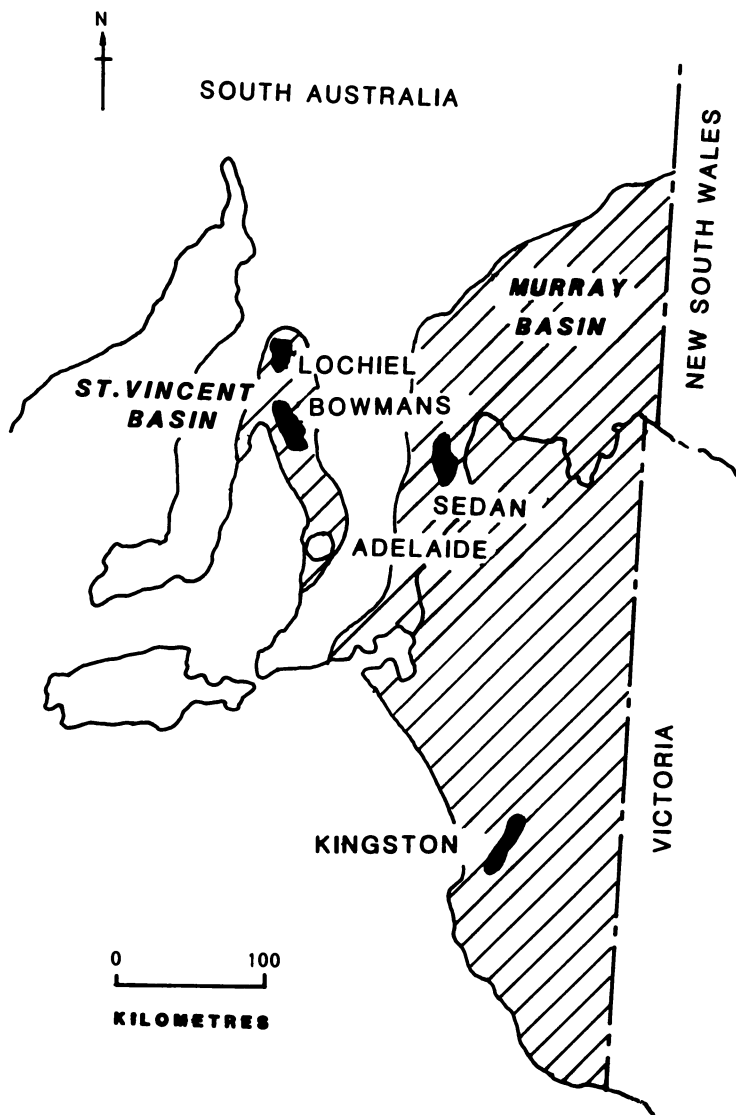


Figure 1. Location of the four lignite deposits in south eastern South Australia in relation to the state capital (Adelaide).

Table II Extractable Inorganics in Lignite Samples

Sample	Extn	Composition (% db)						
		Na	Ca	K	Mg	Al	Cl	S
Bowmans	Acid	1.86	0.62	0.05	0.83	0.28	2.23	3.34
	Water	1.52	0.10	0.02	0.26	0.01	1.98	0.73
	Press	0.93	0.08	0.01	0.26	-	1.90	0.40
Lochiel	Acid	1.52	0.95	0.05	0.80	0.28	0.16	2.18
	Water	1.33	0.02	0.02	0.04	-	0.92	0.56
	Press	0.82	0.07	0.01	0.21	-	1.15	0.43
Sedan	Acid	0.39	1.59	0.05	0.52	0.42	0.01	4.32
	Water	0.39	1.30	1.12	1.19	0.17	0.12	3.87
	Press	0.23	0.05	-	0.55	0.15	0.11	1.38
Kingston	Acid	1.11	1.30	0.12	1.19	0.27	0.01	1.23
	Water	0.28	-	0.01	-	-	0.24	0.07

Acid - acid extractable inorganics

Water - water extractable inorganics

Press - inorganics removed by mechanical dewatering

Mechanical Dewatering.

The analysis of water soluble inorganics present in the lignites can be calculated from the analysis of water contacted with the lignite as described above. It is uncertain whether water leaching induces any chemical changes such as dissociation of ions from the surfaces of lignite or from minerals. It was therefore considered that a more appropriate means of determining the analysis of water-soluble inorganics would be to remove the water from the lignite by mechanical means. Design of equipment capable of mechanically dewatering lignites was obtained from the Grand Forks Energy Technology Centre and CSIRO. Using these designs as a basis, a mechanical press was constructed. The basic criterion for design was that it would dewater a sufficiently large sample of lignite to obtain a suitable volume of water for subsequent analysis.

All the lignite samples were initially crushed to pass 1 mm and contact with the atmosphere was kept to a minimum. A lignite sample was placed in the die. The punch (which transfers the pressure from an Avery Universal Testing Machine to the lignite) was then placed in the die. The lignite was then pressed against a series of water-permeable screens and drainage plates. Under the applied pressure, water was expressed from the lignite sample and exited the dewatering device via the screens and drainage plates, whilst the dewatered lignite was retained on the screens. The expressed water was analyzed by conventional means.

The content of inorganics of the lignite samples is given in Table II with the minerals and their distribution given in Table III.

Table III Minerals and Distribution in Lignite Samples

Sample	Distn Density	Distn	Mineral Species			
			Major	Size Range (μm)	Minor	Size Range (μm)
Bowmans						
-2+0.21mm	med.	even	Si	-500	CaS	-200
			Al,Si	-500	Fe,S	-200
-0.21	med.	uneven	Al,Si	-150	CaS	-100
			Si	-150	NaCl	-5
			FeS	-150		
Lochiel 1						
-2+0.21mm	low	uneven	Si	-500	Fe,S	-200
					Ca,S	-200
-0.21mm	low	uneven	Si	-200	Fe,S	-100
			Al,Si	-200		
Lochiel 2						
-2+0.21mm	med.	even	Al,Si	-200	Fe,S	-200
			Si	-500	Ca,S	-5
Kingston 1						
-2+0.21mm	med.	even	Si (acic)	-20	Ca,S	-20
			Al,Si	-200	Na,Al,Si	-150
-0.21mm	low	uneven	Si (acic)	-20	Al,Si	-20
					Na,Al,Si	-50
Kingston 2						
-2+0.21mm	med.	uneven	Si (acic)	-20	Na,Al,Si	-200
			Al,Si	-500	Fe,S	-200
					Ca,S	-20
Sedan						
-2+0.21mm	low	even	Si	-500	Fe,S	-500
			Ca,S	-500		
			Al,Si	-50		
-0.21	med.	uneven	Ca,S	-200	Fe,S	-200
					Si	-150
					Al,Si	-150

Key to Table III

Elements detected	Species	Elemental Analysis
Si	quartz	SiO_2^*
Si (acic)	acicular quartz	SiO_2
Fe, S	marcasite	FeS_2^*
Ca, S	gypsum	$\text{CaSO}_4 \cdot 2\text{H}_2\text{O}^*$
NaCl	halite	NaCl
Al, Si	kaolinite	$\text{Al}_2\text{O}_3 \cdot 2\text{SiO}_2 \cdot 2\text{H}_2\text{O}^*$
Na, Al, Si	plagioclase	$\text{Na}_2\text{O} \cdot \text{Al}_2\text{O}_3 \cdot 6\text{SiO}_2$

* elements detected using XRD

Discussion

Analytical Techniques

The procedures developed for the analysis of the minerals and inorganics were the result of an extensive series of tests to determine the optimum conditions for these specific sample types. This was then combined with general procedures for the analytical equipment.

SEM-EDS

The equipment and procedures used had several inherent problems including:

1. Poor sensitivity of EDS for elements of low atomic number (especially sodium and magnesium) and an inability to detect elements with atomic numbers less than 10. The software package derived by the authors can derive quantitative analysis from a spectrum taking into account the inherent insensitivity of EDS to those elements whose atomic numbers approach the detection limit.
2. The detection difficulties were then accentuated by the several types of background which were superimposed on the x-ray spectrum of interest. This was overcome by the modelling and subtraction of the background spectrum from the acquired spectrum.
3. Preliminary tests indicated that the distribution of inorganics within a particle could be a function of the rate at which the lignite sample was dried. Rapid drying rates resulted in a concentration of inorganics in the central zone of a particle, whereas slow drying rates resulted in a concentration at the outer perimeter of the particle.
4. To enable quantitative analysis of the inorganics it is necessary to have a known standard. Chemical analysis of the sample to determine the concentration of one species such as chlorine or sulphur provided suitable standards.
5. The chemical analysis does not distinguish between minerals and inorganics in the lignite. Despite this drawback, it was possible to detect trends occurring in the inorganics associated with the lignite.

The use of BSE images on the SEM screen was ideal for the detection of minerals in low rank coals. The difference in atomic number between the major components of the coal matrix (C, H, N and O) and the elements present in the mineral species (Si, Al, Fe, Ca) causes the minerals to appear bright against the dark coal background. Variations in the BSE brightness between minerals was such that the different minerals present were also distinguishable. However, it is difficult to differentiate between quartz and clay (kaolinite) just from a BSE image.

This problem can be overcome by using grain morphology to distinguish between quartz, clay and other minerals. A secondary problem occurs as the low density of the coal matrix allows for a beam penetration to a depth of approximately 10 μm . This means that the BSE image represents a surface volume rather than just a plane.

Minerals which are subsurface are therefore visible, however their brightness is diminished (e.g. subsurface marcasite can have a similar BSE image to clay on the surface).

Analysis of the minerals detected using SEM-EDS was effective with simple minerals, however, determination of clay types was difficult and it was not possible to determine whether a mineral species was anhydrous or hydrated.

XRD

The limitation of an SEM-EDS analysis of minerals is that it cannot characterise the crystal structure of the minerals present. As a result it is difficult to determine some mineral types e.g.

1. differentiating clay types,
2. whether the presence of iron and sulphur is indicative of pyrite, marcasite or FeSO_4 , and
3. minerals which have anhydrous and hydrated forms.

XRD allows the determination of the actual mineral species present. The bulk coal samples resulted in an x-ray pattern with a high background due to the coal matrix. The major mineral species were easily determined, however the minor species could not be detected. As with the SEM-BSE analysis, interpretation of results in a quantitative manner (in relation to the coal) is difficult. The major minerals detected were quartz, kaolinite, gypsum and marcasite.

Minor minerals were not detected as their concentration in the samples was below the detection limits for XRD.

Leaching.

The limitation of water leaching is that some minerals which are not soluble within the coal sample may dissociate on leaching. For the acid leaching, a major problem arises from the dissolution of minerals. This means that both cations exchanged onto the surface are removed as well as ions from the minerals and it is not possible to determine the amount of ions related to the two different environments.

Mechanical Dewatering.

The design of the mechanical dewatering press is such that there is an upper limit to the pressure to which the lignite is subjected. The dewatering pressure is one of the major factors determining the extraction of water, and several good water samples were obtained from the Bowmans, Lochiel and Sedan lignite samples. A suitable sample of mechanically removed water could not be obtained from the Kingston sample.

Data Obtained on South Australian Lignites.

Inorganics

The inorganics analysis given in Table II show that all of the South Australian lignites have high sodium, chlorine and sulphur contents.

The Bowmans lignite has the highest sodium and chlorine levels of 1.86% and 1.98% respectively.

In general the water soluble inorganics consist of predominantly sodium, chlorine and sulphur (as sulphate ion) with lesser amounts of calcium and magnesium. The Bowmans and Lochiel lignites, both from the St. Vincents Basin, have very high sodium, chlorine and sulphur as a consequence of the saline environment in this region. The Sedan lignite in contrast has very high calcium and magnesium concentrations (1.3% and 1.19% respectively). The Kingston lignite exhibits a relatively low concentration of water soluble inorganics.

Acid leaching results give an indication of the total inorganics present in the coals, including water soluble ions, cations exchanged onto the surface functional groups associated with the coal, cations exchanged onto the clay minerals and ions emanating from the dissolution or hydrolysis of minerals.

The water soluble component is easily differentiated, however the other three are not. For the Bowmans, Lochiel and Sedan lignites the acid soluble components (total inorganics - water soluble inorganics) are predominantly cations (Na, Mg, Ca, Al and Fe) which are exchanged onto the lignite surface. In contrast, for Kingston lignite which has the lowest water soluble component, inorganics are associated with or exchanged from the clay minerals.

Analysis of the mechanically removed water showed some significant variations especially with respect to sodium. It can be seen that for Bowmans, Lochiel and Sedan lignites, the sodium content detected by mechanical removal of water is noticeably less than that for the water soluble sodium. This aspect of the occurrence and distribution of sodium (and chlorine) within these samples was discussed in detail in a paper presented by the authors recently (32). The distribution of sodium was found to be a function of the high negative surface charge of the coal surface resulting in adsorption of sodium at this surface.

Minerals.

All of the samples analysed showed, as expected, that the major minerals are quartz, kaolinite, marcasite/pyrite and gypsum. In general the quartz is present in two distinct size ranges; 500 μm and 50 μm .

A major variation was noted in the two Kingston samples where the majority of the quartz is acicular in form and -20 μm in size. The size distribution of the kaolinite is quite variable and again the Kingston sample differed in that most of the kaolinite has sodium associated with it and could therefore be considered a smectite rather than kaolinite. Marcasite is commonly present as a replacement of original coal particles. The gypsum is present mainly in the -20 μm size range. Overall the mineral matter content of the lignites is of the order of 5%-10% (i.e. a medium distribution density).

Acknowledgement.

This research was financed by the South Australian State Energy Research Advisory Committee (SENRAC).

Literature Cited.

1. O'Brien, M.D. In Coal Power '87; Australasian Institute of Mining and Metallurgy, 1987; p.233-240.
2. Williams, R.G. and Manzoori, A.R. *ibid* p. 327-335.
3. Manzoori, A.R. In Australian Coal Science Conference 3; Australian Institute of Energy; 1988; paper B3:1.
4. O'Gorman, J.V. and Walker, P.C., Jr., Mineral Matter and Trace Elements in U.S. Coals. Coal Research Section, College of Earth and Mineral Sciences, Pennsylvania State University, Contract No. 14 - 01 - 0001 - 390, 1972.
5. Ward, C.R. Proc. Australas. Inst. Min. Met. No. 267; 1978, p7-25.
6. Miller, R.N. and Given, P.H. A Geochemical Study of the Inorganic Constituents in some Low-Rank Coals. Pennsylvania State University Report to U. S. Department of Energy, FE-2494-TR-1; 1978.
7. Berkowitz, N. An Introduction to Coal Technology, Academic Press New York; 1979.
8. Miller, R.N., Yarzab, R.F. and Given, P.H., Fuel, 1979, 58, p.4-10.
9. Rigby, G.R. et. al., Quantitative Characterisation of Mineral Matter in a Range of Coals and Coal Generated Materials, NERDDP End of Grant Report No. 144; 1982.
10. Meyers, R.A., Coal Structure, Academic Press, New York; 1982.
11. Badin, E.J., Coal Combustion Chemistry - Correlation Aspects, Elsevier, The Netherlands, 1984.
12. Allen, R.M. and VanderSande, J.B., Fuel, 1984; 63, p.24-29.
13. Raask, E., Mineral Impurities in Coal Combustion, Hemisphere Publishing Corp., New York; 1985.
14. Vorres, K.S., Mineral Matter and Ash in Coal; Symposium Series 301, American Chemical Society, Washington, DC, 1986.
15. Kiss, L.T. and King, T.N., Fuel, 1977, 56, p.340-341.
16. Kiss, L.T. and King, T.N., Fuel, 1979, 58, p.547-549.
17. Perry, G.J., Allardice, D.J. and Kiss, L.T. In The Chemistry of Low Rank Coals, ed. H.H. Schobert, American Chemical Society, Symposium Series 264, 1984, p.3-14.
18. Huffman, G.P. and Huggins, F.E. *ibid.* p.159-174.
19. Reference 14, p.10-40.
20. C. Karr, Analytical Methods for Coal and Coal Products, Academic Press; Vol.I (1978), Vol.II (1980) and Vol. III (1981).
21. Daybell, G.N. and Pringle, N.J.S., Fuel, 1958, 37, p.283-292.
22. Kear, R.W. and Menzies, H.M., BCURA, 1965, 20, No.2, p.53-65.
23. Gluskoter, H.J., Trans SME/ATME, 1967, 238, p.373-379.
24. Skipsey, E., Fuel, 1974; 53, p.258-267.
25. Saunders, K.G., J. Inst. Energy, 1980; p.109-115.
26. Hodges, N.J., Ladner, W.R. and Martin, T.G., J. Inst. Fuel, 1983 56, p.158-169.
27. Pearce, W.C. and Hill, J.W.F., Prog. Energy Comb. Sci., 1986, 12, p.117-162.

28. Herzig, J., Szczepanska, J., Witczak, S. and Twardowska, I., Fuel, 1986, 65, p.1134-1141.
29. Kube, W.R., Schobert, H.H., Benson, S.A. and Karner, F.R., Ref. 17, p.38-51.
30. Benson, S.A. and Holm, P.L., Ind. Eng. Chem. Prod. Res. Dev., 1985, 24, p. 145-149.
31. Miller, R.N. and Given, P.H., Geochim. et. Cosmochim. Acta, 1986, 50, p.2023-2043.
32. Readett, D.J. and Quast, K.B., Ref. 3, Paper A2:3.
33. Electricity Trust of South Australia, South Australian Coalfields, 1986.

RECEIVED November 5, 1990

Chapter 4

Advances in Quantitative Assessment of the Association of Mineral Matter with Coal

Warren E. Straszheim and Richard Markuszewski

Ames Laboratory and Iowa State Mining and Mineral Resources Research
Institute, Iowa State University, Ames, IA 50011

The association of mineral particles with the organic coal matrix is being quantitatively assessed using scanning electron microscope-based automated image analysis (SEM-AIA). Routine SEM analyses of mineral matter for particle size and mineral phase can now be supplemented by SEM-AIA results in which samples are also classified according to the degree of association of the mineral matter with the coal matrix. Such association can be measured either in terms of the mass fraction of the various minerals found in cross sections of the particles or in terms of the relative amount of mineral matter and coal present on the surface of the particles. These measurements can be related to the behavior of the coal during density-based and surface-based physical cleaning processes, respectively. Examples of such association measurements are included for samples of Upper Freeport and Indiana No. 3 coals. Variations in the coal-mineral association the two coals, and even for different minerals within the same coal, are compared to ash reduction and coal recovery during cleaning of these coals by various physical methods.

One of the primary goals of coal beneficiation is the removal of pyrite and other mineral matter in order to decrease the amount of SO₂ emissions, increase the heating value of the coal, and minimize problems caused by ash during and after combustion. Since the ash-forming mineral matter in coal has a wide range of characteristics, and since it is not economically feasible to grind coal to such a small size that all mineral matter is liberated, it is practically impossible to remove all of it during cleaning. Rather, coal is ground and processed only to the extent necessary to liberate and remove sufficient mineral matter to comply with applicable technical and/or environmental constraints. In this context, it is important to know to what degree minerals are associated with the coal.

In order to characterize the cleanability of a coal, washability tests are typically performed for a range of particle sizes and

specific gravities of separation, and coal recovery and mineral matter rejection are measured for each combination. Although such techniques are indicators of possible behavior during density-based separations for a given particle size distribution, they are only indirectly related to particle characteristics and are limited to particle sizes larger than about 60 mesh (250 μm). Since cleanability ultimately depends on the characteristics of mineral matter in individual particles, scanning electron microscope-based automated image analysis (SEM-AIA) techniques have been developed to characterize the mineral matter in more detail and *in situ*.

The computerized SEM-AIA techniques for characterizing mineral particles in coal for size and mineral identity have been developed, refined, and expanded, over several years, with applications to the characterization of several different coals [1-7]. In these techniques, scanning electron microscopy (SEM) is used to observe coal and mineral particles in cross section, energy-dispersive x-ray analysis (EDX) is used to determine the elemental composition of the mineral particles, and automated image analysis (AIA) is employed to characterize a sufficiently large number of particles for good statistics and reproducibility. The size distributions of the mineral particles partially determine the cleanability, since it is generally easier to remove the larger mineral particles. However, the association of mineral particles with the organic coal matrix ultimately determines the cleaning potential. Typically, larger mineral particles are more liberated than are small particles from the coal matrix, and thus they are more easily separated. However, certain minerals, such as calcite, for example, can also be preferentially liberated, regardless of particle size, and thus are physically removable while other mineral grains of the same particle size remain with the coal matrix [3,6].

Therefore, SEM-AIA techniques have been adapted to the characterization of the association of individual minerals with coal. Such techniques have been in use in the mineral industry for several years [8,9]. However, the application of these techniques to coal has lagged, partly due to the difficulty of resolving coal particles from the epoxy mounting media in SEM images. Using backscattered electron (BSE) imaging, conventional epoxy resins exhibit little or no contrast with coal particles. As a result, some novel approaches have been taken to measure the coal-mineral association. Vleeskens et al. [10], instead of using SEM, used optical microscopy in which the coal and epoxy matrix are more easily distinguished. However, in this mode the different mineral grains cannot be easily distinguished, except for pyrite. Therefore, they located pyrite particles and analyzed their perimeters to determine the fraction which was in contact with coal and which was free from coal. Moza and Austin [11] tried doping the epoxy resin with a heavy metal (e.g., barium) to make it stand out from the coal. Even then, there were problems with controlling the doping so that the doped epoxy did not interfere with the detection of minerals such as clay or quartz. With an appropriate epoxy mixture, an elemental analysis was performed for each of several thousand coal-mineral particles to arrive at an average elemental composition for each particle, which was then used as an indicator of coal-mineral association. Although such elemental analyses were helpful in studies on ash behavior, the size of mineral particles and their association with coal were not determined. Therefore, such an approach had limited usefulness in coal preparation. In our own work, the use of carnauba wax was developed as an

alternative and effective mounting medium [12]. It provides sufficient and consistent contrast with the coal so that BSE images can be analyzed automatically.

Experimental

Two bituminous coals of moderate ash content were chosen for this paper to illustrate this method of determining coal-mineral association. The first sample was an Upper Freeport coal with 1.3% moisture, 9.88% ash, and 1.56% total sulfur. The second sample was an Indiana No. 3 coal having 10.5% moisture, 7.35% ash, and 4.26% total sulfur. Both coals had been precleaned at a coarse particle size, ground to minus 325 mesh (44 μm), and then separate samples were cleaned by float-sink and by froth flotation techniques, as described elsewhere [5]. Analyses of the feed coals are included in Table I. In this work, our AIA technique was applied only to the feed coal samples.

Table I. Analyses of Upper Freeport and Indiana No. 3 coals

	<u>Upper Freeport</u>	<u>Indiana No. 3</u>
Proximate Analysis, % (dry)		
Ash	9.88	7.35
Volatile Matter	26.02	40.67
Fixed Carbon	64.10	51.98
Equilibrium Moisture, %	1.34	10.47
Forms of Sulfur, % (dry)		
Total	1.56	4.26
Pyrite	0.95	2.23
Sulfate	0.01	0.07

Because SEM-AIA is often used to explain behavior under specific processing conditions, samples are prepared in the same size in which they are received. Coal samples with their included mineral matter are prepared for image analysis by mixing samples of the dry coal with polyethylene powder (as a diluent) and molten carnauba wax in a volume ratio of 1:2:2. Pellets are then cut along the cylindrical axis to expose a vertical cross section of coal and mineral matter and polished using standard petrographic procedures. The surfaces are coated with 150 \AA of carbon to provide a conductive surface for SEM examination.

Samples were examined with an electron beam of 15 keV and 0.7 nA at magnifications of 200x and 500x using the backscattered electron (BSE) signal. Figure 1 shows a typical BSE image for a coal sample. Use of the BSE signal permits relatively easy differentiation of minerals and coal from each other and from the carnauba wax by using simple brightness thresholds. All particles were characterized for area, total perimeter, and the amount of perimeter in contact with coal, mineral matter, or mounting media. X-ray spectra were then collected for 4 seconds for each of the mineral particles. In order to identify the particles, the integrated intensities for 20 elements

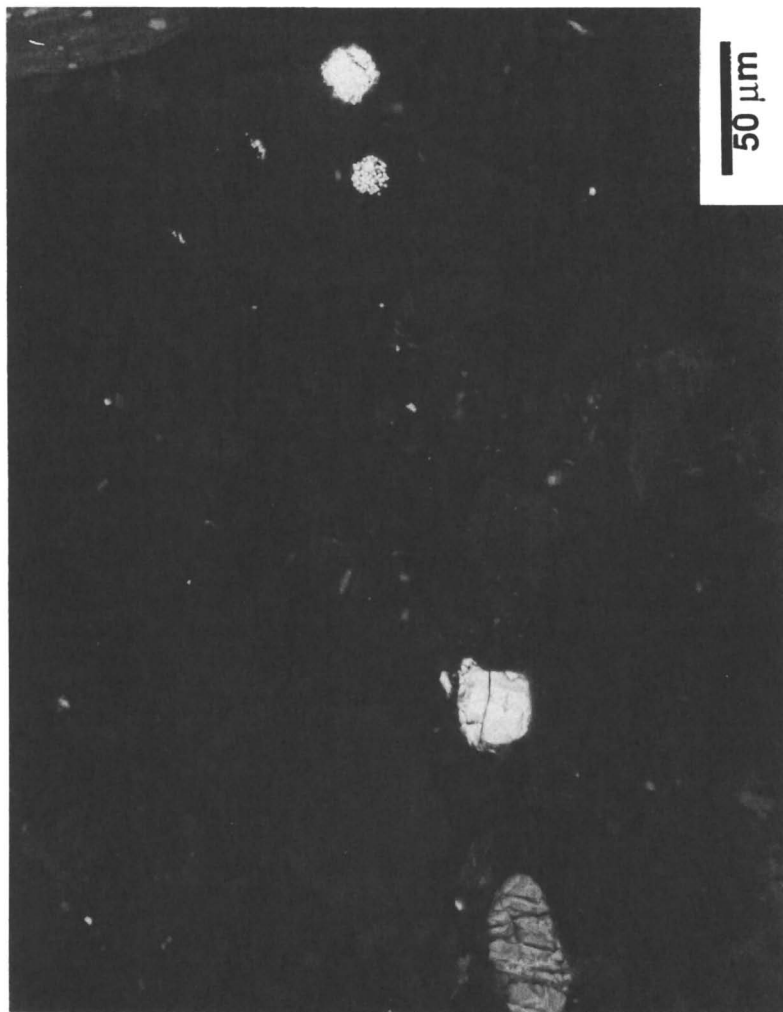


Figure 1. Typical backscattered electron image of 100-mesh Illinois No. 6 coal embedded in carnauba wax.

were compared with a previously prepared table listing ranges of elemental intensities characteristic of minerals found in coal [3,4]. Handbook values of mineral densities were used to convert the results from area fractions to weight fractions.

The SEM-AIA results contain very detailed information for the composite coal/mineral particles and their component parts (i.e., information on size, phase identification, and associations) which can be presented in a number of ways. Tables can be prepared to show the distribution of the sample as a function of particle size and to show the coal-mineral association in terms of bulk properties or in terms of surface properties. For bulk properties, the distribution of coal and minerals is prepared as a function of the total mineral content of the individual particles which can be related to particle density. For surface properties, coal and mineral data are tabulated as a function of the fraction of particle surface covered by mineral matter which can be used to predict the surface properties of the particles and their behavior during surface-based cleaning. Examples of these distributions are given below.

Results and Discussion

Typical distributions of mineral matter according to particle size and mineral phase are given in Figures 2 and 3 for the major phases in the Upper Freeport and Indiana No. 3 coals, respectively. Mineral particle size distributions can be compared to the size of the coal particles to predict the ash reduction potential, since larger mineral particles are likely to be liberated from the coal matrix and thus can be removed during cleaning, while small mineral particles are likely to be associated with the organic matrix and thus tend to remain in the clean coal product. As seen in Figures 2 and 3, most of the mineral matter is rather fine compared to the 44 μm top size (325 mesh) of the sample, and thus might be expected to be rather difficult to remove. Pyrite and quartz particles are a little coarser in the Upper Freeport coal. However, since minerals can be preferentially liberated, it is necessary to analyze directly the association of the mineral matter with the coal rather than inferring behavior from particle size distributions alone.

The first method chosen to express the coal-mineral association results is in terms of the weight fraction of mineral matter in the individual particles, as determined from their cross section. The resulting distribution is comparable to the so-called "grade distributions" used in the mineral industry [8,9]. Such a distribution is included in Table II for the Upper Freeport coal. The data in the table indicate that pyrite is preferentially liberated as compared to quartz or kaolinite. About 78% of the pyrite is in particles containing more than 80% mineral matter, which should be easily removed by density-based separations.

These results have also been plotted in Figures 4 and 5 to show the amount of sample (in %) for each grade. Figure 4 shows the association of coal with mineral matter regardless of the mineral identity, while Figure 5 shows the breakdown of the mineral matter according to mineral phase. Samples with good liberation of minerals from coal should show a clear separation between the coal-rich material on the left and the mineral-rich material on the right side of the figures. As can be seen from Figure 4, most of the mineral matter in this sample is concentrated in the mineral-rich material, but there is some mineral matter found across the entire range of grades.

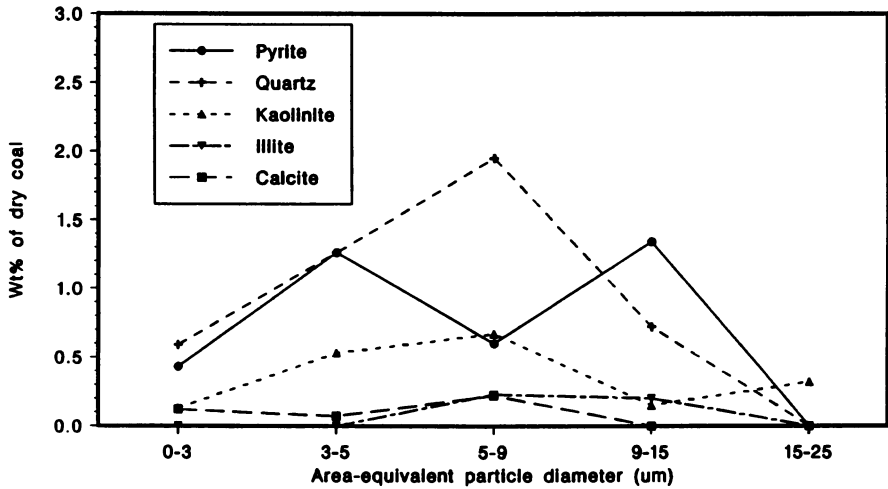


Figure 2. Distribution of selected minerals in Upper Freeport coal as a function of area-equivalent particle diameter (μm).

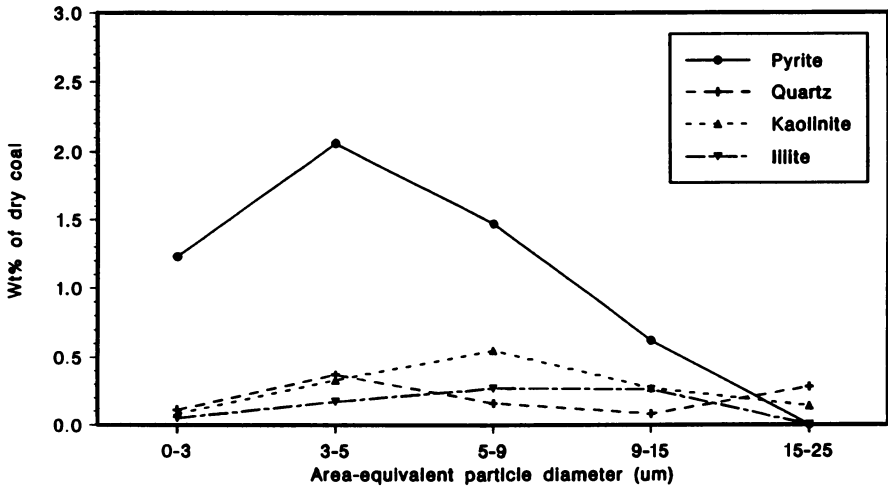


Figure 3. Distribution of selected minerals in Indiana No. 3 coal as a function of area-equivalent particle diameter (μm).

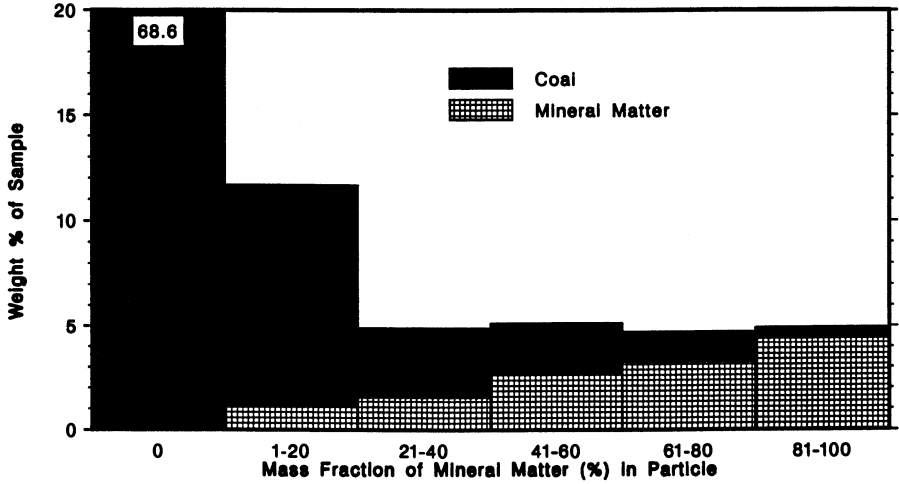


Figure 4. Distribution of coal and mineral matter in Upper Freeport coal as a function of the mineral matter content of the particles.

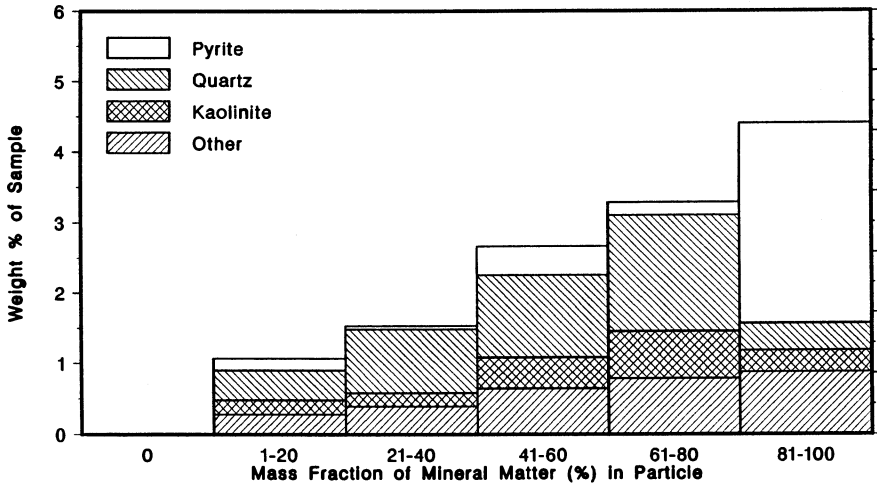


Figure 5. Distribution of individual minerals in Upper Freeport coal as a function of the mineral matter content of the particles.

Table II. Distribution of coal and mineral phases in Upper Freeport coal as a function of particle mineral matter content

	Mineral content of particles, %						Sum
	0	1-20	21-40	41-60	61-80	81-100	
Coal	68.60	10.59	3.38	2.50	1.46	0.53	87.07
Pyrite	0.00	0.17	0.05	0.41	0.18	2.84	3.65
Quartz	0.00	0.42	0.90	1.17	1.65	0.38	4.52
Kaolinite	0.00	0.20	0.19	0.44	0.67	0.31	1.81
Illite	0.00	0.00	0.00	0.00	0.42	0.00	0.42
Other	0.00	0.28	0.39	0.64	0.35	0.87	2.53
Total	68.60	11.66	4.91	5.16	4.74	4.93	100.00

However, Figure 5 illustrates that the general distribution of mineral matter is not the same as that of the pyrite which is liberated to a larger degree.

In addition to expressing coal-mineral association as a function of particle mineral matter content, our most recent efforts have emphasized the determination of coal-mineral association based on particle surfaces. While the previous distributions were measured in terms of bulk properties to provide an indication of the probable cleaning behavior of a coal in a density-based process, they do not lend much insight into cleaning behavior during surface-based processes, such as froth flotation or oil agglomeration. There is no a priori reason to expect that association measured and expressed in terms of bulk composition is generally indicative of association measured in terms of particle surfaces. Therefore, it would also be useful to express results in terms of the proportion of coal (or minerals) present on the surface of the particles.

Figures 6 and 7 show the coal-mineral association for the same Upper Freeport coal sample expressed in terms of the amount of mineral matter on the surface of the particles. There is considerable difference between these two figures and Figures 4 and 5. While Figure 4 shows that about 80% of the mineral matter is present in particles containing more than 40% mineral matter (i.e., less than 60% coal), Figure 6 indicates that only 16% of the mineral matter is associated with particles for which more than 40% of the surface is covered by mineral matter. Indeed, about 70% of the mineral matter is found in particles with more than 80% of the surface covered by coal. Also, the preferential liberation of pyrite noted in terms of bulk composition is absent when association is measured in terms of particle surface.

Thus, the above results for the Upper Freeport coal indicate that density-based processes (e.g., float-sink separation) should be able to remove significant amounts of mineral matter, while surface-based processes (e.g., froth flotation) will likely be unable to reduce the mineral content significantly. Results of cleaning tests reported elsewhere [5] have generally verified these predictions.

Results for the Indiana coal show a distinctly different character. The association distributions are presented in terms of bulk composition in Figures 8 and 9. In general, the mineral matter does

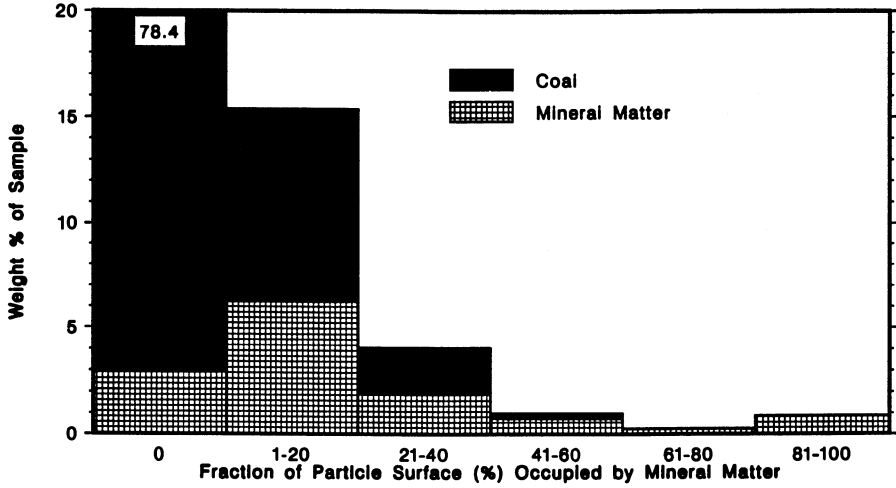


Figure 6. Distribution of coal and mineral matter in Upper Freeport coal as a function of particle surface occupied by minerals.

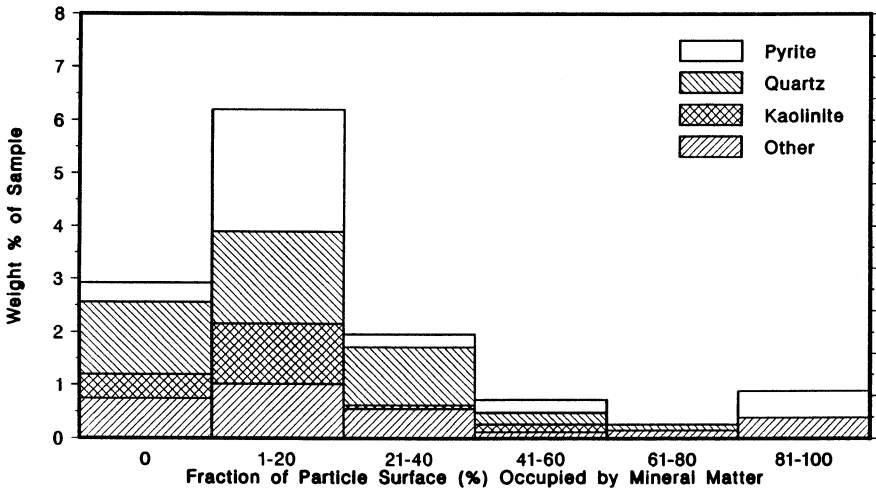


Figure 7. Distribution of individual minerals in Upper Freeport coal as a function of particle surface occupied by minerals.

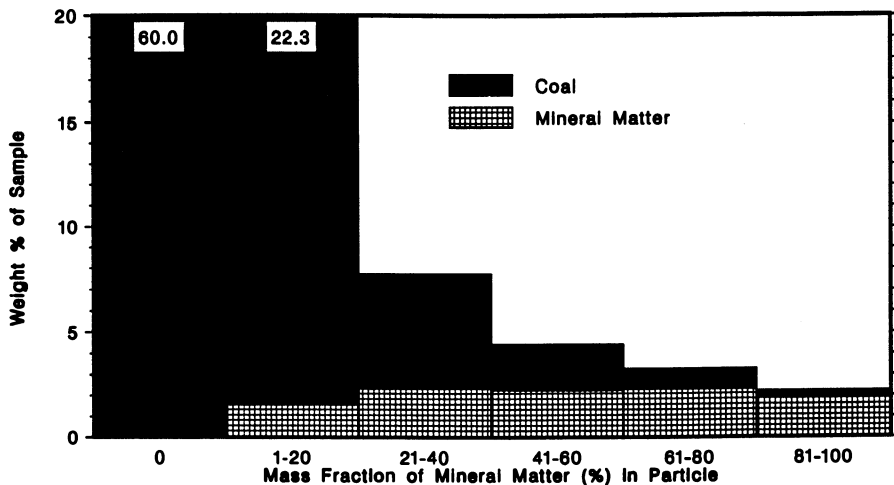


Figure 8. Distribution of coal and mineral matter in Indiana No. 3 coal as a function of the mineral matter content of the particles.

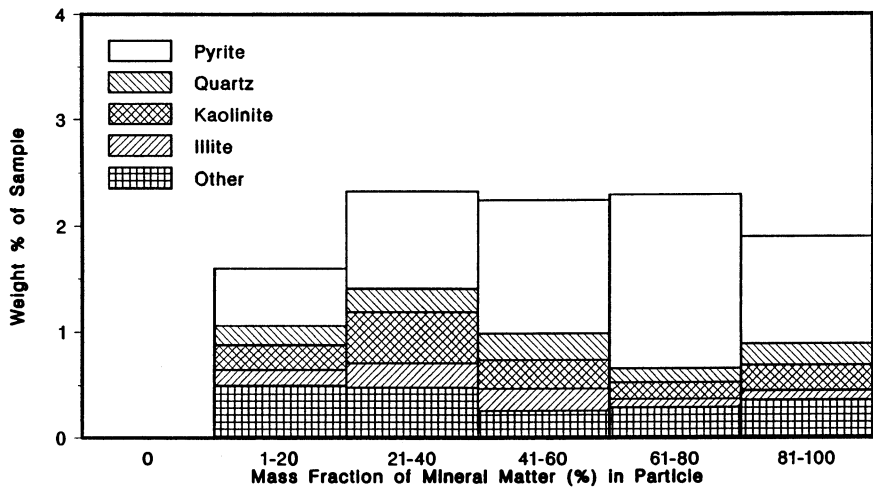


Figure 9. Distribution of individual minerals in Indiana No. 3 coal as a function of the mineral matter content of the particles.

not appear as well liberated as it did for the Upper Freeport coal (compare with Figures 4 and 5). Also, based on these bulk properties, there appears to be no preferential liberation of pyrite as was found for the Upper Freeport coal.

However, the coal-mineral association results for the Indiana coal, when expressed in terms of particle surface in Figures 10 and 11, again show that mineral liberation is less than when the association is considered in terms of bulk properties. But in terms of particle surface, the mineral matter in the Indiana coal appears to be a little better liberated than it is in the Upper Freeport coal. And, like the Upper Freeport sample, no preferential association or liberation of minerals is noted when the association is expressed in terms of particle surfaces.

The above conclusions based on SEM-AIA measurements of association in terms of particle surfaces are somewhat more tentative than the conclusions drawn from bulk association distributions. There are more analytical difficulties when characterizing the particle surfaces than when characterizing the bulk sample. In addition, the factors determining the overall surface nature of a particle are more complex than just the relative amount of the phases present on the particle surface. However, the SEM-AIA results can still provide a useful and heretofore unavailable insight into the nature of mineral matter in coal.

Conclusions

Computerized SEM-AIA techniques can provide insights into the character of a coal and its cleanability that are unavailable by other means. The advantages of this technique stem from its ability to characterize coal and mineral particles *in situ*. For the development of advanced coal cleaning processes, typical washability analyses cannot provide the detail needed since they deal only broadly with the particle character in terms of density. And while similar conclusions regarding preferential mineral liberation or association might be obtained by manual microscopic observation, automated SEM techniques permit the measurements to be performed more quickly and in a quantitative rather than qualitative manner.

Analyses of mineral matter distributions as a function of particle size and mineral type are now practically routine and can provide some indication of coal cleanability. However, when used alone, they do not conclusively indicate the association of minerals with coal. Our recently developed extensions to SEM-AIA techniques can now provide results which show the distribution of phases based on the association of the minerals with coal. Such association can be measured either as the weight fraction of mineral matter in the particle or as the relative amount of surface of the particle occupied by mineral matter. These associations can be related to coal processing behavior and can be used to explain, and possibly even predict, the recovery and quality of product under various cleaning conditions.

Analysis of coal-mineral association in samples of Upper Freeport and Indiana No. 3 coals showed significant differences in the association of minerals with the coal matrix. In terms of bulk properties, the mineral matter was generally more liberated in the Upper Freeport coal than in the Indiana No. 3 coal. Also, based on bulk properties, pyrite was found to be preferentially liberated in the Upper Freeport coal, while no such preferential liberation was observed for minerals in the Indiana No. 3 coal. For both coals, the

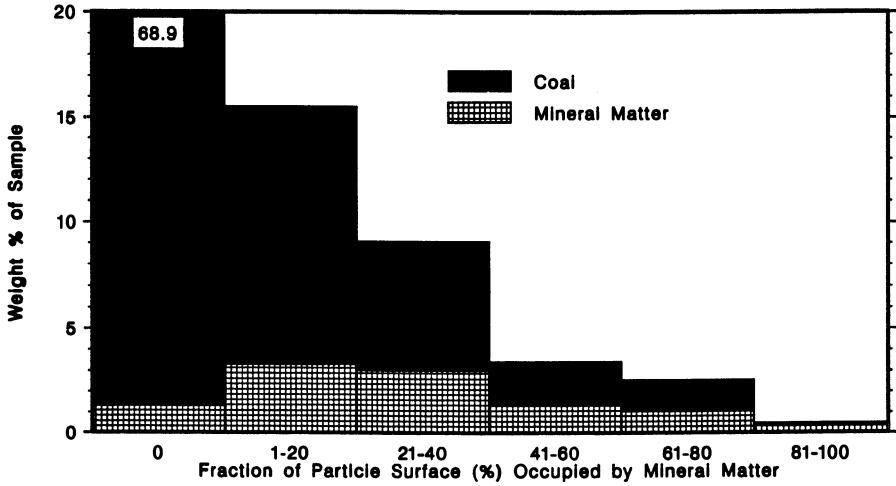


Figure 10. Distribution of coal and mineral matter in Indiana No. 3 coal as a function of particle surface occupied by minerals.

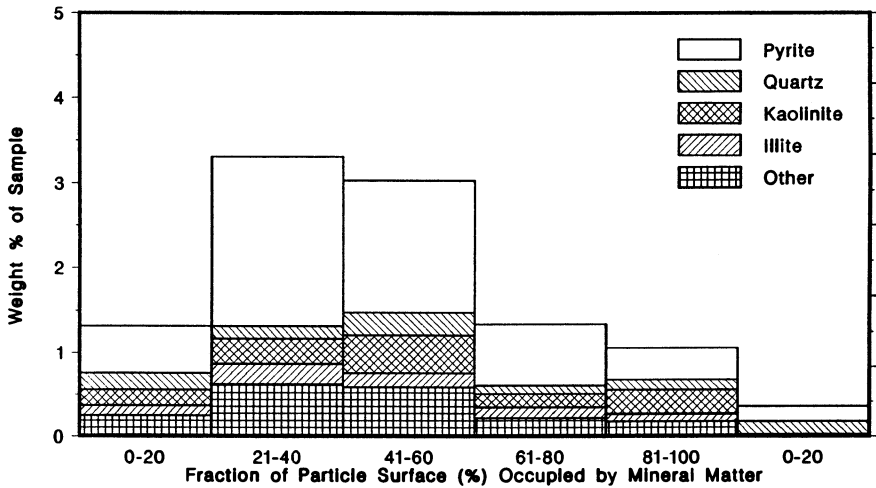


Figure 11. Distribution of individual minerals in Indiana No. 3 coal as a function of particle surface occupied by minerals.

association of minerals with coal was much greater when considered in terms of the particle surfaces. Also, no significant signs of preferential liberation were found when the association was expressed in terms of particle surfaces. Therefore, cleaning by density-based processes would be expected to be somewhat better for the Upper Freeport coal than for the Indiana No. 3 coal, and better for both coals than if surface-based techniques were used for cleaning.

Acknowledgment

Ames Laboratory is operated for the U.S. Department of Energy by Iowa State University under Contract No. W-7405-Eng-82. This work was supported in part by the Assistant Secretary for Fossil Energy through the Pittsburgh Energy Technology Center (PETC), and in part by the U.S. Department of Interior's Mineral Institutes Program administered by the U. S. Bureau of Mines under Allotment Grant No. G1174119.

Literature Cited

1. Huggins, F. E.; Huffman, G. P.; Lee, R. J. In Coal and Coal Products: Analytical Characterization Techniques; Fuller, E. L., Jr., Ed.; ACS Symposium Series No. 205; American Chemical Society: Washington, DC, 1982; pp 239-258.
2. Huggins, F. E.; Kosmack, D. A.; Huffman, G. P.; Lee, R. J. In Scanning Electron Microscopy/1980/I; Johari, O., Ed.; SEM Inc.: Chicago, IL, 1980; pp 531-540.
3. Straszheim, W. E.; Yousling, J. G.; Markuszewski, R. In Mineral Matter and Ash in Coal; Vorres, K. S., Ed.; ACS Symposium Series No. 301; American Chemical Society: Washington, DC, 1986; pp 449-461.
4. Straszheim, W. E. Ph.D. Thesis, Iowa State University, Ames, IA, 1986.
5. Straszheim, W. E.; Younkin, K. A.; Markuszewski R.; Smit, F. J. Am. Chem. Soc. Div. Fuel Chem. Preprints 1988, 33(2), 64-72.
6. Straszheim, W. E.; Markuszewski, R. In Applied Mineralogy; Petruk, W.; Hausen, D.; Hagni, R.; Pignolet-Brandom, S., Eds.; TMS-AIME, New York, (in press).
7. Straszheim, W. E.; Markuszewski, R. Am. Chem. Soc. Div. Fuel Chem. Preprints, 1989, 34(3), 648-655.
8. Petruk, W. In Mineral Processing Design, Yarar, B.; Dogan, Z.M., Eds.; Martinus Nijhoff: Boston, MA, 1987, pp 2-36.
9. Reid, A. F.; Gottlieb, P.; MacDonald, K. J.; Miller, P. R. In Applied Mineralogy; Park, W. C.; Hausen, D. H.; Hagni, R. D., Eds., TMS-AIME, New York, 1985; pp 191-204.
10. Vleeskens, J. M.; Bos, P.; Kos, C. H.; Roos, M. Fuel 1985, 64, 342-347.
11. Moza, A. K.; Austin, L. G. Fuel 1983, 62, 1468-1473.
12. Straszheim, W. E.; Younkin, K. A.; Greer, R. T.; Markuszewski, R. Scanning Microscopy 1988, 2(3), 1257-1264.

RECEIVED November 5, 1990

Chapter 5

Coal Structure

The Problem with Minerals

G. A. Robbins

Consolidation Coal Company, Research and Development, 4000 Brownsville
Road, Library, PA 15129

Fourier transform infrared (FTIR) spectroscopy of coal low-temperature ashes was applied to the determination of coal mineralogy and the prediction of ash properties during coal combustion. Analytical methods commonly applied to the mineralogy of coal are critically surveyed. Conventional least-squares analysis of spectra was used to determine coal mineralogy on the basis of forty-two reference mineral spectra. The method described showed several limitations. However, partial least-squares and principal component regression calibrations with the FTIR data permitted prediction of all eight ASTM ash fusion temperatures to within 50 to 78°F and four major elemental oxide concentrations to within 0.74 to 1.79 wt % of the ASTM ash (standard errors of prediction). Factor analysis based methods offer considerable potential in mineralogical and ash property applications.

Despite considerable effort to understand the chemical nature of the organic and inorganic portions of coal, and substantial advances in instrumentation and methodologies, much of coal's chemical nature remains intractable. This paper reviews methods and their limitations for the determination of specific minerals in coal, and presents results of efforts at Consolidation Coal Company to develop FTIR methods for routine coal mineralogy.

Mineral matter characterization in coal has received considerable attention. Given and Yarzab (1) discussed the problems posed by mineral matter in various coal analyses. Furthermore, mineral matter complicates the chemical treatment of coal. It also has many adverse effects on commercial coal utilization. Coal consumers pay to ship mineral matter, to accommodate its impact on capital equipment and operations, and to dispose of the resultant ash. The impact of coal minerals on utilization motivated Consol's initial interest in mineralogy (2). The results reported here are from a second phase of the FTIR method development, in which extensive improvements were made to the methods.

EXPERIMENTALDescription of Samples

Two coal sample sets and the reference minerals are described below.

Small Data Set. Low-temperature (plasma) ashes (LTAs) were obtained from ten diverse coal samples (Table I), ranging in rank from lignite to lvb. Infrared spectra were obtained of duplicate samples of each LTA. A separate set of duplicates generated (for other purposes) for the first four LTAs listed also was analyzed by FTIR.

Table I. Description of Coals in Small Data Set

Coal	Rank	Seam - Description
P1	hvAb	Pittsburgh - Underground, Clean Coal, Greene Co., PA
EH	hvAb	Elkhorn 3 - Underground, Unwashed, Breathitt Co., KY
I1	hvBb	Illinois 5,6 - Surface, Clean Coal, Jackson Co., IL
SL	Lig	Scranton - Surface, Mercer Co., ND
I2	hvBb	Illinois 6 - Underground, Clean Coal, Jefferson Co., IL
I3	hvBb	Illinois 6 - Surface, Clean Coal, Perry Co., IL
P2	hvAb	Pittsburgh - Underground, Clean Coal, Marshall Co., WV
P3	hvAb	Pittsburgh - Underground, Clean Coal, Monongalia Co., WV
GE	hvAb	No. 2 Gas, Upper and Middle Eagle - Underground, Clean Coal, Raleigh Co., WV
PO	lvb	Pocahontas 3 - Underground, Clean Coal, Buchanan Co., VA

Large Data Set. LTAs were analyzed by FTIR for 50 coals, ranging in rank from lignite to lvb. These were a representative subset of 95 unwashed and clean commercial coals from the eastern, mid-western and western United States and Alberta, Canada. The 50-coal set contained no duplicate coal samples, but different coal samples from the same mine were included.

Reference Minerals. The 42 reference minerals and the mineral classes used are listed in Table II. Most of the minerals were obtained from Ward's Natural Science Establishment, Inc., Rochester, New York. Many of the silicate minerals were American Petroleum Institute (API) standard samples or their equivalents. Numbers given in the table (e.g., kaolinite 4) refer to the API standard designation. When available, several minerals of each type were used for references, to allow for variability in composition, crystallinity, etc.

Methods. Coals ground to -60 mesh were low-temperature (O₂ plasma) ashed in one of three plasma ashers to constant weight for about 100-125 hours for bituminous coals and 200 hours for lower rank coals. Samples were stirred and weighed a minimum of once each 24 hours. The conditions used were 200 watts forward power and 15-20 mL O₂/min (LFE Corp. Model LTA-504 or Denton Vacuum Inc. Model

Table II. Reference Minerals

Main Classes

Kaolin - Kaolinite 4, 5, 6, Dickite 16, 27
 Mica - Biotite, Phologopite, Muscovite
 Illite - Illite 36, Illite-Bearing Shale
 Mixed-Layer Clays - Metabentonite 37, 42
 Montmorillonite - 21, 22A, 22B, 24, 25, 26, 31
 Feldspars - Albite, Anorthite, Orthoclase
 Chlorite - Chlorite
 Misc. Aluminosilicates - Attapulgitite, Halloysite, Pyrophyllite 48
 Quartz - Quartz, Agate
 Fe sulfides - Marcasite, Commercial Pyrite, Mineral Pyrite,
 Pyrrhotite
 Fe oxides - Goethite, Hematite, Magnetite
 Fe sulfate - Difference spectrum weathered minus unweathered pyrite
 Siderite - Siderite
 Calcite - Calcite, Aragonite
 Gypsum - Gypsum, Commercial Drierite (Anhydrite)
 Dolomite - Dolomite

Grouped Classes (used to simplify the final results)

Clays - Kaolin, Illite, M. L. Clays, Montmorillonite, Misc. Alumino-
 silicates
 Other Aluminosilicates - Mica, Feldspar, Chlorite, Quartz
 Sulfate - Fe Sulfate, Gypsum
 Carbonate - Calcite, Siderite, Dolomite
 Fe Altered - Oxides, Sulfate

PE-250 plasma asher) or 280 watts forward power and 90 mL O₂/min (Branson/IPC plasma asher). The latter asher and conditions were used only for ashing small batches of coal (up to eight different samples of 0.5 to 1 g each). When larger batches were ashed, eight dishes containing 2 g each of the same coal were placed in the asher. Ashing containers were made of Pyrex or ceramic.

Mineral standards were hand crushed to -1/4 inch, then ground to a fine powder in a ball mill (alumina elements) or Bleuler Model 526/LFS678 puck mill. The resultant powder was aerodynamically classified in a Bahco Model 6000 micro particle classifier and the finest fraction (#18 throttle) was collected. A size criterion of 90% or more by weight of particles 5 micron and smaller in diameter was used for the mineral standards. Sizes were verified by Coulter Counter. Duplicate 13 mm KBr pellets were prepared and the spectra were weight-scaled by techniques similar to those reported by Painter (3) and Elliot (4). With one exception, all the mineral standard spectra were averages of spectra from duplicate pellets. The one exception was the iron sulfate spectrum, which was obtained as the difference spectrum by subtracting the spectrum of HCl-washed weathered pyrite from that of the weathered pyrite. A weight correction was applied to the difference spectrum.

LTA samples were ground for 30 minutes in a Wig-L-Bug (15mg LTA, 50 mg KBr and 500 mg acetone in an agate vial), dried on a hot

plate at 40°C and then stored in the dessicator. An aliquot of each sample mixture was diluted with KBr, 13 mm pellets were made and the resulting spectra were weight-scaled by techniques similar to those reported by others (3,4). LTAs were not size-classified because of limited quantity. However, the grinding conditions were chosen to give the smallest particles achievable for various reference minerals.

All spectra were run on a Nicolet 7199 FTIR spectrometer equipped to operate in the mid-infrared (wide-band MCT detector). A leastsquares analysis program provided by Nicolet (MCOMP) was extensively modified for efficient routine use with a large number of reference minerals. The reference mineral with the lowest negative concentration in each least-squares decomposition of the LTA spectra was omitted upon each iteration, until only non-negative concentrations were obtained. Generally 12 to 18 minerals remained in the final calculation.

In addition to spectra of the reference minerals listed in Table II, the least-squares components in each iteration included 3 "spectra" representing 1) moisture in KBr blank (obtained by subtraction of 2 KBr blank spectra), 2) a constant baseline offset (1 abs from 4000 to 400 cm^{-1}), and 3) a sloping linear baseline (line from 1 abs at 4000 cm^{-1} to 0 abs at 400 cm^{-1}). The final mineral component concentrations were normalized to 100%, disregarding the contributions of the three artificial components. The normalized least-squares results for each sample were combined with the ash elemental composition of each reference mineral to calculate the elemental composition of the ASTM oxidized ash corresponding to each LTA. This was done by multiplying the concentration of each reference mineral in a sample by the concentration of each elemental oxide in the reference mineral, then summing over each oxide.

For partial least-squares (PLS) or principal component regression (PCR), the infrared spectra were transferred to a DEC VAX 11/750 computer via the NIC-COM software package from Nicolet. This package also provided utility routines used to put the spectra into files compatible with the PLS and PCR software. The PLS and PCR program with cross-validation was provided by David Haaland of Sandia National Laboratory. A detailed description of the program and the procedures used in it has been given (5).

RESULTS AND DISCUSSION

A Critique of Methods for Coal Mineralogy

This survey of five major methods for coal mineralogy and their limitations includes only methods which can provide a "complete" mineral analysis. Methods of limited applicability, such as Mossbauer, are omitted.

X-ray Diffraction. XRD is the most common method used for coal mineralogy (6,7,8). Its major advantage is the ability to unequivocally identify many minerals. The main disadvantages are: 1) reliance on reference minerals, 2) requires careful attention to sample preparation, and 3) low sensitivity to certain minerals (especially many clays) due to poor crystallinity and to particle orientation effects. Many laboratories analyze a separate concentrated clay

American Chemical Society

Library

**1155 16th St., N.W.
Washington, D.C. 20036**

fraction (less than 2 μm or 5 μm). However, sensitivity is still low and other limitations may arise: 1) the separated clay fraction may not be representative, and 2) the separation procedure can alter the sample. The original coal, instead of the LTA, can be analyzed by XRD. However, this is not satisfactory, since sensitivity is even lower. An extensive interlaboratory comparison of XRD results with Illinois 6 coal showed highly variable results (7). That study also included results from FTIR, SEM and other methods.

Infrared Spectroscopy. The use of IR (9,10,11,12) and FTIR (3,4) for coal mineralogy has been reported. Painter and coworkers (3) demonstrated that FTIR can provide a virtually complete analysis. Painter, Brown and Elliott (4), and others (9,10,11) discuss sample preparation, reference minerals, and data analysis. The advantages of IR are: 1) high sensitivity to molecular structure, 2) unequivocal identification of a number of minerals, 3) small sample size (a few milligrams), and 4) rapid analysis time (once LTA is available). Disadvantages include: 1) reliance on reference minerals, 2) requires careful attention to sample preparation, and 3) limited selectivity (discrimination among similar minerals).

The problem with limited selectivity includes some of the minerals which are problems for XRD: illite, muscovite, smectites and mixed-layer clays. Poor crystallinity creates problems with both XRD and FTIR. The IR spectrum of an amorphous material lacks sharp distinguishing features but retains spectral intensity in the regions typical of its composition. The X-ray diffraction pattern shows low intensity relative to well-defined crystalline structures. The major problem for IR is selectivity: for XRD it is sensitivity. In an interlaboratory FTIR comparison (7), two laboratories gave similar results for kaolinite, calcite, and illite, but substantially different results for montmorillonite and quartz.

Electron Beam/X-ray Spectroscopy. Several methods based on point count or automated image analysis (AIA) in scanning electron microscopy-energy dispersive X-ray have been reported (13-18). Point count analysis can determine mineralogy; AIA can also determine the size distribution of the minerals. These methods obtain a point-by-point or particle-by-particle elemental analysis. A mineral distribution and analysis is obtained by classifying each elemental composition into one of the mineral categories. Such methods have several advantages: 1) they can be automated, 2) the composite elemental composition can be checked against that of the bulk sample, 3) it is possible to run coal (not necessary to obtain LTA), and 4) they provide some information on statistical and perhaps spatial, size, or morphological distribution of the minerals. For these reasons, such methods have become more popular in recent years. The major disadvantages are: 1) the chemical information and thus the selectivity is limited, since it uses only elemental composition, 2) it relies on a suitable classification scheme for mineral categories, and 3) data collection can be time-consuming (especially for AIA), requiring many hours per sample.

Optical Microscopy. Optical microscopy is the traditional tool of geologists and petrographers for mineral identification and characterization (19). It has two main advantages: 1) positive identification of minerals can be achieved, and 2) information is obtained on mineral distribution and morphology. However, quantitation is difficult, and the analysis is time-consuming, requires highly trained technicians, and is not amenable to automation. Although in common use in petrographic studies, such methods have been displaced by XRD, IR, and SEM-EDS methods for mineralogical studies.

Thermal Techniques. Thermal techniques, especially differential thermal analysis (DTA) have been used for mineral identification (19) and for coal mineralogy (20). The advantages of thermal techniques are: 1) small sample size, 2) little sample preparation (applicable to whole coals), 3) potentially rapid analysis, and 4) information relevant to combustion behavior may be provided. The disadvantages are: 1) the chemical information is limited, resulting in a lack of selectivity due to overlapping curves for individual minerals, 2) identification/quantification depends on reference minerals (though perhaps less sensitive to such problems than XRD or IR), and 3) it is not developed for quantitative use. Interpretation of thermal data is difficult, but could be improved by appropriate software. Variations, such as using different gases to highlight or suppress features, have been used (20). Detection limits of less than 1 wt % to about 30 wt % were reported for different minerals.

General Comments on Mineralogical Methods. The lack of a measure of quantitative accuracy is a general problem with mineralogy. A major limitation for XRD and IR methods is the use of reference minerals, and the standards used are from geological sources not related to the coal analyzed. This limitation will be avoided by only physical separation of the coal minerals or by data analysis techniques (such as factor analysis) which do not require reference minerals. Many studies have reported successful quantitation of mineral mixtures. This is a necessary, but not sufficient, criterion for a good mineralogical analysis. The differences between mineral mixtures and authentic samples are considerable, and good performance on real samples is not guaranteed. The crucial aspects of SEM-EDS and related techniques are appropriate classification of the elemental data, and obtaining a statistically sufficient number of data points. For classification of data, factor analysis, cluster analysis, or related multivariate techniques appear to be suitable (21).

The IR methods have progressed from hand-drawn baselines and peak height or area for quantitation, to spectral subtraction, to least-squares methods. Least-squares analysis eliminates the reliance on single peaks for quantitation and the subjectivity of spectral subtraction. However, negative concentration coefficients are a problem with least-squares analysis, since they have no physical meaning. Negative components can be omitted according to some criterion and the least-squares process iterated until only

positive concentration coefficients remain. However, this does not ensure that the least-squares solution is a global minimum.

Haaland and coworkers (5) discussed other problems with classical least-squares (CLS) and its performance relative to partial least-squares (PLS) and factor analysis (in the form of principal component regression). One of the disadvantages of CLS is that interferences from overlapping spectra are not handled well, and all the components in a sample must be included for a good analysis. For a material such as coal LTA, this is a significant limitation.

Factor analysis extracts information from the sample data set (e.g., IR spectra) and does not rely on reference minerals. However, because abstract factors have no physical meaning, reference minerals may be needed in target transformations or other procedures to extract mineralogical information. One valuable piece of information obtainable without the use of extraneous data is the number of components required to represent the data within experimental error. Reported applications of factor analysis to mineralogy by FTIR are few (12). However, one commercial laboratory is offering routine FTIR mineral analyses to the petroleum industry, based on related methods (22).

The next section of this paper describes the use of classical least-squares analysis of FTIR data to determine coal mineralogy. This is followed by promising preliminary results obtained using factor analysis techniques.

Results Using Classical Least-Squares

Results of classical least-squares analysis of FTIR spectra of ten coals using forty-two reference minerals were evaluated with regard to reproducibility and accuracy as described below.

Reproducibility. Mineralogical results from the ten-coal set (Table III) are presented as ranges of values. In most cases, the reproducibility is good. Quartz, for example, shows consistently high reproducibility. However, illite, mixed-layer clays and montmorillonite in the first four coals show high variability. These minerals are similar in composition and spectral features. The variability in the FTIR results for these samples is related to variability in the spectral data. The set of ten duplicate spectra gave a pooled SD of 0.03 abs, while the separate set of four duplicate spectra gave a pooled SD of 0.08 abs. Results from the first four samples in the table included the poorer spectral data, while the results from the last six samples were obtained from the better spectra. No specific reason is apparent for the higher error in the four-coal set; however, sampling, instrumental, and environmental factors may have contributed. The reproducibility for total clay content is good, even when variability in individual clay concentrations is high. Iron sulfides, oxides and sulfates also show some variability, particularly in the first and fourth samples.

Accuracy. Although there is no way to measure the accuracy of the FTIR mineralogical results, there are three areas in which it can be addressed (2,4). The first method is to compare pyrite results obtained by FTIR with the conventional ASTM determination. The

Table III. FTIR Mineralogical Results Using Classical Least-Squares, wt % of LTA

Mineral Class	P1 (a)		EH (a)		I1 (a)		SL (a)		I2	
	Min.	Max.	Min.	Max.	Min.	Max.	Min.	Max.	Min.	Max.
Kaolin	25.8	33.9	11.8	16.6	15.1	21.8	1.1	2.9	23.2	25.2
Mica	2.6	6.4	2.9	9.3	0.0	3.3	0.0	0.0	7.6	10.5
Illite	7.1	13.6	20.2	33.8	3.7	47.4	0.0	1.2**	20.8	25.1
Mixed Layer Clays	0.0	11.3*	6.2	16.6	0.0	15.8	0.0	0.0	0.0	0.0
Montmorillonite	4.2	13.4	3.4	5.9	0.0	26.0	15.5	20.4	5.0	9.4
Feldspar	0.0	3.8	0.0	1.3	0.0	0.0	0.0	13.5**	0.0	0.7
Chlorite	0.6	2.5	3.4	4.9	0.0	2.3	0.0	0.0	0.0	0.2
Misc. Clays	1.8	9.8	0.2	2.3	0.0	4.3**	0.0	2.7*	1.7	3.0
Quartz	7.7	13.8	12.5	13.6	11.0	14.6	15.5	20.9	14.1	14.8
Fe Sulfide	9.2	13.2	2.0	5.6	0.0	5.3	4.8	13.1	8.0	8.2
Fe Oxide	4.7	8.7	5.3	9.2	6.8	8.5	0.0	0.3*	5.5	7.3
Fe Sulfate	4.4	11.2	2.9	3.8	0.0	4.5	0.0	0.0	4.3	5.2
Siderite	0.0	0.0	1.5	2.4	0.0	0.0	2.4	5.8	0.0	0.0
Calcite	0.0	0.0	0.0	0.0	0.0	2.8*	0.0	0.0	0.0	0.0
Gypsum	0.0	0.0	0.0	0.5*	0.0	2.3**	34.4	49.2	0.0	0.0
Dolomite	0.0	0.0	0.0	0.0	0.0	0.0	0.0	0.0	0.0	0.0
Grouped Classes										
Clays	54.0	60.0	55.3	59.7	67.7	71.5	19.6	24.9	56.4	57.0
Other Alumino-Silicates	14.6	22.1	20.5	27.1	13.3	17.2	19.5	34.4	23.2	24.8
Sulfates	4.4	11.2	3.2	3.8	2.3	5.0	34.4	49.2	4.3	5.2
Carbonates	0.0	0.0	1.5	2.4	0.0	2.8*	2.4	5.8	0.0	0.0
Fe-Altered	9.3	20.0	8.2	12.4	7.5	13.0	0.0	0.3*	10.7	11.6
Mineral Class	I3		P2		P3		GE		P0	
	Min.	Max.	Min.	Max.	Min.	Max.	Min.	Max.	Min.	Max.
Kaolin	13.3	14.0	17.6	18.6	20.7	21.2	35.3	35.8	21.6	22.5
Mica	6.1	6.7	5.3	5.5	3.6	4.3	12.1	13.1	4.7	7.7
Illite	9.4	10.8	5.3	5.5	10.0	10.4	8.0	9.9	16.6	17.0
Mixed Layer Clays	0.0	0.0	0.0	0.0	0.0	0.0	0.0	0.0	0.0	0.0
Montmorillonite	13.5	13.8	11.7	11.8	4.9	5.9	4.9	5.9	3.1	3.8
Feldspar	3.2	3.8	1.6	2.0	9.7	10.1	2.5	2.7	5.4	6.5
Chlorite	0.0	0.0	0.0	0.0	2.1	2.5	3.6	3.9	5.0	5.5
Misc. Clays	0.0	0.0	2.8	3.3	2.8	3.8	4.0	5.2	0.4	0.6
Quartz	14.2	14.2	8.1	8.1	4.9	6.0	12.2	12.9	6.5	7.1
Fe Sulfide	19.4	19.6	28.0	29.0	20.8	22.3	4.0	5.1	4.4	7.6
Fe Oxide	4.9	5.6	2.9	3.0	4.8	5.7	7.7	8.3	8.8	10.4
Fe Sulfate	9.0	9.3	14.8	14.9	10.8	11.1	1.0	1.8	0.1	0.5
Siderite	3.7	4.0	0.0	0.0	0.6	1.1	0.0	0.0	6.3	6.6
Calcite	0.0	1.6	0.0	0.0	0.0	0.0	0.0	0.0	9.0	9.4
Gypsum	0.0	0.0	0.0	0.0	0.0	0.0	0.0	0.0	1.1	1.6
Dolomite	0.0	0.0	0.0	0.0	0.0	0.1	0.0	0.0	0.0	0.3
Grouped Classes										
Clays	36.9	37.9	37.7	38.9	39.4	40.4	53.7	55.4	42.8	42.9
Other Alumino-Silicates	24.0	24.1	15.3	15.5	20.9	22.1	30.6	32.5	23.1	25.3
Sulfate	9.0	9.3	14.8	14.9	10.8	11.1	1.0	1.8	1.6	1.7
Carbonates	4.0	5.3	0.0	0.0	0.7	1.1	0.0	0.0	15.5	16.0
Fe-Altered	14.2	14.6	17.8	17.8	15.6	16.8	8.7	10.1	9.3	10.5

(a) Four samples run from each of these coals, two samples run from each of the remaining coals.
 * One out of four samples gave a non-zero concentration.
 ** Two out of four samples gave a non-zero concentration.

agreement (Figure 1) is good over the range of 2.9 to 28.1 wt % pyrite in the LTAs from the ten coals, and quite good above 10 wt % pyrite in LTA. Similar results were obtained based on the 475-400 cm^{-1} region for a smaller sample set (2). The present results are based on the 1575-400 cm^{-1} range. The good agreement for the present data set is surprising, since the only spectral feature reported for pyrite in the mid-infrared is at ca. 415 cm^{-1} . In these spectra, the noise level is high near 400 cm^{-1} , and the identification of such a feature is not clear. It appears that the results are derived mainly from baseline curvature (resulting from the Christiansen effect). For all the iron sulfide minerals in the reference set, the baseline absorbance is near zero from ca. 1300 to 400 cm^{-1} , but from 1300 cm^{-1} to 4000 cm^{-1} it curves upward.

The second method for indicating accuracy is to examine the spectral residuals from the least-squares fits (Figure 2, Table IV). The worst case was the lignite (coal SL), the large misfit at ca. 1380 cm^{-1} being due to the omission from the reference minerals of nitrate, presumably produced in the low-temperature ash by fixation of organic nitrogen (23). The reproducibility of the 28 original spectra (pooled SD) was 0.05 abs, slightly higher than the pooled standard fit error of 0.04 abs (without the lignite). However, the ten original duplicate spectra gave a pooled standard deviation of only 0.03 abs, which is slightly lower than the fit errors for most of those samples. In general, the fit error approached the experimental error in the original data.

Table IV. Spectral Fit Errors and Elemental Prediction Errors from FTIR Mineralogy

Coal	Spectral Fit Error (1575-400 cm^{-1}),				SEP Oxide wt % of Ash
	Run 1	Run 2	Run 3	Run 4	
P1	0.028	0.027	0.038	0.041	4.4
EH	0.030	0.033	0.023	0.029	4.3
I1	0.026	0.026	0.029	0.031	4.7
SL	NA	0.250	0.149	0.194	4.1
I2	0.033	0.028			5.2
I3	0.037	0.039			6.7
P2	0.040	0.040			4.4
P3	0.037	0.036			5.5
GE	0.038	0.037			3.4
PO	0.022	0.021			6.2

With SL, pooled std. dev. - 0.093.

Without SL, pooled std. dev. - 0.041.

NA - Not Available.

The third method for assessing accuracy is to calculate an elemental composition for each LTA's corresponding oxidized ash, based on the reference mineral elemental compositions. Reasonably close agreement between the actual (obtained by ICP-AES) and calculated elemental compositions would substantiate (but not prove) the mineral analysis. The standard error of prediction (SEP) for

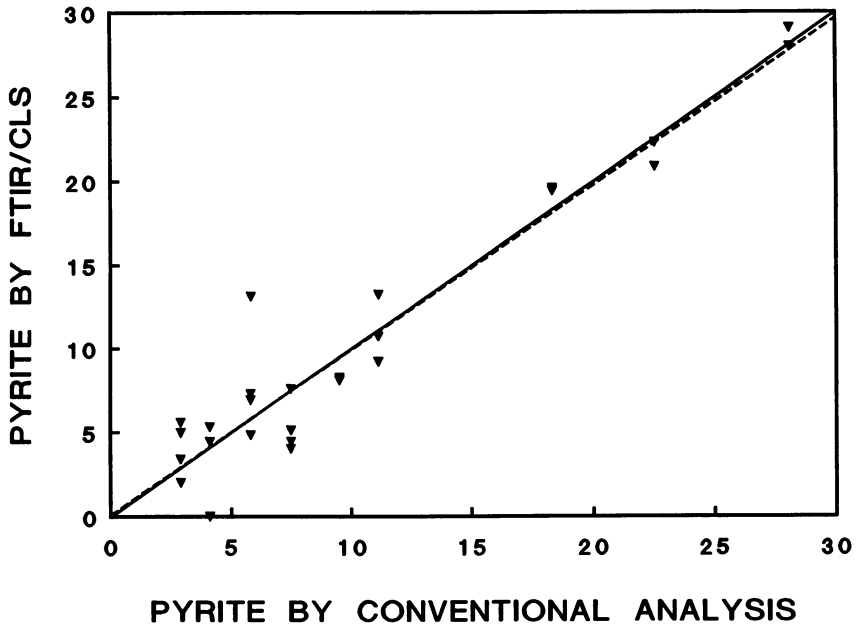


Figure 1. Comparison of FTIR and ASTM Results for Pyrite, wt % of LTA (Solid Line - Parity, Dotted Line - Least-Squares $y = 0.985x + 0.098$).

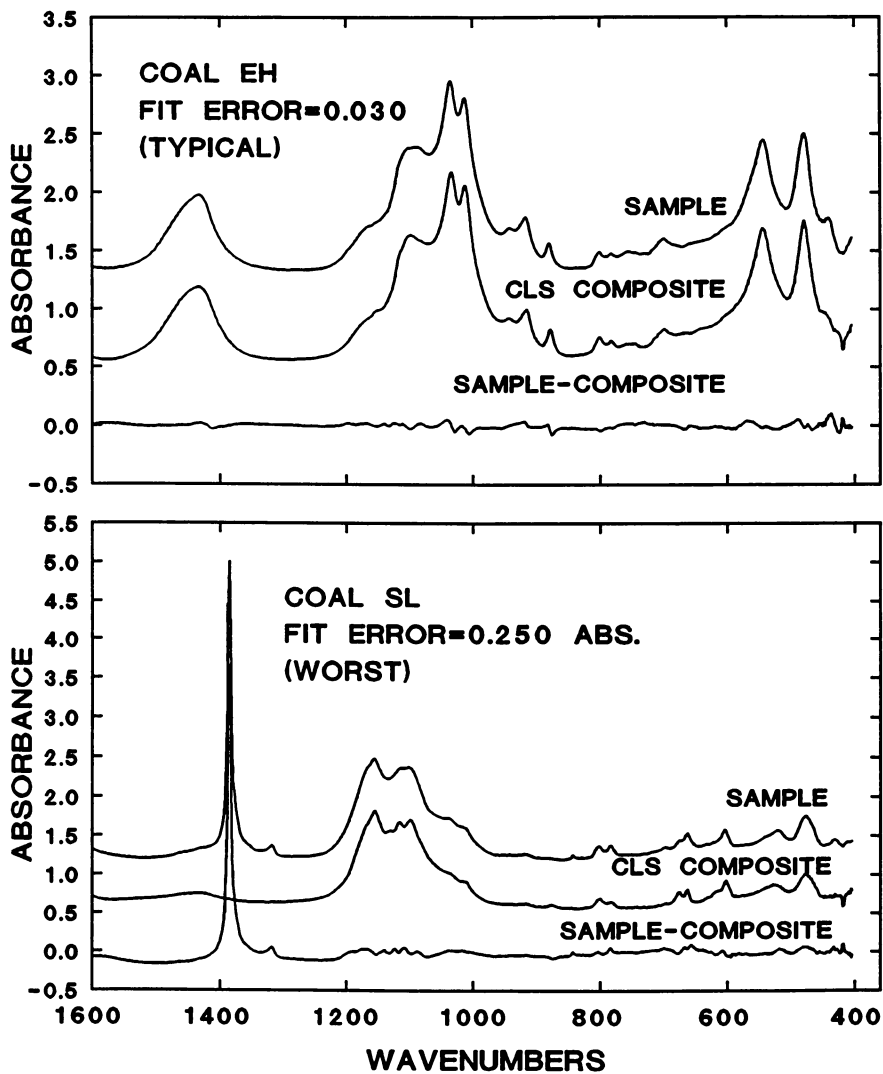


Figure 2. Spectral Residual for Typical (Coal EH) and Worst (Coal SL) Least-Squares Fits. Spectra Shown are Original LTA, Least-Squares Composite, and Difference (Original Minus Composite). LTA and Composite Spectra are Displaced Along the Absorbance Axis for Clarity.

CaO, Fe₂O₃, SiO₂ and Al₂O₃ (Table IV) ranged from 3.4 to 6.7 wt % for the various ashes. The global SEP was 4.8 wt %. By major ash element, the SEP values were 2.8 for CaO, 5.6 for Fe₂O₃, 4.5 for SiO₂ and 5.8 for Al₂O₃. SEP values ranged from 0.3 to 5.7 wt % CaO, 2.3 to 10.3 wt % Fe₂O₃, 0.1 to 11.6 wt % SiO₂ and 3.0 to 5.6 wt % Al₂O₃. Inspection of the elemental results also show some bias. CaO values were usually low, Fe₂O₃ values were usually high, and Al₂O₃ values were always low. Calcite impurities may be present in some of the reference spectra, or something else may interfere with the calcite. The high Fe₂O₃ values, even though the pyrite values appear good, indicate that the determined iron oxides, sulfates, and/or siderite concentrations are too high. Somehow, certain iron minerals seem to be replacing or suppressing the appropriate aluminosilicates in the analysis.

In the next section, the potential for factor analysis and related chemometric techniques for providing improvements in the determination of minerals in coal by FTIR are explored.

Results Using Principal Component Regression (PCR)

PCR is a technique in which principal component analysis (one form of factor analysis) of the spectra is followed by regression of the factor scores to calibrate and predict an independently-measured quantity. Besides the spectral data, these calculations require other data. An accurate mineral analysis of each sample could be used to obtain a calibration. Because this is not possible, one is limited to modeling and predicting other measurable properties such as ash combustion behavior. It is possible to by-pass the mineralogy altogether, and model the desired properties or behavior directly from the LTA spectra. Ash property data which are readily accessible are ASTM ash fusion temperatures (reducing and oxidizing conditions) and ash elemental composition. PLS and PCR are linear models, but are capable of modeling some non-linearities (5). Ash elemental concentrations should be linearly related to intensities of bands in the infrared spectra (under ideal circumstances). Thus, PLS and PCR are expected to do a good job in modeling ash composition. However, ash fusion temperatures are not expected to be linearly related to spectral features.

Infrared data in the 1575-400 cm⁻¹ region (1218 points/spectrum) from LTAs from 50 coals (large data set) were used as input data to both PLS and PCR routines. This is the same spectral region used in the classical least-squares analysis of the small data set. Calibrations were developed for the eight ASTM ash fusion temperatures and the four major ash elements as oxides (determined by ICP-AES). The program uses PLS1 models, in which only one variable at a time is modeled. Cross-validation was used to select the optimum number of factors in the model. In this technique, a subset of the data (in this case five spectra) is omitted from the calibration, but predictions are made for it. The sum-of-squares residuals are computed from those samples left out. A new subset is then omitted, the first set is included in the new calibration, and additional residual errors are tallied. This process is repeated until predictions have been made and the errors summed for all 50 samples (in this case, 10 calibrations are made). This entire set of

calculations is repeated once each time an additional factor is included in the model. The optimum number of factors is near the point at which the residual error reaches a minimum.

Results from these preliminary modeling efforts with the large data set are shown in Table V. These results were obtained with centering (x and y) and scaling (x) as a data pretreatment. Only PCR results are shown, even though the PLS calculations took less computing time and gave slightly better results. The PCR model is preferred because it provides some additional information on our original data set. Results are depicted graphically in Figures 3 and 4 for the best and worst calibrations, respectively. The main measure of the success of these models is the SEP. For ash fusion temperatures, the SEPs ranged from 50 to 78°F. The fusion temperatures at oxidizing conditions generally gave slightly better results than those at reducing conditions. These values represent errors somewhat larger than ASTM repeatability and reproducibility limits. The largest single prediction error for these models was about 200°F. This is no larger than the spread in inter-laboratory results seen in round robin analyses of standard samples. Furthermore, these results appear to be equivalent to the best predictions of ash fusion temperatures available from ash elemental compositions (24,25,26). Many of those models have incorporated ratios, squared terms and log terms to get better results. It appears that the PLS and PCR models work reasonably well for modeling non-linearities in this case.

Table V. Principal Component Regression Calibrations
For Selected Ash Properties

Type	No. of Factors	SEP	Magnitude of Max. Prediction Error	Range of Input Data	
				Minimum Value	Maximum Value
<u>Ash Fusion Temperature, °F</u>					
RID	5	72.4	169.9	1918	2747
RST	5	77.9	153.5	1972	2808
RHT	5	65.9	201.8	2092	2958
RFT	5	56.2	157.6	2127	2968
OID	6	50.5	117.6	2115	2808
OST	5	60.4	149.8	2159	2858
OHT	5	54.0	163.8	2197	2881
OFT	2	61.1	148.1	2218	2769
<u>Ash Element as Oxide, wt %</u>					
SiO ₂	10	1.38	2.81	29.15	56.45
Al ₂ O ₃	13	0.74	1.33	9.12	27.34
Fe ₂ O ₃	8	1.79	3.19	4.33	30.17
CaO	3	1.73	6.88	1.07	30.11

The PCR results for CaO, Fe₂O₃, SiO₂ and Al₂O₃ are quite good, as anticipated. The SEPs for CaO and Fe₂O₃ of 1.7-1.8 wt % are higher than the ASTM reproducibility limits, but the results for

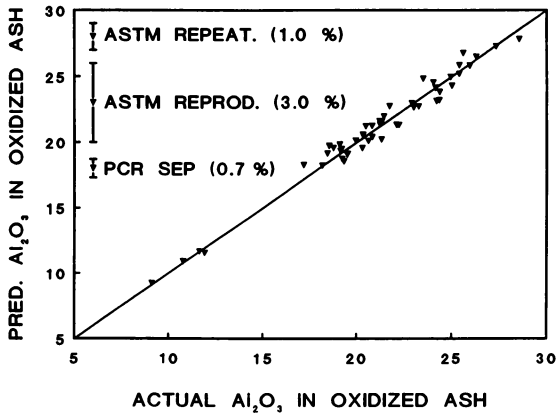


Figure 3. PCR Model Results for Al_2O_3 wt % of Oxidized Ash (Best Model of Ash Properties).

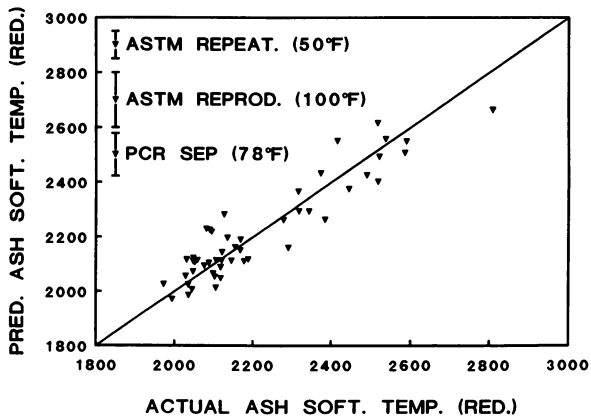


Figure 4. PCR Model Results for Ash Softening Temperature (Reducing), °F (Worst Model of Ash Properties).

SiO₂ and Al₂O₃ are within the ASTM limits for those elements. Note that all these errors are better than the value of 4.8 resulting from the mineralogical analysis. (However, the mineral analysis was not optimized to predict ash elementals.)

The calibrations obtained are valid over a significant range of each property. It is feasible to predict all these properties from the LTA from a small sample of coal, should that be desired. These results mainly show that the methods employed can model other ash properties which are more closely related to large-scale combustion behavior. This is one area where further study is desirable.

Although the software used was not a full-featured factor analysis program, portions of the printed output are useful in studying the spectral data set. Table VI shows some information obtainable from PCR models (large data set) with 5, 10 and 13 factors. In this case, the "factors" are principal components derived entirely from the sample data set. PLS factors are not interpretable in the same manner.

Table VI. Principal Component Information Provided by the PCR Program

No. of Factors	Prediction Residual Sum of Squares (Reconstruction of Original Data)	% of Total Spectral Variance of Data Set
5	89.9	93.5
10	28.1	98.0
13	11.5	99.2

An increase from 5 to 10 in the number of factors representing the original data results in a substantial reduction in the error. Because of the data pretreatment used, the spectral error cannot be directly compared to the experimental error determined from the data set. When five factors were used, two different lignite samples were flagged as possible outliers based on their spectral variances relative to the rest of the data set. With ten factors, one of the lignites was accommodated within the factor model (although ten factors may not have been required to accommodate it). With thirteen factors, both lignites were accommodated.

CONCLUSIONS

Experience in this laboratory has shown that even with careful attention to detail, determination of coal mineralogy by classical least-squares analysis of FTIR data may have several limitations. Factor analysis and related techniques have the potential to remove or lessen some of these limitations. Calibration models based on partial least-squares or principal component regression may allow prediction of useful properties or empirical behavior directly from FTIR spectra of low-temperature ashes. Wider application of these techniques to coal mineralogical studies is recommended.

ACKNOWLEDGMENTS

The author gratefully acknowledges the contributions of others to various aspects of this project. F. P. Burke and R. A. Winschel provided research guidance and helpful advice. M. S. Lancet provided low temperature ash samples and conventional analysis data. Experimental work was performed by J. M. Sarisak, L. L. Anthony, and L. K. Dahm. L. L. Schlutz and D. J. Simmons prepared the manuscript. D. M. Haaland of Sandia National Laboratory provided the PLS and PCR software and gave advice on its use. G. Ritter of Nicolet provided the MCOMP program source code.

LITERATURE CITED

1. Given, P. H.; Yarzab, R. F. Analytical Methods for Coal and Coal Products, C. Karr, Ed.; Academic: New York, 1978, Vol. II; p 3.
2. Robbins, G. A.; Burke, F. P. Proc. 1st Annual Pittsburgh Coal Conference, 1984, p 819.
3. Painter, P. C.; Rimmer, S. M.; Snyder, R. W.; Davis, A. Appl. Spectro., 1981 35, 102.
4. Brown, J. M.; Elliott, J. J. "The Quantitative Analysis of Minerals by Fourier Transform Infrared (FT-IR) Spectroscopy", from Workshop on Application of IR Methods to the Study of Clay Minerals, Clay Mineral Society, 20th Annual Meeting, October 1, 1983, Buffalo, NY.
5. Haaland, D. M.; Thomas, E. V. Anal. Chem., 1988 60, 1193.
6. Renton, J. J. ACS Fuel Chemistry Div. Prepr., 1984, 29(4), 21.
7. Finkelman, R. B.; Fiene, F. D.; Miller, R. N.; Simon, F. O., Eds.; Interlaboratory Comparison of Mineral Constituents in a Sample from the Herrin (No. 6) Coal Bed from Illinois, U.S. Geological Survey Circular 932 (1984).
8. Davis, D. B.; Johnson, L. R.; Mebrahtu, T. U.S. DOE Report DOE/PC/70793--T5, February 1986.
9. Estep, P. A.; Kovatch, J. J.; Karr, C., Jr. Anal. Chem., 1968 40, 358.
10. Tuddenham, W. M.; Lyon, R. J. P. Anal. Chem., 1960, 32, 1630.
11. Stephens, J. D.; Tuddenham, W. M., Am. Lab., 1971, 3, 8.
12. Platbrood, G.; Barten, H. Anal. Chem., 1985, 57, 2504 (1985).
13. Huggins, F. E.; Huffman, G. P.; Lee, R. J. Coal and Coal Products: Analytical Characterization Techniques, ACS Symposium Series, 1982, 205, 239.
14. Straszheim, W. E.; Markuszewski, R. ACS Fuel Chemistry Div. Prepr., 1985, 30(1), 47.
15. Kalmanovitch, D. P.; Montgomery, G. G.; Steadman, E. N. ASME Paper No. 87-JPGC-FACT-4, 1987.
16. Fowkes, W. W. Analytical Methods for Coal and Coal Products, C. Karr, Ed.; Academic: New York, 1978, Vol. II, p 293.
17. Allen, R. M.; VanderSande, J. B. Fuel, 1984 63, 24.
18. Finkelman, R. B. Scanning Microsc., 1988, 9.
19. Zussman, J. Ed. Physical Methods in Determinative Mineralogy, Academic Press, New York (1967).
20. Warne, S. St. J. Analytical Methods for Coal and Coal Products, C. Karr, Ed.; Academic: New York, 1979, Vol. III, p 447.

21. Wangen, L. E.; Peterson, E. J.; Hutchinson, W. B.; Levinson, L. S. in Environmental Applications of Chemometrics, ACS Symposium Series, 53 (1985).
22. Harville, D. G.; Freeman, D. L. SPE Paper No. 18120 (1988), and phone conversations with the authors.
23. Painter, P. C.; Youtcheff, J.; Given, P. H. Fuel, 1980, 523.
24. Gray, V. R, Fuel, 1987, 1230.
25. Slegeir, W. A.; Singletary, J. H.; Kohut, J. F. J. Coal Qual., 1988, 7, 48.
26. Winegartner, E. C.; Rhodes, B. T. J. Eng. Power, 1975, 395.

RECEIVED November 5, 1990

Chapter 6

Chemical Nature of Species Associated with Mobile Protons in Coals

A Study by Field Ionization Mass Spectrometry

Anna Marzec¹ and Hans-Rolf Schulten²

¹Department of Petroleum and Coal Chemistry, Polish Academy
of Sciences, 44-100 Gliwice, 1 Maja 62, Poland

²Department of Trace Analysis, Fachhochschule Fresenius, Dambachtal 20,
6200 Wiesbaden, Germany

With the use of low and high resolution pyrolysis-field ionization mass spectrometry, molecular weight distribution as well as elemental composition were determined of major components of coal material that volatilized in high vacuum of the spectrometer.

The coal, 78% C daf, was heated in the direct introduction system of the spectrometer to the end temperature of 500°C; this led to volatilization yield of the coal corresponding to its mobile phase content which was app. 30 wt % org. mat.

It is assumed that components of the volatilized material represent the coal mobile phase i.e., free molecules originally present in coal as well as fragments that were cleaved from macromolecules by thermal and induced scission of single bonds.

The components are hydrocarbons and oxygen compounds showing high diversity with respect to the content of aromatic rings, from 1 to 5; the alkyl carbon atoms, from 1 to 8; and the molecular weights that are mainly in the range from 230 to 430 Daltons.

Proton n.m.r. investigations of coals swollen in deuterated pyridine showed that the free induction decay /FID/ consists of Gaussian and Lorentzian components related to two populations of protons which have widely different degrees of rotational mobility (1-5). The Gaussian component of FID has been unanimously ascribed to the macromolecular part of the coal matter that is supposed to have very limited rotational mobility. These publications as well as the ensuing debates (6-9) however, reflected the controversy regarding the nature of the Lorentzian /mobile/ protons in coals.

One view is that all Lorentzian protons can be attributed to molecules that are free to rotate in cages of the macromolecular network. Since the free molecules may be differentiated in their sizes and may have restricted freedom of rotation, their spin-spin relaxation times may be also differentiated and account for numerous populations of various mobilities within the group of Lorentzian protons.

The other view which seems to prevail, is that a significant part of the Lorentzian protons, especially those of lower mobility, may be also associated with fragments of the macromolecular network that can rotate due to a single C-C or C-O bond linking such fragment to the network.

The controversy cannot be easily clarified; there is no experimental technique available that could isolate all the free molecules and would leave intact the macromolecular network.

A more realistic approach is a separation of a mixture of free molecules and structural units linked to the network by single bonds, after these bonds have been cleaved by heat treatment of the coal. An insight into the composition of such mixture can provide information on the nature of species that are likely to be associated with the mobile protons. It seems that pyrolysis-field ionization mass spectrometry can be used in order to attain this goal.

Pyrolysis-Field Ionization Mass Spectrometry of Biomaterials. Recently, an improved experimental setup for time-resolved insource pyrolysis /py./ field ionization /f.i./ mass spectrometry /m.s./ has been described (10) and examples of its application to studying various biomaterials have been shown. There is a number of characteristic features of the py.-f.i.m.s. that are

relevant to coal studies. Due to an increase of temperature of a sample in the direct introduction system of the mass spectrometer at heating rates around 1°C per second and recording magnetic scans in 10°C intervals, the volatilized species are not effected by a higher temperature than is needed for their volatilization and detection. High vacuum, 10^{-7}Pa , and short residence time of the volatiles in the ion source of the spectrometer also reduce significantly secondary reactions between the species. The volatiles undergo soft ionization in the high electric field to produce molecular ions, with essentially no fragmentation ions. Hence, the mode of heating and ionization coupled with frequent scanning, can provide information about the composition of materials, even those that are generally assumed to be thermally unstable. For example, application of the py-f.i.m.s. technique to analysis of plant material (11) and organic matter of soil (12) enabled to detect alkanes to C64, hydroxy compounds such as ergosterol /C28/, fatty acids up to C33 and alkyl esters up to C62.

Pyrolysis and Volatilization of Coal in the Mass Spectrometer. Recent studies on mechanistic problems of coal pyrolysis (13) indicated that not only spontaneous thermal scission of inherently weak single bonds is involved in pyrolysis of coal material. A review (13) of data published by various groups provide an argument that induced scission of strong bonds such as Ar-C and Ar-O, also play an important role during pyrolysis. Hence, it is likely that all structural fragments that can rotate due to the presence of a single bond, can also be cleaved off during pyrolysis.

When pyrolysis of coal is carried out in the mass spectrometer in high vacuum of its ion source compartment, volatilization of broken fragments is likely to occur, unless they are of large molecular size. However, a large molecular size of a fragment would also reduce its rotational ability.

The other component of the coal volatilized material are free molecules existing in original coal; this was shown by the py-f. i. m. s studies of coal samples and their pyridine extracts /14/.

Although it is difficult to ascertain whether all free molecules and fragments capable of rotation, are volatilized in the mass spectrometer, this volatilized material certainly represents a high proportion of them.

The present paper shows such py.-f.i.m.s. data for a low rank bituminous coal. More specifically, the molecular distribution of volatilized material as well as elemental composition of its major components, are determined.

Experimental

The coal studied, 78% C and 15.8% O daf, is derived from Carboniferous deposits from the Ziemowit mine in Poland. Its petrographic composition /% vol. dmmf/ is: vitrinite, 60; exinite, 12; and inertinite, 28.

Proton n.m.r. measurements of Zeeman relaxation for the same coal showed (Jurkiewicz, A., Colorado State University, personal communication, 1988) that mobile protons represent 32% of all protons. Assuming that the content of hydrogen in the mobile and immobile phases of the coal is approximately the same, the relaxation measurements indicate that the coal mobile phase content is app. 32 wt % of organic material.

Previously the py.-f.i.m.s. of coals and their pyridine extracts has already been described (14) using this novel technique. About 100 micrograms of ground coal sample was heated in the high vacuum of a combined e.i/f.i./f.d. ion source of a double-focusing mass spectrometer (Finnigan MAT 731, Bremen, FRG). The sample was heated at a constant rate of 24°C/min from 50 to 500°C.

Forty spectra were recorded electrically in the whole temperature range. The f.i. signals of all the spectra were integrated, processed and plotted using the Finnigan Spectro-System 200 to give a summed spectrum. Five measurements of the sample were recorded and their averaged, summed spectrum was finally obtained which is reproducible and representative of the coal.

High mass resolution /h.r./f.i. mass spectrography was carried out using the same py. conditions as above. The photoplate (Q2, Illford, England) was exposed to f.i. ions in the range m/z 60-500 for about 10 min. The resolution obtained was between 10,000 and 20,000 /50% valley definition/ with an average mass accuracy of approximately 0.003 Dalton /3 mmu/. The photographic plate was evaluated with a Gaertner comparator. Mass measurements were calibrated using perfluorokerosene. The accurate mass determinations allow the calculation of the elemental composition of the f.i. ions.

Results and Discussion

The volatilization of the coal pyrolysed in the mass spectrometer to 500°C corresponds to 30 wt % daf. This end temperature had been selected in such way that the yield of volatilization was comparable with the mobile phase content. The temperature also corresponds to a rapid decrease of volatilization. This is shown in Figure displaying the total ion current on heating the

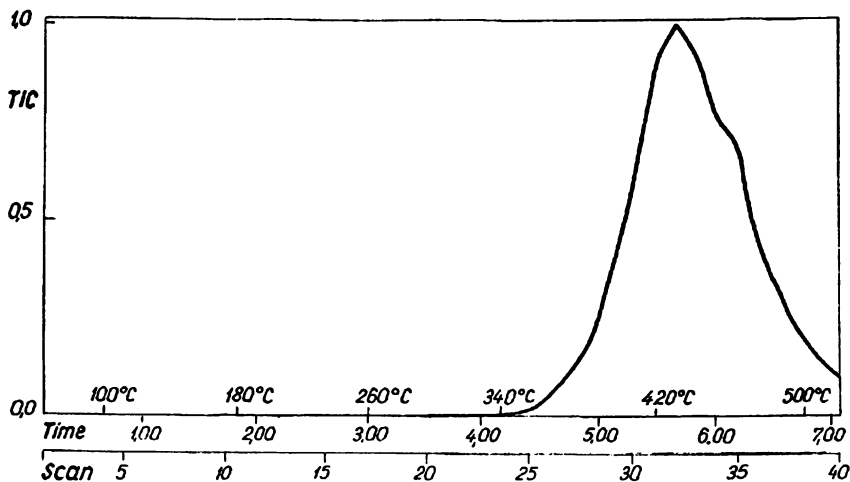


Figure. Total Ion Current TIC /arbitrary units/ versus Temperature and Time of Heating /minutes/ and Scan Number

sample from 50 to 500°C. The volatilization starts at app. 300°C, then it rapidly increases from app. 370°C; after reaching its maximum at ~430°C the volatilization goes quickly down.

The molecular weights of the volatilized components were in the range of 80 to 800 Daltons. However, most intense f.i. signals were found in the much narrower range, from 230 to 430 Daltons; abundances above this range quickly decreased to negligible values. The f.i. mass spectrum in question is not displayed here, since a similar one from another coal was shown elsewhere (14).

High resolution f.i. data are shown in Table. They refer to the major components of the volatilized material; the data for species for which intensities on the photoplate were below 5% are not included, nor are the data for species above 300 Daltons that could not be accurately measured under the selected experimental conditions. Thus, the Table shows elemental composition of the species that account for app. 50 wt % of the volatilized material.

The species represent nearly all homolog series of

Hydrocarbons from C_nH_{2n} to C_nH_{2n-28} ; as well as

Oxygen Compounds from $C_nH_{2n-2}O$ to $C_nH_{2n-30}O$;
and from $C_nH_{2n-6}O_2$ to $C_nH_{2n-26}O_2$.

These formulae refer to compounds that contain one and two rings /such as naphthalene and indene/; three aromatic rings /such as anthracene and cyclopentaphenanthrene/ as well as four aromatic rings /such as pyrene, chrysene/ and five aromatic rings as in benzopyrene.

There are carbon atoms from 1 to 8 in alkyl substituents on the aromatic rings. It is worthy of note that the alkyl substituents are not long. Even if one assumes all alkyl carbons form one alkyl substituent on a ring, a substituent cannot be longer than C₈ for indenenes, C₇ for acenaphthenes, fluorenes and anthracenes and C₆ for benzenes and naphthalenes. Essentially the same applies to alkyl oxygen compounds.

Under the same py.-f.i.m.s. experimental conditions, compounds with normal and branched alkyl chains up to C₃₂ were easily detected in natural waxes (15). Thus, the present results indicate that long alkyl compounds are not major constituents of the coal and discussing the FID signals of coal in terms of its "polyethylene structures" (B. C. Gerstein in reference 8) is not correct for the coal studied and may be not correct for other coals.

In summarizing, the following statements can be made:

- Py.-f.i.m.s. of coal can provide information on chemical nature of species that most likely, contain protons detected by n.m.r. experiments as mobile protons.

Table. ELEMENTAL COMPOSITION OF F.I. MASS SIGNALS DETECTED FOR A LOW RANK BITUMINOUS COAL, 78% C daf

homolog series $C_nH_{2n+z}O_x$ and proposed structure	elemental composition of ions								
C_nH_{2n} ;olefins/ monocyclic alkanes	C_6H_{12}	C_7H_{14}	C_8H_{16}	C_9H_{18}	-	-	-	-	-
C_nH_{2n-2} ;diolefins/ dicycloalkanes	C_6H_{10}	C_7H_{12}	C_8H_{14}	C_9H_{16}	-	-	-	-	-
$C_nH_{2n-2}O$;	$C_6H_{10}O$	$C_7H_{12}O$	-	-	-	-	-	-	-
C_nH_{2n-4} ;triolefins/ tricycloalkanes	C_6H_8	C_7H_{10}	C_8H_{12}	C_9H_{14}	$C_{10}H_{16}$	-	-	-	-
$C_nH_{2n-4}O$;	C_6H_8O	$C_7H_{10}O$	$C_8H_{12}O$	$C_9H_{14}O$	-	-	-	-	-
Number of carbon atoms in alkyl substituents									
	C_0	C_1	C_2	C_3	C_4	C_5	C_6	C_7	C_8
C_nH_{2n-6} ;benzenes	C_6H_6	C_7H_8	C_8H_{10}	C_9H_{12}	$C_{10}H_{14}$	$C_{11}H_{16}$	$C_{12}H_{18}$	-	-
$C_nH_{2n-6}O$;hydro- xy-benzenes	C_6H_6O	C_7H_8O	$C_8H_{10}O$	$C_9H_{12}O$	$C_{10}H_{14}O$	$C_{11}H_{16}O$	$C_{12}H_{18}O$	-	-
$C_nH_{2n-6}O_2$;dihy- droxy-benzenes	$C_6H_6O_2$	$C_7H_8O_2$	$C_8H_{10}O_2$	-	$C_{10}H_{14}O_2$	$C_{11}H_{16}O_2$	-	-	-

Continued on next page

Table. Continued

	C0	C1	C2	C3	C4	C5	C6	C7	C8
C _n H _{2n-10} ;indenes	C ₉ H ₈	C ₁₀ H ₁₀	C ₁₁ H ₁₂	-	C ₁₃ H ₁₆	C ₁₄ H ₁₈	-	C ₁₆ H ₂₂	C ₁₇ H ₂₄
C _n H _{2n-10} O; hydroxyindenes	C ₉ H ₈ O	C ₁₀ H ₁₀ O	-	C ₁₂ H ₁₄ O	C ₁₃ H ₁₆ O	C ₁₄ H ₁₈ O	C ₁₅ H ₂₀ O	-	C ₁₇ H ₂₄ O
C _n H _{2n-10} O ₂ ; dihydroxyindenes	-	C ₁₀ H ₁₀ O ₂	-	C ₁₂ H ₁₄ O ₂	C ₁₃ H ₁₆ O ₂	C ₁₄ H ₁₈ O ₂	-	C ₁₆ H ₂₂ O ₂	-
C _n H _{2n-12} ;naphthalenes -tetrahydrofluorenes	C ₁₀ H ₈	C ₁₁ H ₁₀	C ₁₂ H ₁₂	C ₁₃ H ₁₄	C ₁₄ H ₁₆	C ₁₅ H ₁₈	C ₁₆ H ₂₀	-	-
C _n H _{2n-12} O;hydroxy- naphthalenes/-te- trahydrofluorenes	-	C ₁₁ H ₁₀ O	C ₁₂ H ₁₂ O	C ₁₃ H ₁₄ O	-	C ₁₅ H ₁₈ O	C ₁₆ H ₂₀ O	C ₁₇ H ₂₂ O	C ₁₈ H ₂₄ O
C _n H _{2n-12} O ₂ ;dihydro- xynaphthalenes/-te- trahydrofluorenes	C ₁₀ H ₈ O ₂	-	C ₁₂ H ₁₂ O ₂	C ₁₃ H ₁₄ O ₂	C ₁₄ H ₁₆ O ₂	C ₁₅ H ₁₈ O ₂	C ₁₆ H ₂₀ O ₂	-	-
C _n H _{2n-14} ;acena- phthenes	C ₁₂ H ₁₀	C ₁₃ H ₁₂	C ₁₄ H ₁₄	C ₁₅ H ₁₆	C ₁₆ H ₁₈	C ₁₇ H ₂₀	C ₁₈ H ₂₂	C ₁₉ H ₂₄	-
C _n H _{2n-14} O;hydroxy- acenaphthenes	C ₁₂ H ₁₀ O	C ₁₃ H ₁₂ O	C ₁₄ H ₁₄ O	C ₁₅ H ₁₆ O	C ₁₆ H ₁₈ O	C ₁₇ H ₂₀ O	-	-	-
C _n H _{2n-14} O ₂ ;dihydroxy- acenaphthenes	C ₁₂ H ₁₀ O ₂	-	C ₁₄ H ₁₄ O ₂	C ₁₅ H ₁₆ O ₂	-	C ₁₇ H ₂₀ O ₂	-	C ₁₉ H ₂₄ O ₂	-
C _n H _{2n-16} ;fluorenes	C ₁₃ H ₁₀	C ₁₄ H ₁₂	C ₁₅ H ₁₄	C ₁₆ H ₁₆	C ₁₇ H ₁₈	C ₁₈ H ₂₀	C ₁₉ H ₂₂	C ₂₀ H ₂₄	-

$C_nH_{2n-16}O$;hydroxy-fluorenes	$C_{13}H_{10}O_1$	-	$C_{15}H_{14}O$	$C_{16}H_{16}O$	$C_{17}H_{18}O$	$C_{18}H_{20}O$	$C_{19}H_{22}O$	$C_{20}H_{24}$	$C_{21}H_{26}O$
$C_nH_{2n-16}O_2$; dihydroxyfluorenes	-	$C_{14}H_{12}O_2$	$C_{15}H_{14}O_2$	-	$C_{17}H_{18}O_2$	$C_{18}H_{20}O_2$	$C_{19}H_{22}O_2$	-	-
C_nH_{2n-18} ;anthracenes	$C_{14}H_{10}$	$C_{15}H_{12}$	$C_{16}H_{14}$	$C_{17}H_{16}$	$C_{18}H_{18}$	$C_{19}H_{20}$	$C_{20}H_{22}$	$C_{21}H_{24}$	-
$C_nH_{2n-18}O$; hydroxyanthracenes	-	$C_{15}H_{12}O$	-	$C_{17}H_{16}O$	$C_{18}H_{18}O$	$C_{19}H_{20}O$	$C_{20}H_{22}O$	-	-
$C_nH_{2n-18}O_2$; dihydroxyanthracenes	$C_{14}H_{10}O_2$	$C_{15}H_{12}O_2$	$C_{16}H_{14}O_2$	-	$C_{18}H_{18}O_2$	$C_{19}H_{20}O_2$	-	-	-
C_nH_{2n-20} ; cyclo-pentaphenanthrenes	$C_{15}H_{10}$	$C_{16}H_{12}$	$C_{17}H_{14}$	$C_{18}H_{16}$	$C_{19}H_{18}$	$C_{20}H_{20}$	-	-	-
$C_nH_{2n-20}O$;hydroxy-clopentaphenanthrenes	-	$C_{16}H_{12}O$	-	-	$C_{19}H_{18}O$	-	-	-	-
$C_nH_{2n-20}O_2$;dihydroxy-clopentaphenanthrenes	-	-	-	$C_{18}H_{16}O_2$	-	-	-	-	-
$C_nH_{2n-22}O_2$;pyrenes/fluoranthenes	$C_{16}H_{10}$	$C_{17}H_{12}$	-	$C_{19}H_{16}$	$C_{20}H_{18}$	-	-	-	-
$C_nH_{2n-22}O$;hydroxy-pyrenes-fluoranthenes	$C_{16}H_{10}O$	-	-	-	-	-	-	-	-
C_nH_{2n-24} ;chrysenes	-	$C_{19}H_{14}$	$C_{20}H_{16}$	$C_{21}H_{18}$	$C_{22}H_{20}$	-	-	-	-

Continued on next page

- The results for a low rank bituminous coal show a high diversity of molecular weights for such compounds, from 80 to 800 Daltons; most abundant compounds are in the range from 230 to 430 Daltons;
- The high resolution f.i. data, although limited to major components, also show diverse structures: the number of aromatic rings is from 1 to 5; the number of carbon atoms in alkyl substituents is in the range from 1 to 8.
- This structural diversity must account for a wide range of mobilities of the components of the mobile phase.

Literature Cited

1. Jurkiewicz, A.; Marzec, A.; Idziak, S. Fuel 1981, 60, 1167
2. Jurkiewicz, A.; Marzec, A.; Pislewski, N. Fuel, 1982, 61, 647
3. Marzec, A.; Jurkiewicz, A.; Pislewski, N. Fuel, 1983, 62, 996
4. Barton, W.A.; Lynch, L. J.; Webster, D.S. Fuel, 1984, 63, 1262
5. Kamienski, B.; Pruski, U.; Gerstein, B.C.; Given, P.H. Energy and Fuels 1987, 1, 45
6. Given, P.H.; Marzec, A.; Barton, W.A.; Lynch, L.J.; Gerstein, B.C. Fuel 1986, 65, 155
7. Given, P.H.; Marzec, A. Fuel 1988, 67, 242
8. Axelson, D.E. In NMR of Humic Substance and Coal; /Eds. R.L. Kershaw and M. A. Mikita/, Lewis Pub. Inc.: Chelsea, Michigan, USA, 1987; p 135
9. Derbyshire, F.; Marzec, A.; Schulten, H.-R.; Wilson, M.A.; Davis, A.; Tekely, P.; Jurkiewicz, A.; Bronnimann, Ch.E.; Wind, R.A.; Maciel, G.E.; Narayan, R.; Bartle, K.; Snape, C. Fuel 1989, 68, 1091
10. Schulten, H.-R.; Simmleit, N.; Mueller, R. Anal. Chem. 1987, 59, 2903 and references therein
11. Schulten, H.-R. Simmleit, N.; Mueller, R. Anal. Chem. 1989, 61, 221
12. Hempfling, R.; Schulten, H.-R. Soil Sci. 1988, 146, 262
13. McMillen, D.F.; Malhotra, R.; Nigenda, S.E. Am. Chem. Soc. Div. Fuel Chemistry, Preprints 1987, 32, 180
14. Schulten, H.-R.; Marzec, A. Fuel 1986, 65, 855
15. Schulten, H.-R.; Murray, K.E.; Simmleit, N.; Z. Naturforsch. 1987, 420, 17

RECEIVED January 4, 1991

Chapter 7

Two-Component Concept of Coal Structure

Frank J. Derbyshire¹, Alan Davis², and Rui Lin³

¹Center for Applied Energy Research, 3572 University of Kentucky,
Lexington, KY 40511-8433

²Energy and Fuels Research Center, The Pennsylvania State University,
University-Park, PA 16802

³Unocal Corporation, P.O. Box 76, Brea, CA 92621

The hypothesis that coals can be considered to consist of two component phases has its origins in observations of coal behaviour as well as deriving from the analysis of coals and attempts to define their structure. The results of extensive studies of untreated, preheated and hydrogenated coals, using analytical and microscopic techniques, have allowed some insight into the association between the so-called mobile phase and macromolecular network, and have provided information upon differences in their chemical properties.

The yield of chloroform-soluble extract has been used to indicate the extent of the mobile phase. In untreated coals, only a portion of the mobile phase is readily removable. After mild preheating or mild hydrogenation, there are sharp increases in the yield of extract and accompanying changes in properties. Under these conditions, it is believed that weak bonding between the mobile phase and network is disrupted. The solubilisation of the network requires much higher energy input and necessitates the consumption of hydrogen. The properties of the network components differ significantly from those of the mobile phase and both are coal rank-dependent.

The concept that coals can be usefully considered to consist of two distinct phases of constituents is not new and has been advanced in different ways since the early part of this century. Its revival in recent times is largely attributable to the efforts of the late Peter Given, to whom is owed the now wide use of the terms "mobile phase" and "macromolecular network" (1-3). In broad terms, the mobile phase comprises the smaller molecules in coals, a portion of which is extractable in solvents. The greater proportion of coals is solvent-insoluble and consists primarily of a three-dimensional crosslinked macromolecular network or matrix. The mobile phase is attached to or held within the network by physical constraints and weak bonds.

In 1986, Peter Given organized a "debate in print" by several contributing authors on the nature and extent of the mobile phase as interpreted from ^1H NMR studies (2). He had planned a sequel which was intended to update the NMR work and to introduce findings from other types of investigation. The second debate was completed after Peter Given's death and was published in tribute to his contributions to coal science (3).

Much of the research pursued by the authors of this paper and by their associates has involved studies of the catalytic hydrogenation of coals in the absence of solvent. The technique has been used to elucidate the mechanisms of catalytic coal liquefaction and to provide simultaneously some insight into the structure of coals. Peter Given was directly instrumental in providing the incentive for this research which has extended since 1983. Previous findings were disseminated through several publications (4-8). In this paper, some of the earlier data have been collated with more recent results (9) to provide an account of the relevance of these studies to the two-component concept.

EXPERIMENTAL

Coals covering a range of rank downwards from low-volatile bituminous were examined in solvent-free catalytic hydrogenation over the temperature range 300-400°C and for reaction times up to 60 min. The work discussed here specifically involved four coals which were obtained from the Penn State Coal Sample Bank. These were a subbituminous coal PSOC-1403, and three hvAb bituminous coals, PSOC-1168, PSOC-1266 and PSOC-1510. Characteristics of the coals are summarised in Table I. The reactors were of the tubing bomb type and the initial (cold) hydrogen pressure was 7 MPa. A sulphided Mo catalyst was introduced to the coal by impregnation from an aqueous solution of ammonium tetrathiomolybdate.

Table I. Coal Properties

Penn State Sample	PSOC-1403	PSOC-1266	PSOC-1168	PSOC-1510
Bank No.				
seam	Anderson	L. Kittanning	L. Kittanning	L. Kittanning
county	Campbell	Mehining	Lawrence	-
state	Wyoming	Ohio	Pennsylvania	Pennsylvania
ASTM rank	sub B	hvAb	hvAb	hvAb
mean-maximum reflectance of vitrinite	0.40	0.83	0.83	0.89
moisture (ar wt%)	23.3	3.4	2.4	1.4
mineral matter (a)	-	-	-	-
(dry, wt%) (c)	11.9	6.1	14.5	7.2
	Elemental Composition (% dmmf)			
carbon	72.9	83.2	71.8	77.4
hydrogen	4.5	5.0	4.9	4.9
oxygen (b)	20.4	8.6	18.8	15.2
nitrogen	1.2	2.1	1.6	1.7
organic sulfur	0.9	0.5	2.9	0.8
	Petrographic Composition (Mineral-Free, vol %)			
vitritinite	88	91	88	83
exinitite	2	3	4	10
inertinitite	11	6	7	7

(a) reported as ASTM ash
 (b) by difference
 (c) by low-temperature ashing

The gaseous products, chloroform-soluble extracts and chloroform-insoluble residues were characterized using a range of analytical techniques. A particular advantage of conducting the hydrogenation reactions in the absence of solvent is that microscopy can be used to observe directly the changes wrought in the whole reacted coals and in the extracted residues. Considerable emphasis was placed on this method of analysis using both visible light microscopy and quantitative fluorescence microphotometry. Descriptions of the procedures and techniques have been given earlier (4-9).

CATALYTIC HYDROGENATION

Detailed examination of the composition and distribution of the reaction products over a range of reaction conditions showed that the four coals exhibited certain common trends. Of particular note, there was in each case, a sharp distinction between the events which took place at low and high conversions. The division occurred at a chloroform-solubles yield of approximately 25% wt dmmf coal.

Low extract yields were obtained either by short reaction times at high temperatures or by more extended reaction at low temperatures. The designations of high and low temperature depend upon the individual coal and, more especially upon the coal rank. The evidence accrued in this research has shown that there exists a threshold temperature below which the potential for liquids formation is minimal and above which conversion can proceed at an appreciable rate.

It is supposed that the threshold temperature is determined essentially by the density and nature of the crosslinks in the macromolecular network. This is consistent with evidence showing that the ease of conversion and the selectivity to lower molecular weight liquids increases with decreasing coal rank (10,11). For the subbituminous coal, the rate of liquids formation was negligible at 300°C and became appreciable at 350°C and higher. The bituminous coals began to respond only at temperatures around 400°C. Similar observations have been made in experiments which compared the solvent-free hydrogenation of a lignite and a bituminous coal (12).

During the initial stages of conversion, as the liquid yield increased there were radical changes in the properties of the chloroform-soluble extracts. The atomic ratio, H/C aliphatic hydrogen content and oil to asphaltene (O/A) ratio each increased rapidly at first, passed through a maximum and decreased equally precipitately to a lower value. Illustrations of these changes are presented in Figure 1 and Figure 2 for the O/A ratio and H/C atomic ratio respectively. The progression of

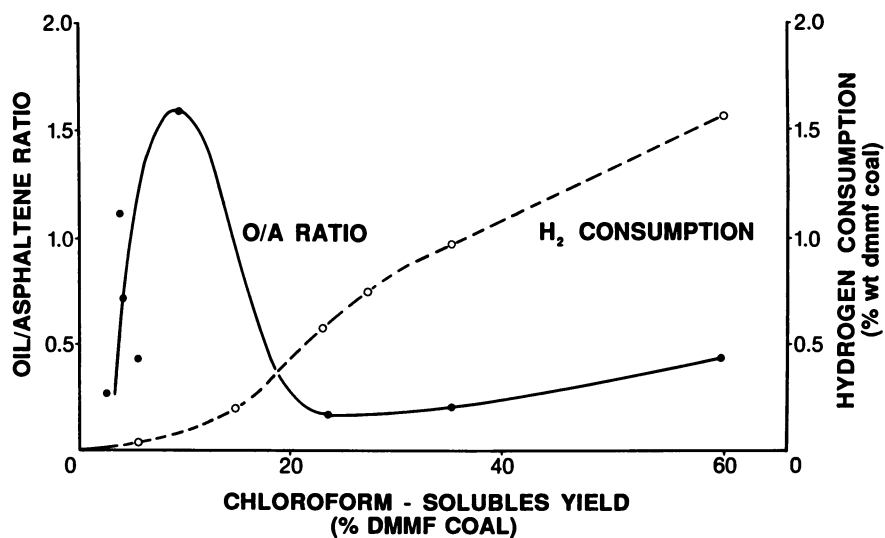


Figure 1. Relationship of H₂ consumption and O/A ratio for hvAb coal, PSOC-1266 (solvent-free hydrogenation; 400°C; 1% wt sulfided Mo; 7MPa H₂ cold).

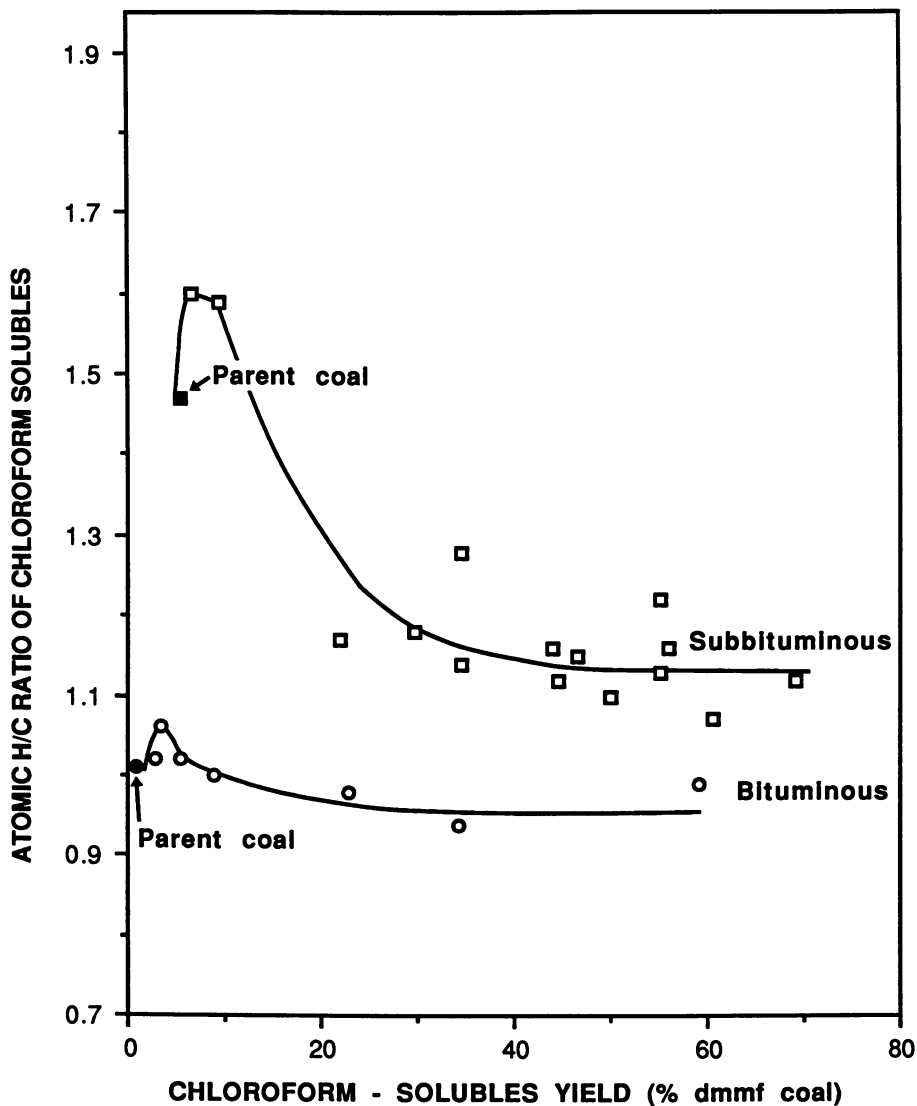


Figure 2. Variation in atomic H/C ratio *versus* chloroform-soluble yields from subbituminous (PSOC-1403) and bituminous (PSOC-1266) coals; (solvent-free hydrogenation; 300-400°C; 5-180 min; 1% wt sulfided Mo; 7 MPa H₂ cold) (data from refs 7 and 8).

aliphatic hydrogen content with chloroform-solubles yield followed a similar trend to that shown for the atomic ratio H/C.

Each of the four coals that were studied exhibited similar behavior, and in each case the three properties passed through early maximum values. Independent of the coal or the measured property, the maxima all occurred between 5-10% wt extract yield and the subsequent decreases were arrested between 20-35% extract yield. No distinction could be made on the basis of coal rank although, admittedly, the number of coals is small.

It is to be noted that the magnitude of the increase in each of the measured properties, between the initial and maximum values, was quite different for the subbituminous coal and the three bituminous coals. Examples of the increases from the initial value (determined for the chloroform-soluble extract from the parent coal) to the maximum are: the O/A ratio increased from 0.8 initial value to 8.0 maximum value for the subbituminous coal, PSOC-1403, and from 0.25 to 1.5 for the bituminous coal, PSOC-1266; the H/C atomic ratio increased from 1.46 to 1.60 for the subbituminous coal, PSOC-1403, and from 1.01 to 1.06 for the bituminous coal, PSOC-1266 (see Figure 2).

For each coal, at the maximum in hydrogen content, or H/C atomic ratio, the aliphatic hydrogen content (determined by ^1H NMR analysis) accounted for over 90% of the total hydrogen. The aliphatic hydrogen contents were 10.5% for the subbituminous coal, PSOC-1403, and 6.9% for the bituminous coal, PSOC-1266. The high aliphatic hydrogen content was associated with the presence of polymethylene chains. The early release of paraffinic material, as n-alkanes and as long chain substituents to aromatic structures, under conditions of mild pyrolysis has been observed in other research (13-15).

Over the initial period of conversion, it was also observed that only small quantities of light hydrocarbon gases were produced. The liberation of carbon oxides, principally CO_2 , was more facile. For both subbituminous and bituminous coals, the yields of CO_2 realised at 300°C were significant, although much higher for the lower rank coal (8,9).

The production of extract yields in excess of 20-35% wt marked the second stage of conversion. Over this period, the H/C atomic ratio and the total aliphatic hydrogen content remained approximately constant or decreased only gradually while the O/A ratio passed through a shallow minimum, Figure 1. The secondary gain in selectivity to oils at high conversions may represent the interconversion of asphaltenes to oils after extended reaction of the primary dissolution products. Other phenomena associated with the progress of the second

stage were that the production of light hydrocarbon gases increased, the aromaticity of the extract progressively increased and oxygen functionalities were eliminated.

Analyses of the chloroform-soluble extracts of the subbituminous coal by Fourier transform infrared spectroscopy (FTIR) showed the presence of a sharp carbonyl absorption peak ($1800-1650\text{ cm}^{-1}$) in the extracts from the parent coal and in those obtained at yields less than about 10% wt dmmf. The peak, which is attributed to ketones and carboxylates, disappeared at higher conversions (16). Whitehurst and co-workers (17) established that carbonyl-containing compounds, such as esters and carboxylates, can cleave under thermal treatment to produce CO , CO_2 and phenols. They concluded that the evolution of these gases during coal liquefaction could originate from the decomposition of similar oxygen functionalities in the coal.

Analyses of the acetylated chloroform-insoluble residues (the acetylation reaction converts aliphatic and aromatic -OH groups to esters, allowing them to be clearly distinguished from water in the FTIR spectra) showed a similar rapid disappearance of the derivatized -OH groups above about 20% chloroform-solubles yield (16).

The consumption of gaseous hydrogen mirrored the changes described above, Figure 1. For the bituminous coals at 400°C , the initial rate of hydrogen uptake was very low. With further reaction, it accelerated, passed through a maximum, and then fell to a lower, more steady value. After about 60 minutes reaction, the total consumption was about 1.5% wt dmmf coal (about 2.0% wt for the subbituminous coal). At the point of transition from the slow initial rate to the accelerating rate, the liquid yields were between 5-15% wt dmmf coal. The acceleration in hydrogen uptake coincided with the end of the first phase of conversion. At this juncture, the total hydrogen consumed was 0.1-0.2% wt. The corresponding figure for the subbituminous coal was about 0.3% wt.

The existence of two stages of conversion has been separately demonstrated in studies by Mobil R & D Corporation where, in non-catalytic solvent liquefaction, two kinetic regimes were distinguished. Initial conversion was rapid with low attendant hydrogen consumption while subsequent conversion was slower and created a much greater demand for hydrogen (18). These findings were re-confirmed in later studies by the same group, when it was further shown that the products first formed were of higher H content and more aliphatic than those generated in the second regime. These observations are illustrated in Figure 3 which shows the change in hydrogen type distribution in the heptane insoluble liquefaction products of a subbituminous coal as a function of a reaction severity parameter (19). The latter is a

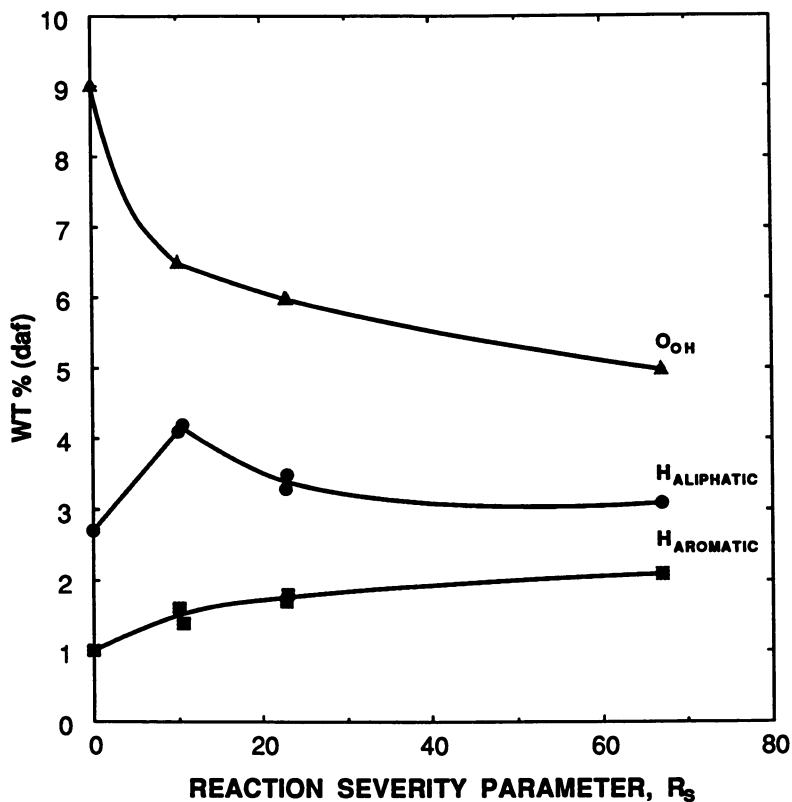


Figure 3. Change in H_{AL} , H_{AR} and O_{OH} with reaction severity (ref. 19: subbituminous coal;) heptane-insoluble product fraction.

composite time-temperature function which was employed to smoothe the effect of temperature fluctuations in short reaction time experiments: maximum duration 6 min. at temperatures up to 460°C. The same research also showed that CO₂ was quickly evolved during liquefaction and that the subbituminous coal consumed more hydrogen than a bituminous coal at the same level of conversion.

The foregoing observations have direct implications to coal structure. In the present work, the production of liquids is facile below about 15% liquids yield and requires little hydrogen consumption. The processes most probably involve the release of species which are physically trapped or are weakly bonded to the insoluble matrix. At high conversions, the products are derived from the breakdown of the macromolecular network. This phase of conversion requires the cleavage and stabilisation of strong bonds, thereby creating an appreciable demand for hydrogen.

The products formed during the two stages are quite different in composition which can account for the rather dramatic swings observed in the extract properties with increasing conversion. The materials first liberated are hydrogen-rich and aliphatic which causes the initial increase in O/A ratio, H/C atomic ratio and aliphatic hydrogen content. Later, as these products are progressively diluted by the addition of more aromatic species emanating from the network, the values of these same measured properties pass through maximum values and subsequently decrease.

FLUORESCENCE MICROSCOPY

The phenomenon of vitrinite fluorescence has been described for 76 humic and vitrinitic materials with levels of organic maturation ranging from peat to low volatile bituminous coal (5,6). Figure 4a shows that fluorescence intensity decreases sharply through the series peat - peat/lignite transitional materials - lignite - subbituminous coal. The so-called primary fluorescence within this range is believed to be due to the presence of fluorophors derived from biopolymers, especially lignin. A second peak in fluorescence intensity (Fig. 4b) commences at about subbituminous rank, is reached in coals with a vitrinite maximum reflectance of about 0.9%, and is largely lost by medium volatile bituminous rank. This "secondary fluorescence" is attributed mainly to the presence of the mobile phase, a conclusion which is supported by a notable parallelism among the trends, in this rank range, of fluorescence intensity, chloroform-solubles yield and Gieseler maximum fluidity (5). The spectral distributions of the secondary fluorescence emissions undergo a red shift due to the

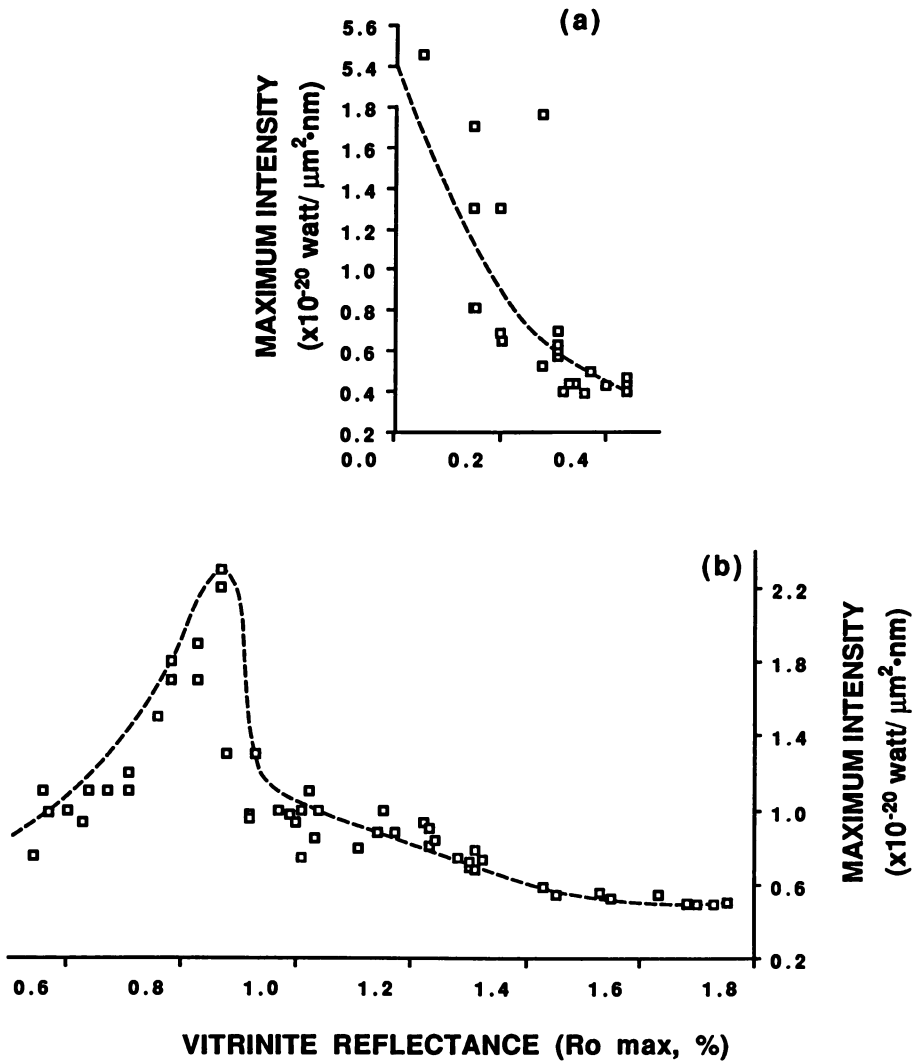


Figure 4. Primary and secondary vitrinite fluorescence (absolute units): (a) primary fluorescence in U-V irradiation, (b) secondary fluorescence in blue-light irradiation.

increasing conjugation of double bonds which accompanies coalification.

After chloroform extraction, coals still demonstrate low levels of residual fluorescence interpreted as being due to entrapped portions of the mobile phase. In Figure 5 the yields of extracts obtained from varying extraction times are plotted against the subsequently determined fluorescence intensity. The figure also shows that mild thermal pretreatment (350°C for 3 min.; N₂ atmosphere) considerably enhanced the intensity of fluorescence and that this was then entirely removed by extended chloroform extraction (6). Apparently the heat treatment disrupts the bonding between the network system and the mobile phase, resulting in increased yield; with reduced energy transfer between the two phases, there is less possibility for intermolecular quenching, so that fluorescence intensity is enhanced.

Brown and Waters (20) showed that the yield of chloroform-soluble extract could be increased several-fold by coal pretreatment which involved rapid heating and cooling. The liberation of additional extract by this means is identical to the situation described above. The enhanced yields reported by Brown and Waters are also of the same order as those corresponding to the initial conversion stage in the catalytic hydrogenation experiments. As this first stage incurred little or no net consumption of hydrogen external to the coal, it is believed that the effects of preheating and of low severity catalytic hydrogenation are equivalent. Brown and Waters concluded that the material derived by preheating was originally present as such in the coals and was not a product of pyrolysis. This is more or less the same definition of the mobile phase as it is understood in the present research.

Just as the untreated bituminous coals showed a parallelism among chloroform-solubles, vitrinite fluorescence intensity and Gieseler plasticity, the products of a single hvAb coal (PSOC-1510), hydrogenated for varying reaction times with a sulfided molybdenum catalyst, showed similar interrelations (Fig. 6). These results, together with the observation that chloroform-extracted coals lose their capability to become thermoplastic (21), are convincing evidence that the mobile phase is a necessary agent in promoting fluid behaviour.

Chloroform extraction of the whole products of dry hydrogenation (400°C; 60 min; 5% Mo; 7 MPa H₂) of PSOC-1266 produced a strongly fluorescent extract and non-fluorescent residue. After drying, the extract was seen under the microscope to contain two components with distinctive fluorescence characteristics (Fig. 7). Component 1 had a fluorescence spectrum very similar to that of the oil (hexane-soluble) fraction of the same

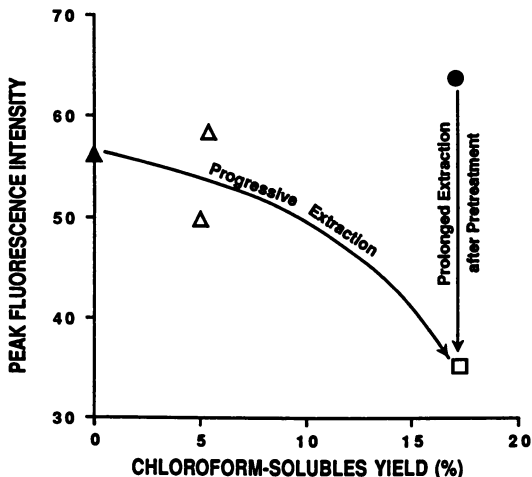


Figure 5. Peak fluorescence intensity of raw (▲) and extracted (Δ) vitrinites versus yield of chloroform extractables. Also shown are data for thermally pretreated vitrinite before (●) and after (□) prolonged chloroform extraction. (Data are from ref. 7.)

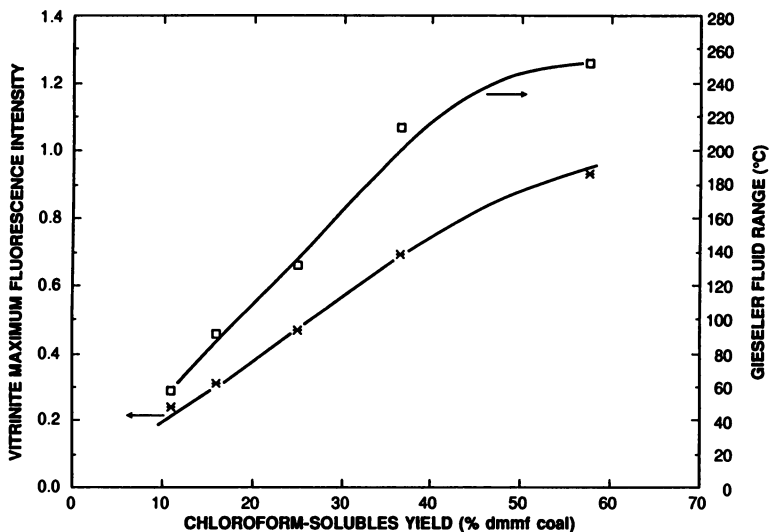


Figure 6. Relations among fluorescence intensity, chloroform-solubles yield and Gieseler plasticity for hydrogenated coal (PSOC-1510; solvent-free hydrogenation, 400 °C; 5-60 min; 1% wt sulfided Mo; 7 MPa H₂ cold).

hydrogenation products; component 2 had a spectrum like that of the corresponding asphaltene fraction which, in addition to a higher peak wavelength, had a very much lower fluorescence intensity than the oil fraction. The observed differences in the fluorescence characteristics of the oil and asphaltene fractions are believed to be due to the more highly condensed materials which constitute the latter.

As reaction conditions became more severe, the fluorescence spectra of the hydrogenated vitrinite underwent a red shift (Fig. 8) from around 600 nm at 350°C to around 680 nm at 400°C. The trend is believed to be due to the production of a higher proportion of asphaltenic material from the vitrinite network, as shown earlier by the reduction in O/A ratio with increasing conversion.

SYNOPSIS

The liquefaction behaviour of the four coals investigated allows a general definition of the mobile phase as that material which is readily liberated by mild thermal treatment. The mobile phase components are richer in hydrogen and significantly more aliphatic than the structural units which comprise the network. The latter are connected by much stronger bonds, necessitating more severe reaction and higher hydrogen consumption to secure their release. The compositions of the mobile phase and network are also dependent upon coal rank.

Fluorescent light microscopy distinguishes between the extractable liquids, which fluoresce strongly, and the matrix, which does not. The disruption of weak bonding effected by thermal treatment, which increased the extract yield, was paralleled by changes in fluorescence intensity. The fluorescence spectra of the extracts also reflect the compositional differences between the mobile phase and the solubilised coal network.

Based upon solubility in chloroform, the mobile phase is estimated to constitute 5-15% wt of the coal. Obviously, this amount will vary if other characterising solvents are used.

It is to be expected that there will be a gradation in the manner in which the smaller molecules are associated with the network. This may involve both physical and chemical forces such as covalent bonds, dispersion forces and hydrogen bonding, and could involve physical entrapment. It is doubtful whether any single technique can distinguish between these different modes of attachment sufficiently clearly to establish a precise boundary. Different energies will be required to disrupt the different types of attachment. It may be significant

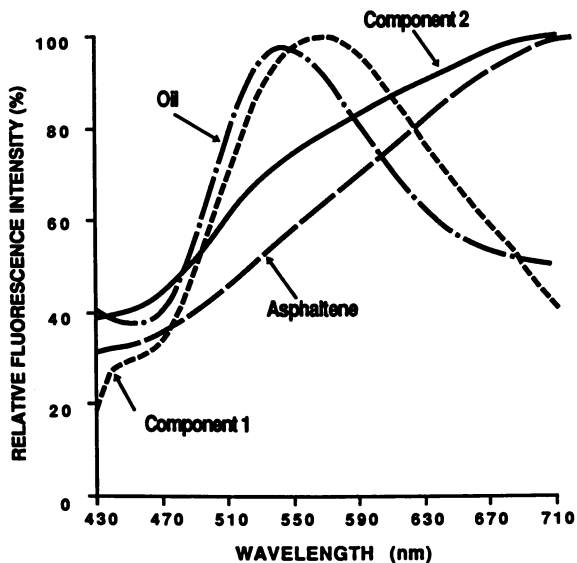


Figure 7. Comparison of fluorescence spectra of two components in chloroform-solubles fraction with oil and asphaltene fractions of hydrogenated coal (PSOC-1266; solvent-free hydrogenation; 400°C; 60 min; 5% wt sulfided Mo; 7 MPa H₂ cold).

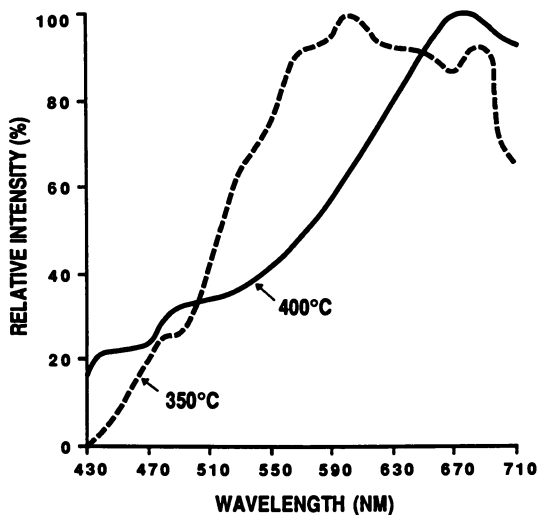


Figure 8. Fluorescence spectra of vitrinite following hydrogenation at 350 and 400°C (PSOC-1266; solvent-free hydrogenation; 60 min; 5% wt sulfided Mo; 7 MPa H₂ cold).

that Brown and Waters (16) found that the increase in chloroform-soluble yield upon coal preheating was dependent upon the pretreatment temperature. A minor peak in the yield was observed at temperatures in the region of 300°C and a second, major one at 400-450°C.

The particular experimental studies, which have been described here, have provided a basis for a practical definition of the boundary of the mobile phase in coals, and some tentative clues to the nature of its association with the network. Inevitably, other research techniques will bring different perspectives.

ACKNOWLEDGMENTS

The authors wish to acknowledge Peter Stansberry and Maite Terrer whose individual and collaborative research work contributed substantially to this paper.

LITERATURE CITED

1. Given, P.H. Prog. Energy Combust. Sci. 1984, 10, 149-158.
2. Given, P.H.; Marzec, A.; Barton, W.A.; Lynch, L.J.; Gerstein, B.C. Fuel 1986, 65, 155-164.
3. Derbyshire, F.J. and others Fuel 1989, 68, 1091-1106.
4. Davis, A.; Derbyshire, F.J.; Finseth, D.H.; Lin, R.; Stansberry, P.G.; Terrer, M.T. Fuel 1986, 65, 500-506.
5. Derbyshire, F.J.; Davis, A.; Lin, R.; Stansberry, P.G.; Terrer, M. T. Fuel Proc. Tech. 1986, 12, 127-141.
6. Lin, R.; Davis, A.; Bensley, D.F.; Derbyshire, F.J. Int. J. Coal. Geol. 1986, 6, 215-228.
7. Lin, R.; Davis, A.; Derbyshire, F.J. Org. Geochem. 1987, 11, 393-399.
8. Derbyshire, F.J.; Terrer, M. T.; Davis, A.; Lin, R. Fuel 1988, 67, 1029-1035.
9. Stansberry, P.G.; Derbyshire, F.J. The Mobile Phase in Coals: Its Nature and Modes of Release, Final Report Part 3, DOE-PC-60811-F3 to the United States Department of Energy. 1988, 223 pp.
10. Derbyshire, F.J.; Stansberry, P.G. Fuel 1987, 66, 1741-1742.
11. Snape, C.E.; Derbyshire, F.J.; Stephens, H.P.; Kottenstette, R.J.; Smith, N.W. Preprints, Am. Chem. Soc., Div. Fuel Chemistry 1989, 34, (3), 793-802.
12. Derbyshire, F.J. Technical Progress Report to US Dept. of Energy. Period Sept. 1985 - Feb. 1986. DOE-PC-60811-9, 10 1986, 30 pp.
13. Snape, C.E.; Ladner, W.; Bartle, K.D. Fuel 1985, 64, 1394-1400.

14. Youtcheff, J.S.; Given, P.H.; Baset, Z.; Sundaram, M.S. Org. Geochem. 1983, 5, 157-164.
15. Calkins, W.H.; Tyler, R.J.; Fuel 1984, 63, 1119-1124.
16. Terror, M.T.; Derbyshire, F.J. The Mobile Phase in Coals: Its Nature and Modes of Release, Final Report Part 1, DOE-PC-60811-F1 to the United States Department of Energy 1986, 113 pp.
17. Whitehurst, D.D.; Farcasiu, M.; Mitchell, T.O.; Dickert, J.J. The Nature and Origin of Asphaltenes in Processed Coals, Electric Power Research Institute Report AF-480 1977.
18. Whitehurst, D.D.; Farcasiu, M.; Mitchell, T.O.; Dickert, J.J. The Nature and Origin of Asphaltenes in Processed Coals, Electric Power Research Institute Report AF-1298 1979.
19. Derbyshire, F.J.; Odoerfer, G.A.; Rudnick, L.R.; Varghese, P.; Whitehurst, D.D. Fundamental Studies in the Conversion of Coals to Fuels of Increased Hydrogen Content, Electric Power Research Institute Report AP-2117. 1981.
20. Brown, H.R.; Waters, P.L. Fuel 1966, 45, 17-39.
21. Dryden, I.G.C.; Pankhurst, K.S. Fuel 1955, 34, 363-366.

RECEIVED November 5, 1990

Chapter 8

Mobile Phase in Coal Viewed from a Mass Spectrometric Perspective

Yongseung Yun¹, Henk L. C. Meuzelaar¹, Norbert Simmleit²,
and Hans-Rolf Schulten³

¹Center for Micro Analysis and Reaction Chemistry, University of Utah,
Salt Lake City, UT 84112

²Chemical and Biological Laboratories, Institut Fresenius, D-6204
Taanusstein-Neuhof, Germany

³Department of Trace Analysis, Fachhochschule Fresenius, Dambachtal 20,
6200 Wiesbaden, Germany

Seven Argonne Premium coal samples ranging from lignite to low volatile bituminous in rank were analyzed by Pyrolysis-Field Ionization Mass Spectrometry (Py-FIMS) in order to determine the existence and structural nature of a thermally extractable "mobile phase". In addition, Curie-point Pyrolysis-Low Voltage Mass Spectrometry (Py-LVMS) was employed to demonstrate the importance of mild oxidation on the thermally extractable mobile phase components.

Py-FIMS results clearly reveal the existence of a thermally extractable, bitumen-like fraction which is chemically distinct from the remaining coal components. In lignite, several biomarker compounds were noticeable in the mobile phase components while bituminous coals contain various alkylsubstituted aromatic compounds in the mobile phase. Blind Canyon coal, which contains 11% resinite, exhibits mobile phase components believed to originate from terpenoid aromatization. Curie-point Py-LVMS results illustrate the importance of the oxidation status of coal for studying the mobile phase since mild air oxidation severely changes the structural characteristics of the thermally extractable mobile phase.

In recent years few topics have generated a more spirited discussion among coal scientists than the issue of the putative binary (mobile + network) phase nature of coals (1). Initially based on NMR observations (2), the concept of a "mobile phase" in coal soon came to encompass a broad range of more or less readily extractable and/or distillable lower molecular weight (MW) components, variously referred to as "guest molecules" (3), "clathrates" (1,4) or simply, and perhaps most succinctly, "bitumen" (5).

None of these terms appears to be completely satisfactory. The concept of "mobility" in NMR spectroscopy is quite different from that in the field of separation science, where mobility generally requires a measurable degree of solubility and/or distillability in liquid or gaseous media, respectively. For example, polymethylene-like moieties, such as found in some coal components (6), are highly "mobile" in NMR terms (1), without necessarily being extractable by solvents or distillable by nondestructive heating.

The term "guest molecules", originally introduced to indicate specifically labeled marker molecules used in NMR studies of coal (7), is equally unsatisfactory for mobile phase components indigenous to the coal itself. Also, there appears to be insufficient evidence for the presence of sizeable quantities of true "clathrates" to rule out other possibilities, e.g., strong noncovalent bonding rather than physical entrapment.

Finally, completely equating the "mobile phase" with solvent (e.g. pyridine) extractable "bitumen" in coal ignores the potential presence of colloidal particulate matter in the pyridine extracts as well as possible solvent-induced scission of weak chemical bonds. Furthermore, the solvent-extractable fraction may well include macromolecular components, such as resinates.

Mass spectrometric observations have thus far played a rather limited role in the "mobile phase" discussions (1) but are starting to shed some light on the key question: is there conclusive evidence for the presence of a chemically and/or physically distinct "mobile phase", as opposed to a continuum of possible molecular sizes and structures?

If the mobile phase is present in a significant concentration, as suggested by the results of solvent extraction studies (1,8), the practical meaning of the mobile phase to coal conversion processes may be profound. In coal liquefaction, two stage processes emphasizing the mobile phase and the macromolecular structure separately could well be most economical. In devolatilization kinetics, at least two sets of kinetic parameters are necessary to model the devolatilization phenomena associated with the mobile phase and the macromolecular structure respectively since the mobile phase components devolatilize at much lower temperatures than the macromolecular structure components (9). In addition, the mobile phase appears to have a significant influence on the thermoplastic properties of coal (5) and thereby on coke quality.

In the context of the present discussion the term "mobile phase" will be used to describe those components which can be thermally extracted ("distilled", "desorbed") under vacuum at temperatures below the thermal degradation range of the coal. The residue, designated as the nonmobile ("network") phase, is thermally degraded in the pyrolysis temperature range. Of course, the onset of pyrolysis may vary considerably, depending on heating rate, rank and coal type (10).

Experimental

Seven ANL-PCS (Argonne National Laboratory - Premium Coal Sample) coals were analyzed by Py-FIMS in time resolved (TR) mode. Conventional characterization data on ANL-PCS coals have been described elsewhere (11). About 100 μg of -100 mesh coal were transferred into a quartz crucible and introduced into the high vacuum (10^{-3} Pa) of the ion source (200°C). The instrumental setup using a Finnigan

MAT 731 double-focussing mass spectrometer, a combined EI/FI/FD/FAB ion source and an AMD Intectra direct introduction system, has been previously described in detail (12). The samples were heated linearly from 50 °C to 750 °C at a rate of 100 K/min. In general, 35 FI mass spectra were recorded in the m/z 50-900 mass range.

In addition, a coal sample was obtained from a fresh channel-cut in the Hiawatha seam in Emery County (Utah) and immersed in water prior to being crushed and milled to <60 mesh in a nitrogen atmosphere and subsequently analyzed by Curie-point pyrolysis low voltage electron ionization mass spectrometry (Py-LVMS) in TR mode. Proximate analysis of Hiawatha coal (hvBb) was 41.42% VM, 42.38% FC, 12.75% ash, 3.45% moisture. In the laboratory oxidation experiment on Hiawatha coal, a 15 g sample of coal was exposed to continuous dry air flow of 80 ml/min through the sintered glass frit distributor at the bottom of the Pyrex glass reactor (104 mm in length and 37 mm o.d.) at 100 °C for 212 h.

The Py-LVMS experiment was performed using an Extranuclear 5000-2 Curie-point Py-MS system. The coal sample was hand ground into a fine, uniform suspension in Spectrograde methanol (5 mg of sample per ml of methanol). A single 5 μ l drop of the suspensions was coated on the ferromagnetic filament (Curie-point temperature 610 °C) and air-dried under continuous rotation for approximately 1 min, resulting in 25 μ g of dry sample on the filament. The filament was inserted into a borosilicate glass reaction tube and introduced into the vacuum system of the mass spectrometer. Directly in front of the open, cross beam type electron ionization chamber the ferromagnetic wire was inductively heated for 6 s at a rate of approximately 100 K/s to an equilibrium temperature of 610 °C (as determined by the Curie-point temperature of the wire). Other MS conditions were as follows: electron impact energy 20 eV, mass range scanned 50-200 amu, scanning rate 1000 amu/s, number of scans 41, total scan time 8 s.

The resulting Py-LVMS spectra were subjected to factor analysis after spectrum calibration. The variance diagram (VARDIA) technique (13) was used to determine the major components showing different time profiles. The major chemical components were visualized in the form of so-called "factor spectra" using the procedure described by Windig *et al.* (14).

Results and Discussion

Is there a chemically and/or physically distinct "mobile phase" in coal as opposed to a continuum of molecular sizes and structures? The temperature-resolved total ion intensity (TII) profile of a Pittsburgh #8 coal in Figure 1 obtained by temperature programmed Py-FIMS shows the presence of a low temperature "hump" which appears to explain 25-30% of the total integrated FI signal intensity in the mass range m/z 50-900. Previously, Chakravarty *et al.* (15) reported a similar profile for Pittsburgh #8 coal obtained by Curie-point pyrolysis in combination with time-resolved low voltage electron ionization (EI) MS and were able to demonstrate that the low temperature hump consisted primarily of homologous series of alkylsubstituted aromatic (e.g., benzenes, naphthalenes, phenanthrenes) and hydroaromatic (e.g., tetralins) compounds. These compounds were interpreted to

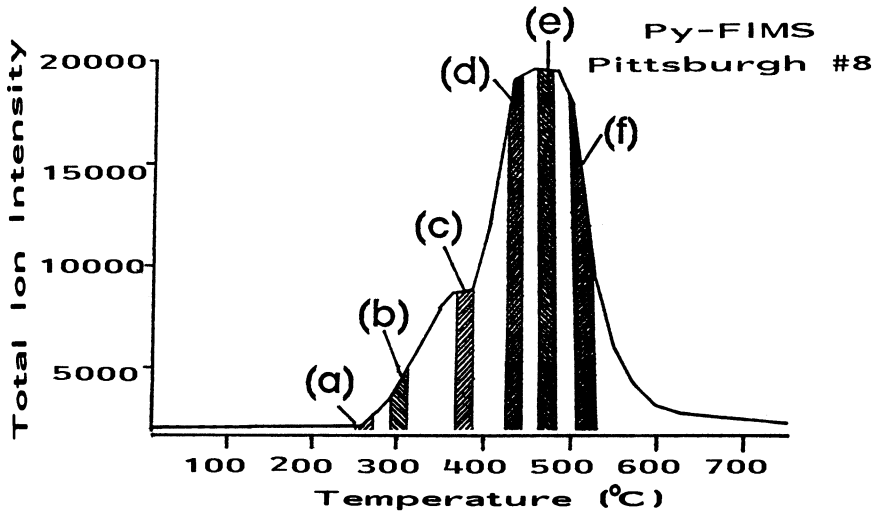


Figure 1. Thermogram of a Pittsburgh #8 coal sample. Crosshatched intervals a-f correspond to molecular weight profiles of FI ions in Figures 3a-f, respectively.

represent the thermally extractable ("vacuum distillable") fraction of the well known "bitumen" component of most high volatile bituminous coals.

More recently, Yun *et al.* (16) confirmed the presence of this low temperature hump in vacuum thermogravimetry (TG)/MS studies of ANL-PCS coals using low voltage EIMS. An important aspect of the latter study was that the mass spectra obtained for the thermally extractable components as well as for the main pyrolysis event were found to be virtually indistinguishable from those observed by Chakravarty *et al.* using Curie-point Py-LVMS, notwithstanding a 5 orders of magnitude lower heating rate (3.3×10^{-2} K/s vs. 1.5×10^3 K/s) and 3 orders of magnitude larger sample (50 mg vs. 25 μ g).

Furthermore, with proper preheating of the transfer zone between pyrolysis and ionization regions, the low voltage EI mass spectra of Pittsburgh #8 coal were shown to be highly similar to the corresponding FI mass spectra in the m/z 50-350 mass range when allowing for known differences in ion transmissivity between the different types of mass spectrometers used (9). In other words, time-resolved TII profiles similar to those shown in Figure 1 as well as to the corresponding mass spectra in Figure 2a have been observed (up till m/z 350) by means of 3 separate Py-MS methods, together covering a broad range of different pyrolysis, ionization and mass spectrometric detection techniques.

The advantages of the FIMS data shown here are that little or no fragmentation of molecular ions occurs during the ionization process and that FI response factors for aromatic and hydroaromatic compounds tend to show relatively little variation (17). In combination with the large mass range and nearly constant ion transmissivity of the magnetic sector instrument used, the FI ion profiles and FI spectra shown in Figures 1 and 2, respectively, are suited for making reliable semiquantitative estimates with regard to the relative yield and molecular weight distribution of coal tar fractions consisting primarily of aromatic and hydroaromatic or alicyclic compounds. Unfortunately, FI response factors for aliphatic compounds show a great deal more variation (18). Consequently, for the purpose of this discussion no attempt will be made to quantitate the contributions or molecular weight distributions of aliphatic components in spite of their well recognized role in coal pyrolysis processes.

Figure 2b clearly show that the alkylsubstituted naphthalenes start to appear at relatively low temperature although the spectrum only accounts for 0.3% of TII. Comparison of the intermediate temperature component ("mobile phase") and high temperature component ("bulk pyrolyzate") spectra in Figures 2c and 2d, respectively, reveals roughly similar average molecular weights ($\bar{M}_n \sim 335$) but rather different MW distributions. Moreover, there are pronounced differences in relative FI signal intensities, especially in the mass range up to m/z 400.

Figure 3 shows the relationships between the temperatures and molecular weight distributions for 6 successive regions of the TII profile in Figure 1. Interestingly, regions a, b and c, primarily representing the low temperature components, show relatively narrow MW distributions around \bar{M}_n values which markedly increase with temperature. This is consistent with the proposed interpretation of the low temperature "hump" as a vacuum desorption and distillation process rather than as a pyrolytic process. By contrast, regions d, e and f, representing the major TII maximum in Figure 1, exhibit much broader MW

Pittsburgh #8 (83.2% C)

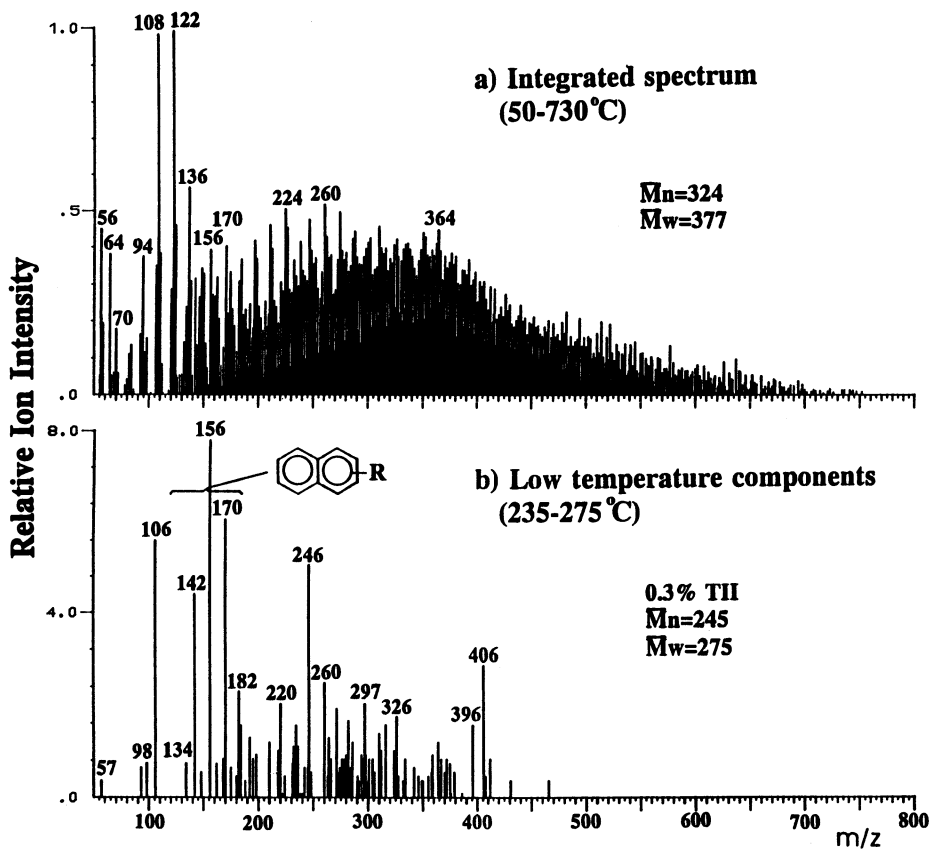


Figure 2. Comparison of Pittsburgh #8 (hvb) coal Py-FI mass spectra recorded over different temperature intervals.

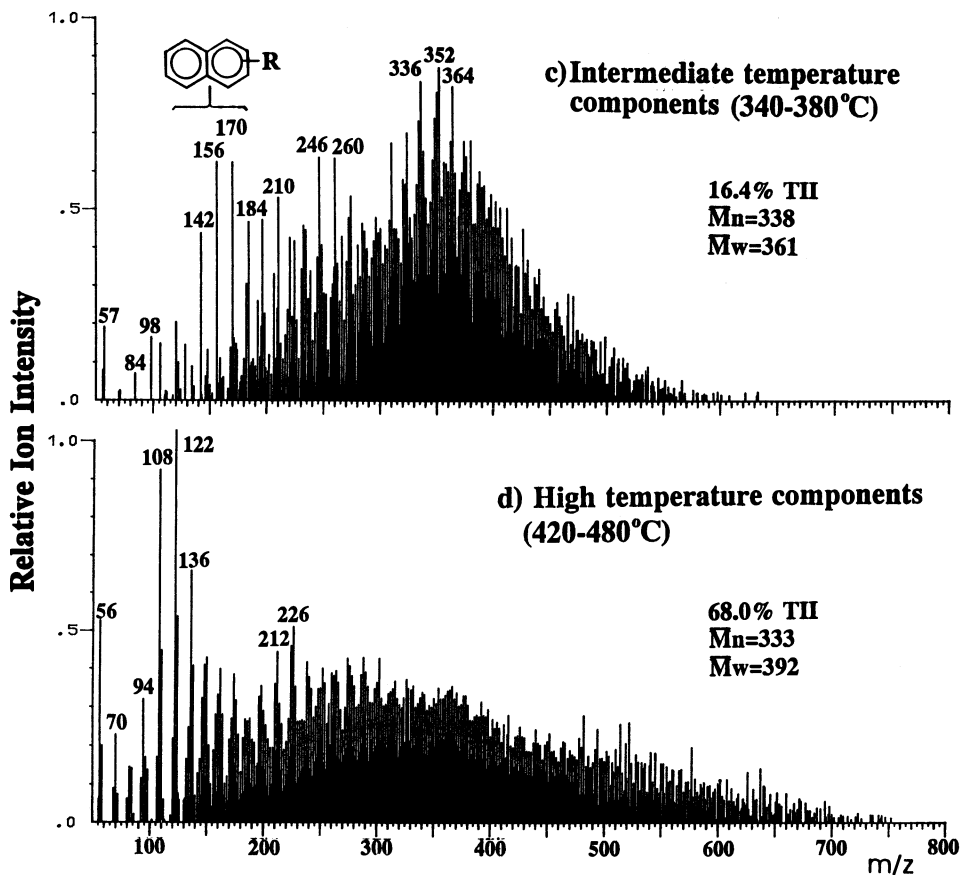
Pittsburgh #8 (83.2% C)

Figure 2. Continued.

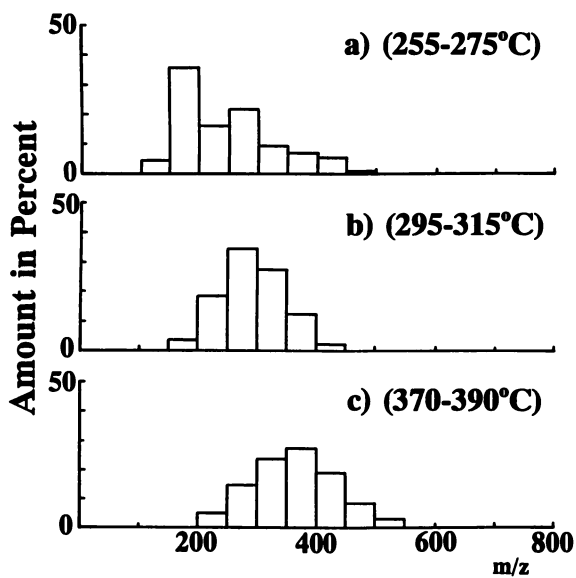


Figure 3. Molecular weight distributions of pyrolyzates in six successive temperature intervals during Py-FIMS analysis of Pittsburgh #8 coal.

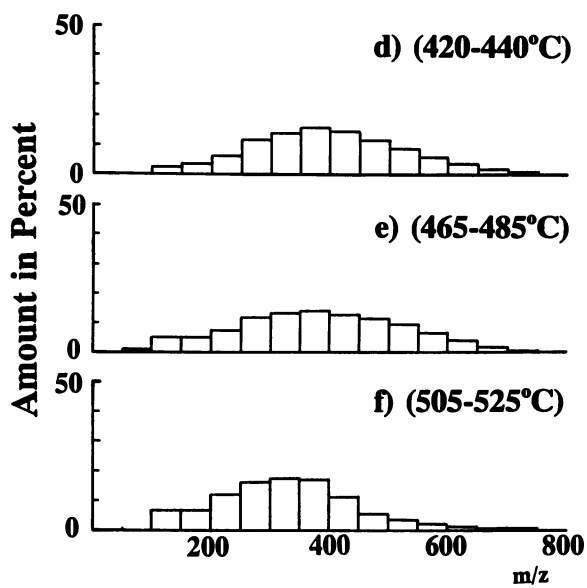


Figure 3. Continued.

distributions characterized by a gradually decreasing average molecular weight of the pyrolyzate. This would seem to be consistent with the proposed interpretation of the major TII peak as the "bulk pyrolysis" event (15).

The transition between c and d is rather abrupt, suggesting that we may indeed be witnessing contributions from two more or less discrete populations of molecules with regard to molecular size distributions. However, in view of the extremely complex interplay between intramolecular and intermolecular, as well as intraparticle and extraparticle, parameters in the experiments described here, the possible presence of a continuum of molecular sizes can certainly not be ruled out at this point.

More informative, perhaps, are the marked differences in relative FI signal intensities between the mass spectra shown in Figures 2c and 2d. In agreement with the previously mentioned results reported by Chakravarty *et al.* (15) and Yun *et al.* (16), the mass spectra of the low temperature component (Figures 2b and c) appear to be dominated by homologous series of aromatic and hydroaromatic compounds. Chemical identification of many of the compounds up to MW 350 has been accomplished by high resolution GC/MS (19, 20), although precise identification of the many possible isomeric structures involved will have to await the availability of suitable reference compounds.

The spectrum of the bulk pyrolysis event in Figure 2d appears to be dominated by hydroxy aromatic compounds, e.g., alkylsubstituted phenols and naphthols. Positive identification of these compounds is much less straightforward, although a surprisingly high degree of correspondence can be found with Py-GC/MS data on Pittsburgh #8 coal (21). Moreover, Chakravarty *et al.* (15) have demonstrated that the main pyrolysis event can be deconvoluted into at least three overlapping events involving vitrinitic moieties in addition to alginite/cutinite-like and sporinite-like components.

In Curie-point Py-LVMS studies of maceral concentrates (22), vitrinitic moieties were shown to be the main source of the hydroxy aromatic components. Thus, the hydroxy aromatic signals observed in Figure 2d appear to be primarily derived from vitrinite-like components by means of pyrolytic processes. Presumably, therefore, the "nonmobile phase", rather than the "mobile phase", is the main source of the phenols observed in TG/MS and Py-MS studies of Pittsburgh #8 coal (9, 16). Further support for this conjecture comes from the observation that phenolic products are also observed in Py-MS analysis of pyridine extracts of Pittsburgh #8 coal known to contain colloidal matter whereas the corresponding tetrahydrofuran extracts, free of colloidal material, produced no phenols (21).

In low-rank coals, such as lignites, vitrinitic components have been shown to produce abundant (alkyl) dihydroxy benzene and methoxy hydroxy benzene compounds of a structural type which can be traced back to fossil lignin moieties (23). In agreement with these earlier studies, the high temperature component spectrum of a Beulah-Zap lignite (Figure 4d) exhibits dominant (alkyl) dihydroxy benzene signals at m/z 110, 124, and 138. The low abundance of FI signals above m/z 200 can be attributed to the more highly crosslinked nature of the macromolecular network phase than the mobile phase in lignites.

As shown in Figures 4b and 4c, the low temperature fraction of Beulah-Zap lignite reveals a completely different type of mass spectrum. From previous studies

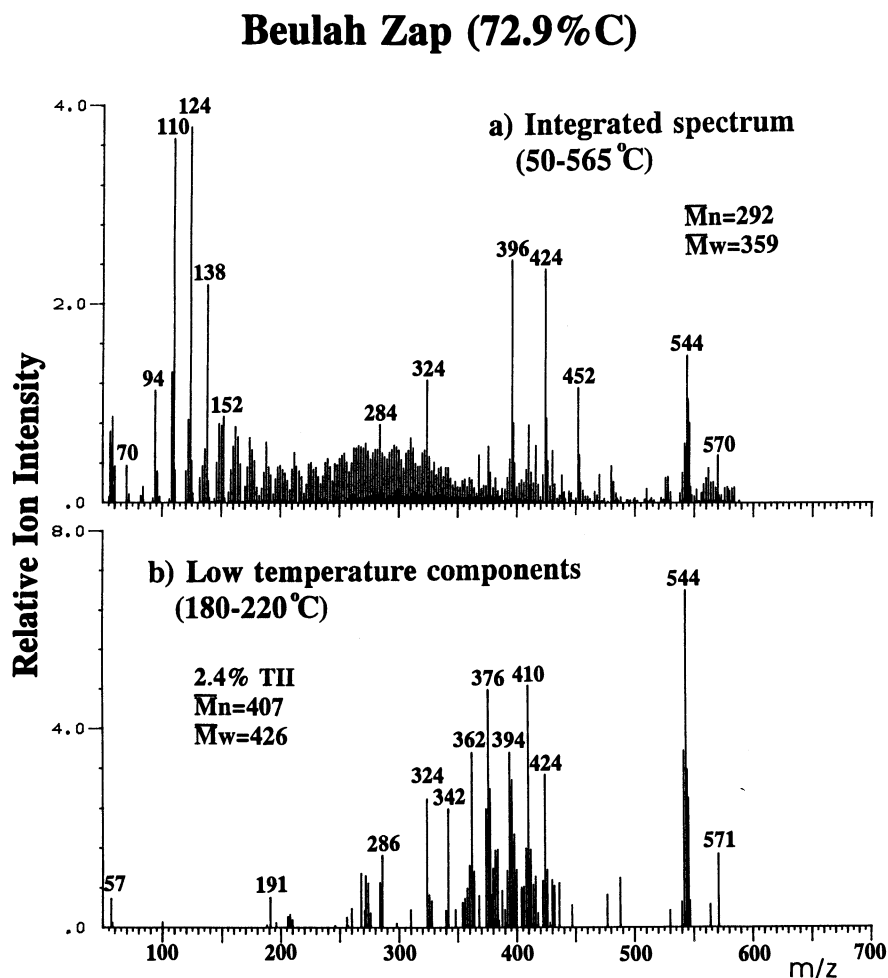


Figure 4. Comparison of Beulah-Zap lignite Py-FI mass spectra recorded over different temperature intervals.

Continued on next page

Beulah Zap (72.9% C)

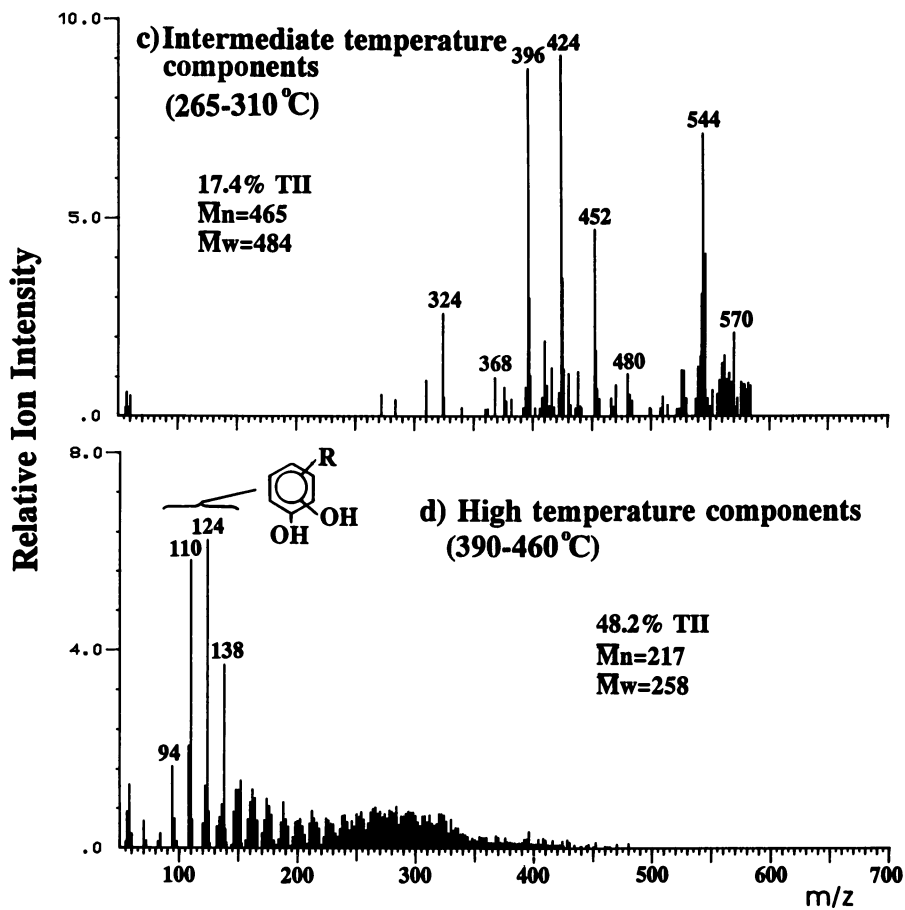


Figure 4. Continued

on soil organic matter by Hempfling *et al.* (24), the FIMS signals in Figures 4b and 4c are known to represent various plant-derived compounds such as n-fatty acids or monomeric esters (m/z 368, 396, 424, 452, 480) and aromatic diesters (m/z 544). Apparently, we are dealing with thermally extractable "biomarker" compounds which have not yet been linked into the macromolecular network phase of the lignite. Furthermore, Figure 4b reveals that the mobile phase in Beulah-Zap lignite contains diterpenoids/pentacyclic hopanes, which was confirmed by the existence of the biomarker at m/z 191.

Figures 5-7 are the spectra exhibiting the thermally extracted mobile phase components over different temperature intervals. All five coals mentioned in Figures 5-7 show distinct mass spectra in the mobile phase compared to the spectra of the macromolecular structure (25) and contain alkylsubstituted naphthalenes in the mobile phase although their relative amounts are dependent on coal characteristics. In general, T_{max} (the temperature where the maximum rate occurs) in Py-FIMS was in the range of 430-470 °C for bituminous rank coals. Around T_{max} , the macromolecular structure of bituminous rank coals is decomposed to yield FI spectrum showing the dominant peaks of alkylsubstituted phenols. Detailed FI spectra of the macromolecular structure for the ANL-PCS coals mentioned in Figures 5-7 are illustrated elsewhere (25).

Illinois #6 at 215-275 °C range exhibits homologous series at m/z 142, 156, 170, 184, 198 (alkylsubstituted naphthalenes), m/z 182, 196, 210, 224, 238 (probably alkylsubstituted tetrahydrophenanthrenes/tetrahydroanthracenes) and m/z 232, 246, 260, 274, 288 (appear to be steranes (26)).

Mobile phase spectra of Blind Canyon coal look rather similar to Beulah-Zap lignite coal with regard to the peaks at m/z 324, 342, 424. Alkylsubstituted naphthalenes components are clearly separated and the other dominant peaks at m/z 310, 324, 342, 356 are believed to originate from triterpenoid aromatization (26). The mass spectra of Blind Canyon coal, which contains 11% resinite, illustrate the importance of depositional environment as well as of rank in determining the components in the mobile phase.

Lewiston-Stockton coal contains the least amount of alkylsubstituted naphthalenes in the mobile phase among six coals except Beulah-Zap lignite coal from the fact that Figure 6a represents only 0.03% of TII. In contrast, Pittsburgh #8 coal appears to contain the largest amount of alkylsubstituted naphthalenes. Lewiston-Stockton coal also appears to contain steranes in the mobile phase as represented by homologous series of m/z 232, 246, 260.

Interestingly, Upper Freeport coal shows two distinct mass spectral patterns in 230-270 °C range (Figure 6c), which contains homologous series at m/z 156, 170, 184, 198 (alkylsubstituted naphthalenes), m/z 216, 230, 244, 258 as well as dominant peaks at m/z 392, 408, 446, 462. The exact structural nature of these peaks needs more scrutiny by GC/MS or high resolution Py-FIMS.

Low volatile bituminous Pocahontas #3 coal shows different early mobile phase components in terms of alkylsubstituted benzenes (m/z 92, 106, 120) and further shows similar components (several homologous ion series) compared to medium volatile bituminous Upper Freeport coal (e.g. at m/z 192, 206, 220, 234; m/z 216, 230, 244, 258; and m/z 266, 280, 294). From the above observations on seven coals, it is clear that there is a chemically and/or physically distinct mobile phase, at

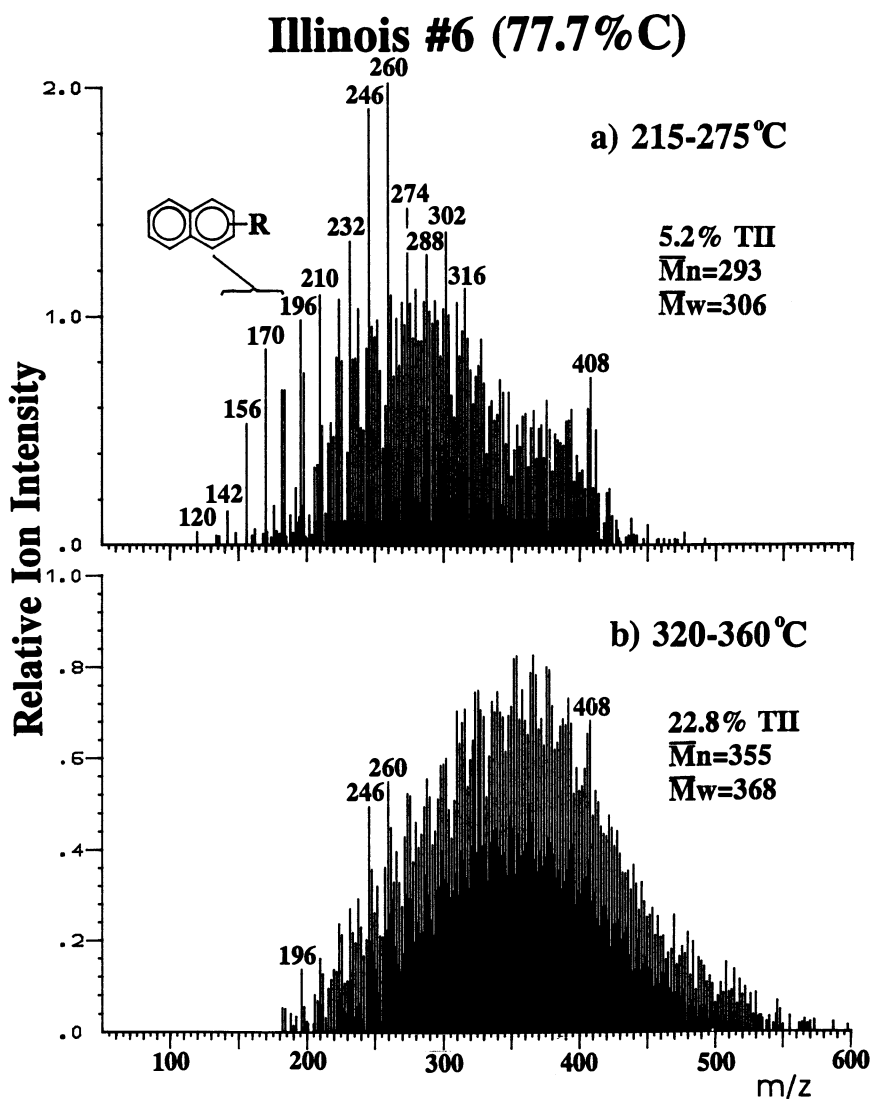


Figure 5. Thermally extracted mobile phase components over different temperature intervals from Illinois #6 and Blind Canyon coals.

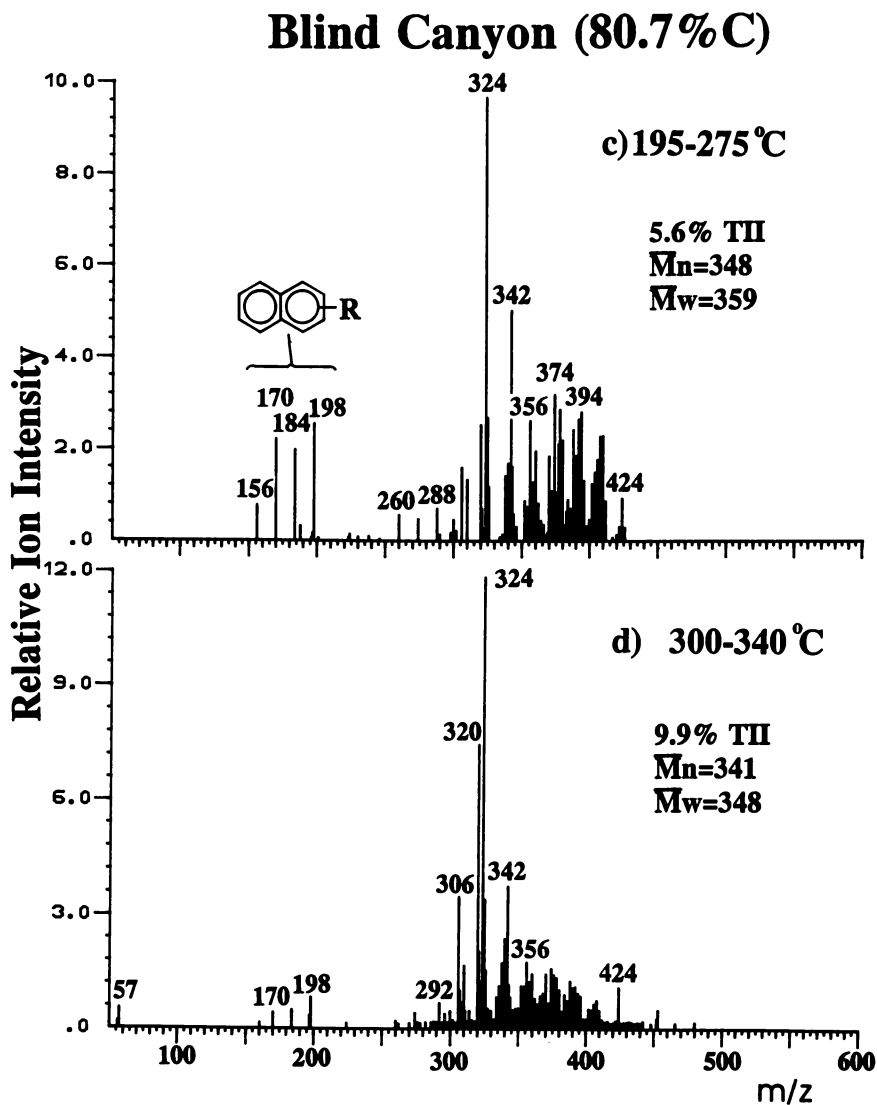


Figure 5. Continued

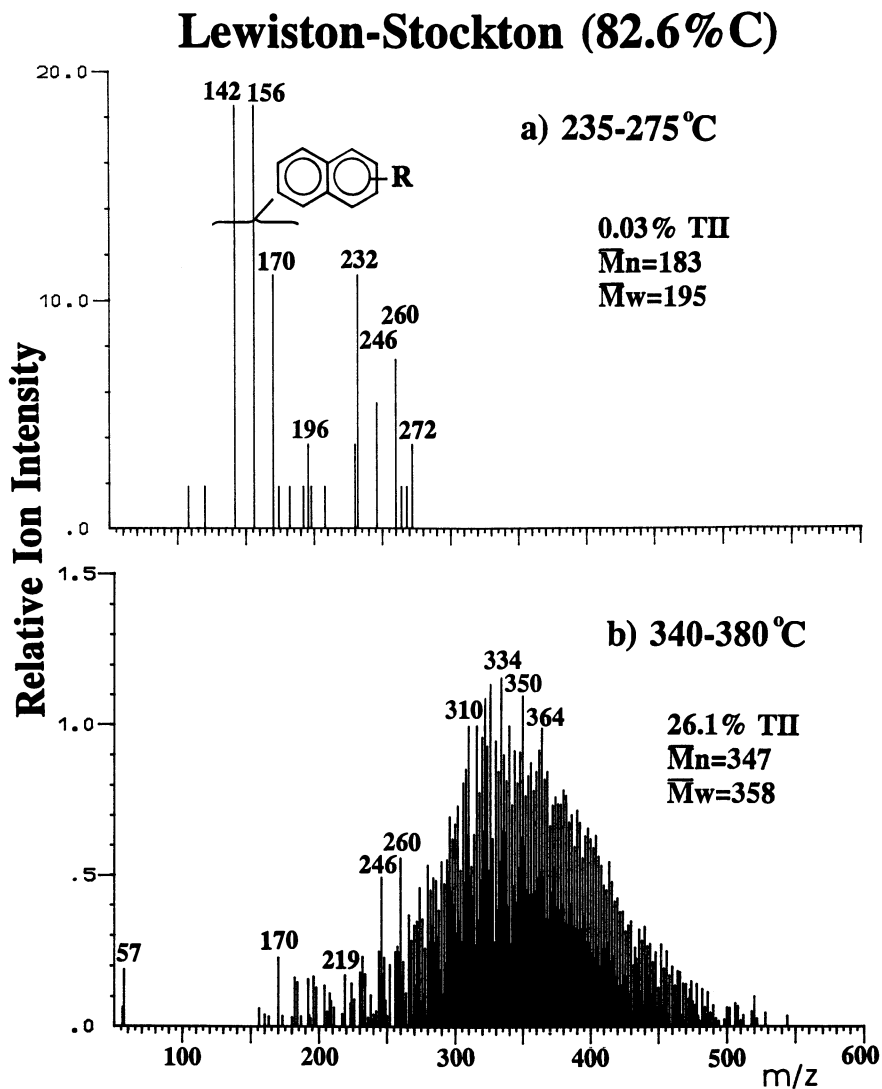


Figure 6. Thermally extracted mobile phase components over different temperature intervals from Lewiston-Stockton and Upper Freeport coals.

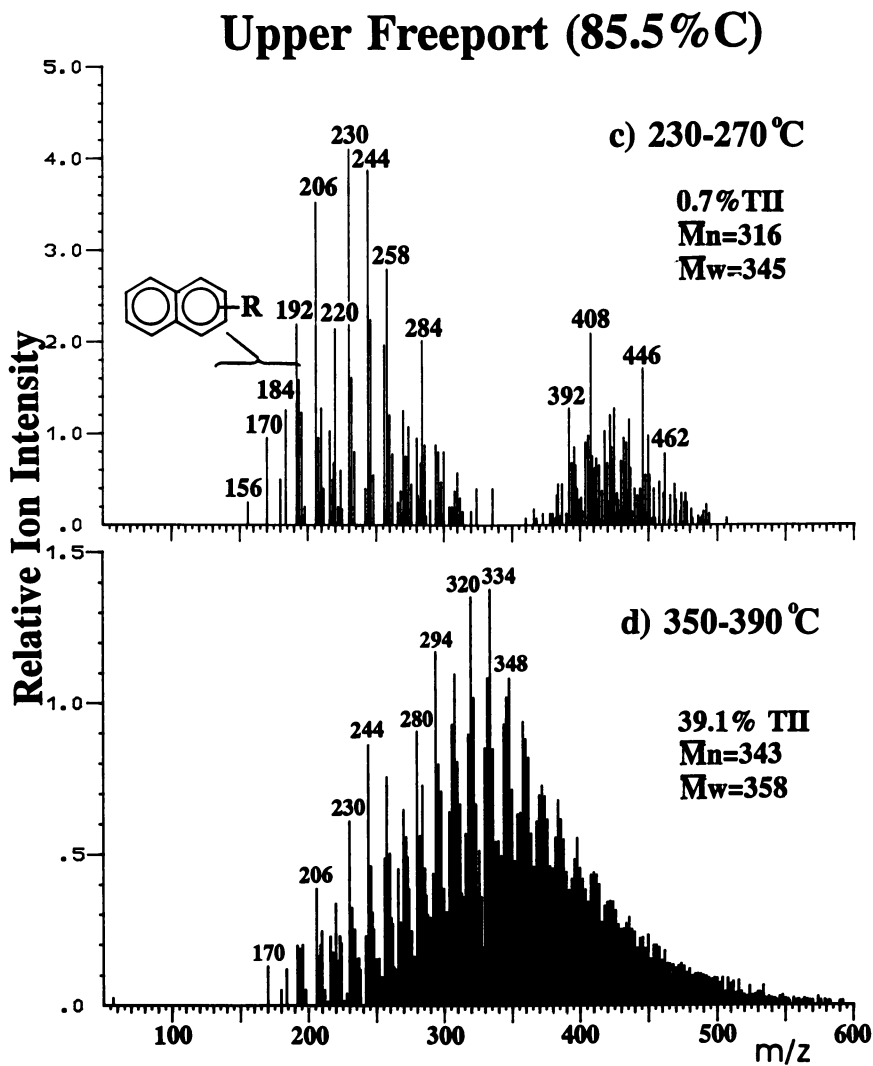


Figure 6. Continued

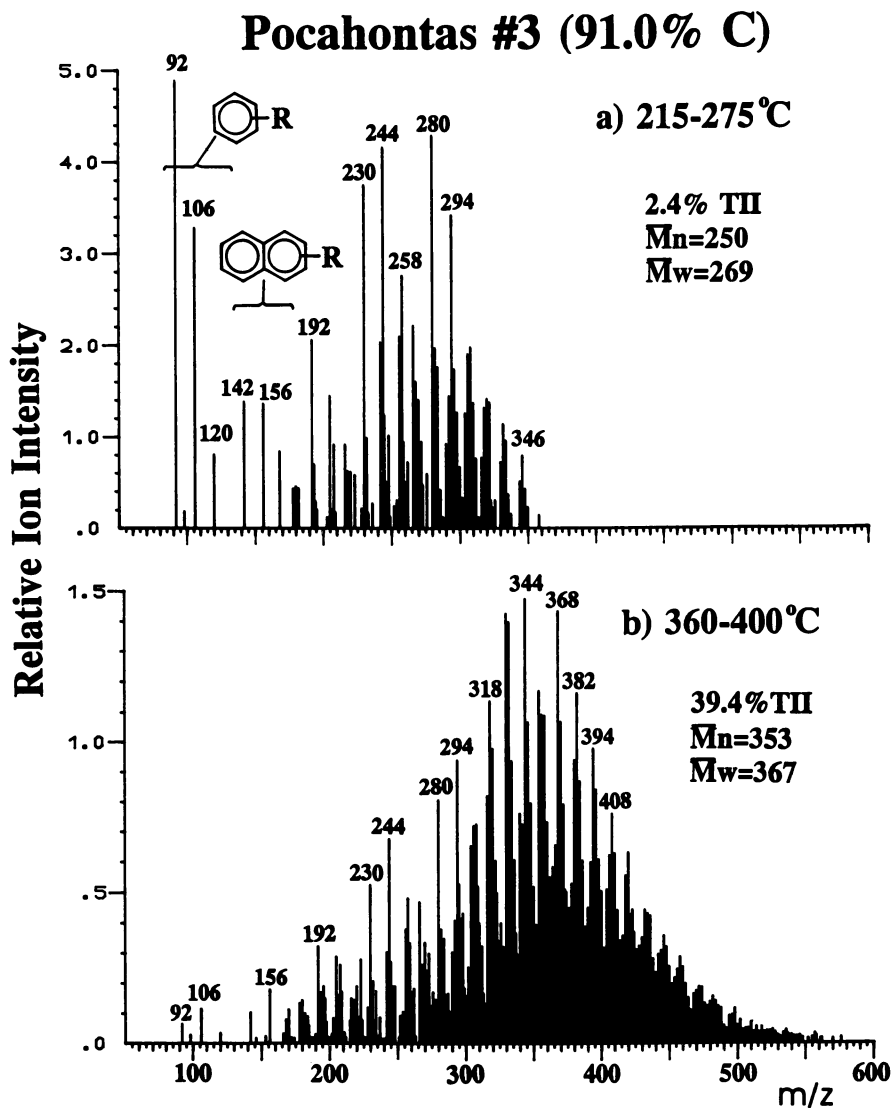


Figure 7. Thermally extracted mobile phase components over different temperature intervals from Pocahontas #3 coal.

least in terms of thermal extraction. Direct comparison with the spectrum on the sample prepared by chemical extraction will definitely help to understand the nature of the mobile phase and to more specifically define the mobile phase.

The above observations point to the importance of rank and depositional environment in defining the molecular characteristics of the "mobile phase" as well as the "network phase" of coals.

To complicate matters further, post-depositional factors, such as "weathering" during storage or transportation, also strongly effect the composition of both phases, as reported by Jakab *et al.* (27). Figures 8 and 9 illustrate the effects of mild oxidation of a Hiawatha (hvb) coal for 212 hours at 100 °C under controlled laboratory conditions, as measured by time-resolved Curie-point Py-LVMS. Both the low temperature hump as well as the bulk pyrolysis event in the weathered coal are markedly reduced. Moreover, the composition and nature of the low temperature components have undergone a dramatic change as illustrated in Figure 9. The alkyl substituted naphthalenes and tetralins dominating the spectrum of fresh channel-cut coal are nearly completely gone. Instead, we now find low MW, oxygen-containing mass signals apparently representing aliphatic carboxylic and carbonylic functionalities, e.g., liberated by low temperature pyrolysis of weak oxygen bonds (27). These observations would seem to indicate that it is pointless to study "mobile phase"/"network phase" phenomena in coal samples of uncertain weathering status. As one example of the importance of weathering, the loss of the typical mobile phase components such as naphthalenes and tetralins appears to coincide with the loss of thermoplastic properties in coal (5). Thus, post-depositional factor such as weathering should be considered as equally important as rank and depositional environment.

Conclusions

Temperature-programmed vacuum pyrolysis in combination with time-resolved soft ionization mass spectrometry allows principally to distinguish between two devolatilization steps of coal which are related to the "mobile" and "non-mobile" phase, respectively. The mass spectrometric detection of almost exclusively molecular ions of the thermally extracted or degraded coal products enables one to study the change of molecular weight distribution as a function of devolatilization temperature. Moreover, major coal components can be identified which are released at distinct temperature intervals.

When limiting our analysis and discussion of mobile phase components to the thermally extractable fraction, we may conclude that the yields and compositions of these products (estimated to constitute 5-15% of dmmf coal weight) are strongly dependent on rank, coal type and weathering status. In coals of hvb and higher rank the nature of the thermally extractable bitumen fraction is consistent with that of a natural pyrolyzate formed by catagenetic processes during the "oil formation window" stage of maturation with subsequent loss of the more reactive oxygen containing moieties. Not surprisingly, in low-rank coals various types of relatively little altered "biomarkers" molecules appear to be important constituents.

Furthermore, artificial "weathering" of coal under carefully controlled conditions in the laboratory reveals a rapid loss of thermally extractable mobile

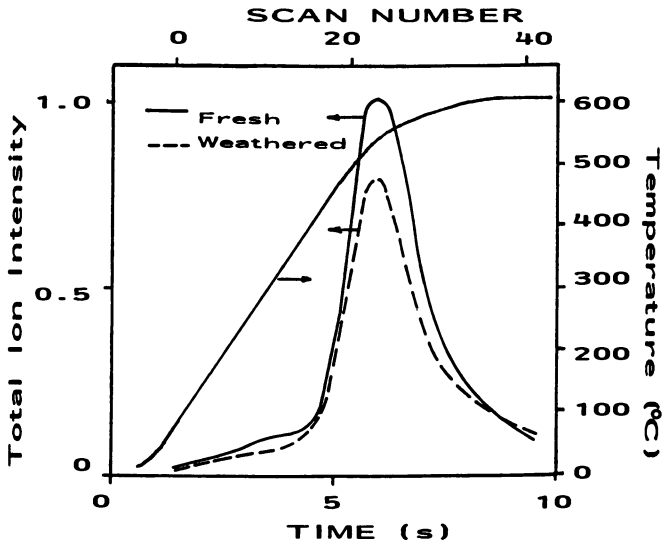


Figure 8. Time-resolved TII profiles of a Hiawatha seam (hvBb) coal obtained by Curie-point pyrolysis in combination with low voltage EIMS.

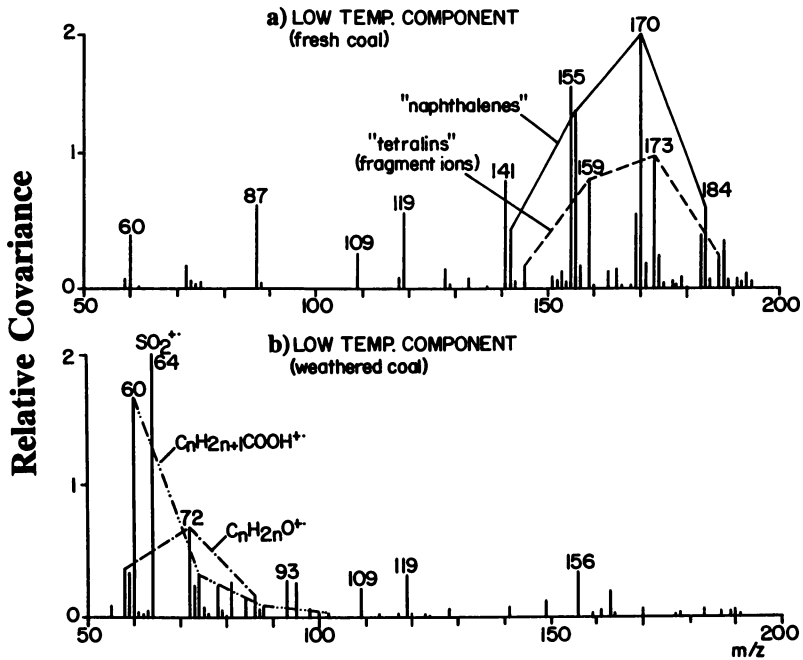


Figure 9. Effect of weathering on low temperature component spectra obtained by low voltage EIMS.

phase components (possibly by "grafting" to the network phase (28)) accompanied by a decrease in total pyrolysis yields. This points out that in future discussions of "mobile phase" phenomena only results obtained on coals of known weathering status, e.g., ANL-PCS coals, should be used.

With regard to the central question whether there exists a chemically and/or physically distinct "mobile phase" in coals, mass spectrometric data on ANL-PCS coals strongly support the presence of a thermally extractable, bitumen-like fraction which is chemically distinct from the remaining coal components.

Acknowledgement

The authors are indebted to Dr. Peter Given, to whose remembrance this paper is dedicated, for his invaluable encouragement, advice and friendship in the early phases of the coal studies leading to the experiments reported in this paper.

The work described here was financially supported by the Advanced Combustion Engineering Research Center (funded by NSF, the State of Utah, 23 industrial participants, and US DOE).

Literature Cited

1. Given, P.H.; Marzec, A.; Barton, W.A.; Lynch, L.J.; Gerstein, B.C. Fuel 1986, **65**, 155-163.
2. Jurkiewicz, A.; Marzec, A.; Pislewski, N. Fuel 1982, **61**, 647-650.
3. Redlich, P.; Jackson, W.R.; Larkins, F.P. Fuel 1985, **64**, 1383-1390.
4. Marzec, A. Fuel Proc. Tech. 1986, **14**, 39-46.
5. Grint, A.; Mehani, S.; Trehwella, M.; Crook, M.J. Fuel 1985, **64**, 1355-1361.
6. Calkins, W.H.; Hovsepian, B.K.; Dyrkacz, G.R.; Bloomquist, C.A.A.; Ruscic, L. Fuel 1984, **64**, 1226-1229.
7. Ebert, L.B.; Long, R.B.; Schlosberg, R.H.; Silbernagel, B.G. ACS Preprints (Div. of Fuel Chem.) 1979, **24(1)**, 104-108.
8. Marzec, A.; Juzwa, M.; Betlej, K.; Sobkowiak, M. Fuel Proc. Tech. 1979, **2**, 35-44.
9. Yun, Y.; Meuzelaar, H.L.C.; Simmleit, N.; Schulten, H.R. submitted to Energy & Fuels.
10. Howard, J.B., In Chemistry of Coal Utilization; Elliott, M.A., Ed.; Wiley: New York, 1981; Chapter 12.
11. Vorres, K.S.; Janikowski, S.K. ACS Preprints (Div. of Fuel Chem.) 1987, **32(1)**, 492-499.
12. Schulten, H.R.; Simmleit, N.; Muller, R. Anal. Chem. 1987, **59**, 2903-2908.
13. Windig, W.; Meuzelaar, H.L.C., Anal. Chem. 1984, **56**, 2297-2303.
14. Windig, W.; Haverkamp, J.; Kistemaker, P.G., Anal. Chem. 1983, **55**, 81-88.
15. Chakravarty, T.; Windig, W.; Hill, G.R.; Meuzelaar, H.L.C. Energy & Fuels 1988, **2**, 400-405.
16. Yun, Y.; Meuzelaar, H.L.C. ACS Preprints (Div. of Fuel Chem.) 1988, **33(3)**, 75-84.
17. Scheppele, S.E.; Grizzle, P.L.; Greenwood, G.J.; Marriott, T.D.; Perreira, N.B. Anal. Chem. 1976, **48**, 2105-2113.

18. Scheppelle, S.E.; Grindstaff, Q.G.; Grizzle, P.L. In Mass Spectrometric Characterization of Shale Oils; Aczel, T. Ed; ASTM STP 902; ASTM: Philadelphia, 1986; pp. 49-80.
19. Later, D.W.; Lee, M.L.; Bartle, K.D.; Kong, R.C.; Vassilaros, D.L. Anal. Chem. 1981, **53**, 1612-1620.
20. Chang, H.K. Ph.D. Thesis, Brigham Young University, Utah, 1989.
21. Meuzelaar, H.L.C. unpublished data.
22. Meuzelaar, H.L.C.; Harper, A.M.; Pugmire, R.J.; Karas, J. Int. J. of Coal Geology 1984, **4**, 143-171.
23. Nip, M.; de Leeuw, J.W.; Schenck, P.A.; Meuzelaar, H.L.C.; Stout, S.A.; Given, P.H.; Boon, J.J. J. Anal. Appl. Pyrol. 1985, **8**, 221-239.
24. Hempfling, R.; Zech, W.; Schulten, H.R. Soil Science 1988, **146**, 262-276.
25. Simmleit, N.; Schulten, H.R., Yun, Y.; Meuzelaar, H.L.C. In Advances in Coal Spectroscopy; Meuzelaar, H.L.C. Ed.; Plenum Publ. Co.: New York, 1990; in press.
26. Philp, R.P. Fossil Fuel Biomarkers, Applications and Spectra; Elsevier: Amsterdam, 1985.
27. Jakab, E.; Windig, W.; Meuzelaar, H.L.C. Energy & Fuels 1987, **1**, 161-167.
28. Meuzelaar, H.L.C.; McClennen, W.H.; Cady, C.C.; Metcalf, G.S.; Windig, W.; Thurgood, J.R.; Hill, G.R. ACS Preprints (Div. of Fuel Chem.) 1984, **29(5)**, 166-177.

RECEIVED November 5, 1990

Chapter 9

Molecular Conformation and Stability of Coal Macerals

Richard Sakurovs, Leo J. Lynch, and Wesley A. Barton

Division of Coal Technology, Commonwealth Scientific Industrial and
Research Organisation, P.O. Box 136, North Ryde,
New South Wales 2113, Australia

Changes in nuclear magnetic resonance measurements of an extensive suite of Australian coals on heating and exposure to pyridine are used to elucidate the molecular conformation of coal macerals. Two types of fusible material are identified in these coals. One is associated with liptinites of all ranks and is typified by fusion commencing at temperatures below 475 K. The other is associated with vitrinites and some inertinites of bituminous coals only and is characterized by a sharp onset of fusion at temperatures above 625 K. The temperature of onset of fusion increases with rank for both types. The effect of pyridine on the molecular stability of bituminous coals at ambient conditions is strongly dependent on maceral composition at $\sim 86\%$ C and on rank at higher carbon contents.

Although the molecular conformation of organic solids profoundly affects their properties, in the case of coals this characteristic has been little studied compared to their chemical composition and functionality. Studies of coal at any level of structure are difficult because of the complex heterogeneity of any particular coal and the great variability of coal types that occur.

Broadly speaking three main concepts are used to model the molecular conformation of coals:

1. Coals as macromolecular three-dimensional crosslinked viscoelastic glassy solids (1,2).
2. Coals as macromolecular/molecular two-phase systems - the host/guest or 'rigid' and 'mobile' phase model (3-5).
3. Coals as paracrystalline substances depicted as having amorphous and ordered 'micellar' regions (6).

The major limitation to the usefulness of each of these concepts (and, no doubt, the necessity for all three) stems from the great variability of coal types. Also, these concepts have mostly been applied only to the vitrinite macerals.

The stability of the molecular conformation of organic solids is determined by the nature and distribution within the molecular network of both covalent crosslinks and the various non-covalent interactions. The latter include localized (e.g. hydrogen bonds) and non-localized electrostatic interactions and the short-range non-polar interactions between molecular units due to the ubiquitous and weak van der Waals induction and dispersion forces (7).

Thus in the case of the aromatic-rich (i.e. vitrinite and inertinite) macerals of coals, if the molecular units are considered to be condensed aromatic and hydroaromatic ring structures, the molecular conformation and stability are determined by the density of covalent crosslinks, the degree of polar functionality and the size and packing geometry of the condensed ring units. The aliphatic-rich liptinite macerals are comprised of a variety of structures including long-chain alkanes, polymerized alicyclic structures and hydroaromatic units (8) so that their conformation is determined largely by covalent crosslinks and probably only to a minor extent by non-covalent interactions.

One means of investigating molecular structures is to determine the extent to which a solid can be destabilized by heat before it decomposes. Significant molecular mobility activated in brown coals at temperatures between 300 and 600 K has been related to the fusion of the extractable, aliphatic-rich fraction of the coals (9). Thermal destabilization of the molecular lattice of aromatic-rich macerals in bituminous coals at temperatures above ~ 600 K is associated with their characteristic thermoplasticity (10). The relationship between the extent of this fusion and the molecular properties of the vitrinite and inertinite macerals, however, is not well understood.

The effects of exposure of organic solids to particular solvents such as pyridine on their conformational stability can also be interpreted in terms of the structural features discussed above. How small nucleophilic molecules disrupt inter- and intramolecular polar interactions in coals thereby 'relaxing' the structural matrix and allowing further solvent penetration has been extensively discussed by Peppas (e.g. 11,12), Larsen (1,13) and Marzec (14-16) and their colleagues. Indeed the extent to which exposure to a polar solvent such as pyridine destabilizes a material's molecular structure is a measure of the extent to which the stability of the material depends on polar interactions. Solvent destabilization of the molecular structure of organic materials can be quantified by simple proton nuclear magnetic resonance (¹H NMR) measurements at ambient temperatures. Such measurements have shown that up to ~ 60% of a coal's molecular structure can be destabilized by pyridine and, by the same token, that at least ~ 40% is impervious to this solvent (15-18).

Recently Quinga and Larsen (19) have considered the role of non-polar interactions in coals. In particular, they pointed out the likely importance of London dispersion forces between planar aromatic units and that the effect of these short-range interactions on the stability of a lattice would increase with increasing size of the molecular units. Thus the greater concentration and growth in average size of these units with increasing rank for bituminous coals would lead to enhancement of the role of the London dispersion

interaction in the stabilization of the molecular lattice of these coals. This process no doubt gives rise to the formation of the ordered graphite-like structures detectable by X-ray diffraction (e.g. 6) and apparently not disrupted by exposure of the coals to pyridine and their resultant swelling (20,21). Also the microscopic conformational and reversible nature of the swelling of coals by pyridine established by Brenner (1) points to these ordered structures existing in microdomains of dimension less than $\sim 10^{-6}$ m.

Strong evidence of the dominant influence of molecular conformation on the properties of coals is implicit in the several data sets which show an extremum in the measured property when plotted against carbon rank. Examples are the extrema which occur in the solid state properties of mass density (22,23) and proton spin-lattice relaxation rate (24) as well as in solvent swelling and extractability (1).

Nuclear Magnetic Resonance Techniques

^1H NMR measurements can distinguish hydrogen in rigid molecular structures of coals, i.e. structures that do not undergo appreciable reorientation and/or translation during time intervals $< \sim 10^{-5}$ s, from hydrogen in mobile structures which possess more rapid molecular motions characteristic of fused or 'rubbery' materials. The data provided by these measurements are presented in this paper in terms of a parameter M_{2T} that measures the extent and degree of molecular mobility. M_{2T} is an empirical second moment of the frequency spectrum of the NMR signal (25), truncated here at 16 kHz (26), and is inversely related to the average molecular mobility of the specimen. Thus the relative decrease in M_{2T} is a sensitive measure of the extent and degree of mobility acquired by rigid molecular structures as a result of their destabilization by thermal or solvent treatment.

The technique of ^1H NMR thermal analysis (25) yields data in the form of M_{2T} pyrograms (typical examples are shown in Figures 1 and 2). The fusibility of a coal can be ranked by the minimum value of M_{2T} ($M_{2T\text{min}}$) attained during the experiment. This parameter measures the instantaneous maximum extent of fusion of the sample on a molecular level and not the total fraction of material that passes through a fused state during heating.

Because the amplitude of a ^1H NMR signal is proportional to the amount of hydrogen present, in the data analyses described below maceral contents which are determined on a volume basis (denoted by vol%) have been converted to a wt% hydrogen basis (denoted by H-wt%) by the method of Lynch et al. (27). In practice, the changes produced in the maceral content values are small except for the coals richest in liptinite.

The Coals

Data have been obtained for an extensive suite of Australian coals by ^1H NMR experiments which probe separately the effects of heat and of exposure to pyridine on the molecular stability of the coals. All coals in the study were comprehensively characterized including

ultimate, chemical (but not direct oxygen) and petrographic compositions.

The coals and coal fractions which have been examined by ^1H NMR thermal analysis are subdivided into two sets:

1. 92 bituminous coals and maceral concentrates with carbon contents of 80 - 90% (daf) and hydrogen contents between 4.1 and 6% (daf). The vitrinite and inertinite (predominantly semifusinite and inertodetrinite) contents of these coals are in the ranges 10 - 98 and 5 - 80 vol% (mmf) respectively. The liptinite content never exceeds 22 vol% and is < 10 vol% in most coals. A suite of 46 bituminous whole coals and maceral concentrates were selected from this set for the pyridine swelling experiments.
2. 10 brown coals with carbon contents of less than 75% (daf). For these coals, liptinite contents vary from 0 to 40 vol%. Inertinite contents are less than 5 vol% except for two coals in which they are ~ 50 vol%.

All coals were ground to $< 500 \mu\text{m}$ and acid-washed to remove HCl-soluble iron (28). The resulting specimens were stored at 255 K under nitrogen. They were dried overnight under nitrogen at 378 K immediately prior to thermal analysis or addition of pyridine.

The thermal analysis experiments involved the collection of ^1H NMR data while coal samples were being heated at 4 K/min to 875 K under non-oxidizing conditions.

In the solvent swelling study each coal was soaked in excess deuterated pyridine in a sealed glass ampoule for approximately two months before NMR measurements were made at room temperature.

Thermal Analysis Data for Representative Coals

In Figures 1 and 2 the M_{2T} pyrograms for seven representative coal specimens are plotted. Analytical data for these materials are listed in Table I.

Table I. Analytical Data for Representative Coals

Coal description	Moisture (%ad)	Ash (%d)	VM (%daf)	C H N S			
				(% daf)			
R30, Vic.	-	0.3	50.7	69.5	5.14	0.57	0.38
Collie, WA	11.9	8.1	39.4	74.4	4.31	1.32	0.91
Amberley, Qld	4.3	12.2	47.3	80.2	6.22	1.60	0.82
Liddell seam, NSW	2.8	5.8	39.5	83.4	5.63	2.19	0.41
Bulli seam, NSW	1.2	8.9	22.4	89.2	4.86	1.62	0.46
Baralaba, Qld	1.4	8.4	12.0	89.7	4.12	1.88	1.18
	$R_{v\text{max}}$ (%)	Vitrinite (%mmf)	Liptinite (%mmf)	CSN ^(a) log (max fluidity, ddp)		Gieseler (b)	
R30, Vic.	-	86	13	-		-	
Collie WA	0.45	51	6	0		-	
Amberley, Qld	0.59	80	18	2		-	
Liddell seam, NSW	0.78	83	6	6.5		2.26	
Bulli Seam, NSW	1.30	46	0	7.5		1.90	
Baralaba, Qld	2.14	63	0	0.5		nd ^(b)	

(a) CSN - crucible swelling number

(b) nd - no detectable movement

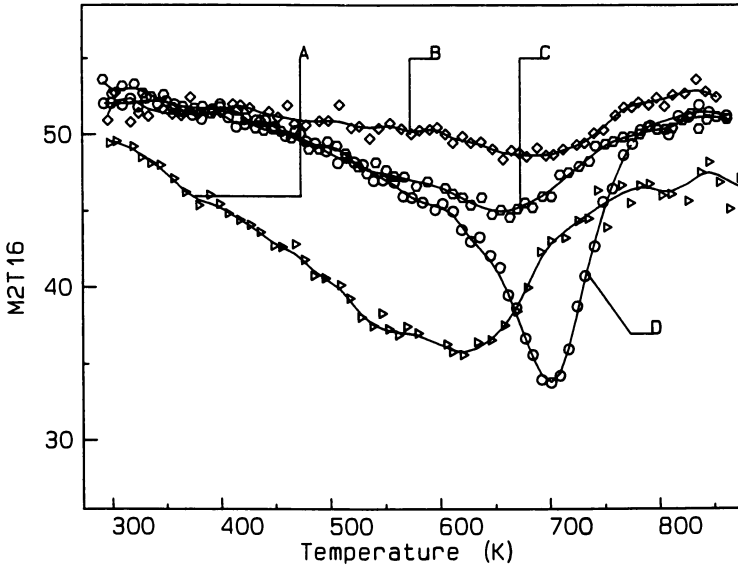


Figure 1. M_{2T} pyrograms of a brown coal (R30) (A), its extracted residue (B), and samples of Collie (C) and Amberley (D) sub-bituminous coals. Analytical data in Table I.

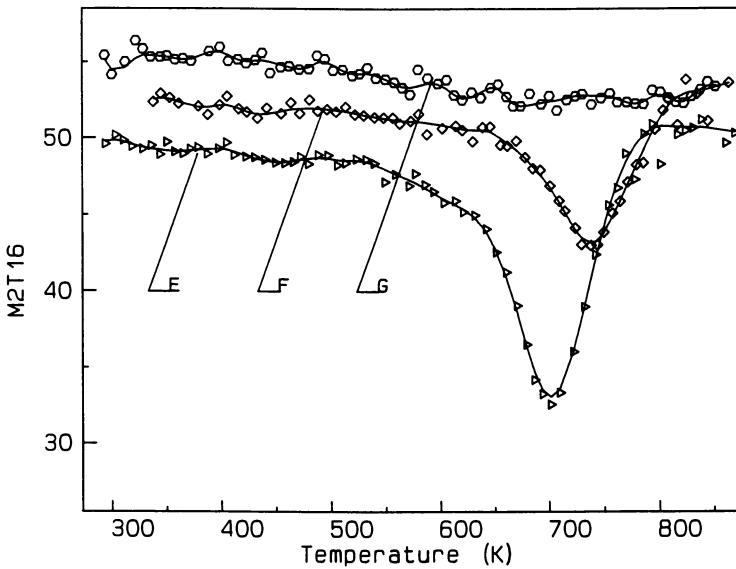


Figure 2. M_{2T} pyrograms of a high-volatile bituminous coal (E), a low-volatile bituminous coal (F) and a semi-anthracite (G). Analytical data in Table I.

The M_{2T} pyrogram of a typical brown coal (Figure 1 (A)) reveals the significant thermally-activated molecular mobility which occurs on heating from room temperature to ~ 600 K. This has been shown to be the result of fusion of the extractable component of such coals (9). The reduction in molecular mobility (increase in M_{2T}) above 600 K results mostly from volatile loss of this 'guest' material. The M_{2T} pyrogram of the extracted residue of a brown coal (Figure 1 (B)), which constitutes usually $>80\%$ of the total coal, exhibits only a low level of thermally-activated molecular mobility. The shallow minimum which does occur in this pyrogram is probably due to fusion of residual 'guest' material. Thus the extract residue or 'host' component of brown coals (considered to be lignin-derived) undergoes no significant fusion during heating to pyrolysis temperatures at 4 K/min. This is consistent with it being a highly crosslinked macromolecular solid.

The M_{2T} pyrograms of two nominally sub-bituminous coals also are recorded in Figure 1. The thermal behaviour of the lower rank Collie specimen (74.4% C) (C) is similar to that of a brown coal containing little extractable 'guest' material, but its fusion is shifted to higher temperatures than that of the brown coals. The higher rank Amberley specimen (80.2% C) (D) clearly shows two fusion transitions. The first parallels that of the Collie coal until the second sharp transition occurs above 600 K. This coal has a high liptinite content (18 vol%) and a correspondingly high hydrogen content. Its high volatile matter value (47.3% daf) ranks it as a sub-bituminous coal but its carbon rank (80.2% C daf) is indicative of a lower rank bituminous coal. The second fusion transition is characteristic of lower rank thermoplastic bituminous coals (see below), but this coal has a crucible swelling number of only 2.

The high-volatile Liddell bituminous coal (Figure 2 (E)) shows little indication of thermally-activated molecular mobility below 500 K. There is some fusion between 500 and 600 K followed by a major fusion transition above 600 K which appears very similar to the high temperature transition of the Amberley coal. This Liddell coal, however, has only 6% liptinite, has a crucible swelling number of 6.5 and exhibits considerable Gieseler fluidity. We therefore attribute this high temperature fusion event to the aromatic-rich macerals of the coal and associate it with the thermoplastic phenomenon. This implies that a stage has been reached in the coalification processes at which aromatic-rich material becomes fusible.

The low-volatile bituminous Bulli coal which contains no liptinite and has significant thermoplastic properties has a M_{2T} pyrogram (Figure 2 (F)) showing only one fusion transition which is lesser in extent and shifted to higher temperatures than that of the Liddell coal. This transition is, of course, attributed to aromatic-rich macerals.

The M_{2T} pyrogram for the Baralaba low-volatile semianthracite (89.7% C) (Figure 2 (G)) shows this material to be totally infusible on heating to pyrolysis temperatures.

Statistical Analysis of All Coal Data

Statistical analyses were applied to the M_{2T} data from both thermal analysis experiments and measurements on coals swollen with pyridine

to estimate values of this parameter for average 'pure' vitrinite, inertinite and liptinite maceral groups. It was assumed that any interactive effects between macerals can be neglected and hence that M_{2T} varies linearly with maceral composition, i.e.

$$M_{2T} = a * \% \text{ vitrinite content} + b * \% \text{ liptinite content} + c. \quad (1)$$

The regression coefficients a, b and c provide calculated M_{2T} values for 'pure' vitrinite ($= 100 * a + c$), 'pure' inertinite ($=c$) and 'pure' liptinite ($= 100 * b + c$).

By applying this analysis at discrete 10 K temperature intervals to the NMR thermal analysis data for the 102 coals (subdivided into brown coals (<75% C), lower rank (80-85% C) and higher rank (85-90% C) bituminous coals), regression coefficients could be obtained as functions of temperature and hence the average M_{2T} pyrograms of the three maceral groups were generated (Figures 3-5). Because these pyrograms are derived statistically from data on coals with a range of thermal properties and whose petrographic specifications are subject to considerable experimental uncertainty (29), they are quantitatively imprecise and can be interpreted only in a broad qualitative manner.

Brown Coals

The host-guest model as it applies to brown coals and as interpreted by Redlich et al. (30) treats such coals as mixtures of two components, termed 'host' (a macromolecular aromatic-rich lignin-derived material) and 'guest' (a largely aliphatic extractable material). Most of the variation in chemical properties of brown coals is attributed to variation in the relative proportion of each component. Redlich et al. (30) devised a procedure for the separation of 'host' and 'guest' material in which the coal is treated in an inert solvent at 600 K under pressure and afterwards extracted with dichloromethane. These authors found all the 'host' materials from a wide range of unweathered brown coals to have similar chemical properties and likewise for the chemical properties of the 'guest' components. ^1H NMR thermal analysis of 'host' materials showed them to be infusible, while the 'guest' materials are fully fusible. The maximum extent of fusion of untreated brown coals as measured by NMR thermal analysis was also found to be linearly related to the yield of 'guest' material from them (30).

The pyrograms of the average 'pure' maceral groups of brown coals (Figure 3) show that the liptinites undergo a substantial degree of fusion on heating whereas vitrinites and inertinites show no evidence of fusion under these conditions. This implies that the 'host' material corresponds to vitrinite and inertinite macerals and the 'guest' material is liptinite. From the above discussion of the properties of the 'host' and 'guest' components, it is concluded that vitrinite macerals in all the brown coals investigated have similar chemical properties, as do liptinites. (Because inertinite contents are low in all but two of the brown coals examined it could not be determined whether the properties of inertinites in all of the brown coals investigated were similar.)

Bituminous Coals

The average 'pure' vitrinites representative of both bituminous coal subsets remain thermally stable below 600 K but, in contrast to vitrinites in brown coals, fuse to a considerable extent at higher temperatures (Figures 4 and 5). The region of greatest fusion is shifted to higher temperatures for the higher rank bituminous coal subset, consistent with the expected rank dependence of coal thermoplasticity (e.g. 31,32). (This is better demonstrated by the plot of the temperature of maximum fusion (as measured by the minimum M_{2T} value) versus mean maximum vitrinite reflectance R_{Vmax} for the individual coals of the set (Figure 6)).

The M_{2T} pyrograms for the 'pure' inertinites representative of the two lower rank coal subsets (Figures 3 and 4) indicate little molecular mobility in the temperature region of coal thermoplasticity (i.e. $> \sim 700$ K). However, the well defined minimum in the corresponding pyrogram for the higher rank bituminous coal subset (Figure 5) reveals a degree of fusibility of inertinites in these coals.

Fusion of the liptinite macerals in bituminous coals commences at lower temperatures and reaches a much greater extent than that of the aromatic macerals (Figures 4 and 5). The greater thermal stability indicated by the much higher fusion temperatures of the bituminous liptinites compared to brown coal liptinites can be explained in terms of these materials having a more highly crosslinked macromolecular structure than the liptinites in the brown coals. This increase with coalification could be the consequence of in situ crosslinking of material or the selective loss of liptinite fractions that are less crosslinked and therefore less inherently stable.

Because liptinites comprise only a small fraction of most Australian bituminous coals, the M_{2T} pyrograms for typical whole coals (Figure 2(E) and (F)) closely reflect the thermal behaviour of the aromatic-rich macerals.

Solvent Destabilization of Bituminous Coals

The destabilization of bituminous coal structures due to exposure to pyridine is measured by the percentage change (decrease) in the value of M_{2T} (ΔM_{pyr}) for the coal after two months soak. In interpreting the results for ΔM_{pyr} we seek to isolate the separate influences of rank and maceral composition. When ΔM_{pyr} for all the coals is plotted against vitrinite content (Figure 7), there is wide scatter and no recognizable trend. However, if the coals are separated into high ($>86\%$ C) and low (80–86% C) rank bituminous subsets (Figure 7), a strong dependence on vitrinite content for the lower rank subset becomes apparent - the greater the vitrinite content the greater the pyridine destabilization. The implication that vitrinite macerals of lower rank bituminous coals are destabilized by pyridine to a greater extent than the corresponding inertinites is confirmed by statistical analysis of the ΔM_{pyr} data for the 28 pyridine-swollen coals with 80–86% C by means of a linear regression analogous to that given by Equation 1. This analysis yields ΔM_{pyr} values of $(23 \pm 4)\%$ and $(9 \pm 3)\%$ for average 'pure'

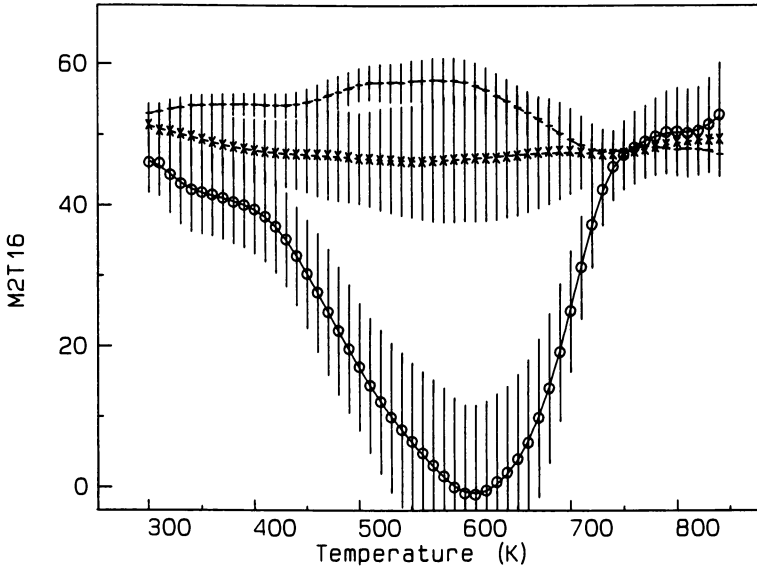


Figure 3. Pyrograms of 'pure' liptinite (o), vitrinite (x) and inertinite (+) for coals with < 75% carbon (daf). The vertical bars denote standard errors.

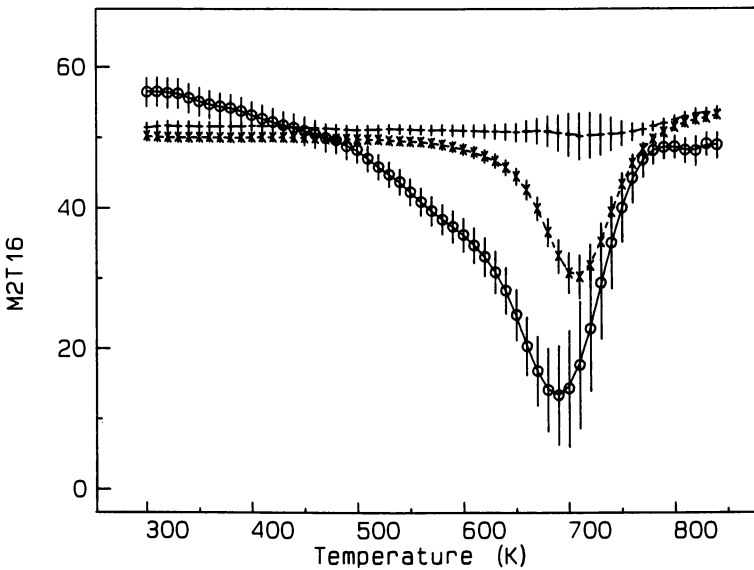


Figure 4. Pyrograms of 'pure' liptinite (o), vitrinite (x) and inertinite (+) for coals with 80-85% carbon (daf). The vertical bars denote standard errors.

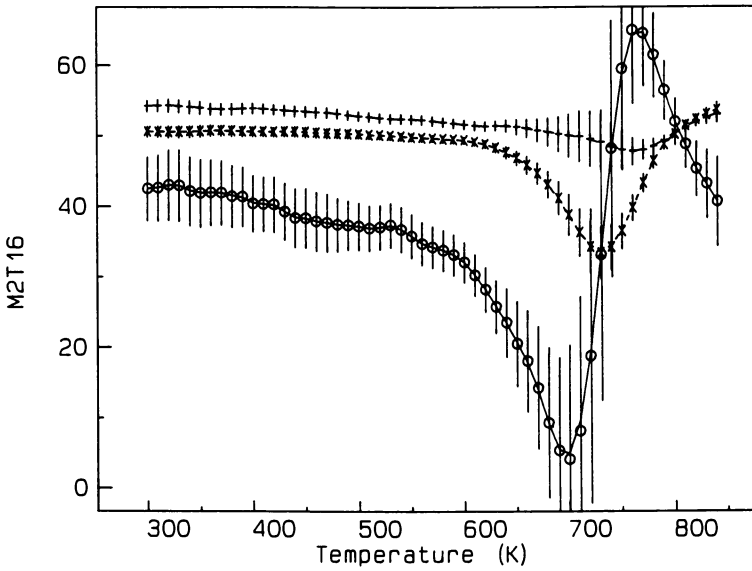


Figure 5. Pyrograms of 'pure' liptinite (o), vitrinite (x) and inertinite (+) for coals with 85-90% carbon (daf). The vertical bars denote standard errors.

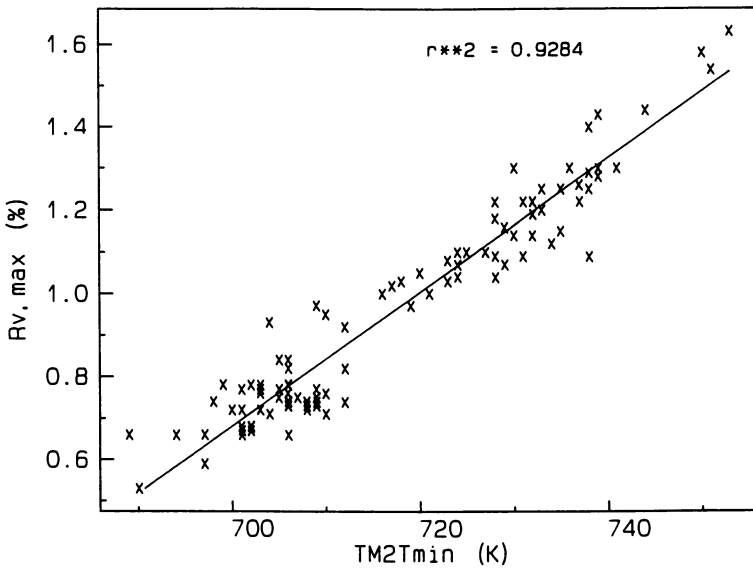


Figure 6. Plot of the temperature of maximum degree of fusion (T_{M2Tmin}) against reflectance (R_{Vmax}) for bituminous coals.

vitrinite and inertinite respectively. A well defined value for 'pure' liptinite is not obtained because of the limited range of liptinite contents.

From Figure 7 it is also apparent that within the bituminous range the lower rank coals are destabilized by exposure to pyridine much more readily than the higher rank coals. Indeed, some higher rank specimens containing ~ 80 H-wt% vitrinite are little influenced by prolonged exposure (Figure 7). This rank effect becomes clearer when ΔM_{pyr} is plotted against carbon content for the vitrinite-rich specimens (>60 H-wt% vitrinite) (Figure 8). Whereas the extent of pyridine destabilization is considerable but variable for vitrinites with <~ 86% C, at higher ranks the vitrinites become increasingly impervious to pyridine and are little affected above 89% C.

A two-parameter linear regression of ΔM_{pyr} with both carbon and vitrinite content for all coals with 86-90 %C that were soaked in pyridine shows that vitrinite content does not contribute significantly to the correlation and hence that maceral composition is of minor importance compared to rank in determining the ability of pyridine to destabilize higher rank bituminous coals.

Comparison of Thermal and Pyridine Destabilization

The relationship between the extent of thermal destabilization of the molecular structures of vitrinite-rich bituminous coals on the one hand and pyridine solvent destabilization on the other is illustrated in Figure 9 in which the ratio of the respective decreases in M_{2T} during heating to the temperature of maximum extent of fusion (ΔM_{heat}) and as a result of soaking in pyridine for two months (ΔM_{pyr}) is plotted against carbon content. Whereas the value of this ratio is independent of rank for coals with <~ 86% C (except for certain coals with relatively high liptinite contents which therefore enhance their overall fusibility), above ~ 86% C it increases markedly, reaches a maximum near 88% C and then falls sharply at higher rank. These trends indicated by the present data reflect both the reduced ability of pyridine to penetrate and destabilize molecular structures in vitrinites with > 86% C (Figure 8) and the rapid decline above ~ 88% C in the extent of fusion of vitrinites at high temperatures as the end of the bituminous range is approached.

Structural Interpretation and Summary

Two distinct types of fusible material occur in coals. One type is aliphatic-rich and associated with the liptinite macerals and the other is contained in the aromatic-rich macerals and particularly the vitrinites of bituminous coals.

In the case of low rank brown coals the aliphatic-rich extractable material fuses at temperatures well below 600 K. With increasing coalification rank the thermal stability of this liptinite material increases and the temperature range of its fusion transition approaches that at which the thermoplastic phenomenon of bituminous vitrinites occurs. The enhanced stability with increasing rank is attributed to greater covalent crosslinking which also would make the material less extractable and resistant to

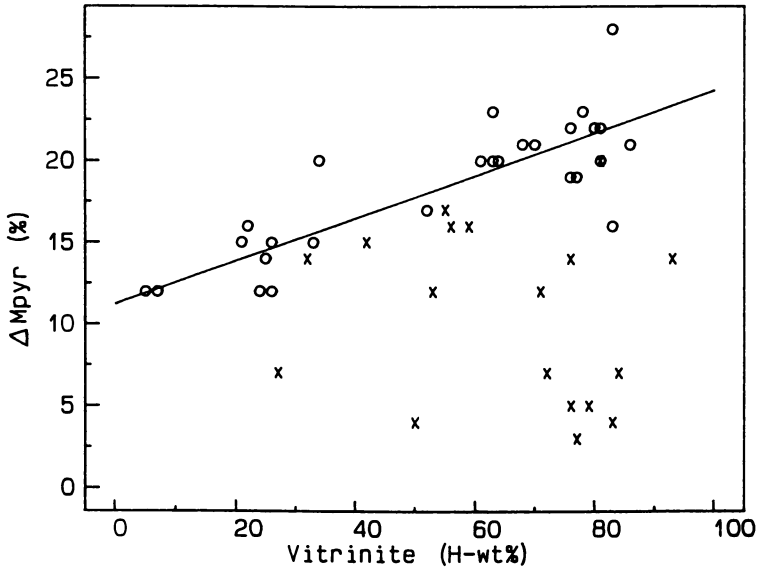


Figure 7. Plot of ΔM_{pyr} against vitritine content (on a wt% hydrogen basis) for bituminous coals with 80-86% C (o) and >86% C (x). The line of best fit to these data for the lower rank subset is shown.

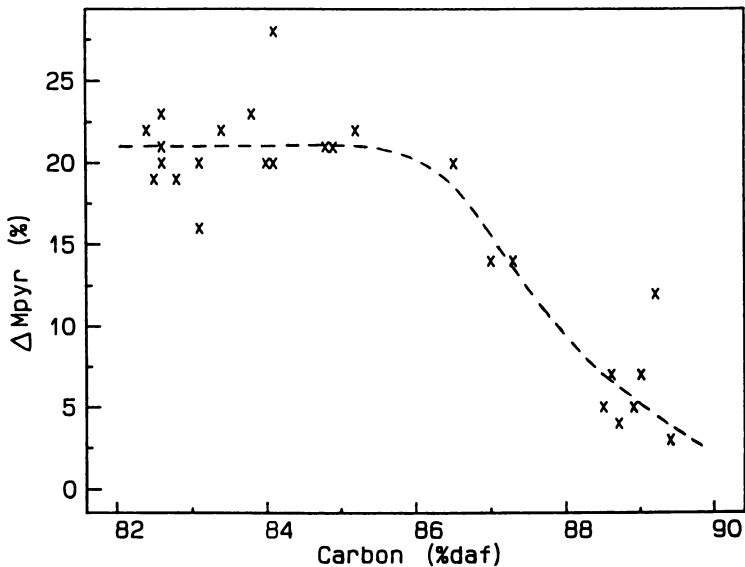


Figure 8. Plot of ΔM_{pyr} against carbon content for vitritine-rich (>60 H-wt% vitritine) bituminous coals.

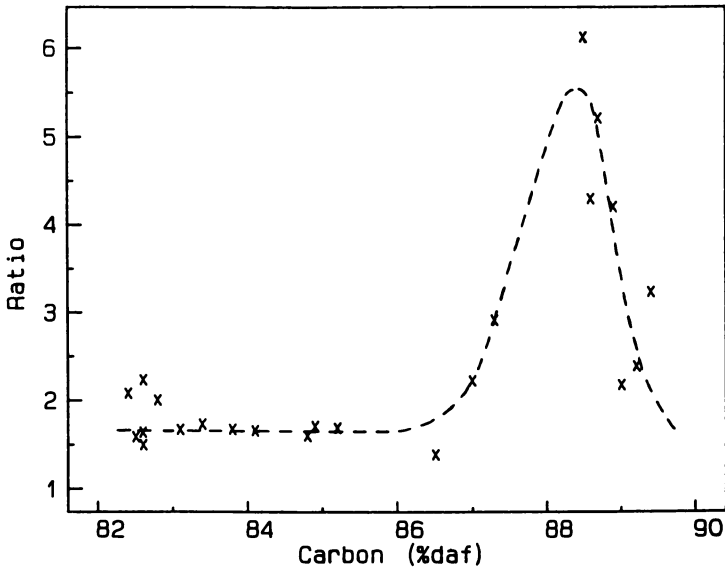


Figure 9. Plot of the ratio of the decreases in M_{2T} due to heating and to exposure to pyridine against carbon content for vitrinite-rich (> 60 H-wt% vitrinite) bituminous coals.

solvent swelling. In the fused state it would remain a crosslinked 'rubbery' material resistant to shear-induced flow.

Fusion of the aromatic-rich macerals is the basis of coal thermoplasticity and its occurrence could be an effective definition of the bituminous range. Fusion of the aromatic-rich structures of low-rank brown coals is inhibited by their high covalent crosslink density. With further coalification these crosslinks are degraded as loss of oxygenated and other functional side groups occurs. A consequence of these processes is the consolidation of the aromatic units into microdomains or 'micelles' (6) with increasing graphite-like order. These microdomains, increasingly stabilized by London dispersion forces, are initially small and poorly ordered. With increasing rank they become larger, more ordered and stable so that their fusion temperature rises. When these structures achieve such a degree of stability that their fusion is inhibited below their temperature of pyrolytic decomposition at heating rates of ~ 20 K/min, thermoplasticity ceases. Acceleration of this stabilization process by the rapid condensation and growth in size of the aromatic units forming the ordered domains at carbon rank $> 87\%$ (33) largely accounts for the decreasing ability of pyridine to destabilize and swell coals at this stage of coalification.

Inertinites are in general more oxygenated and aromatic than their corresponding vitrinites. Their much greater thermal stability and resistance to pyridine destabilization, particularly in lower rank bituminous coals, must relate to their greater covalent crosslink density which also implies that polar interactions have a lesser role in stabilizing their rigid molecular conformation at ambient temperatures. The greater degree of covalent crosslinking in inertinites would also inhibit the development of the ordered microdomains in these macerals compared to that in the vitrinites.

Acknowledgements

Support was provided under the National Energy Research, Development and Demonstration Program (NERDDP). T.P. Maher of the Joint Coal Board provided coal specimens and expert advice. P.J. Redlich (Monash University) supplied brown coals and extracted residues. Maceral concentrates were provided by N. Lockhart, C. Davies, M. Shibaoka, N. Ng and A. Cook. N. Thomas and Z. Lauks performed most of the thermal analysis experiments.

Literature Cited

1. Green, T.; Kovac, J.; Brenner, D.; Larsen, J.W. In Coal Structure; Meyers, R.A., Ed.; Academic: New York, 1982; pp 199-282.
2. Peppas, N.A.; Lucht, L.M. Chem. Eng. Commun. 1984, 30, 291.
3. Given, P.H. In Coal Science; Gorbaty, M.L.; Larsen, J.W.; Wender, I., Eds.; Academic: Orlando, Florida, 1984; Vol. 3, pp 63-252.
4. Marzec, A. J. Anal. Appl. Pyrolysis 1985, 8, 241.
5. Given, P.H.; Marzec, A.; Barton, W.A.; Lynch, L.J.; Gerstein, B.C. Fuel 1986, 65, 155.

6. Hirsch, P.B. Proc. Roy. Soc. (London) 1954, A226, 143.
7. Kauzmann, W. Quantum Chemistry; Academic: New York, 1957; p 503.
8. Neavel, R.C. In Chemistry of Coal Utilization; Elliott, M.A., Ed.; 2nd Suppl. Vol.; John Wiley: New York, 1981; Chapter 3, p 118.
9. Lynch, L.J.; Sakurovs, R.; Webster, D.S.; Redlich, P.J. Fuel 1988, 67, 1036.
10. Lynch, L.J.; Webster, D.S.; Sakurovs, R.; Barton, W.A.; Maher, T.P. Fuel 1988, 67, 579.
11. Peppas, N.A.; Lucht, L.M. Chem. Eng. Commun. 1985, 37, 333.
12. Barr-Howell, B.D.; Peppas, N.A.; Winslow, D.N. Chem. Eng. Commun. 1986, 43, 301.
13. Larsen, J.W.; Green, T.K.; Kovac, J. J. Org. Chem. 1985, 50, 4729.
14. Marzec, A.; Juzwa, M.; Betlej, K.; Sobkowiak, M. Fuel Process. Technol. 1979, 2, 35.
15. Jurkiewicz, A.; Marzec, A.; Pislewski, N. Fuel 1982, 61, 647.
16. Marzec, A.; Jurkiewicz, A.; Pislewski, N. Fuel 1983, 62, 996.
17. Kamienski, B.; Pruski, M.; Gerstein, B.C.; Given, P.H. Energy Fuels 1987, 1, 45.
18. Barton, W.A.; Lynch, L.J. In 1987 International Conference on Coal Science; Moulijn, J.A.; Nater, K.A.; Chermin, H.A.G., Eds.; Coal Science and Technology 11; Elsevier : Amsterdam, 1987; p 37.
19. Quinga, E.M.Y.; Larsen, J.W. Energy Fuels 1987, 1, 300.
20. Bodily, D.M. The Effect of Maceral Properties on the Comminution of Coal; Final Report DOE/PC/70796-12, University of Utah, Salt Lake City, Utah, 1987.
21. Bodily, D.M.; Wann, J-P.; Kopp, V. Prepr. Pap., Amer. Chem. Soc., Div. Fuel Chem. 1986, 31, 300.
22. van Krevelen, D.W. Coal: Typology-Chemistry-Physics-Constitution; Coal Science and Technology 3; Elsevier : Amsterdam, 1981; Chapter 16.
23. Thomann, H.; Silbernagel, B.G.; Jin, H.; Gebhard, L.A.; Tindall, P. Energy Fuels 1988, 2, 333.
24. Yokono, T.; Sanada, Y. Fuel 1978, 57, 334.
25. Lynch, L.J.; Webster, D.S.; Bacon, N.A.; Barton, W.A. In Magnetic Resonance. Introduction, Advanced Topics and Applications to Fossil Energy; Petrakis, L.; Fraissard, J.P., Eds.; NATO ASI Series C124; Reidel : Dordrecht, The Netherlands, 1984; p 617.
26. Webster, D.S.; Sakurovs, R.; Lynch, L.J.; Maher, T.P. Proceedings 1989 International Conference on Coal Science, Japan, 1989, Vol. 2, p 1107.
27. Lynch, L.J.; Sakurovs, R.; Barton, W.A.; Webster, D.S.; Bacon, N.A.; Parks, T. Reactive Inertinite and Coal Carbonization - ¹H NMR Thermal Analysis Studies; NERDDP End of Grant Report, Project No. 662, 1987; Chapter 5.
28. Lynch, L.J.; Sakurovs, R.; Barton, W.A. Fuel 1986, 65, 1108.
29. Australian Standard AS 2856-1986. Coal - Maceral Analysis.
30. Redlich, P.J.; Jackson, W.R.; Larkins, F.P. Fuel 1985, 64, 1983.

31. Brown, H.R.; Hesp, W.R.; Waters, P.L. J. Inst. Fuel 1964, 37, 130.
32. Sakurovs, R.; Lynch, L.J.; Webster, D.S.; Maher, T.P. In 1987 International Conference on Coal Science; Moulijn, J.A.; Nater, K.A.; Chermin, H.A.G., Eds.; Coal Science and Technology 11; Elsevier : Amsterdam, 1987; p 625.
33. Gerstein, B.C.; Murphy, P.D.; Ryan, L.M. In Coal Structure; Meyers, R.A., Ed.; Academic : New York, 1982, pp 87-129.

RECEIVED November 5, 1990

Chapter 10

Direct Determination and Quantification of Sulfur Forms in Heavy Petroleum and Coal

Sulfur K Edge X-ray Absorption and X-ray Photoelectron Spectroscopic Approaches

Martin L. Gorbaty, Graham N. George, and Simon R. Kelemen

Exxon Research and Engineering Company, Annandale, NJ 08801

A Sulfur K Edge X-ray Absorption Near Edge Structure (XANES) Spectroscopy method has been developed for the direct determination and quantification of the forms of organically bound sulfur in nonvolatile petroleum and coal samples. XANES spectra were taken of a number of model compounds, mixtures of model compounds, heavy petroleum and coal samples. Analysis of the third derivatives of these spectra allowed approximate quantification of the sulfidic and thiophenic components of the model mixtures and of heavy petroleum and coal samples. These results are compared with those obtained by X-ray Photoelectron Spectroscopy (XPS).

Although many attempts have been made to determine the forms of organically bound sulfur in nonvolatile and solid hydrocarbonaceous materials, virtually all have involved in one way or another some chemical change to the structures, and leave open questions as to what is being measured (1). While less of an issue for petroleum based samples (2), chemical derivatizations of coal require good mass transport to be sure that the reaction is complete and all products are accounted for. Pyrolysis type experiments (3a) leave open the question as to whether sulfur forms are interconverting (3b). To remove these ambiguities, a direct measurement is required, which must be element specific, environment sensitive, and must be able to observe the entire sample. X-ray Absorption Spectroscopy (XAS) is one such method. In earlier work Hussain et al. (4), Spiro et al. (5), and later Huffman et al. (6,7) demonstrated the potential of sulfur X-ray absorption spectroscopy for the qualitative determination of sulfur forms in coals, however these workers made no attempt at quantification. This report investigates the applications of X-ray absorption near edge structure (XANES) spectroscopy for the purpose of speciating and quantifying the forms of organic sulfur in solids and nonvolatile liquids.

Experimental Section

The details of the XANES experimental setup and data analyses have been described previously (3b,8). All model compounds used in this study were obtained from Aldrich Chemical Company and were used without further purification. The asphaltene samples were prepared from their respective petroleum residua by precipitation from n-heptane following the procedure of Corbett (9). A sample of Rasa coal was generously provided by Dr. Curt White of the Pittsburgh Energy Technology Center.

Results and Discssion

XANES of Model Compounds. Table I lists the first inflection points of the sulfur K edge spectra for a series of model compounds whose structures are believed to be representative of the types of organically bound sulfur found in heavy petroleum and coals. Although the absolute value for the energy calibration contains some uncertainty, the relative precision of the energy scale proved to be reproducible to within less than 0.1 eV. The total span in energy is quite large, being some 12.4 eV between thiohemianthraquinone and potassium sulfate. As might be anticipated (10,11), the first inflections of compounds with more oxidized sulfur are notably higher in energy than for those with reduced sulfur. The sulfur XANES spectra of compounds with similar sulfur electronic environments were found to be similar. For example, dibenzothiophene and benzo thiophene were found to give similar sulfur XANES spectra, whereas dibenzothiophene and thianthrene, whose sulfur atoms are in significantly different environments, exhibit dissimilar sulfur XANES. The XANES spectra of the compounds listed in Table I (3b,8) can readily be used as a fingerprint for the electronic nature of organically bound sulfur, and for distinguishing between the forms of sulfur in the pure compounds.

Examination of Table I reveals that the edge of dibenzothiophene is displaced from that of dibenzylsulfide, the first inflection energy being some 0.6 eV higher for the former compound. From previous XANES data on dibenzothiophene and dibenzylsulfide and physical mixtures of the two, it proved possible to identify each compound in the presence of the other (3b,8). Additionally by simply measuring the heights of the third derivative features at 2469.8 eV and 2470.4 eV relative to the base line in the model compound mixtures, a calibration was established which allowed an approximate estimate of the amounts of each component in hydrocarbon samples to be obtained.

XANES of Petroleum Residua. On the left side of Figure 1 the sulfur K edge spectra for three different petroleum residua and the asphaltene samples prepared from them are shown. While the absorption spectra all appear to be similar, differences are revealed by examining the third derivatives of the spectra, which are shown on the right side of the figure. All the residua samples appear to contain sulfur bound in sulfidic and thiophenic forms, the amount of sulfidic sulfur increasing from sample 1 to sample 3. The asphaltene samples prepared from residua 2 and 3 also appear to contain both forms. Assuming that the composition of the sulfur

Table I. Sulfur K Edge First Inflection Energies (a)

Compound	First Inflection (b) (eV)
K ₂ SO ₄	2478.5
anthraquinone 6-sulfonate(Na)	2477.6
tetramethylenesulfone	2475.6
diphenylsulfone	2474.8
dibenzothiophenesulfone	2474.7
dimethyl sulfoxide	2472.8
tetramethylenesulfoxide	2472.4
2-methylthiophene	2470.6
benzothiophene	2470.4
dibenzothiophene	2470.4
methionine	2470.3
thianthrene	2470.2
dioctylsulphide	2470.1
cystine	2470.1
tetramethylthiophene	2470.0
benzylphenylsulphide	2469.9
dibenzylsulphide	2469.8
2-naphthalenethiol	2469.8
cysteine	2469.2
diphenyldisulphide	2469.2
dibenzylsulfide	2469.1
sulfur	2469.1
iron pyrite	2468.4
thiohemianthraquinone	2466.1

a) Modified from Reference 8.

b) First inflection points were obtained from the position of the lowest energy maximum of the first derivative, and are considered accurate to better than 0.1 eV.

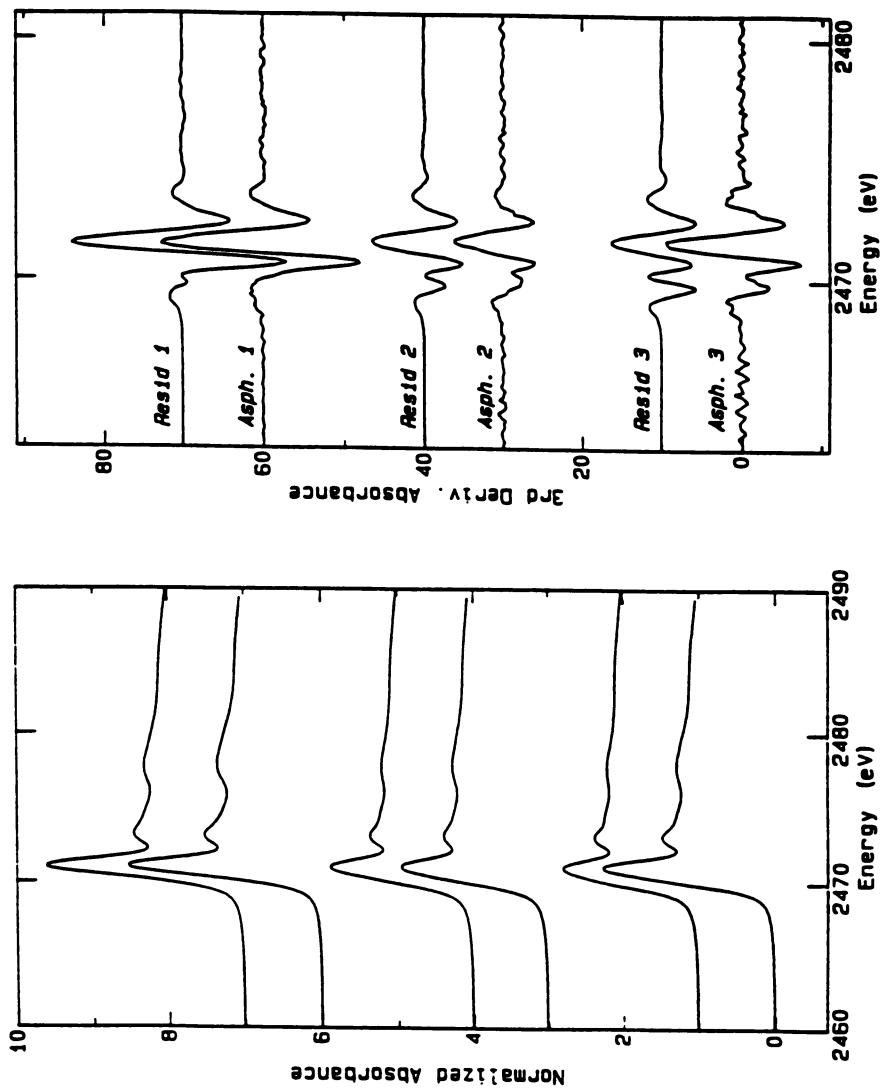


Figure 1. XANES of Residua and Asphaltenes. Left: XANES spectra; Right: 3rd Derivative of XANES spectra

forms in these samples is approximated by the simple two component mixture of dibenzothiophene and dibenzylsulfide models and that any thickness effects are minimal, an estimate of the relative molar quantities of sulfidic and thiophenic forms can be obtained as described above. These approximate values are listed in Table II.

Table II. Approximate Quantification of Organically Bound Sulfur Forms in Heavy Hydrocarbons

Sample	% Sulfidic (± 10)	%Thiophenic (± 10)
<u>Petroleum</u>		
Residuum 1	29	71
Asphaltene 1	0	100
Residuum 2	42(58)	30(42)
Asphaltene 2	43(54)	37(46)
Residuum 3	65	35
Asphaltene 3	50	50
<u>Coal</u>		
Rasa	30	70

In sample 1, it is clear that the predominant form of sulfur in the residuum is thiophenic, while the sulfide forms seem to predominate in residua 2 and 3. In asphaltene samples 1 and 3, the thiophenic sulfur content increases relative to the respective residua, indicating that the molecules containing sulfide sulfur may be more soluble in heptane than those containing thiophenes. For sample 2, there appears to be no such discrimination within the 10% accuracy limits currently established for the XANES analysis.

In the latter case, the totals do not add to 100%. Thickness effects may be responsible for this. Another possible explanation is that a range of slightly different sulfur types, of both sulfidic and thiophenic forms exist in this material, which causes a broadening of the features of the XANES spectrum and making quantification based on mixtures of two model compounds less accurate. In agreement with this possibility, the structure of the third derivative spectra of both the residuum sample 2 and the asphaltene derived from it do appear to be broadened relative to that of the spectra of sample 3 in Figure 1. Since the broadening could be due to structural variations of both forms, the data sets were normalized to 100%, giving a rough approximation of the amounts of sulfidic and thiophenic sulfur, which are shown in parentheses in the table. If it is determined in ongoing studies that the broadening is due to thickness effects, then values reported here for sulfides are overestimates. If non-thiophenic sulfur forms such as disulfides or elemental sulfur are found, the sulfide values for sample 2 will be revised upward.

XPS of Petroleum Residua. XPS sulfur 2p signals from a variety of model compounds have been previously measured to obtain the

instrumental response for single component species as well as to determine the binding energies representative of different sulfur environments (14,15). These model compound results enable the deconvolution of XPS sulfur 2p spectra of complex materials into contributions from sulfide (163.3 eV) and thiophene (164.1 eV) types.

XPS spectra were collected for the same petroleum residua and asphaltene samples used in the XANES studies described above. For all samples the total amount of sulfur relative to carbon as measured by XPS was comparable to that determined by bulk elemental analysis. The spectra were deconvoluted by curve fitting, and the approximate quantifications thus derived are shown in Table III. In agreement with the XANES analysis, residuum sample 1 contains the highest level of thiophenic-like forms and residuum sample 3 the least.

Table III. Mole Percent Sulfide and Thiophenic Sulfur Forms Determined From Analysis of the XPS Sulfur 2p Signal

Sample	% Sulfidic (± 10)	%Thiophenic (± 10)	% Oxidized
<u>Petroleum</u>			
Residuum 1	24	74	2
Asphaltene 1	12	85	3
Residuum 2	33	64	3
Asphaltene 2	26	70	4
Residuum 3	42	55	3
Asphaltene 3	28	67	5
<u>Coal</u>			
Rasa	26	70	4

XANES of Coal. In Figure 2 the XANES spectrum and its third derivative of Rasa coal are displayed and Table II contains the approximate quantification of sulfur types. Rasa coal was chosen for this initial study because it has an unusually high amount of organically bound sulfur, and an unusually low level of pyritic sulfur (12). XANES analysis indicates that about 30% of the sulfur in Rasa coal is sulfidic and 70% is thiophenic. These numbers are in agreement with those found by XPS (14), shown in Table III. Partial confirmation of these values also comes from the work of Kavcic (13), who showed that about 75% of the sulfur in this coal was not reactive toward methyl iodide; this lack of reactivity was attributed to the sulfur being bound in ring structures. Even recognizing the potential or inherent errors of the methyl iodide method such as degree of reaction, possible side reaction, etc., the extent of agreement of the direct and indirect techniques is good.

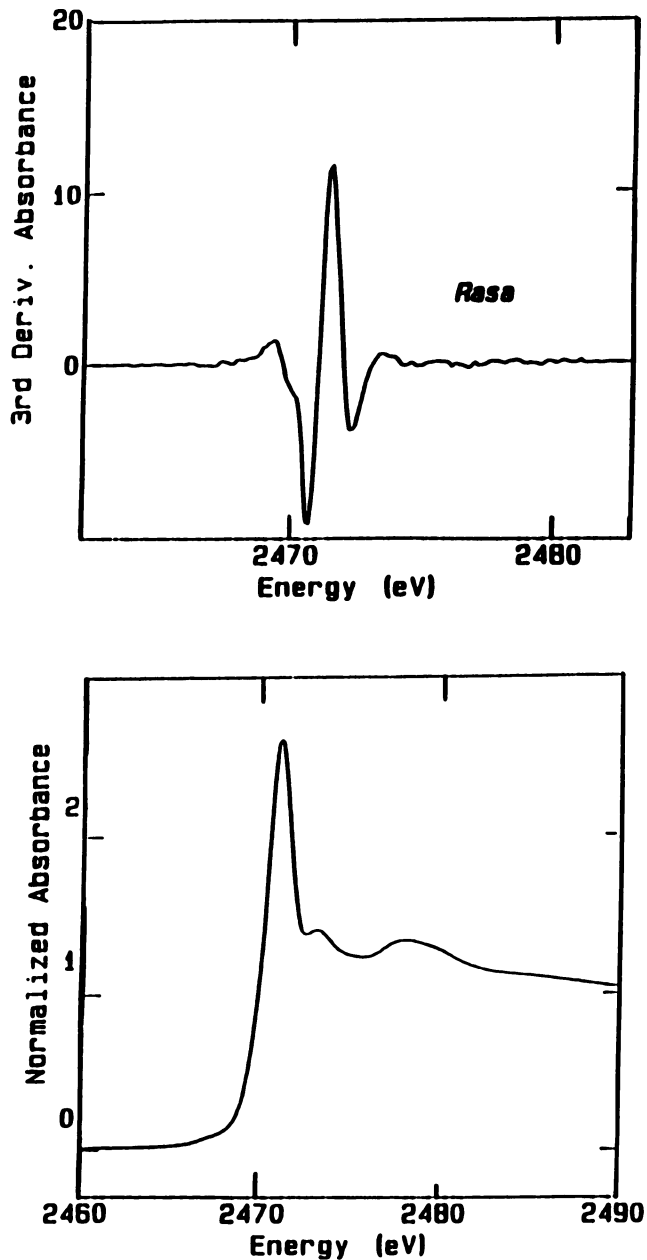


Figure 2. XANES of Rasa Coal; Top: XANES spectrum; Bottom: 3rd Derivative of XANES spectrum.

Comparison of XANES and XPS

Data for the thiophenic sulfur content determined by XANES and XPS for all samples studied are plotted in Figure 3. The solid line in the figure represents the parity situation. Most of the data lie off the parity line in the figure, but in a non-random fashion. The apparent systematic nature of the disparities implies that the differences in the values derived from XANES and XPS arise from the underlying assumptions used in each technique since the experimental precision for both methods is better than differences between the data from XPS and XANES.

Both XANES and XPS results give the same relative ranking for the thiophenic content of any sample, recognizing the currently established accuracy of $\pm 10\%$. For example, either method confirms that petroleum residuum sample 1 contains the most thiophenic sulfur of those studied, and sample 3 the least. Both methods show that thiophenic sulfur concentrates in the asphaltenes prepared from residua 1 and 3, but not in the asphaltenes from residuum 2. However, the quantitative values are different.

There are several potential sources of error. Both methods of analysis use a binary model mixture, composed of sulfidic and thiophenic components. Thickness effects in the XANES of these model systems would alter the calibrations. There may be contributions from species not adequately represented by a simple dibenzothiophene-dibenzylsulfide model. While the XPS data are represented by 163.3 eV and 164.1 eV components, the model compound data base is as yet limited and not sufficient for a definitive interpretation in terms of alkyl sulfide and thiophenic forms. Examination by both XPS and XANES of a wider variety of model compounds and multiple component model compound mixtures will better define the sulfur species represented by these quantification methods.

Conclusions

This work has demonstrated that organically bound sulfur forms can be distinguished and in some manner quantified directly in model compound mixtures, and in petroleum and coal. The use of third derivatives of the XANES spectra was the critical factor in allowing this analysis. The tentative quantitative identifications of sulfur forms appear to be consistent with the chemical behavior of the petroleum and coal samples. XANES and XPS analyses of the same samples show the same trends in relative levels of sulfide and thiophenic forms, but with significant numerical differences. This reflects the fact that use of both XPS and XANES methods for quantitative determinations of sulfur forms are in an early development stage. Work is currently in progress to resolve issues of thickness effects for XANES spectra and to define the possible interferences from pyritic sulfur in both approaches. In addition these techniques are being extended to other nonvolatile and solid hydrocarbon materials.

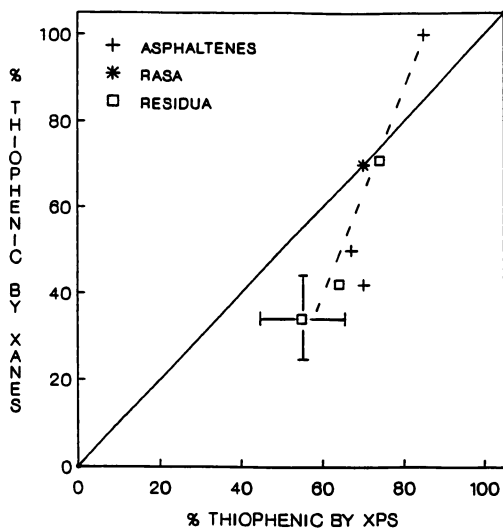


Figure 3. Comparison of XPS and XANES Values for Thiophenic Sulfur Content of Samples Studied.

Acknowledgements

X-ray absorption spectra were recorded at the Stanford Synchrotron Radiation Laboratory, which is funded by the Department of Energy, under contract DE-AC03-82ER-13000, Office of Basic Energy Sciences, Division of Chemical Sciences and the National Institutes of Health, Biotechnology Resource Program, Division of Research Resources. The writers wish to thank Dr. Curt White (PETC) for providing a sample of Rasa coal.

References Cited

1. Van Krevelen, D.W. Coal, Elsevier, Amsterdam, 1961, 171.
2. Rose, K.D.; Francisco, M.A. *J. Am. Chem. Soc.*, 1988, 110, 637.
3. (a) See for example Calkins, W. H. *Energy Fuels*, 1987, 1, 59.
(b) Gorbaty, M. L.; George, G. N.; Kelemen, S. R. in "Geochemistry of Sulfur in Fossil Fuels", ACS Symposium Series, in press.
4. Hussain, Z.; Umbach, E.; Shirley, D.A.; Stohr, J.; Feldhaus J. *Nucl. Instrum. Methods*, 1982, 195, 115.
5. Spiro, C.L.; Wong, J.; Lytle, F.W.; Greigor, R.B.; Maylotte, D.H.; Lamson, S.H. *Science*, 1984, 226, 48.
6. Huffman, G.P.; Huggins, F.E.; Shah, N.; Bhattacharyya, D.; Pugmire, R.J.; Davis, B.; Lytle, F.W.; Greigor, R.B. in "Processing and Utilization of High Sulfur Coals II", Chugh, Y. P. and Caudle, R. D., eds. Elsevier, Amsterdam, 1987, 3.
7. Huffman, G.P.; Huggins, F.E.; Shah, N.; Bhattacharyya, D.; Pugmire, R.J.; Davis, B.; Lytle, F.W.; Greigor, R.B.; *ACS Division of Fuel Chemistry Preprints*, 1988, 33, 200.; Huffman, G.P.; Huggins, F.E.; Mitra, S.; Shah, N.; Pugmire, R.J.; Davis, B.; Lytle, F.W.; Greigor, R.B. *Energy Fuels*, 1989, 3, 200.
8. George, G. N.; Gorbaty, M. L. *J. Am. Chem. Soc.*, 1989, 111, 3182.
9. Corbett, L.W. *Anal. Chem.*, 1969, 41, 576.
10. Frank, P.; Hedman, B.; Carlson, R.M.K.; Tyson, T.; Roe, A.L.; Hodgson, K.O.; *Biochemistry*, 1987, 26, 4975.
11. Bianconi, A. in "X-ray Absorption", D.C. Koningsberger; R. Prins, eds., John Wiley & Sons, New York, 1988, 573.
12. Given, P. H. *Prog. Energy Combust. Sci.*, 1984, 10, 149.; Ignasiak, B.S.; Fryer, J. F.; Jadernik, P. *FUEL*, 1978, 57, 578, and references cited therein.
13. Kavcic, R. *Bull Sci. Conseil Acad. RPF, Yugoslav*, 1954, 2, 12.
14. Kelemen, S. R.; George, G. N.; Gorbaty, M. L. *ACS Div. Fuel Chem. Preprints*, 1989, 34(3), 729.
15. Kelemen, S. R.; George, G. N.; Gorbaty, M. L. *Fuel Process and Technol.*, 1990, in press.

RECEIVED November 5, 1990

Chapter 11

Flory Interaction Parameters for Illinois Number 6 Coal Extracts and Benzene

Leonor Lopez-Froedge, James E. Ball, Min-Wei Chen¹,
and Thomas K. Green

Center for Coal Science, Department of Chemistry, Western Kentucky
University, Bowling Green, KY 42101

Flory interaction parameters (χ) for the untreated and O-alkylated pyridine-extracts of an Illinois No. 6 coal and benzene were determined using an established vapor pressure technique. The extract and O-methylated extracts sorb benzene slowly and behave like glassy materials. A hole-filling/dissolution model for sorption of vapors by glassy polymers was applied to the data in order to separate adsorption from true swelling. The interaction parameters are determined to be 1.5 and 1.2 for the extract and O-methylated extract. O-butylated and O-octylated extracts sorb more benzene and at a faster rate. The presence of the larger alkyl groups lowers the average solubility parameter of the extract, which results in increased swelling by benzene.

Coals are considered macromolecular solids.(1) Although they are not polymers in the sense that they possess a repeating unit, they do possess several fundamental properties typical of synthetic crosslinked polymers.(2) One of these properties is the ability of coals to swell in organic solvents without dissolving.

In recent years, there has been a rapid growth in the number of publications that deal with the solvent swelling of coals. Much of this effort has been directed toward the application of modern polymer and network theories to coals, with the purpose of better understanding their network structures. One of the most fundamental parameters of a network structure is M_c , the number average molecular weight between crosslinks. Consequently, several research groups have attempted to estimate M_c 's for coal from solvent swelling data and the Flory-Rehner equation.(3-9) The equation incorporates both the Flory-Huggins theory of polymer solutions and the Gaussian elastic

¹Current address: East China University of Chemical Technology, Shanghai, People's Republic of China

network theory. An important parameter embodied in the Flory-Huggins theory is the interaction parameter, χ . χ is a thermodynamic parameter describing the free energy of the polymer-solvent interaction. A reliable evaluation of χ is essential to an estimation of M_c for crosslinked networks using the Flory-Rehner equation. Larsen *et al.* have developed a method that relies on regular solution theory to determine χ parameters for nonpolar solvent-coal systems.(6,7) However, few other methods have been developed so that comparisons can be made. It is the purpose of this research to develop such a method.

One of the most common techniques for determining χ parameters for polymer-solvent systems is the vapor pressure method.(10) In this approach, the uncrosslinked polymer is exposed to solvent vapor of known pressure, p . The polymer absorbs solvent until equilibrium is established. χ is related to p and v_2 , the volume fraction of polymer at equilibrium, by the Flory-Huggins equation:(11)

$$\chi = \frac{\ln [(p/p_o)/(1-v_2)] - v_2(1-1/x)}{v_2^2} \quad (1)$$

where p_o is the saturation pressure of the solvent vapor and x is the degree of polymerization or the number of segments in the polymer chain. Measurement of p as a function of v_2 can be used with Equation 1 to obtain values for χ over a wide range of concentrations.

According to Flory-Huggins theory, in the limit of $x \rightarrow \infty$, the critical χ parameter is 0.5.(11) Below this value the polymer and solvent will be miscible in all proportions. Above this value, the solvent will not dissolve the polymer, but will act only as a swelling solvent. Thus, the pure solvent may not dissolve the polymer even though it is not crosslinked. If x is not ∞ , the critical value of χ is larger, but the same qualitative arguments regarding mutual solubility of the solvent and polymer hold. Thus, the application of Equation 1 does not require that the pure solvent be able to completely dissolve the polymer, only that the solvent dissolve into the polymer by an amount that can be measured.

A requirement for application of Equation 1, however, is that the polymer be uncrosslinked. Most vapor sorption studies on coal have been conducted on the covalently crosslinked portion of coals. Under this condition, simultaneous evaluation of χ and M_c must be made. Two groups of researchers have adopted this approach.(8,9) We have adopted an alternative approach by conducting vapor sorption studies on the uncrosslinked portion of the coal. χ parameters can thus be directly calculated from the pressure-sorption data using Equation 1.

The uncrosslinked portion of the coal is obtained by Soxhlet-extraction of the coal with pyridine. Pyridine is a particularly good solvent for coals, and it is thought to remove a majority of the uncrosslinked molecules from the coal matrix. There is evidence that the pyridine-soluble portion is representative of the larger, crosslinked portion,(12) although this aspect remains

controversial.(13) Benzene was chosen as the swelling solvent because it is nonpolar and is not expected to interact specifically with the extract. The Flory-Huggins theory has no provision for such interactions.(11)

Finally, due to the extremely heterogeneous nature of coal, χ parameters derived from Equation 1 can only represent at best an average interaction between a solvent and coal extract. It is also clear that pyridine extracts contain a substantial amount of low molecular weight material. Thus, an estimate of the degree of polymerization, x , which appears in Equation 1, is required.

EXPERIMENTAL

SAMPLE PREPARATION. Dry Illinois No. 6 (Herrin seam, -60 mesh) was used in the sorption studies. Analysis Found: C, 74.37; H, 4.83; N, 1.76; S, 1.76; O (by difference), 8.74; Ash, 8.33 (duplicate). Approximately 10 g of the sample was exhaustively Soxhlet extracted with pyridine. Extractability was 18.7% (wt). The pyridine solution was then filtered through a 0.4 μm filter to insure removal of particulates and colloidal material. The filter did not plug. Most of the pyridine was removed by rotovaporization under reduced pressure at 70-80 °C. Approximately 200 mL of a methanol/water (80/20 vol) mixture and 2 mL of conc. HCl were added to the flask and the mixture was stirred under nitrogen for two days. The solid extract was then filtered and dried under vacuum at 105 °C for 24 hours. Analysis Found: C, 80.0; H, 5.64; N, 1.85; S, 0.70; Ash, 0.30 (duplicate).

O-ALKYLATION PROCEDURE. The extract was O-alkylated according to a method described earlier by Liotta *et al.*(14) using tetrabutylammonium hydroxide and the appropriate alkyl iodide. The extract (1.00 g) was stirred in freshly distilled tetrahydrofuran (THF) (30 mL) under nitrogen for 30 min. A solution of aqueous tetrabutylammonium hydroxide (1.53 M, 2.3 mL, 3.5 mmol base) was then added and this solution was stirred under nitrogen for 30 min. Alkyl iodide (7.2 mmol) was added and the mixture was stirred under nitrogen at room temperature for 2 days. THF and the alkyl iodide were removed by rotovaporization under reduced pressure. The residue was washed with a hot methanol/water mixture (50/50 vol.) until the filtrate was free of iodide (no precipitate with silver nitrate) and tetrabutylammonium cation (no precipitate with sodium tetraphenylborate). The alkylated extract was then dried under vacuum at 105 °C for 24 hours.

FTIR and ^{13}C NMR. FTIR spectra of the O-alkylated extracts were obtained (KBr pellets) using a Nicolet 10DX spectrometer. The O-methylated extract was prepared using ^{13}C -enriched methyl iodide (99% ^{13}C) to enhance the ^{13}C NMR signal of the methyl carbon in the extract. The spectrum was obtained on a pyridine solution of the extract using a Varian XL 300 NMR Spectrometer. Proton decoupling techniques were used and the data was collected in a quantitative mode.

SORPTION EXPERIMENTS. Sorption experiments were carried out using a Cahn 1000 recording balance, with an accuracy of ± 0.03 mg. The balance and its accessories are shown in Figure 1. The instrument is equipped with an MKS Baratron pressure transducer (0-100 torr, 0.15% accuracy) with a digital readout for pressure measurements.

Prior to conducting the sorption experiment, the coal extract (200 mg) was first placed in a Wig-L-Bug capsule and ground for 1 minute under nitrogen. This grinding effectively reduces the extract to a fine powder, which is then used for the sorption experiment. Approximately 50-70 mg of the extract was then placed on the sample pan and the hangdown tube was replaced. The sample was maintained at $30.00 \pm 0.02^\circ\text{C}$ by means of a constant temperature bath which surrounded the hangdown tube.

In a typical experiment, benzene vapor was admitted into the evacuated balance chamber by means of stopcock D. After achieving the desired pressure, stopcock D was closed. The maximum uncertainty in p/p_0 during the course of any one experiment was ± 0.008 units. Equilibrium was judged to be established when there was less than a 1 percent change in weight over a 12 hour period. Total sorption values were reproducible to within $\pm 1\%$.

BET SURFACE AREAS. Surface areas of the unground and ground (Wig-L-Bug; 1 minute) extracts were determined on a Quantachrome B-E-T apparatus. A three-point method was employed, using concentrations of 10, 20, and 30% CO_2 in helium as the adsorbate gases. Approximately 50 mg of the extract were added to the sample cell, which was outgassed for at least 8 hours at a temperature of 105°C . After outgassing was completed, the cell was transferred to the sample station and adsorption of CO_2 was carried out at 78°C . Apparent equilibrium was achieved in less than 30 minutes for each extract. After adsorption, the sample was quickly brought to room temperature to desorb CO_2 . The amount of desorbed CO_2 was measured. The procedure was repeated 3 times and the system was then calibrated using known volumes of pure CO_2 .

DENSITY MEASUREMENTS. The densities of the extract and its O-alkylated derivatives were measured a helium pycnometer.

SOLUBILITY MEASUREMENTS. The solubilities of the extracts were measured in liquid benzene. Approximately 100 mg of the extract was placed in a narrow tube. Excess benzene was added and the tube was shaken. After 24 hours, the tube was centrifuged and the supernatant was removed. Excess benzene was again added and the process was repeated. After 1 week, the insoluble portion was dried and weighed. The percent solubility is based on the weight of the insoluble extract that remained.

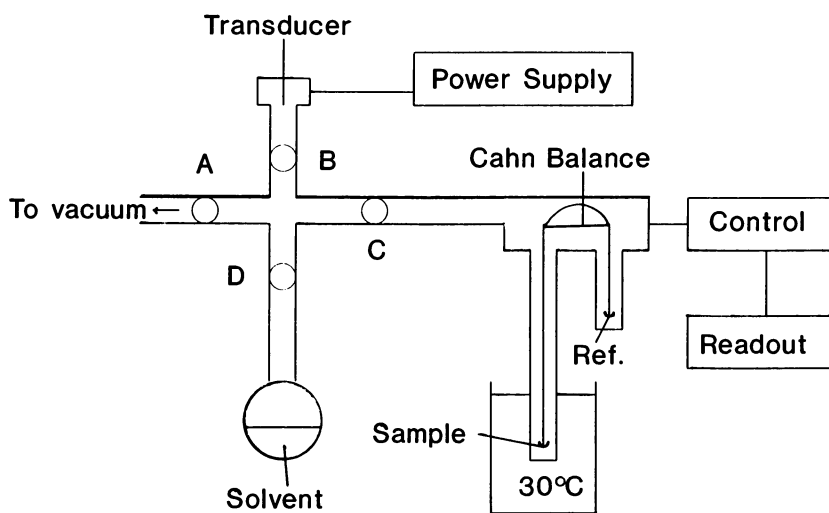
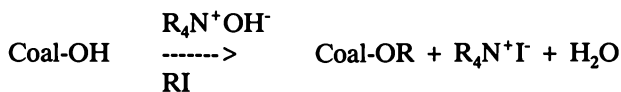


Figure 1. Sorption Apparatus

RESULTS

CHARACTERIZATION of the PYRIDINE-EXTRACT. Pyridine is known to cling to coals. The extract was therefore stirred with a methanol/water/HCl mixture for two days as suggested by Buchanan.(15) Elemental analysis of the extract revealed 1.85% N. The original coal contained 1.92% N (daf) so it is apparent that the methanol/water/HCl treatment followed by drying successfully removed pyridine from the extract. The FTIR spectrum of the extract did not reveal the presence of pyridine.

SYNTHESIS and CHARACTERIZATION of O-ALKYLATED EXTRACTS. Alkylation occurs when tetrabutylammonium hydroxide is used to promote the reaction of the alkyl iodide with the coal in tetrahydrofuran.(14) The alkylation reaction occurs primarily on acidic oxygen functionalities such as phenolic hydroxyl and carboxylic acid groups, as shown below.



The difference in the hydrogen to carbon ratios of the extract and O-alkylated extract was used to establish the number of hydroxyl groups that had reacted. The results are shown in Table I. The predicted H/C ratio is calculated based on the assumption that 4 hydroxyl groups per 100 carbon atoms were alkylated. The agreement between calculated and observed H/C ratio is very good.

TABLE I. H/C Ratios for the Pyridine-extracts of the Illinois No. 6 Coal

Extract	H/C Ratio	
	calcd. ^a	observed
untreated	----	0.84
O-methylated	0.88	0.88
O-butylated	1.00	0.98
O-octylated	1.12	1.12

^a Assuming 4 alkyl groups added per 100 carbon atoms of extract.

FTIR spectra of the alkylated extracts were also obtained. For each derivatized extract, there was a substantial reduction of the OH absorption

band (3300 - 3600 cm^{-1}) compared to the original extract. That it was not entirely absent indicates that a small number of hydroxyl groups were left unreacted or that residual traces of water remain. It is difficult to remove last traces of water from KBr pellets. Careful drying of the KBr pellets of the O-alkylated extracts nearly eliminated the OH absorption band completely. Thus we feel confident that a large majority of the hydroxyl groups were alkylated.

For each alkylated extract, there was an absorption at 1700 cm^{-1} which was absent in the untreated extract. This absorption may be attributed to esters that form from alkylation of carboxylic acids. This interpretation is consistent with the ^{13}C NMR analysis described below. For each O-alkylated extract, there was an increase in the intensity of the C-H absorption bands at 2800-3000 cm^{-1} , consistent with the introduction of aliphatic carbon.

The O-methylated extract was derivatized with 99 percent ^{13}C -enriched methyl iodide. The ^{13}C NMR spectrum of the extract showed a strong absorption at 56 ppm (relative to TMS), which can be attributed to unhindered aryl methyl ethers (67%), a smaller absorption at 60 ppm, attributable to hindered aryl methyl ethers (23%), and a resonance at 51 ppm, assignable to methyl esters derived from carboxylic acids (10%).⁽¹⁶⁾ These results are consistent with those of Liotta *et al.*, who studied the alkylation of whole Illinois No. 6 coal.⁽¹³⁾

SORPTION EXPERIMENTS. The extracts were exposed to benzene vapor at several relative vapor pressures (p/p_0). Two types of sorption experiments were conducted. Experiments in which the benzene vapor pressure is raised from zero to a higher value are termed integral sorptions. Sorption experiments starting with the extract and vapor in equilibrium at a finite, non-zero pressure, and proceeding to a higher pressure, are termed incremental sorptions.

Figures 2-5 show the sorption curves of mass uptake versus time for the extract, O-methylated, O-butylated, and O-octylated extract. Three different experiments are shown in each figure; a single integral sorption and two subsequent incremental sorptions. Both the extract and the O-methylated extract required 30 to 150 hours to reach equilibrium, depending on the particular experiment. The O-butylated extract sorbs benzene considerably faster, requiring less than 20 hours to reach equilibrium at all pressures. Finally, the O-octylated extract required less than one hour to reach equilibrium at each pressure.

EQUILIBRIUM SORPTION VALUES. The equilibrium benzene sorption values for the extracts at the various pressures are presented in Table II. At the lower pressure, total sorption of benzene decreases with increasing size of the added alkyl group. At the higher pressure, the order is reversed.

SORPTION-DESORPTION ISOTHERMS. Sorption-desorption isotherms for the untreated, O-methylated, and O-octylated extracts are presented in Figures 6-8, where the relative vapor pressure of benzene (p/p_0) is plotted against the

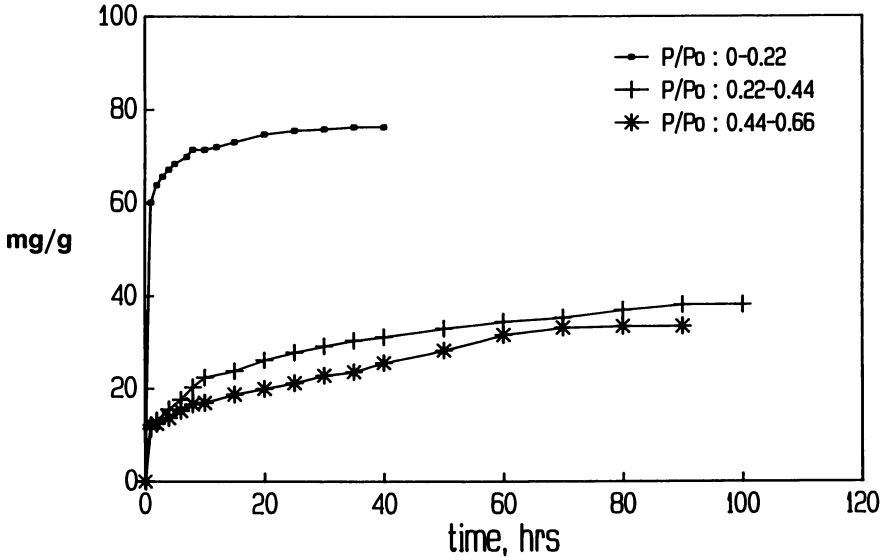


Figure 2. Sorption of Benzene by Pyridine-extract of Illinois No. 6 Coal

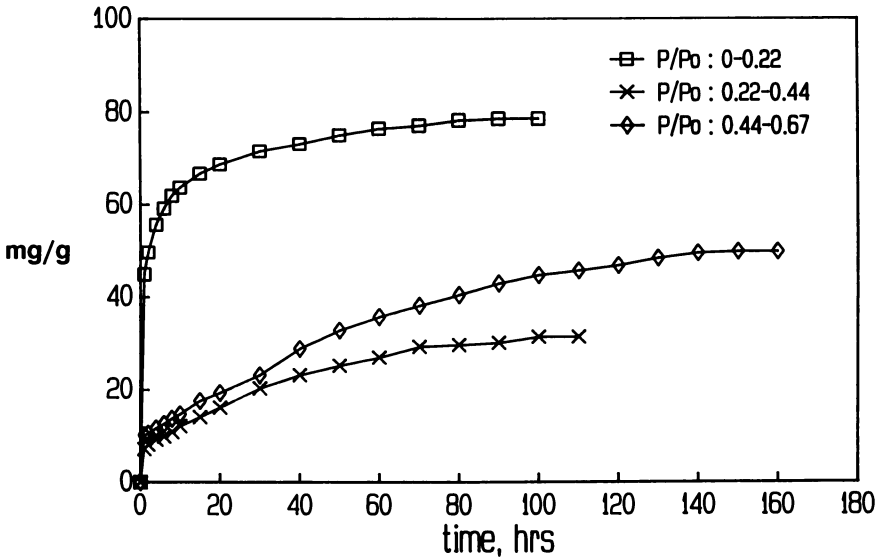


Figure 3. Sorption of Benzene by O-Methylated Extract of Illinois No. 6 Coal

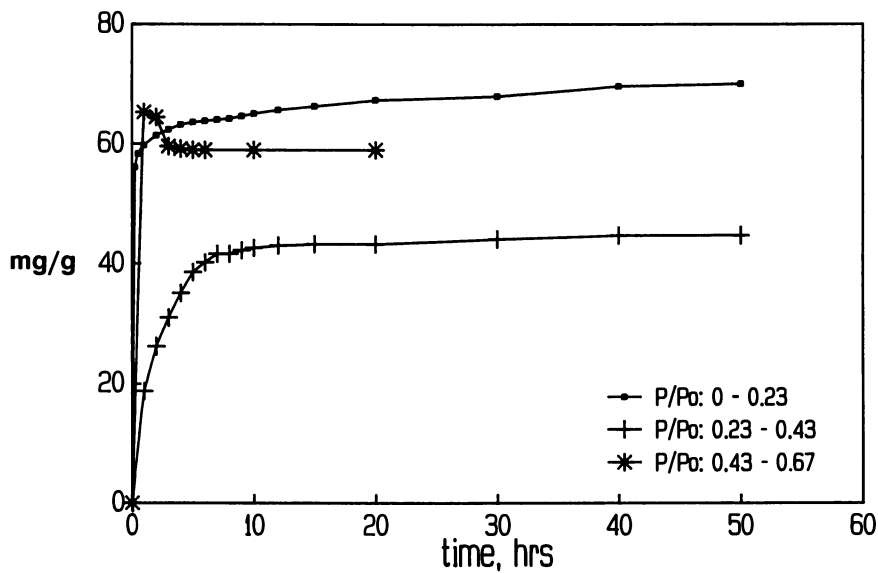


Figure 4. Sorption of Benzene by O-Butylated Extract of Illinois No. 6 Coal

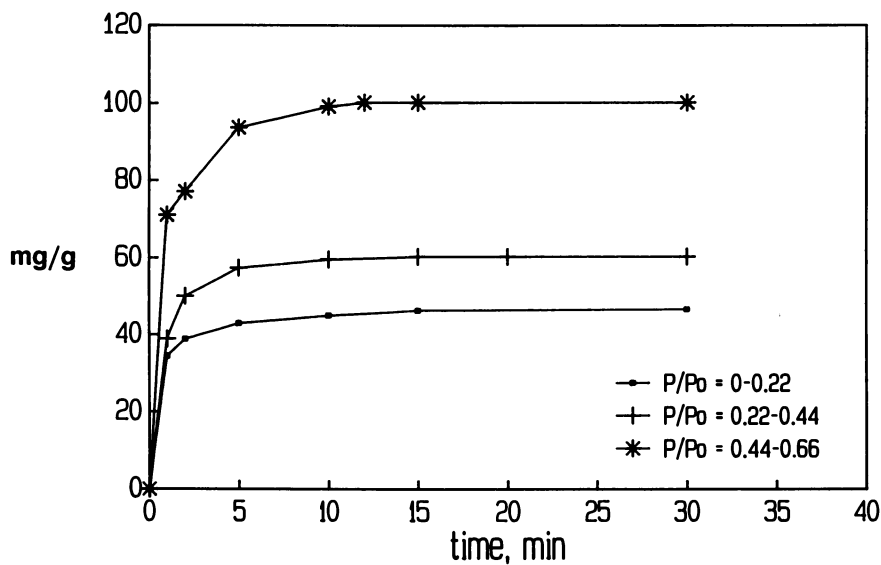


Figure 5. Sorption of Benzene by O-Octylated Extract of Illinois No. 6 Coal

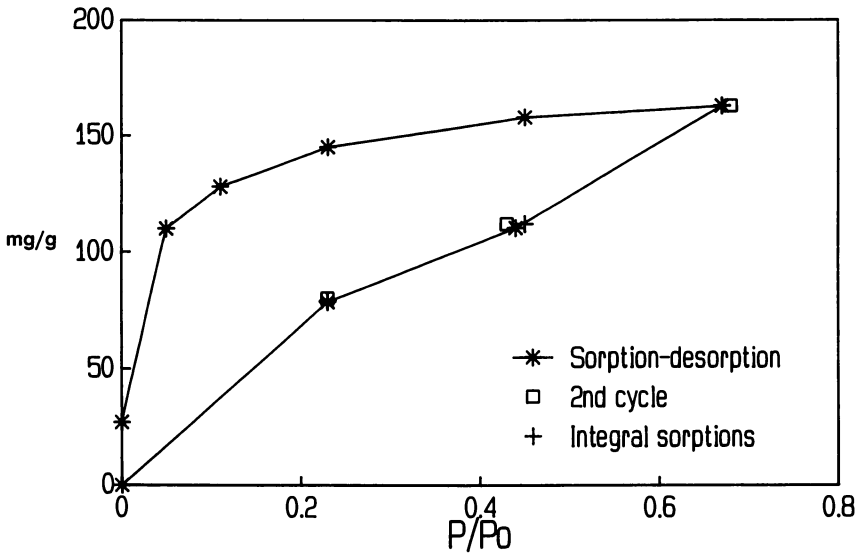


Figure 6. Sorption-desorption Isotherm for Benzene and Extract of Illinois No. 6 Coal

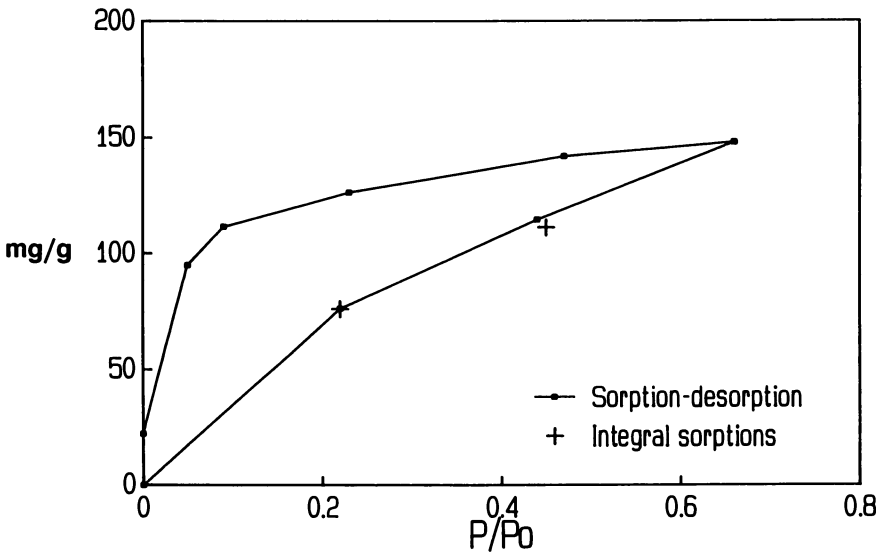


Figure 7. Sorption-desorption Isotherm for Benzene and O-Methylated Extract of Illinois No. 6 Coal

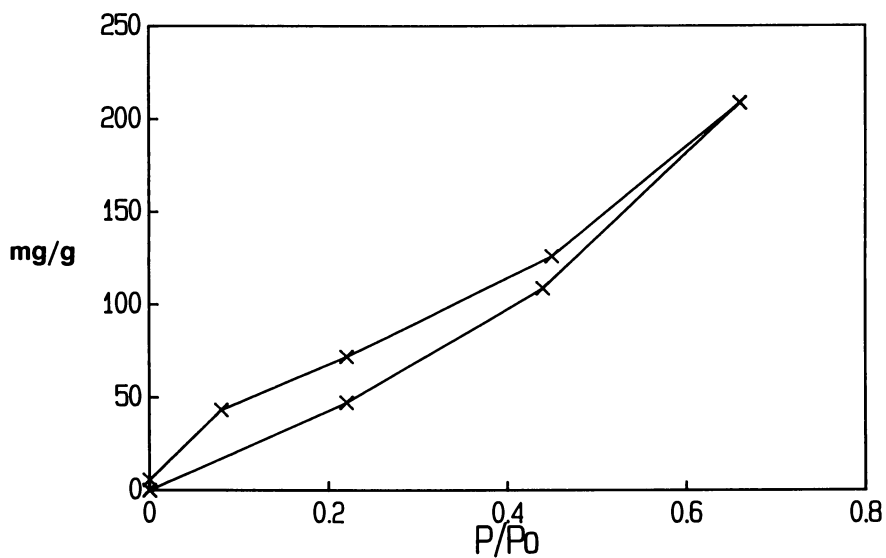


Figure 8. Sorption-desorption Isotherm for Benzene and O-Octylated Extract of Illinois No. 6 Coal

TABLE II. Equilibrium Sorption Values for the Extracts of the Illinois No. 6 Coal and Benzene at 30 °C

Extract\p/p _o	mg/g		
	0.22	0.44	0.66
Untreated	76	114	148
O-methylated	78	110	160 ^a
O-butylated	70 ^b	120 ^c	179 ^a
O-octylated	48	109	208 ^d

^a p/p_o = 0.67

^b p/p_o = 0.23

^c p/p_o = 0.43

^d p/p_o = 0.65

cumulative equilibrium uptake of benzene. Isotherms for the extract and O-methylated extract are characterized by strong hysteresis (non-reversible sorption behavior). For both extracts, a considerable amount of benzene (15-20% wt) cannot be desorbed under vacuum (~0.01 torr, 24 hrs.). However, the benzene could be completely removed from the O-methylated extract by heating to 105 °C under vacuum. Thus, benzene is not irreversibly bound to the O-methylated extract. Once the benzene was driven off, the sorption curve could be reproduced as indicated in Figure 7. We did not apply this procedure to the extract, but we expect it to behave similarly.

The sorption-desorption isotherm for the O-octylated extract is noticeably different. The shape of the sorption curve is concave upward and the hysteresis effect is much less pronounced. Nearly all of the benzene (97% wt) could be desorbed under vacuum at 30 °C. Clearly, this material is responding much differently than the untreated and O-methylated extracts.

DENSITY MEASUREMENTS. Helium densities of the extracts were determined so that the gravimetric sorption data could be converted to volume fractions needed to calculate χ parameters. The results of these measurements are shown in Table III. The density of the extract was observed to decrease with increasing size of the added alkyl group. These results are qualitatively similar to those of Liotta *et al.* (14), who studied the effects of O-alkylation on the physical structure of the native Illinois No. 6 coal.

SURFACE AREAS. CO₂ B-E-T surface areas of the unground and ground extracts were determined. The results are shown in Table III. O-methylation increases the surface area of the extract, but then the surface area of the extract decreases with increasing size of the added alkyl group. The effect of

grinding the extracts in a Wig-L-Bug device for 1 minute is to increase the surface area by 20-30 m²/g.

TABLE III. Helium Densities, CO₂ Surface Areas, and Solubilities of Illinois No. 6 Extracts

	Density, g/mL	Surface Area, m ² /g		Benzene Solubility (wt%)
		Unground	Ground ^a	
Untreated	1.30	78	95	16
O-methylated	1.29	104	124	41
O-butylated	1.24	68	88	77
O-octylated	1.18	11	39	77

^a Ground in a Wig-L-Bug device for one minute.

SOLUBILITY MEASUREMENT. The solubilities of the extracts in liquid benzene at room temperature are shown in Table III. Solubility increases with the size of the alkyl group and appears to reach a limit of 77% soluble.

DISCUSSION

EQUILIBRIUM SORPTION VALUES. The equilibrium sorption values for the extracts at various pressures of benzene are shown in Table II. The results show that O-methylated extract sorbs the most benzene at the lower pressure and that the O-octylated extract sorbs the least. At the higher pressure, the order is reversed. We believe the data shown in Table II reflect changes in the relative amounts of adsorption and absorption (swelling) with increasing size of the added alkyl groups. This interpretation is based on surface area and solubility measurements described below.

The BET CO₂-surface areas of the extracts are shown in Table III. These data show that surface area decreases with increasing size of the added alkyl group. We expect that adsorption of benzene onto surfaces to be most important for the untreated and O-methylated extract and the least important for the O-octylated extract.

Benzene solubilities of the extracts in liquid benzene at room temperature were also measured. The results, shown in Table III, show that solubility increases with increasing size of the added alkyl group. Interestingly, the O-butylated and O-octylated extracts showed the same solubilities in liquid benzene, suggesting that there is a limit to the amount of extract that can be rendered soluble in liquid benzene by O-alkylation. Extrapolating these results to the vapor pressure measurements, we would predict the untreated extract

to swell the least in benzene and the O-butylated and O-octylated extracts to swell the most.

Thus, the data in Table II can be readily explained if one considers the overall sorption process to consist of both adsorption and absorption. At low pressures, adsorption makes a relatively large contribution to the overall sorption process, and the values reflect the relative surface areas of the extracts. At higher pressures, absorption of benzene becomes relatively more important, and the equilibrium sorption values reflect the solubilities of benzene in the extract. It is interesting to note that the O-octylated extract sorbs more benzene than the O-butylated extract at the higher pressure, in spite of the fact that the O-butylated extract has a higher surface area. We conclude that benzene is more soluble in the O-octylated extract.

FLORY INTERACTION PARAMETERS. In order to calculate Flory interaction parameters (χ) from the sorption values presented in Table II, it is necessary first to assume a value of x , the degree of polymerization or the number of segments in the polymer chain. The value of x can be approximated as the ratio of the polymer molar volume to that of the solvent. For a heterogeneous polymer with wide range of molecular weights, the number average degree of polymerization, x_n , should be used.(10) Larsen *et al.* have measured the number average molecular weight of a pyridine-extract of Illinois No. 6 coal to be 1100.(17) Using a density of 1.3 g/mL for the extract, a molar volume of 846 mL/mole is calculated. Using a molar volume of 89 mL/mole for benzene, this yields a x_n of 9.5. O-methylation of the extract should have no significant effect on this value but O-butylation and O-octylation should increase the average molecular weight of the extract by 15% and 30%, respectively. Thus, x_n values of 11.5 and 13.6 were calculated for these extracts. The resulting χ parameters are presented graphically in Figure 9. χ is observed to increase with increasing pressure (or concentration) for all extracts. However, the slope of the curve diminishes with increasing size of the added alkyl group.

As discussed above, we believe adsorption becomes less important and absorption (swelling) becomes more important as the size of the added alkyl group increases. Since the χ parameter describes the "goodness" of the solvent-polymer solution, and has nothing to do with surface interactions, the more reliable χ parameter will be obtained for the O-octylated extract-benzene system. Even so, the ground O-octylated extract possesses considerable surface area and any adsorption of benzene onto surfaces will lead to errors in χ . Sorption experiments were therefore conducted on the unground extract, which possessed only 11 m²/g surface area. χ was determined to be 0.65, which was independent of pressure.

RATE of SORPTION. The overall rate of benzene sorption for the different extracts varies, depending on the size of the added alkyl group (See Figures 2-5). For the extract and O-methylated extracts, equilibrium sorption was achieved in 30 to 100 hours, depending on the experiment. For the O-

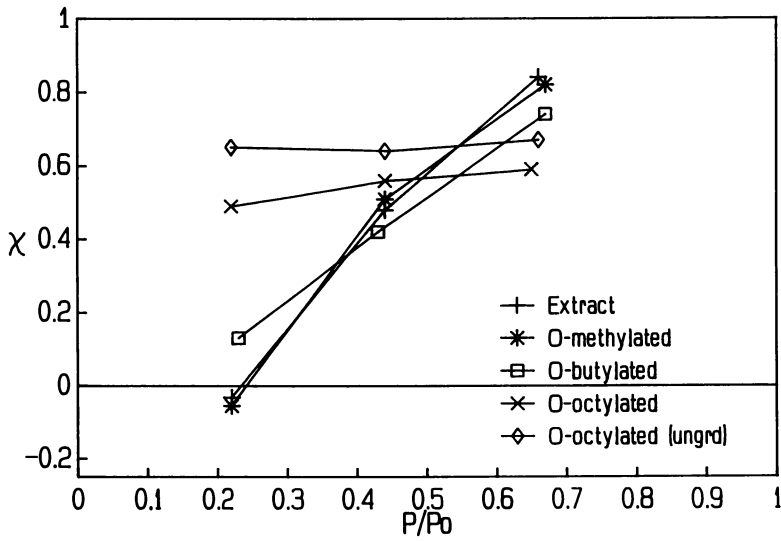


Figure 9. χ Versus Pressure for Benzene-Extract Systems of Illinois No. 6 Coal

butylated extract, equilibrium was achieved in three to ten hours. Sorption of benzene by the O-octylated extract was extremely rapid, requiring less than 30 minutes to reach equilibrium. This shift in sorption behavior might be attributed to the presence of the more flexible alkyl groups. Because of their flexibility, some regions of the alkylated extracts may be somewhat fluid (rubbery) in nature, which allows benzene to diffuse into the extract at a much faster rate.

EXTRACT and O-METHYLATED EXTRACT. The sorption of benzene by the extract and the O-methylated extract is characterized by a rapid, initial uptake followed by a very slow approach to equilibrium. Such sorption behavior is very similar to that of glassy polymers. Thus we have chosen to interpret the sorption curves shown in Figures 2 and 3 in terms of the Berens-Hopfenberg model developed for the sorption of organic vapors into glassy polymers.⁽¹⁸⁾ By doing so, we attempt to correct the total sorption values for surface adsorption in order to calculate χ parameters.

THE BERENS-HOPFENBERG MODEL. The Berens and Hopfenberg model considers the sorption process in glassy polymers as a linear superposition of independent contributions of a rapid Fickian diffusion into pre-existing holes or vacancies (adsorption) and a slower relaxation of the polymeric network (swelling).⁽¹⁸⁾ The total amount of sorption per unit weight of polymer may be expressed as

$$M_t = M_{t,ads} + M_{t,swell} \quad (2)$$

where $M_{t,ads}$ and $M_{t,swell}$ are the contributions of the adsorption and swelling processes, respectively.

The relaxation or swelling process is assumed to be first order in the concentration difference which drives the relaxation and is expressed as

$$M_{t,swell} = M_{\infty,swell} [1 - e^{-kt}] \quad (3)$$

here k is the relaxation rate constant and $M_{\infty,swell}$ is the ultimate amount of sorption due to swelling. The relaxation process is interpreted as a structural reordering or swelling of the polymeric network. It is the swelling term which is of crucial importance to our study.

The slow asymptotic approach to equilibrium exhibited by the extract and O-methylated extract, as shown in Figures 2 and 3, strongly suggest that this process might correspond to the first-order relaxation or swelling process described in the Berens-Hopfenberg model, and that the initial rapid uptake may correspond to hole filling and/or adsorption onto surfaces. If we assume that the hole-filling process is rapid and complete at long times, and that only swelling is taking place, then at long times

$$M_t = M_{\infty,ads} + M_{t,swell} \quad (4)$$

Substituting Equation (3) into (4) yields

$$M_t = M_{e,ads} + M_{e,swell} - M_{e,swell} e^{-kt} \tag{5}$$

Simplifying gives

$$M_e - M_t = M_{e,swell} e^{-kt} \tag{6}$$

and then

$$\ln (M_e - M_t) = -kt + \ln M_{e,swell} \tag{7}$$

A plot of $\ln (M_e - M_t)$ versus time should yield a straight line with an intercept of $\ln M_{e,swell}$.

The results of this analysis are shown in Figures 10 and 11 for the extract and O-methylated extract. Note that a substantial portion of each curve is linear or nearly linear at long times, indicating a first-order process. This is particularly evident for the incremental sorptions where linearity is observed over a 50 to 60 hour period. At short times, the curves clearly deviate from linearity, suggesting that other processes are dominating.

We suggest that the rapid process corresponds to hole-filling and/or adsorption onto surfaces, and that the slow process, which follows first-order behavior, corresponds to swelling of the coal extract. Extrapolation of the linear portion of the curves shown in Figures 10 and 11 to time zero should yield the total uptake of benzene attributed to swelling. The results of this analysis are summarized in Table IV, where the total benzene uptake, M_e , and the uptake attributed to the hole-filling/adsorption and the swelling processes, $M_{e,ads}$ and $M_{e,swell}$, are shown.

TABLE IV. Benzene Sorption Data for Extract and O-Methylated Extract of Illinois No. 6 Coal at 30°C

Pressure Interval p/p_o	Extract (mg/g)			O-Methylated (mg/g)		
	M_e	$M_{e,ads}$	$M_{e,swell}$	M_e	M_{ads}	M_{swell}
0 -0.22	76	64	12	78	56	22
0.22-0.44	38	17	21	32	7	25
0.44-0.66	34	12	22	50 ^a	6	44
Total:	148	93	55	160	69	91

^a $p/p_o = 0.44 - 0.67$

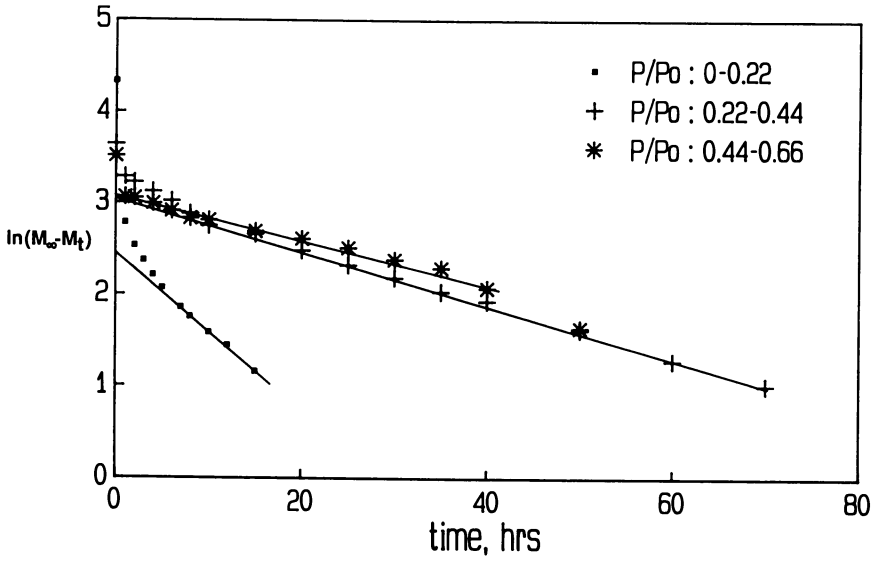


Figure 10. Natural Log ($M_{\infty} - M_t$) Versus Time for Extract of Illinois No. 6 Coal

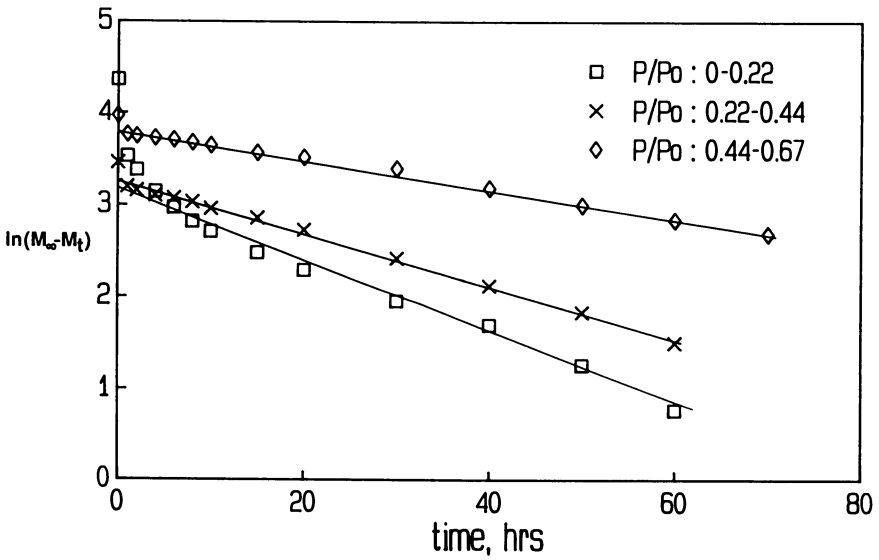


Figure 11. Natural Log ($M_{\infty} - M_t$) Versus Time for O-Methylated Extract of Illinois No. 6 Coal

If this interpretation of the sorption process is correct, it indicates that when the benzene pressure is raised from zero to an activity of 0.22, the dominant process is hole-filling and/or adsorption, with only a relatively minor contribution from actual swelling. However, in subsequent incremental sorptions, the swelling process is clearly dominant. These results are similar to those of Berens and Hopfenberg in their studies on glassy polyvinylchloride.(18) According to their interpretation, the polymer is initially penetrant-free in an integral sorption experiment, and the hole-filling process therefore dominates. Incremental sorptions, however, proceed with polymer in which most of the sorption holes are pre-saturated. The relative contribution of swelling is therefore larger in these experiments.

The swelling data in Table IV can be used to calculate χ parameters for the extract and O-methylated extract using Equation 1. The results are shown in Table V. The χ parameters for both extracts are observed to be positive and independent of pressure or concentration of benzene. The magnitude of the parameters are much larger than that determined for the O-octylated extract (0.65) which is consistent with their lower solubilities in liquid benzene. The χ parameters are much larger than those determined by Larsen *et al.* for the pyridine-extracted Illinois No. 6 coal, which was near 0.3.(6) The reason for this are not clear. However, we note that benzene is a very poor solvent for these pyridine-extracts so large χ parameters are expected.

TABLE V. Volume Fractions of Solvent and χ Parameters for the Illinois No. 6 Coal Extracts and Benzene

p/p_0	Extract		O-Methylated		O-Octylated ^c	
	v_1	χ	v_1	χ	v_1	χ
0.22	0.019	1.6	0.032	1.1	0.051	0.65
0.44	0.050	1.5	0.066	1.2	0.118	0.64
0.66	0.080	1.5	0.12 ^a	1.2	0.220 ^b	0.67

^a $p/p_0 = 0.67$

^b $p/p_0 = 0.68$

^c Determined on unground extract using total sorption values.

Finally, a calculation of the solubility parameter of the extracts can be made using the equation

$$\delta_e = \left[\frac{(\chi - 0.30) RT}{V} \right]^{1/2} + \delta_s \quad (8)$$

where δ_e and δ_s are the solubility parameters of the extract and benzene (9.2 Hildebrands), respectively, and V is the molar volume of benzene (89 mL/mol). The results are summarized in Table VI. Van Krevelen has estimated solubility parameters of coals using a group contribution method and has calculated values ranging from 10.6 to 15.2 Hildebrands.⁽¹⁹⁾ The solubility parameter calculated here for the extract of the Illinois No. 6 coal falls within this range. O-alkylation lowers the solubility parameter as expected. The solubility parameters determined here for the extract and its O-methylated derivative are considerably larger than those determined by Larsen *et al.* for the Illinois No. coal and its O-methylated derivative.⁽⁶⁾ However, only nonpolar contributions to the solubility parameter are measured in their technique. The coal extracts studied here presumably contain a substantial population of hydrogen bonds and other polar interactions, which contribute to the measured solubility parameter using the vapor pressure technique.

Table VI. χ Parameters and Solubility Parameters of Extracts of Illinois No. 6 Coal

	χ	δ_e
Extract	1.5	12.0
O-methylated	1.2	11.7
O-octylated	0.65	10.7

Finally, we note that the χ and solubility parameters of the O-butylated extract are noticeably absent in Table VI. We have attempted to analyze the sorption kinetics according to the Berens-Hopfenberg model in order to correct for adsorption effects, but the treatment yielded unreasonable χ parameters. The reason for this is not clear, but we believe it may be due to the fact that diffusion into the extract is so rapid. Hole-filling and swelling may have comparable rates so that a separation of the two processes is not possible.

CONCLUSIONS

The vapor sorption technique appears to be very promising for determining Flory interaction and solubility parameters of coal extracts. It is clear that surface adsorption of solvent vapor plays a substantial role in the overall sorption process, at least for the extracts studied here. In this regard, the sorption values must first be corrected for adsorption in order to obtain the true swelling values, which are needed to calculate the Flory interaction parameters. If the extract behaves as a glassy material, the Berens-Hopfenberg sorption model for glassy polymers appears useful for making this correction.

The extent to which these Flory interaction parameters apply to the pyridine-insoluble portion of the Illinois No. 6 coal is open to question. We cannot address this aspect fully here, but we have noted that the pyridine-soluble and -insoluble portions of the Illinois No. 6 coal studied here have similar carbon, hydrogen and oxygen contents. Maciel has observed that the aromaticities of the two portions of an Illinois No. 6 coal are similar as well.(12) Based on this alone, it seems that the pyridine-soluble portion is representative of the larger, crosslinked portion, at least for the Illinois No. 6 coal, but this aspect remains controversial,(13) so caution is warranted.

ACKNOWLEDGMENTS

This work was supported by a grant from the U.S. Department of Energy, Grant No. DE-FG22-88PC88924, and the Research Corporation. We thank D. Smith for determining helium densities and R. Porter for obtaining NMR spectra.

LITERATURE CITED

1. Green, T.; Kovac, J.; Larsen, J.W. in Coal Structure; R. A. Meyer, Ed., Academic Press, New York, N.Y., 1982, p. 199.
2. Treloar, L.R.G. The Physics of Rubber of Elasticity; Clarendon Press, Oxford, 1975, pp. 128-139.
3. Sanada, Y.; Honda, H. Fuel 1967, **46**, 451.
4. Kirov, N.Y.; O'Shea, J.M.; Sergeant, G.D. Fuel 1967, **47**, 415.
5. Peppas, N.A.; Lucht, M.L.; "Investigations of the Crosslinked Macromolecular Nature of Bituminous Coals," Final Report, DOE Contract No. DE-F622-78E, 12279, 1980.
6. Larsen, J.W.; Green, T.K.; Kovac, J. J. Org. Chem. 1985, **50**, 4729.
7. Larsen, J.W.; Shauver, S. Energy Fuels 1990, **4**, 74-77.
8. Hsieh, S.T.; Duda, J.L. Fuel 1987, **66**, 170.
9. Nelson, J.R.; Mahajan, O.P.; Walker, P.L. Fuel 1980, **58**, 831.
10. Bonner, D.C. J. Macrol. Sci. - Revs. Macrol. Chem. 1975, C13(2), 263-319.
11. Flory, P.T. "Principles of Polymer Chemistry," Cornell University Press, 1953.
12. Davis, M.F.; Quinting, G.R.; Bronnimann, C.E.; Maciel, G.E. Fuel 1989, **68**, 763-770.
13. Given, P.H. in Coal Science, Vol. 3; M.L. Gorbaty, J.W. Larsen, and I. Wonder, Eds., Academic Press, New York, NY, 1984, pp. 190-204.
14. Liotta, R.; Rose, K.; Hippo, E. J. Org. Chem. 1981, **50**, 277-283.
15. Buchanan, D.H.; Osborne, K.; Warfel, L.C.; Wampang, M.; Lucas, D. Energy Fuels 1988, **2**, 113-170.

16. Botto, R.E.; Choi, C.; Muntean, J.V.; Stock, L.M. Energy Fuels 1987, 1, 270-273.
17. Larsen, J.W.; Mohammadi, M.; Yigirsu, I.; Kovac, J. Geochemica Cosmochimica Acta 1984, 48, 135-141.
18. Berens A.R.; Hopfenberg, H.B. Polymer 1978, 5, 489.
19. Van Krevelen, D.W. Fuel 1966, 45, 229.

RECEIVED November 5, 1990

Chapter 12

Modeling of Coal Structure by Using Computer-Aided Molecular Design

G. A. Carlson and B. Granoff

Fuel Science Division, Sandia National Laboratories,
Albuquerque, NM 87185

Knowledge of coal molecular structure is important in the understanding of coal conversion and coal reactivity. Computer-aided Molecular Design (CAMD) has been used to create and study 3-dimensional models of several postulated coal molecular structures (Given, Wisser, Solomon, and Shinn). Using molecular dynamics calculations, a minimum-energy conformation for each structural model has been determined. Other characteristics of the resulting coal structures such as physical density and hydrogen bond frequency have also been defined. Future applications of this new tool, including combination molecular/macromolecular models and interactions of the models with solvent molecules, will be outlined.

The reactivity of coal is determined in substantial part by its chemical and physical structure. However, coals are very diverse, and even within any given coal type there is considerable heterogeneity. Nonetheless, because of the strong link between structure and reactivity, there have been many attempts to model the molecular structure of various coals. For bituminous coals, the most widely accepted molecular models developed during the past 30 years have been the aromatic/hydroaromatic structures, in which clusters containing about three linked aromatic and/or hydroaromatic rings along with appropriate numbers and types of heteroatoms, are interconnected by hydroaromatic, etheric or aliphatic linkages (1-4). These models incorporate the average chemical and molecular characteristics of coal, and are not intended explicitly to represent actual "coal molecules". They have been derived using all available chemical and structural data on coal (including elemental composition, NMR data on aliphatic/aromatic distribution of carbon and hydrogen, and selective chemical reactions to determine distributions of oxygen, nitrogen, and sulfur functional groups). Data on product distributions from coal liquefaction have provided additional insight into the molecular structures of the clusters and the ways they are interconnected.

A limitation of these molecular structures has been their two-dimensional nature, which necessarily ignores most of the intercluster interactions that occur

within an actual three-dimensional coal structure. Recently, Spiro (5) has constructed space-filling models of several of these structures, to address some of these issues. Using the insights obtained from these models, he identified several steric difficulties in the original structures, and discussed the possible significance of the three-dimensional structures on mechanisms of coal pyrolysis. However, the manipulation of space-filling models, while useful in many ways, does not allow one to determine optimal structural conformations.

Over the past few years, computer-aided molecular design (CAMD) techniques have been developed to provide additional understanding of the structure and properties of complex molecular systems (6). Currently, CAMD techniques are being widely used in the pharmaceutical industry to guide the design and synthesis of a variety of biomolecules (drugs, enzymes, inhibitors, proteins). Using CAMD, one can not only construct a three-dimensional representation of a molecule, but can also convert the structure to an energy-minimized physical conformation, using molecular dynamics techniques. CAMD has been used to study structures of heavy coal liquids (7), but not to examine the energetics of the structures. In this paper, CAMD is used to create three-dimensional models based on several postulated coal structures, and then to identify minimum-energy physical conformations for those models. The energetics are compared and used to rank the models. The physical densities of the models are calculated and compared with experimental data. Finally, the future application of CAMD to macromolecular models of coal and to solvent interactions with coal are discussed.

Method

The CAMD studies described were carried out using BIOGRAF (BioDesign, Pasadena, CA), a molecular modeling software program for simulating organic and biological molecules. BIOGRAF allows the user to build molecules (structures), display them in a variety of formats (stick; dot surface; space-filling), and calculate minimum energy conformations for them. The minimum energy conformations are found using molecular dynamics calculations with a suitable force-field approximation (6). In molecular dynamics, the energy of a structure is evaluated periodically as the atoms are allowed to move relative to one another according to Newton's equations of motion. During the dynamics calculations, structures twist and fold in ways that tend to optimize the non-bonded interactions (van der Waals, electrostatic, ionic, and hydrogen bonds), while maintaining appropriate bond lengths and angles. Dynamics runs usually involve many thousands of evaluation steps, representing the equivalent of many picoseconds of molecular motion. After a dynamics run, the minimum-energy conformation is taken through an additional energy minimization using a conjugate-gradient method. In this process, the atoms of the structure are allowed to move incrementally until a minimum energy is approached. This energy minimum may be a global energy minimum or a local energy minimum, depending on the details of the structure and the extent of the dynamics calculations.

The "temperature" specified for the dynamics calculation defines the atomic velocity distribution. In the current studies, the temperature was allowed to ramp downward from 300 K to 20 K over a 10 ps period (5000 dynamics steps). This allowed the coal structures initially to overcome potential energy barriers between different conformations, and later to approach a minimum energy state.

BIOGRAF supports a number of force fields (AMBER, MM2, and DREIDING). The DREIDING force field, developed for the BIOGRAF

application, was used in the current study. DREIDING is a very general force field that can be used for a large number of atom types. The Dreiding force field calculates the energy as a sum of covalently-bonded interactions (E_s =stretch; E_b =bend; E_t =torsion; and E_i =inversion) and non-covalently-bonded interactions (E_v =van der Waals; E_e =electrostatic; and E_h =hydrogen bonds).

$$E = (E_s + E_b + E_t + E_i) + (E_v + E_e + E_h)$$

Each individual interaction is calculated as the product of a force constant times some function of the departure from equilibrium. For example, for the stretching interaction, $E_s = 1/2 K_s \cdot (R - R_e)^2$, in which K_s is the stretching force constant and R and R_e are the current and equilibrium bond lengths. In DREIDING, the equilibrium values for bond length, angle bend, etc. are defined quite accurately for each atom type. Since bond lengths and angles in minimum-energy structural conformations are not usually significantly different from equilibrium values, it is thus generally possible to determine the relative positions of atoms in a structure (i.e., the structural conformation) with good accuracy. On the other hand, a limitation of DREIDING is that it uses a single force constant for a given type of interaction for all atom types. Thus, for example, one force constant is used to calculate all bond stretches, and a different force constant is used with all angle bending motion. As a result, the energies calculated are most meaningful in a relative, rather than in an absolute, sense.

The BIOGRAF program was run on a MicroVAX II computer equipped with an Evans and Sutherland PS390 graphics terminal. The size of coal structures evaluated, and the duration of molecular dynamics runs, were limited by the available computing speed of this system (a 5000-step, 10-ps molecular dynamics run for a 1040-atom structure, with about 75,000 van der Waals interactions per step, required about 100 hours of computation).

BIOGRAF does not have the capability to determine the physical density of structures. Thus, separate calculations were made of volume elements from which the density could be determined. Using the atomic coordinates produced as output from the BIOGRAF program, the elements of a volume of space containing the structure were identified as structural volume, void volume, or external volume. The structural volume was defined as all volume elements that were "within" the structure, except for the void volume. The boundaries of the structure were defined by the volume elements occupied by its outermost atoms. The void volume was defined as all volume elements that were within the structure, but not within 4 angstroms of any atom. This distance was chosen to represent approximately the size of a probe atom or molecule that might be used in a density determination. The external volume was defined as all other volume elements. Once the volume elements were all identified, the density of the structure was calculated from the molecular weight of the structure, multiplied by Avogadro's number, and divided by the appropriate volume. Densities calculated from the structural volume represent "true" densities, as might be determined experimentally using helium or water displacement. Densities calculated from the structural plus void volume are "particle" densities, as would be measured by displacement of mercury (8).

Results

BIOGRAF was used to create and study three-dimensional models of four postulated bituminous coal molecular structures, those of Given, Wiser, Solomon, and Shinn (1-4). Although other molecular structures have been

described in the literature, these four are representative of the structures that have been developed over the past 30 years.

The Given structure (1) was one of the first structures developed with the assumption of moderate size aromatic/hydroaromatic ring clusters. It continues to be cited as a possible representative coal structure. For CAMD modeling, the Given structure was modified as suggested by Spiro (5) to eliminate a very strained quaternary carbon bond near the center of the structure. The molecular formula was unchanged by this modification. Figure 1a shows the molecular structure from the literature (1), Figure 1b the initially-created computer space-filling model, and Figure 1c the minimum energy conformation attained by the model after 10 ps of molecular dynamics. Significantly, the Given structure is seen to be rather rigid, being constrained by pairs of methylene bridges between aromatic structures.

Figure 2 shows the same set of representations of the Wisser structure (2). For the CAMD study this structure was modified, as Wisser himself later suggested (9), by replacing a -S-S- bridge by a -CH₂-CH₂- bridge. Also, open bonds were capped with methyl groups. Even before energy minimization (Figure 2b), the Wisser structure already had a substantially three-dimensional nature due to steric hindrance by the clusters. Spiro reported (5) he was unable to construct a space-filling model of the Wisser structure without modification, due to steric effects. The minimum-energy conformation (Figure 2c) appears somewhat more compact than the initial structure. The Wisser structure has a higher degree of cross-linking between clusters than the other structures, and this seems to have limited the degree of folding observed after energy minimization.

The Solomon structure (Figure 3), as it appears in the literature (3), consists of three unconnected molecular fragments. It was modified for CAMD study by creating two additional four-ring fragments identical to the first, and connecting one four-ring fragment to each of the three open bonds on the larger fragments. Even with these connections, the Solomon structure remains the most loosely-connected of the four structures. As seen in Figures 3b and 3c, it is nearly two-dimensional as originally constructed, but folds up very substantially during molecular dynamics.

The Shinn structure (Figure 4) represents the most complex coal molecular structure in the literature, consisting of 1306 atoms with a molecular weight of 10023. It includes three isolated clusters (shown enclosed by solid lines in Figure 4a) contained within a larger structure of linked clusters. Shinn's structure was simplified for CAMD modeling by eliminating that fraction identified in his Table 5 as "residue", approximately 20% of the original structure. This simplification facilitated the molecular dynamics runs, which were very time-consuming for this large model. Open bonds at the periphery of the structure were capped with methyl groups. Figures 4b and 4c show that the Shinn structure folded up very substantially during molecular dynamics and energy minimization.

To evaluate further the CAMD results, a number of atomic and chemical parameters from each structure (number of atoms, fractions of aromatic carbon and hydrogen, weight fraction of each atomic species, empirical formula) were compared with the original literature for each structure. This provided a useful check on the accuracy of the computer models. Results of the computer analyses for the four coal structures are given in Table I. The total numbers of atoms only appear as guides to the size and complexity of each structure, and bear no relationship to the size of a "coal molecule" or a decomposition product.

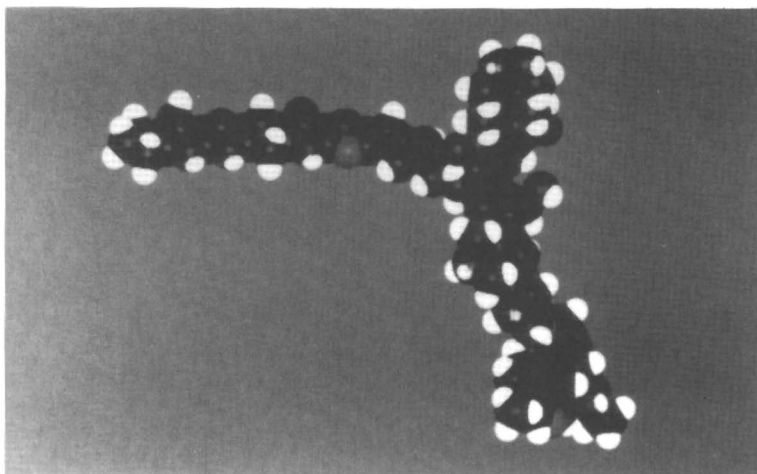
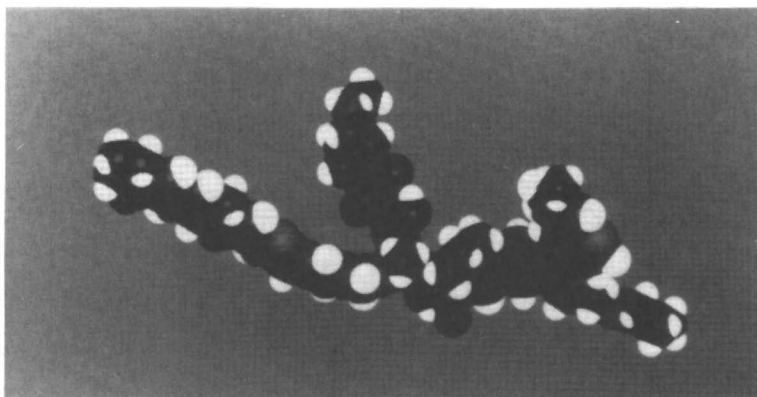
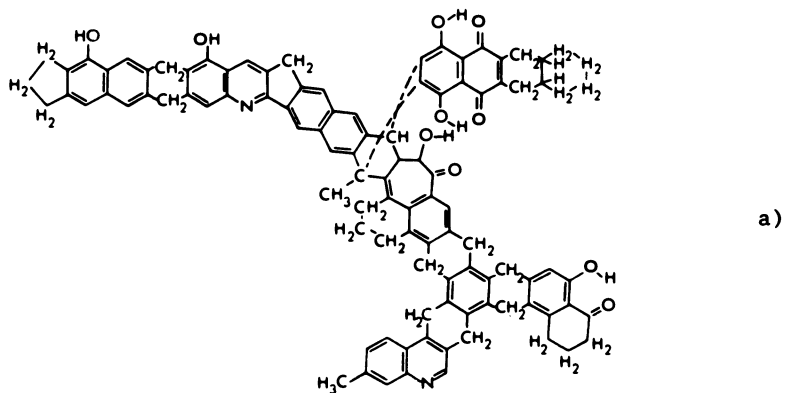


Figure 1. Given structure. a) Structure from literature; b) Initial CAMD-generated structure; c) Energy-minimized structure.

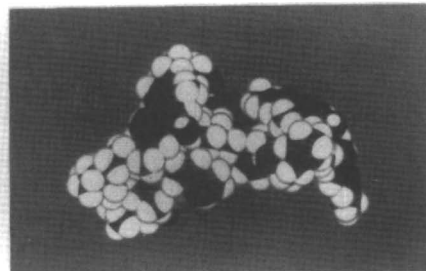
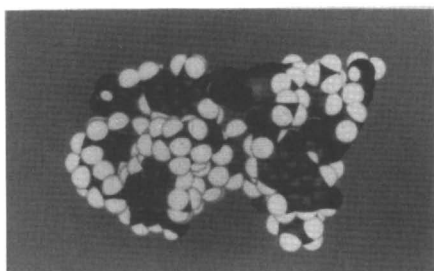
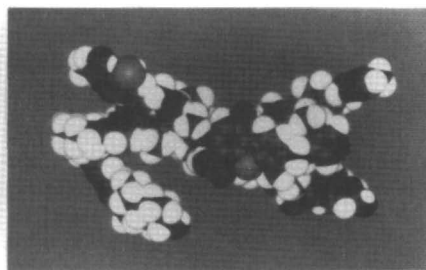
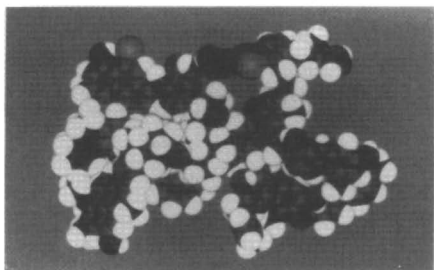
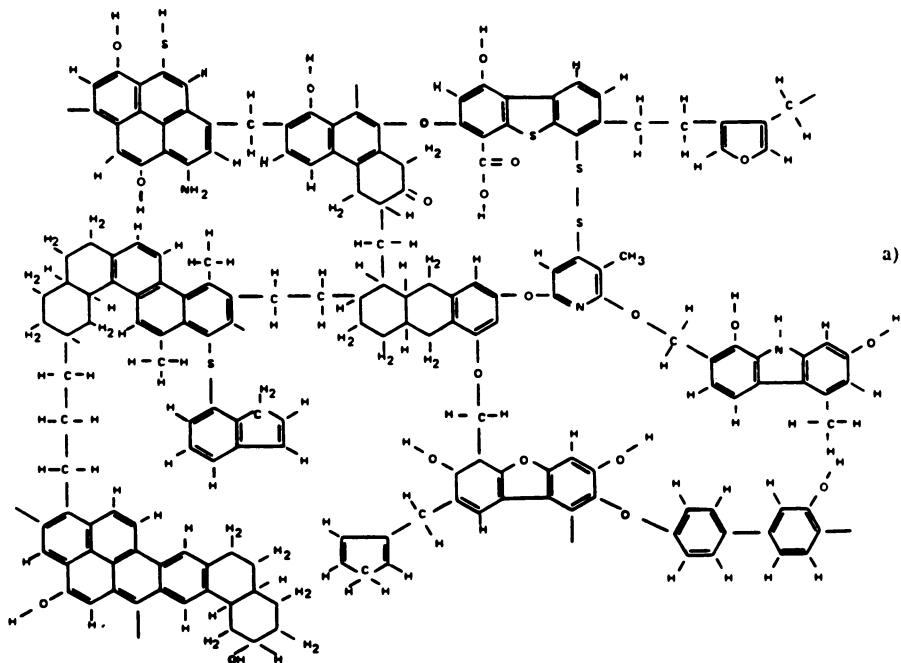
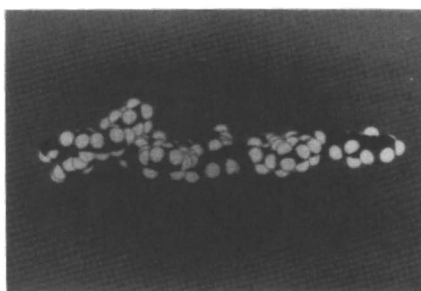
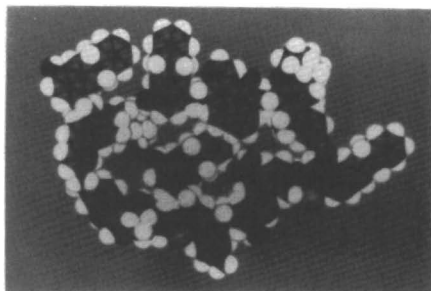
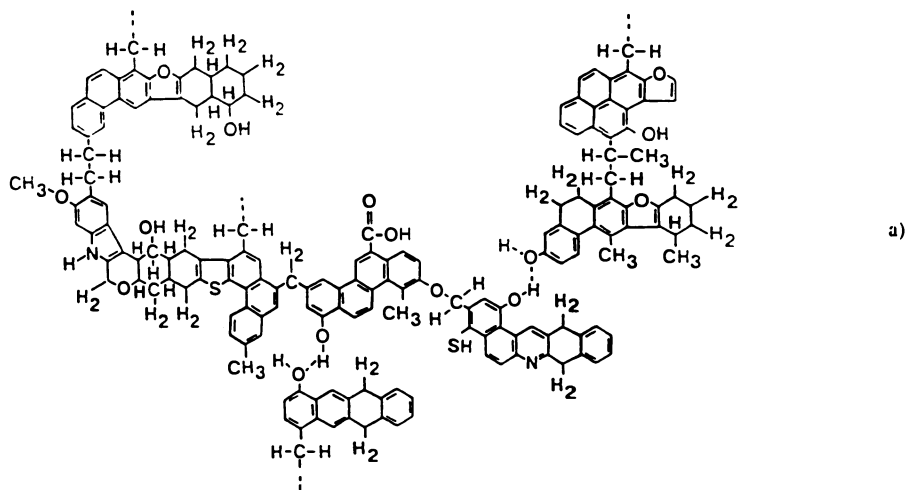
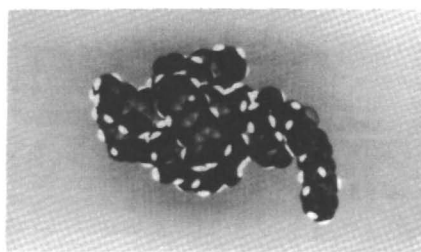
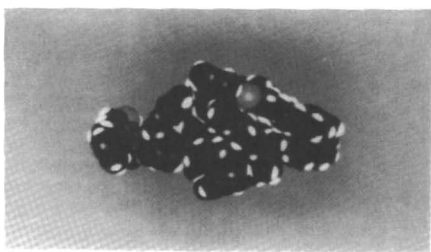


Figure 2. Wiser structure. a) Structure from literature; b) Initial CAMD-generated structure, top and side views; c) Energy-minimized structure, top and side views (same orientation, same scale).



b)



c)

Figure 3. Solomon structure. a) Structure from literature; b) Initial CAMD-generated structure, top and side views; c) Energy-minimized structure, top and side views (same orientation, same scale).

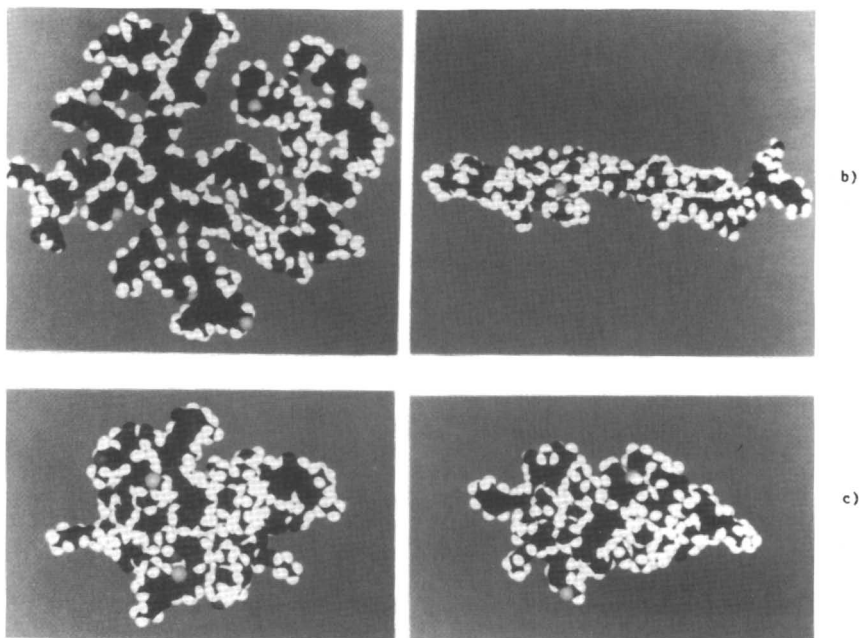
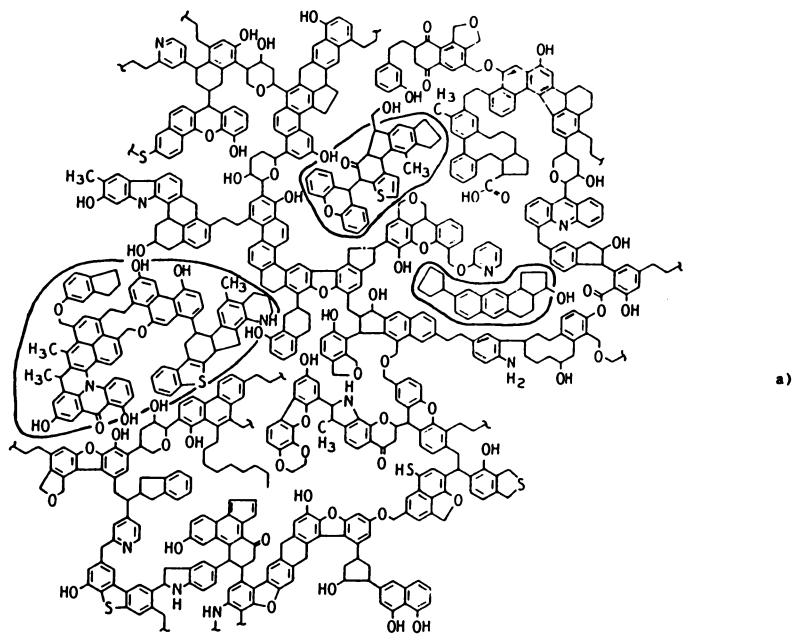


Figure 4. Shinn structure. a) Structure from literature; b) Initial CAMD-generated structure, top and side views; c) Energy-minimized structure, top and side views (same orientation, same scale).

Table I. Coal Structural Parameters

Parameter	Given	Wiser	Solomon	Shinn
Atoms	193	394	396	1040
C_{Ar}/C_{Tot}	0.66	0.70	0.74	0.71
$H_{Ar}/(H_{Ar} + H_{Al})$	0.21	0.28	0.40	0.34
Wt. Fraction (DMMF)				
C	0.820	0.781	0.823	0.795
H	0.053	0.059	0.056	0.056
O	0.107	0.113	0.090	0.113
N	0.019	0.014	0.009	0.014
S	---	0.032	0.021	0.020
Normalized Formula	$C_{100}H_{77}O_{9.8}N_{2.0}$	$C_{100}H_{90}O_{11}N_{1.6}S_{1.6}$	$C_{100}H_{81}O_{8.2}N_{1.0}S_{1.0}$	$C_{100}H_{85}O_{11}N_{1.5}S_{1.0}$
Energy (kcal/atom)	2.01	1.62	1.50	1.55
MW/H-bond	497	212	302	208
Density (g/cc)	1.46	1.28	1.32	1.25

From Table I, a significant difference between the CAMD models is in the fraction of aromatic hydrogen. The value for Solomon's model is too high, being biased upwards by the addition of two highly-aromatic four-ring fragments to the CAMD model. Given, on the other hand, created a structure that would support a low fraction of aromatic hydrogen, to match that based on infrared data available at the time. His value is much lower than those of the other authors and is probably incorrect, judging from more recent FTIR data (10). In order to obtain this low fraction of aromatic hydrogen, Given used pairs of methylene bridges extensively to connect the aromatic clusters. This explains the rigidity of his model, which is a major difference between his and the other structural models.

Also included in Table I is the minimum energy for each structure, determined at the end of molecular dynamics and energy minimization calculations. In order to make the results more easily comparable, the energies are expressed per unit atom. The Given structure is energetically less favorable than the other three by 25-30%. The reason is that the rigidity of the Given structure does not permit the clusters to fold, thus minimizing van der Waals and hydrogen-bond interactions between the clusters.

The energy-minimized structures were also used to estimate the hydrogen-bond density in coal. Based on the total number of hydrogen bonds indicated by BIOGRAF, and using the molecular weight of each coal structure, the average molecular weight per hydrogen bond was determined to be between 208 and 497 (Table I). The Given structure, which did not fold substantially, exhibited the least hydrogen bonding. Further, the hydrogen bonds formed in the Given

structure were between atoms on adjacent rings on the same cluster, and thus did not contribute to intercluster bonding. We can compare the hydrogen-bond density estimated from CAMD analysis with that of Larsen and coworkers (11), who have recently evaluated the macromolecular network structure of two bituminous coals, using solvent-swelling techniques. Using the Kovac equation to analyze the solvent-swelling behavior of unextracted coal, which is largely cross-linked by hydrogen bonds, Larsen estimates an average molecular weight between cross-links of 200-400. Although he claims these data to be only qualitatively correct, they are in good agreement with our computer models.

Density and pore size distributions are properties that have been experimentally measured for various coals and coal macerals (8,12). The densities calculated for the energy-minimized CAMD structures are given in Table I. Since no void volume was found in any of the structures, the densities calculated represent "true" density. With the exception of the Given structure, the densities we have calculated are on the order of those determined for bituminous coal using helium ("true" density), 1.28-1.33 g/cm³ (8), and for vitrinite macerals, the major constituents of bituminous coal, in aqueous solution ("apparent" density), 1.25-1.35 g/cm³ (12). The Given structure, for which a higher density was calculated, is the smallest structure studied and has only surface atoms. Separate studies of model CAMD structures demonstrated that calculated densities for structures with high surface-to-volume ratios (like the Given structure) are typically 5-10% too high. These data, and the calculational method, are still being refined.

To allow us to evaluate porosity in our structures, we have developed the capability to write BIOGRAF-compatible coordinate files of the "structural", "void", and "external" volume grid points. These can then be displayed graphically along with the molecular structure being studied. The structures we have modeled thus far show some surface concavities, but do not show evidence of internal voids large enough to accept solvent molecules or to allow migration of a mobile phase. Since bituminous coals do show substantial porosity (8), this points up a shortcoming in the CAMD studies carried out to date.

Based on all of the data analyzed to date (energetics; folding; physical density; hydrogen bond density), the Shinn, Wisner and Solomon structures appear at this time to be the more favored structures. It is not possible to choose a "best" structure from among them, although the diversity present in the larger Shinn structure would form a rationale for favoring it slightly.

Discussion

CAMD modeling has been used in this study to compare and partially to differentiate several postulated bituminous coal models based on their physical structures, minimum energies, and other characteristics. It is clear from the folding of the CAMD structures after molecular dynamics (especially in Figures 3c and 4c) that simple two-dimensional representations cannot adequately represent the structure of coal. Inter-cluster bonding has a powerful influence on coal structure when three-dimensional models are employed.

On the other hand, it is not possible to determine unequivocally the minimum-energy structure of a given molecular model. For each of the three relatively flexible structures modeled, there was actually a large number of slightly different conformations with similar (low) energies. This suggests first that a number of nearly-equivalent structures might be equally probable in coal, and second, that structures with substantially lower energies than those identified are probably not likely.

Larsen, Cody and coworkers have reported evidence of very little preferred orientation of organic molecules within bituminous coals (13,14). Although the ring structures in the energy-minimized CAMD models show on the average no preferred orientation (some local stacking was observed, especially in the Solomon and Shinn models), the macrostructure is still somewhat anisotropic. If an extended structure based on the several stacked units of the original quasi-planar Shinn structure had been constructed and energy-minimized, the anisotropy would have been more marked. This is consistent with Larsen's experimental observations (13) that vitrinite samples have essentially randomly oriented organic groups (on a macroscopic scale), but at the same time show highly anisotropic mechanical and solvent swelling properties.

In many ways, the molecular models that we have used as the basis for our CAMD studies describe coal structure very well. However, none of the models investigated thus far contains explicit three-dimensional covalent cross-links. Actually, the models we have studied are primarily constructed of long chains of one-dimensionally-linked clusters with a number of short side-chains. However, it has been established on the basis of solvent swelling studies (11,15,16) that bituminous coal is primarily made up from a three-dimensional network of clusters held together by covalent bonds and by an even higher density of hydrogen bonds. These macromolecular models of coal, which are less concerned with the molecular structure than with the ways that clusters are bonded to one another, provide a complementary way of describing coal structure.

We are beginning to develop CAMD models that incorporate the best characteristics of both the molecular and macromolecular models. Our new coal structural model will use coal fragments such as those postulated by Shinn (4), but joined together by three-dimensional covalent cross-links as suggested by Larsen (15). Because these models will be more constrained by the three-dimensional cross-links, they will be less efficient at folding and at filling space. Thus, we anticipate that internal porosity, absent in the present models, will be observed in the new models. We will vary the covalent cross-link density and observe the effect on physical density, internal porosity, and hydrogen bond density. We will also study solvent interactions, both polar and non-polar, with the new structures. We will quantify the changes in structural volume as the internal hydrogen bonds are displaced by solvent hydrogen bonds. The results will be compared with solvent swelling data, and used to provide an independent estimate of effective cross-link density in bituminous coal.

This work represents a first use of CAMD techniques to model coal structure and energetics. The coupling of molecular and macromolecular models represents an exciting future possibility. Obviously, CAMD techniques could also be used to model coals of varying rank. At this time, it is not possible to model chemical interactions using CAMD, since there is no provision for bond-breaking and bond-making. Nonetheless, it appears that CAMD techniques represent a very powerful new tool for studying the nature of coal structure, both molecular and macromolecular.

Acknowledgments

This work was supported by the U. S. Dept. of Energy at Sandia National Laboratories under Contract DE-AC04-76DP00789.

Literature Cited

1. Given, P. H., Fuel 1960, 39, 147.
2. Wisner, W. H., Proc. of the Electric Power Research Institute Conf. on Coal Catalysis, 1973.
3. Solomon, P. R., in New Approaches in Coal Chemistry, Am. Chem. Soc. Symp. Series No. 169, 1981; p. 61.
4. Shinn, J. H., Fuel 1984, 63, 1187.
5. Spiro, C. L., Fuel 1981, 60, 1121.
6. Fruhbeis, H., Klein, R., and Wallmeir, H., Angew. Chem. Int. Ed. Engl. 1987, 26, 403.
7. Robinson, K. K., Proc. of the Electric Power Research Institute Conf. on Coal Structure, 1987, Ch. 3.
8. Mahajan, O. P., "Coal Porosity", in Coal Structure, (R. A. Meyers, ed.), Academic Press, New York, N. Y., 1982; p. 51.
9. Wisner, W. H., NATO ASI Series C 1983, 124, 325.
10. Solomon, P. R., Am. Chem. Soc. Div. Fuel Chem. Preprints 1979, 24(2), 184.
11. Larsen, J. W., Green, T. K., and Kovac, J., J. Org. Chem. 1985, 50, 4729.
12. Crelling, J. C., Proc. 1987 Internat. Conf. on Coal Sci., 1987, p. 119.
13. Larsen, J. W., Am. Chem. Soc. Div. Fuel Chem. Preprints 1988, 33(1), 400.
14. Cody, G. D., Jr., Larsen, J. W. and Siskin, M., Energy and Fuels 1989, 3, 544.
15. Larsen, J. W., Am. Chem. Soc. Div. Fuel Chem. Preprints 1985, 30(4), 444.
16. Brenner, D., Fuel 1985, 64, 167.

RECEIVED November 5, 1990

Chapter 13

Correlation of Coal Properties with Hydroliquefaction Reactivity

A Brief Review

Robert M. Baldwin

Chemical Engineering and Petroleum Refining Department, Colorado
School of Mines, Golden, CO 80401

Since the earliest days of coal liquefaction processing and research, the need for correlations of coal properties with coal reactivity under direct hydroliquefaction conditions has been recognized by coal scientists. This article traces the history of reactivity correlations from the earliest work of Bergius through the classic work at the Bruceton Bureau of Mines during the 1940's to the most recent advances in this subject. Particular emphasis in this review is placed on an examination of the contributions of Professor Peter Given and his co-workers. Reactivity methodologies and techniques for correlation are presented and critically evaluated for utility and applicability as predictive tools.

Early Studies

The first attempts to hydrogenate coal in the laboratory were carried out by Marcelin Berthelot (1) in 1868. The results of subsequent experiments were published by Ipatiev (2) and his co-workers in 1904, in which it was demonstrated that the yield of liquids via high pressure pyrolysis of numerous organic constituents could be markedly enhanced by application of hydrogen. Emil Fischer suggested in 1912 that if coking operations were carried out in a hydrogen atmosphere, an increased yield of hydrocarbons might result. This hypothesis was later confirmed by Franz Fischer and Keller (3), who distilled a bituminous coal in hydrogen under pressure and found that the tar yield was significantly enhanced. Further research on coal hydrogenation was carried out by Fischer and his co-workers at the Kaiser-Wilhelm Institute using for the most part sodium formate and carbon monoxide in the presence of water (4).

Research which would eventually lead to the first "commercial" process for coal liquefaction was in progress as early as 1910 under the direction of Friedrich Bergius. Bergius initially studied the conversion of cellulose and peat in the presence of water, and only later turned his attention to coal. Coals were found to behave in a similar fashion, and Bergius was granted a process patent in 1914 for conversion of coal and other carbonaceous substances. Much of the work of Bergius is summarized in a document published in 1925 (5). In this paper, Bergius first describes the effect of the nature of the coal on the yield of liquid and tars from coal and states that coals containing more than 85% carbon (d.a.f.) gave unacceptably low yields and were hence unsuitable for hydrogenation. In laboratory investigations on a series of 29 British coals of different rank (lignite through anthracite) published in 1928, Graham (6) indicated that no such arbitrary reactivity division was justified. Correlations for hydrogenation yields with coal properties were attempted by Graham using such factors as ultimate carbon, C/H ratio, C/(H-(O/8)) ratio, moisture, oxygen, and fixed carbon. All correlations were deemed to be unsuitable. Beuschleim and Wright (7) in a study of the hydrogenation of 14 U.S. coals and later Gordon (8) also reported similar findings. Francis (9) suggested that the reactivity of coal toward oxidizing agents was an excellent measure of their reactivity towards hydrogen.

Much of the experience in the large-scale German direct coal hydrogenation plants during the 1930's and 1940's was directed towards maximizing the yield and rate of conversion of coal to distillate material (10). Correlations of the performance characteristics of coals utilized in these facilities with coal properties have been published (11,12). Figure 1 presents data on the space-time-yield of gasoline plus middle oil (the latter being characterized by an atmospheric boiling point between 150 and 325 °C). As can be seen, coals with lower carbon content (and correspondingly higher oxygen content) gave higher rates of conversion to distillate.

Macroscopic and Microscopic Coal Constituents

Bergius stated that fusain was the most difficult of the constituents of coal to liquefy. Shatwell and Bowen (13) reported the oil yield from a sample of hand-picked fusain from bituminous coal to be negligible. Wright and Sprunk (14) microscopically analysed the residues from batch hydrogenation of several different U.S. coals, and determined the relative reactivities of the various petrographic constituents. Both Gordon (15) and Heinze (16) stressed the need for reducing the fusain content of

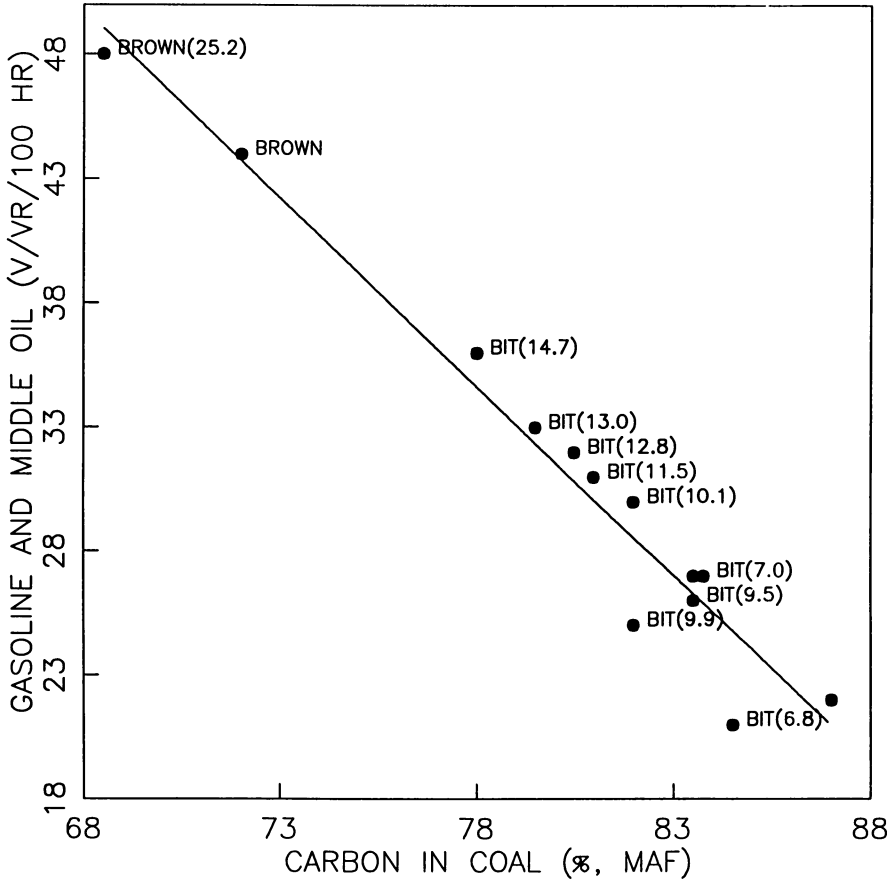


Figure 1: Space-time-yield (volume/volume reactor/100 hours) of gasoline and middle oil for brown and bituminous coals as a function of composition of starting coal. Data from continuous coal hydrogenation facilities operating in Germany during the 1930's.

coals processed in continuous liquefaction plants in order to minimize handling problems in the solids/liquid separations unit operations. Other studies on the effect of the macroscopic properties of coal (vitrain, fusain, clarain, durain) were reported by Shatwell and Graham (17) and Horton et al. (18), with contradictory results.

The first systematic study on the effect of the macroscopic and microscopic coal constituents on coal reactivity was conducted at the Bruceton Bureau of Mines Research Station (now Pittsburgh Energy Technology Center of the US Department of Energy). An extensive treatise on the effect of the petrographic constituents on the reactivity of coal for direct hydrogenation was published by Fisher et al. (19) in 1942. As an integral portion of this research, the behavior of individual maceral groups was determined experimentally, and a correlation developed for liquefaction reactivity. A parity plot for predicted vs. actual yield of residue was presented by Fisher, where "residue" denoted the yield of acetone insolubles after reaction at 445 - 450 °C for 2 hours (initial hydrogen pressure of 2000 psi). Here, the yield of residue was predicted by assuming that the coal constituents would react as follows:

ash and fusain = 100% residue
 opaque attritus = 38% residue
 all other constituents = 0% residue

While this correlation was deemed to be more adequate than previous relationships based solely on rank or carbon content, the deficiencies in terms of chemical differences between macroscopic and microscopic coal constituents for coals of varying rank was recognized by these researchers.

The Work of Peter Given

During the 1970's, Professor Peter Given and his co-workers at Penn State University began a very extensive study of the effect of coal composition on coal reactivity utilizing 104 coals from the U.S. To date, a series of ten papers have been published concerning the coal reactivity studies of Given et al., of which two pertain directly to the subject of reactivity correlations. The first paper (20) dealt with correlations between properties of 104 coals from the Penn State/DOE coal sample bank and conversion of coal to ethyl acetate solubles measured after reaction at 400 °C for one hour in tetralin. This paper introduced the concept of cluster analysis to the subject of reactivity correlation. It was reported that partitioning the samples into three distinct groupings (clusters) markedly improved the total variation accounted for by the multiple linear regression models employed for

correlation of conversion and coal properties. The groupings recommended had the following characteristics:

Group 1: medium sulfur, high rank

Group 2: high sulfur, medium rank

Group 3: low sulfur, low rank

The regression equations developed for correlation of liquefaction conversion and coal properties for each of these groups were as follows:

$$\text{Group 1: Conv} = 34.8 R_o + 50.7 \text{ H/C} + 0.16 V + 30.5 \quad (1)$$

$$\text{Group 2: Conv} = 0.86 \text{ VM} - 22.8 R_o + 1.39 S_t + 39.0 \quad (2)$$

$$\text{Group 3: Conv} = 0.93 \text{ VM} + 0.28 \text{ TRM} - 1.7 \quad (3)$$

where: R_o = vitrinite reflectance

H/C = atomic hydrogen-to-carbon ratio

V = vitrinite content of coal

VM = volatile matter

S_t = total sulfur

TRM = total reactive macerals

The adequacies of these reactivity correlations, expressed as a percentage of the total variation in the data set explained by the model, were 80.0%, 79.2%, and 47.5% respectively. A later paper in the series (21) concentrated on the development of reactivity correlations for a set of 26 high volatile bituminous coals with high sulfur contents, and extended the models previously developed in include analyses of the liquefaction products and coal structural features. These structural features included the usual compositional parameters as well as data from FTIR, ^{13}C -nmr, and the products of oxidation with trifluoroperoxyacetic acid. No significant correlations between liquefaction yields and structural features of the coals were found from this study.

Reactivity Definitions

The traditional parameter that has been used for coal liquefaction reactivity correlations is the point-yield conversion. This parameter is defined by measuring the yield of some solvent-soluble material (THF, pyridine, toluene, etc.) at a fixed reaction time and fixed temperature. This single parameter has been widely utilized by many researchers as the dependent variable in reactivity correlations with coal properties such as volatile matter, H/C and O/C atomic ratios, vitrinite reflectance, maceral distribution, etc. (22-29). As has been recently demonstrated by Shin et al.(30), this parameter can provide meaningful correlations with coal properties for a narrow suite of reasonably homogeneous coals, but the correlations weaken significantly or even disappear if either the time or temperature is changed. Use of a rate constant as a correlational parameter for coal reactivity was proposed by Furlong (31) and Gutmann

(32), and was found to be generally satisfactory for a particular suite of coals within a single rank. This parameter, however, also fails to hold if the temperature is changed (30). An attempt to derive a more universal parameter that could be employed for definition of coal reactivity was made by Shin et al. (33), who combined both static and dynamic reactivity parameters into a single variable.

Many of the compositional parameters utilized as independent variables in the work cited above represented derived coal properties rather than fundamental chemical features. Further, variables traditionally used are often highly correlated with each other (for example volatile matter and hydrogen). As pointed out by Neavel (34), this limits the utility of such parameters in correlational models. Instrumental techniques such as pyrolysis/mass spectrometry (35,36) ^{13}C -n.m.r., FTIR, and ^1H -n.m.r. have also been employed in an attempt to generate a larger data base of compositional information for use in correlation with reactivity. In some cases, the parameters developed from these data are derived from statistical techniques such as principal component and factor analysis, and thus have little if any interpretation or meaning chemically. In this regard, the later work of Neill, Shadle, and Given (37) represents a significant departure from this philosophy in that an attempt was made to correlate both liquefaction chemical properties and coal structural features with the observed liquefaction reactivity.

The lack of significance often found with single-parameter reactivity models has been interpreted to reflect the need for development of multi-parameter models containing functional dependence for reactivity on several compositional parameters. Recently, the use of activation energy as a fundamental parameter for correlation of liquefaction reactivity data has been proposed. Prasad (38) collected reported values for activation energies from other studies, and found a direct correlation between hydroliquefaction activation energy and the H/C ratio of the coal. Shin et al. (39) measured the hydroliquefaction activation energies for conversion of 5 bituminous coals from the Argonne Premium coal collection to THF and toluene solubles. Correlation of these data with fundamental coal chemical properties as determined from ^{13}C -n.m.r. (CP/MAS with dipolar dephasing) and ^1H -n.m.r. (CRAMPS) was successful in developing single parameter reactivity models with very high levels of significance (90%⁺) between the following variables:

Ea (toluene) <---> total oxygen
 Ea (THF) <---> aliphatic hydrogen
 Ea (toluene) <---> protonated aliphatic carbon

These correlations are graphically represented in Figures 2 through 4.

Observations and Conclusions

Coal is an extremely heterogeneous material, both from a macroscopic and microscopic point of view. Correlation of liquefaction reactivity with coal properties is, as a result, inherently difficult and any truly "universal" correlations that will be developed will need to be based

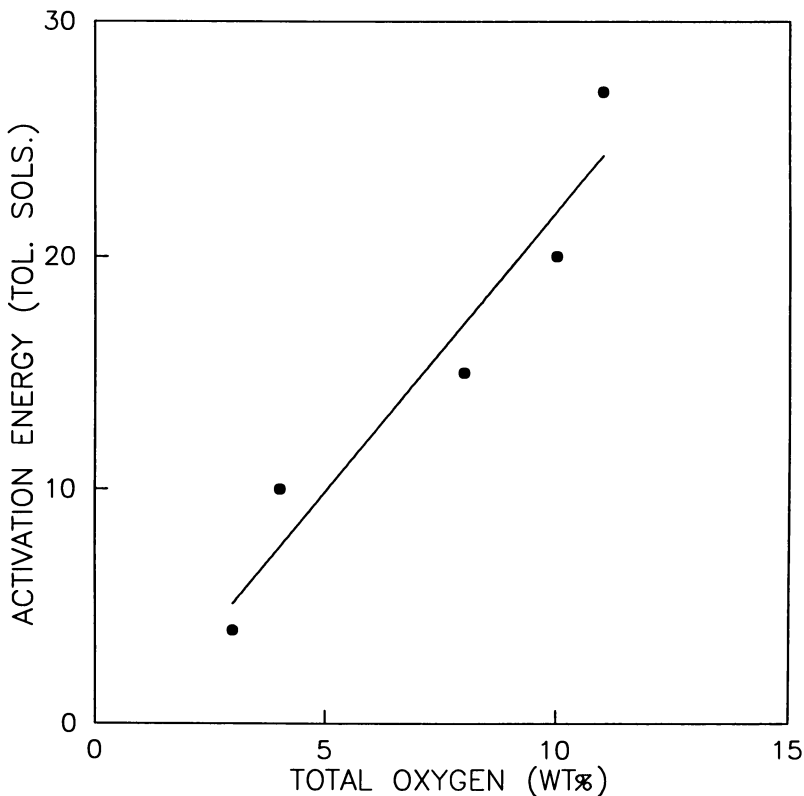


Figure 2: Activation energy for conversion to toluene solubles vs. total oxygen content of Argonne Premium Coal sample bank bituminous coals.

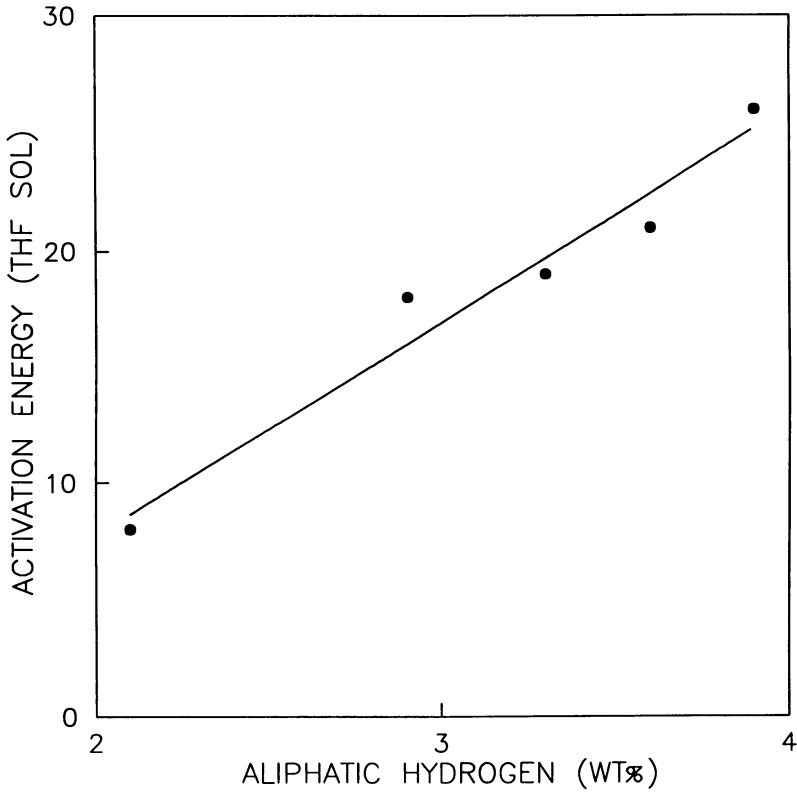


Figure 3. Activation energy for conversion to THF solubles vs. aliphatic hydrogen for Argonne Premium Coal sample bank bituminous coals. Data on proton distribution from Dr. Charles Bronnimann, Colorado State University.

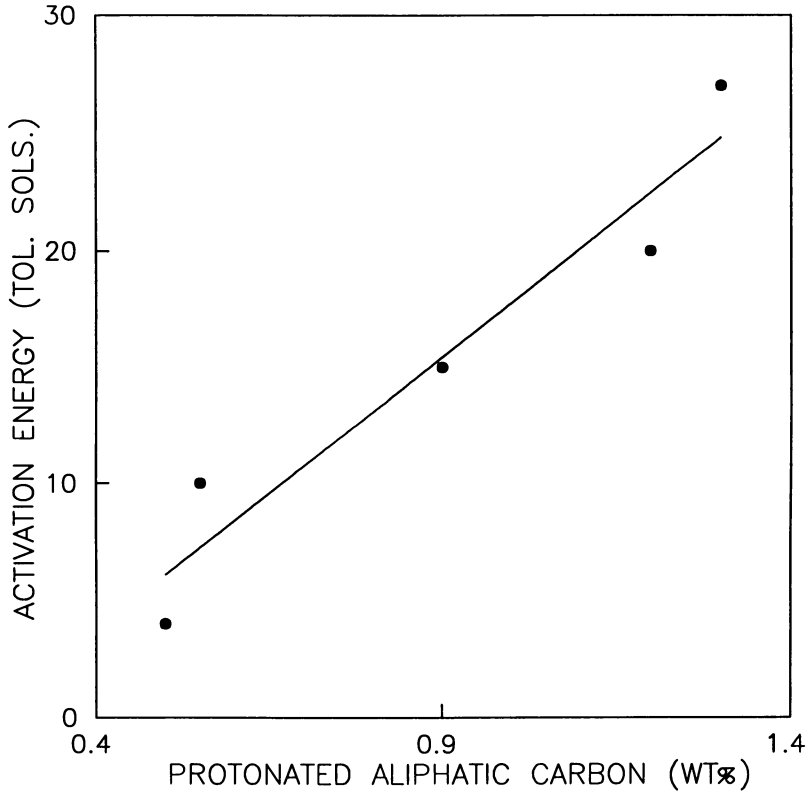


Figure 4: Activation energy for conversion to toluene solubles vs. protonated aliphatic carbon for Argonne Premium Coal sample bank bituminous coals. Data on carbon distribution from Dr. Ronald L. Pugmire, University of Utah.

on fundamental coal chemical and structural information. Lack of this type of information has been a severe limitation for all of the correlational efforts cited in this brief review. If truly predictive models are to be developed, basic data on coal structure will be invaluable. Choice of a reactivity definition employed as the dependent variable in these correlations is probably relatively arbitrary, and may be based totally on purely operational considerations (rate of reaction or extent of reaction) rather than any fundamental considerations. The role of pretreatment processes on reactivity modification (drying, grinding, etc) and mineral matter and matrix effects caused by organic/inorganic interactions needs to be better defined. This is especially true for low rank coals, where the inherently high reactivity of these materials can cause severe processing difficulties leading to artificially low levels of conversion.

Literature Cited

1. Berthelot, M. Bull. Soc. Chim. Fr. 1868, 9, 8
2. Ipatiev, W. Ber deuts. Chem. Ges. 1904, 37, 2961
3. Fischer, F.; Keller, K. Gesamm. Abh. Kohle 1915, 1, 148
4. Fischer, F.; Schrader, H. Brennst-Chemie 1921, 2, 161
5. Bergius, F. Z. kompr. fluss. Gase 1925, 3, 35
6. Graham, J.L. Proc. 2nd Int. Conf. Bituminous Coal 1928, 2, 456
7. Beuschlein, W.L.; Wright, C.C. Ind. Eng. Chem. 1932, 24, 1010
8. Gordon, K. Trans. Inst. Min. Eng. 1932, 82, 348
9. Francis, W.J. Inst. Fuel 1933, 6, 301
10. Wu, W.R.K.; Storch, H.H. USBM Bulletin 1968, no. 633, 17
11. Hupfer, et al. Ludwigshafen Rept. for Jan. 14, 1944, USBM Translation T-142
12. Sherwood, P.W. FIAT Final Report 1947, no. 952
13. Shatwell, H.G.; Bowen, A.R. Fuel 1925, 4, 127
14. Wright, C.C.; Sprunk, G.C. Mineral Industries Experiment Station Bull. 1939, no. 26, Penn State University
15. Gordon, K. Colliery Guardian 1935, 151, 987
16. Heinze, R. Zeit. des Vereines deut. Ingen. 1935, 79, 990
17. Shatwell, H.G.; Graham, J.I. Fuel, 1925, 4, 25
18. Horton, L., Williams, F.A., and King, J.G. Fuel Research and Board Tech. 1935, no. 42
19. Fisher, C.H.; Sprunk, G.C.; Eisner, A.; O'Donnell, H.J.; Clarke, L.; Storch, H.H. U.S. Interior Dept. Tech. Paper 1942, no. 642
20. Yarzab, R.F.; Given, P.H.; Spackman, W.; Davis, A. Fuel 1980, 59, 81

21. Shadle, L.J.; Neill, P.H.; Given, P.H. Fuel 1988, 67, 1465
22. Kessler, M.F. Fuel 1973, 52, 191
23. Mori, K.; Taniuchi, M.; Kawashima, A.; Okuma, O.; Takhashi, T. ACS Div. Fuel Chem. Preprints 1979, 24, no. 2
24. Durie, R.A. ACS Div. Fuel Chem. Preprints 1979, 24, no. 2
25. Gray, D.; Barrass, G.; Jezko, J.; Kershaw, J.R. Fuel 1980, 59, 146
26. Gray, D. Fuel 1978, 57, 213
27. Miller, R.L.; Baldwin, R.M. Fuel 1985, 64, 1235
28. Makabe, T.S. In Proc. 1987 Intl. Conference on Coal Science, Maastricht, The Netherlands, 295
29. Derbyshire, F.J.; Whitehurst, D.D. Fuel 1981, 60, 655
30. Shin, S-C. PhD. Thesis No. 3569, Colorado School of Mines, Golden, CO, 1988
31. Furlong, M.W.; Baldwin, R.M.; Bain, R.L. Fuel 1982, 61, 116
32. Gutmann, M.; Radeck, D.; Konig, M.; Keil, G. Coal Sci. Technol 1987, 11, 187
33. Shin, S-C.; Baldwin, R.M.; Miller, R.L. Energy and Fuels 1987, 1, 377
34. Neavel, R.C. Fuel 1986, 65, 312
35. Baldwin, R.M.; Durfee, S.L.; Voorhees, K.W. Fuel Proc. Tech. 1987, 15, 281
36. Schulten, H.R.; Simmleit, N.; Marzec, A. Fuel 1988, 76, 619
37. Neill, P.H.; Shadle, L.J.; Given, P.H. Fuel 1988, 67, 1459
38. Prasad, G.N.; Wittmann, C.V.; Agnew, J.B.; Sridhar, T. AIChE Jour. 1986, 32, 1288
39. Shin, S-C.; Baldwin, R.M.; Miller, R.L. Energy and Fuels 1989, 3, 193

RECEIVED November 5, 1990

Chapter 14

Influence of Organic Coal Structure on Liquefaction Behavior Under Low-Severity Conditions

Colin E. Snape¹, Frank J. Derbyshire², Howard P. Stephens³,
Richard J. Kottenstett³, and Neil W. Smith⁴

¹Department of Pure and Applied Chemistry, University of Strathclyde,
Glasgow G1 1XL, Scotland

²Center for Applied Energy Research, University of Kentucky,
Lexington, KY 40511-8433

³Sandia National Laboratories, Albuquerque, NM 87175

⁴Department of Chemistry, University of Leeds, Leeds LS2 9JT, England

The influence of coal structure on primary conversions and oil yields in thermolytic extraction with different H-donor and non-H-donor solvents and in dry catalytic hydrogenation has been investigated. Pre-soaking of coal/H-donor solvent slurries at 250°C increased conversions and the level of hydrogen transfer at short contact times (SCT < 10 min.) with 9,10-dihydrophenanthrene demonstrating the importance of solvent accessibility. However, contrary to other studies, prior removal of THF-extractable material (mobile phase) from one bituminous coal actually gave rise to higher conversions to pyridine-solubles for non-donor polynuclear aromatic compounds (PAC), in particular naphthalene, phenanthrene and pyrene. These findings highlight the difficulties in relating primary conversions to coal characteristics. In contrast, oil yields have been found to broadly increase with decreasing rank in both H-donor solvent extraction with a process solvent and dry catalytic hydrogenation. However, in SCT tetralin extraction where poor physical contact between coal and solvent exists, neither total conversion nor oil yield correlates with rank.

The correlation of coal characteristics with liquefaction behaviour has received considerable attention (see, for example refs 1-7) particularly since the renewed interest during the 1970s in the production of liquid fuels and chemical feedstocks directly from coal. As early as 1940, Storch and coworkers(8,9) demonstrated that coals containing up to ~ 87% dmmf C give high yields of soluble products (albeit under severe conditions) and materials which today would be classified as vitrinite and inertinite liquefy readily. More recently, the work of the late Peter Given and coworkers (2,3) on tetralin extraction of US bituminous coals is particularly noteworthy; high sulphur coals of intermediate carbon content gave the highest conversions. However, apart from the lack of precise structural information on the nature of aromatic, aliphatic and heteroatomic groups and low molecular weight (MW) extractable material (mobile phase) in coals, research has been hampered by the fact that the rate and extent of conversion are heavily dependent on the conditions used. Indeed, the recent review by one of the authors (1) indicated that a clear distinction has to

be made between overall or primary conversions (typically pyridine, quinoline or THF-solubles) and distillate or oil yields (toluene or alkane-soluble material). The mobile phase and the nature of H-donor and non-donor solvents all have a profound influence on primary conversions. In contrast, distillate or oil yields often correlate with parameters reflecting the aliphaticity of coals (H/C ratio - 5, decreasing vitrinite reflectance - 6, CH₂ content - 7), better correlations being achieved for low-rank coals if yields are expressed on a "CO₂ free" basis (5). The effects of coal characteristics on conversions are generally much less pronounced under high-severity conditions when a combination of vehicle solvent, hydrogen overpressure and catalyst is employed.

In this paper, a number of low-severity liquefaction regimes are considered. The influence of different H-donor and non-donor solvents on primary conversions without a hydrogen overpressure is discussed in the light of other recent work (10-13). Also, it is demonstrated that oil yields broadly increase with decreasing coal rank in both H-donor extraction and dry catalytic hydrogenation provided that retrogressive reactions are avoided in the initial stages of coal dissolution.

Experimental

Proximate and ultimate analyses of the coals used in this investigation are listed in Table I. Conditions used for the various extraction and hydrogenation experiments are summarised in Table II. All the extractions were carried out in 10 cm⁻³ microreactors using 1 g of coal and 2 g of solvent, the microreactors being heated in fluidised sand baths. H-donor solvent extractions of the Wyodak sub-bituminous coal Illinois No. 6 coal and Point of Ayr coal (UK) were conducted using (i) a Lummus process - derived distillate (nominal boiling range of 340 to 400°C; 91.1% C; 8.7% H and containing approximately 1% donatable hydrogen) and (ii) tetralin with a short contact time (SCT, 10 min). The relatively high temperature of 450°C was used with the process distillate to achieve high oil yields without having a hydrogen overpressure. The product work-up procedure using n-heptane and THF for the process distillate has been described previously (14). For tetralin, the work-up procedure describe below for the model compound solvents was used.

Table I Coal Analyses

	Moisture %	Ash %db	C	H	N % dmmf	O ^a	S _{org}
Pt of Ayr	2.4	10.0	87.2	5.8	1.6	4.4	0.7
Linby	9.8	6.7	83.0	5.0	1.9	8.7	1.0
PSOC 1325	1.2	13.5	90.0	5.0	2.8	1.6	0.6
1296	1.1	20.3	85.7	5.5	1.5	5.8	1.4
1266	3.4	6.1	83.2	5.0	2.1	8.6	0.5
1403	23.3	11.9	72.5	4.5	1.2	20.4	0.9
Wyodak	28.1	8.8	76.0	5.4	1.1	16.9	0.4
Utrillas	6.3	36.8	60.4	4.7	0.6	31.5	2.8

a - by difference
db - dry basis

To investigate factors affecting the initial stages of coal dissolution, extractions were conducted on two UK coals (Linby and Pt of Ayr) at 400°C using a number of model compounds including tetralin, naphthalene, 9,10-dihydrophenanthrene, phenanthrene and pyrene for periods up to 30 min. For Linby coal, the effect of prior Soxhlet extraction with THF on conversions was investigated (extract yield, 6% daf coal). Also, coal/solvent slurries were pre-soaked at 250°C in a number of experiments. Following extraction, the coal/solvent digests were recovered in THF and, after filtration, the THF-insolubles were extracted with either pyridine or quinoline. For the model hydroaromatic compounds, the amount of H transferred during extraction was determined by GC analysis of the products.

Table II. Summary of Liquefaction Experiments

Experiment	Temp °C	Solvent	Solvent to Coal Ratio	Atmosphere Gas	Pressure (cold)
H-donor solvent extraction					
1.	450	Lummus process distillate	2:1	N ₂	30
2.	400	Tetralin ⁺ 9,10 dihydrophen. ⁺	2:1	N ₂	1
Non-donor PAC extraction ⁺	400	Naphthalene, phenanthrene pyrene ⁺	2:1	N ₂	1
Dry catalytic hydrogenation	400	-	-	H ₂	70

Experiment	Residence time min	Solvents used to determine conversions
H-donor solvent extraction		
1. 450°C	30	THF, n-heptane,
2. 400°C	2-30	Pyridine, quinoline, THF
Non-donor PAC extraction ⁺	2-30	Pyridine/quinoline, THF
Dry catalytic hydrogenation	60	Chloroform

+ = with and without a pre-soak period of 60 min, at 250°C

* = before and after THF-extraction of Linby coal

Dry hydrogenations with and without a dispersed sulphided molybdenum (Mo) catalyst (1% loading of Mo) were carried out at 350 and 400°C (15) (Table II) on a suite of five coals comprising of a Spanish lignite (Utrillas), a sub-bituminous coal (PSOC-1403) two hvA bituminous coals (PSOC-1266 and 1296) and a lv bituminous coal (PSOC-1325). To investigate the role played by low MW solvent extractable material (mobile phase) in dry catalytic hydrogenation, a series of experiments was conducted with Utrillas lignite and an Illinois No. 6 coal in which the coals were first extracted with chloroform prior to catalyst impregnation. The quantities of chloroform-soluble material extracted were 2.5 and ~ 5.0% dmmf coal for the lignite and the bituminous coal, respectively.

Results and Discussion

Primary Conversions and Influence of Mobile Phase Yields for the various H-donor and non-donor solvent extractions of Linby coal at 400°C are summarised in Table III; the conversions for the THF-extracted coal include the extracted material. Surprisingly, pre-extraction with THF significantly increases primary conversions in the polynuclear aromatic compounds (PACs) investigated. These findings appear to be contrary to those of other liquefaction (16) and pyrolysis (17) studies where prior removal of chloroform-extractable material significantly reduced conversions. However, Rincon and Cruz (18) have reported recently that pre-swelling coals in THF increases conversions for both anthracene oil and tetralin. The fact that Point of Ayr (87% dmmf C) coal yielded over 80% pyridine-solubles in pyrene (C.E. Snape, unpublished data) without pre-extraction is consistent with the earlier results of Clarke et al (19) for anthracene oil extraction where UK coals

Table III Primary Conversions for Linby coal at 400°C

Solvents	Coal Treatment	Time min.	Yields		Hydrogen consumption (% daf coal)
			Pyridine sols.	THF sols.	
Naphthalene	None	10	51	25	
	"	30	58	29	
	THF-ext.	7	81	24	
	"	30	76	26	
Phenanthrene	None	7	22	15	
	"	30	"	"	
	THF-ext.	7	38	30	
	"	30	"	"	
Pyrene	None	7	24	14	
	"	30	"	"	
	THF-ext.	10	60	47	
	"	30	83	60	
9,10-Dihydro-phenanthrene	THF-ext.	5	55	34	0.5
	"	30	88	83	2.1
	Pre-soak	5	88	53	0.4
	"	30	93	80	1.9
Tetralin	THF-ext.	7	38	25	0.5
	"	30	78	65	1.2
	Pre-soak	7	43	35	0.5
	"	30	75	66	1.3

containing ~85–87% dmmf C and having high free swelling indices gave the highest conversions. It was suggested previously by one of the authors that this could correspond to a minimum in the cross-linking density of bituminous coals (1). However, these latest findings imply that the mobile phase is merely limiting accessibility for larger PACs, such as pyrene, within lower rank bituminous coals.

Conversions to pyridine-solubles for non-THF-extracted Linby coal were much greater with naphthalene than with phenanthrene and pyrene (Table III, pre-soaking at 250°C has little effect on conversions) and, even after THF extraction, naphthalene conversions are comparable to those of pyrene. Although Neavel obtained high yields of pyridine-solubles with naphthalene at short contact times for some US bituminous coals (20), conversions were much lower after longer extraction times. This trend is not evident for Linby coal where little variation in conversion to pyridine and THF-solubles is found for residence times between 10 and 30 min for both the initial and THF-extracted coal samples (Figure 1 and Table III). The trends reported here were certainly not anticipated from previous studies with model PACs (1,21) but yields of THF-solubles for pyrene were considerably greater than those obtained with both phenanthrene and naphthalene (Table III, Figures 1 and 2). This evidence provides strong support for pyrene being an effective "hydrogen-shuttler" (21); the available hydrogen in Linby coal is utilised more effectively with pyrene than with naphthalene and phenanthrene generating significantly higher yields of THF-solubles.

As expected, tetralin and 9,10-dihydrophenanthrene gave much higher yields of THF-solubles after THF extraction than the PACs with the exception of pyrene (Table III). Pre-soaking the coal/solvent slurries at 250°C increased SCT conversions for 9,10-dihydrophenanthrene but not to the same extent for tetralin (Figures 3 and 4) presumably due to poorer physical contact of tetralin with the coal; Narain et al (22) found similar improvement in SCT hydroliquefaction with 1-methylnaphthalene. For 9,10-dihydrophenanthrene, the higher conversion to THF-solubles was not accompanied by an increase in H consumption. However, the conversion at SCT (Figure 3) was no more than that obtained after prolonged extraction (30 min, Table III) with pyrene where no H donation can occur. This agrees with the work of Baldwin and coworkers (23) which showed that oil yields (dichloromethane - DCM; toluene or alkane-solubles) provide more reliable indicators of H utilisation than overall conversions to pyridine (or quinoline) or THF-solubles.

The lower yields of pyridine-solubles obtained with tetralin compared to 9,10-dihydrophenanthrene (Table III) and even to naphthalene and pyrene for the THF-extracted coal (Table III, Figures 1 and 2) again are probably attributable to tetralin being largely vaporised at liquefaction temperatures. Indeed, different trends in primary conversion are evident for the SCT tetralin (400°C) and the higher temperature (450°C) process-solvent extractions (Table IV). The sub-bituminous coal (Wyodak) gives the highest yield of quinoline-insolubles with tetralin consistent with the general trend found in SCT hydroliquefaction by Whitehurst (1,24). In the case of the process solvent, yields of THF-solubles increase with increasing rank (Table IV) although the trend is much smoother than could be realistically expected for a larger suite of coals. Nitrogen containing solvents, such as indoline, have also been found to give significantly higher primary conversions for Wyodak coal (25) than tetralin presumably due to the more effective disruption of hydrogen bonds in the coal. Clearly, solvents which provide good physical contact are essential for low-rank coals to minimise char-forming reactions. In the initial stages of liquefaction these retrogressive reactions are considered to be much more prevalent than for bituminous coals due to the greater numbers of weak covalent bonds giving rise to higher concentrations of free radical species.

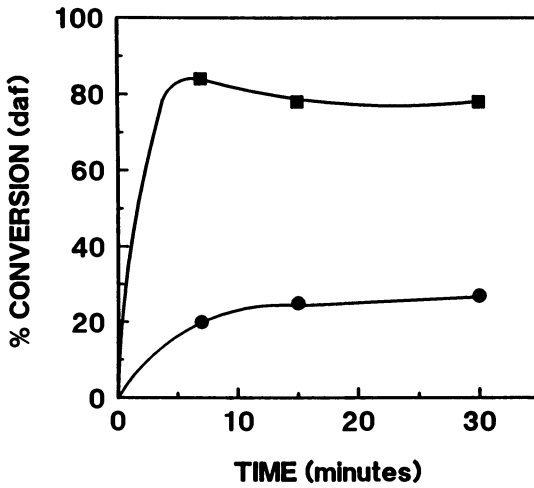


Figure 1. Conversion of THF-extracted Linby coal with naphthalene at 400 °C. ■Pyridine-solubles; and ●THF-solubles.

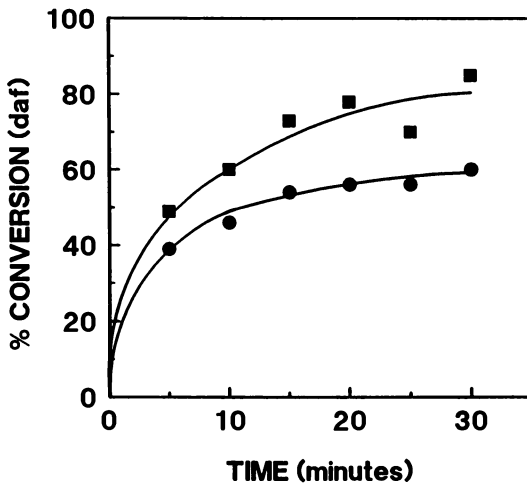


Figure 2. Conversion of THF-extracted Linby coal with pyrene at 400 °C after presoaking at 250 °C for 1 hour. ■Pyridine-solubles; and ●THF-solubles.

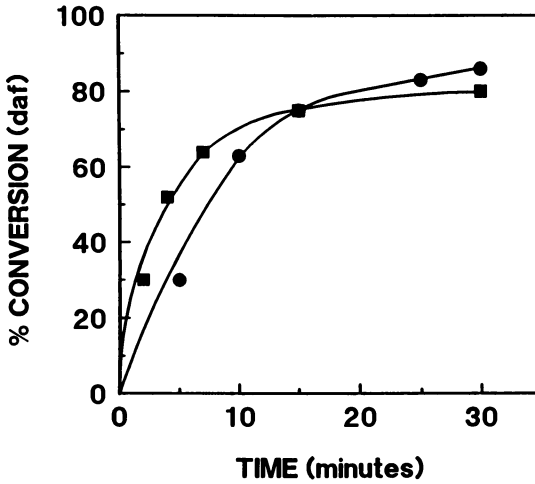


Figure 3. Conversion of THF-extracted Linby coal with 9,10-dihydrophenanthrene at 400 °C to THF-solubles; ● Normal extraction; ■ After presoak at 250 °C for 1 hour.

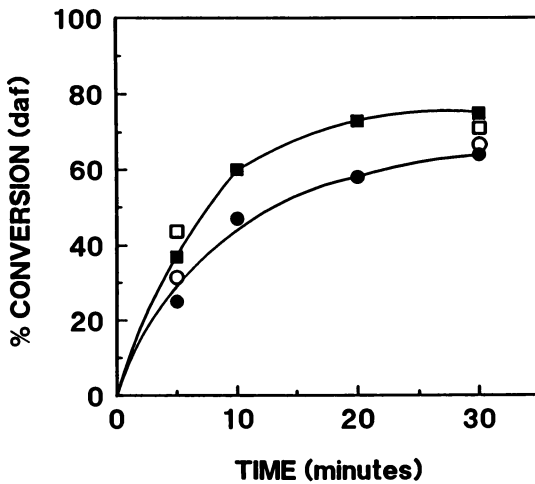


Figure 4. Conversion of THF-extracted Linby coal with tetralin at 400 °C. ■ Pyradine-solubles, normal; □ Pyradine-solubles, after presoak at 250 °C; ● THF-solubles, normal; and ○ THF-solubles, after presoak at 250 °C.

In view of the compelling arguments recently put forward by McMillan and coworkers (12) in support of solvent-mediated hydrogenolysis, it is pertinent to consider whether chemical or physical factors for the different H-donors investigated are responsible for inefficient hydrogen utilisation and, in particular, whether different conversions are evident for a given level of hydrogen donation. Majchrowicz et al (26) demonstrated that by increasing the filling factor for tetralin in autoclaves so that more of the tetralin is in the liquid phase, conversions to THF-solubles increased but the level of hydrogen transfer remained constant. Table III indicates that when 0.5% daf hydrogen has been consumed, the yields of THF-solubles obtained with 9,10-dihydrophenanthrene are considerably higher than with tetralin. Also, the maximum obtainable yield of THF-solubles at 400°C is significantly higher for 9,10-dihydrophenanthrene (Figures 3 and 4). Despite the reservations over the use of THF-soluble yields as indicators of H utilisation, these findings clearly indicate that cleavage of relatively stable C-C bonds via hydrogen radical transfer occurs to a significantly greater extent in 9,10-dihydrophenanthrene.

The results summarised in Table V (27) suggest that removal of some of the mobile phase prior to dry catalytic hydrogenation does not adversely affect chloroform-soluble yields obtained at long reaction times and, in the case of the lignite, the initial rate of conversion may actually be enhanced. Thus, the breakdown of the macromolecular network of coals via catalytic hydrogenation is not strongly dependent on the presence of mobile species.

Table IV H-Donor Solvent Liquefaction Results

Coal	Pt of Ayr	Illinois No. 6	Wyodak
SCT Tetralin - 400°C			
QIs	8	5	26
%daf QS/DCM insols	69	60	35
coal DCM liquids*	20	32	20
			(24)
Process Solvent - 450°C			
THF insols	17.0	3.6	2.1
% daf THF sols/C ₇ insols.	47.5	47.1	35.3
coal C ₇ liquids*	27.6	41.5	39.5
			(47.5)
CO + CO ₂	1.6	1.5	16.8
C ₁ - C ₃ gases	5.5	5.9	6.0

QI = quinoline insolubles

QS = quinoline solubles

C₇ = n-heptane

* = includes water

() = "CO₂ + CO" free basis

DCM = dichloromethane

Table V Influence of Chloroform Pre-extraction on Oil Yields (Chloroform-soluble liquids) in Dry Catalytic Hydrogenation at 400°C

Reaction Time (min.)	Utrillas Lignite		Illinois No. 6	
	Original	Pre-extracted	Original	Pre-extracted
5	50.0	63.7	24.4	8.6
10	59.0	74.3	55.8	22.6
60	66.0	77.8	77.8	73.2

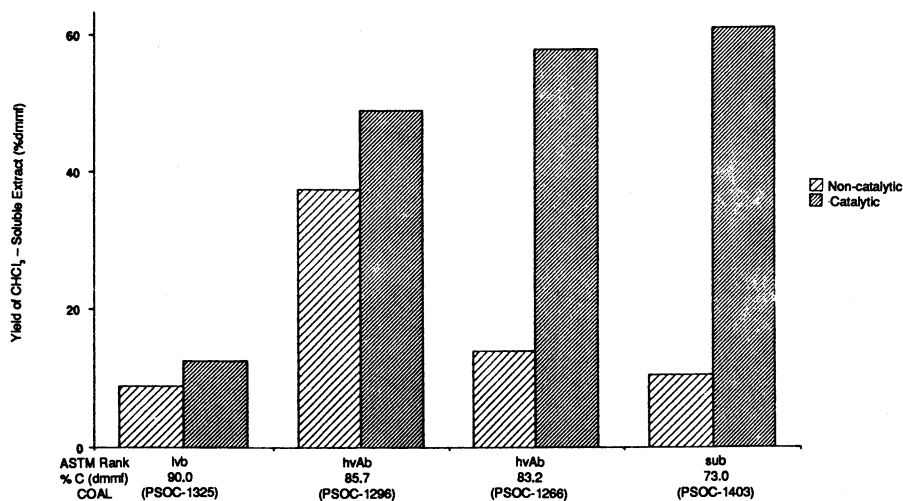


Figure 5. Effect of coal rank and sulphided Mo catalyst on yield of chloroform-soluble liquids in solvent-free hydrogenation at 400 °C.

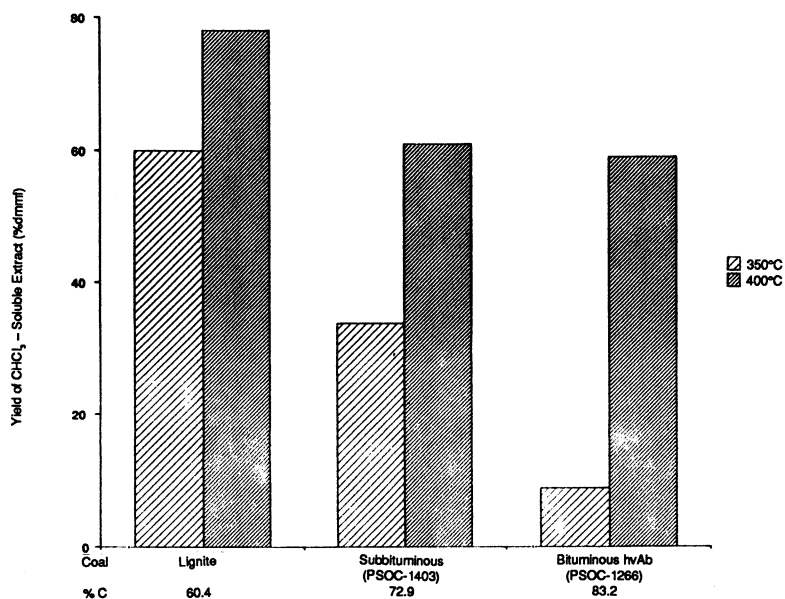


Figure 6. Influence of temperature and coal rank on yield of chloroform-soluble liquids in solvent-free hydrogenation with a sulphided Mo catalyst.

Oil Yields Figure 5 gives the yields of chloroform - soluble liquid products obtained from the dry hydrogenation experiments at 400°C with the sulphided Mo catalyst. Table IV lists oil and gas yields from the process solvent extractions at 450°C. In both regimes, oil yields (chloroform or n-heptane-soluble liquids) generally increase with decreasing rank. Again, the trends are probably much smoother than could be anticipated for a larger suite of coals. For lignites and sub-bituminous coals, it is probably more appropriate to express oil yields on a "CO₂ plus CO free" basis (5) (Table IV), a higher yield then being obtained for Wyodak sub-bituminous coal compared to Illinois No. 6 coal in the process solvent extractions (Table III). Reducing the hydrogenation temperature from 400 to 350°C amplifies the effect of rank on the yields of chloroform-soluble liquids (27) (Figure 6) because of the greater thermal sensitivity of low-rank coals. For catalytic hydrogenation, the trends would not be so acute in the presence of H-donor solvents where conversions tend to be considerably higher.

Although the yield of DCM-solubles increases with increasing rank in SCT tetralin extraction (Table 4, QI + QS/DCM insols), the actual estimated yields of DCM-soluble liquid product are similar for Wyodak and Pt of Ayr coals even after correcting for carbon oxides. Thus, retrogressive reactions encountered in SCT extraction with tetralin for Wyodak coal limit both primary conversions and oil yields. Also, for dry hydrogenation without catalyst oil yields do not correlate with rank (Figure 5), the sub-bituminous coal giving a significantly lower oil yield than one of the hvA bituminous coals. Thus, the catalyst is needed to limit retrogressive reactions promoting cleavage reactions probably by hydrogen radical mediated hydrogenolysis (12). These findings clearly demonstrate the importance of limiting retrogressive reactions in the initial stages of liquefaction for low-rank coals and are in broad agreement with trends obtained under typical SRC-II processing conditions (6) where addition of pyrite is needed to give high oil yields for low-rank coals.

Acknowledgements

The authors thank the US Dept. of Energy (Contract Nos. DE-FE22-83-C60811 and DE-AC04-76DP00789) and the Science and Engineering Research Council with British Coal (CASC studentship for N.W.S.) for financial support.

References

1. Snape, C.E.; Fuel Process. Tech. 1987, **15**, 257-79.
2. Given, P.H.; Spackman, W.; Davis, A.; Jenkins, R.G.; In Coal Liquefaction Fundamentals; Whitehurst, D.D., Ed.; Am. Chem. Soc. Symp. Series 139, 1980; p3-34.
3. Yarzeb, F.; Given, P.H.; Davis, A.; Spackman, W.; Fuel 1980, **59**, 81-92.
4. Baldwin, R.M.; Voorhees, K.J.; Durfee, S.L.; Fuel Process. Tech. 1987, **15**, 282-92.
5. Redlich, P.; Jackson, W.R.; Larkins, F.P.; Fuel 1985, **64** 1383-90
6. Tomlinson, G.; Gray, D.; Neuworth, M.; Proc. Int. Conf. on Coal Science, Sydney, 1985, Pergamon, p 3.
7. Senftle, J.T.; Kuehn, D.; Davis, A.; Brozoski, B.; Rhoads, C.; Painter, P.C.; Fuel 1984, **63** 245-51.
8. Fischer, C.H.; Sprunk, G.C.; Eisner, A.; Clarke, L.; Fein, M.L.; Storch, H.H.; Fuel 1940, **19** 132-38 and 162-72.
9. Hirst, L.L.; Storch, H.H.; Fischer, C.H.; Sprunk, G.C.; Ind. Eng. Chem. 1940, **32**, 1372-79.

10. Keogh, R.A.; Chawia, B.; Tsai, K.J.; Davis, B.H.; Prepr. Am. Chem. Soc. Div., Fuel Chem. 1988, **33(3)**, 333-42.
11. Mochida, I.; Yufu, A.; Sakanishi, K.; Korai, Y.; Fuel 1988, **67**, 114-18.
12. Malhotra, R.; McMillen, D.F.; Prepr. Am. Chem. Soc. Div., Fuel Chem. 1988, **33(3)**, 319-24
13. Chiba, K.; Tagaya, H.; Saito, N.; Energy and Fuels 1987, **1**, 338-43.
14. Stephens, H.P.; Prepr. Am. Chem. Soc. Div., Fuel Chem. 1986 **31(4)**, 314-20.
15. Derbyshire, F.J.; Davis, A.; Lin, R.; Stanberry, P.G.; Terrer, M.T.; Fuel Process. Tech. 1986, **12**, 127-41.
16. Larsen, J.W.; Sams, T.L.; Rogers, B.R.; Fuel 1980, **59**, 666-7.
17. O'Brien, R.J.; Gibbins, J.R.; Kandiyoti, R.; Fuel Process. Tech. 1987, **15**, 71-82.
18. Rincon, J.M.; Cruz, S.; Fuel 1988, **67**, 1162-3.
19. Clarke, J.W.; Kimber, G.M.; Rantell, T.D.; Shipley, D.E.; In Coal Liquefaction Fundamentals; Whitehurst, D.D., Ed.; Am. Chem. Soc. Symp. Series 139, 1980; p 111-129.
20. Neavel, R.C. In Coal Science Vol. 1; Gorbaty, M.L.; Larsen, J.W.; Wender, I; Eds., Academic, 1982; p 1-19.
21. Derbyshire, F.J.; Whitehurst, D.D.; Fuel 1981, **60**, 655-62.
22. Narain, N.K.; Appell, H.R.; Utz, B.R.; Prepr. Am. Chem. Soc. Div. Fuel Chem. 1983 **28(1)**, 161-2.
23. Shin, S.C.; Baldwin, R.M.; Miller, R.L.; Energy and Fuels 1989, **3**, 71-6.
24. Whitehurst, D.D. In Coal Liquefaction Fundamentals; Whitehurst, D.D. Ed., Am. Chem. Soc. Symp., Series 139, 1980; p 133-164.
25. Padrick, T.D.; Lockwood, S.J.; Prepr. Am. Chem. Soc. Div. Fuel Chem. 1984, **29(5)**, 92-8.
26. Majchrowicz, B.B.; Franco, D.; Gelan, J.; de Vlieger, J.J. Proc. 1987 Int. Conf. on Coal Science, Elsevier, 1987, p 207.
27. Derbyshire, F.J.; US DoE Progress Report Sept. 85 - Feb. 86, DoE-PC-60811-9,10, 1986.

RECEIVED November 19, 1990

Chapter 15

Chemistry of Catalytic Preliquefaction

P. R. Solomon¹, M. A. Serio¹, G. V. Deshpande¹, E. Kroo¹,
Harold H. Schobert², and C. Burgess²

¹Advanced Fuel Research, Inc., 87 Church Street, East Hartford, CT 06108

²Fuel Science Program, The Pennsylvania State University,
University Park, PA 16802

Recent experiments at Penn State University showed that for a low rank coal, a low severity "preliquefaction" stage at 350 °C with a catalyst resulted in improved conversion to soluble products in a subsequent "liquefaction" stage at 425 °C. To determine the chemistry responsible for this improvement, FT-IR, NMR, TG-FTIR, FIMS, and solvent swelling were employed to analyze the preliquefaction products. For the best cases, substantial changes were observed in the functional group composition of the residue, (low aliphatic, low carboxyl, and high aromatic), there was a large chloroform extract yield and a high CO₂ yield. The improvement in liquefaction behavior (i.e., conversion to soluble products) appears to be due to loss of the carboxyl groups responsible for low temperature crosslinking without the associated crosslink formation. Model simulations using our FG-DVC network decomposition model show that the reduction in the carboxyl group concentration in the preliquefaction step can significantly enhance the liquefaction yield.

Direct coal liquefaction processes which have been developed over the years have been based on the philosophy of high temperature homolytic cleavage of bonds to yield free radicals which are capped by hydrogen from the donor solvent or hydroaromatic structures in coals. While low rank coals offer the potential of high oil yields because of their small aromatic ring cluster size, it has been observed that under conditions optimized for bituminous coals, low rank coals appear harder to liquefy (1,2). For example, Derbyshire and Whitehurst (3) demonstrated that low rank coals produce very low conversions in short contact time liquefaction in a donor solvent or in long time liquefaction in a non-donor solvent. For low rank coals and lignites, it appears likely that crosslinking reactions associated with oxygen functional groups (4-6) occur before the homolytic cleavage reactions.

In single stage coal liquefaction, bond breaking, crosslinking and hydrogen transfer reactions occur simultaneously. To improve liquefaction, researchers have sought to optimize individual reactions. Recent research on "temperature staged liquefaction" routes, exploring the effects of catalyst and solvent has been

pursued using tubing bomb experiments at Penn State University by Derbyshire, Davis, Schobert and co-workers (7-13). The tubing bomb results (7) showed that for a low rank coal, a low severity "preliquefaction" stage at 350°C in naphthalene with a tetrathiomolybdate catalyst resulted in improved conversion to soluble products with higher fractions of oils in a subsequent higher severity "liquefaction" stage at 425°C.

The objective of this work was the identification of the preliquefaction chemistry through the application of advanced analytical techniques and theoretical models which have been previously employed to understand and predict coal pyrolysis and fluidity behavior. The analytical techniques include three methods to determine the functional group composition of the preliquefaction products: Quantitative Fourier transform infrared (FT-IR) spectroscopy (14-17); cross-polarization-magic angle spinning (CP/MAS) NMR with dipolar dephasing (18-22); and thermogravimetric analysis with detection of the evolved products by FT-IR spectroscopy (TG-FTIR) (23-25). In addition, field ionization mass spectroscopy (FIMS), has been employed to determine the molecular weight distribution of soluble products (26-29) and solvent swelling experiments have been performed to determine the degree of crosslinking in the preliquefaction residua (30,31). Model compounds were studied to investigate decarboxylation reactions under the conditions of the preliquefaction treatment.

The theoretical model describes the break up of the coal macromolecular network under the influence of bond cleavage and crosslinking reactions using a Monte Carlo statistical approach (32-38). A similar statistical approach for coal decomposition using percolation theory has been presented by Grant et al. (39). Such statistical methods have been used for the inverse problem in the polymer literature, i.e., the formation of a macromolecular network by polymerization (40-44). The model was used to determine what effect the removal of crosslinks in the network have on thermal decomposition of the network.

Experimental

Samples. Samples of bituminous and subbituminous coal were provided by the Penn State Coal Sample Bank (PSOC 1504, PSOC 1401, and PSOC 1482) and the Argonne Premium Sample Bank (Zap and Wyodak). The Penn State coals were obtained undried and in lumps of about 12 mm in diameter and were crushed in a glove box under oxygen-free nitrogen to a 0.8 mm maximum size. The crushed coals were subdivided by riffing into a number of 10 g representative samples and sealed in vials under nitrogen. The Argonne coals were provided in sealed vials under argon. Properties of PSOC 1401 for which results are reported here are shown in Table 1.

Preliquefaction and Liquefaction Experiments. Low severity "preliquefaction" and higher severity "liquefaction" tubing bomb experiments were carried out at Penn State University and at Advanced Fuel Research, Inc. The procedure was that described by Derbyshire et al. (7). The preliquefaction was carried out in a tubing bomb at temperatures of 275 and 350°C, and gas pressures of 1000 psi (7 MPa) cold. Coal was impregnated with tetrathiomolybdate catalyst and mixed in a ratio of 1:2 with liquefaction solvent. In most of the experiments, naphthalene was selected as the solvent. Reactions were carried out in tubing bomb reactors of about 20 cm³ capacity which were heated by immersion in a fluidized sandbath. Following preliquefaction, the bomb was cooled and vented to determine the gases evolved by volumetric measurement and gas chromatographic analysis. At that point, either the bomb was opened for analysis of the liquids and solids or a liquefaction step was carried out at a higher temperature before product analysis. The solid and liquid

Table 1 - Coal Properties

Coal	PSOC-1401
Seam	Lower Wyodak
State	Wyoming
ASTM Rank Class (apparent)	Subbituminous
Moisture Content (wt. % (a.r.))	16.3
Mineral Matter	6.5
Elemental Composition Wt.% dmmf	
C	72.7
H	4.5
O ^a	21.4
N	1.1
S	0.3
Sulphur Forms (% dry coal)	
Organic	0.26
Pyritic	0.01
Sulphate	0.00
Total	0.27

^a by Difference

products were worked-up to obtain the yields of insoluble residue (either chloroform or tetrahydrofuran (THF) insoluble), asphaltenes (hexane insoluble, THF-soluble) and oils (hexane-soluble). In these analyses, it was assumed that the naphthalene was part of the hexane solubles.

Analyses

Quantitative FT-IR Analysis. Selected samples of the liquefaction products, total product, the chloroform extracts, the asphaltenes, and the solid residues were analyzed as KBr pellets by FT-IR. The methods employed for quantitative analysis have been described previously (14-17). Measured amounts of sample are mixed with measured amounts of KBr, so that spectra are reported in absorbance units/mg of sample in a 1.33 cm² pellet. A spectral synthesis routine was used to obtain peak areas for individual functional groups and previously determined absorptivities (17) were employed to obtain the reported percentages of each functional group.

TG-FT-IR. Pyrolysis analyses were performed on the preliquefaction solids using thermogravimetric (TG) analysis with on-line analysis of the evolved products (including an infrared spectrum of the condensables) by FT-IR. The TG-FTIR method has been described previously (23-25). The Bomem TG/plus instrument was employed. A sample is continuously weighed while it is heated. A flow of helium sweeps the products into a multi-pass cell for FT-IR analysis. Quantitative analysis of up to 20 gas species is performed on line. Quantitation of the tar species is performed by comparison with the balance reading.

Solvent Swelling and Extraction. The residue samples were extracted with pyridine at the boiling point to obtain the amount and composition of the extract. A portion of the dried, extracted solids was swelled in pyridine in order to estimate the density of crosslinks introduced by the preliquefaction process. The solvent swelling measurements were carried out according to the method of Green et al. (30,31). The amount of swelling of treated coals and chars are compared to that in the raw coal as a relative indication of crosslinking.

FIMS Analysis. Selected extracts were sent for analysis by field ionization mass spectrometry (FIMS) at SRI International. This technique was described by St. John, et al. (26). The sample is heated in a small glass probe. As products vaporize or are released by pyrolysis, they are swept into an ionization source which has regions of very high electric fields. The field ionization induces little fragmentation of the molecules and so provides a determination of the molecular weight of the volatile fragments. Fragments too large to vaporize remain in the probe. The FIMS analysis has been used extensively in our development of the network model for coal decomposition (32-38,45,46).

NMR. NMR analyses were performed on selected samples using dipolar dephasing and off magic angle spinning methods developed at the University of Utah (18-22). This work was performed at the University of Utah under the direction of Professor Ronald Pugmire. The technique allows quantitative analysis of functional groups in the solid coals and chars.

Model Compounds. Model compounds were employed to provide well known materials to study specific chemical reactions or to provide standards to calibrate the analytical techniques. These included 1-naphthoic acid and 2-naphthoic acid to study the reaction of aryl carboxyl groups under preliquefaction conditions.

Results

Product Distribution. Both the products of the preliquefaction and liquefaction stages were analyzed. Variations were made in coal type, (lignite, subbituminous, and bituminous), preliquefaction temperature (275-350°C), gases present (hydrogen, nitrogen, helium), catalyst (tetrathiomolybdate or none), solvent (naphthalene, tetralin or dry) preliquefaction time (30 min - 60 min), and liquefaction time at 425°C (10 min - 30 min).

Results for PSOC 1401 (a Wyodak subbituminous, which was the most frequently studied coal) are presented in Table 2 and Fig. 1. The figure compares liquefaction data (10 min at 425°C) for no preliquefaction, preliquefaction at 275°C (with H₂ and catalyst in naphthalene) and preliquefaction at 350°C (with H₂ and catalyst in naphthalene). **The results show that preliquefaction at 350°C does have a positive effect on the total yield and product quality in liquefaction (much lower residue) while preliquefaction at 275°C causes a negative effect (higher residue).** The reproducibility of the residue determined is $\pm 3\%$, so that 8.5% increase in residue is significant. The results for other coals and conditions are summarized as follows:

- 1) Preliquefaction at 275°C appears to have a negative effect on subsequent liquefaction when compared to results without a preliquefaction step. Preliquefaction results in up to 10% of the coal converted to gases and chloroform solubles. Most coals behaved the same and there was little effect due to the presence of either the catalyst or hydrogen. The solvent was, however, necessary to produce the chloroform extracts as none were produced by a thermal treatment in the absence of a solvent.
- 2) Preliquefaction at 350°C in the presence of a catalyst appears to have a strong positive effect on liquefaction for low rank coals. The largest change due to preliquefaction (high chloroform extract yield, high CO₂ yield) requires both hydrogen and catalyst. Nitrogen and catalyst produce smaller but similar changes, while no catalyst produces much less change and as shown by Derbyshire et al. (7) produces little change in liquefaction. Preliquefaction with no solvent or catalyst produces the least change in the product. Preliquefaction in tetralin produces no improvement over preliquefaction in naphthalene.

FT-IR Functional Group Analysis

Quantitative FT-IR functional group analysis was performed on the starting coals, preliquefaction residua, chloroform extracts, oils, and asphaltenes.

Residua. Analysis of the residua produced with a thermal treatment only (HeD 1401-275 - no catalyst, no solvent, no hydrogen) showed that at 275°C there were no noticeable changes in the FT-IR spectrum from that of the coal. The thermal treatment at 350°C (HeD 1401-350) produced a small reduction in the aliphatic peak at 2900 cm⁻¹. Preliquefaction with solvent at 275°C produced spectra which were independent of whether catalyst was present or hydrogen used. The spectra all showed a reduction in the aliphatics and a slight increase in the ether region but few other changes. The changes are presumably due to the formation and subsequent removal of chloroform solubles, the removal of which leaves a residue which is slightly less aliphatic than the coal.

Results for PSOC 1401, preliquefaction with H₂ and tetrathiomolybdate at

TABLE 2
 TG-FTIR ANALYSIS OF INSOLUBLE FRACTION FROM PRELIQUEFACTION AT 275°C
 AND 350°C, AND LIQUEFACTION AT 425°C
 DRY STARTING COAL BASIS - PSOC1401

CODE	<u>Preliquefaction Stage</u>					
	HELIUM DRY 275	HYDROGEN CATALYTIC 275	HELIUM DRY 350	HYDROGEN CATALYTIC 350	NITROGEN CATALYTIC 350	NITROGEN THERMAL 350
Preliquefaction Temperature	275	275	350	350	350	350
Code	HeD 1401	HC1401-Nap	HeD 1401	HC 1401-Nap	NC 1401-Nap	NT 1401-Nap
Gases	4.9	2.7	11.3	11.2	9.6	--
Chloroform Solubles	0.0	4.0	ND	15.7	12.6	--
Total	4.9	6.7	11.3	26.9	21.6	11.0
CH ₄	0.0	0.0	0.1	0.2	0.1	--
CO	0.2	0.1	0.8	0.4	0.3	--
CO ₂	1.2	2.6	3.5	10.4	8.5	--
H ₂ O	2.9	--	4.7	--	--	--
Tars	0.6	--	2.2	--	--	--
C ₂ H ₆ /C ₃ H ₈	--	0.1	--	0.2	0.1	--

Data reported by Derbyshire. Gases do not include water.

TG-FTIR Analysis

Volatiles	39.2	35.5	29.7	20.8	23.2	30.1
Fixed Carbon	51.2	49.9	52.2	43.8	47.5	50.9
Ash	4.7	7.9	6.8	8.5	7.7	8.0
CH ₄	2.0	0.9	1.8	1.1	1.0	1.2
CO	13.2	11.3	11.3	8.3	9.0	8.7
CO ₂	9.3	7.1	5.8	3.7	4.8	5.5
H ₂ O	9.1	8.0	5.8	5.7	6.1	5.9
Tars*	5.6	7.9	5.0	1.9	2.2	8.8
SO ₂	0.0	0.3	0.0	0.1	0.1	0.0
Preliquefaction + volatiles	44.1	42.2	41.0	47.7	44.8	41.1
Volumetric Swelling Ratio (VSR)	2.1	2.0	1.6	1.8	1.6	

Liquefaction Results

Preliquefaction Solvent

Gases + Oils	18.4	40.6	20.5
Asphaltenes	36.1	43.1	24.5
Conversion	54.5	83.7	45.0
Reaction Time, min	10	10	10

Preliquefaction No Solvent

Gases + Oils	29.8
Asphaltenes	37.9
Conversion	67.7
Reaction Time, min	10

* Volatiles which are solid at room temperature determined by difference.

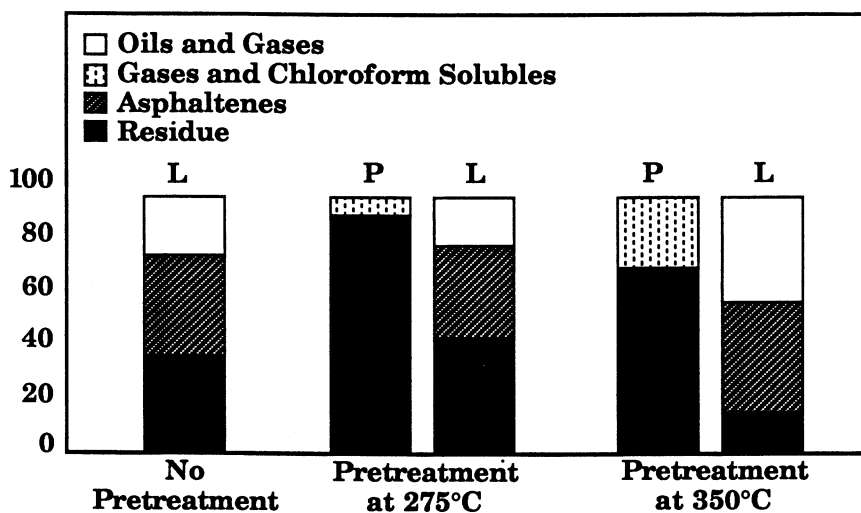


Figure 1. Product Distributions for Preliquefaction and Liquefaction Comparing Results for No Preliquefaction, Preliquefaction at 275°C and Preliquefaction at 350°C. P = Pretreatment and L = Liquefaction. Liquefaction Conditions - 425°C, Mo, Catalyst, Naphthalene Solvent, Hydrogen, Atmosphere (10 min.). Preliquefaction Conditions - Mo, Catalyst, Naphthalene Solvent, Hydrogen, Atmosphere (275°C - 30 min., 350°C - 60 min.).

350 °C, are presented in Fig. 2. The preliquefaction step produced the following changes: 1) decreases in the carbonyl (1700 cm^{-1}) and hydroxyl regions (3400 cm^{-1}) (presumably carboxyl loss); 2) decreases in the aliphatic hydrogen (2900 cm^{-1}); and 3) substantial increases in the aromatic hydrogen ($750\text{--}850\text{ cm}^{-1}$).

The quantitative functional group analysis for PSOC 1401 from these and other spectra are summarized in Fig. 3 and Table 3. The aliphatic hydrogen (Fig. 3a) is found to decrease for solvent treated residues compared to residues formed in the absence of the solvent. The most drastic changes are in the aromatic hydrogen (Fig. 3b), the carbonyl (Fig. 3e), and the one adjacent aromatic hydrogen (Fig. 3g). As can be seen, the major changes are brought about with the catalyst and solvent. These are changes which presumably lead to the improved liquefaction yields.

There are three other cases of interest. The first is HCD 1401-350 which is identical to HC 1401-350 in using hydrogen and a catalyst but no solvent was present. The quantitative functional group analysis is presented in Table 3. It shows the loss in aliphatics and carboxyl, but not the same dramatic increase in the aromatic hydrogen. The second case is NC 1401-350-Tet which was preliquefied in tetralin with a catalyst under a nitrogen atmosphere. The results in Table 3 are very similar to HCD 1401-350 (low aliphatics and low carboxyl). The third case is for the HC 1401-350 residue after it was subsequently heated to 400 °C. This was done to see whether the high aromatic peaks are due to adsorbed naphthalene. The data in Table 3 shows that the functional group composition is almost identical to that in the starting residue. So heating to 400 °C does not change the functional group concentrations and adsorbed naphthalene is not likely.

Our initial conclusion from the FT-IR data on the residua is that it is the reduction in the carboxyl concentration which is most important to the improvements brought about by preliquefaction, and this reduction requires the catalyst but not the solvent and probably not the hydrogen. The major reasons for these conclusions are: 1) pretreatments dry, with naphthalene (with hydrogen and nitrogen) and with tetralin, all reduced the carboxyl concentration, and the dry and naphthalene cases both produced improved liquefaction yields; 2) the presence of hydrogen does not appear to make much difference between HC 1401-350 and NC 1401-350; and 3) the increased aromatics were not present in the dry preliquefaction residue (HCD 1401-350) and so, do not appear necessary for the improvement in liquefaction.

The increase in the aromatic hydrogen appears to result from adducted naphthalene for the following reasons: 1) the peak positions are consistent with adducted naphthalene; 2) the increase is too large to have come from conversion of aliphatic hydrogen to aromatic hydrogen, no increase was seen for NT 1401-350 which had a similar decrease in aliphatic hydrogen; 3) increased aromatic hydrogen due to removal of the carboxyls would not be likely to increase the one adjacent hydrogen peak; and 4) the peak must be due to a tightly bound chemical because it is not removed at 400 °C.

Extracts. Quantitative spectra were obtained for the soluble products of the preliquefaction process. Results for the THF extracts of the residue (asphaltene 1) for HC 1401-350 are presented in Fig. 4 and Table 3. The asphaltenes are very high in carboxyl groups, methyl groups, and aliphatic or hydroaromatic hydrogen. The spectrum does not show very large aromatic peaks; the material appears to contain less than 50% aromatic carbon based on the amount of aliphatic carbon and oxygen present. The THF solubles appear to have carboxyl concentrations about 3/4 of that in the original coal and the HeD 1401-350 run, but much larger than the residues except for the NT 1401-350. They contain significantly less ether oxygen.

TG-FTIR Analysis. The analysis of the volatile products are related to the

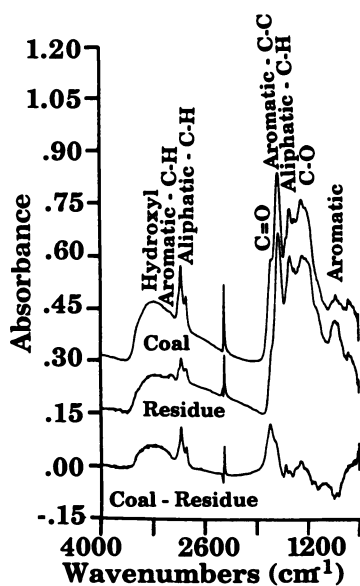


Figure 2. Comparison of FT-IR Spectra for Residue and Parent Coal for PSOC-1401 Wyodak Subbituminous Coal.

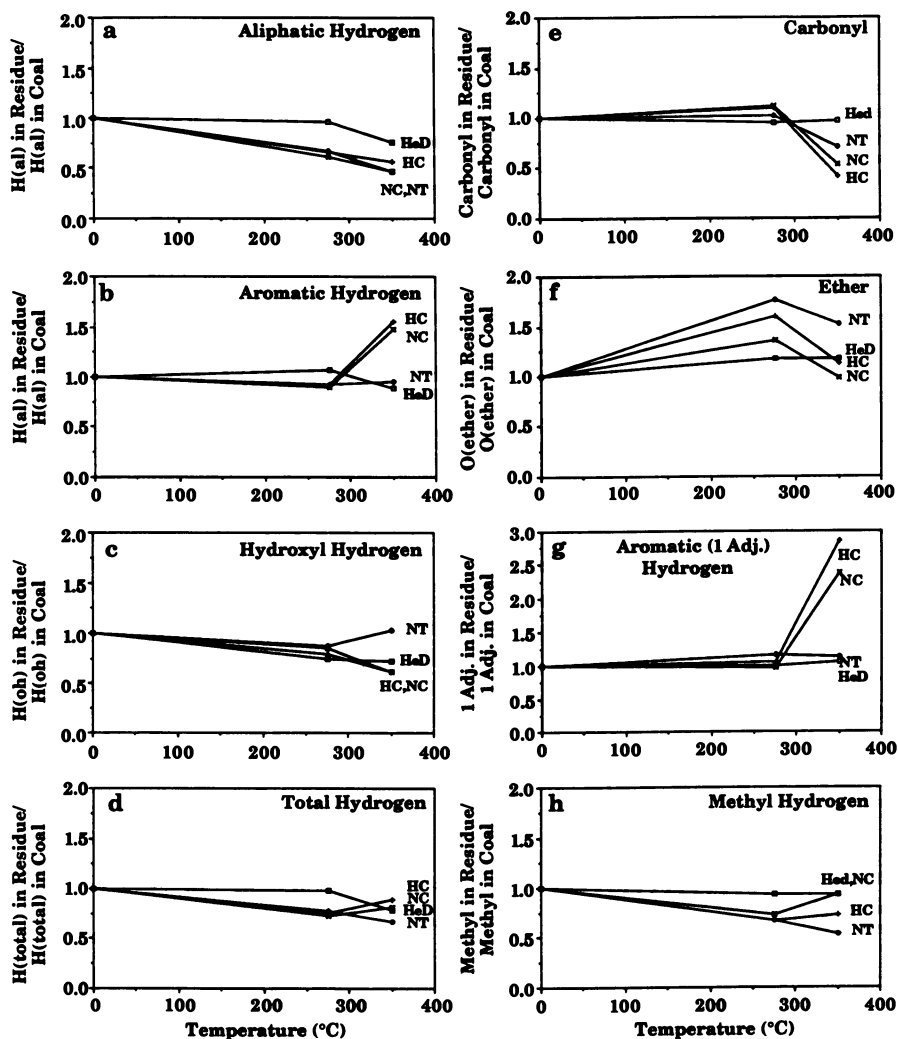


Figure 3. Variations in Functional Group Compositions with Preliquefaction.

Table 3 - Quantitative FT-IR Analysis (Duplicates) of PSOC-1401 Products at 350°C. (wt. % dmmf)

Run	Sample	Hydrogen			Aromatic Hydrogen			Carbon			Carbonyl			Oxygen	
		H _{al}	H _{oh}	H _{ar}	H _{total}	H _{ar} /H _{total}	1 Adj	2 Adj	3 +	C _{al}	Units (Abs. x cm ⁻¹)	O _{oh}	O _{ether}	O _{total}	
PSOC-1401	Coal	2.57	.37	1.44	4.38	.33	.40	.74	.30	17.13	31.33	5.96	4.88	10.84	
PSOC-1401	Coal	2.85	.36	1.49	4.70	.32	.47	.65	.37	19.00	33.32	5.74	5.40	11.14	
HCl401-350-Nap	Residue	1.54	.25	2.27	4.06	.56	1.07	.82	.38	10.27	13.03	4.00	5.25	9.25	
HCl401-350-Nap	Residue	1.50	.26	2.39	4.15	.58	.93	.99	.47	10.00	13.73	4.10	6.25	10.35	
HCl401-350-Nap	400°C Char	1.25	.23	2.64	4.12	.64	.99	1.19	.46	8.33	12.89	3.75	6.00	9.75	
HCl401-350-Nap	400°C Char	1.37	.23	2.27	3.87	.59	.80	1.04	.43	9.13	12.83	3.75	6.40	10.15	
NC1401-350-Nap	Residue	1.29	.28	2.14	3.71	.58	.79	.92	.43	8.60	16.15	4.50	4.75	9.25	
NC1401-350-Nap	Residue	1.22	.30	2.29	3.81	.60	.88	1.01	.40	8.13	18.50	4.75	5.25	10.00	
NT1401-350-Nap	Residue	1.42	.41	1.57	3.40	.46	.46	.65	.46		24.81	6.50	9.00	15.50	
NT1401-350-Nap	Residue	1.10	.42	1.26	2.79	.45	.34	.59	.33	7.39	20.91	6.75	6.50	13.25	
NC1401-350-Tet	Residue	1.82	.18	1.70	3.70	.46	.57	.78	.35	12.13	12.94	2.90	5.50	8.40	
NC1401-350-Tet	Residue	2.04	.22	1.63	3.89	.42	.48	.68	.47	13.60	13.60	3.60	5.60	9.20	
HeD1401-350	Residue	2.03	.25	1.37	3.65	.38	.38	.69	.30	13.53	31.82	4.00	6.00	10.00	
HeD1401-350	Residue	2.07	.25	1.27	3.59	.35	.36	.64	.27	13.80	31.09	4.00	6.00	10.00	
HCD1401-350	Residue	2.09	.14	1.30	3.53	.37	.38	.61	.31	13.93	12.73	2.20	6.40	8.60	
HCD1401-350	Residue	2.38	.16	1.59	4.13	.38	.53	.68	.38	15.87	12.49	2.60	6.90	9.50	
HCl401-350-Nap	Asphaltene-1	7.01	.51	1.18	8.70	.14	.35	.35	.48	46.73	25.30	8.20	2.50	10.70	
HCl401-350-Nap	Asphaltene-1	6.60	.51	1.27	8.38	.15	.40	.36	.51	44.00	22.21	8.20	2.10	10.30	

Nomenclature

HC - Hydrogen Catalytic

NC - Nitrogen Catalytic

HT - Hydrogen Thermal

NT - Nitrogen Thermal

HCD - Hydrogen Catalytic Dry

HeD - Helium Dry

Tet - Tetralin Solvent

Nap - Naphthalene Solvent

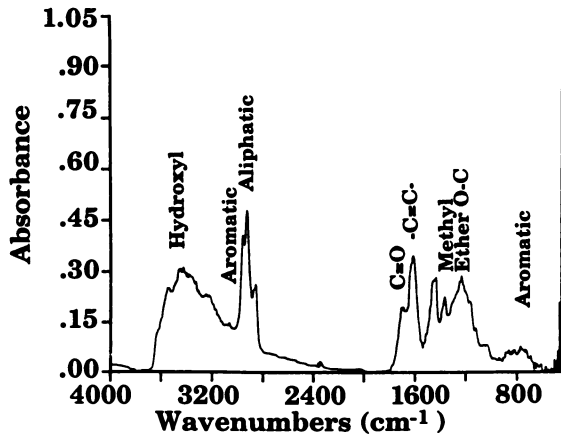


Figure 4. Comparison of FT-IR Spectra of THF Extracts of the Residue (Asphaltene) Formed at 350°C in the Presence of Catalyst and the Presence of Hydrogen.

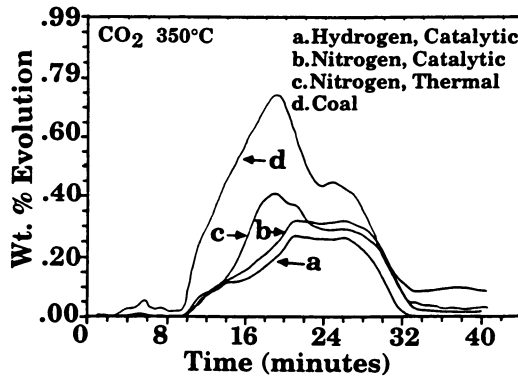


Figure 5. Comparison of CO₂ Evolution Profiles for PSOC-1401 Samples of Coal and Preliquefaction Residue at 350°C from the TG-Plus.

functional group composition of the sample, so the TG-FTIR analysis provides a good complement to the FT-IR functional group analysis. The total gas yields produced in the TG-FTIR analysis are presented in Table 2. It is most useful to compare the data for preliquefaction with solvent and catalyst to the data for thermal treatment in helium without solvent. At 275°C, the most significant affects of the treatment in the solvent is the reduction in methane (50%), a small decrease in CO₂ (~ 25%) and an increase in tar evolved from the preliquefaction residue compared to the evolution from HeD 1401-275. Product evolution from the preliquefaction residue produced using nitrogen and catalyst or nitrogen or hydrogen without catalyst were similar to the hydrogen catalytic case shown. For preliquefaction at 350°C, the reduction in methane evolved from the preliquefaction residue is about the same as for HeD 1401-350, but the reduction in CO₂ is more significant, especially for the hydrogen catalytic case. The tar yields were reduced, but the chloroform solubles were increased compared to the 275°C cases.

Since the FT-IR analysis showed the carbonyl region to change drastically, and the CO₂ yield to decrease in preliquefaction, we consider the CO₂ evolution temperature profile. Figure 5 compares the CO₂ evolution from a number of residua. The major change occurs for the catalytic preliquefaction at 350°C (HC 1401-350 and NC 1401-350). Here a drastic reduction is observed in the CO₂ evolution at all temperatures. This suggests a major chemical change in the carboxyl groups for preliquefaction with a catalyst at 350°C. The nitrogen thermal case shows less of a change.

The TG-FTIR analysis is thus consistent with the FT-IR analysis. The lower carboxyl group concentration brought about by preliquefaction at 350°C with a catalyst and solvent is accompanied by a decrease in CO₂ evolution. The lower aliphatic concentration is accompanied by lower methane and lower tar at 350°C.

Solvent Swelling. The solvent swelling ratio, *Q*, of coal and char has been employed to follow changes which occur in liquefaction (47) or pyrolysis (4-6,48,49). The changes in solvent swelling ratio result from both changes in the solvent interaction parameter and changes in the crosslink density. The former is generally believed to be less important and the solvent swelling ratio has thus been employed as a qualitative measure of the crosslink density.

Results are presented in Fig. 6 as 1 - *x* where

$$x = \frac{Q_{\text{coal}} - Q_{\text{residue}}}{Q_{\text{coal}} - 1} \quad (1)$$

so 1 - *x* = 1 is for sample whose *Q* value is the same as that for the parent coal and 1 - *x* = 0 is for a completely crosslinked residue. The results show that there was a smaller loss in solvent swelling for a catalytic preliquefaction in hydrogen compared to thermal pretreatment without a catalyst or a catalytic pretreatment with nitrogen. This smaller loss in swelling occurs even though more CO₂ (whose evolution is believed to accompany crosslinking) was evolved during the preliquefaction in hydrogen with catalyst. The effect of the catalyst is consistent with the fact that the catalytic treated samples show much greater removal of the carboxyl groups. Since it is believed that carboxyl groups promote crosslinking (4-6), it is expected that these samples will undergo much less additional crosslinking upon further thermal treatment. The charring of HC 1401-350 at 400°C, however, showed a greater loss of swelling than thermal treatment at 400°C. The increase in swelling for the thermally treated sample appears to be due to bond breaking reactions. A similar trend of a reduction followed by an increase in swelling was observed for the Wyodak coal from the Argonne premium sample bank (see Fig. 1 of Ref. 6). The

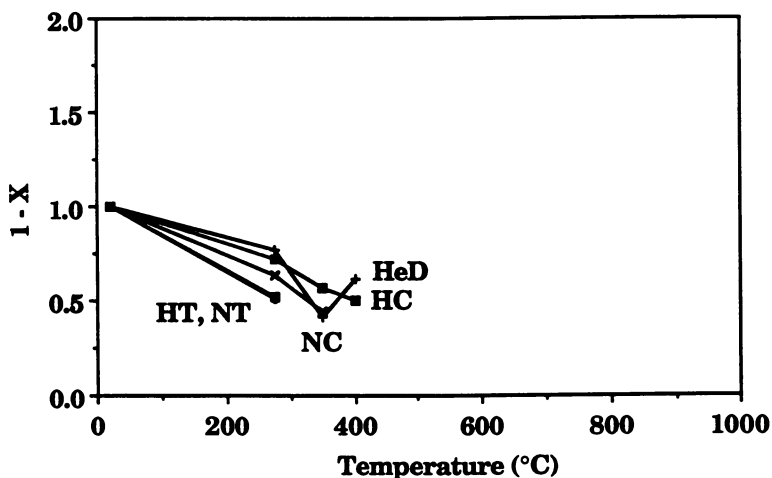


Figure 6. Solvent Swelling Behavior of Preliquefaction Samples.

Table 4 - Carbon Structural Distribution of the Wyodak Subbituminous Coal and the Preliquefaction Residue Formed at 350°C in the Presence of Catalyst and Hydrogen

Sample	f_a	f_a^C	f_a^H	f_{al}	f_{al}^H	f_{al}^*	Carbons/Clusters
Coal	.63	.08	.17	.37	.27	.10	9.7
Residue	.75	.05	.28	.25	.16	.09	12.3

Fractions of sp^2 hybridized carbon and (error estimate).

f_a = total carbon. (± 0.03).

f_a^C = carbonyl - $\delta > 165$ ppm. (± 0.02).

f_a^H = protonated and aromatic. (± 0.03).

Fraction of sp^3 hybridized carbon and (error estimate).

f_{al} = total carbon (± 0.02).

f_{al}^H = CH or CH_2 . (± 0.02).

f_{al}^* = CH_3 or nonprotonated. (± 0.03).

HC 1401-350 residue may not show the effect of bond breaking because of its low aliphatic hydrogen which must be available for free radical stabilization.

FIMS Analyses. FIMS analyses were performed on the chloroform extracts from HC 1401-350 which were separated into hexane solubles (oils plus naphthalenes) and hexane insoluble, THF soluble (**asphaltene 2**). The oil fraction is very volatile with an average molecular weight of 303 AMU on a number average basis. The FIMS spectrum shows the presence of naphthalene, naphthalene dimer and perylene. **These results show that there is significant chemistry going on involving naphthalene dimerization and probably adduction.** The asphaltene fractions showed a higher average molecular weight with only a small amount of naphthalene and no noticeable dimers.

NMR Analysis. NMR analysis was performed on the residue from HC 1401-350. The results are compared to the analysis of the parent coal in Table 4. The data confirm the lower aliphatic content and higher aromatic content in the preliquefaction samples determined by FT-IR. The increase in the aromatic content is in protonated carbon (0.28 for the residue compared to 0.17 for the coal). The major decrease in the aliphatics is in the CH₂ groups (0.27 in the coal vs. 0.16 in the residue). The cluster size in the preliquefaction coal (12.3 carbons) appears to be higher than for the raw coal (9.7). The carboxyl carbon (f_c) in the preliquefaction product (0.05) is also lower than in the raw coal (0.08), consistent with the FT-IR and TG-FTIR results.

Studies with Model Compounds. Since the results of the preliquefaction experiments with a subbituminous coal at 350 °C in the presence of a catalyst showed a significant role of carboxyl groups in preliquefaction chemistry, model compounds with aryl carboxyl groups (1-naphthoic acid and 2-naphthoic acid) were studied. The preliquefaction was carried out at 350 °C for 1 hour in nitrogen with ammonium tetrathiomolybdate (1% Mo) as the catalyst. The starting reaction mixture used was 50% naphthalene, 25% of 1-naphthoic acid and 25% of 2-naphthoic acid (weight basis). The FT-IR spectra (dry, uncorrected) of the starting reaction mixture (spectrum a) and the residue after preliquefaction (spectrum b) are compared in Fig. 7. There is a strong loss in the carbonyl and hydroxyl bands due to the loss of carboxyl groups during the preliquefaction in the presence of the catalyst. A blank run (spectrum c) was done without the catalyst which indicates that the catalyst is necessary to cause the decarboxylation. The CO₂ formation was more than a factor of three higher, due to the presence of the catalyst.

Analysis of the products by GC showed that there was a significant amount of naphthalene dimer in the mixture so that under the conditions of these experiments, significant crosslinking occurs. The model compound experiments thus show that significant decarboxylation occurs in the presence of the catalyst but that it is accompanied by crosslinking. However, the catalyst may also be effective in the breaking of these crosslinks, and this is under further study.

Modeling

The effect of preliquefaction was examined using AFR's FG-DVC (Functional Group - Depolymerization, Vaporization, Crosslinking) model of coal devolatilization (32-38). The model describes the decomposition or condensation of the macromolecular network under the influence of bond breaking and crosslinking reactions. Our model employs a sample macromolecular network in the computer consisting of aromatic ring clusters (monomers) linked by bridges. The bridges are either broken by bond scission reactions or are formed by crosslinking. In the

model, the break-up or solidification of the molecule occurs near a "gel point" where the number of unbroken bonds per ring cluster (monomer), α , reaches a critical value $\alpha_c \approx 0.95$. For bituminous coals, this critical value can be achieved in pyrolysis and the coal melts and becomes fluid. The effects of low temperature crosslinking, which occurs for low rank coals, is to increase α so that in some cases the network cannot come apart by normal pyrolytic reactions.

From the analysis of the results on the preliquefaction chemistry, it was found that the preliquefaction process results in reduction of carboxyl groups, partial crosslinking of the structure and some bond breaking resulting in higher chloroform extractables. The effect of this preliquefaction process on subsequent liquefaction is a high yields of liquids.

The FG-DVC model was employed to examine the effect of the preliquefaction chemistry on subsequent pyrolysis, since it is believed that the improvement in liquefaction must also be observed in pyrolysis. To simulate the effects of preliquefaction, the starting polymer structure of Wyodak coal was modified by putting additional crosslinks (0.13/monomer) to account for partial crosslinking of the structure. The original coal had pyridine solubles of 7.4% but the residue after preliquefaction has THF solubles of 21.5%. To account for this change in the molecular weight distribution of the starting polymer, the oligomer length was decreased from 10 to 4. The donatable hydrogen was kept constant in both cases. The carboxyl content (responsible for early crosslinking) was reduced from 6.9% to 2.9%.

The model was used to compare the coal and preliquefied sample under pyrolysis at 440°C. The results of the simulation are shown in Fig. 8. Comparing Figs. 8a and 8c for the original and modified coals, respectively, we find that while the number of bonds/bead, α , for the unmodified coal does not go below the critical value of 0.95, the value of α for the modified coal does. Figures 8b and 8d compare the fluid fraction of the mixture on pyrolysis at 440°C for original and modified coals, respectively. The modified coal shows a much higher fluid fraction which results in greater fluidity during subsequent liquefaction.

Discussion

There are three possible effects produced in preliquefaction which could lead to improved liquefaction. They are: 1) reduced crosslinking; 2) increased hydrogenation; and 3) increased bond breaking. The experimental results presented above show that effect 1 is the most likely, 2 does not occur and 3 appears to happen to some extent.

Having identified the probable chemical changes responsible for improvements in yield and quality in liquefaction, attention was focused on the reactions which produce the chemical changes. The results raise the following questions and possible answers.

Question 1. What is the chemistry of carboxyl removal? Probable answer. **There are carboxyl groups removed from the residue by conversion to CO₂. There is also a disproportionate share of carboxyl groups removed with the extract.** This occurs only in the presence of the catalyst but with or without the solvent or hydrogen. Fewer crosslinks are formed than would otherwise have been formed with the amount of carboxyl removed. This is confirmed by FT-IR, TG-FTIR, NMR, the model simulation, and experiments with model compounds. Naphthalene adduction could have occurred in the HC 1401-350 case to produce the high aromatic, but carboxyl removed occurred in other cases without this effect. Most of the carboxyl removed is by the formation of CO₂. Decarboxylation is also seen for the model compounds in the presence of the catalyst.

Question 2. What happens to aliphatics? The most probable answer. **There**

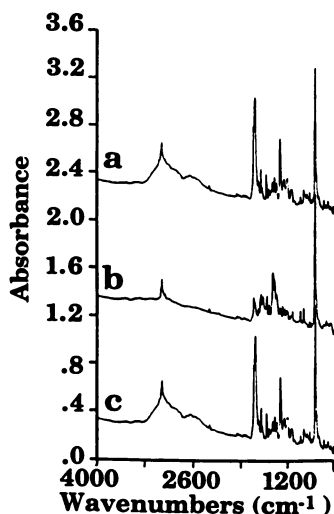


Figure 7. Comparison of FT-IR Spectra of a) Model Compounds Mixture and Residues Obtained by Treating at 350°C in the Presence of Nitrogen and b) Catalysts and c) No Catalysts.

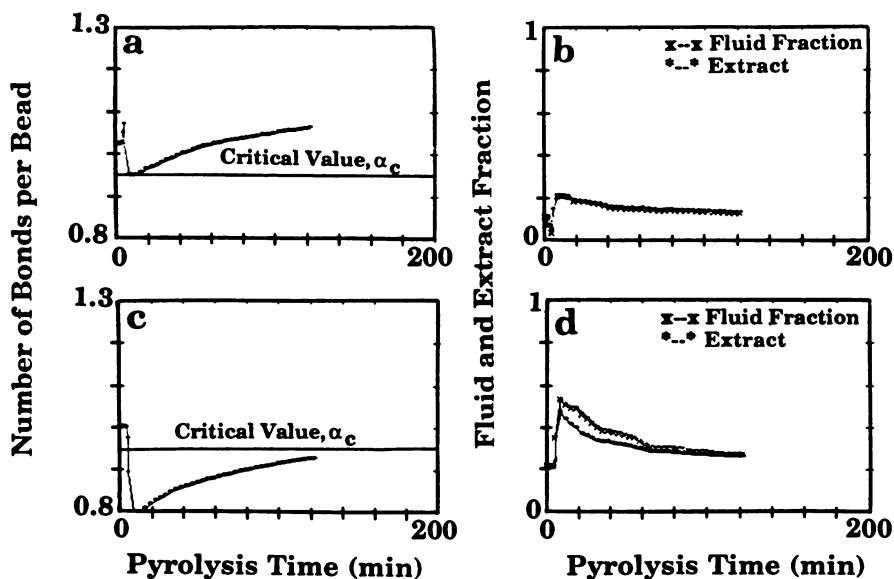


Figure 8. Comparison of Number of Bonds per Bead for a) Original Wyodak Coal (initial crosslinks = 290, initial extract yield = 7.4%, oligomer length = 10 and hard bonds = 200) and c) Modified Wyodak Coal (initial crosslinks = 600, initial extract yield = 21.5%, oligomer length = 4 and hard bonds = 0). b and d Compare the Fluid Fraction and Extract Yield for Original Wyodak Coal and Modified Wyodak Coal, Respectively.

is a reduction in the aliphatics, most likely produced by removal (with the chloroform solubles) of long chain polymethylene and small fragments high in methyl. This is confirmed by FT-IR, TG-FTIR, and NMR.

Question 3. Where do the increased aromatics come from? The most probable answer. Large increases in aromatics were observed in some cases, which are probably due to naphthalene adduction. Conversion from aliphatics is unlikely. The evidence comes from FT-IR, NMR, FIMS and the model compound studies which show that naphthalene adduction occurs.

Question 4. Why is the preliquefied insoluble product so easily liquefied? The most probable answer. The preliquefaction product with the reduced carboxyl groups content is more easily liquefied than the parent coal. Based on the product distribution, solvent swelling data and the model simulation, this improvement results from a reduction in the CO₂ associated crosslinks and from the bond breaking which produces the chloroform solubles. Both effects reduce the total number of bonds linking the network so that the coal can become fluid. If the chloroform soluble fraction is removed after preliquefaction and the residue liquefied, the drastic improvement in the liquefaction is not observed. The model simulation confirms that the residue alone will liquefy slightly better than the parent coal, but not nearly as well as the mixture.

Conclusions

- 1) Preliquefaction of a Wyodak subbituminous coal at 350°C with solvent, catalyst and hydrogen produced the best results, (highest yields and best quality) in subsequent liquefaction for 10 minutes at 425°C. The preliquefaction step produced substantial changes in the functional group composition of the residue, (low aliphatic, low carboxyl, and high aromatic), a large chloroform extract yield and a high CO₂ yield.
- 2) Preliquefaction treatments at 350°C without catalyst or with nitrogen and a catalyst produced results which were not as good as the best case.
- 3) The preliquefaction step did not appear to induce appreciable hydrogenation of the residue even with tetralin as a solvent or a hydrogen gas atmosphere.
- 4) The improvement in liquefaction behavior appears to be due to loss of the carboxyl functional groups usually responsible for crosslinking without the associated crosslink formation.
- 5) Experiments were carried out to test whether carboxyl groups on a model compound were removed under preliquefaction conditions (350°C, tetrathiomolybdate, naphthalene solvent and nitrogen or hydrogen gas). Results showed that almost all of the carboxyl groups were converted to CO₂. This reaction was, however, accompanied by crosslinking. Almost no decarboxylation occurred in the absence of the catalyst.
- 6) Simulations employing the FG-DVC pyrolysis model show that the reduction in the carboxyl group concentration in the preliquefaction step for the Wyodak coal is capable of significantly enhancing the subsequent thermal decomposition of the macromolecular network at higher temperatures. The preliquefaction should thus result in improved liquefaction yields.

Acknowledgement

This work was supported by the U.S. Department of Energy under SBIR Contract

No. DE-AC01-88ER80560. The authors are grateful to Frank Derbyshire for a great deal of advice and help in planning this research effort. We also wish to thank Ronald Pugmire for providing the NMR analysis and Ripudaman Malhotra for providing the FIMS analysis.

References

1. Neavel, R.C., Phil. Trans., R. Soc. Lond., 1981, **A300**, 141.
2. Talib, A., Neuworth, M. and Tomlinson, G., Working Paper No. 84W00279, 1984, The Mitre Corp., VA.
3. Derbyshire, F.J. and Whitehurst, D.D., Fuel, 1981, **60**, 655.
4. Suuberg, E.M., Lee, D., and Larsen, J.W., Fuel, 1985, **64**, 1668.
5. Deshpande, G.V., Solomon, P.R., and Serio, M.A., ACS Div. of Fuel Chem. Preprints, 1988, **33**, (2), 310.
6. Solomon, P.R., Serio, M.A., Deshpande, G.V., and Kroo, E., Energy & Fuels, 1990, **4**, 42.
7. Derbyshire, F., Davis, A., Epstein, M., and Stansberry, P., Fuel, 1986, **65**, 1233.
8. Derbyshire, F.J., Stansberry, Terrer, M.-T., Davis, A., and Lin, R., Proc. Int. Conf. on Coal Science, 1985, pp. 169-172, Sydney, Australia.
9. Derbyshire, F.J., Catalytic Coal Liquefaction by Temperature-Staged Reaction, presented at Direct Liquefaction Contractor's Review Meeting, Pittsburgh, PA, (Oct. 20-22, 1986).
10. Derbyshire, F.J., Davis, A., Lin, R., Stansberry, P.G., Terrer, M.-T., Fuel Processing Technology, 1986, **12**, 127.
11. Davis, A., Schobert, H.H., and Derbyshire, F.J., Enhanced Coal Liquefaction by Low Severity Catalytic Reactions, Technical Progress Report for the period Mar. to May, 1987, U.S. DOE/PETC Contract No. DE-FG22-86PC90910, (6/1987).
12. Davis, A., Schobert, H.H., and Derbyshire, F.J., Enhanced Coal Liquefaction by Low Severity Catalytic Reactions, Technical Progress Report for the period June to Aug. 1987, U.S. DOE/PETC Contract No. De-FG22-86PC90910, (9/1987).
13. Derbyshire, F.J., Davis, A., Epstein, M., and Stansberry, P.G., ACS Div. of Fuel Chem. Preprints, 1986, **31**, (4), 308.
14. Solomon, P.R., in Coal Structure, Advances in Chemistry Series, 1981, **192**, 95.
15. Solomon, P.R., Hamblen, D.G. and Carangelo, R.M., ACS Symp. Series, 1982, **205**, 77.
16. Solomon, P.R. and Carangelo, R.M., Fuel, 1982, **61**, 663.
17. Solomon, P.R. and Carangelo, R.M., Fuel, 1988, **67**, 949.
18. Solum, M.S., Pugmire, R.J., Energy & Fuels, 1987, **1**, 448.
19. Sethi, N.K., Grant, D.M., Pugmire, R.J., J. Magn. Reson., 1987, 71.
20. Solum, M.S., Pugmire, R.J., Grant, D.M., Fletcher, T.H., and Solomon, P.R., Solid State ¹³C NMR Studies of Coal Char Structure Evolution, Western States Section/The Combustion Institute, Pullman, WA, (3/89).
21. Solum, M.S., Pugmire, R.J., and Grant, D.W., ACS Div. of Fuel Chem. Preprints, 1987, **32**, (4), 273.
22. Sethi, N.K., Pugmire, P.J., Grant, D.M., Proceedings Int. Conf. on Coal Sci., 1987, p. 41, Holland.
23. Carangelo, R.M., Solomon, P.R., and Gerson, D.J., Fuel, 1987, **66**, 960.
24. Whelan, J.K., Solomon, P.R., Deshpande, G.V., and Carangelo, R.M., Energy and Fuels, 1988, **2**, 65.
25. Solomon, P.R., Serio, M.A., Carangelo, R.M., Bassilakis, R., Gravel, D.,

- Baillargeon, M., Baudais, F., and Vail, G., "Analysis of the Argonne Premium Coal Samples by TG-FTIR", Energy & Fuels, 1990, accepted for publication.
26. StJohn, G.A. Buttrill, S.E., Jr., and Anbar, M., in ACS Symposium Series 71, Ed., J. Larsen, 1978, 223.
27. Squire, K.R., Solomon, P.R., DiTaranto, M.B., and Carangelo, R.M., ACS Div. of Fuel Chemistry Preprints, 1985, 30, (1), 386.
28. Solomon, P.R. and Squire, K.R., ACS Div. of Fuel Chemistry Preprints, 1985, 30, (4), 346.
29. Solomon, P.R., Squire, K.R., and Carangelo, R.M., Proceedings Int. Conf. on Coal Sci, 1985, p. 945, Sydney, Australia.
30. Green, T.K., Kovac, J., and Larsen, J.W., Fuel, 1984, 63, 935.
31. Green, T.K., Kovac, J., Brenner, D., and Larsen, J.W., in Coal Structure, R.A. Meyers, Ed., Academic Press, NY, 1982, Chapter. 6, p. 199.
32. Solomon, P.R., Hamblen, D.G., Carangelo, R.M., Serio, M.A., and Deshpande, G.V., Combustion and Flame, 1988, 71, 137.
33. Solomon, P.R., Hamblen, D.G., Deshpande, G.V. and Serio, M.A., Proceedings International Coal Science Conference, 1987, p. 601, The Netherlands.
34. Solomon, P.R., Hamblen, D.G., Carangelo, R.M., Serio, M.A. and Deshpande, G.V., Energy and Fuels, 1988, 2, 405.
35. Serio, M.A., Solomon, P.R., Yu, Z.Z., Deshpande, G.V., and Hamblen, D.G., ACS Div. of Fuel Chem. Preprints, 1988, 33, (3), 91.
36. Serio, M.A., Solomon, P.R., and Carangelo, R.M., ACS Div. Fuel Chem. Preprints, 1988, 33, (2), 295.
37. Solomon, P.R., Best, P.E., Yu, Z.Z., and Deshpande, G.V., ACS Div. of Fuel Chem. Preprints, 1989, 34, (3), 895.
38. Solomon, P.R., Hamblen, D.G., and Yu, Z.Z., ACS Div. of Fuel Chem. Preprints, 1989, 34, (4), 1280.
39. Grant, D.M., Pugmire, R.J., Fletcher, T.H., and Kerstein, A.R., "A Chemical Model to Coal Devolatilization Using Percolation Lattice Statistics", submitted for publication.
40. Fischer, M.E. and Essam, J.W., J. Mathematical Physics, 1961, 2, (4), 609.
41. Gordon, M., Proc. R. Soc. London, Ser. A, 1962, 268, 240.
42. Flory, P.J., J. Am. Chem. Soc., 63, 3083, 3097, (1941); see also Principles of Polymer Chemistry, Cornell University Press, Ithaca, NY, 1953, Chapter 9.
43. Stockmayer, W.H., J. Chem. Phys., 1943, 11, 45; 1944, 12, 125.
44. Macosko, C.W. and Miller, Molecular Weights of Nonlinear Polymers, 1976, 2, (2), 199.
45. Solomon, P.R. and King, H.H., Fuel, 1984, 63, 1302.
46. Squire, K.R., Carangelo, R.M., DiTaranto, M.B., and Solomon, P.R., Fuel, 1986, 65, 833.
47. Bockrath, B.C., Illig, E.G., and Wassell-Bridger, W.D., Energy & Fuels, 1987, 1, 227.
48. Suuberg, E.M., Unger, P.E., and Larsen, J.W., Energy & Fuels, 1987, 1, 305.
49. Suuberg, E.M., Otake, Y., and Deevi, S., ACS Div. of Fuel Chem. Preprints, 1988, 33, (1), 387.

RECEIVED November 5, 1990

Chapter 16

Liquefaction Behavior of High-Sulfur Lignites

Ana B. Garcia and Harold H. Schobert

Fuel Science Program, The Pennsylvania State University,
University Park, PA 16802

The hydrogenation reactions of three lignites of widely differing organic sulfur contents were studied using impregnated metal salts as catalysts but no donor solvent. The presence of relatively weak C-S bonds facilitates breakdown of the coal structure. Loss of sulfur proceeds via formation of organosulfur liquids which are subsequently hydrogenated, in reactions similar to hydrodesulfurization on a carbon-supported catalyst. The hydrogen sulfide formed in the reaction helps to catalyze production of liquids.

Previous work in this laboratory has investigated the hydrodesulfurization of Mequinenza (Spanish) lignite, a coal which is of interest for its remarkable organic sulfur content of about 11% on a daf basis. The initial motivation for the study of this coal was to investigate the potential of producing a char of reduced sulfur content for a boiler fuel. In hydrodesulfurization experiments with impregnated molybdenum catalysts, sulfur removals of up to about 70% were obtained (1,2). These results suggested that further efforts to optimize reaction conditions could succeed in removing most of the sulfur. In an ideal process configuration for commercial application, the hydrodesulfurization reaction would remove the organic sulfur as H₂S, leaving the carbon values as a sulfur-free or low-sulfur char suitable for combustion. However, it is inevitable that the reaction of a highly reactive lignite with hydrogen in the presence of a good hydrogenation catalyst will produce some liquids as by-products. In fact, in the experiment in which a sulfur reduction of 70% was achieved, 48% of the lignite was converted to liquid products, although most of the sulfur removed did appear as H₂S. This behavior prompted an examination of the liquefaction reactivity of this lignite, with particular concern for processes leading to the formation of liquids at relatively mild conditions and short reaction times.

It has been known for some time that the yields of desirable products from coal liquefaction can be enhanced by dispersing the hydrogenation catalyst into the coal. For example, in the liquefaction of a high volatile bituminous coal, the total conversion to benzene-soluble material, the asphaltene (hexane-insoluble), and oil yields were all enhanced when the catalyst was impregnated into the coal rather than mixed with the coal as a dry powder (3). In that work, impregnated salts of iron,

nickel, tin, and molybdenum effected two- to three-fold increases in oil yields compared to results obtained when the compounds were added as powders. In the early stages of reaction, the reactants cannot reach the catalyst surface until some breakdown or dissolution of the coal has occurred; thus, in a sense, the catalyst must be transported (*e.g.* by impregnation) to the reactants (4). Earlier work has emphasized the importance of having the catalyst present at the reactive sites when the pyrolytic decomposition of the coal structure begins (5). Our studies of the hydrodesulfurization of the Mequinenza lignite have shown that improved sulfur removal and conversion to liquid products were obtained by impregnating the lignite with water-soluble molybdate or thiomolybdate salts, compared to attempted impregnation with a slurry of insoluble molybdenum disulfide (6). The better conversions to liquids and better sulfur removals obtained with the impregnated salts were attributed to the superior dispersion of these materials, despite the fact that molybdenum disulfide is well known to be a useful hydrogenation catalyst.

Given's study of the liquefaction behavior of 104 high volatile bituminous coals included coal samples of up to 7.3% total sulfur (dry basis) (7). Examination of the data by cluster analysis showed that a factor representing sulfur had a major role in separating the coals into statistically separate groups. Subsequent work, using a set of 26 high volatile bituminous coals with a maximum sulfur content of 7.9% (dry basis), showed no significant relationships of the yields of oils, asphaltenes, or gas to sulfur content (8). The highest organic sulfur content of the coals used in that work was 3.3% (dry basis). The final comment in Given's 1988 paper (8) was that, "the role of sulphur in coals clearly merits further intensive study."

The work reported here used coals of different rank and much milder reaction conditions. Furthermore, a much smaller sample set was used. Therefore, our results are not intended to be a direct extrapolation of previous work (7,8), but rather represent a collateral line of investigation. The results presented here offer some insights into the possibility of exploiting the relatively weak C-S bond for obtaining good liquids yields at mild conditions that might be typical of the low-temperature stage of a temperature-staged liquefaction system.

Experimental

Three lignites were used in this work: Hagel seam lignite from the United States, Cayhiran lignite from Turkey, and the Spanish Mequinenza lignite mentioned above. Some of the characteristics of these lignites are shown in Table I. The principal criterion for the choice of these lignites was to obtain as wide a range of organic sulfur contents as possible. A secondary consideration, having first obtained the desired organic sulfur contents, was to obtain lignites with reasonably comparable carbon and hydrogen contents. The lignite samples were crushed to -60 mesh under oxygen-free nitrogen and stored under nitrogen until impregnated with catalyst or until used in a hydrogenation experiment.

The procedure for conducting the reactions was the same regardless of the gas atmosphere or whether a catalyst was used. All reactions were carried out in microautoclave reactors (tubing bombs) of nominal 30 mL capacity. A 5 g lignite sample of dry lignite was used. No solvent was used in these experiments. The reactor was flushed three times with the desired gas, either nitrogen or hydrogen, before being pressurized to 6.9MPa. The pressurized reactor was then immersed in a sandbath preheated to the desired reaction temperature. The reactor was subjected to vertical oscillation of 2.5 cm at 200 cycles/min for the duration of the reaction. The range of temperatures used in these experiments was 250-325° C; the reaction times were varied from 30 to 240 minutes. At the end of an experiment the reactor was rapidly quenched by immersion in cold water.

Table I. Ultimate and Sulfur Forms Analyses (dry, ash-free basis)
of Lignites Used in this Work

	Hagel	Cayhiran	Mequinenza
Ultimate			
Carbon	71.34	68.15	64.81
Hydrogen	4.50	5.50	5.72
Nitrogen	1.14	2.21	0.96
Organic sulfur	0.79	4.91	11.32
Oxygen (difference)	22.23	19.23	17.19
Sulfur forms			
Total sulfur	0.93	7.34	12.64
Pyritic sulfur	0.10	1.97	1.15
Sulfate sulfur	0.02	0.52	0.14
Sulfide sulfur			0.04
Organic sulfur	0.81	4.91	11.32

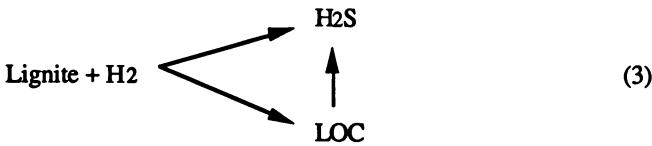
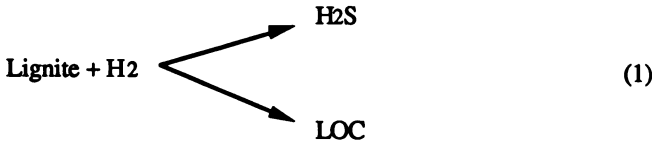
The cooled reactor was vented into a glass expansion bulb from which samples could be withdrawn for gas chromatographic analysis. The reactor contents were washed with tetrahydrofuran (THF) into a dry Soxhlet thimble and were then extracted with THF for about 24 hr under nitrogen. The THF was removed from the extract by rotary evaporation. The solid residue was dried at 100° C for 18-20 hr before weighing. The gas yield was calculated by difference from the weights of the liquids and the THF-insolubles.

For experiments in which a catalyst was used, the lignites were impregnated with a sulfided ammonium molybdate, $(\text{NH}_4)_2\text{MoO}_2\text{S}_2$, reagent grade ammonium tetrathiomolybdate, $(\text{NH}_4)_2\text{MoS}_4$, or with reagent grade nickel sulfate. The sulfided ammonium molybdate was prepared by passing hydrogen sulfide through an aqueous solution of ammonium heptamolybdate for 30 minutes. An amount of the salt sufficient to give the desired catalyst loading was dissolved in sufficient distilled water to give a 1:1 lignite:water ratio. The lignite was slurried in the aqueous solution and stirred for at least 2 hr. Excess water was removed by vacuum freeze drying to a lignite moisture content below 1%. Typically the impregnation procedure was carried out with a large enough batch of lignite to suffice for a series of experiments. The dried, impregnated lignites were stored under nitrogen.

Results and Discussion

Mechanism of Hydrogenation of Mequinenza Lignite. Our initial work focused on the hydrodesulfurization of the Mequinenza lignite; the elucidation of the mechanism of this process then led to a further consideration of the role of organic sulfur in the liquefaction process, presented in the next subsection.

In most experiments the sulfur removed from the Mequinenza lignite appeared in two products, hydrogen sulfide and liquid organosulfur compounds (LOC) present in the THF-soluble extract. There are three mechanisms by which these two sulfur-containing products could be produced from the lignite:



Discrimination among these possible mechanisms can be made by examining the variation of the yields of the two products, LOC and H₂S, as a function of conversion. The analysis follows the method published by Bond (9). In this case, conversion represents the fraction of the sulfur in the lignite converted to both H₂S and LOC, selectivity for either product is the fraction of total sulfur removed from the lignite reporting to that product, and yield is calculated by multiplying conversion by selectivity. These calculations were performed for the reaction of Mequinenza lignite in the presence of sulfided ammonium heptamolybdate, with 1% Mo catalyst loading, using the data presented in Table II. The variations of LOC and H₂S yields with sulfur conversion are shown in Figure 1. (The H₂S yield expressed in Fig. 1 is the percentage of sulfur removed from the Mequinenza lignite as H₂S; this term is distinct from the total H₂S yield, as explained below.) The increase of LOC yield with conversion to a fractional conversion of about 0.5 and its subsequent decrease at higher conversions is a strong indication that the reaction is proceeding by mechanism (2). That is, the hydrodesulfurization proceeds primarily by a breakdown of the lignite structure to produce organosulfur compounds in the initial liquid products; then in a subsequent step these organosulfur compounds are hydrotreated on the catalyst to produce H₂S as the final sulfur-containing product. (These observations do not rule out the possibility that some H₂S is produced by direct hydrogenation of sulfur functional groups in the lignite early in the reaction.) In Table II, the term "total H₂S yield" is used to indicate the amount of gaseous H₂S produced in the hydrodesulfurization reaction *from lignite*, as, for example, grams H₂S per 100 g lignite.

Data from tests at 250, 275, 300, and 325° C were used to calculate pseudo-first order rate constants for the formation of H₂S. These data are expressed on a standard Arrhenius plot (Fig. 2) for which the linear least squares coefficient of determination, r^2 , is 0.98. The apparent activation energy calculated from the slope is 28.5 kcal/mol. This result is in excellent agreement with the recent work of Abotsi, who studied the performance of carbon-supported hydrodesulfurization catalysts (10). Using Ambersorb XE-348 carbon loaded with sulfided ammonium molybdate (3% Mo loading) prepared by the same procedure reported here, Abotsi hydrotreated a coal-derived recycle solvent. The apparent activation energy for

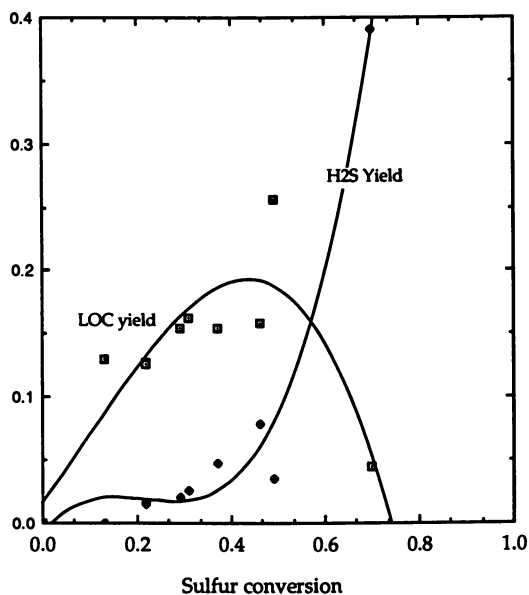


Figure 1. Variation of LOC and H₂S yields as a function of sulfur conversion from Mequinenza lignite.

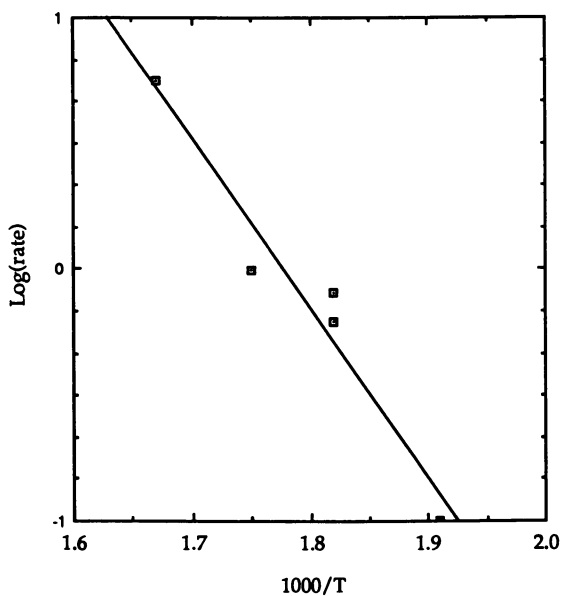


Figure 2. Arrhenius plot of pseudo-first order rates of H₂S production from Mequinenza lignite, with sulfided ammonium molybdate catalyst.

Table II. Reaction Conditions and Results for Hydrogenation of Mequinenza Lignite with Sulfided Ammonium Molybdate Catalyst

Catalyst Loading Wt % daf	Temp. °C	Time hr.	Total in Lignite Wt% (dry)	Total Liquids Yield Wt. % (dry)	Total H ₂ S Yield Wt. % (dry)	Total Sulfur Removed Wt. % (dry)
1.0	250	1.0	11.02	8.8	---	10.8
1.0	275	0.5	10.34	13.0	---	13.1
1.0	275	1.0	11.02	13.5	0.66	22.8
1.0	275	2.0	10.41	16.2	0.67	22.9
1.0	275	4.0	10.41	19.0	0.83	28.6
1.0	300	0.5	10.34	19.1	0.18	23.9
1.0	300	1.0	10.74	20.3	1.05	31.8
1.0	300	1.5	10.74	23.6	1.51	37.1
1.0	300	2.0	10.74	27.7	2.13	45.8
1.0	325	0.5	10.34	33.0	1.40	47.7
1.0	325	1.0	10.74	47.5	5.95	69.9
1.0	350	0.5	10.34	53.6	7.10	77.2
1.5	250	1.0	10.00	11.2	0.14	10.9
1.5	275	1.0	10.00	12.7	0.41	19.3
1.5	300	1.0	10.00	14.9	0.99	22.7
1.5	325	1.0	10.00	35.9	4.73	56.1
2.2	250	1.0	11.03	12.4	0.35	18.2
2.2	275	1.0	11.03	14.2	0.58	21.1
2.2	300	1.0	11.03	20.5	1.57	33.6
2.2	325	1.0	11.03	44.1	6.25	62.6

hydrodesulfurization of the recycle solvent to H₂S on the carbon-supported catalyst was 27.9 kcal/mol. A further characteristic of carbon-supported HDS catalysts is an apparent levelling off of conversions and rates with increased metal loading (11,12). We have shown in previous work that catalyst loadings of up to 4.5% Mo afforded essentially no improvement in sulfur removal relative to that obtained with 1% loading (2).

These results, particularly the indication of a sequential mechanism involving an initial production of liquids which are subsequently hydrotreated on the molybdenum catalyst, were the experimental basis for probing further into the first step - liquids formation - with particular interest in whether the unusually high concentration of organic sulfur in the Mequinenza lignite might have some effect on the liquefaction behavior.

Effects of organic sulfur content on lignite hydrogenolysis. The C-S bond is significantly weaker than the C-C bond. Although data in various reference sources vary slightly, values of 66 and 83 kcal/mole, respectively, are typical (13). These values were the basis for a hypothesis that a coal structure containing a high proportion of relatively weak C-S bonds might be more easily broken apart, relative to a structure with small concentration of C-S bonds, in either thermolysis or hydrogenolysis. To test this hypothesis the three lignites, with organic sulfur contents ranging from 0.8 to 11.3%, were reacted in both hydrogen and nitrogen atmospheres with and without a catalyst.

The relevant experimental results are summarized in Table III. The results for reaction in hydrogen atmosphere show that the liquid yield increases as organic sulfur increases, regardless of whether the lignite was first impregnated with a catalyst. Similar results have been reported for other lignites (with the highest organic sulfur content being 6.0%), but that data was obtained at reaction temperatures of 380-460°C (14). The magnitudes of conversions and product yields

in the dry (i.e., without added solvent) catalytic liquefaction of a subbituminous coal at comparable reaction conditions (15). For reactions in nitrogen atmosphere, where presumably the decomposition of the coal structure would be due entirely to thermal effects, liquid yield also increased with organic sulfur for experiments in the absence of catalyst. This trend was not followed for reactions in nitrogen with the impregnated molybdenum catalyst, for reasons which are not clear. However, the Çayhıran lignite was the only one of the three to produce measurable quantities of H₂S during the reaction in nitrogen atmosphere, suggesting that the organic sulfur functional groups in this lignite might be different from those of the Hagel and Mequinenza lignites. The composition of the gas produced in the treatment of the Çayhıran lignite was 77% CO₂ and 23% H₂S, suggesting that some of the sulfur functional groups in this lignite are readily susceptible to catalytic hydrogenolysis directly to H₂S, rather than breaking apart to form sulfur-containing liquids. Alkyl and aryl thiols and sulfides are readily cleaved by hydrogen; this is a standard laboratory method when Raney nickel is used as the catalyst (16). Diaryl disulfides readily undergo reductive cleavage of the S-S bond to H₂S around 300°C (17). The major organic sulfur functional groups in the young Turkish lignites are in fact considered to be thiols and sulfides (18).

For experiments in the absence of catalyst, both the Hagel and Çayhıran lignites showed an increase in liquid yield for reactions run in hydrogen relative to those run in nitrogen. In the case of the Mequinenza lignite, the liquid yields were essentially identical, within experimental error. This result suggests that the extensive array of C-S bonds enables a facile, thermally induced breakdown of the coal structure which is able to proceed without the intervention of hydrogen.

When reactions were carried out using lignites impregnated with the molybdenum catalyst, a greater yield of liquids was observed, from all three lignites, for experiments in hydrogen relative to those in nitrogen. Furthermore, the improvement in liquid yield, expressed as the difference between the yield in hydrogen and that in nitrogen, itself increased as a function of the organic sulfur content of the lignite. Thus for Hagel lignite the increased liquid yield in hydrogen was 0.7% (i.e., 3.0% in hydrogen vs. 2.3% in nitrogen), while for the Mequinenza lignite the increased yield in hydrogen was 4.5%. Although the yield of liquids increases with organic sulfur content, suggesting that indeed the cleavage of weak C-S bonds may facilitate liquefaction, the increase is not a linear function of sulfur content but becomes much more pronounced at the higher sulfur contents (Fig. 3). This observation suggested that the liquefaction of high-sulfur lignites might be autocatalytic.

The initial hypothesis tested was that the key step facilitating formation of liquids in high yield from the high organic sulfur lignites is the generation of thiols and the subsequent role of thiols in cleaving disulfide structures. The S-S bond is even weaker (51 kcal/mole) than the C-S bond (19). Thiols are easily formed by hydrolytic cleavage of disulfides (20) or other organic sulfur functional groups. Once some thiols had been generated in the reaction, they could then facilitate further reaction of disulfides. In fact, such a disulfide cleavage by thiols is used in biochemical reactions, where such reagents as 2-mercapto-1-ethanol or dithiothreitol (Cleland's reagent) are used to cleave the disulfide linkage in proteins to the free thiol group in cysteine (21). Provided that the disulfide linkages in the lignites are bridging groups, rather than components of cyclic structures (a proviso analogous to the concept of open ethers and closed ethers among oxygen functional groups), the thiols formed by the initial reduction of some of the sulfur groups could then facilitate further depolymerization of the coal structure by reaction with the disulfides.

Table III. Results of Experiments in Hydrogen and Nitrogen at 275°, 6.9MPa Gas Pressure (cold) for 30 min. Results are expressed on a dry, ash-free basis

	Hagel		Çayhıran		Mequinenza	
	H ₂	N ₂	H ₂	N ₂	H ₂	N ₂
Thermal (no catalyst)						
Total conversion	6.0	6.3	4.2	3.0	11.1	12.2
Liquid yield	1.8	1.6	2.4	1.8	11.9	12.1
Gas yield	4.2	4.7	1.9	1.2	-	-
Catalytic						
Total conversion	7.3	5.5	3.5	1.9	16.0	12.6
Liquid yield	3.0	2.3	3.2	1.8	16.4	11.9
Gas yield	4.3	3.2	0.3	0.1	-	0.7

Useful reviews of the kinetics of autocatalytic reactions have recently been published by Mata-Perez and Perez-Benito (22) and by Schwartz (23). For an autocatalytic reaction a plot of r/c , where r is the rate of reaction and c the concentration of reactant, as a function of c should be linear with a negative slope (22). When this analysis is applied to the possibility of autocatalysis of liquids production by LOC, no dependence of r/c on c was found. In fact, least squares "correlation" coefficients were in the range 0.01 - 0.03. Although the initial hypothesis of autocatalysis by thiols is shown to be untenable, an alternative is the possibility of autocatalysis by H₂S.

The review by Trewhella and Grint points out that a factor important in the ability of organic sulfur to enhance liquefaction is the reductive conversion of sulfur functional groups to H₂S (24). As the relative concentration of H₂S increases, improvements are observed in both liquefaction rates and conversions (25). Stenberg and co-workers have examined improvements in liquefaction arising from H₂S catalysis for low-rank coals (26-28). In addition, Stenberg *et al.* also noted an effect of sulfur in the coal on low-rank coal liquefaction conversion. For liquefaction in 1:1 H₂:CO with an anthracene oil solvent at 460°, higher conversion was observed for Martin Lake (Texas) lignite relative to Wyodak subbituminous coal, 75.1 vs. 52.6%, respectively (29). This difference was attributed to the higher sulfur content of Martin Lake lignite (2.2%) relative to the Wyodak coal (0.5%). In fact, for eleven low-rank coals liquefied in this reaction system, the lowest conversions were observed from the coals with the lowest sulfur content and the highest conversion, from the coal with the highest sulfur (29).

A re-examination of our data on Hagel, Çayhıran, and Mequinenza lignite shows clear evidence for autocatalysis by H₂S. Figure 4 is a plot of r/c vs. c for liquids production from Mequinenza lignite with impregnated nickel sulfate catalyst at 275°C. The average H₂S partial pressure in the microautoclave at reaction temperature was 0.14 MPa. Figure 5 shows that the effect is not unique to this reaction temperature and impregnated metal catalyst; these data are for reaction at 325°C with an impregnated sulfided ammonium molybdate catalyst. The average H₂S partial pressure in this system was 1.4 MPa. In both Figures the linear dependence with inverse slope of r/c on c is evident. In these Figures the rate, r , is expressed as the percent of lignite converted to liquids per hour; and the concentration c is the amount of sulfur remaining in the unreacted solid at the time the reaction was stopped.

It has been suggested that organic sulfur is uniformly distributed throughout a coal sample, on the basis of solvent extraction work (30). For example, the sulfur content of extracts produced with various solvents is about the same from one

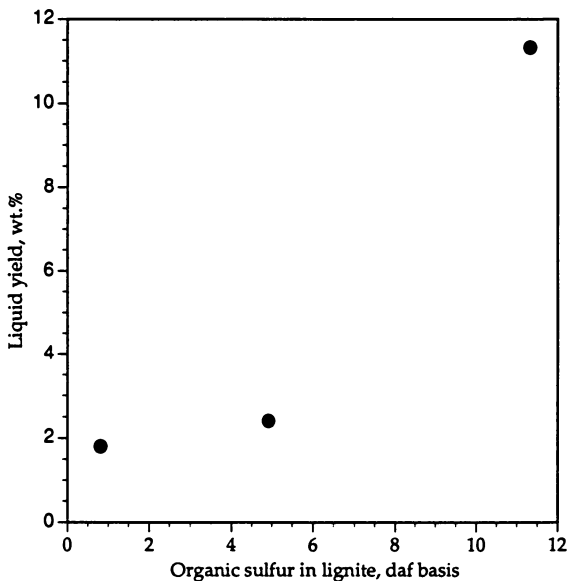


Figure 3. Liquids yield as a function of sulfur content for Hagel, Çayhıran, and Mequinenza lignites, no catalyst, H₂ atmosphere, 275°C.

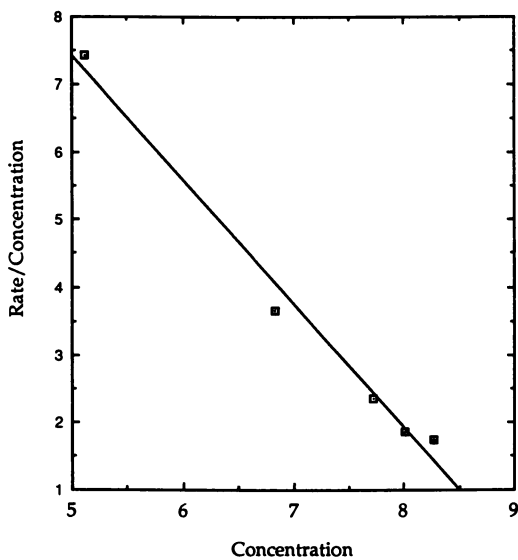


Figure 4. Rate/concentration as a function of concentration for Mequinenza lignite, nickel sulfate catalyst, 275°C, average H₂S partial pressure 0.14 MPa.

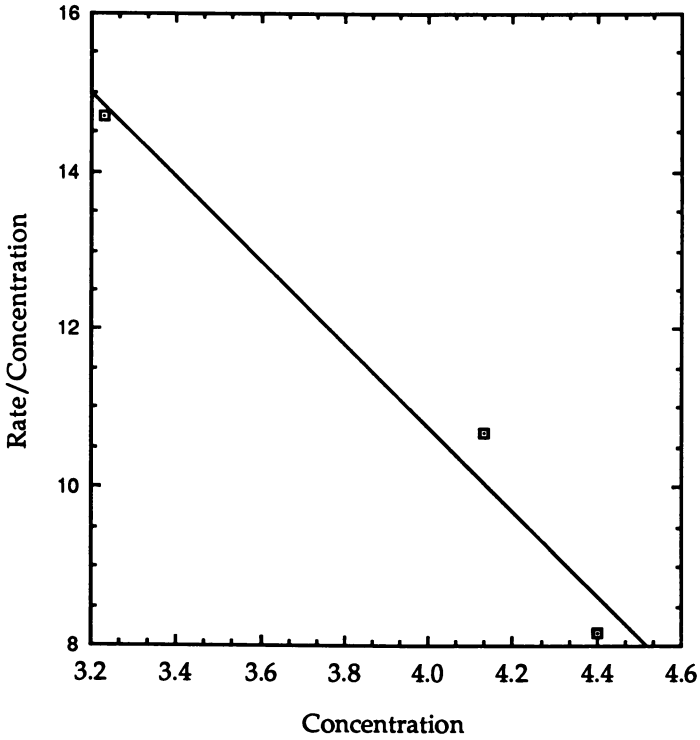
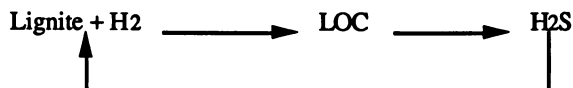


Figure 5. Rate/concentration as a function of concentration for Mequinenza lignite, sulfided ammonium molybdate catalyst, 325°C, average H₂S partial pressure 1.4 MPa.

solvent extract to another, indicating that even though individual solvents may be able to dissolve different portions, or extents, of the coal structure, approximately the same amount of sulfur is removed in each case. It is also recognized that for liquefaction in the absence of added solvent a good dispersion of the catalyst is of special importance in obtaining good conversions (5). The dispersion of the catalyst obtained by the impregnation technique, combined with the inherent dispersion of the sulfur throughout the lignite structure, facilitate the hydrodesulfurization of the LOC with hydrogen to generate H₂S. H₂S only does this HDS process help reduce the sulfur content of the liquid, the H₂S assists by catalyzing further breakdown of the lignite structure. Thus a reaction scheme of the type



appears to be important in the liquefaction of high sulfur lignites.

The work reported here was not undertaken with the specific goal of developing a facile liquefaction process for high sulfur lignites. Nevertheless, liquids yields of >50% were observed in 30 minutes reaction at 350°C from Mequinenza lignite. These promising results suggest that, by taking advantage of the HDS ability of the impregnated metal catalyst and the liquefaction catalysis of the H₂S produced in the process, it may be possible to produce good liquid yields at relatively mild conditions.

Acknowledgements

Dr. Garcia was supported by a postdoctoral fellowship provided by the Spanish Research Council (CSIC). Financial support for the experimental work was provided by The Pennsylvania State University Cooperative Program for Coal Research. The authors are grateful for the sample of Çayhıran lignite provided by the Istanbul Technical University.

Literature Cited

1. Garcia, A. B.; Schobert, H. H. ACS Div. Fuel Chem. Preprints 1988, **33**(1), 241.
2. Garcia, A. B.; Schobert, H. H. Coal Preparation 1989, **7**, 47.
3. Weller, S.; Pelipetz, M. G. Ind. Eng. Chem. Eng. Proc. Devel. 1951, **43**, 1243.
4. Gorbaty, M. L. Fuel, 1978, **57**, 796.
5. Hawk, C. O.; Hiteshue, R. W. U. S. Bur. Mines. Bull. 1965, No. 622.
6. Garcia, A. B.; Schobert, H. H. Fuel, 1989, **68**, 1613.
7. Yarzab, R. F.; Given, P. H.; Spackman, W.; Davis, A. Fuel, 1980, **59**, 81.
8. Neill, P. H.; Shadle, L. J.; Given, P. H. Fuel, 1988, **67**, 1459.
9. Bond, G. C. Heterogeneous Catalysis: Principles and Applications; Clarendon Press: Oxford, 1987; p. 52ff.
10. Abotsi, G. M. K. Ph.D. Thesis, The Pennsylvania State University, University Park PA, 1987.
11. DeBeer, V. H. J.; Duchet, J. C.; Prins, R. J. Catal., 1981, **72**, 369.
12. Duchet, J. C.; VanOers, E. M.; DeBeer, V. H. J.; Prins, R. J. Catal., 1983, **80**, 386.
13. March, J. Advanced Organic Chemistry; John Wiley: New York, 1985; p. 23.

14. Severin, D., Oelert, H. H., and Yildirim, M. E. Proc. 1983 Intl. Conf. on Coal Sci., p. 52.
15. Davis, A.; Derbyshire, F. J.; Schobert, H. H. U.S. DOE Rept. 1987, No. DOE-PC-90910-3.
16. March, J. Advanced Organic Chemistry; John Wiley: New York, 1985; p. 652.
17. Tsai, S. C. Fundamentals of Coal Beneficiation and Utilization; Elsevier:Amsterdam, 1982; Chapter 5.
18. Kara, H.; Ceylan, R. Fuel, 1988, **67**, 170.
19. Pauling, L. College Chemistry; W. H. Freeman: San Francisco, 1964; p. 316.
20. Hudlicky, M. Reductions in Organic Chemistry; Ellis Horwood: Chichester, UK, 1986; p. 87.
21. Loudon, G. M. Organic Chemistry; Benjamin/Cummings: Menlo Park, CA, 1988; p.170.
22. Mata-Perez, F.; Perez-Benito, J. F. J. Chem. Educ., 1987, **64**, 925.
23. Schwartz, L. M. J. Chem. Educ., 1989, **66**, 677.
24. Trewhella, M. J.; Grint, A. Fuel, 1987, **66**, 1315.
25. Hirschon, A. S.; Laine, R. M. Fuel, 1985, **64**, 911.
26. Stenberg, V. I. U.S. DOE Rept. 1988, No. DOE/PC/70787-T11.
27. Stenberg, V. I.; Nowok, J. Chemtech, 1987, **17**, 636.
28. Sondreal, E. A.; Stenberg, V. I.; Willson, W. G. Fuel, 1982, **61**, 925.
29. Stenberg, V. I.; Jones, M. B.; Suwarnasarn, N. J.; Fuel, 1985, **64**, 470.
30. vanKrevelen, D. W. Coal; Elsevier: Amsterdam, 1981; p.171.

RECEIVED December 26, 1990

Chapter 17

Hydroliquefaction of Coal Liquids in Spinning and Falling Basket Autoclaves

Graham Harrison, P. W. Doughty, and S. S. Ali

Department of Applied Sciences, Staffordshire Polytechnic,
Stoke-on-Trent ST4 2DE, United Kingdom

Fresh and used catalysts (CoMo, NiMo, ZnMo and ZnW) were used in hydroliquefaction experiments with batches of Point of Ayr coal liquid. One series of experiments was carried out at 400°C for 2 h with all four of the catalysts using five repeat contacts. A second series used only CoMo over three repeat contacts and considered variations in reaction time and temperature. The performance of the two spinning/falling baskets was compared by investigating the hydrogenation/hydrocracking of phenanthrene at different stirrer speeds, reaction times and reaction temperatures. The analysis schedule made use of vacuum distillation, gas chromatography, carbon, hydrogen and sulphur analysis and specific surface area analysis. Conversions were assessed from the vacuum distillation and gas chromatography data, making use of marker compounds.

Aspects of coal liquefaction have been much researched, particularly with the re-emergence of interest caused by the oil crisis in the 1970's. The type of reactors used in the studies has been various, ranging from small 'bomb' type microautoclaves through larger autoclaves and bench-scale reactors to larger scale pilot or demonstration plants. The use of differently sized and designed high pressure equipment for liquefaction studies further complicates an already complex system and allows only limited comparison of results.

In a continuous reactor, particularly of the trickle bed type, intimate contact between the coal liquid and the catalyst will be maintained throughout the pass of the liquid feed. In an autoclave, particularly of the stirred design, the contact between the liquid and the catalyst will not be as intimate. The action of the stirrer will produce a centrifugal force which will tend to throw the liquid away from the catalyst surface. Consequently, it can be visualised that less strongly adsorbed molecules will spend a shorter time at the catalyst surface so that reaction rates and mechanisms could be very different from those observed in continuous reactor studies. In addition, steady state conditions can be readily investigated in a continuous reactor, whereas for a single contact in an autoclave, steady state conditions may not have been established and changes in catalyst activity will become more relevant.

Autoclaves provide reactors which can be used readily to acquire data from coal liquefaction studies but are less representative of likely commercial plant type reactors than small scale continuous bed-type reactors. Ideally comparisons between reactors are best made by carrying out experiments in various designs of reactors under similar reaction conditions, but, in order to cover the full range of designs adequately, a larger expenditure on equipment (beyond the budgets of most laboratories) would be necessary. However, steps can be taken to cover the

problem by finding whether single contacts in a stirred autoclave can be representative of steady state conditions after running for a particular time or how many contacts at a particular time are required to achieve a steady state condition, i.e. constant catalyst activity. Extrapolating results from autoclave studies to continuous reactors should then become more realistic.

EQUIPMENT FOR EXPERIMENTAL PROGRAMME

All the hydrocracking/hydrogenation experiments were carried out in 500 ml capacity spinning type autoclaves. Two autoclaves of this design were used and the autoclaves were compared in experiments using the model compound phenanthrene, chosen because phenanthrene and its hydro-derivatives represent a large proportion of the solvent which is recycled in coal liquefaction processes.

The design of the autoclaves is relatively unique as the extrudate catalyst is retained in a squat wire mesh basket. The basket is kept above the liquid phase by a bar which can be retracted manually when the basket falls down the magnetically driven stirrer shaft into the liquid phase. The cross-section of the stirrer shaft is such to allow its rotation without moving the basket in its upper position but, on the basket entering the liquid phase, the cross-section changes so that the basket rotates together with the shaft. The stirrer speed is variable and is controlled at a separate box, to which the autoclave control and measuring thermocouples are also attached. The two thermocouples seat alongside each other in a single well and one is used as an override protect; the override temperature is generally set 60-70°C above the control temperature.

The autoclave is heated by a quick-release external unit which has three individually wired elements. Control of the heaters is again effected from the separate control box and the heaters are capable of increasing the temperature from ambient to the working temperature (generally in the range 400-450°C) in about 45 mins. At working temperature, only two of the heaters are required to maintain the temperature within a range of about ±20°C. An exception to this control range occurs on initial release of the basket when an overshoot of 40-70°C can occur. To minimise this overshoot, the basket is released about 50°C below the reaction temperature. The overshoot is probably caused by initial exothermic cleavage of bonds linking aromatic centres and is different for the two autoclaves. This point is considered further later in the chapter.

To be representative of actual process situations, the hydrocracked product was primarily separated by vacuum distillation into acetone/dry ice cold trap fractions and >275, 275-300 and 300-475°C fractions. (Occasionally the top split was taken at 450°C.) Samples of the various fractions were injected through an 'on column' pneumatically sealed assembly onto a 25 m, 0.32 mm OV 101 chromatography column fitted to a Perkin-Elmer Sigma 3B Chromatograph. The temperature was programmed at a ramp rate of 5°C/min between the initial and final temperatures. Quantitative values of yields were calculated by making use of markers to separate the hydrocracked product into 13 groups as indicated in Table I. Selection of these groups was made from the compounds available and some group titles must be viewed as nominal only, whereas other group definitions are more precise. Apart from group 3 (naphthalene), group 9 (phenanthrene), group 10 (anthracene) and group 11 (pyrene), all groups contained many compounds. Probably the groups with the largest uncertainty were groups 11 (hydropyrenes) and 13 (material boiling above pyrene to the top cut temperature).

Two product ranges, defined as material bpt <260°C (groups 1-4) and material bpt <275°C (groups 1-5) have been used for yield comparisons; material in the bpt range 275-475°C was defined as the recycle solvent fraction. The percentage yields were calculated from the following expression:

$$y = \frac{m_c m_c + x_1 m_1 + x_2 m_2 + x_3 m_3}{M}$$

where y is the mass percentage of the particular product group x_c, x_1, x_2 and x_3 are the total percentage areas of peaks in the group occurring in the cold trap fraction and the other three bpt fractions, m_c, m_1, m_2 and m_3 are the masses of the individual bpt fractions and M is the mass of hydrocracked product used for the distillation.

Table I. Definition of Groups for Separating Gas Chromatograms

Group No.	Title	Approximate bpt range °C	Approximate retention time s
1	monocyclics	<185	<120
2	hydronaphthalenes	>185 - 217	>120 - 220
3	naphthalene	218	220
4	methylhydronaphthalenes/ methylnaphthalenes	>218 - 260	>220 - 380
5	dimethyl derivatives of above	>260 - 270	>380 - 510
6	acenaphthene, fluorene	>270 - 280	>510, 580, 680
7	perhydrophenanthrene	>280 -295	>580 - 680
8	hydrophenanthrene	>295 - 315	>680 - 910
9	phenanthrene	336	910
10	anthracene	340	950
11	hydropyrenes	>340 - 400	>950 - 1280
12	pyrene	400	1280
13	>pyrene - 475/450°C	>400 - 475/450	>1280

The distillation fractions were also analysed for their carbon and hydrogen contents using a Leco CHN Determinator which was also used for similar analysis of the used catalysts. The hydrocracked liquid and the used catalysts were analysed for their sulphur contents using a Leco Sulphur Determinator. Some specific surface area analysis by nitrogen adsorption was carried out on the used catalysts using a Micromeritics instrument.

REPEAT CONTACT EXPERIMENTS AT CONSTANT REACTION PARAMETERS

EXPERIMENTAL PROCEDURE

In this series of experiments, the catalysts were used over five repeat contacts with fresh coal liquid. Point of Ayr coal liquid was supplied by the British Coal Corporation, Coal Research Establishment (CRE); one batch of this coal liquid was used in experiments with CoMo and NiMo catalysts and a further batch was used in experiments with ZnMo and ZnW. The catalysts were prepared as extrudates by the technique of incipient wetness which requires stirring the dry alumina support with a set volume of a pre-determined concentration of an appropriate soluble salt of the metal such that the pore space is just taken up by the metals at the required concentration. The alumina support was supplied by Akzo Chemie, The Netherlands and the catalysts were made up to contain 15% WO₃ or MoO₃ and 3% NiO, CoO, or ZnO, expressed as a weight percentage of the weight of support.

For each of the experiments, 4.0 g of catalyst was placed into the basket which was then attached to the autoclave which had been loaded with ~ 100 g of the coal liquid. After sealing the autoclave, it was pressurised to 120 bar with hydrogen. The temperature was raised to the operating temperature of 400°C, at which it was maintained for a further two hours. The basket was released when the temperature reached 350°C and the stirrer speed was maintained at 650 rpm throughout the 2 h run time.

At the end of the experiment, the stirrer and heaters were switched off and the autoclave allowed to cool to room temperature. The autoclave was opened and the liquid contents were removed by suction. The basket was detached and the catalyst removed into a beaker which was placed in an ultrasonic bath. 10 cm³ of dichloroethane was added to the beaker which was agitated in the ultrasonic bath for 15 mins. The solvent was removed by suction filtration, the catalyst was washed with portions of acetone until the washings were colourless and the catalyst was air dried. The liquid product was transferred into a glass jar which was sealed under nitrogen and kept in a refrigerator until required. In order to have a sufficient amount of catalyst for a duplicate experiment on the five contacts and to allow a sample of catalyst to be

retained after each contact for analysis, the following programme of 19 experiments was adopted:- 1st contact - 5 experiments; 2nd contact - 5 experiments; 3rd contact - 4 experiments; 4th contact - 3 experiments; and 5th contact - 2 experiments.

Part of the hydrocracked liquid was vacuum distilled into the fractions defined previously. Initially, a distillation was carried out for each of the 19 experiments, but later a sample was taken from the product combined from each of the duplicate experiments making up the contact. The various fractions were stored in screw cap vials in a refrigerator. For the GC analysis, a sample of each of the fractions was used as an approximately 1% solution (v/v) in cyclohexane.

REPEAT CONTACT EXPERIMENTS AT CONSTANT REACTION PARAMETERS RESULTS AND TRENDS

An example of the data, broken down into the 13 product groups, calculated from the distillation and GC analysis of the hydrocracked liquids from CoMo-catalysed experiments is shown in Table II. It can be seen that the distribution of each of the contacts is similar, reflecting no dependence on repeat contact, even in the case of the first contact which used fresh catalyst. This situation was generally observed for the other catalysts used and a summary of the results for the four catalysts is shown in Table III. The results for ZnW could be interpreted as a gradual decrease in conversion to material bpt <260°C or <275°C. However, this interpretation would depend highly on the reliability of the result for the fifth contact, the two runs of which were carried out on the same autoclave rather than one on each autoclave. The discussion further in the text does indicate that, at shorter contact times, conversions can be dependent upon the autoclave used, and the low value for this fifth contact probably results from this dependence rather than a dependence on contact. Hence it was concluded that, for all the catalysts, conversions to the various bpt materials were independent of repeat contact.

Generally, conversions to material bpt <450°C were in the range of 70-75%. These values would indicate that much of the coal derived material was not converted under the conditions used and that a longer reaction time or a higher reaction temperature would be required to

Table II. Product Distribution for CoMo-Catalysed Experiments over Five Repeat Contacts at 400°C

Group No.	Amount present in hydrocracked product, mass %				
	1st	2nd	3rd	4th	5th
1	2.5	1.6	1.7	2.1	3.8
2	1.9	1.2	1.1	1.7	1.8
3	0.8	0.6	0.5	0.7	0.7
4	3.9	3.9	4.0	4.5	4.1
5	5.8	7.5	8.7	8.1	7.7
6	10.4	8.5	10.3	10.1	7.7
7	4.1	5.3	6.1	6.1	6.5
8	17.9	24.6	23.3	21.9	23.3
9	11.5	10.6	11.0	8.8	8.0
10	1.4	1.1	1.2	0.8	0.8
11	12.8	11.3	8.6	6.2	6.5
12	1.8	-	-	-	-
13	-	-	-	-	-
TOTAL	74.7	76.2	76.4	71.0	71.0
<260°C	9.1	7.3	7.3	9.0	10.4
<275°C	14.8	14.8	16.0	17.1	18.1
<275 - 450°C	59.9	61.4	60.3	53.9	53.1

maximise conversions. These scenarios lead to further repeat contact experiments dealt with later in the text.

The results of carbon and hydrogen analysis of the various bpt fractions for the five repeat contacts using CoMo or NiMo as the catalyst are shown in Table IV as H:C ratios. In all cases, the H:C ratios decrease with the increasing bpt of the fraction, reflecting a gradual increase in the aromatic nature and number of rings of the compounds in the fractions. It is noticeable that the respective values for NiMo and CoMo catalysts are similar and that repeat contact did not influence the results.

Table III. Summary of Product Distribution for Repeat Contact Experiments at 400°C

Catalyst	Contact	Product <260°C	Distribution <275°C	Mass % of total feed	
				275-450°C	>450°C
CoMo	1	9.1	14.8	59.9	25.3
	2	7.3	14.8	61.4	23.8
	3	7.3	16.0	60.4	23.4
	4	9.0	17.1	53.9	29.0
	5	10.4	18.1	52.9	29.0
	Av	8.2	16.2	57.7	26.1
NiMo	1	13.8	20.3	51.4	28.3
	2	7.2	13.2	57.9	28.9
	3	8.9	16.0	57.5	26.5
	4	6.5	13.7	58.4	27.9
	5	5.4	10.6	61.3	28.1
	Av	8.4	14.8	57.3	27.9
ZnMo	1	13.4	21.2	56.3	22.5
	2	14.1	20.3	54.9	24.8
	3	12.4	19.4	55.5	25.2
	4	16.9	23.0	50.3	26.7
	5	10.8	16.7	52.5	30.8
	Av	13.6	20.1	53.9	26.0
ZnW	1	11.7	17.5	56.3	26.2
	2	10.2	15.8	47.9	36.3
	3	9.0	15.0	52.2	32.8
	4	8.9	15.1	58.9	26.0
	5	5.7	9.5	51.8	38.7
	Av	9.0	14.6	53.4	32.0

Table IV. Hydrogen:Carbon Ratios for CoMo and NiMo Catalysed Experiments

Fraction °C	CoMo-catalysed contact no.					NiMo-catalysed contact no.				
	1	2	3	4	5	1	2	3	4	5
CT	1.67	1.68	1.57	1.77	-	-	-	-	1.84	-
<250	1.33	1.42	1.29	1.32	1.30	1.35	1.38	1.33	1.33	1.31
250-275	1.17	1.28	1.20	1.17	1.20	0.96	0.98	0.92	1.00	1.02

Table V summarises the data of the sulphur analysis of the hydrocracked liquids and the various bpt fractions for CoMo and NiMo catalysed experiments. The sulphur contents of neither the total hydrocracked liquids nor the individual bpt fractions showed any dependence on repeat contact or catalyst type. The values did show that the sulphur concentrated in the recycle solvent fraction (275-450°C), suggesting that, even under the relatively strong conditions used, certain sulphur-containing compounds will survive to be recycled in the solvent. However, the sulphur content of the coal liquid feed was reduced by about 50% and the sulphur content of the likely upgradable product was low.

Table V. Sulphur Content of Hydrocracked Liquids and Distillation Fractions for CoMo and NiMo Catalysed Experiments

	Fraction °C					Sulphur Content(%)				
	CoMo catalysed contact no.					NiMo catalysed contact no.				
	1	2	3	4	5	1	2	3	4	5
CT	-	0.01	-	-	-	0.01	-	-	-	-
<250	0.01	0.02	0.03	0.03	0.03	0.02	0.02	0.02	0.02	0.02
250-275	0.02	0.03	0.03	0.03	0.03	0.03	0.03	0.03	0.02	0.03
275-450	0.29	0.22	0.26	0.27	0.25	0.25	0.20	0.21	0.20	0.23
HL*	0.32	0.41	0.32	0.29	0.37	0.37	0.32	0.32	0.32	0.29

* indicates total hydrocracked liquid

The data for the carbon, hydrogen, sulphur and specific surface area for all four catalysts are summarised in Table VI. Only the sulphur contents of the Mo-containing catalysts showed any dependence on repeat contact. The sulphur content increased with contact number, reflecting gradual sulphidation of the metal content. For the ZnW catalyst, the sulphur content reached a relatively constant value after the first contact, the value corresponding to sulphidation of the Zn content only, suggesting that the level of H₂S produced by desulphurisation was inadequate to cause sulphidation of the metal content.

The carbon content of the used catalysts and the H:C ratios of the deposited material were independent of contact number, indicating a rapid rate of carbon deposition early in the first contact and thereafter no further deposition. Although the specific surface area measurements show significant scatter, there is no obvious trend with contact, reinforcing the point made above. The used catalysts had a significantly lower specific surface area than the fresh catalysts (250-255 m²/g) and the results suggested that CoMo and NiMo catalysts were reduced to a greater extent. However, the Zn-containing catalysts were reduced to a greater extent. However, the Zn-containing catalysts had been washed further with successive portions of quinoline and toluene before analysis. In addition, samples of used CoMo and NiMo catalyst were subjected to this additional washing as well as being preheated for 1h at 400°C in a stream of nitrogen. Analysis of these further treated samples gave specific surface area analysis values in the range 150-175 m²/g suggesting that careful pretreatment of used catalyst samples is needed before they are subjected to specific surface area analysis. It should be noted that the carbon contents of these catalysts only showed a small decrease and their H:C ratios were unaffected. The lower H:C ratios for the Zn-containing catalysts probably result from the use of a different batch of coal liquid for these experiments.

Table VI. Analysis of Used Catalysts

Contact No.	Catalyst % C deposited				Contact No.	Catalyst % S deposited			
	CoMo	NiMo	ZnMo	ZnW		CoMo	NiMo	ZnMo	ZnW
1	17.4	16.5	20.9	18.4	1	2.56	2.75	2.95	0.75
2	20.7	16.4	21.2	18.8	2	3.47	3.75	3.66	0.77
3	19.3	20.9	20.2	22.2	3	4.00	3.99	4.42	0.80
4	24.0	15.7	20.0	19.1	4	4.27	4.46	4.13	0.80
5	19.8	21.9	20.0	19.4	5	4.57	4.52	3.96	0.77

Contact No.	Catalyst H:C ratio				Contact No.	Catalyst specific surface area m ² /s			
	CoMo	NiMo	ZnMo	ZnW		CoMo	NiMo	ZnMo	ZnW
1	1.6	1.3	1.0	1.2	1	92	67	134	117
2	1.4	1.5	1.1	1.1	2	73	83	118	130
3	1.4	1.2	1.0	1.2	3	44	50	150	98
4	1.3	1.6	1.0	1.2	4	44	87	158	178
5	1.4	1.2	1.2	1.2	5	46	40	109	122

REPEAT CONTACT EXPERIMENTS UNDER VARIOUS REACTION PARAMETERS.

These experiments used only three contacts, requiring three runs for the first and second contacts and two runs for the third contact. The experiments all used CoMo as the catalyst and are denoted by the following: 4006.0, 6 h with oxide catalyst; 4302.0, 430°C, 2 h with oxide catalyst, and 4302.5, 430°C, 2 h with presulphided catalyst. The experimental and analytical procedures were essentially the same as adopted previously except for the 430°C experiments in which the basket was released at 375°C rather than 350°C.

A summary of the product distribution is shown in Table VII. As was found previously, there was no obvious dependence of any of the product groups on repeat contacts. Conversions to the low bpt material (<260 or <275°C), and total conversions were higher than for 2 h at 400°C. The amounts of <260 and <275°C material for 2 h at 430°C were similar to those for 6 h at 430°C both for oxide and presulphided catalysts. However, the amount of the recycle solvent fraction was lower for 2 h at 430°C for the oxide catalyst, as was the overall conversion to <475°C material.

The data for the carbon and hydrogen analyses of the various distillation fractions for runs 4006.0 and 4302.5 are summarised in Table VIII. Again there is a gradual decrease in the hydrogen:carbon ratio with increasing bpt of the fraction and there is no dependence on repeat contact. Generally, the longer run time seems to have promoted more hydrogenation, with the hydrogen contents being slightly higher for the 6 h experiments. However, the increase in reaction temperature from 400 to 430°C combined with presulphiding the catalysts also induced greater hydrogenation when the results in Tables VIII and VI are compared.

Sulphur analysis of the liquids and analyses of the used catalysts revealed the same type of trends as are expounded for the experiments at 400°C. Therefore, for all of the repeat contact experiments, irrespective of catalyst or experimental condition, constant catalyst activity was achieved after a single contact so that results from single contacts in autoclaves of the design used in this investigation would be representative of steady state liquefaction conditions, enabling the autoclaves to be used for the rapid accumulation of liquefaction data.

Table VII. Summary of Product Distribution for Repeat Contact Experiments under Various Reaction Parameters

Run No.	Contact No.	Product Distribution Mass %			
		Fraction °C			
		<260	<275	275-475	>475
4006 0	1	13.9	19.7	57.7	22.6
	2	12.2	19.9	58.7	21.4
	3	10.7	18.7	59.4	21.9
	Av	12.2	19.4	58.3	22.0
4302 0	1	14.5	23.6	50.6	25.8
	2	14.4	24.6	50.9	24.5
	3	12.4	20.8	53.8	25.4
	Av	13.8	23.0	51.8	25.2
4302 5	1	13.8	19.3	57.7	23.0
	2	12.4	17.8	59.7	22.5
	3	15.6	22.4	55.7	21.9
	Av	13.9	19.8	57.7	22.5

Table VIII. Carbon and Hydrogen Analysis of Distillation Fractions from Experiments 4006.0 and 4302.5

Fraction °C	Contact No.	Composition (mass %) and H:C Ratios					
		4006.0			4302.5		
		C	H	H:C	C	H	H:C
CT	1	85.9	12.8	1.79	86.5	12.9	1.79
<275		88.6	10.0	1.36	90.3	9.8	1.30
275-300		89.7	9.2	1.23	91.8	8.5	1.11
300-475		91.7	8.0	1.05	93.0	7.2	0.93
>475		91.8	5.8	0.76	93.3	5.4	0.69
CT	2	85.5	13.6	1.91	85.5	13.4	1.88
<275		90.2	10.2	1.36	90.1	9.8	1.31
275-300		90.8	9.2	1.22	91.2	8.7	1.14
300-475		92.2	8.1	1.05	92.2	7.7	1.00
>475		92.0	6.0	0.78	93.4	5.4	0.73
CT	3	86.1	13.8	1.92	85.6	13.3	1.86
<275		88.8	10.2	1.38	89.9	9.9	1.32
275-300		90.1	9.7	1.29	91.3	8.3	1.09
300-475		91.7	8.0	1.05	92.4	7.5	0.97
>475		91.3	6.4	0.84	93.5	5.5	0.71

COMPARISON OF AUTOCLAVE PERFORMANCES FOR HYDROGENATION OF PHENANTHRENE.

During the repeat contact studies, it was noted that, although the autoclaves were of the same design, significantly different results (in terms of conversions to material bpt <260 or 275°C) could be obtained depending on which autoclave was used. The differences were particularly noticeable over short contact times at 400°C. In order to assess the factors contributing to these differences, the two autoclaves were compared for the hydrogenation of phenanthrene at different stirrer speeds at different temperatures over different reaction times. All experiments used 100 g of phenanthrene and 4 g of catalyst (CoMo) and were operated at an initial cold pressure of hydrogen of 120 bar. The liquid product was analysed by gas chromatography by which the amounts of phenanthrene and the di, tetra, octa (sym and asym) and perhydro-derivatives were identified. Some of the remaining peaks were identified, eg butyltetralin, biphenyl and ethyltetralin; these are products of the hydrocracking of phenanthrene and it was assumed that the remaining unidentified peaks also resulted from hydrocracking.

The relative performances of the two autoclaves were compared by the use of ratios. Three ratios were derived utilising (a) the unconverted phenanthrene, denoted by P; (b) the amounts of the various hydro-derivatives of phenanthrene multiplied by the relative number of hydrogens added, eg % tetrahydrophenanthrene 4, denoted by HP; (c) the total content of hydrocracked compounds, denoted by C. These ratios would indicate the 'reactivity' of the autoclaves and their relative abilities towards hydrogenation and hydrocracking.

EFFECT OF STIRRER SPEED

Table IX summarises the data for experiments operated at 420°C for 2 h at the three stirrer speeds 200, 400 and 600 rpm. It can be seen that the values are closest to unity at 600 rpm, a value of one, indicating equal performance. The autoclave providing the higher conversion of phenanthrene also showed the higher ability for hydrogenation. The values relating to cracking were inconclusive, but did show the near unity value at 600 rpm. The extent of conversion tended to increase with increasing stirrer speed, as did the amount of hydrogenation with the contents of all the hydrophenanthrenes increasing, but the amount of hydrocracking tended to decrease.

Table IX. Autoclave Performance Comparator Ratios - Influence of Stirrer Speed

Speed rpm	Performance Comparator		
	P	HP	C
200	1.25	0.78	1.23
400	1.18	0.92	0.77
600	1.05	0.98	0.99

EFFECT OF REACTION TEMPERATURE

Table X summarises the data for experiments operated at 400 rpm for 2 h at 380, 420 and 440°C. The results confirm the comments above regarding the relative performances of the autoclaves with again the ratios for assessing hydrocracking ability being inconclusive but indicating that the autoclave showing the higher hydrogenation ability had a lower hydrocracking ability. The extent of cracking increased with temperature, particularly between 420 and 440°C when the amount of cracking tended to increase by a factor of 2. Between 420 and 440°C the proportions of di, tetra, per and sym-octahydrophenanthrene decreased significantly, but the content of asym-octahydrophenanthrene decreased only slightly.

Table X. Autoclave Performance Comparator Ratios - Influence of Reaction Temperature

Temperature °C	Performance Comparator		
	P	HP	C
380	1.09	0.96	1.28
400	1.06	0.96	1.31
420	1.18	0.96	0.77
440	1.04	0.82	1.32

EFFECT OF REACTION TIME

Table XI summarises the results for experiments conducted at 400 rpm at 400°C for 2, 6 and 18 h. Similar observations about the comparative performances of the autoclaves were found with a positive indication of increasing hydrogenation capability with decreasing hydrocracking ability. For both autoclaves, the concentrations of di, tetra and sym-octahydrophenanthrene decreased with increasing time, but the concentration of asym-octahydrophenanthrene was roughly constant and only fell between 6 and 18 h. The amount of cracking increased with increasing time, reaching a value of over 50% with the autoclave giving the higher amount of cracking; for the other autoclave, the value was almost 40% after 18 h.

Table XI. Autoclave Performance Comparator Ratios - Influence of Reaction Time

Time, h	Performance Comparator		
	P	HP	C
2	1.06	0.96	1.31
6	1.17	0.76	1.50
18	1.12	0.66	1.29

DISCUSSION

The largest differences in the conversion to material bpt <260 or <275°C between the two autoclaves occurred in the initial experiments at 400°C over 2 h. From the results where the two autoclaves were compared for hydrogenation/hydrocracking of phenanthrene, it might be expected that a longer running time or a higher reaction temperature would induce larger differences. Consequently, the differences must not be arising from the production of the lower bpt material from the hydrocracking of polynuclear aromatic compounds. Evidence to support this suggestion arises from the NMR analysis of the distillation fractions which shows that the levels of phenanthrene and hydrophenanthrene in the hydrocracked products were similar to those found in the coal liquid feed.

Proton and ¹³C NMR analysis of asphaltene fractions of extracts produced by dissolution of coal in hydrogenated anthracene oil at 400°C have indicated average molecular structures containing aromatic clusters linked by ether, methylene or phenyl-phenyl bridges (1). These types of bonds are readily cleaved in the presence of catalysts of the type used in the hydroliquefaction experiments (2) and it seems likely that in the early stages, these cleavage reactions are predominating over hydrogenation to produce the lower bpt material. As time progresses, hydrogenation/hydrocracking reactions will become significant. Unfortunately, the relative abilities of the two autoclaves towards these bridge cleavages were not measured.

However, there is a temperature overshoot when the baskets are released and the autoclave with the larger overshoot produces the higher conversions to lower bpt material.

Since the conversions from the first contact are similar to those from other contacts, deposition must occur rapidly during the first contact and thereafter remain relatively constant. Thus, for the type of autoclave used in this study, deactivation appears to occur in a matter of minutes rather than hours and definitely faster than has been reported for pilot plant operation using trickle bed reactors; for instance Kang and Johanson (3) reported a time of 50 h for a H-coal process pilot plant. It would also seem that deactivation resulted from the cleavage reactions, probably because the rate of cleavage was faster than the rate of hydrogen donation, resulting in polymerisation reactions occurring. This fact may suggest that hydroliquefaction should operate initially at a lower temperature and for trickle bed or ebullating bed reactors, a temperature gradient increasing from the input to the output should be incorporated in the design.

The choice of catalyst for liquefaction processes is important and the results presented here allow some comparison of catalyst performances. From the first series of experiments, CoMo and NiMo can be compared, as can ZnMo and ZnW, but the two pairs cannot be compared directly because different batches of coal liquid were used. Generally CoMo induced a greater conversion to material bpt <450°C and to material bpt <275°C. The conversions to material bpt <260°C were about the same and the H:C ratios of the various distillation fractions were also similar. There were similar levels of decomposition of carbon and sulphur on the catalysts and the sulphur contents of the hydrocracked liquids were also similar. Thus, overall CoMo was slightly better than NiMo for the type of autoclave used in this study. Experiments catalysed by ZnMo resulted in higher conversions than those catalysed by ZnW. Since there was little difference between the catalysts regarding the other parameters measured, Mo-containing catalysts are better than W-containing catalysts for promoting hydroliquefaction.

CONCLUSIONS

The results have shown that spinning/falling basket autoclaves can be used effectively for gathering data on coal hydroliquefaction, a single contact being representative of steady state conditions. As with other types of reactors for coal liquefaction, the catalysts were deactivated to a constant activity but the rate of deactivation was much more rapid in the autoclaves. Caution must be applied when comparing results from reactors of different design as even similar design autoclaves can produce different results. However, although there were differences in results, the two autoclaves showed the same trends, which may suggest that trends found on one type of reactor would be similar to those on another, but specific results may be very different.

ACKNOWLEDGEMENTS

The authors acknowledge the financial support provided by the Science and Engineering Research Council and British Coal (Grant Reference No. GR/D 41163) and the supply of chemicals by Akzo Chemie, The Netherlands (catalyst support) and British Coal, Coal Research Establishment (coal liquid).

REFERENCES

1. Cahill, P. and Harrison, G. Second International Rolduc Symposium on Coal Science, 2125, May 1989, paper 39.
2. Ouchi, K. and Makabe, M. Proceedings of 1989 International Conference on Coal Science, Tokyo, Japan, 23-27 October 1989, p 833.
3. Kang, C.C. and Johanson, E.S. 'Liquid Fuels from Coal', Academic Press, p 89 (1979).

RECEIVED November 5, 1990

Chapter 18

Hydrogen Transfer Reactions in Model Systems Representative of Recycle Solvents

Kevin Bate and Graham Harrison

Department of Applied Sciences, Staffordshire Polytechnic,
Stoke-on-Trent ST4 2DE, United Kingdom

Phenanthrene was hydrogenated under various conditions of temperature, pressure and time with a selection of bimetallic and monometallic catalysts. From the G.C. analysis of the product, the contents of the various hydro-derivatives were established and related to reaction conditions. Certain compounds resulting from cracking were also identified. Other aromatic compounds, which together with phenanthrene generate much of the H-donor content of process recycle solvents, were also hydrogenated under constant conditions. A chemical test method using sulphur as a hydrogen acceptor was used for assessing the donatable hydrogen contents of samples of the hydrogenated aromatic compounds and compared with approaches using G.C. and NMR.

Thermal cleaving of bonds during coal dissolution generates free radicals which require stabilising if massive coking is to be prevented. In coal liquefaction processes, stabilisation is usually provided by using a solvent which is capable of donating hydrogen. The British Coal liquefaction process, developed by its Coal Research Establishment, separates coal dissolution from catalytic hydrocracking of the coal liquid to form a two-stage process. Thus, in the first stage, the recycled process solvent becomes depleted of its H-donor compounds and this depletion is made up during the second stage by hydrogenation. Consequently, in the second stage, there is a 'conflict of interests' in that the solvent needs only to be hydrogenated but the dissolved coal fragments need to be hydrocracked. Too severe reaction conditions will result in a loss of the solvent fraction because hydrocracking reactions will predominate and too mild conditions will result in low conversions to lower boiling point material suitable for upgrading to transport fuels.

The start-up solvent for the CRE process is hydrogenated anthracene oil which contains a high proportion of phenanthrene and its hydro-derivatives. On continuous recycling, the composition of the solvent changes but high levels of the previously mentioned compounds remain. The lower temperature of the distillation fraction taken for recycling as solvent may also change from time to time and will be dictated by the need to maintain a solvent balance for the process. Thus, the solvent fraction could contain significant levels of substituted naphthalenes and their hydro-derivatives and pyrene plus its various hydro-derivatives, the relative proportions of which will depend upon the lower and upper temperatures taken for the recycled fraction. The recycle solvent will also contain appreciable levels of compounds based on fluorene and fluoranthene. Although the list of compounds previously mentioned does not

contain the only compounds found in a recycle solvent, it constitutes a major part of it so that studies using these compounds should form a reasonable description of actual process solvents.

A successful two-stage liquefaction process will need to maintain a relatively consistent H-donor capability in its recycle solvent and should react positively to rectify variations in the consistency outside acceptable limits. In order to react to these variations, the process will need the ability to adjust reaction parameters (e.g. pressure, temperature, throughput, catalyst activity), probably according to its H-donor ability. Hence there is a need to monitor the H-donor content of the solvent.

Several methods have been proposed for measuring the hydrogen donor content of process solvents, with probably the most popular approach adopting quantitative NMR spectroscopy (1-8). Amongst the other approaches, the use of hydrogen acceptors in chemical tests has been suggested. For instance, Bockrath et al (9) used dibenzylmercury as a source of benzyl radicals to which hydroaromatic compounds would donate hydrogen. Aiura et al (10) used sulphur as the hydrogen acceptor and found good agreement with results calculated from NMR spectroscopy. A chemical method is more realistic of the hydrogen donation. The NMR approaches can often involve tedious calculations and generally require ^{13}C NMR data which can take a long time to accumulate.

EXPERIMENTAL

Hydrogenation of model aromatic compounds. All the hydrogenation experiments were carried out in 500 cm³ capacity spinning/falling basket autoclaves manufactured by Baskerville Scientific Ltd. Detail of the autoclaves is provided elsewhere in this book (Harrison, Doughty and Ali). Apart from further experiments with phenanthrene, all the experiments used a γ -Al₂O₃ supported 15% Mo/3% Co commercial catalyst supplied by Akzo Chemie, The Netherlands. Typically 75 g of the model compound was hydrogenated with 5.0 g of catalyst at a feed pressure of 10 MPa hydrogen for 2 h at 400°C. The heat up time was 45mins and the autoclave was allowed to cool overnight. The further experiments with phenanthrene considered variations in pressure, time, temperature and catalyst type; the catalysts used were laboratory prepared by the technique of incipient wetness which impregnates the alumina extrudate support (supplied by Akzo Chemie, The Netherlands) with appropriate soluble salts of the metals in the calculated concentration and volume to give 15 wt % of Mo or W and 3% of Ni, Co or Zn, based on the mass of support used. The amounts of phenanthrene and catalyst used were the same as those stated earlier.

The products from the hydrogenation experiments were subjected to gas chromatography and NMR spectroscopy. Gas chromatography used ~ 1% solutions in cyclohexane which were injected through an 'on column' injector onto an 0V 101 25 mm x 0.32 mm capillary column fitted to a Perkin-Elmer Sigma 3B Dual FID Chromatograph coupled to a JJ CR 600 Pen Recorder and a LDC 300 Peak Area Integrator. The chromatograph was programmed with a start temperature of 80°C and a ramp rate of 5°C/min. ^1H and ^{13}C NMR spectra were recorded on a Jeol Model PFT-90Q spectrometer fitted with a 10 mm probe. All solutions were made up in chloroform-d and TMS was added as an internal standard for ^1H NMR; the chloroform-d peak at 76.99 was used as the standard for ^{13}C spectra. To facilitate quantification of ^{13}C NMR, the paramagnetic relaxation agent, chromium acetylacetonate, was added and 10,000 acquisitions were gathered at a 3 s delay between the 90° pulses; a gated decoupling was used during acquisitions. Some mass spectrometry to assist peak identification of the gas chromatograms was kindly carried out by CRE.

Reaction of Hydrogenated Products with Sulphur. These experiments were conducted in a 10 cm³ capacity tube-type microautoclave (manufactured by Baskerville Scientific Ltd) fitted with a 0-10 bar Schaevitz pressure transducer linked to a digital read-out. The microautoclave sat in its own electrical heater and its temperature was controlled by a thermocouple linked to a read-out. The pressure of H₂S was monitored and once it became

constant, the microautoclave was rapidly cooled to room temperature. A note of the cold pressure was made before the H₂S pressure was released and the contents removed. In order to relate the H₂S pressure to the hydrogen donor content, calibration experiments were carried out using 9,10-dihydrophenanthrene as the H-donor.

RESULTS AND DISCUSSION

Hydrogenation of Phenanthrene (Variation in time, temperature and pressure)

These experiments used a 15% Mo/3% Ni catalyst and the experimental conditions and final pressures at the reaction temperature are summarised in Table I. In run 2, the pressure was frequently re-intensified to 180 bar so that this pressure was maintained for most of the duration of the experiment.

Table I. Experimental conditions for hydrogenation of phenanthrene

Run Number	Temperature °C	Initial Pressure MPa	Time h	Final Pressure MPa
1	400	20	24	9
2	350	18	24	18
3	300	20	24	13
4	300	20	24	11
5	300	20	18	15
6	300	20	21	13
7	275	20	24	13
8	300	20	24	13

From the GC analysis supplemented by some GC/MS, the following compounds were identified: phenanthrene (P), 9,10-dihydrophenanthrene (H₂P), tetrahydrophenanthrene (H₄P), symmetrical octahydrophenanthrene (s-H₈P), antisymmetrical octahydrophenanthrene (a-H₈P), perhydrophenanthrene (H₁₄P) and the cracking products (C) - butyltetralin (BT), diphenyl (BP), ethyltetralin (ET) and tetralin (T). Figure 1 shows the chromatogram trace from run 3 (300°C, 20 Pa, 24 h). The peak for H₂P at 867 s was close to a s-H₈P peak at 860 s and on occasions these peaks were not resolved. Three peaks were identified for this experiment as H₁₄P but, as can be seen from Figure 2, actually six peaks can be assigned as H₁₄P in agreement with Allinger et al ⁽¹¹⁾ who proposed six geometric isomers of H₁₄P; Figure 2 shows the GC/MS information for run 2 which yielded a relatively high content of H₁₄P. The total amount of the above list of compounds generally accounted for >95% of the peaks.

The results of the GC analysis are shown in Table II. The extent of cracking at 300°C or less was relatively low, accounting for <10% of the product if the unidentified peaks were assumed to be from cracking. On increasing the temperature to 350°C, cracking became only slightly more intensive but at 400°C almost 40% of the product was not phenanthrene and its hydroderivatives. Normally, the hydrocracking stage of the CRE process is operated at temperatures >400°C so that it might be expected that loss of recycle solvent would occur because of cracking.

Although the amount of cracking was generally low, some comments can be asserted about the reactions taking place. The detection of diphenyl may indicate some cracking of H₂P initially to form ethyldiphenyl or dimethyldiphenyl followed by alkyl elimination reactions. The absence of butylnaphthalene would suggest that H₄P was not cracked but the butylnaphthalene peak may not have been separated from other peaks as was noted by Haynes ⁽¹²⁾. Butyl and ethyl tetralins would arise from the hydrocracking of H₈P, but whether one or both isomers was involved was impossible to assess. These two compounds could also be derived from H₄P.

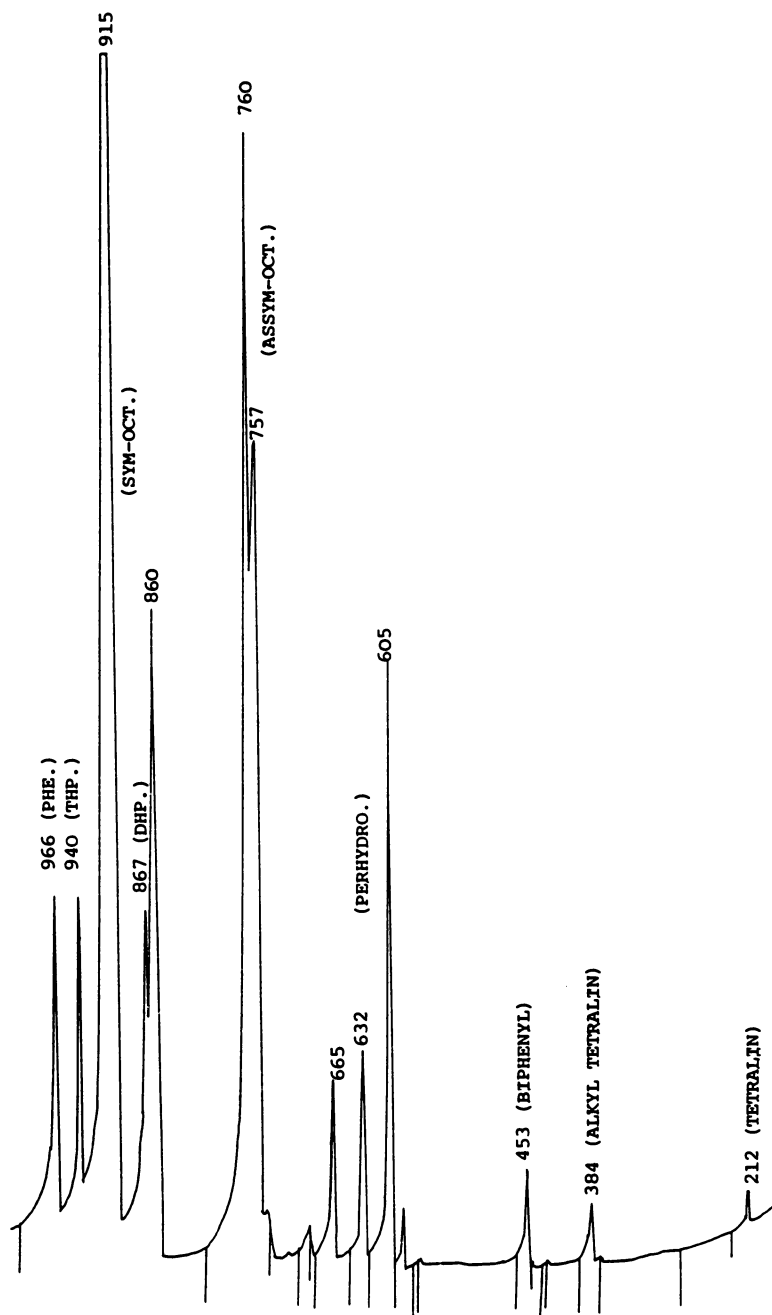


Figure 1. Gas chromatogram of product from phenanthrene hydrogenation run 3 (300°C for 24h).

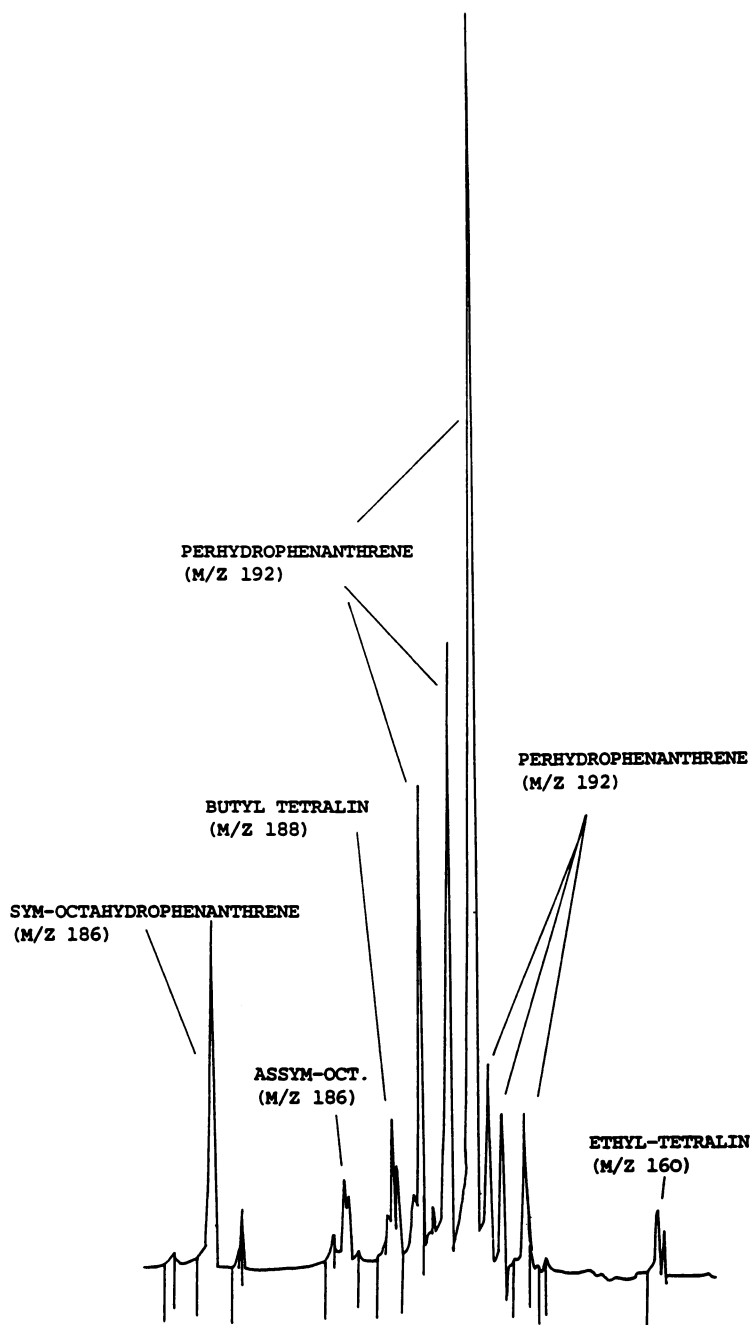


Figure 2. GC/MS of product from phenanthrene hydrogenation run 2 (350°C for 18h).

Table II. GC analysis of products from hydrogenation of phenanthrene under various reaction conditions

Run No.	Composition of hydrogenated product (wt % of recovered liquid)									
	P	H ₂ P	H ₄ P	s-HgP	a-HgP	H ₁₄ P	BP	BT	ET	T
1	12.7	1.9	8.7	12.8	14.2	12.9	3.6	0.9	3.0	7.1
2	0.2	0.4	0.4	6.9	2.7	78.9	4.2	-	2.0	0.8
3	3.7	6.0	2.0	49.0	27.6	9.6	0.3	0.9	0.5	0.2
4	0.7	3.1	3.1	40.1	15.7	26.8	2.5	1.7	1.0	0.3
5	13.3	2.2	4.0	45.8	25.0	2.9	0.8	1.9	0.4	0.6
6	4.8	4.2	2.7	51.5	27.1	7.8	0.2	1.0	-	-
7	7.6	3.2	3.5	50.3	24.9	10.2	0.2	1.7	0.8	-
8	4.6	3.6	3.6	50.1	27.7	9.2	0.3	1.0	-	-

Hydrogenation of phenanthrene (Variation of catalyst type)

Hydrogenation experiments were conducted at 400°C and 20 MPa for 2 h with a number of mono and bimetallic catalysts, all on an acidic alumina support. Rate constants were calculated by assuming first order reaction kinetics for the disappearance of phenanthrene. The values for the rate constants and the results of the GC analysis (phenanthrene and its hydroderivatives) are summarised in Table III.

Table III. Gc analysis of products and first order rate constants for hydrogenation of phenanthrene

Catalyst	Composition of hydrogenated product (wt %)						Rate constant (h ⁻¹)
	P	H ₂ P	H ₄ P	a-HgP	s-HgP	H ₁₄ P	
Al ¹	86.0	6.7	4.0	-	2.3	-	0.07
Ni (3%)	72.3	10.1	7.3	0.8	0.9	-	0.16
Co (3%)	80.6	9.5	4.8	0.2	0.6	-	0.11
NiMo (3%/15%)	21.5	1.1	18.9	12.9	32.8	8.5	0.77
CoMo (3%/15%)	19.9	6.7	19.0	14.1	25.8	9.2	0.81
ZnMo (3%/15%)	21.3	9.2	18.9	13.8	23.5	8.6	0.77
NiMo ² (3%/15%)	17.2	3.2	18.9	13.9	28.2	10.4	0.88
NiW (3%/15%)	48.1	4.0	16.2	4.9	21.5	1.6	0.37
NiMo (3%/10%)	21.5	1.4	17.5	13.4	28.4	9.2	0.77
NiMo (3%/5%)	30.7	-	16.4	11.0	34.2	6.3	0.59
NiMo (1%/15%)	17.7	2.3	18.5	13.5	31.6	11.4	0.87
NiMo ³ (3%/15%)	13.4	3.5	20.5	13.2	29.3	13.4	1.00
CoMo ³ (3%/15%)	12.5	-	17.7	14.0	31.0	18.1	1.04

1 - alumina support only; 2 - commercial catalyst; 3 - presulphided catalysts

It can be seen that the alumina support itself caused only a small amount of hydrogenation because of the absence of transition metal sites. The rate constant was increased by about a factor of 2 when 3% of Co or Ni was impregnated on the catalyst, but the rate was

considerably slower than for the bimetallic catalysts, particularly Mo-containing bimetallic catalysts. The three Mo-containing catalysts 3%/15% NiMo, CoMo and ZnMo had similar rate constants which were more than two times greater than the value for 3%/15% NiW; consequently, bimetallic Mo catalysts are much more active towards hydrogenation than bimetallic W catalysts.

Reducing the Mo content of the NiMo catalyst from 15 to 10% did not reduce the rate constant, but the rate constant did decrease when the Mo content was reduced further to 5%. The rate constant was not reduced when the Ni content was reduced to 1%. Presulphiding both the 3%/15% NiMo and CoMo caused a significant increase in the rate constant. However, the major change in the composition of the product was an increase in the H₁₄P content and a reduction in the P content. The level of H₁₄P needs to be kept low to maintain a good concentration of hydrogen donors and it is preferable to restrict hydrogenation even if this does result in a higher content of phenanthrene which, at least, could act as a hydrogen shuttler.

The results in Table III did show variation in the H₂P and s-HgP contents. For instance, 3%/15% ZnMo gave 9.2% H₂P and 23.5% s-HgP, whereas 3%/15% NiMo gave 1.1% H₂P and 32.8% s-HgP. The reason for these differences was that the GC peaks for these two compounds were often difficult to separate and it can be seen that the total percentage of the two compounds was roughly equal for both catalysts.

Hydrogenation of other polycyclic aromatic compounds found in recycle solvents. These experiments were carried out at 400°C at 17 MPa for 2 h using a commercial 3%/15% CoMo catalyst. The first order rate constants are shown in Table IV; it can be noticed that no values are reported for acenaphthylene and dibenzothiophene as hardly any of the starting compounds remained after the reaction and polymerisation was evident for both compounds.

Table IV. First order rate constants for hydrogenation of some polycyclic aromatic compounds with CoMo

Compound	Amount remaining (wt %)	Rate constant (h ⁻¹)
acenaphthylene	0	-
dibenzothiophene	<0.5	-
fluoranthene	19	0.83
1-methylnaphthalene	18	0.86
2-methylnaphthalene	23	0.73
phenanthrene	20	0.80
pyrene	41	0.45
fluorene	44	0.41
dibenzofuran	63	0.23
carbazole	80	0.11

Hydrogenation of pyrene Hydrogenation experiments were carried out with an oxide and a presulphided catalyst and the analysis of the products is shown in Table V, from which it can be seen that the distribution of the products for both catalysts was similar. The principal hydrogenation products were dihydropyrene and hexahydropyrene and lesser amounts of the tetra and decahydro-derivatives were also detected. Two isomeric forms were found for both the hexahydro and decahydro-derivatives. For the hexahydro-derivatives, 1,2,3,6,7,8 hexahydropyrene was the more abundant (ratio 4:3).

Table V. Gc analysis of products from hydrogenation of pyrene with oxide and presulphided CoMo catalysts

Compound	Composition of product (wt %)	
	Oxide	Presulphided
pyrene	41.3	42.1
dihydropyrene	23.1	23.6
tetrahydropyrene	3.8	4.0
hexahydropyrene	27.5	27.6
decahydropyrene	5.1	5.2
others	4.3	2.5

Cracking reactions produced only 3.5% of the product and most of the cracked product was substituted hydrophenanthrenes. One product positively identified was s-HgP resulting from the initial hydrocracking of one or both of the forms of decahydrophenanthrene which have low resonance stabilisation energies. This type of cracking reaction would not be unfavourable and could produce a better hydrogen donor compound.

Hydrogenation of fluorene Hydrogenation of fluorene provided, 34 wt % hexahydrofluorene, 6 wt % perhydrofluorene and 16 wt % cracked material as well as 44 wt % unreacted fluorene. The cracked material consisted largely of diphenyl with smaller proportions ortho methyl-substituted diphenyl. These products arise from cracking of the central five-membered ring. Compounds produced from hydrogenation of these compounds were also identified as well as small amounts of cycloalkanes.

Hydrogenation of acenaphthylene During the experiment, a great deal of polymerisation occurred and only the acetone-soluble part of the product was analysed. This part contained 18 wt % acenaphthene, 62 wt % dimethylnaphthalenes and 20 wt % other material. An experiment carried out at 300°C also showed considerable polymerisation with a similar distribution of material in the acetone-soluble fraction; in both experiments, no starting material was identified in the product. The major product was 1,9-dimethylnaphthalene and the other material showed GC peaks with retention times from tetralin to methyltetralin.

The instability of the five-membered ring will make acenaphthene a poor hydrogen donor in spite of the fact that the loss of two hydrogen atoms would produce a fully conjugated compound. Seshadri et al.⁽³⁾ recognised this fact and eliminated the contribution from acenaphthene when quantifying the hydrogen donor content of the recycle solvent; however, it would seem that the content of acenaphthene would be low unless significant amounts were produced during coal dissolution.

Hydrogenation of fluoranthene Fluoranthene was relatively reactive towards hydrogenation with over 80 wt % reacting. Only 30% of this 80% was positively identified as being hydrofluoranthene-derivatives, of which the major form was tetrahydrofluoranthene, known to be a good H-donor. Notwithstanding this comment, the region where many of the unidentified peaks occurred would suggest that they could have been hydrofluoranthenes and therefore fluoranthene and its hydro-derivatives could have a significant role in coal liquefaction.

Hydrogenation of 2-methylnaphthalene The main product resulted from hydrogenation of the unsubstituted ring to give 2-methyl - 5,6,7,8-tetrahydronaphthalene whose content at 30.6 wt % was over twice that of 2-methyl - 1,2,3,4-tetrahydronaphthalene (14.8 wt %) resulting from hydrogenation of the methyl-substituted ring. The next major product at 10.7

wt % was tetralin; since the naphthalene content was relatively low (1.2 wt %), it seems that methyl abstraction from an unsaturated ring would be less likely than abstraction from a saturated ring, suggesting that tetralin resulted from elimination of CH₃ from 2-methyl-1,2,3,4-tetrahydronaphthalene. The high proportions of methyltetralins in the product would contradict the mechanism by Patzer et al.⁽¹⁴⁾ who reported abstraction of CH₃ from methyl-naphthalene prior to hydrogenation.

Small amounts of 1-methylnaphthalene (0.6 wt %) and 1-methyltetralin (0.2 wt %) were detected, indicating some migration of the CH₃ group from the two to the one position. Some isomerisation of 2-methyltetralin through the methyltetralyl radical was indicated by the formation of the dimethylindan derivative (3.8 wt %).

Hydrogenation of 1-methylnaphthalene Hydrogenation of the unsubstituted ring was again favoured giving 49 wt % of the 5,6,7,8-hydroderivative compared with 22 wt % of the 1,2,3,4,-hydroderivative. The amount of tetralin (2 wt %) was considerably less than for 2-methylnaphthalene, but the amount of naphthalene (4 wt %) was somewhat higher. The amount of dimethylindan isomerisation product (1.5 wt %) was less than for 2-methylnaphthalene and there was no evidence for migration of the CH₃ group.

Hydrogenation of heterocycles Hydrogenation experiments were carried out with the fluorene related heterocycles, dibenzothiophene, dibenzofuran and carbazole showing the following order of reactivity: dibenzothiophene > fluorene > dibenzofuran > carbazole. The product from the hydrogenation of dibenzothiophene, as with acenaphthylene, was a black viscous liquid, indicative of polymerisation. The acetone-soluble fraction of this liquid contained mainly diphenyl and phenylcyclohexane. Sulphur analysis of the whole product showed a sulphur content of only 0.1% compared with the 8.7% of the starting material.

For dibenzofuran, no diphenyl was detected in the product, but phenylcyclohexane and bicyclohexane were detected. Therefore, hydrogenation of at least one of the rings was necessary before ring opening took place. A similar conclusion was found for the analysis of the product from hydrogenation of carbazole. There was evidence for the formation of the hexahydro-derivatives of the two compounds which could make both these compounds effective hydrogen donors.

QUANTIFICATION OF DONATABLE HYDROGEN

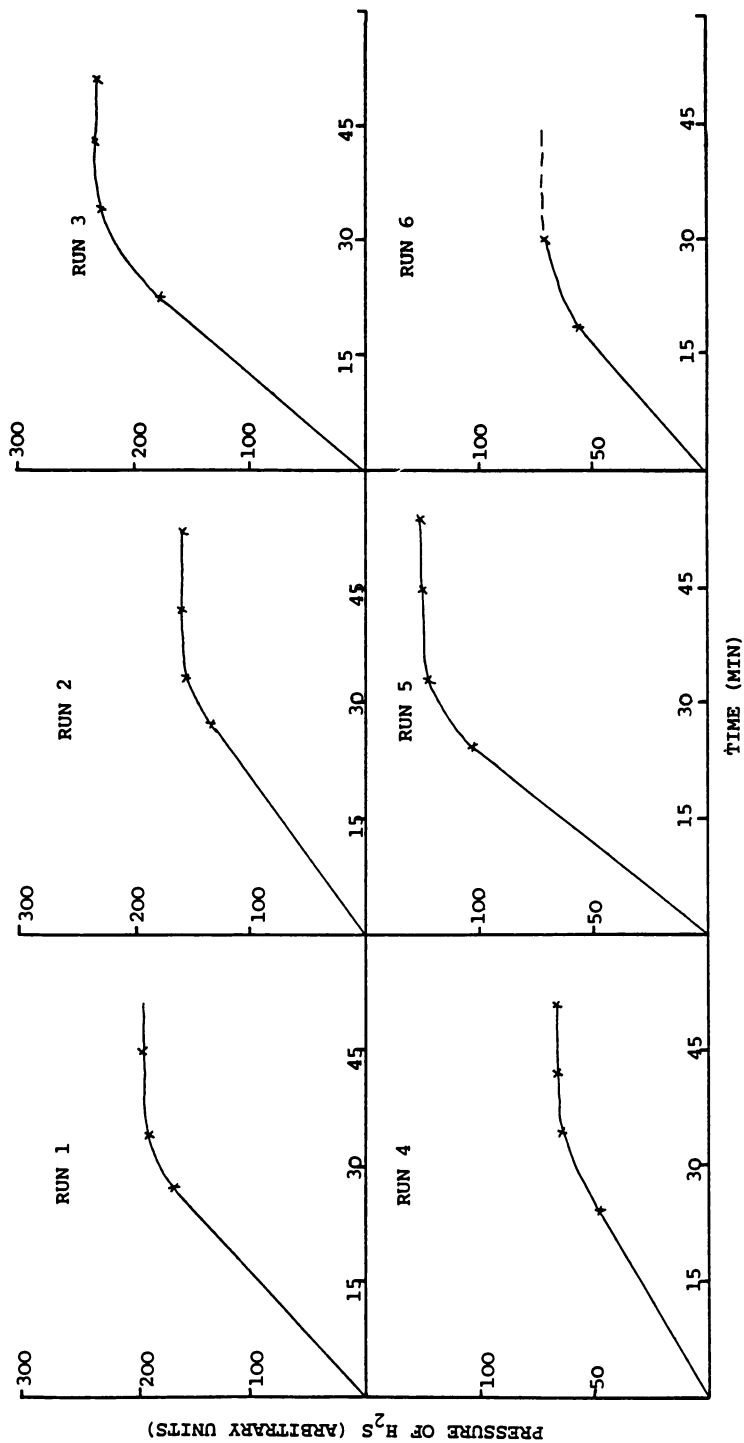
Chemical test using sulphur as an hydrogen acceptor Sulphur will readily accept donatable hydrogen to produce H₂S whose partial pressure will be proportional to the concentration of H-donors. This reaction provides a simple method for monitoring H-donors contents and initial experiments showed that only small amounts of sulphur and the hydrogen donor compound were needed for the reaction. The method was calibrated using 0.5 g of sulphur with various amounts of 9,10 dihydrophenanthrene (H₂) which were reacted at 275°C in a 10 cm³ microautoclave. Plots of pressure vs. time (Figure 3) indicates that an equilibrium pressure was reached in 30 mins or less.

Figure 4 shows plots of pressure reading vs mass of H₂P for the pressure readings at temperature and when cold and for both cases a linear relation was observed. Least squares analysis of the data provided the following equations:

$$\begin{array}{ll} x = 0.00455y - 0.1154 & r = 0.9971, \text{ at } 275^{\circ}\text{C} \\ \text{and } x = 0.00636y - 0.0266 & r = 0.9976, \text{ when cooled} \end{array}$$

where x is the mass of H₂P and y the pressure reading. These equations were used to quantify the H-donor contents of samples from the various hydrogenation reactions.

Quantification by NMR spectroscopy The approach used by Clarke et al.⁽¹⁾ was adopted but the hydroaromatic range was extended from 22.5-50 ppm to 20-50 ppm; this extension was necessary because the addition of 150 mg of chromium acetylacetonate to quench Nuclear

Figure 3. Plots of H₂S pressure vs. time.

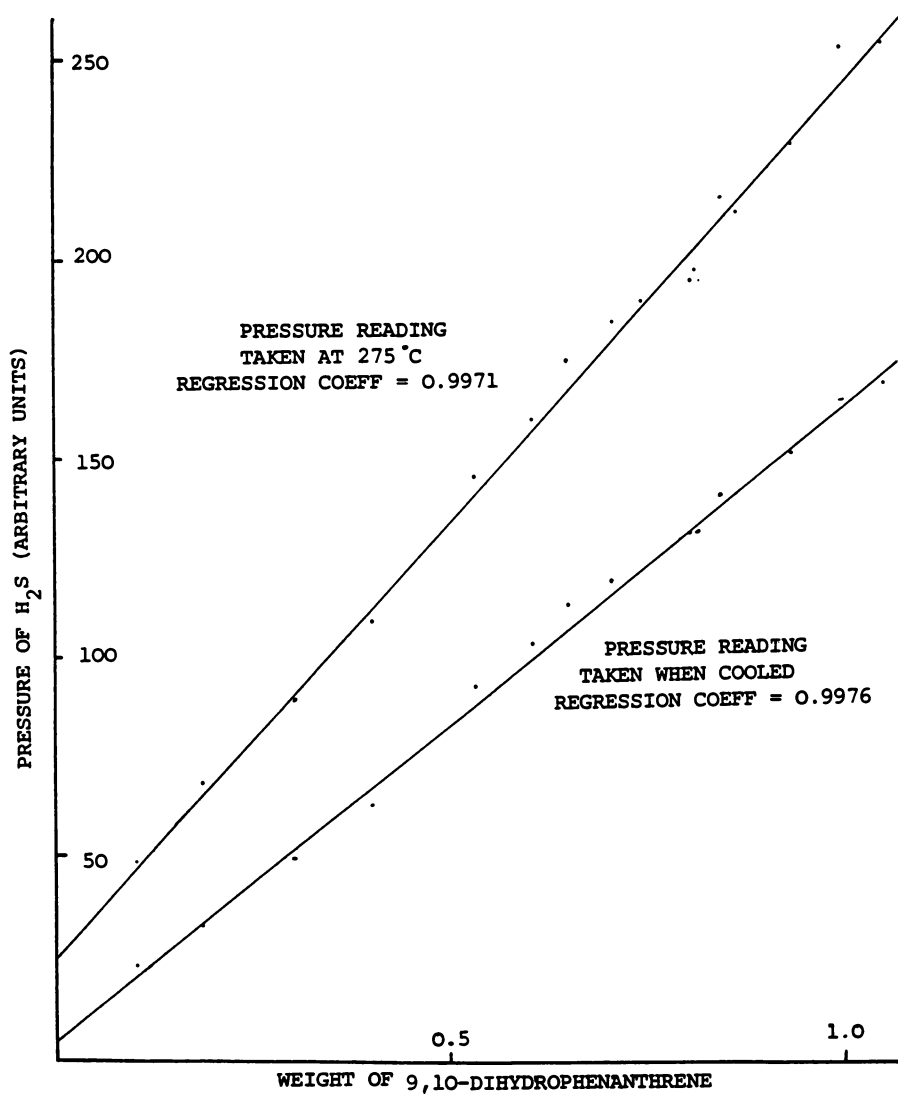


Figure 4. Calibration graph for sulphur method for H-donor quantification.

Overhauser Enhancement caused some downfield shift. The approach needs an assessment of the saturates content which is normally achieved by solvent elution chromatography. However, for our analysis, the saturates content was assessed from the GC analysis.

Quantification by GC Since in most cases a large percentage of the peaks on the chromatograms were identified, direct quantification of the H-donor content could be made from GC analysis of the hydrogenated samples.

COMPARISON OF THE THREE APPROACHES

Table VI summarises the data for the quantification of the H-donor content for samples from the hydrogenation of pyrene, phenanthrene, 1-methylnaphthalene, 2-methylnaphthalene and fluorene. It can be seen that agreement between the three approaches was generally good, the S-method tending to produce the higher values and NMR spectroscopy the lower values. The values for the hydrogenated fluorene sample did show a wide variation compared with the other samples. The values obtained from GC could have underestimated the H-donor content because of the relatively large proportion of peaks that remained unidentified; some of these peaks could have resulted from hydroaromatic compounds and could account for the difference between the results from GC and NMR but not the difference in the value for the S-method. The product from the sulphur test did contain some black insoluble material, indicative of the occurrence of some polymerisation, and GC analysis of the acetone-soluble part of the product did show the formation of some higher boiling point material (retention time 1918 s) with the consequent disappearance of some of the lower boiling point material. Therefore, other reactions than dehydrogenation of hexahydrofluorene to fluorene occurred; these reactions may have produced gaseous alkanes which would contribute to the pressure reading. Unfortunately, analysis of the gas mixture after the reaction was not possible. Further experiments are now in hand to assess the other reactions occurring, but the fact that these reactions did occur even at 250°C (cf 400°C used for coal dissolution) may suggest that hydrofluorenes may not be good hydrogen donors. Furthermore, the content of hydrofluorenes in recycle solvents is not very large so that the error caused by their presence in tests with recycle solvents should not be very large. For the other samples, GC analysis of the products showed that the peaks characterised as hydroaromatic were greatly reduced with a consequent increase in the peak for the parent aromatic. Peaks characterised as perhydro, ie saturates, remained relatively the same, indicating that these compounds did not influence the quantification by the S-method.

Table VI. Comparison of approaches for measuring H-donor content; of various hydrogenated aromatic compounds

Parent aromatic	Donatable hydrogen (wt %)		
	S-method	GC	NMR
Pyrene	1.87	1.86	1.77
Phenanthrene	2.09	1.94	1.86
1-methylnaphthalene	2.09	2.07	2.08
2-methylnaphthalene	1.87	1.15	1.62
Fuorene	2.44	0.96	1.23

Conclusions

The results have shown that, for the hydrogenation of the aromatic compounds providing a large proportion of the H-donors in recycle solvents, the extent of cracking (apart from acenaphthylene and dibenzothiophene) was relatively small at 400°C. Consequently, at this temperature for a run time of 2 h with catalysts normally applied to coal hydroliquefaction, loss

of recycle solvent should be small and compensated by the formation of similar material from coal fragments. From the hydrogenation experiments with phenanthrene, it seems that Mo-containing catalysts will be more effective than W-containing catalysts for solvent rehydrogenation. Presulphiding the Mo-containing catalysts did increase the rate of hydrogenation but induced greater hydrogenation to saturates which are ineffective H-donors. However, presulphiding the catalysts could reduce the reaction time for the hydrocracking stage because of the improved rate for solvent rehydrogenation depending upon the balance between the rate of hydrocracking of coal fragments and solvent rehydrogenation.

Apart from the hydrogenated fluorene sample, the chemical test method using sulphur as an hydrogen acceptor has proved to be successful for measuring donatable hydrogen contents. The method requires only a small amount of sample, can be carried out in a relatively short time and uses relatively simple equipment and inexpensive materials. The GC approach would be unsuitable for process recycle solvents because of the complex chromatograms and the difficulty in identifying all peaks. The NMR approach uses ^{13}C NMR, which requires more expensive equipment and a long time to accumulate a good spectrum, and needs a separate, time-consuming determination of the saturates content. Results to be published at a later date have indicated that the sulphur method can be used to determine the H-donor content of actual process recycle solvents providing good agreement with values calculated from ^{13}C NMR. The method is also more representative of the actual situation in coal dissolution in that it places the recycle solvent under hydrogen donation conditions.

Acknowledgements

The authors would like to express their gratitude to the Science and Engineering Research Council and the British Coal Corporation for their financial support (grant reference number GR/D 41163), to the Coal Research Establishment for carrying out and interpreting the GC/MS analysis and to Akzo Chemie, The Netherlands, for the supply of catalysts and the catalyst support.

References

1. Clarke, J.W. Randell, T.D. and Snape, C.E. Fuel 61 707 (1982)
2. Ladner, W.R. and Snape, C.E. Fuel 57, 658 (1978)
3. Seshadri, K.S. Ruberto, R.C. Jewell, D.M. and Malone, H.P. Fuel 57, 111 (1978)
4. Seshadri, K.S. Ruberto, R.C. Jewell, D.M. and Malone, H.P. Fuel 57, 549 (1978)
5. Bianco, A.D. Zaninelli M and Garadi E. Fuel 65, 1062 (1986)
6. Delpuech, J.J. Nicole, D. Danbenfield J.M. and Boudd, J.C. Fuel 64, 325 (1985)
7. Curtis, C.W. Guin, J.A. Hale, M.A. and Smith, N.L. Fuel 64, 461 (1988)
8. Smith, B.E. Proc. Int. Conf. Coal Science, Maastricht, Holland, October 1987 p.212
9. Bockrath, B.C. and Bittner E. Proc. Int. Conf. Coal Science, Pittsburg, USA, October 1983, p 212
10. Aiura, M. Massunga, T. Moriya, K. and Kageyama, Y. Fuel 63, 1163 (1984)

11. Allinger, N.L. Gorden, B.J. Tyminski, I.J. and Wuesthoff, M.T. *J. Org Chem* 36,739 (1971)
12. Haynes Jnr, US Dept of Commerce, Rep No. NSF/RA-770322 (1978)
13. Patzer, J.F. Farranto, R.J. and Montagna, A.A. *Eng Chem. Proc. Des Dev* 18, 625 (1979)

RECEIVED November 5, 1990

Chapter 19

Production of Filtered Coal Extract Solution with Very Low Levels of Mineral Matter

M. Cloke and Z. N. Aquino

Department of Chemical Engineering, University of Nottingham,
Nottingham NG7 2RD, United Kingdom

In two-stage coal liquefaction processes, the coal is digested in a solvent in the first stage and then hydrocracked in the second stage in order to increase the hydrogen-to-carbon ratio and the yield of distillate material. At some point in the process, mineral matter and undissolved residual material must be removed, and the processes used for this step are usually filtration or solvent de-ashing, with the latter taking the form of anti-solvent or critical solvent de-ashing. The de-ashing step can occur either after the first or second stages (1). The major advantage of de-ashing before the second stage is that it reduces catalyst deactivation due to both carbon deposition and trace element deposition, as reported by Stohl and Stephens (1). However, even when de-ashing is carried out before the second stage, deactivation of the catalyst still occurs initially due to carbon deposition and, over the life of the catalyst, but at a much lower rate, due to trace element deposition (1-6). In the case of carbon deposition the cause is not known, although there is some evidence linking high molecular weight species to carbon deposition (1-7). The mineral matter in the coal is largely removed by the de-ashing process, but not completely; thus, metallic trace elements are present in the coal extract solution and go forward to the hydrocracking stage, where some deposit, causing irreversible catalyst deactivation.

The British Coal process is a two-stage process with filtration as the de-ashing step occurring between the digestion and hydrocracking stages (8). In the process, powdered coal (< 200 μm) is digested in process-derived hydrogenated anthracene oil (HAO) at about 400°C and 15-20 bar pressure. Different solvent-to-coal ratios can be used, but 2:1 is the most common. During the digestion there is no addition of hydrogen gas and the pressure is autogenous, controlled by venting light-ends and non-condensibles. Following digestion, the mixture is filtered through a pressure filter to give a filtered coal extract solution. For a solvent-to-coal ratio of 2:1, this normally produces an extract solution with an ash level of about 500-600 ppm. This solution is then fed to a catalytic hydrocracker, which is run at temperatures of 400-430°C and a hydrogen pressure of 150-200 bar, using a Ni/Mo on alumina catalyst or similar. This catalyst is subject to the deactivation processes previously described.

Previous work in this laboratory (9-12) has shown that, by altering various parameters in the liquefaction process, the ash level of the filtered coal extract solution

can be reduced to levels as low as 60 ppm. It has also been shown (13) that the insoluble portion of solvent extractions used to characterise the filtered extract solution contain a high proportion of the trace elements originally present in the extract. The solvents used were pentane, toluene and THF, and with toluene, for example, about 80% of the metallic trace elements originally present in the filtered extract solution precipitated out with the insolubles.

In this paper, a description will be given of the previous work carried out to find ways to reduce metallic trace elements in the filtered extract to low levels. This will be compared with new work where solvent precipitation was carried out on filtered extract solution as an alternative method of producing low levels of trace elements.

PREVIOUS WORK

One of the aims of the work carried out in this laboratory was to investigate the deposition of trace elements on the hydrocracking catalyst. To this end, a continuous laboratory hydrocracker was installed and, to provide feed material for this, a 2-1 autoclave and pressure filter were also installed. It was noticed on the initial runs with the autoclave that the ash level of the filtered extract solution was considerably lower, at 100-200 ppm, than that normally obtained by British Coal, at 500-600 ppm. The reason for this difference was not known, so an investigation was carried out which found that the lower ash levels could be produced by a higher digestion pressure. Table 1 shows some of the results obtained, which have been previously published (10). Note that throughout all the experiments described in this paper the coals used were Point of Ayr and Calverton, whose analyses are given in Table 2, and that the HAO to coal ratio used was always 2:1. Hence, ash analyses in the coal extract solution are comparable.

Table 1 Effect of digestion pressure and filtration temperature on the ash of the filtered extract solution

Coal	HAO Batch	Digestion pressure (bar)	Filtration temperature (°C)	Extract ash (ppm)	Conversion (%)
Pt. of Ayr	1	40	265	100	83
Pt. of Ayr	1	35	265	130	83
Pt. of Ayr	1	30	265	140	83
Pt. of Ayr	1	20	265	200	82
Pt. of Ayr	1	15	265	250	84
Pt. of Ayr	1	10	265	470	86
Calverton	2	40	265	340	83
Calverton	2	30	265	350	82
Calverton	2	20	265	360	85
Calverton	2	10	265	580	83
Pt. of Ayr	2	35	265	240	83
Pt. of Ayr	2	40	180	80	82

Table 2 Analyses of Point of Ayr and Calverton coals

	Proximate Analysis			Elementary Analysis				
	VM (wt% db)	Ash (wt% db)	Moisture (%)	C	H	N	O	S
Pt. of Ayr	31.6	13.1	3.5	82.7	5.2	1.8	7.5	2.8
Calverton	35.5	6.8	7.0	82.1	5.8	1.5	9.0	1.6

Table 1 shows that as the digestion pressure is increased the extract ash decreases. With Calverton coal the decrease in ash level is less marked, but these results coincide with the use of the second batch of HAO. Point of Ayr coal also shows an increase in ash level with the second batch of HAO. However, by reducing the filtration temperature a low ash level is again observed. Many other similar experiments have been carried out (10,14) using different coals and further combinations of digestion pressure and filtration temperature, and the effect is always confirmed with the requirement that digestion pressure be above about 30 bar. Optimisation is achieved by reducing the filtration temperature where different HAO and coal combinations are used.

The effect on overall conversion is slight and again this has been confirmed in many different experiments. However, there does appear to be a slight reduction in conversion with increased digestion pressure and reduced ash levels. This gives some support to the theory that the effect is caused by a precipitation of ash-bearing material from retained low-boiling material at higher digestion pressures.

In another series of experiments in this laboratory (11), it was found that the particle size of the coal fraction used affected the ash level in the filtered coal extract solution. In these experiments, the coal sample, which is nominally < 200 μm , was divided into different size fractions by sieving, and each fraction digested using the normal procedure. Table 3 shows the results obtained with Point of Ayr and Calverton coals. Note that the Point of Ayr coal was a different batch to that used for the results described previously, with a similar analysis except for ash, which was higher at 19 %.

Table 3 Ash levels in coal and filtered coal extracts for different sized coal fractions

	Ash Level (ppm)	
	Calverton coal	Pt. of Ayr coal
0-200 μm coal	68000	190000
0-50 μm coal	76400	257000
50-75 μm coal	61400	227000
75-105 μm coal	60700	191000
105-149 μm coal	54100	176000
149-200 μm coal	43400	58000
0-200 μm extract	485	280
0-50 μm extract	581	1014
50-75 μm extract	390	344
75-105 μm extract	460	522
105-149 μm extract	564	238
149-200 μm extract	535	237

The results in Table 3 show that for each coal the mineral matter content increases with a decrease in size fraction. The filtered extracts produced in the 0-50 μm range show a higher level for both coals. The effect is more pronounced with Point of Ayr coal and clearly shows the deleterious effect of fine material. There is clearly scope for reducing ash levels in the extract by rejecting the fine material prior to digestion. The material which is less than 50 μm represents some 30-50 % of the coal and further work investigating the effect of size fractions below 50 μm could be of benefit. It was also found that conversion increased with increasing size fraction, which is of significant benefit and probably due to the increased concentration of pyrite in the larger-sized fractions.

The effect of the quality of the solvent has also been investigated in terms of the saturates content (14). This was prompted by some similar work carried out by Kimber (15). The saturates content of the HAO is measured by the quantity of material passing through a silica gel column with n-pentane as eluent. Generally, as saturate levels increase, the amount of donatable hydrogen in the solvent decreases and the conversion decreases. However, it was also found that as saturate levels increase the ash level in the filtered extract solution decreases. Some results using Calverton coal are shown in Table 4. The HAO samples used were made up by mixing, in the required proportions, the 8 and 22 % samples.

From Table 4, the reduction in ash content with increase in saturates content is clear, in spite of the higher ash level of the 22 % saturates HAO. The conversion peaks at 12 % saturates, which was unexpected and cannot be explained, except that many factors affect conversion and this could be the result of some other factor or a combination of factors. However, the reduction in conversion from 16 % saturates onwards is clear.

So far, no mention has been made of the individual trace elements. At the beginning of this work, it was found that the proportions of the trace elements in the ash vary from original coal to filtered coal extract solution. Some of the original results for Point of Ayr coal are shown in Table 5 (9).

The results in Table 5 show a large increase in proportion of Mn and Ti, and increases for Mg and Ca from coal to extract. Fe stays about the same and all the others decrease. Previous work (2) has also shown that the elements which increase in proportion also deposit readily and steadily on the hydrocracking catalyst. Thus, any method which reduces the ash level in the filtered extract solution needs to be, if at all possible, selective towards Mn, Ti, Ca, Mg, and Fe. In the case of digestion pressure, as shown by the results above, most trace elements do not significantly change their proportion as the ash level decreases, except for Mn where the situation becomes worse and Mg where there is some improvement. Liquefaction of different-sized coal fractions has little effect on the distribution of elements in the ash as the overall ash level decreases. However, with the use of HAO with different saturates levels, there is a distinct increase in the levels of Ti with decreasing ash level, but a significant decrease in Mn.

Thus, the previous work gives different ways of reducing the overall ash level in the filtered extract solution, with indications of the effect on individual trace elements. However, all these methods require alteration to process parameters and it was thought that it might be useful to provide an alternative which would be an add-on to the existing process. The observation that solvent insolubles of filtered extract contain high proportions of trace elements could provide the basis for a method based on solvent de-ashing of a filtered extract. These results are described in the next section.

Table 4 Ash levels and conversions in the filtered extract solutions produced using HAO of different saturates level

	Filtered extract solutions						HAO samples	
	8	10	12	14	16	18	8	22
Saturates content of HAO (%)	8	10	12	14	16	18	8	22
Ash content (ppm)	364	331	317	290	221	209	73	165
Conversion (%)	81	82	87	84	76	56	-	-

Table 5 Trace element analysis of coal and extract ashes

	Filtered extract solution				Coal
	35	20	15	10	-
Digestion Pressure (bar)	130	200	250	470	131000
Ash content (ppm)					
Proportion of metal in ash (%)					
Al	3.3	5.1	6.9	4.2	11.3
Ti	8.4	6.9	8.9	5.1	0.5
Si	1.0	1.4	1.2	0.7	17.0
Ca	12.1	10.3	7.3	11.1	3.5
Mn	7.4	4.5	3.7	2.5	0.1
Fe	13.7	18.0	14.9	13.6	13.6
Mg	3.5	5.2	10.6	8.5	1.5
Na	0.3	0.3	0.2	0.3	0.3
K	0.1	0.1	0.1	0.1	2.0

SOLVENT PRECIPITATION OF TRACE ELEMENTS

Experimental

Materials

The coal used was Point of Ayr, supplied preground to $-200\ \mu\text{m}$ by British Coal. An analysis of the coal is given in Table 2. The HAO solvent used was also supplied by British Coal.

Procedures

Liquefaction to produce filtered extract solution was carried out in a 2-l autoclave under the conditions described previously and elsewhere (9). Solvent precipitation experiments using the filtered extract solution were carried out in a 0.2-l autoclave. The extract and solvent were mixed together cold, in the autoclave, and heated to the extraction temperature in a fluidised sand bath. The mixture was agitated at the required temperature for 20 minutes and then filtered through a pressure filter containing a nomex cloth, at the extraction temperature, using the pressure in the autoclave or an applied nitrogen pressure. In some experiments, the solvent was injected, under pressure, into extract solution already at the required temperature.

Analysis

Ash yields of the liquid products were determined by evaporating a sample (25 g) in a platinum crucible until coke formed. The ashing was completed in a muffle furnace at 850°C .

Trace element analysis was carried out on the ash by fusing with lithium metaborate, followed by dissolution in 10 % hydrochloric acid. The resulting solution was analysed using atomic emission and absorption spectrometry (AA). The method has been described previously (9).

Simulated distillation analysis was carried out on the extract and filtrate produced after precipitation, focusing on the fractions which boiled below 350°C . A Perkin Elmer model 8500 GC fitted with a wide-bore, OV-1 capillary column, 25 m long and $0.53\ \mu\text{m}$ in diameter, was used. The oven temperature was held at 40°C for 1 minute and then increased at a rate of 4°C per minute to 250°C , where the temperature was held. There was no split on the injection and a FID detector was used. Initial fractionation of the samples was carried out by vacuum distillation.

Results and Discussion

Reduction in ash levels

In the first series of experiments toluene was used as the solvent and the extractions were carried out at a temperature of 110°C . The ratio of extract to toluene was varied and a blank run was also carried out with no toluene added. This was to make certain that no precipitation was occurring as a result of cooling and reheating.

From the results in Table 6 it can be seen that by increasing the quantity of toluene used then the amount of material precipitated is increased and the ash level of the filtrate decreases. It is clear, from the filtrate mass, that there is still a significant quantity of toluene remaining, which might be expected at the temperature used. To allow for this, an equivalent extract ash is calculated as shown in Table 6. This figure also shows a steady decrease as the mass of toluene used increases. The mass of cake obtained

shows that there would be a significant loss of product by precipitation if this method were to be used to remove trace elements. The extract solution in this series of experiments had a "high" ash value of 560 ppm. In the next set of experiments, the extract solution had a lower ash value of 180 ppm, and the effect of varying the precipitation temperature was studied.

Table 6 Extraction of coal extract solution with toluene - effect of toluene-to-extract ratio

Temperature of extraction : 110°C

Ash of original coal extract solution : 560 ppm

Mass extract	(g)	56	55	61	55	55
Mass toluene	(g)	56	32	25	11	0
Ratio extract/toluene		1:1	1.7:1	2.5:1	5:1	BLANK
Mass cake	(g)	18.7	15.4	3.0	1.5	0
Filtrate - mass	(g)	81.3	66.1	79.0	62.3	
- ash	(ppm)	70	140	380	470	550
Equivalent						NO
extract ash	(ppm)	110	160	490	530	EFFECT

$$\text{Equivalent extract ash} = \frac{(\text{mass filtrate} \times \text{filtrate ash})}{\text{mass extract}}$$

Table 7 shows that, as the temperature of extraction is increased, the mass of cake decreases but the equivalent extract ash increases. However, it would seem that a significant reduction in the amount of material precipitated can be obtained without a large increase in the ash level of the filtrate. This is especially seen in the increase in temperature from 100 to 138°C.

Table 7 Extraction of coal extract solution with toluene - effect of temperature

Ratio extract/toluene : 1.67:1

Ash of original coal extract solution : 180 ppm

Extraction temperature	(°C)	100	138	175	200
Mass extract	(g)	50	50	47	50
Mass cake	(g)	20.4	10.0	6.9	3.4
Filtrate - mass	(g)	51.6	59.1	55.7	50.1
- ash	(ppm)	60	70	80	140
Equivalent					
extract ash	(ppm)	60	70	100	140

The average value for the THF insolubles of a filtered extract solution produced in this laboratory is 2-4 % and it was found (13) that about 60 % of the trace elements were precipitated out with the insolubles. Thus, it was considered that THF might give low ashes in the filtrate with less material precipitated. Table 8 shows the results obtained when THF was used as the solvent. The results obtained were disappointing, in that there was little reduction in ash level. It may be that lower temperatures or more solvent are required. However, both would reduce the practicality of using THF.

Table 8 Extraction of coal extract solution with THF

Ash of original coal extract solution : 180 ppm

Extraction temperature (°C)	122	103	66	66
Mass extract (g)	50	50	50	50
Mass THF (g)	30	30	30	50
Ratio extract/THF	1.67:1	1.67:1	1.67:1	1:1
Mass cake (g)	4.1	4.8	4.8	9.5
Filtrate - mass (g)	55.1	59.3	69.6	81.5
- ash (ppm)	120	130	160	110
Equivalent extract ash (ppm)	130	150	220	180

The final solvent to be tried was pentane. In the normal insolubles test, the pentane insolubles is normally over 25 % for the filtered extract solution. In the runs that were carried out with pentane, there were many operational problems, mainly associated with the large quantities of material precipitated. The filtrates produced contained very low levels of trace elements, but it was considered that the large amounts of material precipitated, most of which was difficult to remove from the autoclave, ruled this out as a potential solvent.

Thus, the only reasonable results were obtained with toluene, and in this case control could be exercised by adjusting either the ratio of extract to toluene or the temperature. In a real process, the solvent would probably be injected into the hot extract. This was simulated using a nitrogen over-pressure to inject toluene into the autoclave, and it was found that the results were similar to those obtained when solvent and extract were mixed cold. Use of this solvent precipitation method would result in a loss of product, as indicated by the weight of filter cake obtained. However, this material is mainly preasphaltenic and thus difficult to upgrade in the hydrocracking stage. In a commercial coal complex, some coal would be required to burn in boilers, etc. and for the production of hydrogen. The precipitated material could be used in this way so that in the process as a whole, the loss is minimal.

Trace element concentrations

As indicated previously, it is important to look at the individual trace elements in the coal extract solution. Table 9 shows the concentration of trace elements in the ash from the original extract and the filtrate produced after toluene extraction. This was for an extract with an ash level of 350 ppm, extracted with toluene at 165°C to give a filtrate with an ash level of 100 ppm. The results show that there are some differences, with Ca reducing and Fe and Ti increasing their proportions. However, the changes are not great and it would be expected that if the filtrate were fed to the hydrocracker it would deposit trace elements as observed previously (2), except, of course, there would be a smaller quantity overall.

Nature of the extract solution after precipitation

When toluene extractions were carried out at 110°C, it was clear from the mass obtained, that toluene remained in the filtrate. With the higher temperature extractions, remembering that the filtration was also carried out at the higher temperature, the mass of filtrate was accordingly lower, since most of the toluene boiled off from the filtrate.

Table 9 Trace element analysis

Proportion of Element in Ash (%)	Original Extract	Filtrate after Toluene extraction
	Al	5.5
Ti	1.8	4.0
Si	4.0	2.8
Ca	25.6	15.2
Mn	3.0	4.5
Fe	3.8	8.2
Mg	5.4	5.4
Na	1.5	2.4
K	0.5	0

However, examination of the filtrate showed that it was much more fluid than the original extract and it appeared that some toluene remained in it. To investigate this, analysis of the extract and filtrate were carried out by an initial vacuum distillation followed by GC analysis of the distillate. The results are shown in Table 10.

Table 10 Simulated distillation of the fraction boiling to 350°C of extract and filtrate after extraction with toluene at 165°C

Extract:toluene ratio	Original Extract	Filtrate		
	-	1.6:1	2.5:1	3.3:1
		(% distilled)		
0-100°C	0.5	0.1	0.1	0.1
0-150°C	1.2	0.1	0.1	0.1
0-200°C	7.0	5.1	4.2	4.2
0-250°C	19.3	32.9	20.0	21.1
0-300°C	54.6	78.5	64.1	67.5
0-350°C	100	100	100	100

From the results in Table 10 it can be seen that for the filtrate obtained after precipitation with toluene, that the fraction boiling to 150°C decreases. This is contrary to what was expected, in that the fluidity of the filtrate would indicate some retention of toluene, but the distillation shows otherwise. The fraction from 200-300°C shows an increase after precipitation, which again is difficult to explain in terms of a simple precipitation of high molecular weight species. In a different set of experiments, a larger quantity (about 4 l) of material was prepared by precipitation of insolubles from filtered extract solution using toluene. To characterise the product, it was tested for pentane, toluene and THF insolubles. Following this, the material was stored in a vessel for about 2-3 weeks at 150°C prior to use. It was found that some of the material had evaporated and the extract was less fluid. The insolubles content was retested and it was found that the pentane insolubles had increased from 26 to 32 %; the toluene insolubles from 8.5 to 9.8 %; and the THF insolubles decreased from 2.0 to 1.8 %. It would thus appear that

over the period in question lower molecular weight material was lost. This indicates that initially after precipitation, there is a retention of toluene, but it is not freely in solution. The toluene is probably adducted to other material, giving the increase in the higher boiling ranges and in the pentane solubles. This material is, however, easily lost from the solution, as indicated by the above results.

CONCLUSIONS

Several options have been outlined for the reduction of mineral matter to low levels in filtered extract solution. These are mainly applicable to the British Coal process, but have implications for other 2-stage processes. By running the digestion at a pressure above about 30 bar and reducing the filtration temperature as required, low levels of trace elements have been obtained with a series of different coals and HAO solvents. Discarding the fine fraction of the coal from the feed to the digester will also result in lower levels of trace elements in the extract solution, as will increasing the saturates content of the HAO. However, in the latter case this may also lead to reduced overall conversion.

An alternative to adjusting process conditions is to have a secondary solvent precipitation stage. Toluene was found to be the best solvent tried and, again, low levels of trace elements were obtained. Using this method, however, there is a loss of product, but this is mainly high molecular weight species, which are difficult to hydrocrack and are probably responsible for deposition of carbonaceous material on the catalyst.

ACKNOWLEDGEMENTS

The work described in this paper was largely funded by the Science and Engineering Research Council, UK. The assistance of British Coal in their supply of materials and useful information is gratefully acknowledged.

LITERATURE CITED

- 1 Stohl, F.V. and Stephens, H.P. Ind. Eng. Chem. Res. 1987, **26**, 2466
- 2 Cloke, M., Hamilton, S. and Wright, J.P. Fuel 1987, **66**, 678
- 3 Stiegel, G.J., Tischer, R.E., Cillo, D.L. and Narain, N.K. Ind. Eng. Chem. Prod. Res. Dev. 1985, **24**, 206
- 4 Ahmed, M.M. and Crynes, B.L. I.Chem.E. Symposium Series No. 62 1980, L1
- 5 Freeman, G.B., Adkins, B.D., Moniz, M.J. and Davis, B.H. Applied Catalysis 1985, **15**, 49
- 6 Cillo, D.L., Stiegel, G.J., Tischer, R.E. and Narain, N.K. Fuel Proc. Tech. 1985, **11**, 273
- 7 Yoshimura, Y., Hayamizu, K., Sato, T., Shimada, H. and Nishijima, A. Fuel Proc. Tech. 1987, **16**, 55
- 8 Davies, G.O. Chem. Ind. (London) 1975, **15**, 560
- 9 Cloke, M. Fuel 1986, **65**, 417
- 10 Cloke, M. and Wright J.P. Fuel 1989, **68**, 683
- 11 Cloke, M. and Wright J.P. Fuel Proc. Tech. 1989, **23**, 173
- 12 Cloke, M. and Wright J.P. Fuel (awaiting publication)
- 13 Cloke, M. and Wright J.P. Fuel 1988, **67**, 1648
- 14 Cloke, M. and Wright J.P. Fuel Proc. Tech. 1990, **24**, 203
- 15 Kimber, G.M. Int. Conf. Coal Science, Pergamon, Australia, 1985, 106

RECEIVED November 5, 1990

Chapter 20

Effect of Mild Chemical Pretreatment on Liquefaction Reactivity of Argonne Coals

R. L. Miller, Robert M. Baldwin, O. Nguanprasert, and D. R. Kennar

Chemical Engineering and Petroleum Refining Department, Colorado School of Mines, Golden, CO 80401

Mild pretreatment of four coals from the Argonne Premium Coal Sample Bank using alkyl alcohols and hydrochloric acid has been investigated as a method for improving liquefaction reactivity. Our technique mildly alkylates the coal (< 0.5 alkyl groups added/100 carbon atoms) and adds small amounts of chlorine which may act as a dissolution catalyst. Infrared spectroscopic studies of the treated and untreated coals indicated that alkylation occurred at phenolic and carboxylic sites within the coal, but no evidence of alkylation at carbon sites was noted. Mild pretreatment with methanol or propanol and HCl improved liquefaction reactivity for each coal studied over a range of reaction severity and conversion levels. The enhancement was far greater per unit of methyl group addition than achieved using either Sternberg's reductive alkylation or Liotta's oxygen alkylation techniques.

Much of the recent research in direct coal liquefaction seeks to develop methods for dissolving coal at low reaction severity (defined as temperatures below 350 °C and pressures of 1000-1500 psig). Most of these efforts have been prompted by several incentives that exist for converting coal at milder reaction conditions than those utilized in conventional processes, including:

- * Reduced hydrocarbon gas make resulting in reduced feed gas consumption and enhanced hydrogen utilization efficiency
- * Suppressed retrogression of primary coal dissolution products resulting in enhanced distillate yield and residuum product quality
- * Residuum which is less refractory and thus amenable to upgrading in a conventional second-stage hydrocracker
- * Substitution of less expensive off-the-shelf vessels, piping, and pumps in place of costly, custom-designed units

Researchers at several locations including the Pittsburgh Energy Technology Center (1), the University of North Dakota Energy and Environmental Research Center (2), Carbon Resources, Inc. (3), and the Colorado School of Mines (4) have investigated various methods for improving coal reactivity and liquid yields at mild reaction conditions. These studies showed that coal can be readily converted to tetrahydrofuran (THF) soluble products via selective chemical attack rather than thermal bond scission, but that the rate and extent of coal dissolution at mild conditions is strongly dependent upon intrinsic coal reactivity. Thus the problem of optimizing low severity liquefaction performance becomes one of maximizing coal reactivity at these conditions.

The objective of this paper is to present recent research results in which mild chemical pretreatments such as methanol/HCl are being evaluated as methods for improving intrinsic coal reactivity prior to liquefaction. The basis for this work derives from studies by Sternberg (5), Larsen (6), Sharma (7), Liotta (8), and others where alkylation was utilized as a method for rendering coal soluble in THF or toluene to aid in structural analysis. Results from Sharma's work are particularly pertinent, since they demonstrated the ability to alkylate coal using alkyl alcohols such as methanol rather than exotic and expensive chemical reagents such as tetrabutylammonium hydroxide, aluminum trichloride, methyl iodide, etc. Limited work has been reported which relates increased solvent solubility of alkylated coal to enhanced liquefaction reactivity. Schlosberg et al. (9) measured the reactivity of mildly alkylated Wyodak subbituminous and Illinois #6 bituminous coals in tetralin at 427 °C, 1500 psig hydrogen pressure and 130 minutes reaction time. A 10-21 wt% (maf and alkyl group-free basis) increase in cyclohexane soluble conversion was noted for the alkylated coals.

Experimental Procedure

Pocahontas #3 low volatile bituminous coal, Illinois #6 high volatile bituminous coal, Wyodak subbituminous coal, and Beulah-Zap lignite from the Argonne Premium Coal Sample Bank were used as feed coals in these experiments. Ultimate analyses for these coals are listed in Table I. Coal samples were stored under argon in sealed ampules prior to use in pretreatment and liquefaction experiments.

Table I

Ultimate Analysis of Feed Coals

Wt% Dry Basis	Pocahontas #3	Illinois #6	Wyodak	Beulah-Zap
Carbon	86.7	65.7	68.4	65.9
Hydrogen	4.2	4.2	4.9	4.4
Nitrogen	1.3	1.2	1.0	1.0
Sulfur	0.7	4.8	0.6	0.8
Oxygen	2.3	8.6	16.3	18.2
Ash	4.8	15.5	8.8	9.7
Coal Rank	LVB	HVB	Subbit.	Lignite

Three chemical pretreatment methods were evaluated in this study. Most of the pretreatment experiments were performed using a liquid phase technique we developed based on gas phase alkylation chemistry reported by Sharma (7). Coal was pretreated by suspending 5 g of undried coal in 40 cm³ of alkyl alcohol and 0.1 cm³ of concentrated HCl catalyst in a 100 cm³ round bottom flask and continuously stirring the coal/methanol slurry on a magnetic stirring plate for a prescribed period of time (usually 3 hrs.). The flask was connected to a cooling water condenser to reduce alcohol losses by evaporation. Several experiments were completed in which dry nitrogen was used to blanket the coal/alcohol slurry; elemental analyses of the treated coals showed no difference in the extent of coal oxidation when the system was purged with nitrogen and when it was vented to the atmosphere. After pretreatment, most of the excess alcohol was decanted off and the moist coal sample washed with three 50 cm³ aliquots of fresh alcohol to remove residual acid. Any remaining alcohol was recovered by roto-evaporation and vacuum drying (50 °C, 0.1 torr, 24 hrs.). Untreated coal samples were vacuum dried at the same conditions before liquefaction. After drying, all treated and untreated coal samples were stored at room temperature in a vacuum desiccator (0.1 torr) prior to analysis or liquefaction. Reactor runs were scheduled so that each coal sample was stored in the desiccator for less than 12 hours before use.

For comparison purposes, samples of Wyodak coal were also pretreated using standard procedures developed by Sternberg pretreated using standard procedures developed by Sternberg (5) and Liotta (8). The Sternberg technique involved reacting coal in a THF slurry with potassium metal in the presence of naphthalene, which acted as an electron transfer agent. The product, a coal polyanion, was then reacted with an alkylating agent (ethyl iodide in our experiments) to obtain the alkylated coal product. Following alkylation, the coal sample was roto-evaporated to remove excess THF, washed with methanol, and exhaustively extracted with water prior to vacuum drying (50°C, 0.1 torr, 24 hours). Depending upon coal rank, as many as 10-15 alkyl groups per 100 carbon atoms may be added to the coal at both carbon and oxygen sites via Sternberg reductive alkylation, with corresponding pyridine solubility increases of nearly 95 wt% (5).

The Liotta procedure involved slurrying coal in an aqueous solution of tetrabutylammonium hydroxide to remove acidic protons, followed by addition of methyl iodide as alkylating agent. This mixture was then stirred vigorously for 12-72 hrs. depending upon the extent of alkylation desired. After alkylation, the moist coal sample was roto-evaporated to remove excess THF and methyl iodine, followed by exhaustive extraction with water to remove tetrabutylammonium iodide produced during alkylation. Finally, the treated coal was vacuum dried (50°C, 0.1 torr, 24 hours) before use.

Carbon analyses were performed on each pretreated coal sample using a Carlo-Erba model 1106 CHN analyzer to measure the extent of alkylation as computed from the following formula:

$$\text{Extent of alkylation} = \frac{C_3 - C_1}{C_2 - C_1} \times 100$$

(g alkyl group/100 g maf coal)

where: C₁ = wt% carbon (maf basis) in untreated coal
 C₂ = wt% carbon in alkyl group
 C₃ = wt% carbon (maf basis) in treated coal

The extent of alkylation could then be easily converted by material balance to a basis of number of alkyl groups added per 100 carbon atoms in the treated coal.

Liquefaction reactivity experiments were conducted in a 20 cm³ tubing bomb reactor attached to an agitator and immersed in a fluidized sandbath. Table II lists reaction conditions used in these runs. A non-hydrogen donor vehicle (1-methylnaphthalene, 1-MN) and a hydrogen donor vehicle (9,10-dihydrophenanthrene, DHP) were used as solvents (2/1 solvent/coal wt. ratio). Coal conversion was monitored using THF extraction data corrected for the intrinsic THF solubility of untreated and treated coals.

Table II
Liquefaction Reaction Conditions Studied

Temperature:	315°C, 350°C, 400°C
Initial Pressure:	65 atm (cold)
Reaction Time:	30 min.
Feed Gas:	hydrogen
Solvents:	1-methylnaphthalene 9,10-dihydrophenanthrene
Solvent/Coal wt. ratio:	2/1
Catalyst:	none

Solubility measurements of untreated coals, treated coals, and liquefaction products were conducted at ambient conditions and consisted of these steps: 1) sonicating the liquid products from the tubing bomb reactor in excess THF for 10 min., 2) centrifuging the mixture at 2000 rpm for 15 min., and 3) decanting THF-soluble products and excess THF from the THF-insoluble residuum. This procedure was repeated at least two times or until no additional THF-soluble products were recovered. Remaining THF insolubles were dried at 100°C for 24 hrs to remove residual THF, weighed, and finally ashed. Coal conversion to THF soluble products was computed as follows:

$$\text{Coal conversion (wt\% maf basis)} = \frac{M_f - M_p}{M_f} \times 100$$

where: M_f = mass of maf THF-insoluble coal charged

M_p = mass of maf THF-insoluble products recovered
(corrected to satisfy the ash balance)

Photoacoustic Fourier Transform Infrared Spectroscopy (PAFTIR) was used to monitor functional group changes within selected treated coal samples. The photoacoustic technique allows direct measurement of powdered solid state spectra without errors caused by low transmittance signals or variations in surface morphology. Depending upon signal strength, PAFTIR spectra generally describe solid properties to depths of about 40 angstroms.

Results and Discussion

Alkylation Studies. Several preliminary experiments were completed to compare the extent of alkylation obtained with our coal pretreatment method to that obtained with Sternberg and Liotta alkylation. Results for Wyodak coal are summarized in Table III. Clearly, our procedure provides a very mild alkylation treatment compared with the other two methods and does not appear to be sensitive to differences in alkyl chain length (methyl vs. propyl). The increase in THF solubility was also small; this result again suggests only a small extent of alkylation and, in addition, shows that only minimal ion exchange (for example Ca^{++} by H^+) occurred in the coal mineral matter. The effect of each pretreatment method on low severity liquefaction reactivity is discussed in the next section.

Table III
Results From Ambient Pretreatment Experiments
Using Wyodak Coal

Method	Alkyl Group	Alkyl Groups Added Per 100 C Atoms	Wt% THF Solubility
None	---	---	2.3
Present study *	methyl	0.2	5.6
Present study *	propyl	0.3	6.5
Liotta **	methyl	6.2	18.8
Liotta ***	methyl	11.9	27.0
Sternberg	ethyl	3.3	24.7

* 3 hrs. pretreatment time
 ** 12 hrs. alkylation time
 *** 24 hrs. alkylation time

Liquefaction Reactivity Studies. To study the influence of coal rank on the reactivity enhancement effectiveness of our pretreatment method, samples of the four Argonne coals were treated with a mixture of n-propanol and HCl (100/1 wt. ratio) for three hours. At these conditions, Pocahontas coal was essentially unreactive, while less than 0.5 propyl groups per 100 carbon atoms were added to each of the other three coals. Low severity liquefaction conversion results for the treated coals using 1-methylnaphthalene solvent are shown in Figure 1. Data for the corresponding untreated Argonne coals are included in this figure for ease of comparison. Propylation of each coal enhanced conversion to THF soluble products, although the effect increased dramatically with decreasing coal rank (and increasing oxygen content). This result suggests that our pretreatment procedure preferentially alkylates coal at oxygen sites rather than carbon sites in the coal structure.

Figure 2 summarizes results from a series of low severity experiments using Wyodak coal which was pretreated with HCl and either methanol, ethanol, n-propanol, n-butanol, or isobutanol (100/1 alcohol/acid wt. ratio, 3 hrs.). These data suggest only a slight effect of alkyl group chain length on reactivity enhancement indicating that cheaper, commodity alcohols such as methanol may be used successfully as the pretreatment agent. This result indicates the potential for considering mild chemical pretreatment on a larger process scale, although the net consumption of methanol and HCl must be better estimated before pretreatment costs can be determined.

Figure 3 shows the effect of reaction temperature on the liquefaction reactivity of methylated (3 hrs, 100/1 methanol/HCl wt. ratio) and untreated Wyodak coals using DHP solvent. Mildly treating the coal (approx. 0.2 methyl groups added/100 carbon atoms) resulted in THF conversion improvements of about 21 wt% at 315°C, 23 wt% at 350°C, and 14 wt% at 400°C. Clearly, mild pretreatment enhances reactivity over the entire range of observed conversion levels. This result is very significant since it shows that our pretreatment procedure is beneficial at conversion levels of commercial interest, and thus, represents more than a laboratory curiosity.

Figure 4 compares the effect of our mild pretreatment technique with low severity reactivity enhancement data for Wyodak coal samples alkylated using the Liotta and Sternberg methods. As shown, our method provided a significant reactivity improvement at very low extent of alkylation compared with the other two techniques. This result was puzzling, and in fact, seemed to suggest that some other effect was contributing to the observed reactivity behavior. To investigate this possibility, we performed several additional pretreatment experiments, results of which are summarized in Figure 5. Without HCl addition, methanol pretreatment of Wyodak coal provided a very slight extent of alkylation (< 0.05 methyl groups/100 carbon atoms) and liquefaction reactivity was nearly unaffected. Christensen (10) observed similar alkylation behavior with Beulah lignite. Replacing methanol with acetone or hexane (two reagents which cannot act as alkylating agents in this system) reduced the reactivity enhancement compared with the methanol/HCl treatment, but did improve reactivity compared with the untreated coal. Finally, replacing HCl with acetic acid resulted in less reactivity improvement, probably because of differences in acid strength. Although not shown in Figure 5, pretreatment with methanol/H₂SO₄ actually decreased liquefaction reactivity and sulfur was incorporated into the treated coal, indicating the formation of sulfones.

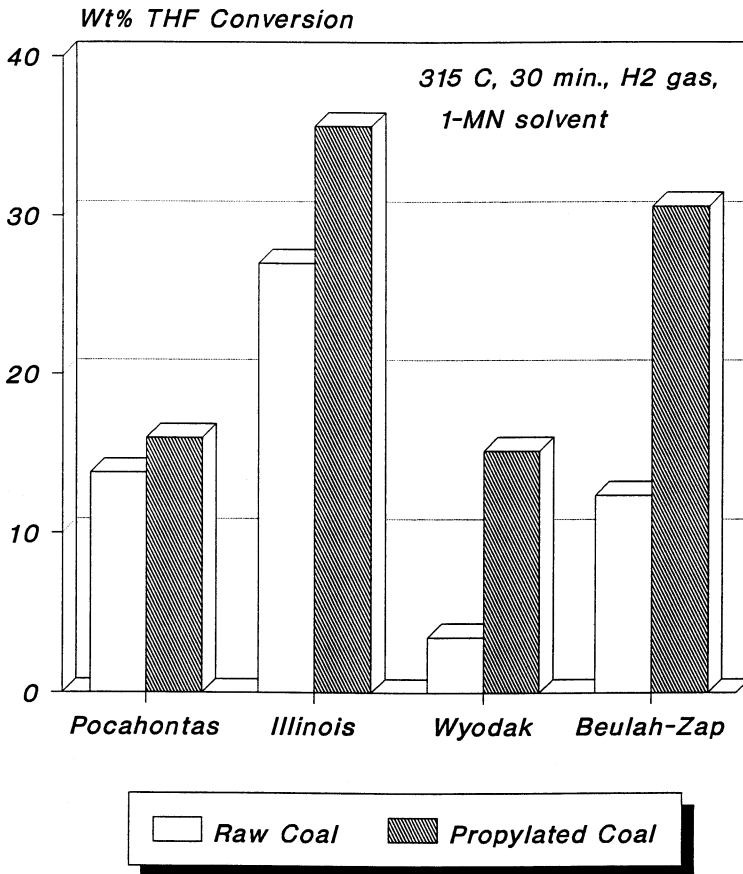


Figure 1. Effect of Mild Propylation on Liquefaction Reactivity of Four Argonne Coals at Low Severity Reaction Conditions.

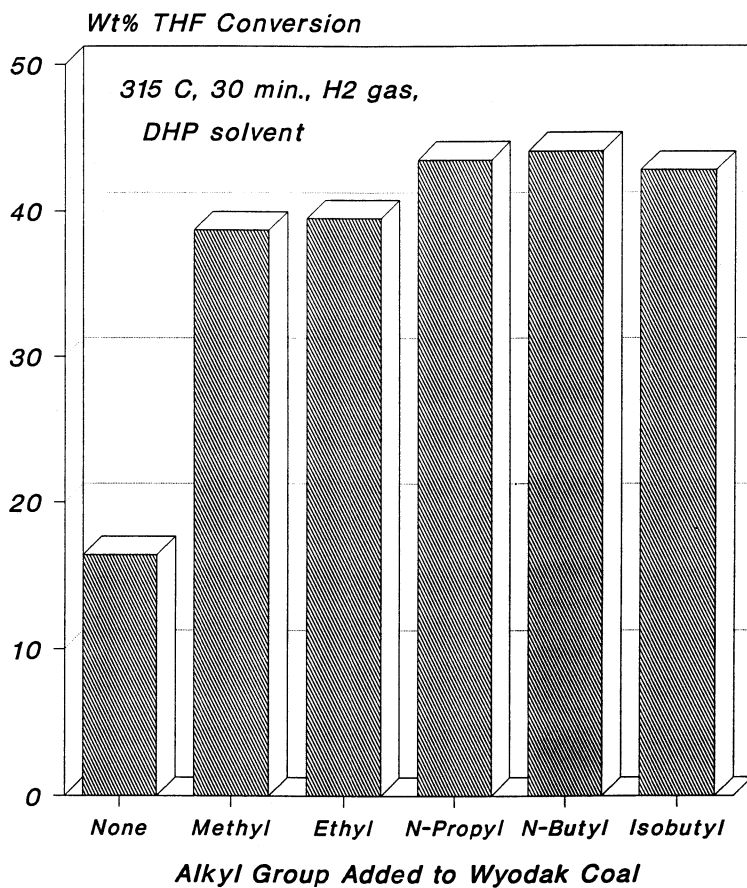


Figure 2. Effect of Alkyl Group Size on Coal Liquefaction Reactivity of Treated Wyodak Coal at Low Severity Reaction Conditions.

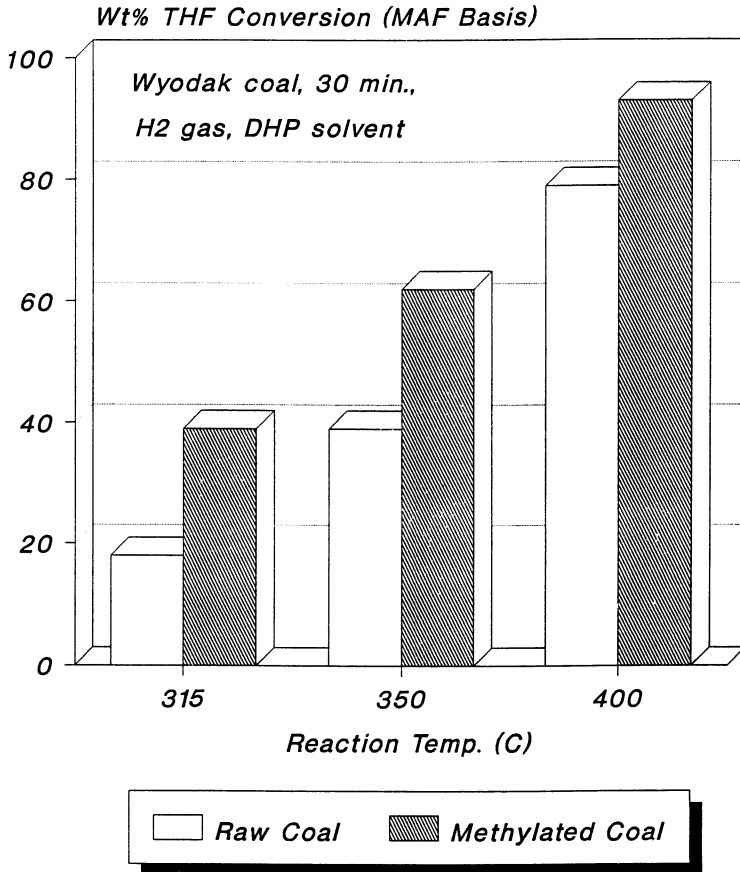


Figure 3. Effect of Reaction Temperature on Liquefaction Reactivity of Methylated and Untreated Wyodak Coal.

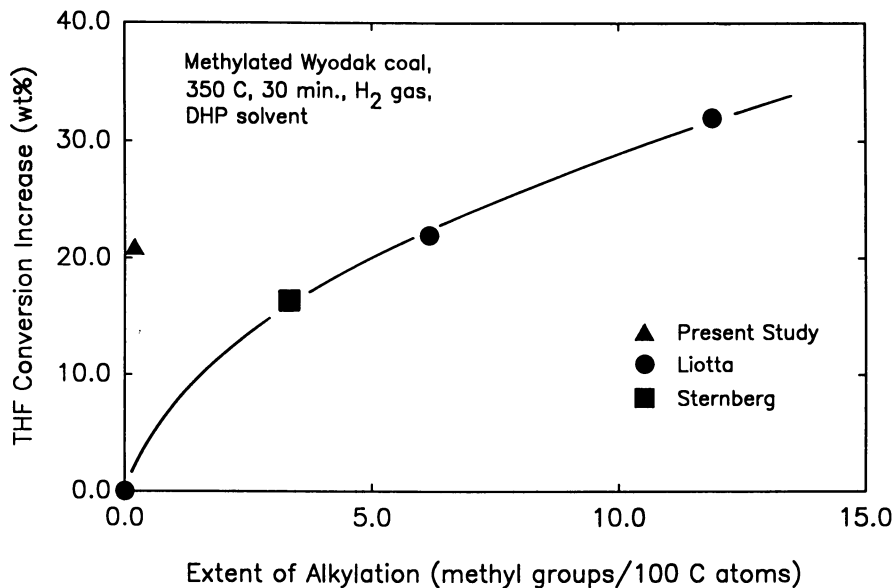


Figure 4. Liquefaction Reactivity Enhancement as a Function of Alkylation Extent for Three Pretreatment Methods.

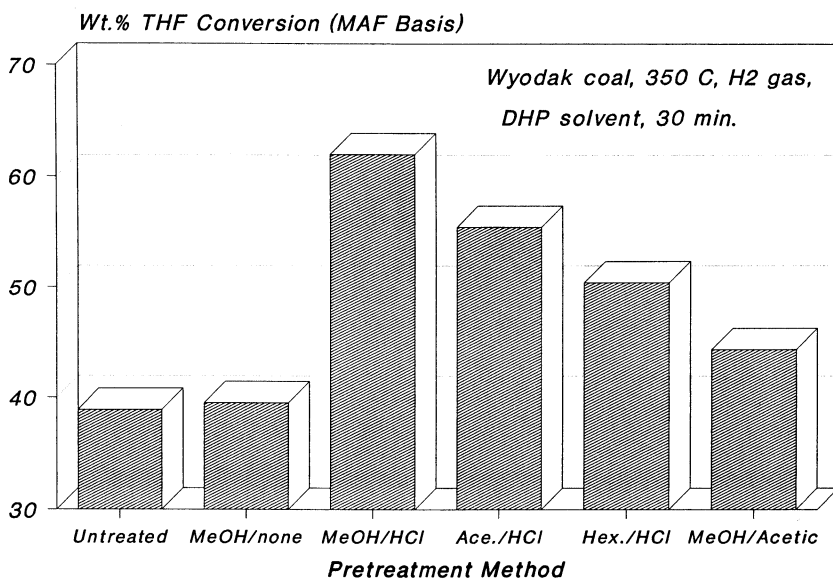


Figure 5. Effect of Various Pretreatment Methods on Enhancement of Low Severity Wyodak Coal Liquefaction Reactivity.

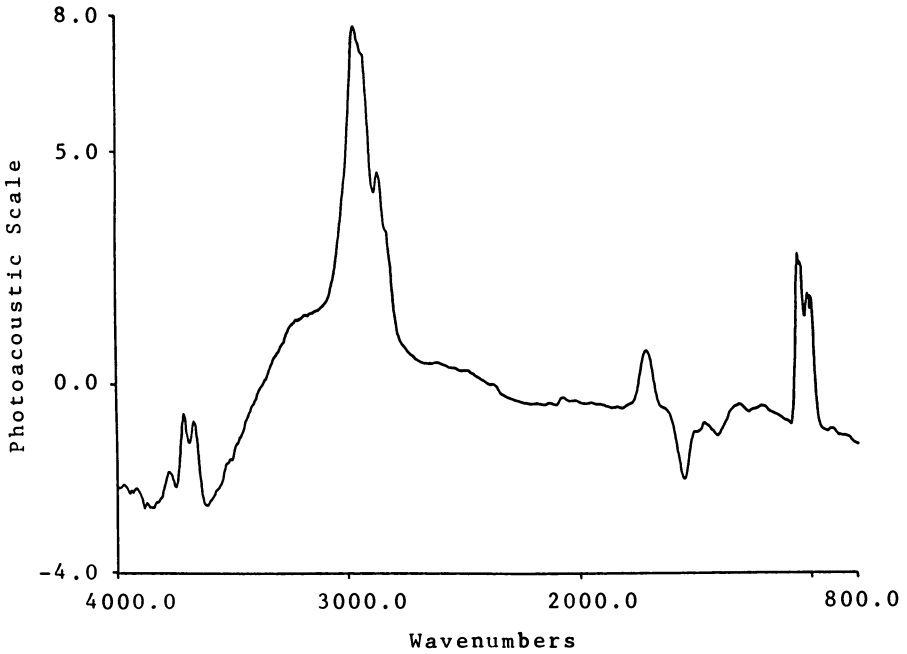
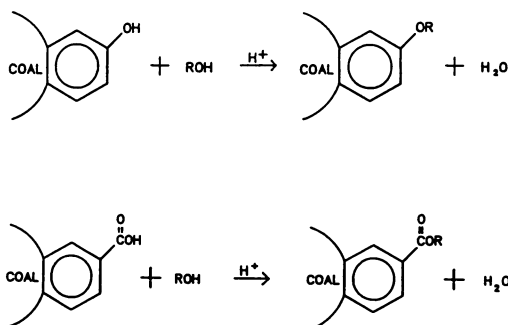


Figure 6. Subtractive Photoacoustic Fourier Transform Infrared Spectrum of Propylated Wyodak Coal.

Taken together, these data suggest that both alkylation and the presence of chlorine ions contributed to the observed liquefaction reactivity enhancement. Although the data are preliminary, we believe that iron pyrite and perhaps other species in the coal mineral matter may be chlorinated to form metal chlorides such as FeCl_3 ; such species are known to be active coal conversion catalysts (11,12).

PAFTIR Studies. In an attempt to begin studying possible reaction mechanisms governing our mild pretreatment method, we analyzed several untreated and treated coal samples using Photoacoustic Fourier Transform Infrared Spectroscopy. Figure 6 shows the unweighted subtractive spectrum (treated coal spectrum minus untreated coal spectrum) for propylated Wyodak coal (3 hrs, 100/1 n-propanol/HCl wt. ratio). Several important features can be identified in this spectrum: 1) reduced O-H stretching in the $3200\text{--}3600\text{ cm}^{-1}$ region, 2) increased aliphatic C-H stretching between 2800 and 3000 cm^{-1} , 3) appearance of the C=O ester stretch near 1700 cm^{-1} , 4) disappearance of the C=O carboxylate stretch near 1550 cm^{-1} , and 5) appearance of C-O aliphatic and aromatic stretches near 1000 cm^{-1} . Spectra from coal samples alkylated using the Liotta procedure (known to be selective to alkylation at oxygen sites only) showed similar characteristics to those identified in Figure 6.

These observations are consistent with the dehydration and esterification reactions shown below:



Both reactions act to reduce hydrogen bonding within the coal structure which may have a direct positive impact on liquefaction reactivity. More indirectly, these reactions lower the concentration of OH species in coal-derived products and hence, reduce the extent of retrogressive condensation via ether bridge formation. Reducing production of THF-insoluble condensation products increases the net THF-soluble coal conversion observed during the liquefaction experiment. None of the spectra from coals pretreated with alkyl alcohols and HCl showed any significant evidence of alkylation at carbon sites in the coal.

Acknowledgments

We wish to acknowledge financial support from the U.S. Department of Energy under Contract No. DE-AC22-88PC88812.

Literature Cited

1. Bockrath, B.C.; Illig, E.C.; Finseth, D.H.; Sprecher, R.F. Prepr. Pap.- Am. Chem. Soc., Div. Fuel Chem. 1984, 29(5), 76.
2. Farnam, S.A.; Wolfson, A.C.; Miller, D.J.; Gaides, G.E.; Messick, D.D. Prepr. Pap.-Am. Chem. Soc., Div. Fuel Chem. 1985, 30(2), 354.
3. Porter, C.R.; Knudson, C.L.; Rindt, J.R. Prepr. Pap.- Am. Chem. Soc., Div. Fuel Chem. 1986, 31(4), 70.
4. Miller, R.L.; Baldwin, R.M. Prepr. Pap.- Am. Chem. Soc., Div. Fuel Chem. 1986, 31(4), 152.
5. Sternberg, H.; Delle Donne, C.L. Fuel 1974, 53, 172.
6. Larsen, J.W.; Kuemmerle, E.W. Fuel 1976, 55, 162.
7. Sharma, D.K.; Sarkar, M.K.; Mirza, Z.B. Fuel 1985, 64, 449.
8. Liotta, R. Fuel 1979, 58, 724.
9. Schlosberg, R.H.; Neavel, R.C.; Maa, P.S.; Gorbaty, M.L. Fuel 1980, 59, 45.
10. Christensen, R.J. Ph.D. Dissertation, Texas A&M University, College Station, Texas, 1987.
11. Derbyshire, F.J. Catalysis in Coal Liquefaction: New Directions for Research; IEA Coal Research: London, June 1988.
12. Anderson, L.L.; Miin, T.C. Fuel Proc. Tech. 1986, 12, 165.

RECEIVED November 5, 1990

Chapter 21

Dispersed Catalysts for Coal Liquefaction

Albert S. Hirschon and Robert B. Wilson, Jr.

Inorganic and Organometallic Chemistry Program, 333 Ravenswood Avenue, SRI International, Menlo Park, CA 94025

Dispersed catalysts formed from aqueous metal salt impregnation and organometallic precursor techniques were investigated for conversion of Illinois #6 and lignite coals into soluble products. The organometallic precursors were found to be exceptionally active and provide the greatest yields of toluene soluble products. We believe the key to effective catalysis is the use of catalyst precursors that give high dispersion and do not require high temperature activation. A positive correlation between loss of oxygen in the final product and extent of conversion was found. Low temperature hydrogenations (300°C) of impregnated coals show that the highly dispersed catalysts seem to aid in forming tetrahydrofuran-soluble materials. Results from hydrogenolysis studies suggest that these catalysts will not break weak links in the coal matrix at these low temperatures, so that a possible alternative is that these dispersed catalysts prevent retrogressive reactions. Higher temperature conversions (400-425°C) were also conducted using either tetralin as a donor solvent, or hexadecane as a non-interacting non-donor solvent. The organometallic impregnation gave conversions to toluene-soluble material in the hexadecane which were almost as high as in tetralin, suggesting that with a well dispersed catalyst, expensive conversion solvents are not necessary for high conversions.

Although great progress has been made in converting coal to distillable liquids in high yields, the products are still not competitive with petroleum. A major problem is that under the severe conditions for bond-breaking during coal liquefaction, retrogressive reactions take place that produce char and coal liquids that are difficult to hydrotreat (1-6). For instance, phenolics are thought to polymerize into polymeric furans during the liquefaction process. For low-rank coals, the carboxylates are thought to be an important factor in these retrogressive reactions. Thus the heterocyclic compounds in the coal liquids produced from coal make coal liquids difficult to upgrade. In order to hydrotreat these materials such high temperatures and hydrogen pressures are required that the valuable aromatic-containing materials in the coal liquid are concurrently hydrogenated.

Dispersed catalytic liquefaction has several distinct advantages over thermal or conventional supported catalytic liquefaction. In the presence of hydrogen, a suitably dispersed catalyst can provide a highly reducing environment within the coal matrix, thus eliminating the need for a good hydrogen-donating solvent. An added advantage to these catalysts is that they can promote certain bond cleavage reactions during the liquefaction step. If they can aid in removing the heteroatoms, namely oxygen and nitrogen, during the early stages in coal liquefaction, then the detrimental regressive reactions would be minimized. Thus a better quality coal liquid product would be produced that would be easier and less expensive to hydrotreat.

Many workers have investigated non-supported high dispersion catalysts (7-16). Most work on dispersed catalysts has focused on metal salts such as ammonium molybdate, pyrites, or oil-soluble catalysts such as molybdenum naphthenate. Derbyshire et al. have conducted considerable research utilizing the $(\text{NH}_4)_2\text{MoO}_4$ and $(\text{NH}_4)_2\text{MoS}_4$ aqueous impregnation methods at low temperatures where they have shown that these dispersed catalysts can effectively utilize hydrogen to aid in subsequent conversions (8-10). The problem with most dispersed catalysts that have been tested is that they are only activated at high temperatures. For instance, ammonium tetrathiomolybdate decomposes to MoS_3 at low temperatures. However, the more active form is MoS_2 is formed at much higher temperatures ($\geq 350^\circ\text{C}$) (17-18). In a similar manner, the molybdenum naphthenate needs to be transformed into MoS_2 . The importance of the correct stoichiometry has been emphasized by Montano et al. (19,20). They have suggested in work on iron sulfide catalysts that the pyrite (FeS_2) must be transformed to pyrrhotite, Fe_{1-x}S , ($0 < x < 0.125$) before it is catalytically active. Under coal liquefaction conditions, the sulfur must diffuse out of the pyrite to allow the transformation to occur. In contrast, when the precursor is $\text{Fe}(\text{CO})_5$, sulfur diffuses into the iron to form highly dispersed pyrrhotite.

Due to the competing retrogressive and bond-breaking reactions occurring during coal liquefaction, having highly dispersed catalysts already in the correct stoichiometry and active state should be essential to produce high quality coal liquids. Since we have been successful in increasing the activities of hydrotreating catalysts by use of organometallic precursors to form highly dispersed catalysts, we are very interested in using these same techniques for direct liquefaction catalysis (21-24). Thus the following work describes our efforts to compare and apply high dispersion techniques to coal liquefaction.

Experimental

The coals used were PSOC 1098 Illinois #6 and Beulah-Zap North Dakota lignite from the Argonne coal bank. The analytical data of these coals are shown in Table I. The ratio of catalyst to coal was approximately 0.6 mmoles of metal per gram of coal. The organometallic catalysts were molybdenum(II) acetate dimer, $\text{Mo}_2(\text{OAc})_4$, obtained from Strem, molybdenum(II) allyl dimer $\text{Mo}_2(\text{OAc})_4$, was prepared by the method of Cotton and Pipal (25). The NiMo supported catalyst was prepared by addition of bis(1,5-cyclooctadiene) Ni(0) (Strem) to sulfided Mo on alumina (22). $\text{Cp}_2\text{Mo}_2(\mu\text{-SH})_2(\mu\text{-S})_2$, referred to as $\text{MoS}_2(\text{OM})$, was prepared by modification of method of Dubois et al. (26), and $\text{Cp}_2\text{Mo}_2\text{Co}_2(\mu_3\text{-S})_2(\mu_4\text{-S})(\text{CO})_4$, $\text{CoMo}(\text{OM})$ was prepared by the method of Curtis et al. (27). Pentacarbonyl iron was obtained from Aldrich, and the sulfur-containing iron cluster, $(\mu\text{-S}_2)\text{Fe}_2(\text{CO})_6$, Fe_2S_2 , was prepared by the method of Bogan et al. (28). Ammonium tetrathiomolybdate, $\text{MoS}_4(\text{Aq})$, was obtained from Alfa Chemicals, and the CoMo dimer, $\text{CoMo}(\text{Aq})$ was prepared by the method of Konigs and Muller et al. (29-31). The organometallic catalysts were impregnated into the coal in tetrahydrofuran (THF) with the exceptions of $\text{Mo}_2(\text{OAc})_4$

where toluene was used, and the iron complexes, where the reaction solvent was used. The solvent was removed by evaporation under vacuum. The molybdenum salt was added as an aqueous solution. For low temperature hydrogenation reactions, 1 g coal was treated for 4 h at 300°C under hydrogen (500 psig cold) as a suspension of 10 mL hexane in a 45-mL Parr bomb. The extent of reaction was monitored by THF extraction. The coal liquefaction experiments were conducted in a 300 mL Autoclave Engineers stirred reactor using 5.0 g of coal, 30 g of liquefaction solvent, and 500 psig hydrogen. For the aqueous impregnation, it was found that the yields could be increased by not completely drying the aqueous impregnated coals. Temperatures of either 400°C or 425°C for 20 minutes using either tetralin or n-hexadecane were used for these conversions. The conversions were calculated from the amount of toluene-insoluble material and are based on daf basis, or the carbon balance, as in the case of the lignite.

Table I. Ultimate and Proximate Analyses of Coals

Coal	Illinois #6	North Dakota Lignite
Ultimate Analysis (Wt % Dry Basis)		
Carbon	67.48	65.85
Hydrogen	4.82	4.36
Nitrogen	1.22	1.04
Sulfur	3.98	0.80
Ash	15.86	9.72
Proximate Analysis (Wt %, As Received)		
Moisture	4.19	32.24
Ash	15.20	6.59
Volatile Matter	33.68	30.45

Results and Discussion

Good coal liquefaction catalysts should also have good hydrogenolysis activities, and therefore, we have looked at methods to improve hydrotreating catalysts. For instance, highly dispersed hydrogenolysis catalysts were prepared by impregnating homogeneous organometallic complexes on an alumina support. The molybdenum(II) allyl dimer is a highly reactive organometallic complex capable of reacting with the surface OH groups on the alumina support (32). The advantage of these methods are that one can create "surface confined" highly dispersed, small particle sized catalysts throughout the support. In contrast, the conventional incipient wetness technique tends to cause large metal clusters to be formed, leaving a low surface area of active catalyst, and thus much lower activities. Table II compares the hydrodenitrogenation (HDN) activities of a NiMo catalyst prepared by the above organometallic approach (OM) using molybdenum(II) allyl dimer, with that prepared by a conventional incipient wetness approach (conv). We have been testing the catalysts as improved HDN hydrotreating catalysts using quinoline as a model. The HDN pathways of quinoline contains two routes to HDN products; one leading to propylbenzene (PB), and the other to propylcyclohexane (PCH). The turnover frequency, TF (moles substrate/moles of metal in catalyst/hr) for the disappearance of tetrahydroquinoline (THQ) and appearance of the hydrocarbon products PB and PCH is listed in Table II. Here, the TF for formation of PCH has

increased from 8.2 to 26.5 and the TF for formation of PB has increased from 0.3 to 1.4. The increased activity is due to a highly dispersed organometallic complex, yielding a high-surface-area catalyst and using the minimum amount of metal. Also note that when a less active catalyst precursor is used, $\text{Mo}_2(\text{OAc})_4$, the HDN activity is far less. The method of preparation and activation of both these complexes were similar, and most likely could not explain the differences in reactivity. We believe the difference in this case is due to a low dispersion of $\text{Mo}_2(\text{OAc})_4$ on the alumina support due to its lack of reactivity with the surface OH molecules. Differences in particle size and dispersion due to method of preparation have been well documented. For instance, Thompson and Carvill recently estimated the particle size of MoS_2 formed from an organometallic molybdenum thiolate precursor to be less than 15Å (33). In contrast, estimates of particle sizes from aqueous impregnation techniques have been in the hundreds of Angstroms (34). Thus the effective surface area and therefore the effective reactivity must be far greater for catalysts formed from the proper organometallic precursors. Generally, the temperature regime of these catalysts for hydrogenolysis of C-N-C and C-O-C linkages is 350°C and above; however, we have found that CoMo catalysts will break C-O bonds as low as 300°C, and thus for the purposes of our coal conversions may be the superior coal liquefaction catalyst.

In order to determine the effect of these dispersed catalysts, we examined both high temperature and low temperature reactions, to gain insight into their relative effectiveness in different conditions. The low temperature reactions were conducted in hexane, as an inert solvent. Such reactions should be much like the dry pyrolysis reactions described by Derbyshire. Table III lists comparisons of the molybdenum complexes prepared by both aqueous impregnation and by organic solutions of organometallic clusters. Ammonium tetrathiomolybdate was chosen as the water-soluble precursor since it is thought to be an excellent hydrogenation and liquefaction catalyst and also can be used to form mixed metal sulfide clusters which may be used as hydrogenolysis catalysts (29-31). For comparison, we used an organometallic sulfido complex, $\text{Cp}_2\text{Mo}_2(\mu\text{-SH})_2(\mu\text{-S})_2$. This complex is an excellent choice as a precursor since it is an easily prepared oil-soluble sulfided molybdenum catalyst and is similar in stoichiometry to the MoS_2 , which is considered the active liquefaction catalyst. As with the aqueous molybdenum salt, it also can be used to form a mixed metal sulfide cluster which can be used to examine the feasibility of a homogeneous organometallic cluster similar to a hydrogenolysis catalyst such as CoMo.

Table III lists the THF solubilities of Illinois #6 obtained as a function of catalyst and method of impregnation. As shown in these data, the impregnation by the wet impregnation technique did little in terms of changes in THF solubility. These results are disappointing in that we had hoped that the impregnation of molybdenum, and especially with mixed metals would aid in cleaving heteroatoms at low temperatures and thus increase the solubility. However, the combination of mixed metals from the aqueous precursors actually gave an insoluble precipitate, thus decreasing the surface area, and most likely decreasing the effectiveness of the catalysts. However, the impregnations with the organometallic complexes and subsequent hydrogenations gave improved THF yields for both the Mo and CoMo complexes, increasing from $\approx 8\text{-}11\%$ for the aqueous baseline to 16-17% for the organometallic pretreatments. Model studies demonstrate that the molybdenum catalysts would not break any heteroatom linkages at these temperatures with the exception of phenolics. The only catalysts that would break these linkages would be the CoMo catalysts; however, no difference was observed between the reactivities of the corresponding CoMo and Mo catalysts, suggesting that the reason for the increased solubilities after the organometallic impregnation is most likely due to increased hydrogenation reactions and perhaps removal of phenolics which may cause retrogressive reactions.

Table II. Turnover Frequencies for Quinoline HDN^a

Catalyst	Precursor	THO	TF ^b	
			PCH	PB
NiMo	Conv	67.4	8.2	0.3
NiMo(OM)	Mo ₂ (OAc) ₄	41	3.4	0.5
NiMo(OM)	Mo ₂ (allyl) ₄	111	26.5	1.4

^aReaction of 10 mL of 0.0197 M quinoline in n-hexadecane and 0.100 g catalyst at 350°C and 500 psig H₂.

^bTF - moles reactant or product/total moles metal/h.

Table III. THF Solubility of Impregnated Coal^a

Pretreatment	Mo%	X% ^b	THF Sol. (wt%)
None	0	0	10
MoS ₄ (aq)	5.0	0	11
MoS ₂ (OM)	4.0	0	16
CoMo(aq)	5.6	1.6	7
CoMo(OM)	-- ^c	-- ^c	17

^aIllinois #6 coal (1.0 g) was impregnated with ammonium tetrathiomolybdate (0.20 g, 0.77 mmol) in 10 mL of water at 250°C for 30 minutes. For the mixed metals, 0.385 mmol of metal salt was added.

^bX refers to the second metal.

^cAnalysis not determined.

The coal liquefaction experiments in tetralin were conducted with a high ratio of tetralin to coal (6 to 1). Therefore, we would expect that the effect of the catalyst in terms of providing a reducing environment or forming an active solvent should be minimized. Thus, any differences we see in conversions should primarily reflect the effect of the catalyst promoting bond breaking reactions (although one could argue that the catalyst is producing low concentrations of reactants derived from the solvent that are actually producing the bond breaking).

Table IV lists some results for conversion of coal into toluene soluble material at 400 and 425°C. The effect of the aqueous molybdenum impregnations for coal conversions at 400°C were found to be quite minimal, with an average increase in coal conversions of only 5%. The molybdenum acetate dimer, $\text{Mo}_2(\text{OAc})_4$ gave a similar increase of about 6%; and the organometallic molybdenum sulfido dimer $\text{Cp}_2\text{Mo}_2(\mu\text{-SH})_2(\mu\text{-S})_2$, provided still greater conversions, with an increase of 13%. The mixed metal catalysts also gave enhanced conversions, with the $\text{CoMo}(\text{aq})$ and $\text{CoMo}(\text{OM})$ impregnations giving a 10% and 19% increase in conversions, respectively. The differences between the organometallic catalyst are even greater when the liquefaction experiments were done at 425°C. The convertibility increased to 84% TS for the $\text{MoS}(\text{OM})$ catalyst, compared to only 69% for the non-catalyzed conversion and 76% for the coal impregnated with aqueous Mo. Thus from these results we see that the organometallic precursors give higher conversions than the catalysts derived from aqueous impregnation techniques, with the highest conversion with the molybdenum sulfido dimer which is already in the correct stoichiometry to form the active MoS_2 catalyst. Additionally, as with hydrotreating catalysts, the mixed metal CoMo catalysts show higher degrees of conversions than the respective Mo catalysts.

To further expand on the differences between these catalysts, conversions were conducted in a non-reactive solvent, n-hexadecane. The advantage of conversions in this solvent is we can distinguish between the effects of the solvent and the catalyst, since tetralin easily allows high conversions because of its H-donating capacity and ability to mediate radical hydrogen transfer reactions. In fact, the inability of the catalysts to significantly increase conversions in tetralin may actually be because of competitive reactions with tetralin. Thus reactions using the inert solvent will eliminate these possible competing reactions, and will be much like pyrolysis reactions. As shown in Table IV and Figure 1a, the $\text{Mo}(\text{aq})$ impregnation increases the conversion from 25% to 41%, while the $\text{Mo}(\text{OM})$ catalyzed conversion gives a 54% yield. This high conversion in hexadecane is significant, in that it is approximately the same as in tetralin at 400°C, suggesting that if the catalyst is well enough dispersed and active, good conversion solvents are not necessary.

Iron catalysts are effective catalysts, although not nearly as effective as the molybdenum catalysts, and are thought to work in a different manner. For instance, the molybdenum catalysts are good hydrogenation catalysts, whereas the iron catalysts appear to function by removing oxygen functionalities. For these reactions, $\text{Fe}(\text{CO})_5$ was compared to the iron sulfido dimer, $(\mu\text{-S}_2)\text{Fe}_2(\text{CO})_6$, designated as Fe_2S_2 . These catalysts were used at the same amounts as used for the molybdenum catalysts, so that lower conversions were expected. In tetralin, both catalysts gave similar conversions for the Illinois #6 as the base-line case, with the $\text{Fe}(\text{CO})_5$ catalyst giving 47% conversion and the Fe_2S_2 catalyst 49% conversion. Interestingly, the TS product of the Fe_2S_2 catalyst was a tar while the product from the $\text{Fe}(\text{CO})_5$ catalyzed reaction was a brittle solid. Experiments with model compounds have shown that the $\text{Fe}(\text{CO})_5$ tends to form tars as well as metal carbides and oxides, whereas the $[\text{SFe}(\text{CO})_3]_2$ shows no evidence of polymerization reactions or other products besides iron sulfides, and we suggest that further investigation of these products will show that later gives a better quality product. The conversions in hexadecane using Fe_2S_2 are slightly higher (29%) than those

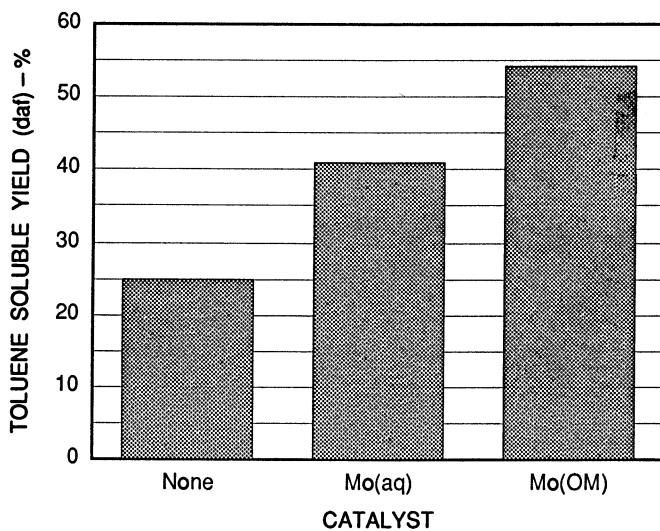
Table IV. Conversion to Toluene Soluble Products^a

Catalyst	Solvent	T (°C)	% TS	%O
None	Tetralin	400	48	6.0
MoS ₄ (Aq)	Tetralin	400	53	4.8
MoS ₂ (OM) ^b	Tetralin	400	61	4.6
Mo ₂ (OAc) ₄ (OM) ^b	Tetralin	400	56	4.8
CoMo(Aq)	Tetralin	400	58	5.6
CoMo(OM) ^b	Tetralin	400	67	4.4
Fe(CO) ₅	Tetralin	400	47	5.0
Fe ₂ S ₂	Tetralin	400	49	5.1
None	Tetralin	425	69	4.0
MoS ₂ (OM) ^b	Tetralin	425	84	2.3
MoS ₄ (Aq)	Tetralin	425	76	4.0
None	Hexadecane	400	25	--
Fe(CO) ₅	Hexadecane	400	24	--
Fe ₂ S ₂	Hexadecane	400	29	--
Mo(aq)	Hexadecane	400	41	--
MoS ₂ (OM)	Hexadecane	400	54	--
None ^c	Hexadecane	425	24	11.6
Fe(CO) ₅ ^c	Hexadecane	425	41	11.0
Fe ₂ S ₂ ^c	Hexadecane	425	39	10.9

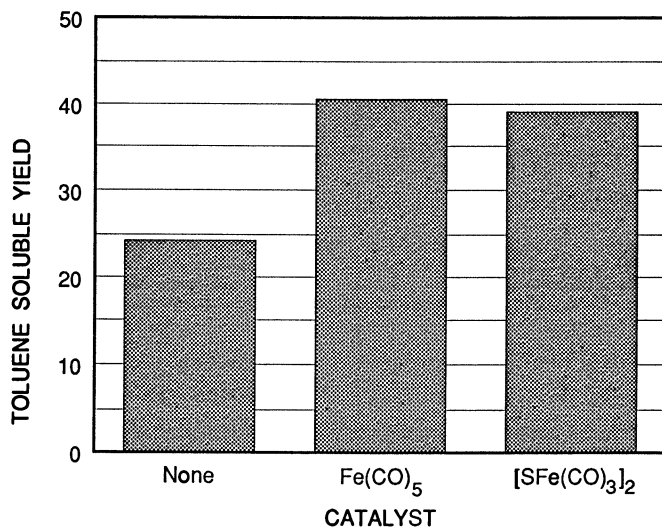
^aReaction conducted in 300-mL autoclave of 5 g Illinois #6 coal in 30 g of tetralin and 500 psi H₂ at 400°C/20 min.

^bOM refers to organometallic precursor.

^cNorth Dakota lignite from Argonne coal bank.



(a) Conversion of Illinois #6 coal with molybdenum catalysts in hexadecane at 400°C.



(b) Conversion of Texas lignite with iron catalysts in hexadecane at 425°C.

daf = Dry-ash-free, Mo(aq) = molybdenum sulfide salt,
 Mo(OM) = organometallic complex (sulfido molybdenum complex).

Figure 1. Coal conversion using various catalysts.

with $\text{Fe}(\text{CO})_5$ (24%) and base line case of 25%. However, these conversions are still similar, and therefore we compared these catalysts for the conversion of lignite, which having larger amounts of oxygen functionalities, should be more susceptible to these catalysts. As shown in Figure 1b, both of these catalysts are quite effective, even in n-hexadecane, with both increasing the conversion by approximately 15%. Thus the iron complexes appear to be best suited towards low rank coals, presumably due to their increased oxygen functionalities.

The oxygen content of the TS product of the catalyzed conversions were found to be lower than those of the non-catalyzed runs. For instance, the molybdenum catalyzed reactions have the lowest oxygen content of 4.6 to 4.8% oxygen, the iron catalyzed reactions give a 5% oxygen content, and the base line runs have an oxygen content of 6-6.5%. The mixed metal organometallic CoMo catalyst produced the lowest oxygen content of 4.4%, consistent with the high HDO activity of CoMo catalysts. The nitrogen content does not seem to be much changed, with the molybdenum catalyzed conversions actually showing a slightly higher nitrogen content. The lower oxygen content is one of the goals of our work, since many of the retrogressive reactions are thought to center through this group. In future work we hope to determine whether the reduction of oxygen occurs during the preconversion reactions as we speculate, or during the more severe reactions during coal conversion.

The nature of the coal impregnated with the catalysts was also examined through use of X-ray diffraction methods. Attempts were made by SEM to determine the dispersion of the molybdenum catalyst by looking both at the starting impregnated coal and the residue of the coal after conversion. However, due to the low concentration of molybdenum and the fact that the X-ray diffraction pattern of molybdenum and sulfur overlap, the dispersion of molybdenum could not be distinguished from the background sulfur. However, the fact that we did see a highly dispersed spectrum and no islands of molybdenum (or sulfur), would indicate that our methods prevented segregation of the catalyst during the dispersion or during the catalytic conversions. Another observation was that the molybdenum in the coal impregnated by aqueous techniques was notably associated with oxygen, presumably as the metal oxide, whereas the molybdenum formed from the organometallic method was not, and was only associated with sulfur. Thus the organometallic method apparently formed the final product which was in the fully sulfided state, (the more active state). The X-ray diffraction pattern of both residues was very weak, and could not be identified, other than they appeared to be similar to a metal sulfide pattern. The X-ray diffraction patterns of the iron complexes were quite similar, showing in both cases, the pattern of pyrrhotite. Thus to form this product iron carbonyl must extract the sulfur from the coal, whereas the sulfido dimer is already in the correct stoichiometry for the product. As with the molybdenum complex, we believe that having the catalyst in the active state as early as possible during the conversion process will aid yields and quality of product. We hope to be able to better understand such effects in future work.

Conclusions

Comparison of the aqueous and organometallic techniques shows that the organometallic route is superior both for hydrotreating reactions and for coal liquefaction reactions. We view this enhancement with the organometallic complexes as the ability to be better dispersed than the aqueous impregnation techniques. The highest activity with the molybdenum sulfido complex, we believe, is because the catalyst was impregnated in a highly active form, and thus does not

require subsequent activation during the liquefaction step. In fact, the sulfido complex has been shown to be active for hydrogenations at room temperature (26). The advantages of our methods are (1) the catalyst can be readily impregnated into the coal and (2) we can design a catalyst such that it transforms directly into the correct stoichiometry for the active form of the catalyst. An important aspect of highly dispersed catalysts are that they can effectively catalyze coal conversion even in poor liquefaction solvents, thus making them very attractive in processes such as coprocessing where inexpensive liquefaction media such as resids are used. Additionally, these types of highly dispersed catalysts should allow researchers an ideal probe to better investigate the mechanism of coal liquefaction by controlling the amount of retrogressive and bond-breaking reactions. In future work, we hope to investigate the scope of these highly active catalysts, and prepare soluble mixed metal clusters which should enhance the liquefaction of coal still further.

Acknowledgements

The authors gratefully acknowledge the partial support of this work by the Department of Energy under Contracts No. DE-FG22-85PC80906 and DE-FG22-87PC79936.

Literature Cited

1. Whitehurst, D. D.; Mitchell, T. O.; Farcasiu, M. Coal Liquefaction--The Chemistry and Technology of Thermal Processes (Academic Press 1980, N.Y.), pp. 207-272 and references cited therein.
2. Sullivan, R. F. ACS Fuel Preprints 1986, **31**(4) 280-293.
3. Sullivan, R. F.; Frumkin, H. A. ACS Fuel Preprints 1986, **31**(2) 325-339.
4. Moroni, E. C. ACS Fuel Preprints 1988, **33**(3) 198-201.
5. Moroni, E. C. ACS Fuel Preprints 1988, **33**(1) 384-386
6. Neuwirth M. B.; Moroni, E. C. Fuel Processing Technology 1984, **8**, 231-239.
7. Garg D.; Givens, E. ACS Fuel Preprints 1983, **28**(5), 200-209.
8. Derbyshire, F. J.; Davis, A.; Epstein, M.; Stansberry P. Fuel 1986, **65**, 1233-1240.
9. Derbyshire, F. J.; Davis, A.; Lin, R.; Stansberry, P.; Terrer, M.-T. ACS Fuel Preprints 1985, **30**(4), 326-332.
10. Mastral, A.; Derbyshire, F. Fuel 1988, **67**, 1477-81.
11. Ha, B.; Ruether, J.; Smith, D.; Mima, J. ACS Fuel Preprints 1988, **33**(3), 343-350.
12. Snape, C. E.; Bolton, C. ACS Fuel Preprints 1988, **33**(3), 351-356.
13. Cugini, A.; Ruether, J.; Cillo, D.; Krastman, D.; Smith, D. ACS Fuel Preprints 1988, **33**(1), 6-19.
14. Curtis, C.; Pellegrino, J. ACS Fuel Preprints 1988, **33**(1), 376-383.
15. Derbyshire, F. J. ACS Fuel Preprints 1988, **33**(3), 188-197
16. Curtis, C.; Pellegrino, J. ACS Fuel Preprints 1988, **33**(1), 376-383.
17. Cotton F. A.; Wilkinson, G. Advanced Inorganic Chemistry 3rd Ed. (Interscience Publishers, N.Y. 1972), p948-9.
18. Satterfield C. N.; Gueltekin, S. Ind. Eng. Chem. Proc. Des. and Dev. 1981, **20**, 62-68.
19. Montano P.; Bommannavar, A. J. Mol. Catal., 1983, **20**, 393.
20. Montano, P. ACS Fuel Preprints 1986, **31**(2), 226.
21. Hirschon, A. S.; Wilson Jr., R. B.; Laine, R. M. ACS Fuel Preprints 1986, **31**(1) 310-317.
22. Hirschon, A. S.; Wilson Jr., R. B.; Laine, R. M. ACS Petr. Preprints 1987, **32**(2) 268-270.

23. Hirschon, A. S.; Wilson Jr., R. B.; Laine, R. M. Advances in Coal Chemistry, N. P. Vasilakos, Ed., 1988, Theophrastus Publications S. A., Athens, Greece, 351-366.
24. Hirschon, A. S.; Wilson Jr., R. B.; Laine, R. M. Appl. Catal. 1987, **34**, 311-316.
25. Cotton, F. A.; Pipal, J. R. J. Am. Chem. Soc. 1971, **93**, 5441-5445.
26. Cowens, B. A.; Haltiwanger, R. C.; DuBois, M. R. Organometallics 1987, **6**, 995-1004.
27. Curtis M. D.; Williams, P. D. Inorganic Chem. 1983, **22**, 2261-2.
28. Bogan, Jr., L. E.; Lesch, D. A.; Rauchfuss, T. B. J. Organometallic Chem. 1983, **250**, 429-438.
29. Konings, A. J. A.; Valster, A.; de Beer, V. H. J.; Prins, R. J. Catal. 1982, **76**, 466-472.
30. Muller, A.; Diemann, E.; Heinsen, H.-H. Chem. Ber. 1971, **62**, 975-980.
31. Muller, A.; Ahlborn, E.; Heinsen, H.-H. Z. Anorg. Allg. Chem. 1971, **386**, 102-106.
32. Yermakov, I. Cat. Rev.-Sci. Eng. 1976, **13**, 77-120.
33. Thompson, L. T.; Carvill, B. T. American Chemical Society 198th National Meeting, Miami Beach, Florida, September 10-15, 1989.
34. Keely, W. M.; Jerus, P.; Dienes, E. K.; Hausberger, A. L. Catal. Rev. Sci. Eng. 1984, **26**, 485-502.

RECEIVED November 15, 1990

Chapter 22

Effects of Oxidation and Weathering on Char Formation and Coal Combustion

Stephen L. Bend¹, Ian A. S. Edwards, and Harry Marsh

Department of Chemistry, Northern Carbon Research Laboratories,
University of Newcastle upon Tyne, Newcastle upon Tyne NE1 7RU, United
Kingdom

This study shows that limited oxidation at 373 K or weathering (ambient) of coal feedstock reduces the thermoplastic properties of a coal. This is manifest as a transformation in char type, from cenospheres to 'inertoids', at high rates of heating (10^4 – 10^5 K s⁻¹) in an Entrained Flow Reactor at 1273 K. The specific types of char are related to the chemical structure of the coal and an inverse relationship exists between the occurrence of cenospheric chars and the atomic O/C ratio of the oxidised or weathered coal from which they are derived.

The oxidation or weathering of coal dramatically influences and alters inherent properties. The effect that oxidation has upon the coking and caking properties of coals, through the loss of plasticity and fluidity, is well documented in the literature (e.g. 1,2). However, few studies discuss effects of oxidation of pulverised-coal feedstock upon pulverised coal combustion. With an ever increasing world trade in coal that requires the temporary stockpiling of coal, at some stage during the shipment of coal to various points of usage, the effects of oxidation upon coal feedstock must be addressed. There are no grounds for assuming that the properties and utilisation characteristics for steam coal are fixed and remain constant throughout time.

Nandi *et al.* (3), in their investigation into the role of inert coal macerals in pulverised fuel combustion, determined that the combustion efficiency of coal was inversely related to the (organically) inert content of the coal feedstock during pilot-scale combustion experiments. Within their category of 'inert' material was what they considered to be particles of oxidised vitrinite. Hamilton (4) comments on differences induced in the appearance of chars produced by heated grid pyrolysis following the laboratory storage of coal for one year. Mahajan *et al.* (5), Jenkins *et al.* (6), and Tromp *et al.* (7) investigated oxidation effects upon 'swelling coal' (mvb rank) using oxidation temperatures ranging from 320–573 K (typically 393–470 K). They comment upon the subsequent enhancement in reactivity, increase in porosity, loss of thermoplasticity and a significant decrease in the production of n-alkane homologues during Curie-point pyrolysis. However, few studies to date (8) have investigated the oxidation and weathering of pulverised-coal feedstock and

¹Current address: Energy Research Unit, University of Regina, Regina, Saskatchewan S4S 0A2, Canada

the differences wrought upon pyrolysis behaviour, char characteristics and the combustion of char using an Entrained Flow Reactor (EFR) and high rates of heating.

Because the mechanisms of oxidation are complex and apparently differ above and below temperatures of 340 to 350 K (2.9-12), this study investigates the comparative differences between and the effects of oxidation at 373 K and weathering, due to exposure to atmospheric conditions, upon char formation and char combustion.

OBJECTIVES.

The overall objective of this study is to investigate the effect of oxidation at 373 K, using static air, and weathering, under atmospheric conditions, upon the pyrolysis and combustion of pulverised coal feedstock using laboratory-based equipment. More specifically:

1. To study and examine the effects of oxidation at 373 K and weathering upon the morphology of associated chars and their physical and structural characteristics using an Entrained Flow Reactor at 1273 K.
2. To study and examine the effects of oxidation at 373 K and weathering upon the subsequent combustion of the char using an Entrained Flow Reactor at 1273 K and possible relationships between the structure of the parent coal and the characteristics of the associated char.

EXPERIMENTAL.

Coals Used and Sample Preparation. Two coals were selected for this study. The first ('A') is a British Coal class 500 and represents a caking coal, whereas the second ('B') is a class 700 which is used as a steam-raising coal within a 1,730 MW coal-fired generating station. An outline of their respective characteristics is given in Table I.

Table I. Selected coal characteristics of coals 'A' and 'B'

Coal	R ₀ max (%)	Rank (ASTM)	Proximate Analyses			Elemental Analyses				Calorific Value MJ kg ⁻¹ (gross)
			VM (wt% dry basis)	FC	Ash	C	H	N	O	
A	0.93	hvAb	35.6	59.3	5.1	81.0	5.3	1.7	12.5	33.6
B	0.76	hvBb	37.2	58.0	4.8	80.5	5.2	1.9	12.4	31.4

The freshly mined samples of coal were received in lump form (>10 cm) within hours of being mined. They were crushed to < 2.5 mm in a mechanical jaw crusher, then sieved in a glove box under nitrogen to a top size of 1.18 mm and subsequently subdivided into twelve individual samples, representing four sample suites, two per coal with six individual samples. One set of five samples from each coal was evenly distributed as a 'monolayer' on flat trays and placed in a covered container in the open air and exposed to the atmosphere. The second set of five samples from each coal was evenly distributed upon flat individual trays and placed in a large heated receptacle and oxidised at 373 ± 5 K in static air. The sixth sample from each coal suite was analysed immediately and used as the datum sample. Samples of weathered and oxidised coal were removed periodically for analysis, thereby providing the oxidised and 'weathered' samples. The coals were crushed and sieved to the required size fractions under an atmosphere of nitrogen in a glove box.

Analytical Techniques. A Stanton Redcroft STA 780 Thermal Gravimetric Analyser was used for all proximate analyses (13). Calorific value determinations were obtained using a Gallenkamp Adiabatic bomb calorimeter. A Carlo Erba 1160 elemental analyser was used for the analysis of carbon, hydrogen and nitrogen, oxygen (plus sulphur) being determined by difference. The infra-red spectra of the coals were obtained using a Nicolet 20 SXB Fourier-transform infrared spectrometer with the KBr pellet technique. All coal petrographic analyses were conducted using a Leitz MPV3 microscope photometer. Vitrinite reflectance (% R_0 random) was determined on crushed particulate (< 212 μm) mounted blocks and based upon 100 measurements on the sub-maceral telocollinite; maceral analyses were also conducted on crushed particulate-mounted blocks, using a Swift point-counting device with a total of 500 individual counts and interpoint and interline distances of 50 μm and an overall magnification of x 800.

Chars were produced from the coals (38 to 75 μm size fraction) in a vertical, electrically heated, Entrained Flow Reactor [EFR] (Figure 1.) using nitrogen at 1273 ± 5 K with heating rates of $10^4 - 10^5$ K s^{-1} . The gas flow rate was 38 l min^{-1} creating laminar flow conditions and thereby producing the required coal particle residence time of 1 second, the sample feed rate being 0.5 g min^{-1} . The cross-sectional morphology and optical texture of the char form the criteria for their classification, which is based upon a modified system proposed by Bailey and Diessel (Bailey, J. G. and Diessel, C. F. K., 1987: presentation to Committee of the I. C. C. P.). An outline of the char classification used, their respective criteria and characteristics are given in Table II. The quantitative analyses of the chars were achieved using a Swift point-counter and a Leitz MPV3 microscope photometer, at an overall magnification of x 800, in conjunction with the classification table presented in Table II. The internal (macro) porosity of each char was derived by Image Analysis using transmitted light microscopy on thin sections (5 μm thick) of epoxy mounted char. A Jeol JSM T-20 scanning electron microscope (SEM) was used to examine the surface topography of selected chars. The surface area analysis of selected chars was obtained by adsorption of carbon dioxide using the single point method (14). Char combustion was achieved using the EFR at 1273 ± 5 K with air as the gasification medium. The proportion of un-burnt carbon within the combustion product was determined using the 'ash-tracer technique' (15).

RESULTS.

Oxidation and Weathering Effects upon Coal Structure. The proximate analyses of oxidised coals 'A' and 'B' show an initial rapid loss in volatile matter content with a subsequent gradual decrease in the rate of loss as the duration of oxidation increases (16). The levelling-off after 32 days suggests that no further significant decrease in volatile matter content yield occurs beyond that time at 373 K. The rate of volatile matter loss was greater for the oxidised series of coals than for those weathered over a similar period of time. Like the oxidised coal suites, the levelling off between 32 and 52 weeks suggests that further decrease in volatile matter content yield would be slight following weathering under ambient conditions.

The trends for volatile matter content yield are associated with a similar decrease in elemental hydrogen and carbon in preference to oxygen, although the rate at which carbon and hydrogen decrease is dependent upon the severity of the conditions of oxidation or weathering, as noted previously (17,18). Figure 2 illustrates the reversed trend in the atomic O/C ratios induced by oxidation (at 373 K) or weathering, compared to the normal decrease in the atomic O/C ratio associated with coalification (18), illustrating that the O/C

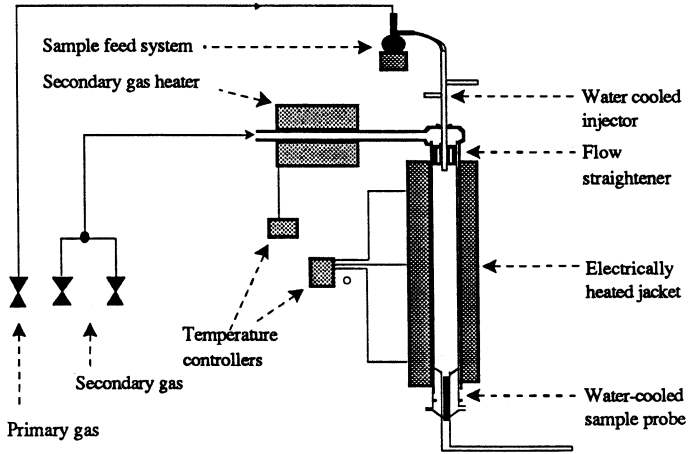


Figure 1. A Schematic representation of the Entrained Flow Reactor apparatus.

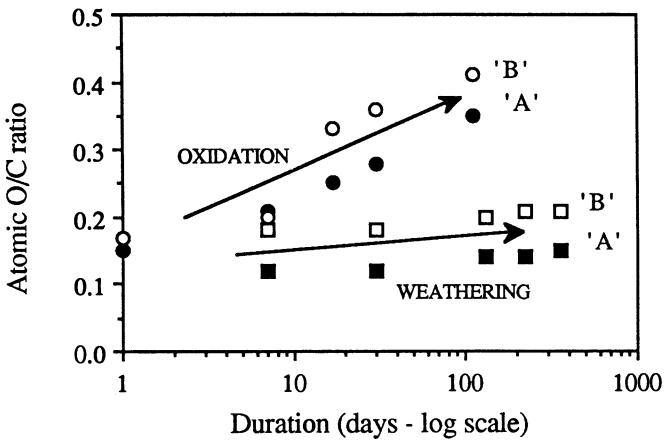


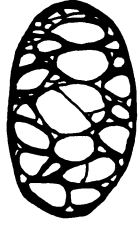



Figure 2. The Atomic O/C ratios for the oxidised and weathered coals against the log of time.

Table II. Char Morphology Nomenclature, Classification, Criteria And Typical Profiles (after Bailey and Diessel 17)

Class	Sub-class	Optical Texture	Criteria
Coal Particle	Unchanged- -with pore development		-no softening, no vesiculation little change in vitrinite reflectance. -softening, some vesiculation but recognisable as coal.
Cenosphere	Mono-	Isotropic or Anisotropic	-spherical - subspherical in shape, single chamber, no secondary or tertiary vesiculation within the char wall, porosity $\geq 70\%$.
	Tenui-	Isotropic or Anisotropic	-spherical - subspherical in shape, one large chamber, some secondary or tertiary vesiculation within the char wall, char wall thickness $\leq 5\mu\text{m}$, porosity $\geq 65\%$.
	Crassi-	Isotropic or Anisotropic	-spherical - subspherical in shape, one large chamber with pronounced secondary or tertiary vesiculation within the char wall, wall thickness $\geq 5\mu\text{m}$, porosity $\geq 65\%$.
Cenospheropore		Isotropic or Anisotropic	-subspherical to elongate, consisting of more than one large rounded chamber, char wall thickness $\geq 5\mu\text{m}$, porosity $\geq 65\%$.
Network	Tenui-	Predominantly Isotropic	-elongate to oblong, consisting of many sub-parallel elongate chambers, char wall thickness $\leq 5\mu\text{m}$, porosity $\geq 65\%$.
	Crassi-	Isotropic or Anisotropic	-elongate to oblong, consisting of many sub-parallel elongate chambers, char wall thickness $\geq 5\mu\text{m}$, porosity $\leq 65\%$.
	Mixed-	Isotropic or Anisotropic	-variety of shapes or porosities, char wall thickness and/or optical texture.
Solid	Inertoid	Predominantly Isotropic	-solid, massive particle with no vesiculation, coal precursor material not recognisable, high reflectance: solid, massive particle with no vesiculation.
	Fusinoid	Predominantly Isotropic	-coal precursor material recognisable as fusinite, high reflectance.
Fragment	(no equivalent) < 10 μm .		
Typical Profiles:			
	Cenosphere	Cenospheropore	Network
			
			Solid 50 μm

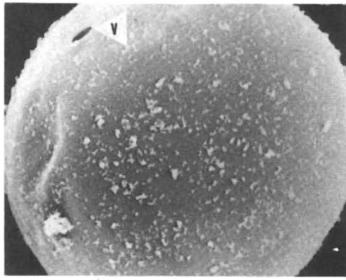
ratios increase for both the oxidised and weathered coals at the expense of hydrogen and carbon, but at different rates over the same period of time.

The removal of hydrogen is supported in this study by Fourier transform infrared spectroscopy (FT-ir), which indicates that the main processes occurring during the oxidation of coals 'A' and 'B' are the progressive removal of aliphatic hydrocarbons and the inclusion of oxygen-bearing functionalities within the molecular structure of the coal. The removal of aliphatic hydrocarbons, such as $=\text{CH}_2$ and $-\text{CH}_3$ and CH- groups, is indicated by a decrease in the absorption bands occurring at 2920, 2850 and 1435 cm^{-1} (19.23) for both oxidised coal suites. The absorption bands occurring between 1580 cm^{-1} and 1750 cm^{-1} are attributed by other workers to specific oxygen-bearing functional groups, which include carboxylic acids [1580-1590 cm^{-1}] (19.24) ketones [1620-1700 cm^{-1}] (12.25) carbonyls in acids [1690-1718 cm^{-1}] and anhydrides [1770 cm^{-1} and 1843 cm^{-1}] (21.26)

In contrast, the weathered series of coals show a markedly different trend, the most notable difference being the development of a pronounced, broad, absorption band at $\approx 3380 \text{ cm}^{-1}$ after a period of 19 weeks, attributable to OH- stretching vibrations (20.26); this trend is more pronounced within the weathered 'B' coal series. The OH- stretching band diminishes for both coals exposed to the atmosphere for periods in excess of 19 weeks in this study, although it is not clear whether this is attributable to changes in ambient conditions (i.e. seasonal variations) or is due to the formation of ether and/or ester linkages. Also, in contrast to the oxidised coal series (373 K/air), the slight decrease in aliphatic CH- stretching bands at 2920-2850 cm^{-1} occurs over a longer period of time with respect to the weathered 'A' series with little apparent change for the weathered 'B' series within the resolution of the associated spectra.

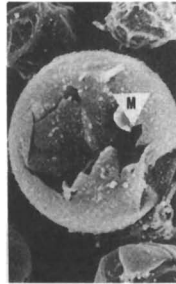
The effect of oxidation at 373 K or weathering upon vitrinite reflectance values induces changes in the determined values that reflect the severity (temperature) of the conditions used. The oxidised (373 K) coals show an increase to approximately 20 to 25% above the original values for the fresh coals after a period of three months (i.e. 0.93 to 1.16%, 0.76 to 0.98%). In contrast, the reflectance values for the weathered coals decrease over a similar period of time, from 0.93% and 0.76 to 0.86% and 0.68% for coals 'A' and 'B' respectively, in agreement with the work of Puetmann *et al* (27). Clearly, the temperature used within this study governs the structural changes occurring during the oxidation or weathering of coals 'A' and 'B'. This would support the growing consensus of opinion that different oxidative processes occur above and below 70 to 80°C (340-350 K).

Char Morphology And Combustion: Oxidation Effects. The transformation in char morphology, due to the pyrolysis of progressively oxidised coals in the EFR, is shown in Plate 1 for coals of the 'A' series and the nomenclature used defined in Table II. Coal 'A' generates a predominance of optically anisotropic, single chambered, cenospheric chars upon pyrolysis at 1273 K when fresh (Plate 1a). The char produced from the fresh coal 'A', possess only the occasional large single vent, with indications that the closure of small devolatilisation vents ($< 2 \mu\text{m}$) due to thermal annealing has occurred. However, after a period of oxidation for 7 days (Plate 1b) the initial high proportion of cenospheric char is replaced by chars exhibiting a more complex internal multi-chambered structure, i.e. *cenosphere network*, which are ultimately replaced by dense *inertoid* chars (Plate 1c) exhibiting no internal macro-porosity or particle swelling. Using averaged values, the internal porosity (void space) for each of the recognised classes of char decreases from +70% (cenospheres), through 65% (tenuinetwork) and 45% (crassinetwork) down to less than 20% for those within the solid inertoid class. The transformations in char



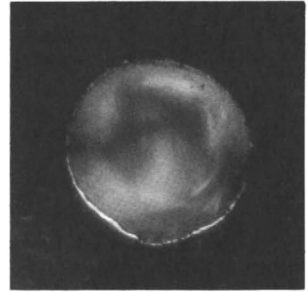
1a (i)

50µm



(ii)

100µm



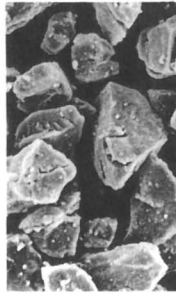
(iii)

50µm



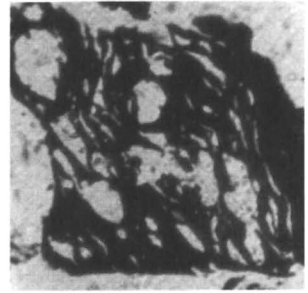
1b (i)

7.5µm



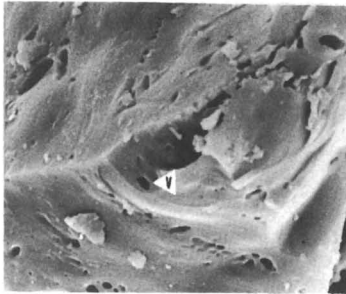
(ii)

100µm



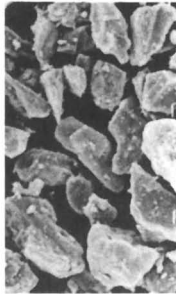
(iii)

25µm



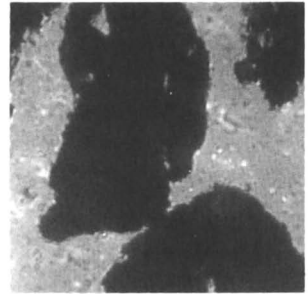
1c (i)

7.5µm



(ii)

100µm



(iii)

25µm

Plate 1. Scanning Electron Microscope and Optical Microscope Micrographs of selected char from oxidised 'A' series coals. 1a., char produced from fresh coal. 1b., char from coal oxidised for 17 days. 1c., char from coal oxidised for 112 days. V, devolatilisation vent, M, mechanical damage.

morphology, due to oxidation, is accompanied by the development of visible porosity on the outer surfaces of chars as shown in the SEM micrographs (Plate 1). Furthermore, increases in visible porosity within the outer char wall, due to oxidation, is accompanied by significant increases in micro-porosity indicated by an increase in surface area from 60 to 250 m² g⁻¹ for the 'A' series and from 160 to 270 m² g⁻¹ for the 'B' series.

Coal 'A' is associated with a greater caking propensity than coal 'B' and therefore the effect of progressive oxidation is more pronounced for coals of the 'A' series through a noticeable loss of swelling and softening characteristics, accompanied by an elimination of all visible optical anisotropy within the char after the oxidation of the parent coal for one week. However, the replacement of cenospheres by chars of lower thermoplasticity is common to both coal series (Figures 3 and 4).

The char burn-out characteristics (Figure 5), measured by the proportion of unburnt carbon remaining within the char combustion residue, show a marked decrease in the level of unburnt carbon due to the progressive oxidation of the parent coal within the first 7 days. This coincides with a marked decrease in optical anisotropy, a decrease in the proportion of cenospheric chars and an increase in the proportion of network chars and an increase in surface area; although despite differences in their initial unburnt carbon levels (28.0% and 2.2% for coals 'A' and 'B' respectively) during that initial period of oxidation the trends relating to char burn-out characteristics are somewhat similar. However, differences exist between the 'A' and 'B' series in their relative combustion efficiencies following prolonged oxidation at 373 K beyond 17 days (Figure 5). The level of unburnt carbon within the extensively oxidised coals of the 'B' series significantly increases, exceeding the initial unburnt carbon value of 2.2% for the fresh coals, whereas the unburnt carbon levels within the extensively oxidised 'A' series coals show only a modest increase (<1.6%). This suggests that the oxidation of a caking coal (i.e. 'A' series), for a limited period of time, significantly improves char gasification through the formation of chars associated with an isotropic optical texture (more disordered structure) and increased char wall porosity. However, there appears to be a point beyond which char burn-out (gasification) is not improved by the oxidation (373 K/air) of parent coals and consequently levels of unburnt carbon increase within the combustion residue, the extent of which is possibly related to the original coal rank and is discussed below.

Char Morphology And Combustion: Weathering Effects. The changes in char characteristics, due to weathering, are less severe and more gradual than those changes induced by oxidation at 373 K over the same period of time (Figures 6 and 7). For example, the weathering of coals 'A' and 'B' for 32 weeks produces a similar distribution in char type than can be achieved in 1 day at 373 K (Figures 3 and 4), with no apparent change in the proportion of cenospheres due to the weathering of the parent coals during the initial four week period (Figures 6 and 7). Similarly, the elimination of optical anisotropy and increase in visible char-wall porosity within chars produced from weathered coals 'A' and 'B' is much more gradual.

Coals of the weathered 'A' series show a significant improvement in char burn-out during the initial four week period (Figure 8), with unburnt carbon levels decreasing from 29% to 7%. Beyond that initial period the rate at which char gasification is enhanced by weathering of the parent coal decreases, generating an asymptotic curvilinear relationship. In contrast, the decreasing levels of unburnt carbon for the weathered 'B' series exhibit a more linear relationship over the total duration of weathering, decreasing from 2.2% to almost zero (0.4%) after one year.

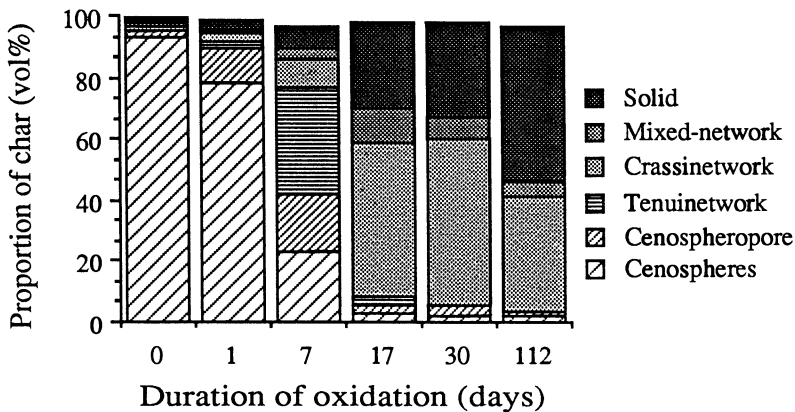


Figure 3. Coal series A and the change in char type with oxidation (373 K).

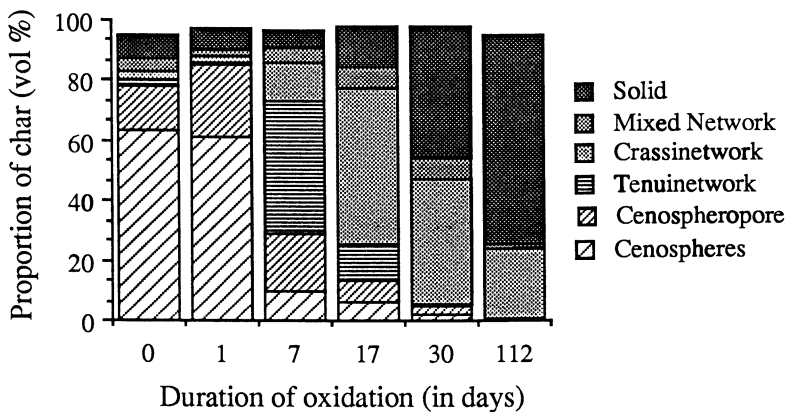


Figure 4. Coal series B and the change in char type with oxidation (373 K).

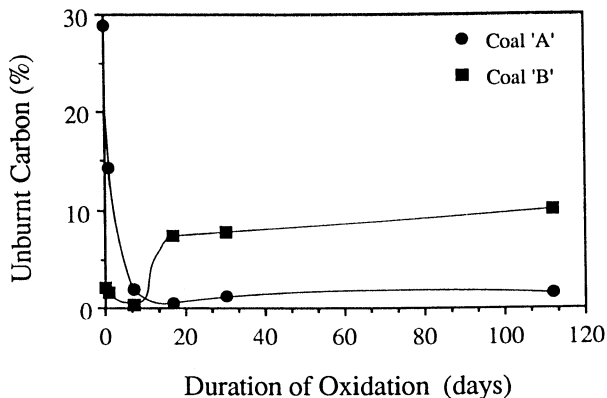


Figure 5. The changes in the level of unburnt carbon within the combustion product of char derived from coals of the oxidised series A and B.

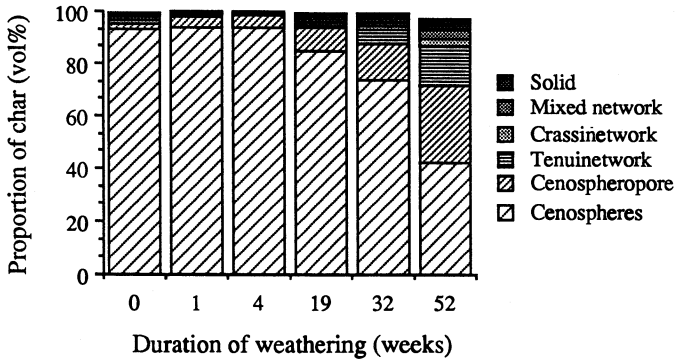


Figure 6. Coal series A and the change in char type with weathering.

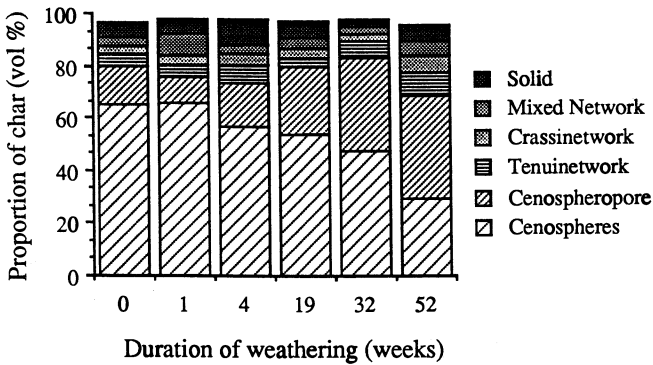


Figure 7. Coal series B and the change in char type with weathering.

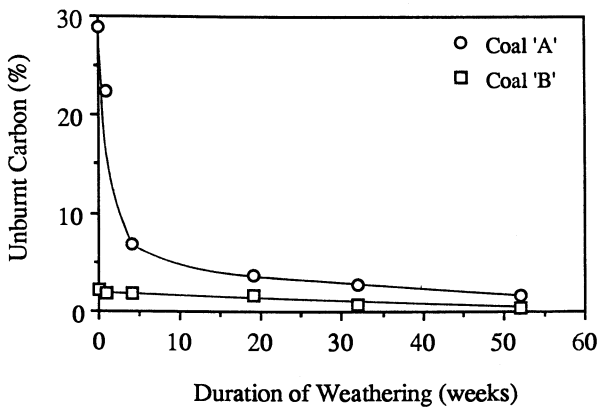


Figure 8. The changes in the level of unburnt carbon within the char combustion product derived from the weathered coal series A and B.

DISCUSSION.

Oxidation And Weathering Effects Upon Char Characteristics and Combustion.

It is a current axiom that the oxidation of a caking coal reduces subsequent thermoplasticity and fluidity upon heat treatment at slow rates of heating. At high rates of heating (10^4 to 10^5 K s⁻¹) the effects are somewhat similar. The formation of cenospheres from fresh vitrinite-rich coals during pyrolysis in an EFR indicates the formation of a *bubble-like* structure of minimum surface energy by a 'fluid' devolatilising material (metaplast). A comparison of the characteristics of the chars produced from oxidised or weathered coals, by rapid heating (10^4 to 10^5 K s⁻¹) at 1273 K, indicates that the progressive oxidation or weathering of high volatile bituminous coals leads to the gradual elimination of inherent fluid properties, an increase in density and the production of chars from metaplast of increased surface energy (i.e. non-spherical). The changes in char morphology as a direct consequence of oxidation or weathering can be illustrated thus:



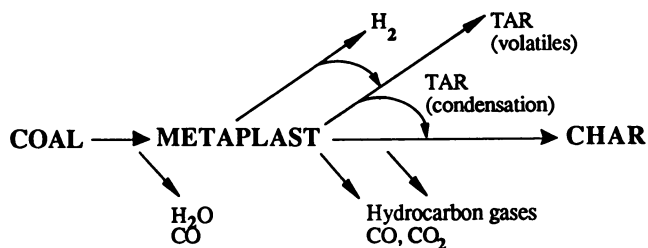
A loss of metaplast fluidity during pyrolysis is further evidenced by the appearance of devolatilisation vents ($< 2 \mu\text{m}$) within the outer wall of the char (Plate 1). A characteristic previously discussed by Mahajan *et al.* (5) and Maloney and Jenkins (6) is the inhibition of thermal 'annealing' due to the oxidative pre-treatment of the parent coals. The premise is that the absence of small devolatilisation vents, within the outer char walls, is attributable to the closure of devolatilisation vents through the maintenance of metaplast fluidity. Alternative devolatilisation theories, such as 'jet release' or 'evaporative' mechanisms and the collapse of preexisting pores due to surface tension effects are also suitable theories that can account for the lack of small devolatilisation vents in chars formed from caking coals. This study concurs with the work of Mahajan *et al.* (5) that the limited oxidation (or weathering) of parent coals increases the surface area of the char and increases the outer char wall porosity. This is possibly due to an increase in localized devolatilisation, or alternatively through the maintenance and enlargement of preexisting pores in non-softening particles that are derived from highly oxidised coals. Of further significance concerning the enhancement of gasification rates, is the creation of char in which the molecular structure of the char becomes increasingly disordered in response to the weathering or oxidative pre-treatment of parent coals. This is demonstrated within the oxidised 'A' series by the transformation in optical texture from chars exhibiting anisotropic fine grained mosaics to optically isotropic chars. It is believed that optically isotropic chars contain a greater number of edge carbons, structural defects and available surface area than optically anisotropic char. Therefore, the enhancement in gasification and reduction in the level of unburnt carbon during char combustion can be attributed to the development of an accessible porosity and a probable increase in available surface area. However, differences in the relative combustion performance of the chars of this study suggest that there is a point beyond which char burn-out (gasification) is not improved by the oxidation of parent coals. This is attributed to the formation of dense particles that have a very limited pore size distribution (i.e. predominantly micropores) and therefore inaccessible to reacting gases within the residence time permissible. Consequently levels of unburnt carbon increase within the combustion residue. The transformations in char characteristics and the loss of thermoplastic properties due to oxidation or weathering,

described above, can be related to transformations within the chemical structure of the parent coals and subsequent particle behaviour during pyrolysis.

Relationships Between Coal Properties, Char Morphology and Combustion.

FT-ir spectroscopy indicates that the most recognizable structural changes occurring within coals 'A' and 'B' due to oxidation or weathering is the loss of aliphatic groups (-CH-, -CH₂, -CH₃-) and the inclusion of oxygen-bearing functionalities. The rates at which such changes occur and the nature of the oxygen-bearing functional groups are strongly dependent upon the severity (i.e. temperature) of the conditions employed. The atomic O/C ratios of coals 'A' and 'B' increase due to oxidation or weathering, but at different rates that also reflect the severity of the oxidising or weathering conditions. Such changes in the chemical structure of the parent coals can be related to the generation of specific types of char. The formation of cenospheres, which are characterised by pronounced swelling, low char wall porosity, low surface area and an anisotropic optical texture, is inversely related to the atomic O/C ratio of the parent coal, either as a function of oxidation or weathering (Figure 9). The formation of chars of lower thermoplasticity (e.g. network) bear a normal relationship to the O/C ratio of the parent oxidised or weathered coal. Similarly, the level of unburnt carbon within the char combustion product can be related to the atomic O/C ratio of the parent coals (Figure 10), irrespective of whether the parent coals were oxidised at 373 K or weathered under ambient conditions; in each case the level of unburnt carbon attains a minimum value (i.e. almost complete char gasification) where the O/C ratio for parent coals is approximately 0.20. This value coincides with the the virtual elimination of char optical anisotropy and the development of multi-chambered, fenestrated chars of high internal porosity. Similar relationships exist for fresh, vitrinite rich coals of different rank (28).

The loss of fluidity has been linked to concomitant decreases in the concentration of aliphatic CH groups, which have been favoured as the major source of donatable hydrogen during pyrolysis considered necessary to saturate radicals formed during bond scission. During pyrolysis the coal structure decomposes through the thermal dissociation of weak bridges (e.g. methylene), creating radicals that are either stabilised, primarily through hydrogen addition to form stable volatile species, or recombine forming char (29,30). This is represented through an adaptation of the model proposed by Unger and Suuberg (31):



The reduction in thermoplasticity of the metaplast is possibly the result of the promotion of aromatisation/char condensation reactions at the expense of the production of stable volatile species during coal pyrolysis. In this way, the generation of specific char types at 1273 K in the EFR can be related to the proportion of elemental oxygen within the original coal structure of the oxidised or weathered coal particle; below an atomic O/C ratio of ≈ 0.15 the predominant char is that of the cenosphere variety due to the maintenance of metaplast fluidity during pyrolysis.

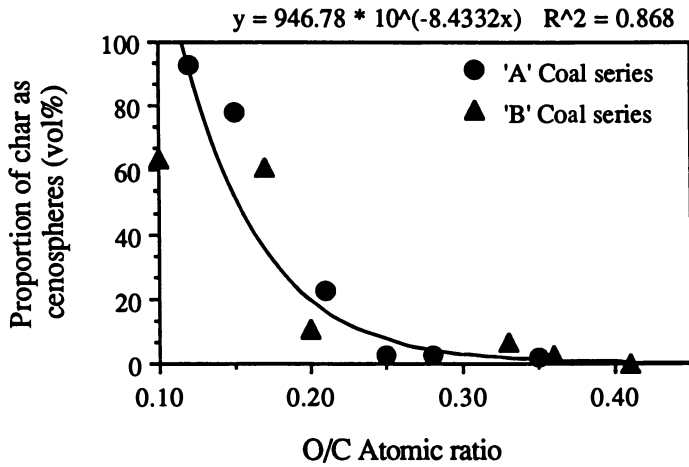


Figure 9. The proportion of char occurring as cenospheres and the O/C atomic ratios for the oxidised coals (373 K).

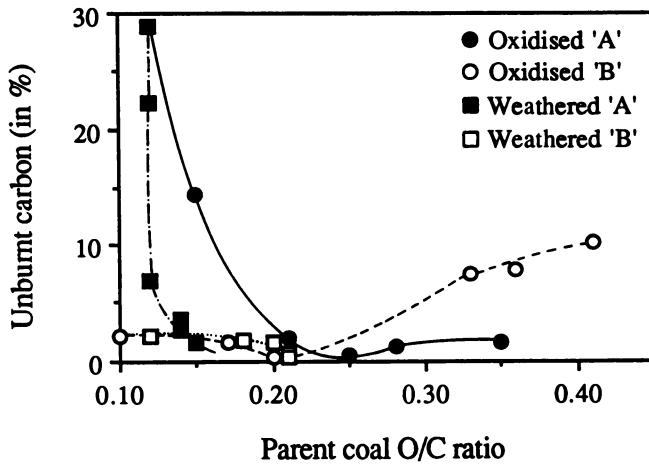


Figure 10. The relationship between unburnt carbon within the char combustion product and the atomic O/C ratio of the parent coals.

Such correlations have important bearings on the current level of understanding regarding the mechanisms of pyrolysis devolatilisation and char formation. Furthermore, standard forms of analyses are subject to oxidation or weathering effects and this study demonstrates that correlations between levels of unburnt carbon and vitrinite reflectance (33) maybe potentially misleading unless the affects of oxidation or weathering are considered.

CONCLUSIONS.

1. Progressive oxidation or weathering of coal affects the physical and structural characteristics of chars produced during coal pyrolysis at 1273 K in an EFR. The transformation in char morphology can be related to the loss of thermoplastic properties, as a direct consequence of oxidation or weathering. The oxidation at 373 K or weathering of coal under ambient conditions for limited periods of time forms highly vesiculated, fenestrated chars with high surface areas, a reduction in swelling and an isotropic optical texture. Extensive oxidation at 373 K produces dense chars that undergo little devolatilisation.

2. The changes in char morphology can be related to the properties of the parent coal, in that an inverse relationship exists between the O/C ratio of the parent coal and the formation of cenospheric char. Similarly, relationships exists between levels of unburnt carbon within the char combustion residue and the O/C ratio of the parent coal. The oxidation or weathering of a caking or weakly caking coal significantly increases rates of char gasification, apparently due to the development of an accessible porosity within the char wall material and an isotropic optical texture.

However, the question whether the combustion of oxidised or weathered pulverised coal would maintain a self-sustaining flame in a full-size industrial boiler at maximum load cannot be addressed within the present study. The inhibition of volatile matter release, due to the promotion of char condensation reactions during coal pyrolysis, suggests that this may not be the case, a point pertaining especially to the more severely oxidised coals (i.e. 373 K for 112 days). Clearly there is need for future work within this area of pulverised coal combustion.

Acknowledgments.

This study was funded in part by the Commission of the European Communities, Non-Nuclear Energy R and D Programme, Contract No. EN3F.0040.UK(H). One of us (SLB) would like to thank Mr. Jim Pearson of British Coal for kindly providing the samples of fresh coal, Mr. C. Spracklin for conducting the surface area analyses and Mrs. B. Crawford for assisting with the Scanning Electron Microscopy.

Literature Cited

1. Schmidt, L. D. In Chemistry of Coal Utilisation, Lowry, H. H. Ed., John Wiley and Sons. New York, 1945; Volume 1, 627-676.
2. Larsen, J. W.; Lee, D.; Schmidt, T.; and Grint, A. Fuel. 1986, 65, 595-96.
3. Nandi, B. N.; Brown, T. D.; and Lee, G. K. Fuel. 1977, 56, 125-30.
4. Hamilton, L. H. Fuel. 1981, 60, 909-13.
5. Mahajan, Om. P.; Komatsu, M. and Walker, Jr., P. L. Fuel. 1980, 59, 3-10.
6. Jenkins, R. G.; Nandi, S. P. and Walker, Jr. P. L. Fuel. 1973, 52, 288-93.

7. Tromp, P. J. J.; Kapteijn, F.; Boon, J. J. and Moulijn, J. A. In Int. Conf. on Coal Science; Moulijn J. A.; Nater, K. A. and Chermin, H. A. G. Eds.; Elsevier Science Pubs: B.V. Amsterdam, 1987; 537-41.
8. Maloney, D. J. and Jenkins, R. G. Fuel. 1985, 64, 1415-22
9. Albers, G.; Lenart, L. and Olert, H. H. Fuel. 1977, 53, 47-53.
10. Chamberlain, E. A. C.; Barrass, G. and Thirlaway, J. T. Fuel. 1976, 55, 217-23.
11. Jakab, E.; Hoesterey, B.; Windig, W., Hill, G. R. and Meuzelaar, H. L. C. Fuel. 1988, 67, 73-9.
12. Martin, R. R.; MacPhee, J. A.; Workinton, M. and Lindsay, E. Fuel. 1989, 68, 1077-79.
13. Ottaway, M. Fuel. 1982, 61, 713-16.
14. Field, D. J. PhD Thesis. University of Newcastle upon Tyne. 1989.
15. Nskala, N., Walker, P. L. and Essenhigh, R. H. The Characteristics of Chars Produced by Pyrolysis Following Rapid Heating of Pulverised Coal. Technical Report 2, 1977, Pennsylvania State University, Contract No. E(49-18)-2030.
16. Bend, S. L., Edwards, I. A. S. and Marsh, H. In Recent Advances in Coal Science: A Symposium in Remembrance of P. Given. ACS Preprints 34. No. 3. Miami Beach, 1989. 923-30
17. Axelson, D. E., Mikula, R. J. and Munoz, V. A. In Int. Conf. on Coal Science; Moulijn J. A.; Nater, K. A. and Chermin, H. A. G. Eds.; Elsevier Science Pubs: B.V. Amsterdam, 1987; 419-22.
18. van Krevelen, D. W. and Schuyer, J. Coal Science; Elsevier: Amsterdam, London, New York, Princeton. 1957.
19. Bouwman, R. and Frericks, I. L. C. Fuel. 1980, 59, 315-22.
20. Rhoads, C. A.; Senftle, J. T.; Coleman, M. M.; Davis, A. and Painter, P. C. Fuel. 1983, 62, 1387-92.
21. Calemma, V.; Rausa, R.; Margarit, M. and Girardi, E. Fuel. 1988, 67, 764-65.
22. Zawadzki, J. Carbon. 1987, 16, 491-97.
23. Senftle, J. T.; Kuehn, D.; Davis, A.; Brozowski, B.; Rhoads, C. and Painter, P. C. Fuel. 1984, 63, 245-50.
24. Fuller, M. P., Hamadeh, I. M., Griffiths, P. R. and Lowenhaupt, D. E. Fuel. 1982, 61, 529-36.
25. Painter, P. C.; Snyder, R. W.; Pearson, D. E. and Kwong, J. Fuel. 1980, 59, 282-85.
26. Tooke, P. B. and Grint, A. Fuel. 1983, 62, 1003-08.
27. Puettmann, W.; Steffens, K. and Kalkreuth, W. In Int. Conf. on Coal Science; Moulijn J. A.; Nater, K. A. and Chermin, H. A. G. Eds.; Elsevier Science Pubs: B.V. Amsterdam, 1987; 411-14.
28. Bend, S. L. PhD Thesis. University of Newcastle upon Tyne. 1989.
29. Jüngten, H. Fuel. 1984, 63, 731-37.
30. Moulijn, J. A. and Tromp, P. J. J. in: 'New Trends in Coal Science'; Yürüm, Y. Ed.; Kluwer Academic Press: Dordrecht, Boston, London. 1986; 433-80.
31. Unger, P. E.; Suuberg, E. M. 18th Symp. (Int.) on Combustion. The Combustion Institute, Pittsburgh. 1981, 1203-11.
32. Jüngten, H. Erdöl und Kohle Erdgas. 1987, 40, No. 3, 153-65.
33. Bailey, J. G.; Tate, A.; Diessel, C. F. K. and Wall, T. F. Fuel. 1990, 69, 225-39.

RECEIVED November 5, 1990

Chapter 23

Effect of Air Oxidation on Aliphatic Structure of Coal

J. T. Joseph and O. P. Mahajan

Amoco Oil Research Department, Amoco Research Center,
Naperville, IL 60566

Oxidative weathering of coal affects its structure and properties, and as a result its utilization. For example, weathering adversely affects liquefaction yield, cokability, calorific value, and beneficiation. However, little is known about the chemistry of coal weathering. This paper discusses the effect of air oxidation on the aliphatic bridges that connect the aromatic-hydroaromatic units in coal; it is expected that the oxidation process simulates accelerated natural, ambient temperature weathering of coals. The aliphatic bridges play a significant role in coal liquefaction and weathering alters them. We have demonstrated, by acid-catalyzed transalkylation reactions and by gas chromatography-mass spectrometry (GC-MS) analysis of the products, that air oxidation reduces concentrations of several types of straight chain and branched chain aliphatic bridges. Infrared spectroscopic analysis shows that these bridges are converted to carbonyl and carboxyl groups. Plausible mechanisms for these transformations have been suggested.

It is well known that weathering of coal induces irreversible structural changes that are detrimental to its utilization. For example, weathering decreases solvent extraction yields¹, liquefaction yield^{2,5}, and hydrocarbon yield during pyrolysis⁶. It also reduces fluidity^{3,7,8} and calorific value⁹, and causes poor coking behavior^{10,11}. Irreversible changes in surface properties, that in turn affect coal beneficiation, also occur during weathering^{12,13}. Effects of oxidative weathering on coal properties have been recently reviewed by Berkowitz¹⁴ and by Gray and Lowenhaupt¹⁵.

Relatively little is known about the chemistry of coal weathering. It is known that the oxygen content of coal increases during weathering¹⁶. The changes in structural features due to weathering/air oxidation have mostly been monitored by infrared spectroscopy. Rhoads et al.¹⁷ and others^{18,19} have observed an increase in the carbonyl absorption with a simultaneous decrease in the aliphatic C-H absorption during oxidation at 398° K and above. However, Martin and Chao found that during the

weathering of Argonne Premium coal samples (73.0-85.6% C, daf) under ambient conditions the carbonyl absorption increases while the C-H absorption in the aliphatic region remains unaffected²⁰. Liotta et al. found that the concentrations of ether and carboxylic acid groups increase upon prolonged ambient temperature weathering of Illinois #6 coal¹⁶. Painter et al. also have noted formation of carbonyl and carboxylic acid groups with concurrent decrease in aliphatic C-H intensity during the initial stages of air oxidation of a highly caking Pennsylvania coal¹⁸.

Our interest was to determine the fate of the aliphatic bridges during coal weathering. The aliphatic carbon structure, especially the bridges, play a significant role in coal liquefaction. The macromolecular network structure of bituminous and lower rank coals contains part of the aliphatic structure as methylene and polymethylene bridges connecting aromatic/hydroaromatic clusters. During liquefaction, these relatively weak bridges undergo cleavage, while the hydroaromatic units provide part of the hydrogen for capping the free radicals produced by thermal decomposition¹. Therefore, the changes in aliphatic carbon distribution in coal during weathering can influence its liquefaction behavior.

Currently, there are no accurate methods available for quantifying the aliphatic bridges in the coal macromolecule. Quantitative nature of the application of infrared (IR) spectroscopy is limited to certain general types of functional groups or bond types. Nuclear magnetic resonance spectroscopy, despite the success of dipolar dephasing techniques to decipher the extent of substitution on carbon atoms, is still inadequate to distinguish distinct structural entities^{21,22}.

In our studies, we have used acid-catalyzed transalkylation of coal using phenol and boron trifluoride, first reported by Heredy and Neuworth²³, to quantify the aliphatic bridges in coals and monitor changes in these bridges during air oxidation. It is assumed that during the transalkylation reaction, most of the methylene and polymethylene bridges are transferred to phenol. Since extensive solubilization is achieved by transalkylation, the information obtained from the analyses of the soluble products can provide useful information about coal structure. Although there are side reactions associated with the transalkylation reaction²⁴, we believe that it is adequate for comparing the relative features of raw and weathered coals. In addition to transalkylation, we have also used infrared studies to monitor the changes occurring during air oxidation at 383° K. It is expected that this oxidation simulates accelerated natural, ambient temperature weathering of coals.

EXPERIMENTAL

Coal Samples. Three bituminous coals, namely, San Juan (New Mexico), Illinois #6, and Elkhorn (Kentucky) were used in the present study. Most of the studies were done on the San Juan coal. The coals were collected from the freshly exposed mine faces. The samples were immediately transferred at the mine face to containers under a nitrogen atmosphere. The containers were closed tightly, sealed, and stored at 277° K. The grinding and sieving were done under a nitrogen atmosphere. The ground and riffled samples were kept in glass jars, sealed under nitrogen, and stored in a refrigerator at 277° K. The proximate and ultimate analyses of the coal samples are given in Table I.

Coal Oxidation. The coal samples, ground to -325 standard mesh, were subjected to oxidation in the laboratory by heating them at 383° K in an air oven for 16 hours. This treatment will be referred to as "air oxidation" and the coal sample thus treated will be referred to as *oxidized coal*.

TABLE I. Proximate and Ultimate Analyses of Coals

	<u>San Juan</u>	<u>IL #6</u>	<u>Elkhorn</u>
<u>Proximate Analysis (wt %, dry basis)</u>			
Ash	11.4	11.8	6.6
Volatile Matter	44.2	39.7	38.7
Fixed Carbon	44.4	48.5	54.8
<u>Ultimate Analysis (wt %, dry, mineral matter-free basis)</u>			
Carbon	78.9	78.9	85.4
Hydrogen	6.0	5.4	5.7
Nitrogen	1.6	1.2	1.8
Sulfur	1.0	4.4	0.7
Oxygen (by diff.)	12.4	10.0	6.3

Transalkylation. The procedure for transalkylation was essentially the same as that used by Heredy and Neuworth²³. Briefly, coal(10 g) was slurried with phenol (100 g, Aldrich) in a three-necked round-bottomed flask equipped with a condenser and a thermometer, and heated to 373° K using a water bath. Boron trifluoride, BF₃ (Matheson) was bubbled through the coal-phenol slurry for 6 hours. The effluent gases were passed through saturated solution of sodium carbonate to neutralize the acids. At the end of 6 hours, BF₃ flow was stopped and the flask was purged with N₂ to remove any unreacted BF₃ and gaseous hydrogen fluoride produced by the hydrolysis of BF₃. The reaction mixture, which now was a viscous suspension, was poured into 1 liter of ice-cold water. Sodium carbonate was added to the aqueous slurry with vigorous stirring until the aqueous layer was neutral. The neutralized reaction mixture was extracted successively with ether and toluene. Preliminary analyses by gas chromatography (GC) and high pressure liquid chromatography (HPLC) indicated that the ether extract contained predominantly phenol and small quantities of coal-derived products. The toluene extract also contained phenol, but had a much larger proportion of coal-derived materials than the ether extract.

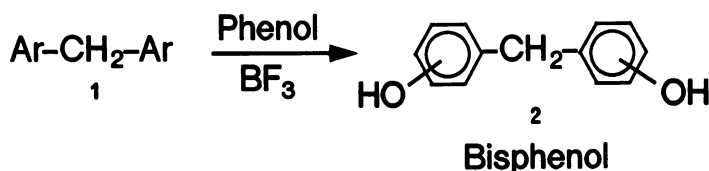
Product Analyses. The ether and toluene extracts from the transalkylation reactions of fresh and oxidized coals were analyzed by gas chromatography-mass spectrometry (GC-MS) on a VG-7070HS mass spectrometer in the electron impact mode. The mass spectrometer was interfaced with a Hewlett-Packard 5790 gas chromatograph. The GC column was a 35 meter long capillary with DB-1 as the stationary phase. A temperature program of 423-623° K at 8°/minute was used during the analysis. It was suspected that some of the high molecular weight phenolic compounds produced

during the reaction may not be volatile enough for GC analysis. Therefore, the reaction mixture was silylated using *N,O*-bis(trimethylsilyl)fluoroacetamide (BSTFA)²⁵ prior to analysis. Silylation of phenols converts them to silyl ethers, whose boiling points are considerably lower than those of the phenols. This procedure thus makes high molecular weight phenols more amenable to GC analysis. *Bis*-2- and *bis*-4-hydroxyphenyl methane were used as internal standards for quantification.

RESULTS AND DISCUSSION

Transalkylation involves the transfer of alkyl groups between aromatic nuclei, usually in the presence of strong Lewis acids. Heredy and Neuworth²³ used this reaction to "depolymerize" coal. As a result of the reaction of coal with BF_3 and phenol, the solubility of coal in phenol or pyridine increased substantially. Various modifications of this reaction have since been reported^{26,27}. Transalkylation reactions in the presence of trifluoromethane sulfonic acid and aromatic hydrocarbons have recently been used by Benjamin et al.²⁸ and Farcasiu et al.²⁹ to identify structural features in coals and heavy petroleum ends, respectively.

It is believed that during transalkylation the aliphatic side chains and bridges transfer from coal, without rearrangement, to the aromatic substrate such as phenol or toluene. A typical reaction is depicted in Scheme I.

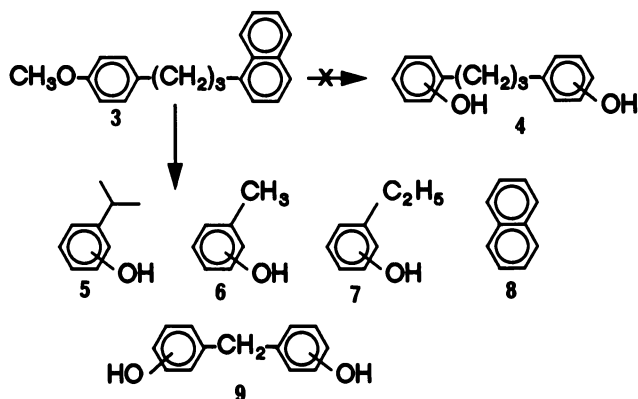


Scheme I. Transalkylation

For the above reaction to occur, the aromatic nuclei in compound 1 should carry activating groups, such as hydroxyl, alkoxy, or fused ring aromatics^{24,30}. As a result of reaction with BF_3 and phenol, the macromolecular structure of coal should undergo rupture at the aliphatic bridges, and these bridges are transferred to phenol molecules to produce bisphenols. Analysis of the bisphenols should provide information on the aliphatic bridges present in coal structure.

In model compounds, the aliphatic side chains on aromatic nuclei transalkylate without rearrangement^{31,32}. However, the reaction of aliphatic bridges is more complicated. For example, transalkylation of 1-(4-methoxyphenyl)-3-(2-naphthyl)

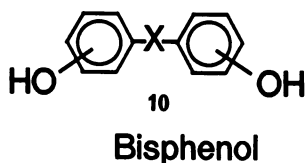
propane (Compound 3) under BF_3 -phenol reaction conditions does not produce the expected 1,3-bishydroxyphenyl propane (Compound 4)²⁴. Instead, it gives a variety of products (Compounds 5-9) resulting from the rearrangement and fragmentation of the trimethylene bridge in Compound 3, as shown in Scheme II. However, it should be pointed out that the bisphenol 9 is the major product. Formation of naphthalene (Compound 8) is interesting because it clearly indicates complete detachment of the bridging group from the naphthalene moiety in the parent compound.



Scheme II. Side Reactions During Transalkylation

Because of the above considerations, it is not possible to determine the exact nature and concentration of the aliphatic bridges as they are present in coals by analysis of the transalkylation products. However, a comparison of the relative concentrations of the various aliphatic bridges in different coal samples and how they change during weathering is possible. Specifically, our aim was to compare the relative concentrations of methylene and polymethylene bridges in fresh and oxidized coals, so that the effect of oxidative weathering on these bridges could be assessed.

Numerous bisphenols of the general structure 10 were detected in both the ether and toluene extracts of the transalkylation products from the fresh and oxidized coal samples.



X = straight or branched chain aliphatic bridge

Table II contains a list of the aliphatic bridges detected in the toluene extract. Compounds with methylene bridges were predominant in the products from the fresh coal. This is consistent with the results of Benjamin et al.²⁸. It is interesting to note that several branched chain bridges appear in the transalkylation products from both the fresh and oxidized coals.

TABLE II. Bridges Detected in the Transalkylated Products

<u>Bridge</u>	<u>Formula</u>
Methylene	-CH ₂ -
Ethylene	-CH ₂ -CH ₂ -
Methylmethylene	-CH(CH ₃)-
Ethylmethylene	-CH(CH ₂ CH ₃)-
Propyl methylene	-CH(CH ₂ CH ₂ CH ₃)-
Methylethylene	-CH(CH ₃)-CH ₂ -
Ethylethylene	-CH(CH ₂ CH ₃)-CH ₂ -
Butylmethylene	-CH(CH ₂ CH ₂ CH ₂ CH ₃)-

Such bridges in coal structure have been reported only recently. Alkyl substituted methylene and ethylene bridges have been detected in a Wyodak coal by Benjamin et al.²⁸. In the present study, some of the branched chain bridges may have been formed by rearrangement of the straight chain bridges during transalkylation²⁴.

The relative concentrations of several types of hydrocarbon bridges, namely methylene(-CH₂-), ethylene(-CH₂-CH₂-), methyl methylene (-CH(CH₃)-), methyl ethylene(-CH(CH₃)-CH₂-), ethyl methylene (-CH(CH₂CH₃)-), and propyl methylene (-CH(CH₂CH₂CH₃)-) in the fresh and oxidized San Juan coal are compared in Table III.

TABLE III. Relative Concentrations of Aliphatic Bridges in Transalkylated Products from Fresh and Oxidized San Juan Coal

<u>Aliphatic Bridge</u>	<u>Relative Concentration</u>		<u>Ratio: Fresh/Oxidized</u>
	<u>Fresh</u>	<u>Oxidized</u>	
-CH ₂ -	5.16	0.85	6
-CH ₂ -CH ₂ -	1.80	0.13	14
-CH(CH ₃)-	1.08	0.17	6
-CH(CH ₃)-CH ₂ -	1.04	0.11	9
-CH(CH ₂ CH ₃)-	0.67	0.09	7

The concentrations are reported as a fraction of the toluene extract from the transalkylation reaction. As a result of oxidation, concentrations of the most abundant bridges, namely methylene, ethylene, methyl methylene, and ethyl methylene groups are reduced by factors of 6, 14, 6, and 9, respectively. The differences in the

concentrations of larger bridges were not measured because of their low abundance in the transalkylated products.

The results in Table III clearly indicate that the aliphatic bridges have been altered significantly by oxidation. The question is: what are these bridges converted to? By infrared analysis, Liotta et al. have detected increases in carboxylic acid groups and ether linkages after long term ambient temperature weathering of an Illinois #6 coal¹⁶. Rhoads et al.¹⁷ and Painter et al.^{18,33} have obtained infrared spectroscopic evidence for a decrease in the aliphatic stretching intensity (2900 cm^{-1} region) and an increase in the carbonyl stretching (1700-1765 cm^{-1} region) after air oxidation of a highly caking Pennsylvania coal. They speculate the formation of ester groups, in addition to ketones and carboxyl groups, as a result of extended air oxidation at about 373°K. Jakab et al. have reported that oxidation of subbituminous coals causes changes in both the aliphatic and aromatic structures of coal³⁴. By Curie point pyrolysis GC-MS they detected an increase in carbonyl groups in the coals oxidized in air at 373° K. In addition, they found decreased yields of alkyl naphthalenes and phenols from the oxidized coal compared to the fresh coal. The decrease was attributed to condensation reactions involving alkyl aromatics and phenolic fragments resulting in large clusters. Gethner has speculated that formation of aldehydes, ketones, esters, and ethers is likely during oxidation of coals at 373° K³⁵. Recently, Fuller has obtained high temperature infrared spectroscopic data which indicate that during air oxidation at 473° K or above¹⁹, several surface groups such as ketones, aldehydes, carboxylic acids, and anhydrides of carboxylic acids are formed.

We have examined the infrared spectra of three coals before and after overnight oxidation in air at 383° K. The infrared spectra of the fresh coals, their corresponding oxidized samples, and the difference spectra between the oxidized and fresh coals are given in Figures 1-3. Several changes due to oxidation are observed. The most significant changes are the enhanced carbonyl absorptions in the 1700 cm^{-1} region, and decreases in the aliphatic C-H absorptions in the 2850-2950 cm^{-1} (CH stretching) and 1450 cm^{-1} (CH_2 bending) regions. These changes are quite discernible in the difference spectra. Minor changes are observed in the aromatic CH vibrations in the 750-850 cm^{-1} region as well, especially in the Elkhorn coal.

With regard to the results of our infrared study, a word of caution is appropriate. The large decreases in the concentration of the aliphatic bridges after oxidation, as measured by transalkylation (Table III), cannot be expected to match those indicated in the difference infrared spectra between oxidized and fresh coals. This is because the spectra measure the total aliphatic content of the samples, namely aliphatic bridges, hydroaromatics, and aliphatic side chains. In contrast, results in Table II show differences in relative concentrations of the aliphatic bridges, which represent only a part of the total aliphatics. Furthermore, concentrations measured by transalkylation correspond to only the soluble fractions of the reaction products; some of the more complex transalkylation products may be retained in the residue itself.

Our transalkylation studies show that the concentrations of methylene and other aliphatic bridges decrease during air oxidation. The infrared analysis shows that carbonyl groups are produced during the oxidation process. Therefore, it is quite likely that under our oxidation conditions the aliphatic bridges are converted to carbonyls and/or carboxylic acid groups.

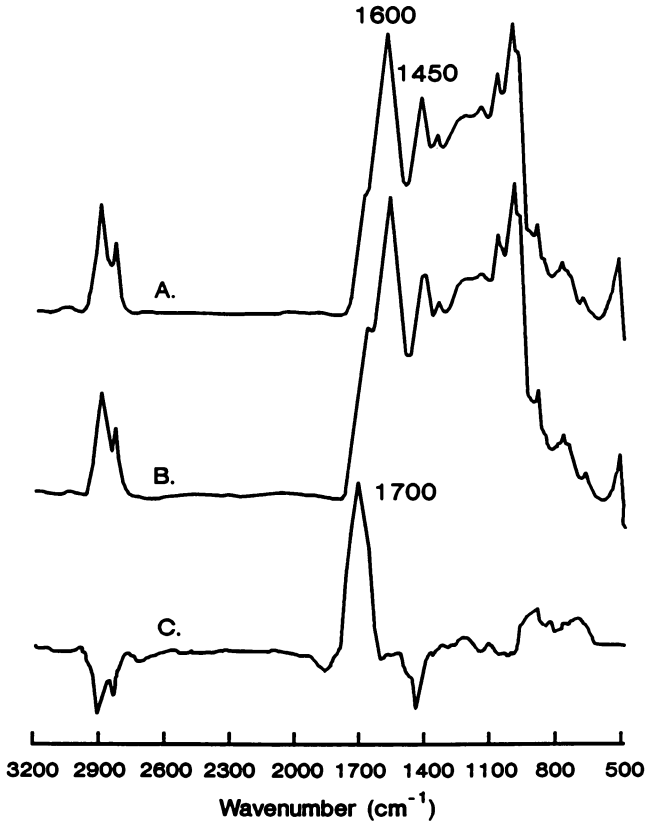


Figure 1. Infrared spectra of San Juan coal

A. Fresh coal, B. Weathered coal, and C. Difference spectrum (B-A).

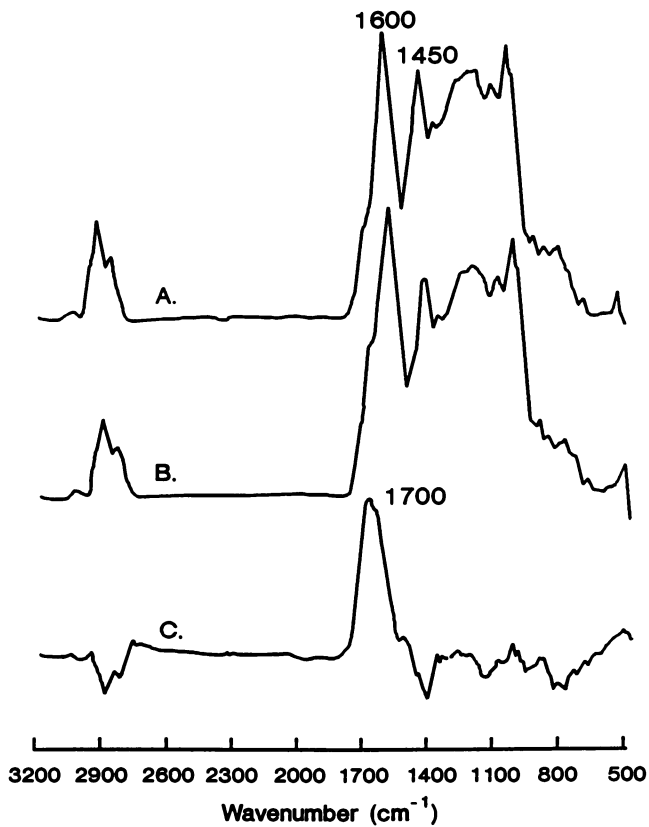


Figure 2. Infrared spectra of Illinois #6 coal
A. Fresh coal, B. Weathered coal, and C. Difference spectrum (B-A).

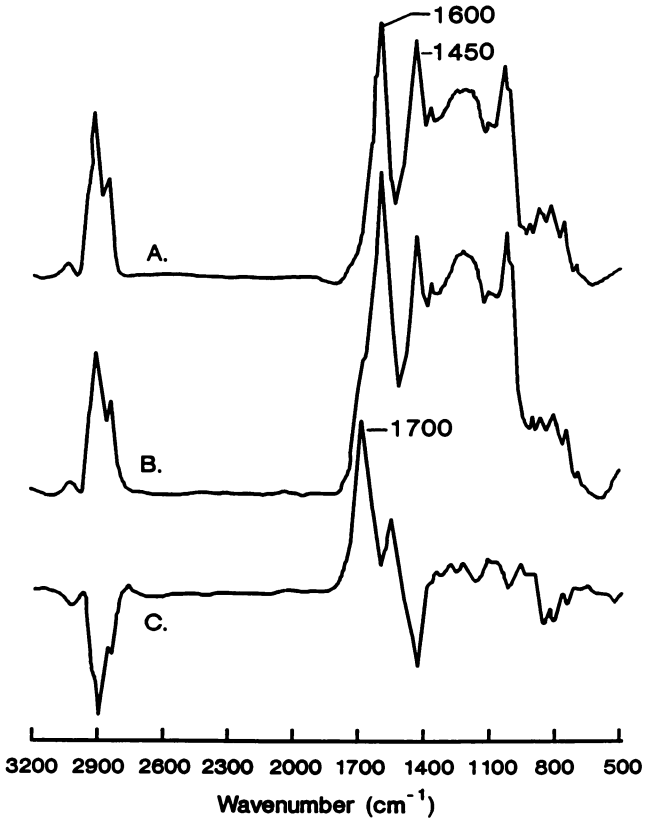
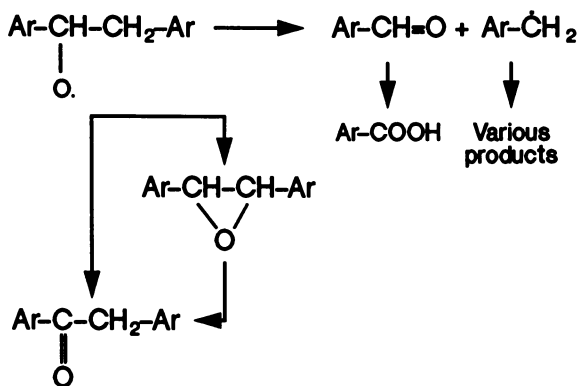


Figure 3. Infrared spectra of Elkhorn coal

A. Fresh coal, B. Weathered coal, and C. Difference spectrum (B-A).



Scheme V. Possible Oxidation Pathways(contd.)

There is ample evidence in the literature for conversion of reactive hydrocarbons to carbonyl compounds by autoxidation⁴³⁻⁴⁹. In coals, the final products of autoxidation under the conditions used in the present study could be a mixture of carbonyl and carboxylic acid surface groups. Under mild oxidation conditions, a different set of functional groups such as ethers as proposed by Liotta et al.¹⁶ or epoxides as suggested in Scheme V could be formed. There are numerous examples of alkoxy radicals rearranging to epoxides⁵⁰⁻⁵². Choi and Stock have shown that ethers can be produced from benzhydrol structures, which are invoked as intermediates in Scheme IV³³. At higher temperatures, the epoxides and ethers are unstable and may rearrange to carbonyl compounds.

CONCLUSIONS

Air oxidation of coal causes a significant decrease in the concentration of aliphatic bridges as determined by acid-catalyzed transalkylation of coal with phenol. Infrared analysis of the raw and oxidized coals indicate that the hydrocarbon bridges are converted to carbonyl groups. Plausible explanations have been offered for the formation of carbonyl groups from aliphatic bridges.

ACKNOWLEDGEMENTS

The authors wish to thank J. E. Duffield, Cynthia Neu and Jean Schaap for technical assistance; R. E. Pauls and R. W. McCoy for GC and HPLC analysis; G. G. Jones for GC-MS analysis, and A. B. Mossman for helpful discussions.

LITERATURE CITED

1. Buchanan, D. H.; Warfel, L. C.; Mai, W.; Lucas D. Am. Chem. Soc.; Div. Fuel Chem., Preprints 1987, 32(1), p 146.
2. Neavel, R. C. Fuel 1976, 55, 237.
3. Chang, C. Y.; Guin, J. A.; Tarrer, A. R. J. Chinese Chem. Soc. 1981, 28, 155.
4. Whitehurst, D. D.; Mitchell, T. O.; Farcasiu, M. Coal Liquefaction: The Chemistry and Technology of Thermal Process, Academic Press, New York, 1980, p 112.
5. Senftle, J. T.; Davis, A. International Journal of Coal Geology 1984, 3, 375.
6. Meuzelaar, H. L. C.; McClennen, W. H.; Cady, C. C.; Metcalf, G. S.; Windig, W.; Thurgood, J. R.; Hill, G. R. Am. Chem. Soc.; Div. Fuel Chem., Preprints 1984, 29(5), p 166.
7. Larsen, J. W.; Lee, D.; Shawver, S. E.; Schmidt, T. E. Gas Research Institute, Annual Report, February 1984.
8. Johnson, R. A.; Cooney, R. P. Aust. J. Chem. 1983, 36, 2549.
9. Orenbach, M. S.; Anchugova, N. A. Khim. Tverd. Topl. 1983, 2, 19.
10. Crelling, J. C.; Schrader, R. H.; Benedict, L. G. Fuel 1979, 58, 542.
11. Sarkar, S. Fuel 1980, 59, 450.
12. Vargha-Butler, E. I.; Zubovits, T. K.; Smith, R. P.; Tsim, I. H. L.; Hamza, H. A.; Neuman, A. W. Colloids Surf. 1984, 8, 231.
13. Wu, M. M.; Robbins, G. A.; Winschel, R. A.; Burke, F. P. Am. Chem.Soc.; Div. Fuel Chem., Preprints 1987, 32(1), p 408.
14. Berkowitz, N. Sample Selection, Aging, and Reactivity of Coal, R. Klein and R. Wellek, Eds., Wiley-Interscience, New York, 1989, Chapter 5, pp 217-251.
15. Gray, R. J.; Lowenhaupt, D. E. Sample Selection, Aging, and Reactivity of Coal, R. Klein and R. Wellek, Eds., Wiley-Interscience, New York, 1989, Chapter 6, pp 255-334.
16. Liotta, R.; Brons, G.; Isaacs, J. Fuel 1983, 62, 781.
17. Rhoads, C. A.; Senftle, J. T.; Coleman, M. M.; Davis, A.; Painter, P. C. Fuel 1983, 62, 1387.
18. Painter, P. C.; Coleman, M. M.; Snyder, R. W.; Mahajan, O. P.; Komatsu, M.; Walker, P. L., Jr. Applied Spectroscopy 1981, 35, 106.
19. Fuller, E. L., Jr.; Smyrl, N. R. Am. Chem. Soc.; Div. Fuel Chem., Preprints 1988, 33(4), p 691.
20. Martin, K. A.; Chao, S. C. Am. Chem. Soc.; Div. Fuel Chem., Preprints 1988, 33(3), p 136.
21. Pugmire, R. J.; Woolfenden, W. R.; Mayne, C. L.; Karas, J.; Grant, D. M. Am. Chem. Soc.; Div. Fuel Chem., Preprints 1983, 28(1), p 103.
22. Murphy, P. D.; Cassidy, T. J.; Gerstein, B. C. Fuel 1982, 61, 1233.
23. Heredy, L. A.; Neuwirth, M. B. Fuel 1962, 41, 221.
24. Joseph, J. T.; Mahajan, O. P. Fuel 1985, 64, 1321.
25. Stalling, D. L.; Gehrke, C. W.; Zumwalt, R. W. Biochem. Biophys. Res. Comm. 1968, 31, 161.
26. Ouchi, K.; Imuta, K.; Yamashita, Y. Fuel 1965, 44, 29.
27. Yurum, Y.; Yiginsu, I. Fuel 1981, 60, 1027.
28. Benjamin, B. M.; Douglas, G. C.; Cannonico, D. M. Fuel 1984, 63, 888.
29. Farcasiu, M.; Forbus, T. R.; La Pierre, R. B. Am. Chem. Soc.; Div. Pet. Chem., Preprints 1983, 28(2), p 279.
30. Larsen, J. W.; Lee, D. Fuel 1983, 62, 918.

31. Heise, R.; Tohl, A. Justus Liebigs Ann. Chem. 1982, 270, 155.
32. Bakoss, H. J.; Roberts, R. M. G.; Sadri, A. R. J. Org. Chem. 1982, 47, 4053.
33. Painter, P. C.; Snyder, R. W.; Pearson, D. E.; Kwong, J. Fuel 1980, 59, 282.
34. Jakab, E.; Windig, W.; Meuzlaar, H. L. C. Energy and Fuels 1987, 1, 161.
35. Gethner, J. S. Fuel 1985, 64, 1443.
36. Gaddelle, C.; Clement, G. Bull. Soc. Chim. Fr. 1968, #1, 44.
37. Lloyd, W. G. Methods in Free Radical Chemistry, Vol. 4, E. S. Huysen, Ed., Marcel-Dekker, New York, 1973, Chapter 1, p 22.
38. Retkofsky, H. L.; Hough, M. R.; Maguire, M. M.; Clarkson, R. B. Coal Structure, M. L. Gorbaty and K. Ouchi, Eds.; Am. Chem. Soc. Symposium Series #192, 1981, Chapter 4.
39. Petrakis, L.; Grandy, D. W.; Jones, R. B. Fuel 1982, 61, 21.
40. Dack, S. W.; Hobday, M. D.; Smith, T. D.; Pilbrow, J. R. Fuel 1984, 63, 39.
41. deVries, H. A. W.; Bokhoven, C.; Dormans, H. H. Brennst. Chem. 1959, 50, 289.
42. Lynch, B. M.; Lancaster, L.; MacPhee, J. A. Am. Chem. Soc.; Div. Fuel Chem., Preprints 1987, 32(1), p 138.
43. Benson, S. W. J. Chem. Phys. 1961, 34, 521.
44. Nangia, P.; Benson, S. W. J. Am. Chem. Soc. 1964, 86, 2770.
45. Jones, J. H.; Allendorf, H. D.; Hutton, D. W.; Fenske, M. R. J. Chem. Eng., Data 1961, 6, 620.
46. Fish, A. Proc. Roy. Soc.(London) 1966, A293, 378.
47. Fish, A. Proc. Roy. Soc.(London) 1967, A298, 204.
48. Zeelenberg, A. P.; Bickel, A. F. J. Chem. Soc. 1961, 4014.
49. Russel, G. A. J. Am. Chem. Soc. 1979, 79, 3871.
50. Fish, A.; Haskell, W. W.; Read, I. A. Proc. Roy. Soc.(London) 1969, 313, 261.
51. Shaw, R.; Trotman-Dickenson, A. F. J. Chem. Soc. 1960, 3210.
52. Trimm, D. L.; Cullis, C. F., J. Chem. Soc. 1963, 1430.
53. Choi, C. Y.; Stock, L. M. J. Org. Chem. 1984, 49, 2871.

RECEIVED November 5, 1990

Chapter 24

Plastofrost Technique for Studying the Carbonization of Coal

A Reexamination

A. J. Royce, P. J. Readyhough, and P. L. Silveston

Coal Research Laboratory, Department of Chemical Engineering,
University of Waterloo, Waterloo, Ontario N2L 3G1, Canada

The Plastofrost technique initially proposed in the early 1960's is a method of visually examining the coal to coke transformation during carbonization as well as assigning temperature ranges to these transformations. The technique has been modernized and applied to several problems; 1) the roles of the bitumen phase and metal salts in coal softening and fusion during coal-bitumen co-processing, 2) measurement of the plastic range of coking coals and 3) investigation of rheological measurements of those coals. It appears to be a useful technique and warrants much more use.

The Plastofrost technique was developed by Ritter and Juranek (1, 2) in West Germany during the early 1960's to observe the coal-to-coke transformation (softening, pore development and resolidification), and the interaction of coal macerals at different degrees of carbonization. Changes in the coal particles occurring at increasing temperatures during carbonization are made visible, and if captured on film, produce a time-temperature record of the process. Although hailed as a useful tool by researchers, the Plastofrost technique enjoyed just a brief period of popularity. Since the 1960's the technique has not been mentioned in the coal science literature. Nevertheless, the technique appears to have many applications and so deserves a re-examination.

Our objectives in this paper are to describe the Plastofrost technique and the modifications we have made, illustrate the information obtained, and examine the range of scientific and technical questions this procedure can be used on.

The principle of the Plastofrost technique is to produce a temperature difference across a coal sample so that the bottom of the sample reaches at least 550°C, even though the top of the sample has not yet attained 350°C. The bottom temperature ensures that

semicoke forms so that the coke texture can be observed, while limiting the top temperature to 350°C leaves coal in an unaltered state. Placing thermocouples in the sample gives the temperature profile at the time when the bottom reaches 550°C and heating is discontinued; the maximum temperature at each point in the sample is known thereby and a temperature can be assigned to each visible stage of the coal to coke transformation found when the sample is split open and inspected.

Heating of the sample is unidirectional just as in a coke oven. However, in the Plastofrost unit, the sample is heated from the bottom. It differs, therefore, from a coke oven in the direction of gas flow with respect to the temperature front. Some of the gas in a coke oven will move through the hot zone, and undergo further cracking, whereas in the Plastofrost, gas flow is only into the cooler region of the sample. The significance of this difference is not known. Nevertheless, movement of the temperature front through the sample makes the Plastofrost a better model of a coke oven than a dilatometer or a plastometer whose designs provide uniform heating.

Equipment

Figure 1 shows a schematic (elevation) of the Plastofrost apparatus as modified for the present study. The two main components are the heater and the coking attachment. The heater consists of a nickel-plated copper slab in which four 300 watt cartridge heaters are enclosed. A chromel/alumel thermocouple insulated with ceramic tubing placed 5 mm beneath the top surface of the slab measures the temperature (see Fig. 1). The bead of the TC is at the centre of the slab. Figure 2 is a photograph of the assembled apparatus.

The coking attachment comprises a baseplate; a coking cylinder; and a ram. The coking cylinder has an inside diameter of 41 mm and a height of 75 mm. Wall thickness is 3 mm. The cylinder can be separated vertically into halves and has ten evenly spaced holes, 5 mm centers, along each side of the vertical split. Ceramic tubes (2.5 mm o.d.) are placed in these holes, as shown in the figures, and chromel/alumel thermocouples are inserted so that the measuring junctions are located along the axis of the cylinder. Halves of the cylinder are clamped together as shown as well in the figures.

The cylinder fits into an insert in the baseplate. This plate measures 110 mm x 110 mm and is 6 mm in thickness. Three 6.3 mm rods, 115 mm in height extend from the base plate to the retainer for the ram. The ram itself is 10 mm thick and has a diameter of 39.75 mm, just slightly less than the inside diameter of the coking cylinder so that it can easily compact and retain the coal within the cylinder. It is fitted with a 76.5 cm long "T-shaped" handle, threaded through the retainer. Thus the ram can be raised or lowered to provide any desired degree of compaction in the coal.

The coking attachment is placed in a snug fitting inset on the top plate of the furnace. This is stepped as shown in the figure to reduce heat flow to the cylinder walls. The furnace provides unidirectional heating to the sample in the cylinder from the bottom upwards. Figure 3 is a photograph of the disassembled Plastofrost showing the parts described above. Modifications of the original design were the seating, ram support, and in design of the heating

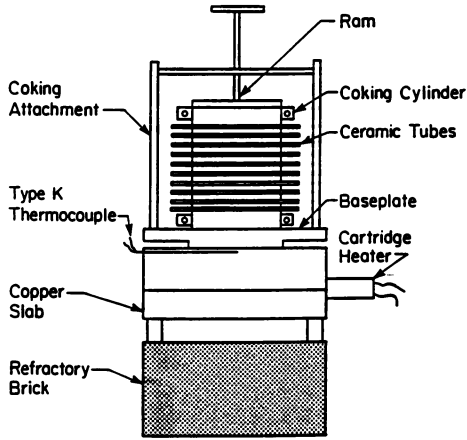


Figure 1. Schematic of the Plastofrost apparatus.

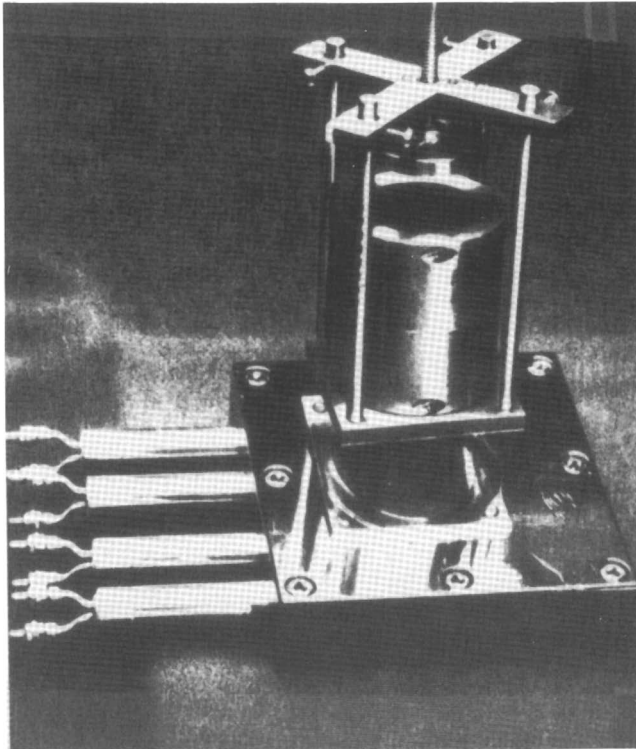


Figure 2. Photograph of the assembled Plastofrost unit.

slab. The seating was changed to minimize heat flow to the cylinder walls, while the slab was redesigned to increase the maximum rate of heating and improve temperature uniformity.

A microcomputer based control and data acquisition system is required to monitor the 10 thermocouples in the sample and to control the heater temperature. For the latter, the rate of change of the thermocouple in the slab was used and power to the cartridge heaters varied. Details are given by Duever (3) and in a WCPD report (4).

Heater and coking attachment were well insulated and placed in a tight fitting box that could be flushed with nitrogen. The complete system was used in a fume hood as devolatilization occurs during a run. The microcomputer was located next to the fume hood.

Procedure

Prior to loading, an aluminum foil was placed in the coking cylinder and ceramic tubes, 5 cm in length, were fitted in to the holes located in the coking cylinder. The cylinder was placed on the baseplate before coal was added. A sample of air dried, ground coal, weighing 85 grams, was incrementally packed into the cylinder using the ram to guarantee a constant packing density. Usual density employed was of 0.9 g/cm^3 . The attachment was then suitably insulated using fibrefax and insulating tape. Insulation was needed to ensure a uniform radial temperature distribution. The ten chromel/alumel thermocouples were inserted into the ceramic tubes and connected to a junction strip as the last step. In several experiments, only 66.5 g of coal were used to give a density of 0.76 g/cm^3 .

The samples were heated in air until the temperature in the lowest level of the coal reached 200°C . At that time nitrogen was introduced into the test chamber to prevent oxidation of the sample. The heater operated thereafter at the maximum heating rate until its temperature reached 400°C . The temperature in the lowest level of the packed coal sample at this time was usually about 250°C . Above 400°C the furnace heating rate was controlled at $3^\circ\text{C}/\text{min}$. Heating continued until the temperature in the lowest level of the coal just above the heating slab reached about 550°C . At this time, the heater was turned off, the coking apparatus removed from the heating slab, and left to cool in an inert atmosphere until the temperature at all levels fell below 200°C . The foil wrapped sample then was impregnated using a polyester resin sometimes thinned with acetone. After hardening the sample was cut into two pieces perpendicular to the ceramic tubes using a diamond-tipped circular saw. Each half was impregnated with polyester resin again, but this time under vacuum. Figure 4 compares sawed and impregnated sections.

The final step in sample preparation was grinding and polishing. The former followed the recommendations of the Bituminous Coal Research Inc. (5). The exposed face of the coked samples were polished to produce scratch-free surfaces suitable for microscopic examination using three polishing stages, each of three minutes duration. After each polishing stage, an ultrasonic cleaner was used to remove all polishing or grinding particles. Using a Zeiss UNIVERSAL Research Microscope, Plastofrost samples were examined by reflected light using parallel polars and a $1/4 \lambda$ plate inserted

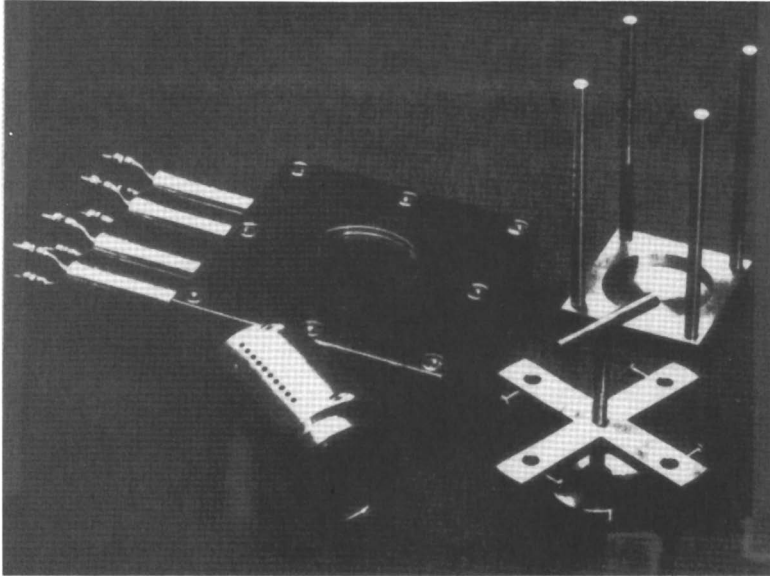


Figure 3. Photograph of the disassembled Plastofrost unit showing the different parts.

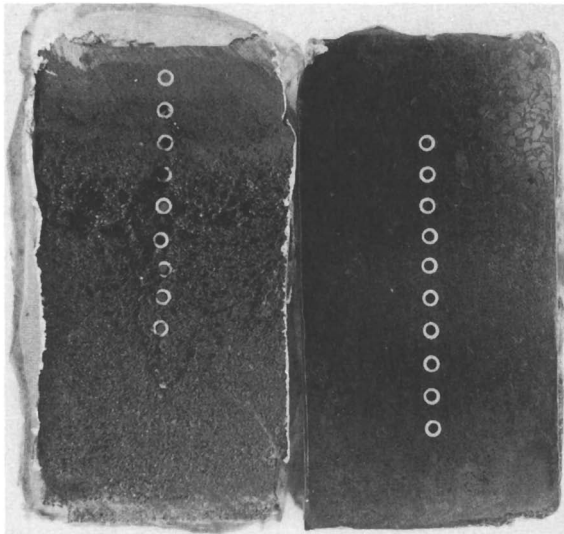


Figure 4. Sections of the Plastofrost sample showing the ceramic tubes holding the thermocouples; Left: cut section, but not impregnated; Right: polyester impregnated section.

between the specimen surface and the analyzer to characterize the samples in terms of their optical texture. A strip 5 mm wide on either side of the center axis of the cylinder was examined. Juranek et al. (6) measured the temperature profile perpendicular to the center axis and found that within such a strip, deviation from the temperature along the center axis was within 3°C.

The first step in the microscopic evaluation was to determine the relative positions of the ceramic tubes making use of a stage micrometer. These tubes held the thermocouples during the tests so that the temperatures at the tube positions were known. Then samples were examined under the microscope to observe the softening characteristics of the coal, its resolidification, and the nature of the coke formed. This was accomplished by identifying the following transitions found by Ritter and Juranek (1, 2) and Juranek (6) to be common to coking goals:

1. The first appearance of pores in the individual grains.
2. The initial fusion of the grains.
3. The point at which there is a significant increase in the proportion of pores.
4. The completion of fusion where individual grains are no longer distinguishable.
5. The development of anisotropic semicoke.

With the aid of the stage micrometer, positions could be assigned to each of these changes to the nearest tenth of a millimeter and the temperatures for each transition could be estimated from the temperature record.

Completion of fusion and a significant increase in pores are relatively gross characteristics and could easily be identified at 50X magnification. Determinations of initial pore development and grain fusion were more difficult and generally required higher magnifications of 100 and 200X. The anisotropic nature of the semicoke was observed at 200 and 500X magnification. The development of anisotropy in the softened coal mass is an indication of decreasing viscosity. With increasing time and temperature, anisotropic domains grow and may form large regions of uniform orientation. Thus, since these domains should not change above the resolidification point, the point at which domains cease to grow and change should be the resolidification temperature.

Further details of procedure are available (3, 4). Several experiments were performed using coal-bitumen slurries. A different procedure had to be developed to prepare samples from slurries. Fluidity of the slurry during heating was a problem. A paper at recent ACS Symposium (7) discusses this procedure. An extended discussion appears in a report in the public domain (10).

Plastofrost Observations

As mentioned above, some of the carbonization stages are easily identified. One of these is the completion of fusion. Figure 5b shows the observed completion of fusion in a cretaceous LVB sample. The black and dark grey regions are unfilled and resin filled pores or interparticle voids respectively, while the light grey, largely featureless, region is the fused vitrinite. Boundaries between bordering vitrinite macerals have disappeared and bridges connect

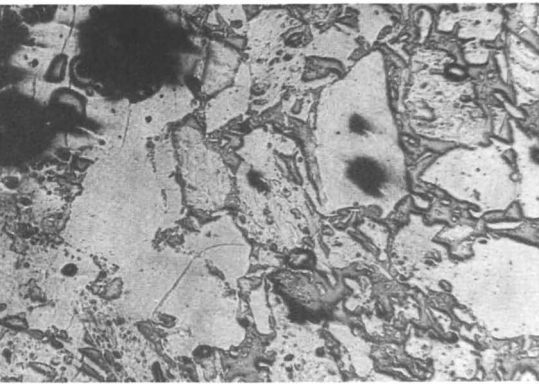
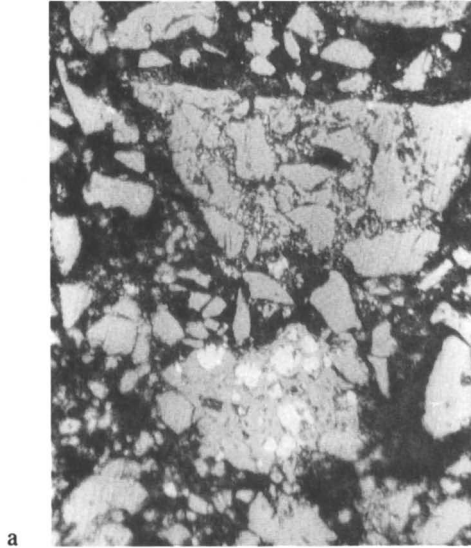


Figure 5. Softening and fusion appearance; a) vitrinite enriched cretaceous LVB at 330 °C; b) completion of fusion (422 °C) for a vitrinite enriched cretaceous LVB coal.

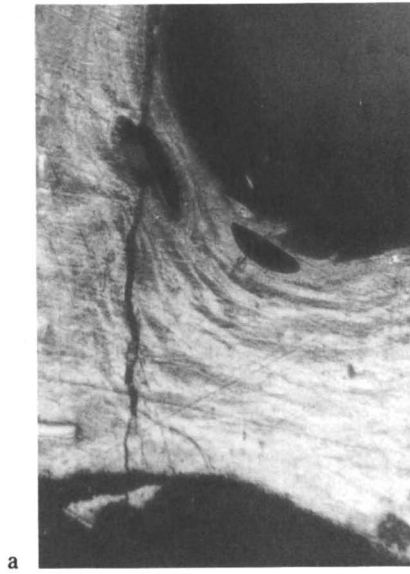
well separated macerals. Devolatilization pores are the irregular sized, semicircular regions in the vitrinite macerals. A distinct inertite maceral, probably semi fusinite, is at the lower left border of the photo. Stress cracks arising during cooling are also visible. The sample prior to softening and fusion appears in Figure 5a at the same magnification.

Use of $1/4 \lambda$ plate with parallel polarizers permits the texture of the cooled molten phase and the semi coke to be observed. Figure 6 shows the texture of the anisotropy for 3 samples. Magnification of all samples is 200X. The left-hand figure shows elongated, flow domain texture at 458°C that is typical of both carboniferous and cretaceous LVB coals. Texture has been interpreted by Grint et al. (8). Surprising is that this anisotropy is seen at a temperature 25°C below the temperature of maximum dilatation measured using a Ruhr dilatometer for the coal (4). The coal must still be fluid at this temperature. Thus, the texture represents either structure in the softened or molten coal or formed as the coal solidifies on cooling in the sample preparation procedure. Appearance of anisotropy prior to the temperature of maximum dilatation, that is, while the coal was still plastic, occurred with both cretaceous and carboniferous MVB coals. It did not occur with the HVB samples. For these coals, the temperature of maximum dilatation coincided with the temperature of the first appearance of anisotropy so that the latter temperature does signal semicoke formation for this rank of coal.

Coal rank (vitrinoid mean reflectance) affects texture of the semi coke strongly. Figure 6b shows well developed medium grain mosaic anisotropy surrounding a pore in the lower part of the photomicrograph. The coal used for this sample was a cretaceous HVB which had an enriched vitrinite content. The fine to coarse grain texture is typical for the HVB coals. The temperature reached at the point where the photomicrograph was taken was 550°C . The texture seen in Figure 6b contrasts well with the texture for an LVB sample shown in Figure 6a.

Figure 6c is taken from another, as yet unpublished study of coal carbonization during co-processing of bitumen and coal (7). The circular black region is a resin filled devolatilization pore surrounded by bitumen semicoke. Fused vitrinite is the bright region with very little texture. The photomicrograph suggests that neither the bitumen or the plastic coal are mutually soluble and the presence of bitumen does not interfere strongly with the fusion of vitrinite macerals.

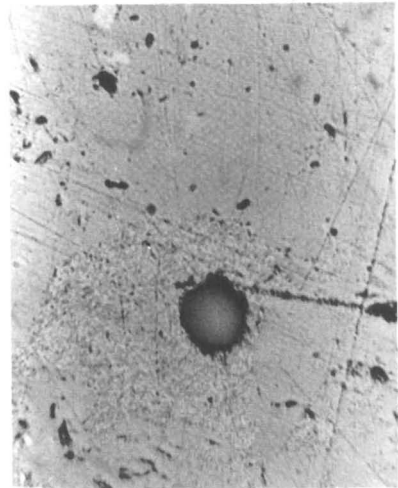
It is evident from the discussion above that the Plastofrost technique can furnish information on 1) whether or not a coal or coal blend undergoes softening, fusion and flow as it is heated through the carbonization range of temperatures, 2) temperatures at which the five stages of coal transformation occur for that coal or blend, 3) the size and distribution of the devolatilization pores, and 4) pore wall thickness which is thought to bear on coke strength and reactivity. With suitable microscopes, the technique can identify macerals present in the coal, their size distribution and the behaviour of each maceral class as it goes through carbonization.



a



b



c

Figure 6. Semicoke texture; a) flow domain anisotropy in a LVB semicoke; b) fine grain mosaic anisotropy in a HVB semicoke; c) vacuum bottoms and carboniferous MVB coal at 554 °C (coal 30% by weight).

It can also identify texture of the semi coke formed as illustrated in Figure 6. If a binder is used with a coal, the Plastofrost technique can determine the coal-binder interaction and the texture of coke formed from the binder phase. Although not considered in studies undertaken at Waterloo, the axial location of the thermocouples in the sample holder makes the Plastofrost procedure capable of measuring coal-coke conductivity as a function of coal, temperature and compaction pressure, with just a modest redesign of the heating slab.

Plastofrost Applications

The discussion in the previous section of what can be observed by the Plastofrost technique indicates potential applications of the techniques. These are collected in Table I. Only several of these potential applications have been studied by us. In this section, our work will be briefly examined and references to more complete reports will be given. Beginning with Duever's study (3, 9), the Waterloo Coal Research laboratory has applied the Plastofrost to three problems: 1) measuring the effect of metal salts on coal particle fusion during bitumen coal co processing, 2) assessing the accuracy of the dilatometric plastic range, and 3) exploration of the failure of rheological tests to predict the good coking performance of North American cretaceous coals. In the first of these applications (10), two cretaceous and two carboniferous coals were used along with a heavy bitumen (vacuum bottoms). Plastofrost samples were prepared from the coals with 0, 5 and 20 wt% metal salts, the vacuum bottoms, and slurries of 30 wt% coal in the vacuum bottoms with metal salt levels of 0, 5 and 20 wt%. It was found that the salt delayed initial fusion of the coal grains and completion of

Table I. Potential Applications of the Plastofrost Technique

-
- Influence of additives (inorganic salts) or mineral matter on coal softening, fusion and semicoke texture
 - Coal-binder interaction during carbonization
 - Softening, fusion and semicoke texture for different coals and coal blends
 - Measurement of the plastic range of different coking coals and coal blends
 - Influence of weathering, grain size on softening and fusion behaviour of coals
 - Effect of coal handling (beneficiation) on softening and fusion behaviour of coals
 - Maceral behaviour and interaction on carbonization
 - Mesophase development during carbonization
 - Relation of coke strength (stability) to coke texture, pore size distribution, pore wall thickness
 - Coal/coke conductivity as a function of carbonization and/or compaction
-

fusion. Also, the anisotropic texture of the semicoke was diminished by the salt. The presence of vacuum bottoms suppressed coal fusion, probably by physically separating the coal grains. Fusion is also slightly suppressed at 20 wt% additive; 5 wt% seemed to have little effect. Dissolution of vitrine in the bitumen was not observed. The coal and vacuum bottom phases carbonize separately yielding distinct, but well bonded semicokes. Figure 6c illustrates this observation. Anisotropic texture of the vacuum bottoms coke is strongly diminished by the presence of the finely ground coal. The micrographs suggest that the metal salt impregnated coals expel the salt on softening. This salt collects on the maceral surfaces and may physically interfere with the fusion process.

The second and third applications employed the same Plastofrost data taken with two suites of HVB to LVB coals of the carboniferous and cretaceous eras. The coals were split by gravimetric means into vitrinite enriched and depleted samples. In our study of dilatometry plastic ranges (11), it was found that the plastic range agrees well with the range obtained from the Plastofrost initial softening and first appearance of anisotropy temperatures for coals showing positive total dilatations and HVB coals with high vitrinite content. This is illustrated in Figure 7. With the exception of several HVB coals, the dilatometer seriously underestimates the plastic range of poorly or non-dilatating coals. The explanation for this is that dilatometry does not correctly measure the softening temperature of many coals. Only with HVB coals do the estimates of initial softening temperature by the two techniques agree.

As discussed earlier, the Plastofrost estimate of the resolidification temperature (semicoke formation) is incorrect for MVB and LVB coals. Thus, that technique does not give the "real" plastic range. The best estimate seems to come from using the Plastofrost measurement of the initial fusion temperature and the dilatometer reading of the temperature of maximum dilatation.

The third Plastofrost application (4) investigated the observation (12, 13) that rheological tests on certain bituminous coals of cretaceous origin indicate that these coals should have poor coking quality even though commercial use and ASTM Sole Heated Oven tests show that these coals produce good quality coke. The Plastofrost observations indicate cretaceous bituminous coals exhibit all the carbonization stages seen in good coking coals. Temperatures of the carbonization stages did not differ greatly between the carboniferous and cretaceous coals as well. The plastic range of the latter coals is generally smaller for the LVB coals; the difference approaches 55°C. It was concluded that the problem with the rheological tests lies with the assumption that contraction and dilatation depend only on fluidity of the coal. These changes probably reflect the viscosity of the softening coal and the size and distribution of the inert macerals in the coal.

Three years experience with the Plastofrost technique indicate measurements are reproducible, provided the same observer makes the readings. However, sample preparation is slow and measurements have a subjective element because different observers obtain different stage temperatures from the same sample.

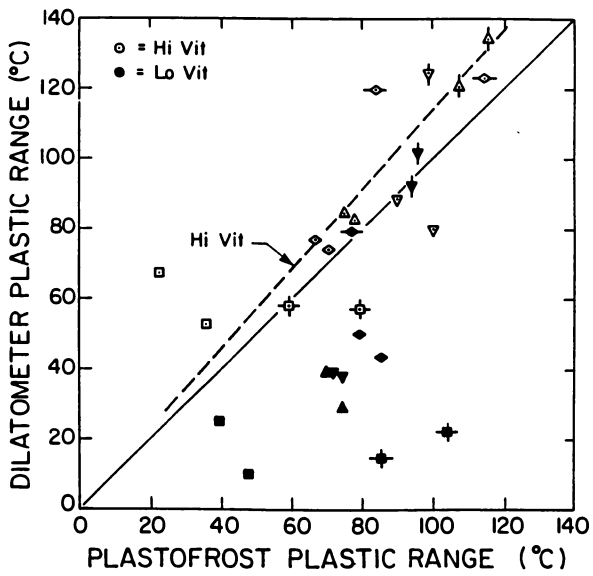


Figure 7. Cross plot of dilatometric and Plastofrost plastic ranges.

Acknowledgements

Much of the work discussed above was performed under contract awarded by the Canada Departments of Supply and Services and Energy, Mines and Resources to the Waterloo Centre for Process Development. Dr. J.T. Price of CANMET was the supervising scientist on these contracts. His active participation was very much appreciated.

References

1. Ritter, H.; Juranek, G. Eine Neue Method zur Untersuchung und Berschreibung des Erweichungsverhaltens von Kohlen; Brennstoff Chemie., 1960, 41 (6), 170.
2. Ritter, H.; Juranek, G. Ueber das Erweichungsverhalten von Kohlen im Bereich der Oberen Esskohlen bis Unteren Fettkohlen, Brennstoff Chemie., 1960, 42, 17.
3. Duever, P.D. An Investigation of Coal Rheology with a Plastofrost Apparatus, MSc Thesis, Department of Chem. Eng., University of Waterloo, Canada, 1986.
4. Waterloo Centre for Process Development. A Plastofrost study of Western Canadian coking coals, Final Report prepared for the Canada Department of Supply and Services and the Canada Department of Energy, Mines and Resources, Ottawa, Canada, 1989.
5. Berry, W.F.; Cole, D.L. Preparation and Polishing of Coal and Coke for Petrographic Analysis, Bituminous Coal Research Inc., Pennsylvania, 1965.
6. Juranek, G.; Bussmann, B.; Seifert, G. Ueber das erweichungsverhalten von Kohlen Verschiedener Inkohlung; Brennstoff Chemie., 1963, 44 (4), 97.
7. Royce, A.; Readyhough, P.J.; Silveston, P.L.; Fouda, S.A. Effects of Iron Salts on the Carbonization of Coal-Bitumen Slurries, Symp. on the Chemistry of the Carbonization of Petroleum Feedstocks, Div. of Petroleum Chemistry, ACS Los Angeles Meeting, Sept. 26-30th, 1988.
8. Grint, A.; Swietlik, U.; Marsh, H. Carbonization and Liquid-crystal (Mesophase) Development-9. The Co-carbonization of Vitraains with Ashland A200 Petroleum Pitch, Fuel, 1979, 58, 642.
9. Duever, P.D.; Silveston, P.L.; Readyhough, P.J. Application of a Modified Plastofrost Apparatus to Coal Rheology, CIM Bulletin, 1987, 80 (901), 60-62.
10. Waterloo Center for Process Development Final Report for Cyclone Engineering Sales Ltd. - Plastofrost Measurements, Univ. of Waterloo, Waterloo, Canada, 1988.
11. Royce, A.; Readyhough, P.J.; Silveston, P.L. Plastic Range of Coking Coals Preprint, Coal Characterization for Conversion Processes Symposium, Rolduc, Netherlands, May 22-25, 1989.
12. Berkowitz, N.; Fryer, J.F.; Ignasiak, B.S.; Szladow, A.J. Behaviour Differences Between Carboniferous and Cretaceous Bituminous Coals of Similar Rank, Fuel, 1974, 53 (2), 141.
13. Leeder, W.R.; Coakden, J.R.; Price, J.T.; Botham, J.C. Prediction of Coke Quality with Special Reference to Canadian Coals, Proc. Ironmaking Conference (AIME), 1979, 38, 385.

RECEIVED November 5, 1990

Author Index

- Ali, S. S., 225
 Aquino, Z. N., 250
 Baldwin, Robert M., 171,260
 Ball, James E., 137
 Barton, Wesley A., 111
 Bate, Kevin, 236
 Bend, Stephen L., 284
 Burgess, C., 193
 Carlson, G. A., 159
 Chen, Min-Wei, 137
 Cloke, M., 250
 Davis, Alan, 72
 Derbyshire, Frank J., 72,182
 Deshpande, G. V., 193
 Doughty, P. W., 225
 Edwards, Ian A. S., 111
 Garcia, Ana B., 213
 George, Graham N., 127
 Gorbaty, Martin L., 127
 Granoff, B., 159
 Green, Thomas K., 137
 Harrison, Graham, 225,236
 Hatcher, Patrick G., 9
 Hirschon, Albert S., 273
 Joseph, J. T., 299
 Kelemen, Simon R., 127
 Kennar, D. R., 260
 Kottenstett, Richard J., 182
 Kroo, E., 193
 Lerch, Harry E. III, 9
 Lin, Rui, 72
 Lopez-Froedge, Leonor, 137
 Lynch, Leo J., 111
 Mahajan, O. P., 299
 Markuszewski, Richard, 31
 Marsh, Harry, 284
 Marzec, Anna, 61
 Meuzelaar, Henk L. C., 89
 Miller, R. L., 260
 Nguanprasert, O., 260
 Quast, Keith B., 20
 Readett, David J., 20
 Readyhough, P. J., 313
 Robbins, G. A., 44
 Royce, A. J., 313
 Sakurovs, Richard, 111
 Schobert, Harold H., 1,193,213
 Schulten, Hans-Rolf, 61, 89
 Serio, M. A., 193
 Silveston, P. L., 313
 Simmleit, Norbert, 89
 Smith, Neil W., 182
 Snape, Colin E., 182
 Solomon, P. R., 193
 Stephens, Howard P., 182
 Straszheim, Warren E., 31
 Wilson, Robert B., Jr., 273
 Yun, Yongseung, 89

Affiliation Index

- Advanced Fuel Research, Inc., 193
 Amoco Research Center, 299
 Colorado School of Mines, 171,260
 Commonwealth Scientific Industrial and
 Research Organisation, 111
 Consolidation Coal Company, 44
 Exxon Research and Engineering
 Company, 127
 Fachhochschule Fresenius, 61,89
 Institut Fresenius, 89
 Iowa State University, 31
 The Pennsylvania State University,
 1,72,193,213
 Polish Academy of Sciences, 61
 Sandia National Laboratories, 159,182
 South Australia Institute of Technology, 20
 SRI International, 273
 Staffordshire Polytechnic, 225,236
 U.S. Geological Survey, 9
 University of Kentucky, 72,182
 University of Leeds, 182
 University of Newcastle upon Tyne, 284
 University of Nottingham, 250
 University of Strathclyde, 182
 University of Utah, 89
 University of Waterloo, 313
 Unocal Corporation, 72
 Western Kentucky University, 137

Subject Index

A

- Acenaphthylene, effect of catalyst on hydrogenation, 243
- Acid-catalyzed transalkylation of coal, quantification of aliphatic bridges, 300
- Activation energy, measurement of property–reactivity relationships, 176,177–179*f*
- Air oxidation
definition, 301
effect on aliphatic structure of coal
coal oxidation procedure, 301
coal sample preparation, 300
oxidation, effect on IR spectra, 305,306–308*f*
oxidation mechanisms, 309–310
product analytical procedure, 301–302
proximate and ultimate analyses of coals, 300,301*t*
transalkylation, 301–305
- Aliphatic bridges in coal macromolecule, quantification methods, 300
- Aliphatic structure of coal
effect of air oxidation, 299–310
role in coal liquefaction, 300
- Argonne coals, effect of mild chemical pretreatment liquefaction reactivity, 260–271*f*
- Autoclaves, use in coal liquefaction, 225

B

- Benzene, Flory interaction parameters, 138–156
- Berens–Hopfenberg model
benzene sorption data, 153*t*,155
extract analysis, 153,154*f*
Flory interaction parameter calculation, 155–156*t*
O-methylated extract analysis, 153,154*f*
sorption per unit weight of polymer, 152–153
- BIOGRAF, 160,161
- Biomaterials, pyrolysis–field ionization MS, 62–63
- Bitumen, definition, 89

Bituminous coals

- molecular conformation and stability, 118,119–120*f*
solvent destabilization, 118,121,122*f*
- British Coal process, description, 250
- Brown coals, molecular conformation and stability, 117,119*f*

C

- Carbonization of coal, studying via plastofrost technique, 313–324
- Catalytic hydrogenation of coals
acetylated chloroform-insoluble residues, 79
aliphatic hydrogen content, 78
chloroform-soluble extracts, 79
consumption of gaseous hydrogen, 75
H₂ consumption and oil-to-asphaltene ratio vs. chloroform-solubles yield, 75,76*f*,78
H/C ratio vs. chloroform-solubles yield, 75,77*f*,78
implications for coal structure, 81
low extract yields, 75
progress to second stage of conversion, 78–79
threshold temperature, 75
two stages of conversion, 79–81
- Catalytic preliquefaction chemistry
aliphatics, reduction, 209,210
aromatics, increase, 210
chemistry of carboxyl removal, 209
field ionization MS analyses, 207
field ionization MS analytical procedure, 196
- Fourier-transform IR analysis
extracts, 200,204*f*
residues, 197,200–203*t*
- Fourier-transform IR analytical procedure, quantitative, 196
- model compound(s), 196,206
modeling, 206,208,209*f*
NMR analysis, 206,207*t*
NMR procedure, 196
preliquefaction and liquefaction experiments, 194,196
preliquefied insoluble product liquefaction, 210

Catalytic preliquefaction chemistry—

Continued

- product distribution, 197,198*t*,199*f*
- sample preparation, 194,195*t*
- solvent swelling, 205,206*f*,207
- solvent swelling and extraction procedure, 196
- thermogravimetric–Fourier-transform IR analysis, 196,200,204*f*,205
- Catechols, component of ancient coalified wood samples, 17
- Char formation, effect of oxidation and weathering, 284–297
- Clathrates, definition, 89
- Coal
 - association of mineral matter, quantitative assessment, 31–42
 - lack of information on chemical nature, 44
 - mineral matter, problems in analysis, 44
 - pyrolysis and volatilization in MS, 63–64
 - swelling ability in organic solvents without dissolving, 137
- Coal beneficiation, goals, 31
- Coal extracts, Flory interaction parameters, 138–156
- Coal hydrogenation, 171–172
- Coalification, advances, 3
- Coalification of wood, process, 9
- Coalified wood, identification of lignin-derived pyrolysis products, 10
- Coal liquefaction, *See* Liquefaction of coal
- Coal mineralogy, *See* Mineralogy of coal
- Coal property–hydroliquefaction reactivity relationships
 - activation energy, 176,177–179*f*
 - early studies, 171–172,173*f*
 - Given, Peter, work, 174–175
 - macroscopic and microscopic coal constituents, 172,174
 - point–yield conversion, 175–176
 - space–time–yield of gasoline plus middle oil vs. starting coal composition, 172,173*f*
- Coal Research Establishment coal liquefaction process
 - solvent, 236–237
 - stages, 236–237
- Coal science, advances in analytical instrumentation, 3–4

Coal structure

- modeling using computer-aided molecular design, 159–169
 - two-component concept, 73–87
 - Coking, transitions, 318
 - Combustion efficiency of coal, relationship to inert content of coal feedstock, 284
 - Combustion of coal, effect of oxidation and weathering, 284–297
 - Computer-aided molecular design for coal structure modeling
 - advantages and disadvantages, 167–168
 - applications, 160
 - coal structure parameters, 162,166*t*,167
 - energetics, 166*t*
 - folding, 166*t*
 - Given structure, 161–162,163*f*
 - hydrogen bond density, 166*t*,167
 - importance, 5
 - method, 160–161
 - physical density, 166*t*,167
 - Shinn structure, 161–162,166*f*
 - Solomon structure, 161–162,165*f*
 - Wiser structure, 161–162,164*f*
 - Continuous reactor, use in coal liquefaction, 225
 - Cresols, component of ancient coalified wood samples, 17,18*f*
- D
- De-ashing, removal of mineral matter, 250
 - Dimethylphenols, component of ancient coalified wood samples, 17,18*f*
 - Dispersed catalytic liquefaction of coal
 - advantages and disadvantages, 274
 - conversion to toluene-soluble products, 278,279*t*,280*f*
 - experimental materials, 274–275
 - experimental procedure, 275
 - hydrodenitrogenation activities, 275,277*t*
 - impregnated coal, nature, 281
 - molybdenum vs. iron catalysts, 278,280
 - oxygen content, 281

Dispersed catalytic liquefaction of coal—

Continued

- solubilities vs. catalyst and method of impregnation, 276,277*t*
- turnover frequency, 275–276,277*t*
- ultimate and proximate analyses of coals, 274,275*t*

Donatable hydrogen quantification

- chemical test using sulfur as hydrogen acceptor, 244,245–246*f*
- GC, 247
- NMR spectroscopy, 244,247

E

Electron beam–X-ray spectroscopy, analysis of coal mineralogy, 48

F

Flory interaction parameters for coal extracts and benzene

- Berens–Hopfenberg model, 152–156
 - Brunauer–Emmett–Teller surface area determination, 140
 - ¹³C-NMR procedure, 139
 - calculation, 150,151*f*
 - density measurement(s), 140,148
 - equilibrium sorption values, 143,148*t*,149–150
 - extract and *O*-methylated extract, 152
 - Fourier-transform IR procedure, 139
 - O*-alkylated extract synthesis and characterization, 142*t*,143
 - O*-alkylation procedure, 139
 - pyridine extract characterization, 142
 - rate of sorption, 150,152
 - sample preparation, 139
 - solubility measurement(s), 140,149
 - sorption–desorption isotherms, 143,146–147*f*,148
 - sorption experimental procedure, 140,141*f*
 - sorption experimental results, 143,144–145*f*
 - surface areas, 148,149*t*
- Fluoranthene, effect of catalyst on hydrogenation, 243
- Fluorene, effect of catalyst on hydrogenation, 243

Fluorescence microscopy of coals

- fluorescence intensity vs. chloroform-extractables yield, 83,84*f*
 - fluorescence intensity vs. chloroform-solubles yield vs. Gieseler plasticity, 83,84*f*
 - fluorescence spectra of components of chloroform-solubles fraction, 83,85,86*f*
 - fluorescence spectra of vitrinite, 85,86*f*
 - primary and secondary vitrinite fluorescence, 81,82*f*,83
- Fusain, liquefaction, 172,174
- Fusible material in coals, types, 121
- Fusion of aromatic-rich macerals, basis of thermoplasticity, 124

G

Gaussian component of free induction decay, description, 62

Given, Peter Hervey

- career, 1–2
 - coal composition, effect on coal reactivity, 174–175
 - coal studies, 1–2
 - death, 2–3
 - education, 1
 - liquefaction reactivity, correlation with structure, 5
 - Pennsylvania State University, 1–2
 - work and personal life, 1
- Given structure, computer-aided molecular design, 1,161–162,163*f*
- Given symposium
- comparisons to 1964 conference topics, 3–5
 - sponsors, 3
- Guest molecules, definition, 89

H

Heteroatom incorporation and distribution in coal, advances from 1964 to 1989, 5

Heterocycles, effect of catalyst on hydrogenation, 244

High-sulfur lignites, liquefaction behavior, 214–223

Hydrogenation of coal, studies, 171–172

Hydrogenation of Mequinenza lignite

- Arrhenius plots, 216,217f,218
- mechanism, 215–216
- product yields vs. sulfur conversion, 216,217f
- reaction conditions and results, 216,218t

Hydrogen transfer reactions in model systems representative of recycle solvents

- catalyst type, effect, 241–243t,244
- comparison of approaches, 247t
- donatable hydrogen, quantification, 244,245–246f,247
- experimental conditions for phenanthrene hydrogenation, 238t
- GC of phenanthrene hydrogenation product, 238,239f
- GC–MS of phenanthrene hydrogenation product, 238,240f
- hydrogenated product reactions with sulfur, procedure, 237–238
- methods, 237
- model aromatic compound hydrogenation procedure, 237
- temperature, effect, 238,241t

Hydroliquefaction of coal liquids in

- spinning–falling basket autoclaves
 - autoclave performances, comparison, 233–234t,235
 - catalyst, effect, 235
 - experimental equipment, 226–227
 - groups for separation of GCs, definition, 226,227t
 - reaction time and temperature, effect on autoclave performance, 233,234t
 - repeat contact experiments at constant reaction parameters
 - experimental procedure, 227–228
 - H/C ratios, 229t
 - product distribution, 228–229t
 - sulfur content, 230t
 - used catalysts, analysis, 231t
 - repeat contact experiments at varying reaction parameters
 - C and H analysis, 231,232t
 - product distribution, 231,232t
 - stirrer speed, effect on autoclave performance, 233t
- Hydroliquefaction reactivity, parameters, 175**

Hydrosulfurization of Mequinenza lignite

- effect of salts, 214
- ideality, 213

I**Inorganics in South Australian lignites**

- coal samples, 21,22t
 - content, 24t,27–28
 - leaching procedure, 22–23
 - mechanical dewatering procedure, 24,27
 - scanning electron microscopic analysis, disadvantages, 26–27
 - scanning electron microscopic procedure, 21–22
 - X-ray diffraction analysis, advantages, 27
 - X-ray diffraction procedure, 22
- Interaction parameter**
- determination techniques, 138
 - vapor pressure determination method, 138
- IR spectroscopy, analysis of coal mineralogy, 48**

L**Least-squares analysis, classical, results for coal mineralogy, 50–55**

- Lignin, biochemical and chemical alteration during burial, 9
- Lignin-derived compounds, in pyrolysis products of low-rank coals, 10
- Lignin-derived structural units in ancient coalified wood samples
- catechol content, 17
- cresol content, 17,18f
- dimethylphenol content, 17,18f
- experimental procedure, 11
- methoxyphenol content, 11–17
- phenol content, 17,18f
- pyrograms
- buried cedar wood, 13,16f
- Carboniferous lignitic wood from Moscow Basin, 17,18f
- Cretaceous lignitic wood samples, 13,14–15f
- samples, 10,11t
- solid-state ¹³C-NMR spectra, 11,12f,13

- Lignin from angiosperms and gymnosperms, composition, 9
- Lignite, South Australian, *See* South Australian lignites
- Lignite hydrogenolysis, effect of organic sulfur content, 218–223
- Liotta procedure, description, 262
- Liquefaction behavior, correlation of coal characteristics, 182–183
- Liquefaction behavior of high-sulfur lignites experimental materials and procedure, 214–215
- hydrogenation mechanism for Mequinenza lignite, 215–216,217f,218t
- organic sulfur content, effect on hydrogenolysis, 218–223
- ultimate and sulfur form analyses of lignites, 214,215t
- Liquefaction of coal
- dispersed catalysts, use, 273–281
- free radical stabilization, 236
- hydrogenation catalyst, effect, 213–214
- methods at low reaction severity conditions, advantages, 260
- reactors, 225
- studies, 171–172
- Liquefaction reactivity, effect of mild chemical pretreatment of Argonne coals, 260–271f
- Lorentzian component of free induction decay, description, 62
- Low-rank coals
- catalytic preliquefaction for oil yield improvements, 193–210
- categories of noncarbonaceous material, 21
- M**
- Macromolecular structures of coals, advances from 1964 to 1989, 4
- Mequinenza lignite, hydrogenation mechanism, 215–216,217f,218t
- Metallic trace element reduction in filtered extract
- coal fraction size, effect on ash levels in coal and filtered coal extracts, 252t,253
- digestion pressure and filtration temperature, effect on ash, 251t
- Metallic trace element reduction in filtered extract—*Continued*
- Point of Ayr and Calberton coals, analyses, 251,252t
- previous work, 251–254t
- solvent precipitation of trace elements, 255–259
- solvent quality, effect on ash levels and conversions in filtered extract solutions, 243t
- trace element analysis of coal and extract ashes for Point of Ayr coal, 253,254t
- Methods for coal mineralogy
- advantages and disadvantages, 49–50
- electron beam—X-ray spectroscopy, 48
- IR spectroscopy, 48
- optical microscopy, 49
- thermal techniques, 49
- X-ray diffraction, 47–48
- Methoxyphenol(s), component of ancient coalified wood samples, 11–17
- Methoxyphenol biomarkers, survival, 10
- 1-Methylnaphthalene, effect of catalyst on hydrogenation, 244
- 2-Methylnaphthalene, effect of catalyst on hydrogenation, 243–244
- Mild chemical pretreatment effect on liquefaction reactivity of Argonne coals
- alkyl group size, effect, 265,267f
- alkylation extent, effect on reactivity enhancement, 265,269f
- alkylation studies, 264t
- carbon analytical procedure, 262–263
- chemical pretreatment method, procedure, 262
- coal conversion to soluble products, 263
- experimental procedure, 261–264
- feed coals, ultimate analysis, 261t
- liquefaction reaction conditions, 263t
- liquefaction reactivity studies, 265,266–269f,271f
- mild propylation, effect, 265,266f
- photoacoustic Fourier-transform IR spectroscopy, 270,271f
- pretreatment method, effect on reactivity enhancement, 265,269f
- reaction temperature, effect, 265,268f
- studies, 261
- Mineral(s) in South Australian lignites coal samples, 21,22t

Mineral(s) in South Australian lignites—*Continued*

- content and distribution, 24,25*t*,28
- leaching analysis, limitation, 27
- leaching procedure, 22–23
- mechanical dewatering
 - advantages, 27
 - procedure, 24
- scanning electron microscopic analysis, disadvantages, 26–27
- scanning electron microscopic procedure, 21–22
- X-ray diffraction analysis, advantages, 27
- X-ray diffraction procedure, 22
- Mineral matter associated with coal
 - measurement methods, 31–33
 - scanning electron microscopic based automated image analysis, 32–42
- Mineral matter characterization in coal, problems, 44
- Mineralogy of coal
 - accuracy of results, 50,52*t*,53–54*f*,55
 - classical least-squares analysis, results, 50–55
 - experimental procedure, 46–47
 - large data set, 45
 - methods, 47–50
 - principal component regression, results, 55,56*t*,57*f*,58*t*
 - reference minerals, 45–46*t*
 - reproducibility of results, 50,51*t*
 - sample description, 45
 - small data set, 45*t*
- Minor elements in coals, advances from 1964 to 1989, 4
- Mobile phase, 73
- Mobile phase in coal, definition, 89
- Mobile phase in coal via MS
 - experimental procedure, 90–91
 - molecular weight distributions of pyrolysates vs. temperature, 93,96–97*f*,98
 - oxidation, effect, 107,108*f*
 - temperature
 - effect on Beulah–Zap lignite, 98–101
 - effect on MS, 93–95*f*
 - temperature-resolved total ion intensity profile, 91,92*f*,93
 - thermally extracted mobile-phase components vs. temperature, 101–107
- Mobility, definition, 90

Molecular conformation of coal(s)

- determination, 112
- modeling concepts, 111
- Molecular conformation of coal macerals
 - bituminous coals, 118,119–120*f*
 - brown coals, 117,119*f*
 - coal data, statistical analysis, 116–117
 - coal samples, 113–114
 - NMR techniques, 113
 - structural interpretations, 121,124
 - thermal analytical data for coals, 114*t*,115*f*,117
- Molecular structure of coals
 - limitations, 159–160
 - modeling, 159
- MS, studies of mobile phase in coal, 90–107

N

- Number-average molecular weight between cross-links, estimation, 137–138

O

- Optical microscopy, analysis of coal mineralogy, 49
- Organic coal structure effect on liquefaction behavior under low-severity conditions
 - chloroform preextraction, effect on yields, 189*t*
 - coal analyses, 183*t*
 - coal rank and sulfided Mo catalyst, effect on yield, 190*f*,191
 - conversion with 9,10-dihydro-phenanthrene, 186,188*f*
 - conversion with naphthalene, 186,187*f*
 - conversion with pyrene after presoaking, 186,187*f*
 - conversion with tetralin, 186,188*f*
 - experimental procedure, 183–185
- H-donor solvent liquefaction results, 186,189*t*
- liquefaction experiments, summary, 183,184*t*,185
- oil yields, 190*f*,191
- primary conversions, 185–189

Organic coal structure effect on liquefaction behavior under low-severity conditions—*Continued* temperature and coal rank, effect on yield, 190*f*,191

Organic sulfur content, effect on lignite hydrogenolysis catalysts, effect, 218–219 distribution, 220,223 liquid yield vs. sulfur content, 219,221*f* organic sulfur, distribution, 220,223 rate/concentration vs. concentration, 220,221–222*f* results, 218–219,220*t*

Organically bound sulfur in nonvolatile and solid hydrocarbonaceous materials, determination methods, 127

Oxidation effect on char formation and coal combustion aliphatic hydrocarbons, removal, 289 analytical techniques, 286,287*f*,288*t* atomic O/C ratios vs. time, 286,287*f*,289 char, proportion occurring as cenospheres, 295,296*f* char classification, criteria, and characteristics, 286,288*t* char morphology, change, 294–295 char type, change, 291,292*f* coals and characteristics, 285*t* entrained flow reactor apparatus, schematic representation, 286,287*f* hydrogen, removal, 289 relationship among coal properties, char morphology, and combustion, 295,296*f*,297 relationship between unburnt carbon and atomic O/C ratio, 295,296*f* sample preparation, 285 scanning electron microscopic and optical microscopic micrographs, 289–291 study objectives, 285 temperature, effect, 289 unburnt carbon within combustion product, change in level, 291,292*f*

Oxidized coal, definition, 301

P

Particle densities, definition, 161

Phenols, component of ancient coalified wood samples, 17,18*f*

Plastofrost technique for studying coal carbonization apparatus, 314–317*f* applications, 322–324*f* assembled unit, photograph, 314,315*f* development, 313 dilatometric plastic range accuracy, assessment, 322–323,324*f* disassembled unit, photograph, 314,316,317*f* experimental procedure, 316,317*f*,318 information obtained, 320,322 metal salt, measurement of effects on coal particle fusion, 322–323 observations, 318–322 principle, 313–314 rheological test failure, exploration to predict good coking performance, 322–323 sawed and impregnated sections, photograph, 316,317*f* schematic representation of apparatus, 314,315*f* semicoke texture, 320,321*f* softening and fusion appearance, 318,319*f*,320

Point-yield conversion definition, 175 measurement of property–reactivity relationship, 175–176

Polycyclic aromatic compounds, effect of catalyst on hydrogenation, 242*t*

Principal component regression description, 55 results for coal mineralogy, 55,56*t*,57*f*,58*t*

Pyrene, effect of catalyst on hydrogenation, 242,243*t*

Pyrolysis–field ionization MS of biomaterials features, 62–63 species associated with mobile protons ion coals, 64–70

Pyrolysis of coal in MS, components, 63

S

Scanning electron microscopic based automated image analysis of mineral matter associated with coal applications, 32

- Scanning electron microscopic based
 automated image analysis of mineral
 matter associated with coal—*Continued*
 backscattered electron image, typical, 33,34*f*
 coal and mineral distribution vs.
 mineral matter content, 35,37*f*,38*t*,40*f*
 coal and mineral distribution vs. particle
 surface occupied by minerals,
 38,39*t*,41,42*f*
 composition of sample coals, 33*t*
 experimental materials, 33
 experimental procedure, 33,35
 mineral distribution vs. area-equivalent
 particle diameter, 35,36*f*
 mineral distribution vs. mineral matter
 content of particles, 38,40*f*,41
 mineral distribution vs. particle surface
 occupied by minerals, 41,42*f*
- Shinn structure, computer-aided molecular
 design, 161–162,166*f*
- Solomon structure, computer-aided
 molecular design, 161–162,165*f*
- Solvent precipitation of trace elements
 analytical procedure, 255
 ash levels, reduction, 255,256–257*t*
 experimental materials and procedure, 255
 extract solution after precipitation,
 nature, 257,258*t*,259
 temperature, effect, 256*t*
 tetrahydrofuran, effect, 256,257*t*
 toluene-to-extract ratio, effect, 255,256*t*
 trace element concentrations, 257,258*t*
- Solvent swelling, determination, 205,206*f*,207
- Sorption of benzene
 behavior for extract and *O*-methylated
 extract, 152
 Berens–Hopfenberg model, 152–156
 curves, 143,144–145*f*
 experiments, 143
 rate, 150,152
- South Australia, coal and lignite basins,
 20,23*f*
- South Australian lignites
 minerals and inorganics, 20–28
 typical analyses, 21,22*t*
- Species associated with mobile protons in
 coal via field ionization MS
 elemental composition, 66,67–70*t*
 experimental materials and procedure, 64
 hydrocarbons, 66
- Species associated with mobile protons in
 coal via field ionization MS—*Continued*
 molecular weights, 65
 oxygen compounds, 66
 volatilization vs. temperature and time
 of heating, 65*t*
- Spinning–falling basket autoclaves,
 hydroliquefaction of coal liquids, 225–235
- Stability of coal(s)
 determination, 112
 nonpolar interactions, effect, 112–113
 solvents, effect, 112
- Stability of coal macerals
 bituminous coals, 118,119–120*f*
 brown coals, 117,119*f*
 coal data, statistical analysis, 116–117
 coal samples, 113–114
 NMR techniques, 113
 solvent, effect on bituminous coals,
 118,121,122*f*
 thermal analytical data for coals, 114*t*,115*f*,117
 thermal and pyridine destabilization,
 comparison, 121,123*f*
- Sternberg technique, description, 262
- Sulfur forms in heavy petroleum and coal,
 127–135
- T**
- Thermal techniques, analysis of coal
 mineralogy, 49
- Trace elements, solvent precipitation,
 255–259
- Transalkylation
 aliphatic bridges, concentrations in
 products, 304*t*,305
 bisphenol, detection, 303
 bridges in products, detection, 304*t*
 description, 302
 scheme, 302
 side reactions, 302
- True densities, definition, 161
- Two-component concept of coal structure
 catalytic hydrogenation, 75–81
 characteristics of coals, 73,74*t*
 experimental procedure, 73,75
 fluorescence microscopy, 81–86
- Two-phase concept of coal structure,
 advances from 1964 to 1989, 4–5

Two-stage coal liquefaction processes,
description, 250

V

Vapor pressure method for interaction
parameter determination, theory, 138
Vapor pressure technique, Flory interaction
parameter determination, 138–156
Volatilization of coal in MS, components,
63–64

W

Weathering effect on char formation and
coal combustion
analytical techniques, 286,287f,288t
atomic O/C ratios vs. time, 286,287f,289
char, proportion occurring as
cenospheres, 295,296f
char classification, criteria, and
characteristics, 286,288t
char morphology, change, 294–295
char type, change, 291,293f
coal properties, char morphology, and
combustion, relationship, 295,296f,297
coals and characteristics, 285t
entrained flow reactor apparatus,
schematic representation, 286,287f
sample preparation, 285
scanning electron microscopic and
optical microscopic micrographs,
289–291
study objectives, 285

Weathering effect on char formation and
coal combustion—*Continued*
temperature, effect, 289
unburnt carbon and atomic O/C ratio,
relationship, 295,296f
unburnt carbon within combustion product,
change in level, 291,293f
Weathering of coal
chemistry, 299
detrimental effects, 299
Wiser structure, computer-aided molecular
design, 161–162,164f

X

X-ray absorption near-edge structure
spectroscopic (XANES) determination of
sulfur forms in heavy petroleum and coal
coal, 132,133f
comparison to XPS, 134,135f
experimental procedure, 128
first inflection energies of sulfur K
edge spectra, 128,129t
model compounds, 128
organically bound sulfur forms in heavy
hydrocarbons, quantification, 131t
petroleum residues, 128,130f,131t
X-ray diffraction, analysis of coal
mineralogy, 47–48
X-ray photoelectron spectroscopic (XPS)
determination of sulfur forms in heavy
petroleum and coal
comparison to XANES, 134,135f
petroleum residues, 131,132t

Production: Paula M. Betard and Margaret J. Brown
Indexing: Deborah H. Steiner
Acquisition: Cheryl Shanks
Cover design: Tina Mion

Printed and bound by Maple Press, York, PA